OFFICE OF CIVILIAN RADIOACTIVE WASTE MANAGEMENT
SCIENTIFIC ANALYSIS COVER SHEET

1. QA: QA

MW 9/26/2002

2. Scientific Analyses Title
Thermal Testing Measurements Report

3. DI (Including Revision Number)
ANL-NBS-HS-000041 REV00

4. Total Attachments	5. Attachment Numbers - Number of pages in each
N/A	

	Print Name	Signature	Date
6. Originator	R. Wagner	SIGNATURE ON FILE	26 Sep 02
7. Checker	P. Persoff	SIGNATURE ON FILE	09/26/02
8. QER	S. Harris	SIGNATURE ON FILE	9/26/02
9. Responsible Manager/Lead	Y. Tsang	SIGNATURE ON FILE	9/26/02
10. Responsible Manager	J. Wang	SIGNATURE ON FILE	9/26/02

11. Remarks

Block 6:
Contributions to Sections 1, 2, 3, 5, 7, and 8 by R. Wagner and Y. Tsang; Section 4 by R. Wagner, Y. Tsang, and T. Vogt; Section 6 by R. Wagner, Y. Tsang, W. Lin, J. Case, M. Conrad, L. DeLoach, B. Freifeld, F. Homuth, R. Jones, S. Levy, B. Marshall, J. Peterson, S. Sobolik, T. Vogt, and K. Williams.

Technical Contact/Department:

Revision History

12. Revision/ICN No.	13. Description of Revision/Change
REV00	Initial Issue

INTENTIONALLY LEFT BLANK

CONTENTS

CONTENTS (Continued)

CONTENTS (Continued)

CONTENTS (Continued)

CONTENTS (Continued)

CONTENTS (Continued)

CONTENTS (Continued)

LIST OF FIGURES

(Note: Figures that contain input data are traceable to DTNs in Tables 4-1, 4-2, or 4-3.)

LIST OF FIGURES (Continued)

LIST OF FIGURES (Continued)

LIST OF FIGURES (Continued)

LIST OF TABLES

(Note: Tables that contain data are traceable to Input-DTNs in Tables 4-1, 4-2, or 4-3.)

LIST OF TABLES (Continued)

LIST OF TABLES (Continued)

ACRONYMS

2D	two-dimensional
3D	three-dimensional
AE	acoustic emission
AR	activity ratio
ASTM	American Society for Testing and Materials
BH	borehole
BSC	Bechtel SAIC Company, LLC
C	chemical
CDEX	cross-drift extensometers
CIP	cast-in-place
CRWMS	Civilian Radioactive Waste Management System
DCS	Data Collection System
DKM	dual-permeability model
DLS	detailed line surveys
DOE	U.S. Department of Energy
DST	Drift Scale Test
DTN	data tracking number
EA	Engineering Assurance
EC	electrical conductivity
ECM	equivalent continuum model
EDX	energy-dispersive X-ray spectroscopy
EPA	U.S. Environmental Protection Agency
ERT	electrical resistivity tomography
ESF	Exploratory Studies Facility
F	Fluoride
FKM	fluoroelastomer
FLAC	Fast Lagrangian Analysis of Continua
FM	fracture monitoring
FSO	full scale output
FTP	file transfer protocol
FWP	field work package
FY	fiscal year
G	general
GHFM	guarded heat flow meter
GPR	ground penetrating radar

H	hydrological
HF	hydrogen fluoride
HFT	heat-flux transducer
IC	Ion Chromatography
ICP/AES	Inductively Coupled Plasma and Atomic Emission Spectroscopy
IR	infrared
ISS	Integrated Science Solutions
LANL	Los Alamos National Laboratory
LBNL	Lawrence Berkeley National Laboratory
LBT	Large Block Test
LLNL	Lawrence Livermore National Laboratory
LVDT	linear variable displacement transducer
M	mechanical
M&O	Management and Operating Contractor
MCTE	mean coefficient of thermal expansion
MDL	method detection limits
ME	mean error
MFC	mass flow controllers
MINC	multiple interacting continua
MOP	multiple offset profile
MPBX	multiple-point borehole extensometer
NIST	National Institute of Standards and Techno1ogy
NRC	Nuclear Regulatory Commission
OCRWM	Office of Civilian Radioactive Waste Management
PLT	Plate Loading Test
PPM	parts per million
QA	quality assurance
QER	Quality Engineering Representative
QP	Quality Procedure
QIP	Quality Implementing Procedure
RBLC	rock-bolt load cells
REKA	**r**apid **e**stimation of thermal conductivity (**k**) and thermal diffusivity (**a**lpha)
RH	relative humidity
RMR	Rock Mass Rating
RMS	Root Mean Square
RPC	Records Processing Center
RTD	resistant temperature device
RTV	room-temperature vulcanized

SEM	scanning electron microscope
SHT	Single Heater Test
SMF	Sample Management Facility
SN	scientific notebook
SNL	Sandia National Laboratory
T	thermal
TCA	thermal conductivity apparatus
TC	thermocouple
TDMS	Technical Data Management System
TDS	total dissolved solids
THM	thermal-hydrological-mechanical
Tptp	Topopah Spring Tuff
Tptpmn	Tertiary-Miocene (Age), Paintbrush (Group), Topopah Spring Tuff (Formation), Crystal-Poor (Member), Middle Nonlithophysal (Zone)
TTF	Thermal Test Facility
U	uranium
USBR	U.S. Bureau of Reclamation
USGS	U.S. Geological Survey
XRD	X-ray diffraction
YMP	Yucca Mountain Site Characterization Project
ZOP	zero offset profile

INTENTIONALLY LEFT BLANK

1. PURPOSE

The purpose of the Thermal Testing Measurements Report (Scientific Analysis Report) is to document, in one report, the comprehensive set of measurements taken within the Yucca Mountain Project Thermal Testing Program since its inception in 1996. Currently, the testing performed and measurements collected are either scattered in many level 3 and level 4 milestone reports or, in the case of the ongoing Drift Scale Test, mostly documented in eight informal progress reports. Documentation in existing reports is uneven in level of detail and quality. Furthermore, while all the data collected within the Yucca Mountain Site Characterization Project (YMP) Thermal Testing Program have been submitted periodically to the Technical Data Management System (TDMS), the data structure—several incremental submittals, and documentation formats—are such that the data are often not user-friendly except to those who acquired and processed the data.

The documentation in this report is intended to make data collected within the YMP Thermal Testing Program readily usable to end users, such as those representing the Performance Assessment Project, Repository Design Project, and Engineered Systems Sub-Project. Since either detailed level 3 and level 4 reports exist or the measurements are straightforward, only brief discussions are provided for each data set. These brief discussions for different data sets are intended to impart a clear sense of applicability of data, so that they will be used properly within the context of measurement uncertainty. This approach also keeps this report to a manageable size, an important consideration because the report encompasses nearly all measurements for three long-term thermal tests. As appropriate, thermal testing data currently residing in the TDMS have been reorganized and reformatted from cumbersome, user-unfriendly Input-Data Tracking Numbers (DTNs) into a new set of Output-DTNs. These Output-DTNs provide a readily usable data structure, including graphical displays and comprehensive spreadsheets. In some cases, there was no need to reformat or restructure Input-DTNs so they remained unchanged.

Thermal testing measurement data come from the characterization (pre-heating/baseline and post-cooling) and testing (heating and cooling) phases of the Large Block Test (LBT), the Single Heater Test (SHT), and the Drift Scale Test (DST). Since the LBT and SHT are completed, all phases of those two tests are addressed. DST measurements addressed in this report include pre-heating and the entire four-year heating phase, which ended January 14, 2002. Discussion of measurements from the ongoing cooling phase will be included in future revision(s) of this report.

The objective of the YMP Thermal Testing Program is to gain a more in-depth understanding of the coupled thermal (T), hydrological (H), mechanical (M), and chemical (C) processes. Satisfaction of this objective will ultimately lead to better understanding of how thermally driven coupled processes would affect the performance of the waste packages and the flow and transport of radionuclides (and consequently, the performance of the repository). The robust study of coupled-process behavior in the YMP Thermal Testing Program required a pioneering effort involving a blend of laboratory and field testing, along with numerical analyses using various process models. This program also utilized an approach to progress from smaller-simpler-shorter testing to larger-more complex-longer testing. For example, the Single Heater

Test served as a "shakedown" test for the DST in which several measurement concepts and devices were evaluated and improved while coupled processes were being studied. This strategy ensured advanced understanding of coupled-process behavior from refined and improved DST measurements and analyses.

The YMP Thermal Testing Program, which was initially described in the Site Characterization Plan (U.S. Department of Energy [DOE] 1988 [100282]), identified seven types of tests. In 1994, the YMP thermal testing program was re-evaluated, resulting in two phases of test consolidation. The first phase, documented in the report entitled *In-Situ Thermal Testing Program Strategy* (DOE 1995 [130104]), presented five types of *in situ* thermal tests, including the LBT and the SHT. The second phase of test consolidation, documented in the report entitled *Updated In Situ Thermal Testing Program Strategy* (CRWMS M&O 1997 [111106]), was a more fundamental approach that included consideration of thermally driven coupled processes and related parameters. Additional scope included laboratory tests, analogs, modeling, performance confirmation monitoring, and a restructured suite of *in situ* thermal tests. The DST was developed from this second phase of test consolidation.

The LBT, located in Fran Ridge, southeast of Yucca Mountain, is described in the *Large Block Test Final Report* (Lin et al. 2001 [159069]). The heating phase of the LBT started in February 1997 and continued until March 1998, at which time the heaters were turned off. Cooling-phase measurements at the LBT were made until September 1998. Upon completion of the post-cooling characterization of the LBT block, a final report was prepared (Lin et al. 2001 [159069]).

The SHT, located in Alcove No. 5 of the Exploratory Studies Facility (ESF), is described in the *Characterization of the ESF Thermal Test Area* (CRWMS M&O 1996 [101428]), *Single Heater Test Status Report* (CRWMS M&O 1997 [101540]) and *Single Heater Test Final Report* (CRWMS M&O 1999 [129261]). The heating phase of the SHT started in August 1996 and continued for 275 days until May 1997. The cooling phase continued until January 1998, at which time post-cooling characterization of the test block commenced. Laboratory tests, modeling, analyses, and documentation were completed, and the final report (CRWMS M&O 1999 [129261]) was submitted to the DOE in October 1999.

The DST is described in the following reports: *Drift Scale Test Design and Forecast Results* (CRWMS M&O 1997 [146917]) and *Drift Scale Test As-Built Report* (CRWMS M&O 1998 [111115]). The results from characterizing the test block are contained in the *Ambient Characterization of the Drift Scale Test Block* (CRWMS M&O 1997 [101539]). Early results of the DST are discussed in the *Drift Scale Test Progress Report No. 1* (CRWMS M&O 1998 [108306]). The heating phase of the DST started in December 1997 and lasted approximately four years until January 14, 2002. DST measurements through the entire four-year heating phase are reported in this Scientific Analysis Report. Cooling phase measurements are planned for future revision(s) of this report.

Discussion of the thermal testing measurements in this report is organized first under the heading of the three tests: LBT, SHT, and DST; and then under the four processes: T, H, M, and C. Miscellaneous measurements and observations are also discussed. Although the list of measurement types is comprehensive, it is neither practical (because of finite report length) nor necessary to thoroughly discuss all data sets. For example, the DST measured temperatures come

from nearly 2,700 thermal sensors distributed throughout the test block and collected hourly, resulting in approximately 100 million measurements. Therefore, as appropriate for each measurement type, only a representative discussion of the test data behavior is presented. Readers are referred to user-friendly Output-DTNs for comprehensive data sets that include complementary graphics.

The depth of the following discussions concerning the 12 basic measurement groups (three thermal tests and four processes) is dictated by their respective data characteristics. In general, discussions of thermal and mechanical measurements tend to be comparatively short, although the respective Output-DTNs contain comparatively large amounts of data. This condition reflects the inherent simplicity or straightforwardness of temperature and displacement measurements that are recorded frequently (hourly) on a data acquisition system. Conversely, discussions of hydrological and chemical measurements tend to be lengthier, while their Output-DTNs are comparatively small. The smaller output data sets result from measurements collected comparatively infrequently (monthly or longer) on a nonintegrated data acquisition system. The more lengthy discussion in the chemical-measurements sections relate to sampling procedures that have great relevance to the data collected. Also, in certain hydrological measurements, detailed explanations are needed for the complex data reduction that occurs as the data are transformed from Input-DTN data to more useful and functional Output-DTN data. Furthermore, since several level 3, level 4, and other technical documents exist (see prior comments on LBT, SHT, and DST reports), discussion of the measurement process was intentionally limited. More specifically, discussion of calibration, measurement technique, and scientific notebook entries, was, for the most part, not included in this report. Also, complete interpretations of the massive amount of measurement data acquired in the YMP thermal testing diagram was not attempted in this report.

Uncertainty associated with most measurements is also discussed. These discussions are restricted to actual measurements and data reduction. If quantifiable uncertainties were cited, then either references to manufacturer's specifications were provided or they were referred to as "estimates." Standard error analyses (mean and standard deviation) were provided for applicable measurements such as repetitive measurements of laboratory or field parameters. Test measurements of a response for a specific location and time are not applicable for standard error analyses. Additional information on measurement uncertainties can be located via directions in DTNs cited in the first footnote of Tables 4-1, 4-2, and 4-3. This information, among other things, provides detailed discussions of scientific notebooks and calibration relationships relevant to uncertainties of thermal testing measurements. The approach taken provides sufficient discussion of uncertainties for end-users of thermal testing measurements such as process modelers. Uncertainty related to modeling and analyses between measured and simulated data will be discussed in Model Reports related to TH, THC, and THM process models. Also included in this report are summaries of three white papers involving in-depth investigations of unexpected or unusual behavior not uncommon in large-scale, long-term field testing such as the DST. The summaries are in Sections 6.3.2.6, 6.3.3.7, and 6.3.4.5.

The measurements documented in this Scientific Analysis Report were conducted under the *Technical Work Plan for: Unsaturated Zone Sections of License Application Chapters 8 and 12* (BSC 2002 [159051]) and *Test Plan for: Drift Scale Test* (BSC 2002 [158190]).

The report is organized as follows: Section 2 addresses the applicability of the QA program. Section 3 discusses the use of controlled and baselined software. Section 4 provides a tabulation of technical product inputs (i.e., Input-DTNs) that were used to develop technical product outputs (i.e., Output-DTNs). Assumptions used in the scientific analyses are documented in Section 5. Discussion of the thermal test measurements for each of the three thermal tests are provided in Section 6. Summary and sources of Inputs-DTNs, software, and cited references are presented in Sections 7 and 8, respectively.

2. QUALITY ASSURANCE

The activities documented in this Scientific Analysis Report were determined to be subject to the requirements of the U.S. DOE Office of Civilian Radioactive Waste Management (OCRWM) *Quality Assurance Requirements and Description* (DOE 2002 [159475]). It was prepared in accordance with AP-SIII.9Q, *Scientific Analyses*. Specifically, this investigation of thermal test measurements is consistent with the direction delineated in the *Technical Work Plan for: Unsaturated Zone Sections of License Application Chapters 8 and 12* (BSC 2002 [159051]) and the *Test Plan for: Drift Scale Test* (BSC 2002 [158190]) which were prepared in accordance with AP-2.27Q, *Planning for Science Activities*, and AP-SIII.7Q, *Scientific Investigation Laboratory and Field Testing*, respectively.

The document identifier was obtained as per AP-6.1Q, *Controlled Documents*. Input DTNs were documented in accordance with AP-3.15Q, *Managing Technical Product Input*s. Data not already in the Technical Data Management System (TDMS) were submitted to the TDMS in accordance with AP-SIII.3Q, *Submittal and Incorporation of Data to the Technical Data Management System*. Software, as applicable, was obtained, controlled, and documented as per AP-SI.1Q, *Software Management.* Process controls on specific uses of electronically stored information, including information residing in an electronic information management system or on electronic media, were evaluated as per AP-SV.1Q, *Control of the Electronic Management of Information*.

The methods used for control of electronic management of data are in accordance with those specified in the *Technical Work Plan for: Unsaturated Zone Sections of License Application Chapters 8 and 12* (BSC 2002 [159051]). Specifically, electronic management of information is controlled under the following organization-specific procedures: YMP-LBNL-QIP-SV.0, *Management of YMP-LBNL Electronic Data* for Lawrence Berkeley National Laboratory (LBNL); 033-YMP-QP-3.8, *Control of the Electronic Management of Data* for Lawrence Livermore National Laboratory (LLNL); and LANL-YMP-QP-S5.01, *Electronic Data Management*, for Los Alamos National Laboratory (LANL).

For work done by the U. S. Geological Survey (USGS), four electronic databases on work stations/personal computers are in use by the USGS Environmental Science Team. The databases are backed up on a fixed schedule and whenever blocks of new data are added. Backed-up files are stored on fixed and removable magnetic media and removal optical media. Backup media are kept in secure areas remote from the workstations/personal computers. Backup is also provided by hard copies of original raw data and by laboratory notebooks. Completeness and accuracy of data input are assured through multiple checking steps. A final check is attained by retrieving data from the database and physically checking it against the original input records. Any errors are corrected and the records are rechecked after correction. Records of this checking process are maintained. Data packages submitted to the TDMS are prepared by outputting the data from the databases commonly through spreadsheets. It is not necessary to rekey the data once they are in the databases and have undergone final checks.

For work done by Sandia National Laboratories (SNL), the requirements of AP-SV.1Q were met by the following measures: Computers used for processing and storing information will be

password-protected. All files will be backed up on magnetic media monthly or oftener as needed. Backup media will be labeled with the date and time of backup, DOE serial number of the computer backed up, system utility used to perform the backup, and format of the magnetic media. Information transfers from one computer to another was done by magnetic media, internet, or local network, using file transfer protocol (FTP) or attachments to e-mail on the same system. These transfer methods are quite dependable and generally error-free. In most cases, such transfers are between computers that use a common operating system and storage format. In these cases, the name, date, and file size was visually checked. ASCII files was also be verified by visual comparison of the data. All such visual checks was documented in a scientific notebook maintained in accordance with AP-SIII.1Q, *Scientific Notebooks*.

For work done by Integrated Science Solutions (ISS), the requirement of AP-SV.1Q was met by the following measures: Computers used for processing and storing information will be password-protected. All files will be backed up on magnetic media monthly or oftener as needed. Backup media was labeled with the date and time of backup, DOE serial number of the computer backed up, system utility used to perform the backup, and format of the magnetic media. Information transfers from one computer to another was done by magnetic media, internet, or local network, using FTP or attachments to e-mail on the same system. These transfer methods are quite dependable and generally error-free. In most cases, such transfers are between computers that use a common operating system and storage format. In these cases, the name, date, and file size was visually checked. ASCII files was also verified by visual comparison of the data.

Scientific notebooks, as applicable, were used as per AP-SIII.1Q. As required, this Scientific Analysis Report includes the quality level of the thermal testing measurements as per AP-2.22Q, *Classification Criteria and Maintenance of the Monitored Geologic Repository Q-List.* The conclusions of this report do not affect the repository design or permanent items.

A checker and Bechtel SAIC Company, LLC (BSC) Quality Engineering Representative (QER) reviews were conducted per AP-SIII.9Q. In addition, an LBNL technical review and Engineering Assurance (EA) review were performed per YMP-LBNL-QIP-6.1, *Document Review*. Upon completion, an interdisciplinary review was conducted in accordance with AP-2.14Q, *Review of Technical Products and Data*. Upon approval of the checking and interdisciplinary reviews, this Scientific Analysis Report was processed in accordance with AP-6.1Q. Modifications, as applicable, resulting from the DOE's review were implemented as per AP-7.5Q, *Submittal, Review, and Acceptance of Deliverable*s. The records required by Sections 6.1 and 6.2 of AP-SIII.9Q were collected and submitted to the Records Processing Center in accordance with AP-17.1Q, *Record Source Responsibilities for Inclusionary Record*s. The records listed in Section 6.3 of AP-SIII.9Q were dispositioned by the Record Source per requirements in AP-32.4, *Records Retention and Disposition*.

Relevant Technical Implementing Procedures are listed in Section 8.2.

3. USE OF SOFTWARE

As per Section 5.3 and Attachment 3 – Item 3 of AP-SIII.9Q, the use of software applies to those activities associated with the scientific analyses of this report. Basically, the scientific analyses for this report involves restructuring, as needed, Input-DTNs into more user-friendly Output-DTNs. This process involves only limited use of commercial off-the-shelf graphic packages and spreadsheet software which is exempt from the control requirements of AP-SI.1Q, *Software Management.* Nonetheless, computations using the standard functions of commercial software need to be discussed as per Attachment 3 – Item 3 of AP-SIII.9Q. The software used for the scientific analyses of this Scientific Analysis Report (in restructuring Input-DTN into Output-DTN) are Microsoft EXCEL: Versions 97 and 2000, operating systems Windows 98, Windows NT and Windows 2000. The input and output data are listed respectively in the Input-DTN and Output-DTN columns of Tables 6.1-1, 6.2-1 and 6.3-1.

In majority of data presented in Tables 6.1-1, 6.2-1 and 6.3-1 the process involved in going from the input data in the Input-DTN column to the output data in the Output-DTN column involves simple reorganization, sorting and no calculation. The exceptions are:

1. For the air-permeability data where the data reduction processes is described in Sections 5.1. The specific Output-DTNs are:

    - LB0208AIRKSHTC.001 in Table 6.2-1
    - LB0208AIRKDSTH.001 in Table 6.3-1

    The input data are as listed in the respective Input-DTN columns and the equation used is Eq. 5.1-1

2. For the smoothed MPDX displacement and strain data where the smoothing process is discussed in Section 5.2. The specific Output DTNs are:

    - SN0207F3912298.037 in Table 6.3-1
    - SN0208F3912298.039 in Table 6.3-1
    - SN0203F3912298.038 in Table 6.3-1

    The input data are as listed in the respective Input-DTN columns and smoothing process is as discussed in Section 5.2.

INTENTIONALLY LEFT BLANK

4. INPUTS

The following discussion provides a listing of Input-DTNs for measurements of characterization and test data from each of the three thermal tests (Large Block Test (LBT), Single Heater Test (SHT), and Drift Scale (DST)). Since many of these DTNs were developed in an incremental manner during the duration of each test, several DTNs need to be accessed to examine measurements for the duration of the already completed thermal tests (LBT and SHT) and the four-year heating phase of the DST. This cumbersome aspect of many of the following Input-DTNs has been corrected with restructured and better organized Output-DTNs listed in Tables 6.1-1, 6.2-1, and 6.3-1. The following tables identify the locations of the Input-DTNs in this document's text, which is also consistent with tables and figures cited in their respective sections.

Applicable criteria and applicable codes and standards used in this Scientific Analysis Report are also discussed below.

4.1 DATA AND PARAMETERS

4.1.1 LARGE BLOCK TEST

Table 4-1 provides Input-DTNs for characterization and test measurements from the LBT, along with where they were cited in this report. In the third column under the heading "Type," the data are grouped according to the four processes: thermal (T), hydrological (H), mechanical (M), and chemical (C), plus a fifth category, "general" (G).

4.1.2 SINGLE HEATER TEST

Table 4-2 provides Input-DTNs for characterization and test measurements from the SHT, along with where they were cited in this report. In the third column under the heading "Type," the data are grouped according to the four processes: thermal (T), hydrological (H), mechanical (M), and chemical (C), plus a fifth category, "general" (G).

4.1.3 DRIFT SCALE TEST

Table 4-3 provides Input-DTNs for characterization and test measurements from the DST along with where they were cited in this report. In the third column under the heading "Type," the data are grouped according to the four processes: thermal (T), hydrological (H), mechanical (M), and chemical (C), plus a fifth category, "general" (G).

4.2 CRITERIA

There are no criteria from requirement documents that are identified as specific for this Scientific Analysis Report.

4.3 CODES AND STANDARDS

No specific formally established codes and standards have been identified as applying to this Scientific Analysis Report. Although some standards were used to obtain thermal testing measurements, this activity was upstream of the Input-DTN submittal, which would make it outside the scope of this report (See Section 1). Also, refer to key references cited in Section 1 and corresponding background discussion in the Input-DTNs for information on applicable standards.

Table 4-1. Input-DTNs for the Large Block Test[1]

Input-DTN [DIRS]	Description	Type[2]	Q Status	Report Location		
				Text	Figures	Tables
LL980918904244.074 [135872]	Heater Power, Temperature, Relative Humidity, and Gas Pressure	T,H	Q	6.1.1.1 6.1.1.2 6.1.2.3	6.1.1.1-1 6.1.1.2-1 6.1.1.2-2 6.1.2.3-1 6.1.2.3-2	
LL980913304244.072 [145385]	Electrical Resistance Tomograms	H	Q	6.1.2.1	6.1.2.1-2 6.1.2.1-3	
LL981001604244.079 [158261]	Electrical Resistivity	H	Q	6.1.2.1		
LL980919304244.075 [145099]	Neutron Logging	H	Q	6.1.2.2	6.1.2.2-1 6.1.2.2-2 6.1.2.2-3	
LL950812704242.017 [158237]	Porosity, Saturated and Dry Density	H	non-Q[3]	6.1.2.4		6.1.2.4-2
LL960905204244.022 [158244]	Laboratory Matrix Permeability	H	Q	6.1.2.4		6.1.2.4-1
LL981208404244.092 [158263]	X-ray Radiography	H	Q	6.1.2.4	6.1.2.4-1	
LL980919404244.076 [148630]	Rock Mass Displacements	M	Q	6.1.3.1 6.1.3.2	6.1.3.1-2	
LL960400404244.012 [158271]	Fracture Mapping	G	Q	6.1.4.1	6.1.4.1-1	
LL960400504244.013 [158274]	Fracture Mapping	G	Q			
LL960400604244.014 [158275]	Fracture Mapping	G	Q			
LL960400704244.015 [158276]	Fracture Mapping	G	Q			
LL981202305912.004 [158270]	Bacterial Transport	C	non-Q[4]	6.1.4.3		

NOTE: [1] DTNs: LA0106FH831151.002 [158230] and LA0106FH831151.003 [158229] provide access via Records Processing Center (RPC) to all thermal and mechanical data collected in LBT Data Collection System (original/electrical and converted/engineering units). These non-qualified DTNs also provide access (RPC) to pertinent supporting material such as scientific notebooks and calibration relationships.

[2] T=Thermal, H=Hydrological, M=Mechanical, C=Chemical, G=General/Miscellaneous.

[3] The status of the data is classified as non-Q because the data reporting was preliminary. Hence, these data should only be used for corroborative purposes.

[4] These data deal with bacteria abundance and bacterial types that are secondary to the primary objective of understanding the coupled processes. They should only be used for reference purposes.

Table 4-2. Input-DTNs for the Single Heater Test[1]

Input-DTN [DIRS]	Description	Type[2]	Q Status	Report Location		
				Text	Figures	Tables
SNF35110695001.001 [158315] and LL970805504244.043 [158313]	XYZ Coordinates of Boreholes and Sensors	T,H,M,C	Q	6.2	6.2-2	6.2-2
SNF35110695001.008 [113812]	Heater Power	T	Q	6.2.1.1	6.2.1.1-1	
SNF35110695001.008 [113812]	Temperature – Heating and Initial Six Months of Cooling	T	Q	6.2.1.2	6.2.1.2-1 6.2.1.2-2 6.2.1.2-3 6.2.1.2-4	
SNF35110695001.009 [113819]	Temperature – Last Two Months of Cooling	T	Q			
SNL22080196001.001 [109722]	Thermal Conductivity	T	Q	6.2.1.3		6.2.1.3.-1
LL970101004244.026 [158281]	Electrical Resistance Tomography	H	Q	6.2.2.1	6.2.2.1-1 6.2.2.1-2	
LL970505404244.031 [148609]	Electrical Resistance Tomography	H	Q			
LL971002904244.044 [158286]	Electrical Resistance Tomography	H	Q			
LL980105204244.049 [148610]	Electrical Resistance Tomography	H	Q			
LB980901123142.003 [119016]	Ground Penetrating Radar Data	H	Q	6.2.2.2	6.2.2.2-1 6.2.2.2-2 6.2.2.2-3	
LL980106904244.051 [118963]	Neutron Logging	H	Q	6.2.2.3	6.2.2.3-1 6.2.2.3-2	
LB960500834244.001 [105587]	Pre-Heating Air Injection	H	Q	6.2.2.4		6.2.2.4-1 6.2.2.4-2 6.2.2.4-4
LB980120123142.008 [158280]	Air Injections in Boreholes 16 and 18, Part 1 of 4	H	Q	6.2.2.4	6.2.2.4-1	
LB970500123142.001 [158293]	Air Injections in Boreholes 16 and 18, Part 2 of 4	H	Q			
LB0204SHAIRK3Q.001 [159543]	Air Injections in Boreholes 16 and 18, Part 3 of 4	H	Q			
LB971000123142.001 [118965]	Air Injections in Boreholes 16 and 18, Part 4 of 4	H	Q			
LB980901123142.001 [118999]	Post-Cooling Air Injection and Gas Tracer Testing	H	Q	6.2.2.4		6.2.2.4-3 6.2.2.4-4 6.2.2.4-5
LB980901123142.002 [119009]	Temperature, Relative Humidity, Gauge Pressure (Passive Monitoring)	T,H	Q	6.2.2.4	6.2.2.4-2 6.2.2.4-3 6.2.2.4-4	
LB970500123142.003 [131500]	Pre-Heating Laboratory Saturation, Porosity, Bulk Density Gravimetric Water Content	H	Q	6.2.2.5		6.2.2.5-1 6.2.2.5-2
LL970709004244.035 [127312]	Pre-Heating Laboratory Porosity, Relative Humidity, and Water Saturation	H	Q	6.2.2.5	6.2.2.5-1	6.2.2.5-3
LB980901123142.006 [119029]	Post-Cooling Laboratory Saturation, Porosity, Bulk Density Gravimetric Water Content	H	Q	6.2.2.5	6.2.2.5-2	6.2.2.5-4

Table 4-2. Input-DTNs for the Single Heater Test[1] (continued)

Input-DTN [DIRS]	Description	Type[2]	Q Status	Report Location		
				Text	Figures	Tables
SNF35110695001.008 [113812]	Standard MPBX Displacements – Heating and Initial Six Months of Cooling	M	Q	6.2.3.1	6.2.3.1-3	6.2.3.1-1 6.2.3.1-2
SNF35110695001.009 [113819]	Standard MPBX Displacements – Last Two Months of Cooling	M	Q	6.2.3.1	6.2.3.1-3	6.2.3.1-1
LL980109904243.015 [158299]	Optical MPBX Displacements	M	Q	6.2.3.1		
SNF35110695001.010 [158300]	Rock Mass Deformation Modulus – Borehole (Goodman) Jack	M	Q	6.2.3.2		6.2.3.2-1
SNF35110695001.008 [113812]	Rock Bolt Load – Heating and Initial Six Months of Cooling	M	Q	6.2.3.3		6.2.3.3-1
SNF35110695001.009 [113819]	Rock Bolt Load – Last Two Months of Cooling	M	Q			
SNL22080196001.001 [109722]	Laboratory Thermal Expansion	M	Q	6.2.3.4		6.2.3.4-1 6.2.3.4-2
SNL22080196001.002 [158306]	Pre-Heating Laboratory Unconfined Compressive Strength, Dry Bulk Density, Poisson's Ratio, Youngs Modulus, Saturated Bulk Density, Seismic Velocity	M	Q	6.2.3.4		
SNL22080196001.003 [119042]	Post-Cooling Laboratory Thermal Conductivity, Thermal Expansion, Unconfined Compressive Strength, Dry Bulk Density, Poisson's Ratio, Young's Modulus	T, M	Q	6.2.3.4		6.2.3.4-1 6.2.3.4-2 6.2.3.4-3
SNF35110695001.008 [113812]	Rock Mass Thermal Expansion	M	Q	6.2.3.5		6.2.3.5-1
LL970101104244.027 [158309]	Chemical Abundance Data	C	non-Q[3]	6.2.4.1	6.2.4.1-1	6.2.4.1-1
LL970409604244.030 [111481]	Chemical Abundance Data	C	non-Q[3]			
LL970703904244.034 [111482]	Chemical Abundance Data	C	non-Q[3]			
LL971006604244.046 [148611]	Chemical Abundance Data	C	non-Q[3]			
LA0009SL831151.001 [153485]	Fracture Mineralogy	C	Q	6.2.4.2		6.2.4.2-1 6.2.4.2-2 6.2.4.2-3
LB970100123142.002 [158288]	Infrared Images, Part 1 of 5	T, H	Q	6.2.5.2		
LB970400123142.001 [158289]	Infrared Images, Part 2 of 5	T, H	Q			
LB970700123142.002 [158295]	Infrared Images, Part 3 of 5	T, H	Q			
LB971000123142.002 [158296]	Infrared Images, Part 4 of 5	T, H	Q			
LB980120123142.001 [158297]	Infrared Images, Part 5 of 5	T, H	Q			

NOTE: [1] DTN LA0002FH6001WP.001 [158278] provides access via Records Processing Center (RPC) to all thermal and mechanical data collected in SHT Data Collection System (original/electrical and converted/engineering units). This non-qualified DTN also provides access (RPC) to pertinent supporting material such as scientific notebooks and calibration relationships.

[2] T=Thermal, H=Hydrological, M=Mechanical, C=Chemical, G=General/Miscellaneous.

[3] These four sets of data are classified as non-Q due to the disposition of a non-conformance report regarding measurement and testing equipment. Hence, these data should only be used for corroborative purposes.

Table 4-3. Input-DTNs for the Drift Scale Test[1]

Input-DTN [DIRS]	Description	Type[2]	Q Status	Report Location		
				Text	Figures	Tables
MO0002ABBLSLDS.000 [147304]	XYZ Coordinates of Boreholes and Sensors	T,H,M,C	Q	6.3	6.3-2 6.3-3 6.3-4 6.3-5 6.3-6 6.3-7 6.3-8 6.3.3.1-1	6.3-2
MO9807DSTSET01.000 [113644]	Heater, Power, Current, Voltage, Temperature: November 7, 1997 – May 1998	T	Q	6.3.1.1 6.3.1.2	5.2-2 6.3.1.1-1 6.3.1.2-1 6.3.1.2-2 6.3.1.2-3 6.3.1.2-4 6.3.1.2-5 6.3.1.2-6 6.3.1.2-7 6.3.1.2-8 6.3.1.2-9	
MO9810DSTSET02.000 [113662]	Heater, Power, Current, Voltage, Temperature: June 1998 – August 1998	T	Q			
MO9906DSTSET03.000 [113673]	Heater, Power, Current, Voltage, Temperature: September 1998 – May 1999	T	Q			
MO0001SEPDSTPC.000 [153836]	Heater, Power, Current, Voltage, Temperature: June 1999 – October 1999	T	Q			
MO0007SEPDSTPC.001 [153707]	Heater, Power, Current, Voltage, Temperature: November 1999 – May 2000	T	Q			
MO0012SEPDSTPC.002 [153708]	Heater, Power, Current, Voltage, Temperature: June 2000 – November 2000	T	Q			
MO0107SEPDSTPC.003 [158321]	Heater, Power, Current, Voltage, Temperature: December 2000 – May 2001	T	Q			
MO0202SEPDSTTV.001 [158320]	Heater, Power, Current, Voltage, Temperature: June 2001 – January 14, 2002	T	Q			
SNL22100196001.006 [158213]	Thermal Conductivity as Function of Saturation	T	Q	6.3.1.3		
SN0203L2210196.007 [158322]	Thermal Expansion Thermal Conductivity DST Specimens	T,M	Q	6.3.1.3		6.3.1.3-1 6.3.1.3-2
LL980411004244.060 [159107]	DST Baseline REKA Probe Measurements. Temperature Measurements using REKA Probes: 11/14/97 - 7/31/98.	T	Q	6.3.1.4		
LL980411104244.061 [159111]	DST Baseline REKA Probe Measurements for Thermal Conductivity and Diffusivity. VA Supporting Data	T	Q	6.3.1.4		
LL980902104244.070 [159109]	DST Baseline REKA Probe Measurements for Thermal Conductivity and Diffusivity. Probe 1 from Borehole #153, Probe 2 from Borehole #152, Probe 3 from Borehole #151.	T	Q			

Table 4-3. Input-DTNs for the Drift Scale Test[1] (continued)

Input-DTN [DIRS]	Description	Type[2]	Q Status	Report Location		
				Text	Figures	Tables
UN0106SPA013GD.003 [159115]	DST REKA Probe Acquired Data for Thermal Conductivity and Diffusivity: 05/01/1998 to 04/30/2001	T	Q	6.3.1.4		
UN0106SPA013GD.004 [159116]	DST REKA Probe Developed Data for Thermal Conductivity and Diffusivity: 05/01/1998 to 04/30/2001	T	Q			
UN0109SPA013GD.005 [159117]	DST Rapid Evaluation of K and Alpha (REKA) Probe Acquired Data for Thermal Conductivity and Diffusivity: 05/01/2001 to 08/31/2001	T	Q			
UN0112SPA013GD.006 [159118]	DST REKA Probe Acquired Data for Thermal Conductivity and Diffusivity: 09/01/2001 to 12/31/2001	T	Q			
UN0201SPA013GD.007 [159119]	DST REKA Probe Developed Data for Thermal Conductivity and Diffusivity: 05/01/2001 to 12/31/2001	T	Q			
LL000804023142.009 [158325]	Water Saturation	H	Q	6.3.2.1	6.3.2.1-1 6.3.2.1-2	
LL980108804244.052 [158332]	Electrical Resistivity	H	Q	6.3.2.1		
LL980406404244.057 [113782]	Electrical Resistance Tomography	H	Q			
LL990702704244.099 [113872]	Electrical Resistivity	H	Q			
LL980808604244.065 [113791]	Electrical Resistance Tomography	H	Q			
LB990630123142.005 [129274]	Ground Penetrating Radar Data	H	Q	6.3.2.2	6.3.2.2-1	
LB000121123142.004 [158338]	Ground Penetrating Radar Data	H	Q			
LB000718123142.004 [153354]	Ground Penetrating Radar Data	H	Q			
LB0101GPRDST01.001 [158346]	Ground Penetrating Radar Data	H	Q			
LB0108GPRDST05.001 [158440]	Ground Penetrating Radar Data	H	Q			
LL020710223142.024 [159551]	Neutron Logging	H	Q	6.3.2.3	6.3.2.3-1 6.3.2.3-2	
LB970600123142.001 [105589]	Active DST Pre-Heating Air Injection, Part 1 of 2	H	Q	6.3.2.4		6.3.2.4-1
LB980120123142.005 [114134]	Active DST Pre-Heating Air Injection, Part 2 of 2	H	Q	6.3.2.4		6.3.2.4-2
LB980120123142.004 [105590]	Active Baseline Air Injections in Boreholes 57-61, 74-78, 185-186	H	Q	6.3.2.4	6.3.2.4-2 6.3.2.4-3 6.3.2.4-4	6.3.2.4-3

Table 4-3. Input-DTNs for the Drift Scale Test[1] (continued)

Input-DTN [DIRS]	Description	Type[2]	Q Status	Report Location		
				Text	Figures	Tables
LB980420123142.002 [113706]	Active Hydrology Testing for Boreholes 57-61, 74-78, 185-186; Air Injection and Gas Tracer Tests	H	Q	6.3.2.4	6.3.2.4-2 6.3.2.4-3 6.3.2.4-4 6.3.2.4-8	
LB980715123142.002 [113742]	Active Hydrology Testing Data (Air Injection) Collected from 12 Hydrology Boreholes: March 1998 to May 1998	H	Q	6.3.2.4	6.3.2.4-2 6.3.2.4-3 6.3.2.4-4	
LB981016123142.002 [129245]	Active Hydrology Testing for Boreholes 57-61, 74-78, 185-186; Air Injection Tests: June 1998 to August 1999	H	Q			
LB990630123142.001 [129247]	Active Hydrology Testing by Air Injection: September 1998 to May 1999	H	Q	6.3.2.4	6.3.2.4-2 6.3.2.4-3 6.3.2.4-4 6.3.2.4-5 6.3.2.4-6	
LB000121123142.002 [158337]	Active Hydrology Testing by Air Injection: June 1999 to October 1999	H	Q	6.3.2.4	6.3.2.4-2 6.3.2.4-3 6.3.2.4-4	
LB000718123142.002 [158341]	Active Hydrology Testing Data (Air Injection) Collected from 12 Hydrology Holes: November 1, 1999 to May 31, 2000	H	Q	6.3.2.4	6.3.2.4-1 6.3.2.4-2 6.3.2.4-3 6.3.2.4-4	
LB0101AIRKDST1.001 [158345]	Active Hydrology Testing Data (Air Injection) Collected from 12 Hydrology Boreholes: June 1, 2000 to November 30, 2000	H	Q	6.3.2.4	6.3.2.4-2 6.3.2.4-3 6.3.2.4-4	
LB0108AIRKDST5.001 [158438]	Active Hydrology Testing Data (Air Injection) Collected from 12 Hydrology Boreholes: December 1, 2000 to May 31, 2001	H	Q			
LB0203AIRKDSTE.001 [158348]	Active Hydrology Testing Data (Air Injection) Collected from 12 Hydrology Boreholes: June 1, 2001 to January 2002	H	Q			
LB980420123142.001 [113696]	Passive Monitoring Data for Boreholes 57-61, 74-78, 185-186: Nov 1997 to Feb 1998	H	Q	6.3.2.4	6.3.2.4-7	
LB980715123142.001 [113733]	Passive Monitoring Data Collected from 12 Hydrology Boreholes: March 1998 to May 1998	H	Q			
LB981016123142.001 [158353]	Passive Monitoring Data for Boreholes 57-61, 74-78, 185-186 Taken from June 1998 to Aug 1998, 3rd Quarter	H	Q			
LB990630123142.002 [158355]	Passive Monitoring Data (Relative Humidity, Pressure, Temperature): September 1998 to May 1999	H	Q			
LB000121123142.001 [158335]	Passive Monitoring Data (Relative Humidity, Pressure, Temperature): June 1 through October 31, 1999	H	Q			

Table 4-3. Input-DTNs for the Drift Scale Test[1] (continued)

Input-DTN [DIRS]	Description	Type[2]	Q Status	Report Location		
				Text	Figures	Tables
LB000718123142.001 [158340]	Passive Monitoring Data Collected from 12 Hydrology Boreholes Test: November 1, 1999 to May 31, 2000	H	Q	6.3.2.4	6.3.2.4-7	
LB0101H2ODST01.001 [158347]	Passive Monitoring Data Collected from 12 Hydrology Boreholes: June 1, 2000 to November 30, 2000	H	Q			
LB0108H2ODST05.001 [158441]	Passive Monitoring Data Collected from 12 Hydrology Boreholes: Dec. 1, 2000 to May 31, 2001	H	Q			
LB0203H2ODSTEH.001 [158351]	Passive Monitoring Data Collected from 12 Hydrology Boreholes: June 1, 2001 through end of Heating Phase Jan. 14, 2002	H	Q			
LB980912332245.002 [105593]	Gas Tracer Test and Estimated Porosity	H	Q	6.3.2.4		6.3.2.4-5 6.3.2.4-6
LB970500123142.003 [131500]	Laboratory Saturation, Porosity, Bulk Density, Particle Density, Gravimetric Water Content Data from Dry Drilled and wet drilled Cores in the DST and SHT	H	Q	6.3.2.5		6.3.2.5-1 6.3.2.5-2
LL020502523142.020 [159105]	Laboratory Measured Electrical Properties of the DST Samples as a Function of Saturation at 95ºC	H	Q	6.3.2.5		
LL981109904242.072 [118959]	Saturated and Dry Bulk Density Permitivity	H	Q	6.3.2.5	6.3.2.5-1 6.3.2.5-2	6.3.2.5-3
SNF39012298002.002 [159114]	Measurements of Displacement Data for the Drift Scale Test (with results from 11/1/1997 through 5/31/1998)	M	Q	6.3.3.1 6.3.3.2	5.2-1 5.2-3 5.2-4 6.3.3.1-2 6.3.3.1-3 6.3.3.1-4 6.3.3.1-5 6.3.3.1-6	
SNF39012298002.006 [158419]	MPBX and CDEX Displacement June 1998 – August 1998	M	Q			
SNF39012298002.010 [158367]	MPBX and CDEX Displacement September 1998 – May 1999	M	Q			
SN0001F3912298.014 [153841]	MPBX and CDEX Displacement June 1999 – October 1999	M	Q			
SN0007F3912298.018 [158374]	MPBX and CDEX Displacement November 1999 – May 2000	M	Q			
SN0101F3912298.024 [158400]	MPBX and CDEX Displacement June 2000 – November 2000	M	Q			
SN0107F3912298.029 [158408]	MPBX and CDEX Displacement December 2000 – May 2001	M	Q			
SN0203F3912298.033 [158361]	MPBX and CDEX Displacement June 2001 – January 14, 2002	M	Q			

Table 4-3. Input-DTNs for the Drift Scale Test[1] (continued)

Input-DTN [DIRS]	Description	Type[2]	Q Status	Report Location		
				Text	Figures	Tables
SNF39012298002.004 [153837]	MPBX and CDEX Displacement Corrected for Thermal Expansion November 9 1997 – May 1998	M	Q	6.3.3.1 6.3.3.2	5.2-1 5.2-3 5.2-4 6.3.3.1-2 6.3.3.1-3 6.3.3.1-4 6.3.3.1-5 6.3.3.1-6	6.3.3.6-5
SNF39012298002.008 [153839]	MPBX and CDEX Displacement Corrected for Thermal Expansion June 1998 – August 1998	M	Q			
SNF39012298002.012 [153840]	MPBX and CDEX Displacement Corrected for Thermal Expansion September 1998 – May 1999	M	Q			
SN0001F3912298.016 [153842]	MPBX and CDEX Displacement Corrected for Thermal Expansion June 1999 – October 1999	M	Q			
SN0007F3912298.020 [158388]	MPBX and CDEX Displacement Corrected for Thermal Expansion November 1999 – May 2000	M	Q			
SN0101F3912298.026 [158402]	MPBX and CDEX Displacement Corrected for Thermal Expansion June 2000 – November 2000	M	Q			
SN0107F3912298.031 [158413]	MPBX and CDEX Displacement Corrected for Thermal Expansion December 2000 – May 2001	M	Q			
SN0203F3912298.035 [158363]	MPBX and CDEX Displacement Corrected for Thermal Expansion June 2001 – January 14, 2002	M	Q			
SNF38040197001.001 [159130]	Strain-gage and Anchor Locations	M	Q	6.3.3.3	6.3.3.3-1	
SNF39012298002.003 [158417]	Ground Support System Strain: November 9, 1997 – May 1998	M	Q	6.3.3.3	6.3.3.3-2	
SNF39012298002.007 [158365]	Ground Support System Strain: June 1998 – August 1998	M	Q			
SNF39012298002.011 [158368]	Ground Support System Strain: September 1998 – May 1999	M	Q			
SN0001F3912298.015 [158372]	Ground Support System Strain: June 1999 – October 1999	M	Q			
SN0007F3912298.019 [158387]	Ground Support System Strain: November 1999 – May 2000	M	Q			
SN0101F3912298.025 [158401]	Ground Support System Strain: June 2000 – November 2000	M	Q			
SN0107F3912298.030 [158409]	Ground Support System Strain: December 2000 – May 2001	M	Q			
SN0203F3912298.034 [158362]	Ground Support System Strain: June 2001 – January 14, 2002	M	Q			
SNF39012298002.005 [158418]	Ground Support System Strain Corrected for Thermal Expansion: November 9, 1997 – May 1998	M	Q			
SNF39012298002.009 [158366]	Ground Support System Strain Corrected for Thermal Expansion: June 1998 – August 1998	M	Q			

Table 4-3. Input-DTNs for the Drift Scale Test[1] (continued)

Input-DTN [DIRS]	Description	Type[2]	Q Status	Report Location		
				Text	Figures	Tables
SNF39012298002.013 [158369]	Ground Support System Strain Corrected for Thermal Expansion: September 1998 – May 1999	M	Q	6.3.3.3	6.3.3.3-2	
SN0001F3912298.017 [158373]	Ground Support System Strain Corrected for Thermal Expansion: June 1999 – October 1999	M	Q			
SN0007F3912298.021 [158391]	Ground Support System Strain Corrected for Thermal Expansion: November 1999 – May 2000	M	Q			
SN0101F3912298.027 [158407]	Ground Support System Strain Corrected for Thermal Expansion: June 2000 – November 2000	M	Q			
SN0107F3912298.032 [158414]	Ground Support System Strain Corrected for Thermal Expansion: December 2000 – May 2001	M	Q			
SN0203F3912298.036 [158364]	Ground Support System Strain Corrected for Thermal Expansion: June 2001 – January 14, 2002	M	Q			
LB980120123142.007 [158352]	Acoustic Emissions: Baseline and Heating	M	Q	6.3.3.4	6.3.3.4-1 6.3.3.4-2	
LB980420123142.004 [113717]	Acoustic Emissions: Baseline and Heating	M	Q			
LB990630123142.004 [158360]	Acoustic Emissions: Baseline and Heating	M	Q			
LB000121123142.005 [158339]	Acoustic Emissions: Baseline and Heating	M	Q			
LB000718123142.005 [158343]	Acoustic Emissions: Baseline and Heating	M	Q			
LB0101ACEMDST1.001 [158344]	Acoustic Emissions: Baseline and Heating	M	Q			
LB0108ACEMDST5.001 [158437]	Acoustic Emissions: Baseline and Heating	M	Q			
SNL23030598001.003 [158422]	Creep Testing of Concrete Liner	M	Q	6.3.3.5	6.3.3.5-1	
SN020312210196.007 [158322]	Laboratory Thermal Expansion	M	Q	6.3.3.5		6.3.3.5-1 6.3.3.5-2
SNL02100196001.001 [158420]	Elastic Constants and Strength Properties	M	Q	6.3.3.5		6.3.3.5-3
SNL23030598001.001 [158370]	Elastic Constants and Strength of Concrete	M	Q	6.3.3.5		6.3.3.5-4 6.3.3.5-5
SN0011F3912298.022 [158392]	Rock Mass Displacement Pressure Data Plate Load Test October 16-17 2000	M	Q	6.3.3.6		6.3.3.6-1
SN0011F3912298.023 [158399]	Rock Mass Displacement Pressure Data in Modulus October 16-17 2000	M	Q	6.3.3.6		6.3.3.6-2

Table 4-3. Input-DTNs for the Drift Scale Test[1] (continued)

Input-DTN [DIRS]	Description	Type[2]	Q Status	Report Location		
				Text	Figures	Tables
GS970608314224.007 [158430]	Rock Mass Rating and Rock Mass Quality	M	Q	6.3.3.6		6.3.3.6-2 6.3.3.6-3 6.3.3.6-4
SNF32020196001.010 [158314]	Rock Mass Quality	M	Q			
SNF32020196001.015 [158434]	Rock Mass Quality	M	Q			
MO0207AL5WATER.001 [159300]	Water Sampling in Alcove 5 (Results from 2/4/1997 through 4/20/1999).	C	Q	6.3.4.1		6.3.4.1-1
MO0101SEPFDDST.000 [153711]	Field Measured Data of Water Samples from the Drift Scale Test	C	Q			
SN0203F3903102.001 [159133]	Drift Scale Test Water Sampling (with Results from 4/17/2001 through 1/14/2002)	C	Q			
MO0005PORWATER.000 [150930]	Perm-Sample Pore Water Data	C	Q	6.3.4.1		6.3.4.1-2
LL001100931031.008 [153288]	Aqueous Chemistry of Water Sampled from Boreholes of the Drift Scale Test (DST)	C	Q			
LL001200231031.009 [153616]	Aqueous Chemistry of Water Sampled from Boreholes of the Drift Scale Test (DST)	C	Non-Q[3]			
LL020302223142.015 [159134]	Aqueous Geochemistry of DST Samples Collected from HYD Boreholes.	C	Q			
LL020405123142.019 [159307]	Aqueous Geochemistry of Condensed Fluids Collected During Studies of Introduced Materials	C	Q			
LB980420123142.005 [111471]	Isotope Data for CO_2 from Gas Samples Collected from DST: February 1998	C	Q	6.3.4.2		6.3.4.2-1 6.3.4.2-3
LB980715123142.003 [111472]	Isotope Data for CO_2 from Gas Samples Collected from DST: June 4, 1998	C	Q	6.3.4.2		6.3.4.2-1 6.3.4.2-3
LB981016123142.004 [113278]	Isotope Data for CO_2 from Gas and Water Samples: June 1998 to September 1998	C	Q			
LB990630123142.003 [111476]	Isotope Data for CO_2 from Gas and Water Samples: September 1998 to May 1999.	C	Q			
LB000121123142.003 [146451]	Isotope Data for CO_2 Gas Samples Collected from the Hydrology Boreholes: August 9, 1999 Through November 30, 1999	C	Q			
LB000718123142.003 [158342]	Isotope Data for CO_2 Gas Samples Collected from the Hydrology Boreholes: April 18, 2000 Through April 19, 2000.	C	Q			

Table 4-3. Input-DTNs for the Drift Scale Test[1] (continued)

Input-DTN [DIRS]	Description	Type[2]	Q Status	Report Location		
				Text	Figures	Tables
LB0102CO2DST98.001 [159306]	Concentration and Isotope Data for CO_2 and H_20 from Gas Samples Collected from Hydrology Boreholes: May and August 1999, April 2000, January and April 2001	C	Q	6.3.4.2	6.3.4.2-1	6.3.4.2-1 6.3.4.2-2 6.3.4.2-3
LB0108CO2DST05.001 [156888]	Concentration and Isotope Data for CO_2 and H_20 from Gas Samples Collected from Hydrology Boreholes: May and August 1999, April 2000, January and April 2001	C	Q			
LB0203CO2DSTEH.001 [158349]	Concentration/Isotope Data for CO_2/H_20 from Gas Samples Collected from Hydrology Boreholes up to End of Heating	C	Q	6.3.4.2		6.3.4.2-1 6.3.4.2-3
LB0206C14DSTEH.001 [159303]	Carbon 14 Isotope Data from CO_2 Gas Samples Collected from DST	C	Q			
LA9912SL831151.002 [146449]	Percent Coverage By Fracture-Coating Minerals in Core ESF-HD-TEMP-2	C	Q	6.3.4.3		6.3.4.3-1
LA0201SL831225.001 [158426]	Chemical, Textural, and Mineralogical Characteristics of Sidewall Samples from the Drift Scale Test.	C	Q	6.3.4.3		
LA0009SL831151.001 [153485]	Fracture Mineralogy of the ESF Single Heater Test Block, Alcove 5	C	Q			
LA0201SL831225.001 [158426]	Chemical, Textural, and Mineralogical Characteristics of Sidewall Samples from the Drift Scale Test.	C	Q			
GS011108312322.008 [159136]	Uranium Concentrations and 234u/238u Activity Ratios Analyzed Between February 1, 1999 and August 1, 2001 for Drift-Scale Heater Test Water Collected Between June 1998 and April 2001, and Pore Water Collected Between March 1996 and April 1999.	C	Q	6.3.4.4	6.3.4.4-1 6.3.4.4-2	
GS011108312322.009 [159137]	Strontium Isotope Ratios and Strontium Concentrations in Water Samples from the Drift Scale Test Analyzed from March 16, 1999 to June 27, 2001.	C	Q	6.3.4.4	6.3.4.4-3	
SN0203F3903102.001 [159133]	Drift Scale Test Water Sampling (With Results from 4/17/2001 Through 1/14/2002)	C	Q	6.3.4.5		6.3.4.5-1
LL020405123142.019 [159307]	Aqueous Geochemistry of Condensed Fluids Collected During Studies of Introduced Materials.	C	Q			

Table 4-3. Input-DTNs for the Drift Scale Test[1] (continued)

Input-DTN [DIRS]	Description	Type[2]	Q Status	Report Location		
				Text	Figures	Tables
LARO831422AQ97.002 [158431]	DST Borehole Video Logging	G	Q	6.3.5.2		

NOTE: [1] DTNs LA9908FH6001WP.001 [158319], LA0111FH831151.002 [158317], LA0208FH831151.001 [159515], and LA0208FH831151.002 [159308] provide access via Records Processing Center (RPC) to all thermal and mechanical data collected in DST Data Collection System (original/electrical and converted/engineering units). These non-qualified DTNs also provides access (RPC) to pertinent supporting material such as scientific notebooks and calibration relationships.

[2] T=Thermal, H=Hydrological, M=Mechanical, C=Chemical, G=General/Miscellaneous

[3] This data set is classified as non-Q due to the disposition of a Deficiency Report. Hence, these data should only be used for corroborative purposes.

5. ASSUMPTIONS

As per Attachment 3-Item 5 of AP-SIII.9Q, assumptions apply to those activities associated with the scientific analyses of the Scientific Analysis Report. The scientific analyses for this report involve mainly restructuring, as needed, Input-DTNs (that presently reside on the TDMS) into more user-friendly Output-DTNs. These transformations of Input-DTNs to Output-DTNs in most instances consisted of straightforward reorganizing, reformatting, and/or graphic representation that did not invoke significant assumptions. But for a few groups of measurements, more extensive data reduction was needed to achieve the objective of converting the content of the Input-DTNs into Output-DTNs in a format that is more useful to the end-users. For these measurements, assumptions associated with the data reduction are discussed below.

Discussions of the bases for the assumptions in this Scientific Analysis Report are grouped into two categories (Sections 5.1 and 5.2) in which each assumption is essentially identical and can be stated as follows: "It is assumed that the significant reduction of measurements from the appropriate Input-DTNs to the Output-DTNs has been properly conducted."

5.1 AIR-PERMEABILITY ANALYSIS

Assumption: The development of air permeabilities (Output-DTN) from air-injection flow rates and pressure responses (Input DTNs) assumes air behaves as an ideal gas; a finite line source can represent a borehole injection interval; air flows are mainly through fractures; and air flows are governed by Darcy's law.

Basis: The following discussion pertains to measurements described in Sections 6.2.2.4 and 6.3.2.4. Based on the detailed discussion below, further confirmation of this assumption is not required.

During air-injection testing, local permeability is estimated from the steady-state pressure response to a constant-flux gas injection. An analytical solution for the steady-state pressure response of a constant flow-rate injection in a finite line source is applied to estimate gas permeability near the wellbore. The solution was adapted from the steady-state analytical solution for ellipsoidal flow of incompressible fluid from a finite line source (Hvorslev 1951 [101868]) in an infinite medium ($L/r_W >> 1$) and is as follows:

$$k = \frac{P_{SC} Q_{SC} \mu \ln\left(\frac{L}{r}\right) T_f}{\pi L (P_2^2 - P_1^2) T_{SC}} \qquad \text{(Eq. 5.1-1)}$$

where:

- k = permeability (m^2)
- P_{SC} = pressure at standard conditions(1.013×10^5 Pa)
- Q_{SC} = flowrate at standard conditions(m^3/s)
- μ = dynamic viscosity of air (1.81×10^{-5} Pa · s at 20°C)

L = length of air injection zone (m)
r_w = radius of borehole (m)
T_f = temperature of formation (^{o}K)
P_2 = steady state pressure (Pa)
P_1 = ambient pressure (Pa)
T_{SC} = temperature at standard conditions (293.16° K)

Equation 5.1-1 is discussed in Section 8.1.1.1 of the *Single Heater Test Final Report* (CRWMS M&O 1999 [129261]). It assumes a finite length and finite radius cylindrical injection source, surrounded by a homogeneous medium of infinite extent. Gas is assumed to be ideally compressible. Alternative conceptualizations of the flow field geometry are possible and yield estimates of permeability that may vary by a factor of two or three from the above solution.

For Equation 5.1-1 to be valid in a fractured media, fractures must be dense and form an effective continuum at the scale at which the test is performed. This assumes that the fractures play the role of interconnected pores in a porous media and do not act as discrete features. In cases where the assumptions of an effective continuum are not valid, Equation 5.1-1 still yields a useful quantitative value that reflects the rock-mass gas injectivity. Here injectivity is defined as a measure of the formation's ability to permit gas flow. Changes in permeability (or formation injectivity) during heating and cooling are indicative of changes in fracture liquid saturation, or opening and closing of fractures from THM coupling. As fracture saturation increases or fractures close, gas injectivity decreases. Similarly a decrease in fracture liquid saturation or fracture opening will lead to an increase in gas injectivity. For both the SHT and DST, changes in permeability will be reported as a ratio of measured permeability to the baseline value, established prior to the start of heating.

The user of the permeability estimates should understand the limitations of a continuum model in interpreting measurements performed in a heterogeneous formation, such as the Topopah Spring middle nonlithophysal tuff. An example of model limitations is a block of rock that contains only a single transmissive feature. An injection test can be performed with a straddle packer that spans length L of formation that includes this single transmissive feature, leading to an estimate of permeability, k. If a shorter injection interval is tested, for example $L/10$, where this same single transmissive feature is straddled, the estimate for the formation permeability will yield a value of $k*\ln(10)$. In a case such as this, it is erroneous to assume that Equation 5.2-1 will provide an accurate estimate of formation permeability. However, by repeatedly performing measurements using the same testing configuration, changes in permeability can be tracked as thermal testing proceeds. For both the SHT and the DST, the air-permeability test intervals were kept fixed between quarterly air-injection tests, excluding the DST zones that varied as a result of pneumatic-packer failures.

5.2 MULTI-POINT BOREHOLE EXTENSOMETER (MPBX) DISPLACEMENTS AND STRAIN ANALYSIS

Assumption: It is assumed that noisy/erratic data can be eliminated on the basis of "smoothing."

Basis: The following discussion pertains to measurements described in Section 6.3.3.1. Based on the detailed discussion below, further confirmation of this assumption is not required.

The MPBX and strain data are meant to provide a measure of rock deformation caused by thermal expansion and mechanical stresses in the rock surrounding the Heated Drift. The MPBX and strain data were expected to have a "smooth" appearance, with any discontinuities likely relating to sudden movements along fractures. However, many of the data traces exhibit "noise" which makes the data difficult to read and interpret.

In general, there are two types of noise that have been identified in the MPBX data. One type is identified by either a wildly oscillating mean value with no discernable pattern, or by values that go outside the expected range of displacement values. These data values are understood to be "bad data", where the gage is experiencing either temporary or permanent incorrect readings. The second type is identified by data that has a discernable pattern (typically, the pattern would follow a curve fit to the top "edge" of the data on a displacement-versus-time curve), and the data oscillates at values below the predominant curve. A closer examination of the individual MPBXs revealed the following generalizations:

- Displacement and temperature data in boreholes collared in the crown (MPBXs 3-5, 7-9, 11-13) had substantial oscillations with this pattern.

- Temperature data in boreholes collared in invert (MPBXs 6, 10, 14) had almost no unusual oscillations.

This examination of the MPBX data noted a peculiar unidirectional nature to the oscillations in the temperature data: when the mean temperature was below the boiling point (96°C), the oscillations were upward to a ceiling of 96°C; similarly, for mean temperatures above 96°C, the oscillations were downward to a floor of 96°C. Furthermore, it was noted that these oscillations were occurring in the MPBXs collared in the crown (3-5, 7-9, 11-13), and not in those collared in the invert (6, 10, 14).

Apparently, the oscillations in the displacement data are being affected by temperature oscillations in the MPBX borehole, caused by water recirculation within the borehole. Water vapor enters the borehole above the boiling isotherm. (This is possible, even though the MPBX boreholes were sealed with an aluminum liner coated with Teflon, because of gaps in the liner for anchor placement.) The thermocouples (TCs) at locations far above the collar experience water condensation, which raises temperatures toward the ceiling at 96°C. The liquid water then falls down the borehole; there are sufficient gaps around the anchors for liquid water to pass through. Eventually, this water vaporizes in the regions closer to the Heated Drift, causing temperatures there to drop to the 96°C floor. The recirculating water, which alternately boils, rises, condenses, and falls in a cyclic fashion in the borehole, causes the Invar connecting rods to shrink/expand, resulting in real changes in voltages in the linear variable displacement transducers (LVDTs), which correspond to the temperature extremes.

The changing temperatures at the MPBX head also affect the calibration constants of the LVDTs based on the temperature at the collar. It is thought that the surrounding rock mass is negligibly affected by these temperature oscillations, and thus the oscillating MPBX measurements do not

represent the actual rock behavior. To use the MPBX data to validate thermal-mechanical models, or to use them to derive rock-mass thermal-mechanical properties, the true rock-mass behavior must somehow be extracted from the noisy data. It is this requirement that led the thermal test team to attempt to smooth the MPBX data.

There are several issues that make a scientifically based algorithm for smoothing the MPBX data a complex matter: the contraction/expansion of the Invar rods, the effect of temperature on the LVDT, the need to capture true fracture deformation events, and other causes of unlikely data values. Therefore, to attempt to provide smooth data for use in validating thermal-mechanical models, a simplified approach using technical judgment was used. Under this approach, the acquired MPBX measurements from the LVDTs, as calculated by the Data Collection System, were corrected for the thermal expansion of the Invar connecting rods in essentially the same manner as the developed MPBX data that are regularly submitted to the TDMS. The acquired MPBX and temperature data, and the corrected MPBX data, were listed in an Excel spreadsheet, one for each MPBX. Then, several steps were taken to smooth the data. First, based on the technical judgment of the analyst, sections of data that were considered unusable were deleted. Typically, these data were either the results of a problem with the gage itself: failure, erratic voltage readings, etc. Then, other sections of noisy data were identified using a 0.3 mm difference between values at six-hour intervals. If the behavior of the identified data matched the assumed behavior caused by the recirculating water, then that range of values was discarded. Figures 5.2-1–5.2-4 show the following steps in this process for MPBX9: original thermally corrected displacement data, temperature data, and smoothed data using this method.

While discarding data, it was important to retain information that may represent other physical processes, such as a sudden permanent shift that may indicate fracture slippage or closure. This procedure is somewhat subjective, but it does allow for a reduction of the MPBX data to a reasonable and functional format.

This procedure for smoothing the MPBX data was used for MPBX data through 7/31/2000 (i.e., through 971 days of heating). For this report, an additional step was taken—the maximum (or minimum, where applicable) value for consecutive ten-day windows was taken from the data, to provide a user-friendly format for modeling purposes. Figure 5.2-4 shows the final smooth data for MPBX9; this format will be used for the rest of this report. The Output-DTN for all smoothed DST MPBX data for the heating phase of the DST is provided in Table 6.3-1.

The strain data (measured on the surface of the cast-in-place concrete liner) was also smoothed but in a less complex manner than applied to the MPBX displacements. The noisy/erratic strain data was usually smoothed by retaining the maximum value, but, in some cases, the minimum value was selected. The Output-DTN for all smoothed DST strain data for the DST heating phase is provided in Table 6.3-1.

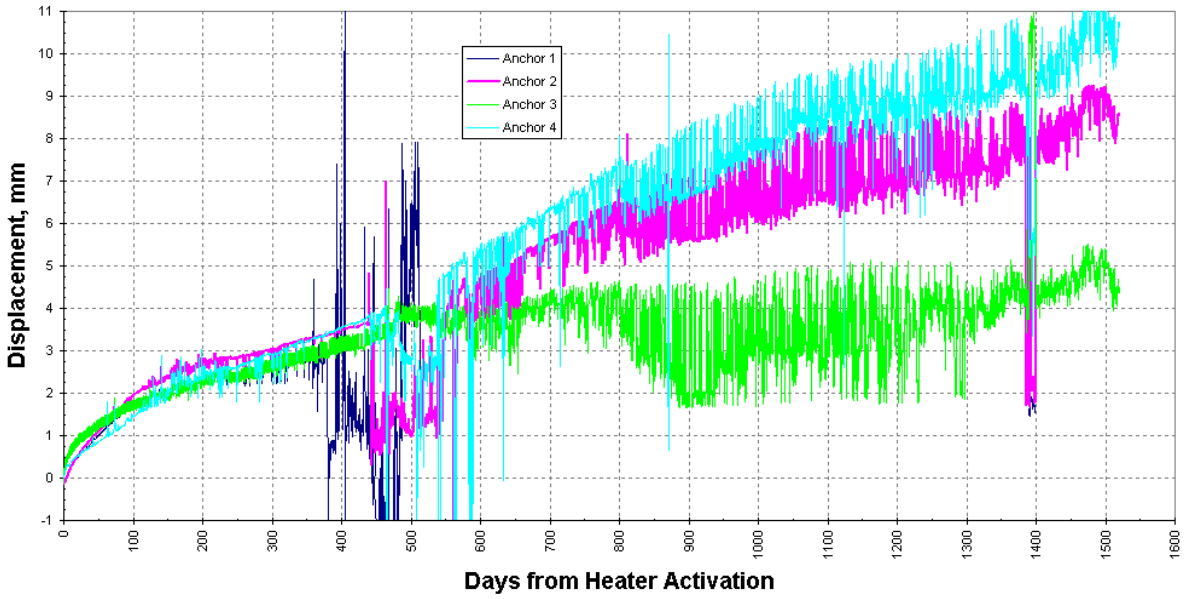

Figure 5.2-1. Original Thermally-Corrected Displacement Data for DST Borehole 156 (MPBX9)

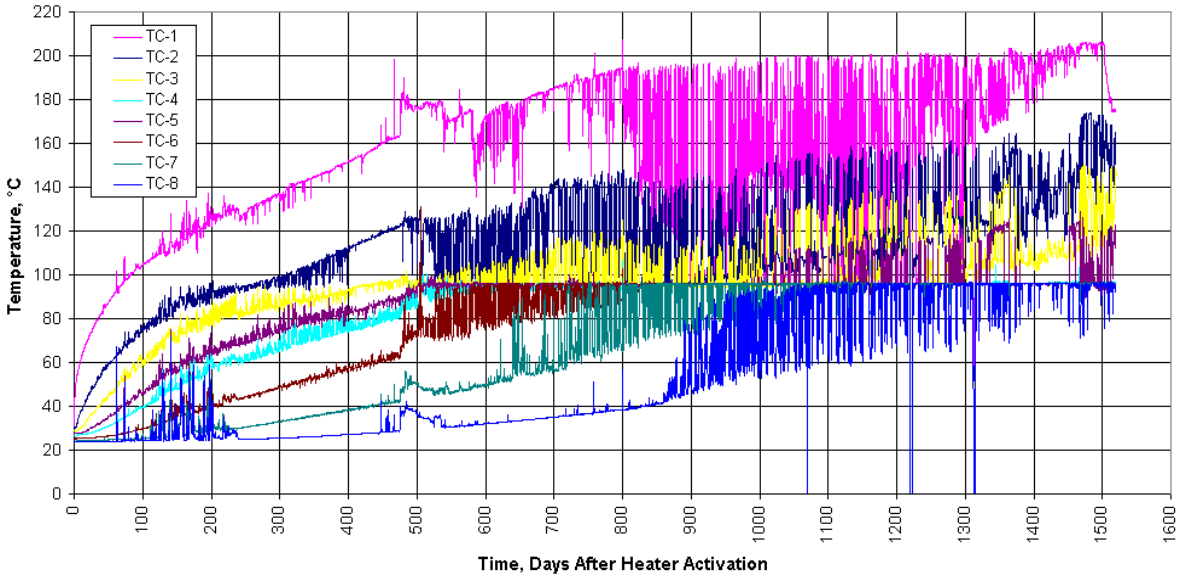

Figure 5.2-2. Temperature Data for DST Borehole 156 (MPBX9)

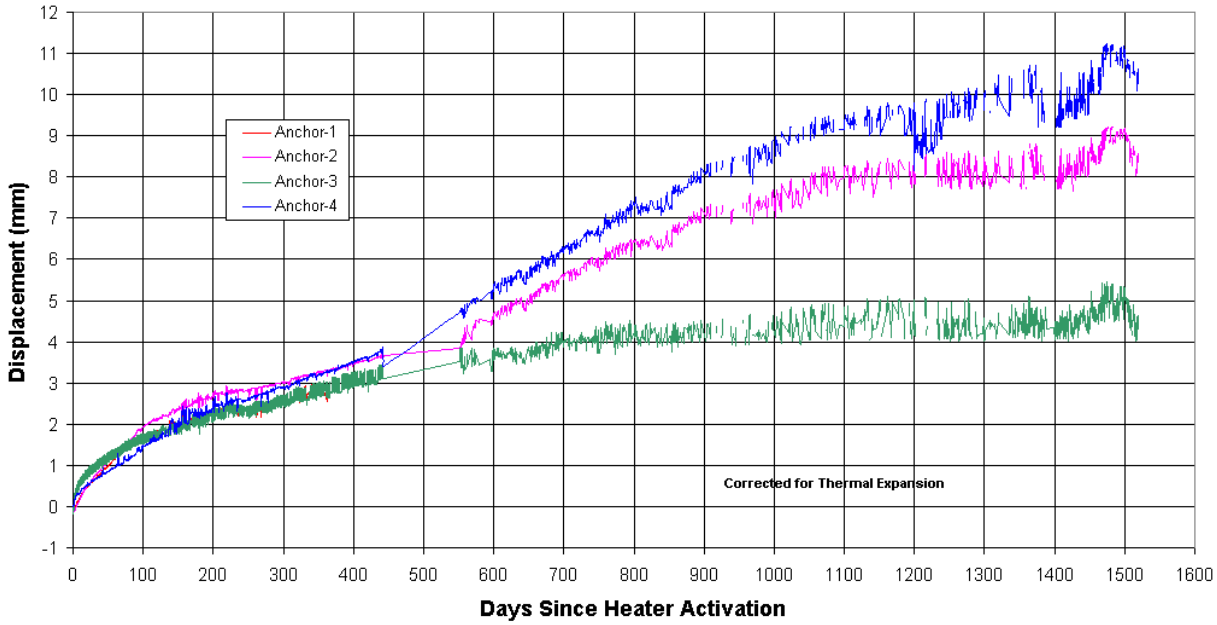

Figure 5.2-3. Intermediate Smoothed Displacement Data for DST Borehole 156 (MPBX9)

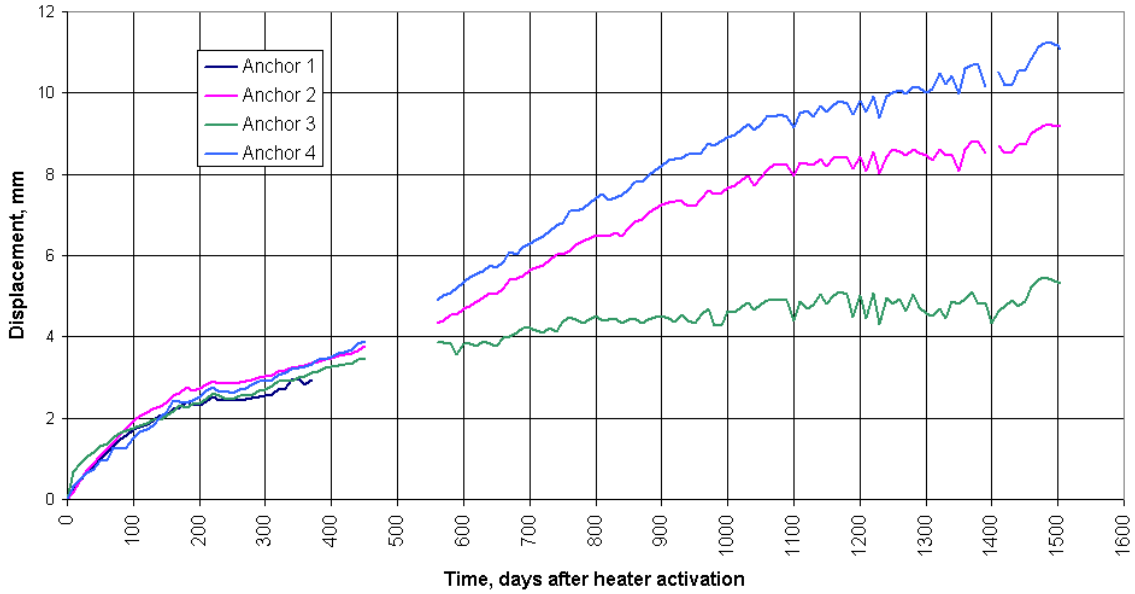

Figure 5.2-4. Final Smoothed Displacement Data for DST Borehole 156 (MPBX9)

6. DISCUSSION OF MEASUREMENTS

Scientific analysis is defined in Section 3.13 of AP-SIII.9Q as a study that investigates scientific phenomena or parameters. The scientific phenomena investigated are the thermal-hydrological-mechanical-chemical behavior measured in each of the three thermal tests (LBT, SHT, and DST). Parameters in this report reflect laboratory and field measurements that characterized the respective test blocks for each of the three thermal tests. As discussed in Section 1, data collected within the YMP Thermal Testing Program must be readily usable to end users such as those representing the Performance Assessment Project, Repository Design Project, and Engineered System Sub-Project. Since either detailed level 3 and level 4 reports exist or the measurements are straightforward, only brief discussions are provided for each data set. These brief discussions for different data sets are intended to impart a clear sense of applicability of data, so that end users will be able to use and interpret these data properly within the context of measurement uncertainty. This approach also keeps the report to a manageable size, an important consideration since it encompasses nearly all measurements for three long-term thermal tests. As appropriate, thermal testing data currently residing in the TDMS have been reorganized and reformatted from cumbersome, often not user-friendly Input-DTNs into a new set of Output-DTNs. These Output-DTNs provide data structure including graphical displays and comprehensive spreadsheets. In some cases, there was no need to reformat or restructure Input-DTNs so they remained unchanged.

Discussion of the thermal testing measurements in this report is organized first under the heading of the three tests: LBT, SHT, and DST; and then under the four processes: thermal (T), hydrological (H), mechanical (M), and chemical (C). Miscellaneous measurements and observations are also discussed. Although the list of measurement types is comprehensive, it is neither practical (because of finite report length) nor necessary to thoroughly discuss all data sets. For example, the DST-measured temperatures come from nearly 2,700 thermal sensors distributed throughout the test block and collected on an hourly basis, resulting in approximately 100 million measurements. Therefore, as appropriate for each measurement type, only a representative discussion of the test data behavior is presented. Readers are referred to user-friendly Output-DTNs for comprehensive data sets that include complementary graphics.

The following discussions concerning the 12 basic measurement groups (three thermal tests and four processes) are dictated by their respective data characteristics. In general, discussions of thermal and mechanical measurements tend to be comparatively short, although the respective Output-DTNs contain comparatively large amounts of data. This condition reflects the inherent straightforwardness of temperature and displacement measurements that are recorded frequently (hourly) on a data acquisition system. Conversely, discussions of hydrological and chemical measurements tend to be lengthier, while their Output-DTNs are comparatively small. The smaller output data sets result from measurements collected comparatively infrequently (monthly or longer) on a nonintegrated data acquisition system. The more lengthy discussion in the chemical measurements sections relate to sampling procedures that have much relevance to the data collected. Also, in certain hydrological measurements, detailed explanations are needed for the complex reduction that occurs as the data are transformed from Input-DTNs to more useful and functional Output-DTNs.

In addition, uncertainty associated with most measurements is discussed. These discussions of uncertainty are restricted to actual measurements and data reduction. If quantifiable uncertainties were cited, then either references to manufacturer's specifications were provided or they were referred to as "estimates." Standard error analyses (mean and standard deviation) were provided for applicable measurements such as repetitive measurements of laboratory or field parameters. Test measurements of a response for a specific location and time are not applicable for standard error analyses. Additional information on measurement uncertainties can be located via directions in DTNs cited in the first footnote of Tables 4-1, 4-2, and 4-3. This information, among other things, provides detailed discussions of scientific notebooks and calibration relationships relevant to uncertainties of thermal testing measurements. The approach taken provides sufficient discussion of uncertainties for end-users of thermal testing measurements such as process modelers. In cases where uncertainty is redundant among two or all three thermal tests, the initial discussion of uncertainty is referenced. Uncertainty related to modeling and analyses between measured and simulated data will be discussed in Model Reports related to TH, THC, and THM process models. Also included in this report are summaries of three white papers involving in-depth investigations of unexpected or unusual DST behavior not uncommon in large-scale, long-term field testing. They are found in Sections 6.3.2.6, 6.3.3.7, and 6.3.4.5.

6.1 LARGE BLOCK TEST (LBT)

The LBT is a controlled test to provide data for a better understanding of the coupled thermal-hydrologic-mechanical-chemical processes in a heated unsaturated rock mass. The LBT was conducted at the outcrop of the middle nonlithophysal unit of the Topopah Spring tuff (Tptpmn) at Fran Ridge, Nevada. A $3 \times 3 \times 4.5$ m high column of the rock mass was isolated from the outcrop at the eastern slope of Fran Ridge (See Figure 6.1-1). The base of the column is still connected to the ground. The block was heated from February 28, 1997, to March 10, 1998. A natural cooling phase started on March 10, 1998, until the termination of the data acquisition on September 30, 1998.

Tables 4-1 and 6.1-1 provide a listing of LBT Input-DTNs and Output-DTNs, respectively. The Output-DTNs provide either test measurements or parameter values and related graphics and coordinates of the sensors used in the test measurements. Table 4-1 also provides the Q-status of the measurements, as well as the text, figures, and tables in this report where Input-DTNs are cited.

For ease of thermal modeling, a one-dimensional thermal field (having thermal gradient dependent only on the z direction) within the block was created by line heaters used to simulate a planar heat source located at a height of approximately one-third of the total height of the block (1.75 m from the base of the block). A heat exchanger system was used to maintain a constant temperature, about 60°C, on the top surface of the block. This system consisted of an aluminum plate fitted with heating/cooling coils mounted on the top of the block. This plate was connected to a heat exchanger to allow thermal control of the top surface.

To achieve a one-dimensional thermal-hydrological process in the z direction, a layer of room-temperature vulcanized (RTV) rubber and Viton were installed on the block sides to minimize moisture flux. Three layers of thermal-insulation materials were installed on the outside of the

moisture barrier. All of the sensor boreholes were sealed by cement grout, packers, or a RTV/ Teflon™ membrane.

Sensors in the block measured heater power, temperature, moisture content, mechanical deformations, thermal conductivity and diffusivity, relative humidity, and gas pressure. Air permeability was measured before the heating and at the end of the heating phase. Figures 6.1-2 to 6.1-5 show the sensor boreholes in the top and sides of the block. There are no sensor boreholes in the south side of the block. The assessment of the chemical process in the block was achieved by comparing the mineralogical changes in the core samples obtained before and after the test. Small blocks of the rock were obtained from the proximity of the large block for conducting laboratory tests to determine hydrologic and mechanical properties. Microbial survivability and migration were also investigated. These measurements and observations will be described in greater detail in the following subsections. Table 6.1-2 shows the XYZ coordinates of the collar and bottom of all of the boreholes in the LBT.

The LBT data collection system (DCS) recorded thermal and mechanical data hourly for the most part. The acquired data consists of both original (measured electronic values) and converted (engineering units). Two packages of data were submitted to the Records Processing Center (RPC) and corresponding DTNs (LA0106FH831151.002 [158230] and LA0106FH831151.003 [158229]) were also obtained. These DCS-DTNs are considered non-qualified because they are stored in the RPC but they do identify compact discs of identical qualified data that are distributed to the Thermal Test Team. These DCS-DTNs also identify scientific notebooks (SNs) that provide details of LBT measurements including calibration information. These DCS-DTNs are reduced and re-structured and periodically submitted to the TDMS resulting in many of the Input-DTNs introduced below and listed in Table 4-1. As discussed in Sections 1 and the introduction to Section 6, these Input-DTNs are further refined, reduced, and restructured before being resubmitted to the TDMS as Output-DTNs (see Table 6.1-1). In summary, the end user has access to three levels of data for LBT thermal, mechanical measurements: DCS-DTNs, Input-DTNs, and Output-DTNs. For most future applications, it is anticipated that end users will access the Output-DTNs because they are more user friendly.

6.1.1 LBT Thermal Measurements

The block was heated by electrical heaters in the five heater boreholes, which formed a horizontal plane 2.74 m below the block top. The heater boreholes are EH1 to EH5 as shown in Figure 6.1-4. The temperature was measured in boreholes within the block as well as on the block surfaces. The temperature boreholes within the block are shown as TT1 and TT2 in Figure 6.1-2, NT1 to NT4 in Figure 6.1-3, and WT1 to WT3 in Figure 6.1-5. *In situ* thermal conductivity [k] and diffusivity [α] were measured by using Rapid Evaluation of K and Alpha (REKA) probes in three boreholes. The REKA boreholes are TR1 in Figure 6.1-2 and WR1 and WR2 in Figure 6.1-5. The following sections will present the heater power, temperature, and thermal conductivity and diffusivity of the block.

A detailed discussion of the LBT thermal measurements is provided in Section 5 of the *Large Block Test Final Report* (Lin et al. 2001 [159069]). Input-DTNs and Output-DTNs for thermal measurements are provided in Tables 4-1 and 6.1-1, respectively.

6.1.1.1 Heater Power

6.1.1.1.1 Results: Heater Power

The heater in each of the five heater boreholes (EH1 to EH5 as in Figure 6.1-4) was energized to 450 W on February 28, 1997. The power output of one of those heaters as a function of time is shown in Figure 6.1.1.1-1, as an example. The power output of the other heaters was similar to this one. Spikes in this figure were due to short-duration power outages, which did not affect the test significantly. The data gaps at 133 to 136 days and at 280 to 283 days were caused by malfunction of the data acquisition unit. The power was maintained approximately constant, at about 450 W, until about Day 222, when the power was reduced to reach a near steady-state temperature in the block. The temperature at TT1-14 was maintained fairly constant at about 135°C (see Figure 6.1.1.2-1) for the remainder of the test. Toward the end of the test, the power had to be increased back to nearly 450 W to maintain the 135°C temperature in the test block. This was probably caused by a cooler ambient temperature at that time. The heater power data are in the Technical Data Management System (TDMS) under DTN: LL980918904244.074 [135872].

6.1.1.1.2 Measurement Uncertainty: Heater Power

The accuracy of the watt transducers used in measuring the heater power is conservatively estimated to be less than 2% at 500 W full span. This degree of uncertainty is considered typical. The uncertainty is less than the power fluctuations associated with routine oscillations of power supply from the local utility as shown in Figure 6.1.1.1-1.

6.1.1.2 Temperatures

The temperature measurements included the spatial and temporal variation of the temperature in the block and the thermal gradient on the block surfaces. Resistance temperature devices (RTDs) were used to measure temperatures in the block and on the block surface. Within the block, temperature was measured in nine RTD boreholes and five heater boreholes: TT1 and TT2, NT1 to NT4, EH1 to EH5, and WT1 to WT3, as shown in Figures 6.1-2 to 6.1-5, respectively. The RTD boreholes were instrumented with RTDs at 20 cm spacing. This was accomplished by grouting a bundle of RTDs with cement in each of the temperature boreholes. The RTD numbering always started from the bottom of a borehole. For example, TT1-1 is the RTD at the bottom of the vertical RTD borehole TT1, and NT1-14 is the RTD near the collar of the horizontal RTD borehole NT1, which was drilled from the north face of the block to a distance of about 30 cm from the south face of the block. In addition, five RTDs were placed in a thin-walled stainless-steel tube to test the feasibility of their being calibrated or replaced during the test. The stainless-steel tube was grouted along with the RTD bundle in-borehole TT1. Three RTDs were placed in each of the five heater boreholes approximately 0.6, 1.5, and 2.4 m from the collar. The thermal gradient to determine heat flux out of the block across the block surface was measured by a pair of RTDs on both sides of a 1.2 cm thick Ultratemp™ insulation panel. Ultratemp™ panels were mounted in zones on the four vertical faces of the block, on the outside of the Viton sheet. Temperature measurements on the top of the block were performed to verify that the heat exchanger controlled the top temperature at about 60°C during the test.

For the discussion of the temperatures within the block during the test, only the temperature measured in the grouted boreholes will be used. The entire set of the temperature data is available in the TDMS under the DTN: LL980918904244.074 [135872].

6.1.1.2.1 Results: Temperatures

The spatial distribution of the temperature in the LBT shows that the block was heated nearly unidirectionally in the z direction. The temperature in the two vertical RTD boreholes will be used to illustrate the temperature history in the block during the test. Figures 6.1.1.2-1 and 6.1.1.2-2 show the temperature history at RTDs TT1-14 and TT2-14, respectively. TT1-14 and TT2-14 are at 5 and 10 cm below the heater plane, respectively. The location of boreholes TT1 and TT2 can be found in Figure 6.1-2. The temperatures at TT1-14 are about 10°C greater than those at TT2-14, mainly because TT1-14 is about 5 cm closer to the heater plane than TT2-14. All of the sharp drops in temperature that occurred before 100 days since heating are related to power outages. TT1-14 represents the highest measured temperature in the rock of the LBT.

As shown in Figure 6.1.1.2-1, the temperature at TT1-14 increased rapidly with time at the early stages of the heating. The temperature increased mainly from heat conduction. Rate of increase for the temperature decreased with time, mainly because of the decrease in thermal gradient at the RTD location as the thermal front expanded with time. When the temperature reached the boiling point of water, which is about 96°C at the elevation of Fran Ridge, the rate of temperature increase was significantly decreased. This decrease was caused by consumption of energy in the vaporization of the pore water in the rock. During the 20-day period between Day 30 and Day 50, the temperature at TT1-14 increased from about 96°C to about 98°C. After Day 50, the temperature at TT1-14 increased faster with time, indicating that most of the pore water had vaporized. Then at Day 105 (June 13, 1997) the temperature dropped to near the boiling point of water. This is the onset of the first of the two thermal-hydrological (TH) events. The second TH event occurred at Day 186 (September 2, 1997). The temperature fluctuations in those TH events indicated condensate refluxing. On Day 220 (October 6, 1997), the heater power started to ramp down to keep the TT1-14 temperature at approximately 137°C. The heaters were turned off on March 10, 1998, to start a natural cooling phase. The data acquisition was terminated on September 30, 1998.

Figure 6.1.1.2-2 shows a temperature history at TT2-14 similar to that of TT1-14. The temperature at TT2-14 remained at 97.4°C for about 37 days (Day 75–Day 112). Then the temperature increased to, and remained at, about 99°C for 16 days. Because the temperature at TT2-14 was at the boiling point of water when the first TH event occurred, the temperature at TT2-14 was not affected by that event. The rest of the temperature history at TT2-14 was very similar to that at TT1-14.

6.1.1.2.2 Measurement Uncertainty: Temperatures

The accuracy of the RTD is within 0.3^{o}C (Section 5.1 of Single Heater Test Status Report (CRWMS M&O 1997 [101540])). With consideration of other factors, such as the location of the RTDs, the accuracy of the measured temperature in the LBT is estimated to be within 1.5°C. The RTD bundles were grouted in the boreholes; therefore, some of the RTDs may not have had direct contact with the borehole wall.

Additional uncertainty may be introduced into the heat flux calculation. The heat flux of a region is represented only by the measurement at one point. The thermal conductivity of the Ultratemp™ sheet, which is given by the manufacturer, and the measured thermal gradient were used to calculate the heat flux. No attempt was made to assess the variation of the insulation property and any effect of the field operation on the insulation effectiveness.

6.1.2 LBT Hydrological Measurements

The hydrologic measurements presented in this section include the field-measured moisture content, gas pressure, relative humidity, air permeability; and the laboratory-determined hydrologic parameters. The moisture content in the block was determined by electrical resistance tomography (ERT) and neutron logging. Neutron logging provides accurate determination of the moisture content within about a 10 cm radius distance from a borehole. The ERT provides 2-D distribution of the moisture content on a larger scale with less accuracy. The two methods were used to complement each other. Neutron logging was conducted periodically in 15 neutron boreholes: TN1-TN5 (Figure 6.1-2), NN1-NN6 (Figure 6.1-3), and WN1-WN4 (Figure 6.1-5). ERT electrodes were mounted in the vertical ERT borehole near the center of the block top and on the block sides. ERT was also periodically conducted on the large block periodically. Gas pressure and relative humidity were monitored in the four hydrologic boreholes: TH1 (Figure 6.1-2), NH1 (Figure 6.1-3) and WH1-WH2 (Figure 6.1-5). Air permeability was measured in the hydrologic borehole TH1 before the block was cut, before the heating started, and at the end of the heating phase. Cross-borehole permeability between some of the boreholes was also measured before heating.

Small blocks of the rock were collected in the proximity of the large block for laboratory tests of parameters. These include density, porosity, water permeability, moisture-retention curves, and fracture flow and matrix-imbibition visualization using X-ray radiography.

A detailed discussion of the LBT hydrological measurements is provided in Section 6 of the *Large Block Test Final Report* (Lin et al. 2001 [159069]). Input-DTNs and Output-DTNs for hydrological measurements are provided in Tables 4-1 and 6.1-1, respectively.

6.1.2.1 Electrical Resistance Tomography (ERT)

ERT is a geophysical imaging technique that can be used to map subsurface resistivity (Daily and Owen 1991 [159126]; Lin et al. 2001 [159069], pp. 6-3 and 6-6). The ERT measurements consisted of a series of voltage and current measurements from buried electrodes, using an automated data collection system. The data were then processed to produce ERT tomograms. The images of resistivity change can be used, along with the measured temperature field and what is known of initial conditions in the rock mass, to estimate moisture change during heating. ERT electrodes were placed at approximately 0.3 m spacing in horizontal and vertical grooves on all four sides of the block, as shown in Figures 6.1.2.1-1 and 6.1-4 and along bore ERT (Figure 6.1-2). This arrangement of electrodes allowed imaging of two intersecting perpendicular vertical planes and tow parallel horizontal planes, about 1.25 m above and below the horizontal heater plane.

The ERT tomograms can be found in the TDMS under the DTN: LL980913304244.072 [145385] and LL981001604244.079 [158261]. Some of the resistivity images reconstructed late in the experiment (and the moisture changes inferred from them) are questionable because of the sparse data. As the rock mass dehydrated, the contact impedance between the electrodes and the rock increased dramatically, and data quality declined. Having fewer usable data results in a poorly constrained reconstruction that might look smeared or washed out. This is particularly noticeable in the vertical planes beginning early in 1998. Even though the test lasted until the end of September 1998, only the images up to March 19, 1998, are valid.

6.1.2.1.1 Data Processing

Section 6.1.2.1 of the *Large Block Test Final Report* (Lin et al. 2001 [159069]) provides detailed descriptions of the ERT methodology and data reduction procedures. Some of the important features of the 2-D algorithm used for ERT are briefly described. The algorithm (LaBrecque et al. 1996 [159047]) solves both the forward and inverse problems to find the smoothest resistivity model that fits the field data to a prescribed tolerance. Resistivity values assigned in this way to each pixel in the mesh constitute the ERT tomograms. Although the mesh is of a large region around the electrode arrays, only the region inside the ERT electrode array is used in the calculations of moisture content, because the region outside the array is poorly constrained by the data.

The ratio of the measured electrical resistivity data during the test (both the heating phase and the cooling phase) to that of the pre-heating phase is chosen to represent the changes in the rock's electrical resistivity. This was done pixel by pixel within the image plane. This approach tends to reduce the effects of anomalies that do not satisfy the 2-D assumptions of the resistivity model because the 3-D effects tend to cancel in the ratio, since they are contained in both pre-heating and heating/cooling data.

Resistivity of the rock is influenced by changes in moisture content, porosity, cation exchange capacity, solutes in the pore water, and temperature. Moisture content and temperature effects are expected to be most significant. An increase in temperature or moisture causes a resistivity decrease. However, there may be regions where the increasing temperature and decreasing pore-water resistivity were opposed by the rock mass drying, which increases the resistivity. Our goal in this section is to use the images of resistivity change along with the measured temperature to estimate moisture change during the test. See Section 6.1.2.1.2 of the *Large Block Test Final Report* (Lin et al. 2001 [159069]) for a detailed description of how the changes in moisture content were calculated from the resistivity changes.

Waxman and Thomas (1974 [101736]) describe a model for electrical conduction in partially saturated shaly sands typical of oil reservoirs (intended for oil field data) that accounts for conduction through the bulk pore water as well as conduction through the electrical double layer near the pore surface. This model can predict temperature dependence of the resistivity, but several of the model parameters must be empirically determined and are not available for tuff. Roberts and Lin (1997 [101710]) suggest that the Waxman model provides reasonably good estimates of resistivity for saturations greater than 20%. Waxman-Thomas model 1 converts the electrical resistivity changes to saturation changes, assuming that the primary pathway of

electrical current is through the water in the open pore space; Waxman-Thomas model 2 assumes that the primary pathway is through the double layer.

Changes in saturation are estimated by using both models 1 and 2 (Waxman and Thomas 1974 [101736]). This approach should provide bounds to the domain of possible saturations that may be present. However, if the cation exchange capacity, porosity, or water resistivity varies significantly across the ERT image plane, it is possible that model 1 results would be more accurate. In fact, we believe that model 1 is more representative of the rock mass for two reasons. First, the saturation estimates based on this model are in better agreement with those of the neutron log where those data are available. Second, model 2 occasionally predicts a saturation greater than 1, which, of course, is nonphysical. For that reason, only the saturation change tomograms of model 1 are presented in DTN: LL980913304244.072 [159109].

6.1.2.1.2 Results: ERT

Figure 6.1.2.1-2 shows the saturation ratios (defined as current moisture content to pre-heating initial moisture content) in the two horizontal planes. Blank spaces indicate data sets that did not converge. The changes in moisture content initially are very small and increase in magnitude and extent as the test proceeds. Both horizontal imaging planes are 1.37 m from the heater plane; therefore, no significant drying in these planes is expected. Notice, however, that there are some asymmetries between the two planes. Through June 25, 1997 (117 days into heating), the upper plane (above the heater elevation) shows significantly less change from initial conditions than the lower plane. This asymmetry possibly resulted from heterogeneities in the block.

Drying started to appear as early as May 22, 1997, in the lower plane. The anomalies were localized and linear in shape. Clearly, this drying is a result of the high temperatures, but the effects recorded in these images appear different above and below the heater plane. Above the heater, drying appears later and appears to form anomalies with rounded outlines. The linear shape may be caused by the matrix drying around a planar fracture that cuts through the image plane. Other anomalies of dehydration occur in both planes; some are quite prominent and some are minor. They all support the notion that the dehydration front is steadily advancing from the heater plane into both image planes, but that the process is affected by rockmass heterogeneities.

Figure 6.1.2.1-3 shows the changes in the moisture content in the two vertical planes. As expected, the most obvious feature is the drying zone surrounding the heaters. Although drying is not clearly associated with the heaters until May 22, 1997 (about 83 days into heating), once formed, the drying zone is the dominant feature in either image plane all the way through the last data of cool-down (March 19, 1998). This large dry zone around the heater persists until the late heating phase in February 1998, when it breaks up, apparently because of excessive impedence associated with drying.

Once formed, the heater dry zone is not smooth and planar, reflecting the heater geometry. Instead, it is very irregular in shape, with many appendages. There is also a tendency for the dry zone to be relatively flat on top and bottom early in the test, but convex on top and concave on the bottom late in the test. The asymmetry may be attributed to rock heterogeneities arising from fractures, though no convincing correlation is found between these features in the ERT images to the major fractures mapped in the block.

6.1.2.1.3 Measurement Uncertainty: ERT

Geophysical methods, including ERT, are intended to give qualitative estimates of drying and wetting. The ERT image represents integration of the saturation distribution over a relatively large area, and is therefore bound to be less accurate than neutron logging. There are many factors that affect the uncertainty of the ERT results:

- The measurements of electrical voltage and current in the field are accurate, relative to other factors.

- Measured temperatures within the image region are used for the ERT data reduction. Although the temperature can be measured very accurately at the RTD locations, interpolations are necessary to provide a 2-D temperature field suitable for the ERT. The interpolation will introduce uncertainty in the temperature field, especially with significant heterogeneity in the rock mass.

- The current ERT data reduction does not directly consider the cation exchange capacity of the rock. The cation exchange capacity is indirectly considered when the laboratory measured relationship among the electrical resistivity, water saturation, and temperature is used to check Waxman-Thomas model of electrical resistivity and water saturation, which was developed for the case of shale sands. The validity of this model for welded tuff has been only partially checked by the laboratory data of welded tuff (Roberts and Lin 1997 [101710]).

- The laboratory resistivity data of welded tuff indicate that the Waxman-Thomas model tends to overpredict dryness for saturations less than 20%.

- The inversion algorithm used to reconstruct the tomographs smooths the data. Therefore, the structures observed are “smeared” versions of the true target.

- The effect of the thermal fracturing on the electrical resistivity was not considered by the Waxman-Thomas model.

- The resistivity ratios were calculated using a 2-D algorithm; natural heterogeneities such as fractures tend to be 3-D. Changes in resistivity occurring along fractures may be distorted by use of the 2-D algorithm.

- Metallic sensors in the block may reduce sensitivity to resistivity changes occurring in the block.

- The Waxman-Thomas models do not account for changes in water resistivity caused by rock/water chemical interactions. If chemical reactions cause changes in the concentration or types of ions in the water, or change the porosity because of mineral precipitation or dissolution, the estimated saturation changes will be in error.

6.1.2.2 Neutron Logging

Neutron logging was used to measure the moisture content in the rock through the various phases of the LBT. The neutron probe contains a source of high-energy neutrons and a detector for slow (thermal) neutrons. Neutron counts were measured in each hole at 10 cm intervals. The hydrogen in the water in the rocks slows down the neutrons, making them detectable. Thus, higher counts (or a positive difference in counts relative to background or pre-heating levels) indicate higher water content (or increased water content over background). Calibrations were conducted of the neutron tool in a liner-grout and liner-RTD-grout assemblies (identical to that used in the boreholes) to known moisture contents. Water content is calculated from the neutron counts using the calibration results. Under ambient conditions, the sampling volume surrounding the probe has a diameter of approximately 12 cm (Lin et al. 2001 [159069], Section 6.1.2.1.2); this volume diameter increases as moisture content decreases.

Neutron logging was conducted in some of the vertical boreholes in the potential location of the block, before the boundary of the block was cut. This was to assess the initial moisture content in the outcrop. Then, after the cutting of the block boundary, the neutron logging was repeated to assess the changes in the moisture content resulting from the cutting. Cutting the block boundary using water had no significant effect on the moisture content of the block. Background moisture saturation levels were determined to be about 60 to 80%, for a laboratory-determined porosity of about 11%. Before the heating was started, the baseline moisture content in every neutron borehole was established. Then, during the heating phase and the consequent cooling phase of the test, neutron logging was conducted about once per month. In all cases, neutron counts were obtained at every 10 cm spacing in each borehole. The neutron counts were converted to fraction volume water content by using calibration results.

Neutron logging was conducted in the five vertical boreholes (TN1 to TN5, as shown in Figure 6.1-2), six horizontal boreholes from the north face (NN1 to NN6 in Figure 6.1-3), and four horizontal boreholes from the west face (WN1 to WN4 in Figure 6.1-5) after the completion of the installation of sensors (pre-heating) in February 1997. The neutron boreholes were equipped with a Teflon™ liner, and the space between the liner and the borehole wall was sealed with cement grout. Moisture content was determined with both the Teflon liner and the cement grout in place. The pre-heating measurement established the baseline so that the effect of heating the block on its moisture content could be determined. The neutron tool was calibrated in a 3.81 cm diameter borehole, with the Teflon liner/grout assembly exactly the same as in the neutron boreholes of the LBT. The neutron tool was calibrated both with and without Teflon liner and cement grout conditions. It was determined that the Teflon liner/grout assembly had no major effect on the determined moisture content. This is not surprising because the neutron boreholes in the LBT are designed in such a way that the thickness of the annular cement grout is minimal, only about 0.3 cm (Lin et al. 2001 [159069], p. 6-14).

A complete set of the raw neutron counts, the location of measurements in each borehole, and the converted difference fraction volume water content are in the TDMS under the DTN: LL980919304244.075 [145099].

6.1.2.2.1 Results: Neutron Logging

The difference fraction volume water content in TN3 during the test is presented in this section in graphical form, so that the process of moisture movement can be analyzed. The difference fraction volume water was calculated by subtracting the baseline fraction volume water from that measured during the test.

Figure 6.1.2.2-1 shows the pre-heating (baseline) fraction-volume-water content in TN3 as a function of depth from the top of the block, respectively. This is an example of the baseline water content in the neutron borehole. Generally, the initial moisture content in the region near the collar is less than that in the borehole. The variation in the initial moisture content in each borehole is probably caused heterogeneity in the rock mass.

Figures 6.1.2.2-2 and 6.1.2.2-3 show the difference fraction volume water in borehole TN3, as a function of depth from the top of the block. These are examples to illustrate the variation in the moisture content in the block as measured by neutron logging. Data for the other boreholes can be found in DTN: LL971204304244.047 [113894]. In these figures, the positive fraction volume water means gaining moisture content; the negative fraction volume water means losing moisture content. Generally, the vertical boreholes have a well-defined dryout zone developed after 48 days of heating at the heater plane, which was at about 2.74 m from the top of the block. The dryout zone widened with time, and the extent of the drying also increased with time, because of the continuous heating. The widths of the maximum dryout zones, as measured at the half of the depth of the dryness in the five vertical boreholes, ranged from 1.49 to 1.69 m. It is fair to say that the width of the dryout zone is quite uniform. There was not much change in the extent of the dryness after Day 361 of heating. There were some variations in the shape of the tip of the dryout zone among those five vertical neutron boreholes. The dryness in those five vertical boreholes ranged from -0.07 to -0.09 fraction volume. Those variations among the five vertical boreholes illustrate the effect of heterogeneity in the block on the movement of moisture. Those figures do not show significant rewetting during the cool-down phase.

The variation of the moisture content among the north-face neutron boreholes and the west-face neutron boreholes are similar, and are consistent with that shown in TN3. Generally, the variation of the moisture content was uniform across the block. The variation of the moisture content in the horizontal neutron boreholes depends on the vertical location of the borehole.

The data also showed that the moisture movement in the block was almost one-dimensional. A well-defined dryout zone was developed at the heater plane. The neutron results did not show significant rewetting during the cool-down phase. Fractures have important roles in the localized movement of the moisture (Lin et al. 2001 [159069], pp. 6-14 and 6-16).

6.1.2.2.2 Measurement Uncertainty: Neutron Logging

Neutron logging provides comparatively more accurate measurement of water content than ERT and GPR measurements. But the volume or cross-sectional area covered by the neutron measurement, which is approximately a 15 cm radius from the borehole, is less than ERT and GPR. The variation of the moisture content in the cement grout between the Teflon liner and the

borehole wall may have some effect on the neutron counts. But the effect is small in the LBT because the thickness of the grout column is only about 0.3 cm.

6.1.2.3 Passive Monitoring—Gas Pressure and Relative Humidity

Gas pressure and relative humidity were measured in the four hydrology boreholes: TH1, NH1, WH1, and WH2. Packers were installed in those boreholes to pack off zones for the measurements. Each pack-off zone was about 0.46 m in length. One Humicap™ was installed in each pack-off zone, and a pressure line was installed to bring the gas pressure to a pressure transducer outside of the block. There were three pack-off zones in TH1: one each in NH1, WH1, and WH2. Detailed discussion of these measurements can be found in Section 9.2 of the *Large Block Test Final Report* (Lin et al. 2001 [159069]). The gas pressure and the relative humidity data can be found in the TDMS under the DTN: LL980918904244.074 [135872].

6.1.2.3.1 Results: Gas Pressure and Relative Humidity

Since the pressure transducer outputs were all very noisy, only the relative humidity (RH) and temperature measured by the Humicap sensors will be presented. The Humicap sensors in the first two packed-off zones of the vertical borehole (TH1) also performed unreliably during the LBT. The discussion below, therefore, focuses on the third zone of the vertical borehole and the horizontal boreholes. The Humicap in WH1 and WH2 are the only two sensors that performed for the entire test period. Figures 6.1.2.3-1 and 6.1.2.3-2 show the temperature and relative humidity respectively as measured in WH2 (borehole WH2 is at about 0.5 m above the heater plane). These figures are used as examples of the humidity sensor data. Other humidity sensors functioned similarly.

The WH2 temperature (Figure 6.1.2.3-1) results agree well with the temperatures measured by the RTDs. The initial RH was about 90% and remained high until slightly past 125 days (Figure 6.1.2.3-2). The relative humidity values fell to about 25% by about 230 days. This decrease is consistent with the moisture content measured by neutron logging. Neutron logging in TN3 (Figure 6.1.2.2-3) shows that more than 3% fraction volume water was lost between 130 days and 334 days of heating. This amount of moisture loss was almost half of the total moisture loss at that location in that borehole. The small number of humidity sensors deployed in the LBT limited the conclusive information about the TH process that can be drawn. However, the temperature and RH records from borehole WH2 clearly show that a dry zone extended 0.5 m or more above the heater plane after 135 days. Higher in the block, at 1.5 m above the heater plane (borehole WH-1), boiling conditions were never reached, and RH remained high throughout the LBT. Data also show that rewetting of dry zone was very slow following heater turn-off.

6.1.2.3.2 Measurement Uncertainty: Relative Humidity

The accuracy of humidity measurement is about 2–3% and the RTD temperature measured by the humidity sensor is accurate to within 0.3°C (Section 5.1 of the *Single Heater Test Status Report* (CRWMS M&O 1997 [101540])). But the primary uncertainty in the measurement may result from the conditions in the borehole, such as the sealing of the packer. In a highly fractured rock mass, sealing of a borehole by packers is likely to be incomplete. It is very difficult to provide a quantitative uncertainty caused by the leak through the packers.

6.1.2.4 Laboratory Parameters—Matrix Permeability, Density, Porosity, Micro-Pore Structure, Fracture Flow and Matrix Imbibition Visualization

Small blocks of the rock at the LBT site were collected for laboratory testing of hydrologic properties and processes. Those hydrologic properties include density, porosity, water permeability, and moisture-retention curves. The hydrologic process investigated was fracture flow and matrix imbibition. Section 3.5.1.3 of the *Large Block Test Final Report* (Lin et al. 2001 [159069]) carries the description of the laboratory tests in greater details. Here, the methods of the laboratory tests are briefly discussed and the results summarized.

Matrix Permeability

The water permeability of the Topopah Spring tuff samples obtained from Fran Ridge was measured in the laboratory as a function of temperature. The technique of measuring the permeability was the steady-state flow-through method. Core samples of about 2.54 cm in diameter and 5.1 cm in length were prepared from small block SPC00504573 collected at Fran Ridge during the excavation of the large block, with core identification numbers SPC00504573.4 and SPC00504573.5. The test sample was first saturated with water. Then the sample was encapsulated in a membrane, which separated the sample from the confining pressure fluid. The sample assembly was placed within a pressure vessel with independently controlled confining pressure, pore-water pressure, and temperature. The sample was brought to an equilibrium of certain temperature, confining pressure, and pore pressure.

A differential pressure across the length of the sample was created to cause a flow. The steady-state flow rate was measured. Permeability was calculated using Darcy's equation, assuming the pore pressure gradient is linear. The measurement equipment used in the permeability measurement included a confining pressure transducer, pore pressure transducer, differential pressure transducer, and thermocouple to measure temperature. Flow rate was determined by letting water flow into a container on a balance. The weight of the balance corresponded to the volume of water that has flowed through the sample and is recorded by a computer, along with all the other data such as time, temperature, differential pressure, pore pressures, and confining pressure. Because the flow rate was low, it was necessary to consider the rate of evaporation from the collection bottle. This was found to be linear with time over a period of about one week. The water lost due to evaporation was 4.13 mg/hour. This lost water was added to the balance reading for a specific period of time when calculating permeability. The matrix permeability data can be found in the TDMS under the DTN: LL960905204244.022 [158244].

Density, Porosity and Micro-Pore Structure

Section 3.5.1.3.3 of the *Large Block Test Final Report* (Lin et al. 2001 [159069]) presents the porosity and the micro-pore structure of the LBT samples. The porosity was determined by calculating the difference between the dry density and the water-saturated wet density, divided by the water density (the Gravimetric method). The micro-pore size distribution was determined by mercury-injection porosimetry, another conventional method in the study of rock pore structure. The density and porosity data from the dry-and-saturation method can be found in the TDMS under the DTN: LL950812704242.017 [158237].

Fracture Flow and Matrix Imbibition Visualization

Section 3.5.1.3.4 of the *Large Block Test Final Report* (Lin et al. 2001 [159069]) presents the laboratory experiments using X-ray radiography to visualize fracture flow and matrix imbibition. The samples used in those visualizations were machined from small blocks obtained at the LBT site. A vertical tensile fracture was induced in the middle of the sample block of 2.5 cm thickness, oriented so that the plane of the fracture was parallel to the direction of X-ray transmission. At the top and bottom of the sample were chambers for ponding and collection of water. X-ray radiographs were taken periodically to image water movement into the fracture and rock matrix. A total of seven experiments were conducted. The experimental conditions included isothermal with and without shim, and at thermal gradients with shim. The role of the shim is to increase the aperture of the induced fracture. The X-ray radiograph data can be found in the TDMS under the DTN: LL981208404244.092 [158263].

6.1.2.4.1 Results: Matrix Permeability, Density, Porosity, Micro-Pore Structure, Fracture Flow and Matrix Imbibition Visualization

Matrix Permeability

The water/matrix permeability data of intact core sample SPC00504573.4 are summarized in Table 6.1.2.4-1. The permeability of the intact Topopah Spring tuff sample was less than 10^{-18} m^2. This permeability value is consistent with that measured in cores from Yucca Mountain (Lin and Daily 1984 [101393]). It is also shown in Table 6.1.2.4-1 that intact sample permeability was not a strong function of temperature. This is also consistent with that reported by Lin and Daily (1984 [101393]).

Density, Porosity and Micro-Pore Structure

Table 6.1.2.4-2 shows the porosity of the LBT samples. The porosity ranged from 0.08 to 0.14, with a mean of 0.104 for the 36 samples. The porosity of the 33 samples determined from the mercury injection porosimetry ranged from 0.08 to 0.20 with a mean of 0.115, which agreed well with that determined by dry-and-saturation method.

Fracture Flow and Matrix Imbibition Visualization

At room temperature, imbibition occurred chiefly through the matrix for the unshimmed fracture, with a roughly v-shaped wetting front. During the shimmed fracture experiment, water flowed along the fracture length first, then imbibed horizontally into the matrix.

Under a thermal gradient, water flowed down the fracture quickly. There was significant lateral imbibition into the matrix from the fracture. Penetration of the boiling zone by the water depends on the water head.

Figure 6.1.2.4-1 shows two images to illustrate the effect of water head on the fracture flow and matrix imbibition. In those two cases, the lower 6–7 cm from the bottom of the sample was the boiling zone. The convention used for the difference images is that darker colors or shades indicate relatively high X-ray attenuation and the presence of water, while the lighter areas correspond to lower attenuation and relatively dry areas. For a small water head of about 0.26 m,

the water wetted almost the entire fracture first, followed by imbibition into the matrix, as shown in Figure 6.1.2.4-1 (left image). Within 7.2 hours of ponding, the water penetrated about 3 cm into the boiling zone. Figure 6.1.2.4-1 (right image) shows that when the water head was increased to 0.46 m, the water flowed through the entire length of the fracture within minutes and continued to flow through the boiling region. Not much imbibition into the matrix was observed in this case. The difference in water head was enough to force water through the boiling zone without significant imbibition.

6.1.2.4.2 Measurement Uncertainty: Matrix Permeability; Density, Porosity, Fracture Flow and Matrix Imbibition Visualization

Matrix Permeability

The factors contributing to permeability uncertainty include the measurement accuracy of flow rate, differential pressure, and temperature. Those measurements are all fairly accurate. The propagated error in the permeability through Darcy's equation is small. This uncertainty does not include sample variation and scaling effects when the parameter is applied to the field.

Density and Porosity

The uncertainty of determining the density and porosity of a sample includes the uncertainty in the sample weight and volume, as discussed in the previous subsection, Moisture-Retention Curves.

Fracture Flow and Matrix Imbibition Visualization

The fracture flow and matrix imbibition experiments were intended to be qualitative observations. The main source of uncertainty is the similar X-ray attenuation caused by either increased water content or the forming of potassium iodide crystals.

6.1.3 LBT Mechanical Measurements

6.1.3.1 Multi-Point Borehole Extensometers (MPBX) Displacements

The three-dimensional view of the six MPBX boreholes in the block is shown in Figure 6.1.3.1-1. For the location of those boreholes in the top, north, and west sides of the block, see Figures 6.1-2, 6.1-3, and 6.1-5, respectively. Section 7.1.1 of the *Large Block Test Final Report* (Lin et al. 2001 [159069]) presents the MPBX measurements in detail. Each extensometer consists of three or four borehole anchors connected to linear variable displacement transducer (LVDTs) at the collar by invar rods. The anchors are numbered such that anchor 1 is nearest and anchor 4 is farthest from the collar. The anchors are spring-loaded to the borehole wall. Each anchor is connected to a LVDT at the collar by one invar rod. Any movement of the rock at an anchor transferred to the LVDT at the collar. Therefore, the extensometers measure linear displacement relative to the surface collar. In the data reduction, the thermal expansion of the invar rod was corrected from the raw displacement data by using the manufacturer's invar rod thermal-expansion coefficient and the measured temperatures in TT1 and TT2.

Pre-heating MPBX measurements were conducted for several days before the heaters were energized on February 28, 1997. The LVDTs were zeroed before the heating was started. All of the extensometers performed well during the first few weeks, but problems developed over time, beginning with NM-2, which is located near the heater plane. NM2 failed after about 40 days of heating. About 100 days into the heating phase, two more MPBXs (TM1 and NM1) failed. Before the heating phase ended, at about 375 days, TM2 and NM1 were repaired. Three out of the six MPBX provided complete sets of displacement data for the entire duration of the test.

A detailed discussion of the LBT mechanical measurements is provided in Section 7.1 of the *Large Block Test Final Report* (Lin et al. 2001 [159069]). The Input-DTN for mechanical measurements are provided in Table 4-1. The Input-DTN for these MPBX displacements is LL980919404244.076 [148630].

6.1.3.1.1 Results: MPBX Displacements

Figure 6.1.3.1-2 shows a typical example of the displacement data as a function of time. This is the displacement measured at the #4 anchor of WM2. Also shown in the figure is the temperature measured at TT2-22, which was about the same distance from the heater plane as WM2. Positive displacement means expansion; negative displacement means contraction. The measured displacement in the block tracked the temperature well indicating that the block expanded as a result of heating.

The horizontal displacements near the base of the block were small, essentially the same in the two horizontal directions, and were recovered during cool-down. The horizontal displacements near the top of the block were large, isotropic, and were only partially recovered. The vertical displacement was fairly small but only partially recovered during cool-down.

6.1.3.1.2 Measurement Uncertainty: MPBX Displacement

There are several potential sources for measurement uncertainty in the displacement measurements presented in this section. These uncertainties, quantifiable and non-quantifiable, are listed below:

Quantifiable

- The accuracy of the instrumentation.
- The conversion of the electrical output to engineering units. The uncertainty from these equations, and the computational (round-off) error inherent in the data conversion software, are negligible.
- The physical location of the gages in the test region. The location uncertainty is particularly important in regions of high temperature gradient, of which hydrological and thermal expansion behavior are thought to be strong functions for certain temperature ranges.
- The uncertainty related to the choice of method for computing thermal expansion of Invar rods based on measured temperatures along MPBXs is difficult to estimate. The

magnitude of any discretization error is likely not large enough to affect the general trends in thermal-mechanical deformation of the rock illustrated by the data.

Non-quantifiable

- Electrical interference, such as spurious signals from power surges, can cause low-magnitude noise, unexplained meandering in the data, or high-magnitude spikes.

- Unidentified sensor or MPBX assembly stability issues, which have caused a few LVDTs or vibrating wire gages to either produce "bad" data for an extended period of time before returning "good" data, or to have an unexplained shift in magnitude while maintaining expected rates of behavior on both sides of the shift.

- Degradation or failure of the instrumentation.

6.1.3.2 Fracture Monitoring

Deformations of several major fractures that intersect the surface of the LBT block were monitored using three-component fracture monitors. The purpose of these sensors was to monitor the movement of fractures to gain information about the magnitude and direction of fracture deformation during the test, especially as it relates to TH behavior.

Linear variable displacement transducers (LVDTs) were used to measure the displacements in the three-component surface fracture monitor. The sensors were mounted in T-shaped slots cut into the block, visible in Figure 6.1-1. The slots were cut so that one LVDT would measure aperture change or deformation across the fracture in the plane of the face, while the other two LVDTs would measure sliding in orthogonal directions, parallel and perpendicular to the face. The fractures chosen were oriented perpendicular to the face as much as possible; thus the information can be used to supply estimates of fracture deformation parameters, such as dilation with sliding. See Section 7.1.3 of the *Large Block Test Final Report* (Lin et al. 2001 [159069]) for detailed discussion of fracture monitoring. The Input-DTN for fracture monitoring is LL980919404244.076 [148630].

6.1.3.2.1 Results: Fracture Monitoring

The fracture monitoring (FM) data show that the vertical and horizontal fractures responded somewhat differently. The major horizontal fracture near the top opened coincidentally with the TH event at Day 105. Both vertical and horizontal fractures showed closing during the thermal recovery from the TH events, that is, during periods of apparent condensate refluxing. Initial response for several of the FMs was associated with temperature at the heater plane. FM data indicate that the top of the block moved to the east. Most of the FM deformation was not recovered. The FM data are somewhat inconsistent with the MPBX data, as FMs indicate more deformation in lower portions of the block and less deformation in the upper portions of the block.

6.1.3.2.2 Measurement Uncertainty: Fracture Monitoring

The factors contributing to uncertainty in fracture monitoring include the accuracy of the LVDT, the rigidity of the mounting brackets, limited number of the monitoring points, the effects of the environmental conditions on the fracture monitor, the heterogeneity in the rock, and the apparent movement on the block surface. Similar to the MPBX, LVDTs are accurate. The uncertainty caused by the rest of these factors can only be assessed qualitatively. The mounting brackets and their posts in the rock have to be rigid. Fractures are more complex than planes. Limited number of measuring points cannot fully describe the movement of the fractures. The expansion and contraction of the fracture monitor owing to environmental temperature variations may cause significant uncertainty. Because the fractures are not really orthogonal to the block sides, the monitored movements on the block surface are apparent movements, not the true movements.

6.1.4 LBT Miscellaneous Measurements and Observations

Fracture mapping and qualitative observations were included in the LBT. Observations from boreholes included assessments of fracture flows and microbial survivability and migration. Fracture mapping and the activities in the observation boreholes, as well as microbial survivability and migration, will be summarized here.

A detailed discussion of the LBT miscellaneous measurements is provided in the *Large Block Test Final Report* (Lin et al. 2001 [159069]). *Large Block Test Final Report* (Lin et al. 2001 [159069]). The Input-DTN and Output-DTN for miscellaneous measurements are provided in Tables 4-1 and 6.1-1, respectively.

6.1.4.1 Fracture Mapping

Fracture mapping served many purposes: to characterize the test block, to help interpret test results, and to compare with the fracture characteristics of the Exploratory Studies Facility (ESF). Section 4 of the *Large Block Test Final Report* (Lin et al. 2001 [159069]) presents the fractures mapped in the block. Fractures were carefully mapped on the block surface (four sides and top). Information on the fracture was also collected from video logs of boreholes. On the block surface, fractures were mapped using a 30 × 30 cm grid system on all four vertical sides and the top of the block. The fracture locations were digitized, and fracture segment nodes were assigned x-y-z values. These discrete data points were then input into a 3-D modeling code (EarthVision™ Version 5.0). From the borehole video logs, the depths at which the fracture enters and exits the borehole were recorded, as well as the strike, dip, dip direction, aperture, and magnitude of the features. Appendix C of the *Large Block Test Final Report* (Lin et al. 2001 [159069]) carries information of all borehole video logs. EarthVision generated the trace of the fractures on the block surface and created fracture planes in the block. The fracture information can be found in the TDMS under the following DTNs: LL960400404244.012 [158271], LL960400504244.013 [158274], LL960400604244.014 [158275], and LL960400704244.015 [158276].

6.1.4.1.1 Results: Fracture Mapping

Major fractures were identified based on the size, extent, continuity, and other considerations. The major fractures were then grouped into six systems according to their strike and dip. Figure 6.1.4.1-1 shows 3-D views of all of the major fractures in the block. The fractures in the LBT were dominated by high-angle fractures. This is similar to the fractures in the ESF of Yucca Mountain. However, the fracture orientation in the block is somewhat different from that in the ESF.

6.1.4.1.2 Measurement Uncertainty: Fracture Mapping

The fractures were mapped by hand with tape measures and by viewing video logs, which have a measuring tape in the image. The accuracy of the measured location and extent of the fractures are about a few millimeters. The major uncertainty is in the continuity of the fractures within the block. EarthVision uses interpolation to extend a fracture between the block surface and the boreholes. But in reality, a fracture may be discontinued or have abrupt changes in its strike and dip. It is impossible to assess the accuracy of the fracture model generated by EarthVision without taking the block apart.

One more important point may be the effect of the fractures on the coupled thermal-hydrological-mechanical-chemical processes. This is not an uncertainty issue of the fracture mapping per se, but is an uncertainty in the use of the fracture data. For example, a major fracture, as indicated by its appearance, may not be an effective flow path for the thermal-hydrological process, or a dominant discontinuity for the thermal-mechanical process. The fracture surface roughness was not examined during the fracture mapping. The effect of the fractures on the thermal-chemical process is not clear.

6.1.4.2 Video Observation of Boreholes

Four observation boreholes, NO1, NO2, EO3, and WO5, were installed near the bottom of the block. See Figures 6.1-3, 6.1-4, and 6.1-5 respectively for the location of these boreholes.

6.1.4.2.1 Results: Video Observation of Boreholes

Section 9.1 of the *Large Block Test Final Report* (Lin et al. 2001 [159069]) carries detail description of the observations performed in these observation boreholes. Briefly, these observation boreholes were equipped with a Pyrex™ tube with ink marks on its top. The Pyrex tube was put in a half-PVC pipe, cushioned by one piece of white cloth. The Pyrex tube was to allow access to a video camera for viewing fracture flows in a borehole. The ink marks on the Pyrex tube and the white cloth under the tube were to provide markers of fracture flow. Observations were performed periodically. It was obvious very early that the moisture in the tube prohibited any meaningful direct observation by a video camera. Most of the observations were performed by examining the ink marks on the tube and the ink stains on the white cloth. Many discrete markers (ink stains) were observed in the white cloth. But it was also obvious that condensation on the tube dissolved away a significant portion of the ink marks.

6.1.4.2.2 Measurement Uncertainty: Video Observation of Boreholes

These observations have qualitative uncertainties, which are inherent to visual observations of geologic features.

6.1.4.3 Microbial Observation

Section 9.3 of the *Large Block Test Final Report* (Lin et al. 2001 [159069]) provides a detailed summary of the findings concerning microbial survivability and migration. Microbes were collected from the rock at the LBT site and cultured to be double-drug resistant. The labeled microbes were placed in the heater boreholes and the two vertical boreholes identified as LBL-1 and LBL-2 in Figure 6.1-2. The purpose was to test the survivability of the microbes and their migration in the heated, partially saturated rock environment. The observation performed was to periodically sample the moisture on the Pyrex tube and the white cloth cushion in the observation boreholes mentioned above. The data on the microbial types, abundance, and growth rates can be found in the TDMS under the DTN: LL981202305912.004 [158270].

6.1.4.3.1 Results: Microbial Observation

Basically, the microbes were found in the observation boreholes, which were about 1.5 m below the heater boreholes. This observation indicates that the microbes survived the heating and traveled with drainage water to the observation boreholes.

6.1.4.3.2 Measurement Uncertainty: Microbial Observation

The microbial observation was intended to be qualitative and scoping. Uncertainty assessment for the qualitative activity is not meaningful.

Figure 6.1-1. The LBT Block of Topopah Spring Tuff at Fran Ridge

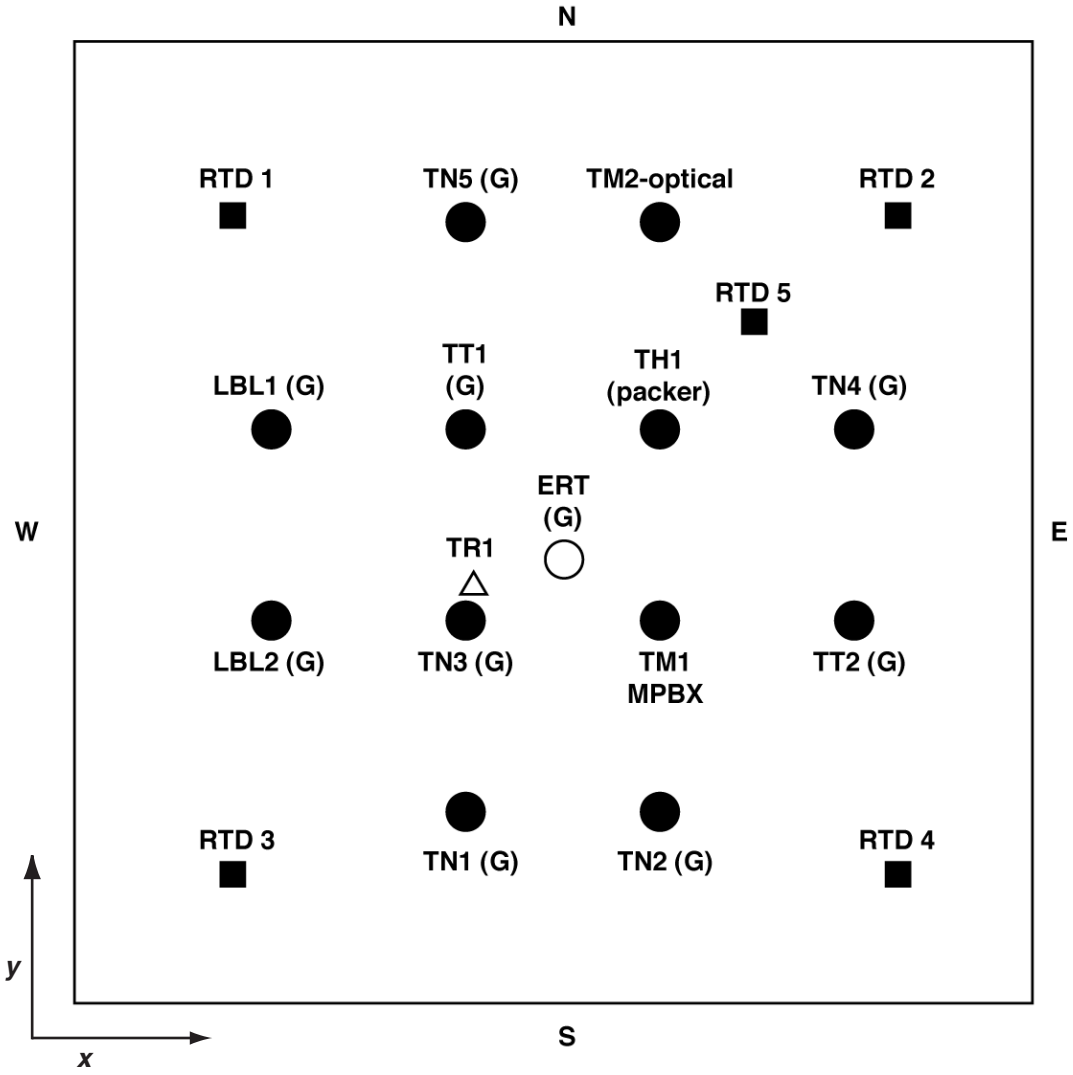

TT# – Temperature measurements – borehole
RTD# – Temperature – Surface mounted RTD
LBL# – Open holes used by LBL for air and then grouted
TN# – Neutron holes lined and grouted
TR1 – REKA probe – grouted
TM# – Mechanical – MPBX borehole
ERT – ERT electrode hole, grouted
TH# – Hydrologic hole with packers
G – Grouted

Figure 6.1-2. LBT Vertical Boreholes Drilled from the Top of the Block

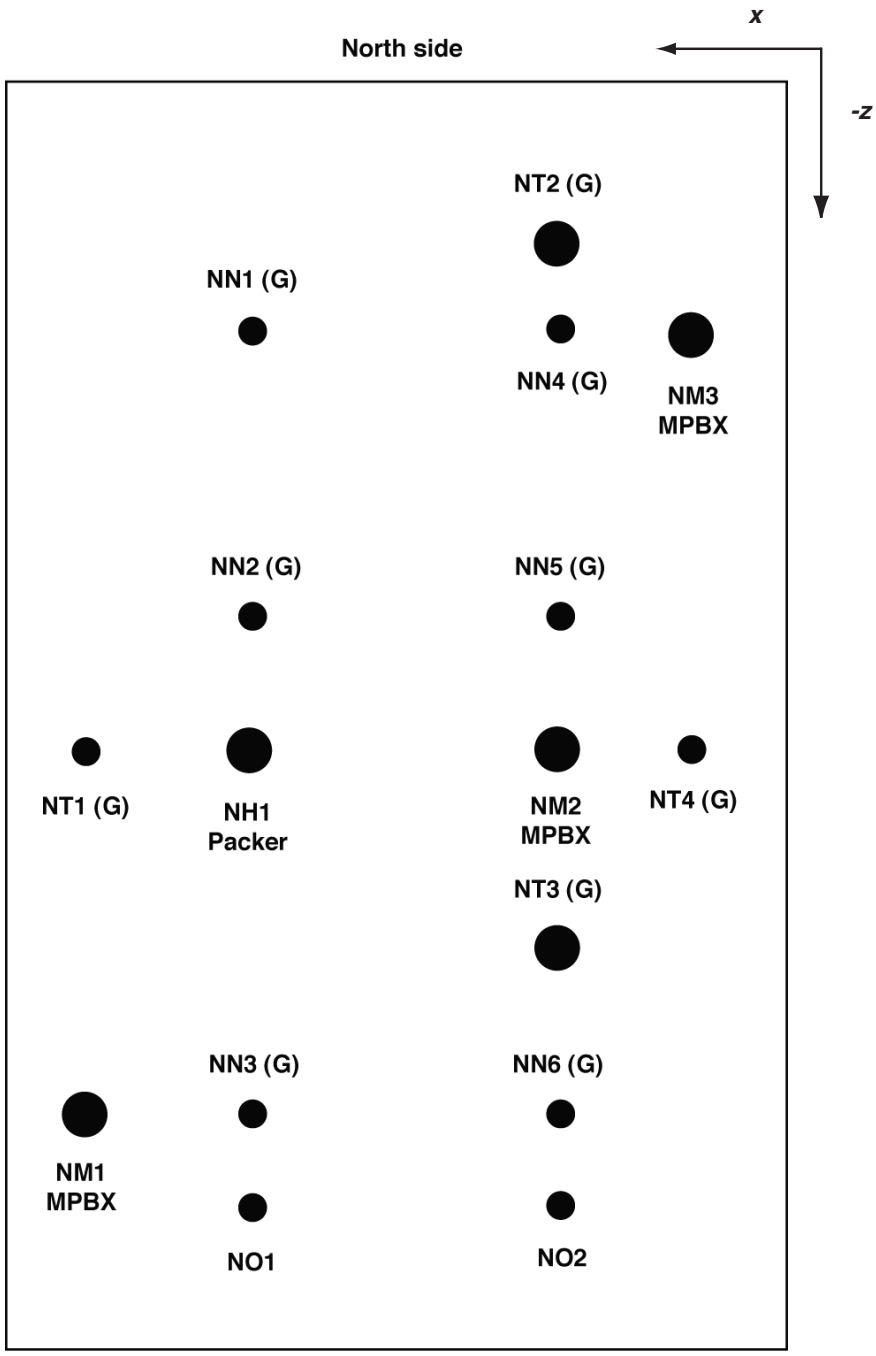

NN# – North side neutron hole – lined and grouted
NT# – North side temperature (RTD bundle) all grouted
NM# – North side mechanical
NO# – North side observation hole
NH# – North side hydrology – packer assembly installed

Figure 6.1-3. LBT Sensor Boreholes Drilled from the North Side of the Block

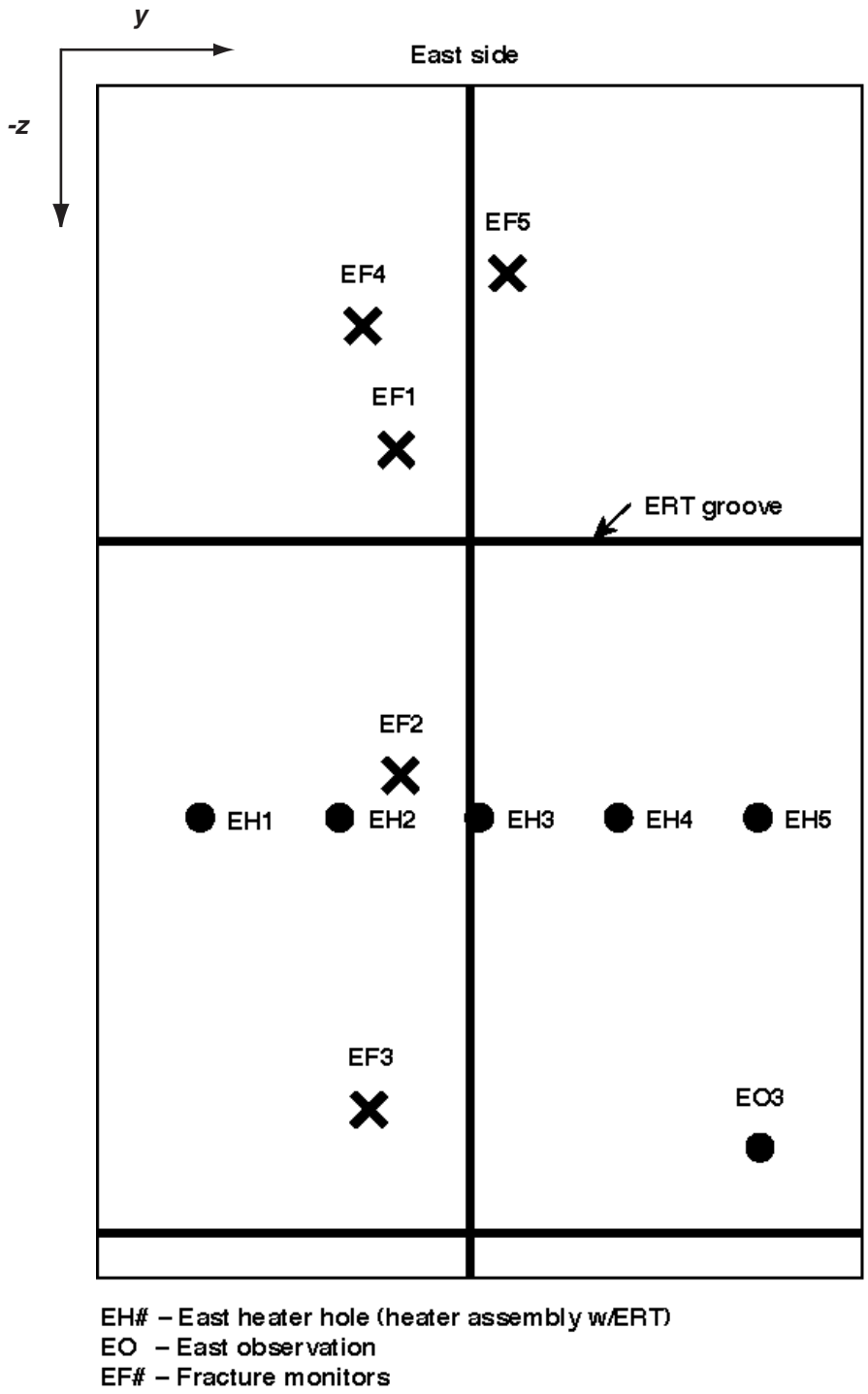

Figure 6.1-4. LBT Boreholes Drilled from the East Side of the Block

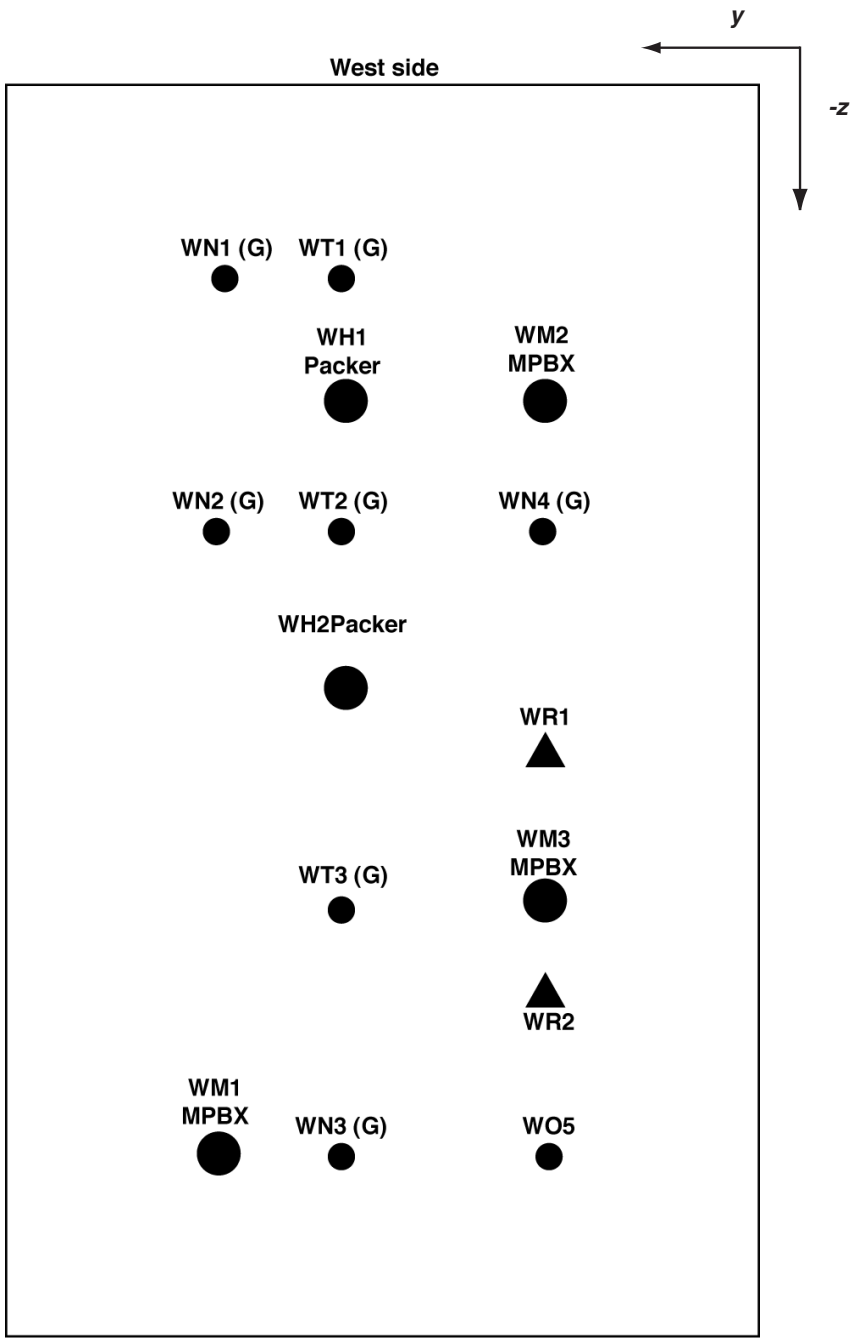

WN# – West side neutron hole – lined and grouted
WT# – West side temperature (RTD bundle) grouted
WH# – West side horizontal – packer assembly installed
WM# – West side mechanical (MPBX) hole – grouted
WO# – West side observation hole
WR# – West side REKA borehole

Figure 6.1-5. LBT Sensor Boreholes Drilled from the West Side of the Block

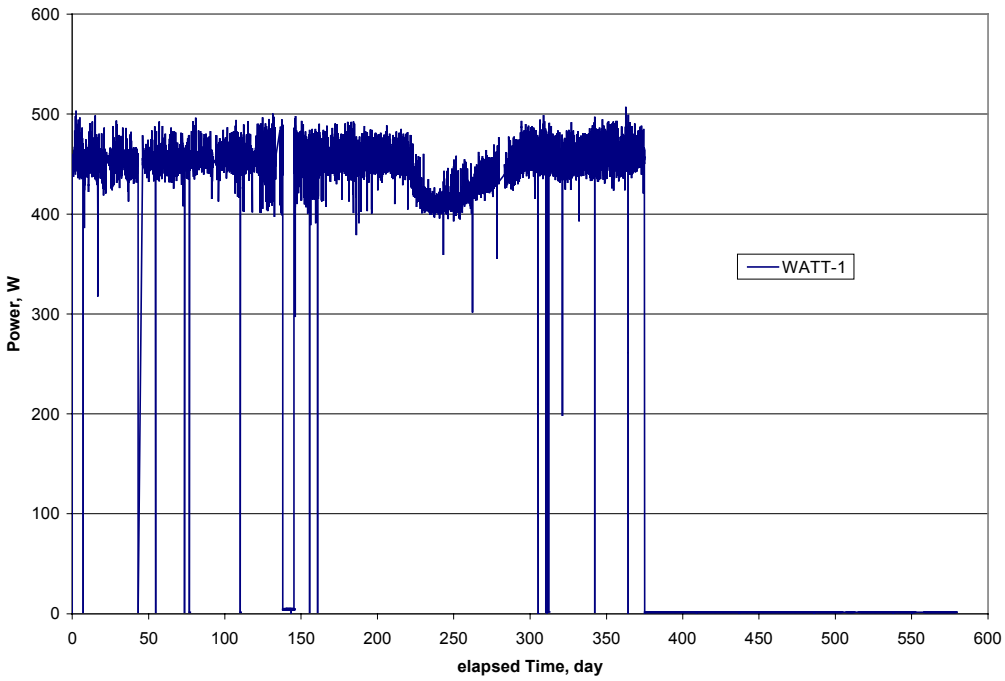

Figure 6.1.1.1-1. The Power History of the LBT Heater EH1

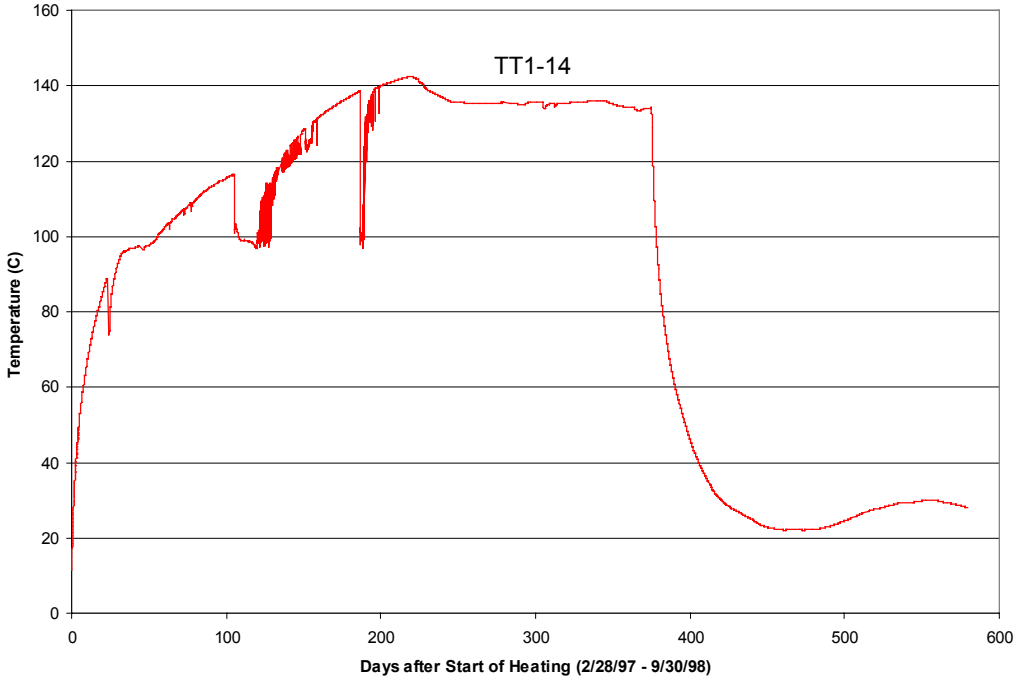

Figure 6.1.1.2-1. Temperature History at LBT TT1-14

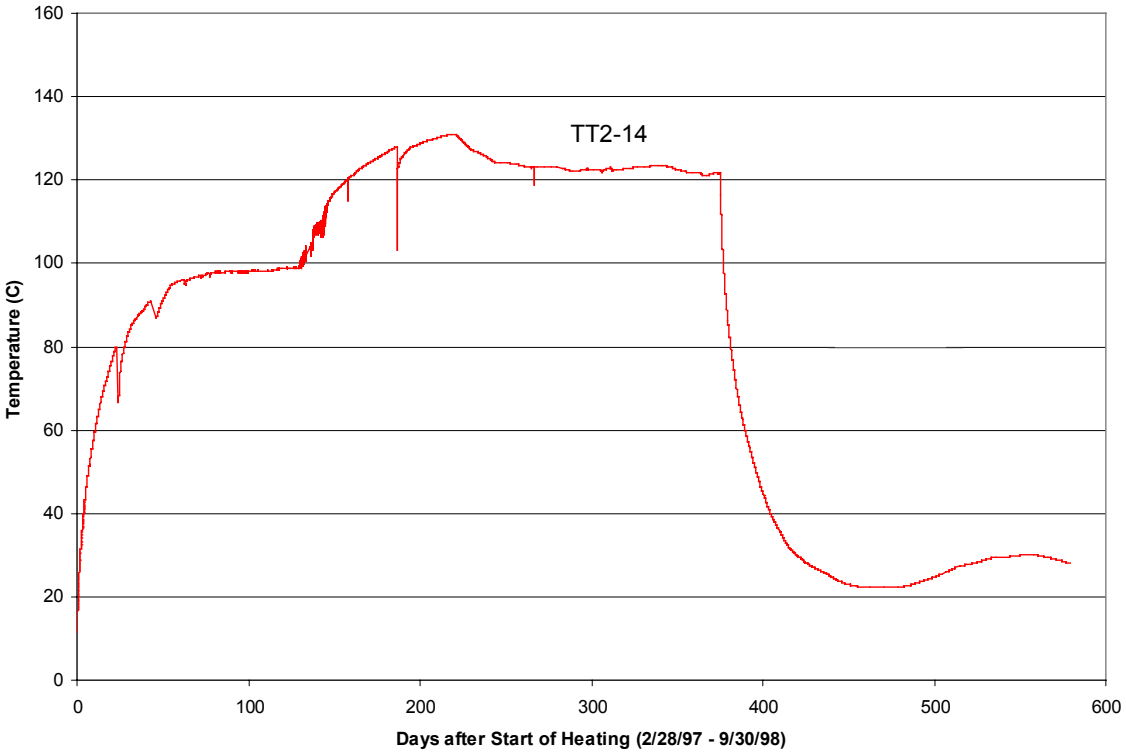

Figure 6.1.1.2-2. Temperature History at LBT TT2-14

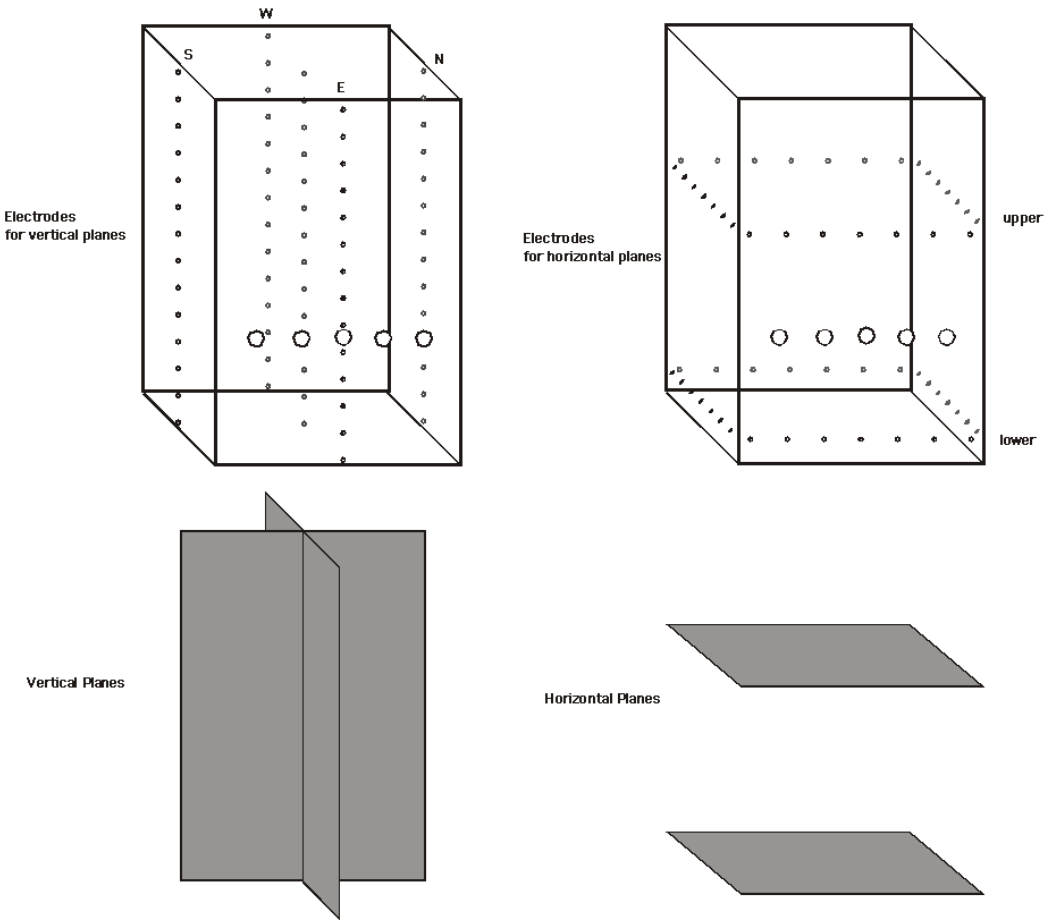

Figure 6.1.2.1-1. LBT Layout of ERT Electrodes

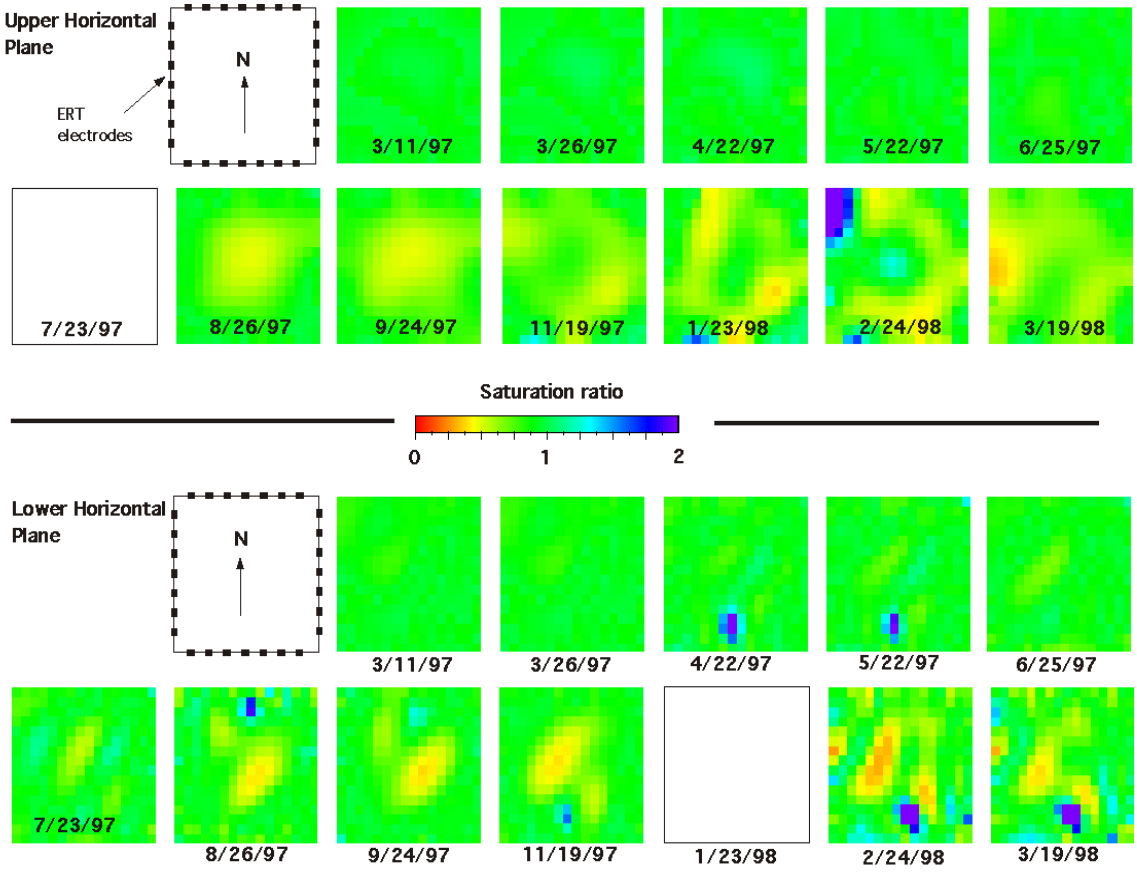

Figure 6.1.2.1-2. Distribution of Moisture Content in Two Horizontal Planes from LBT ERT

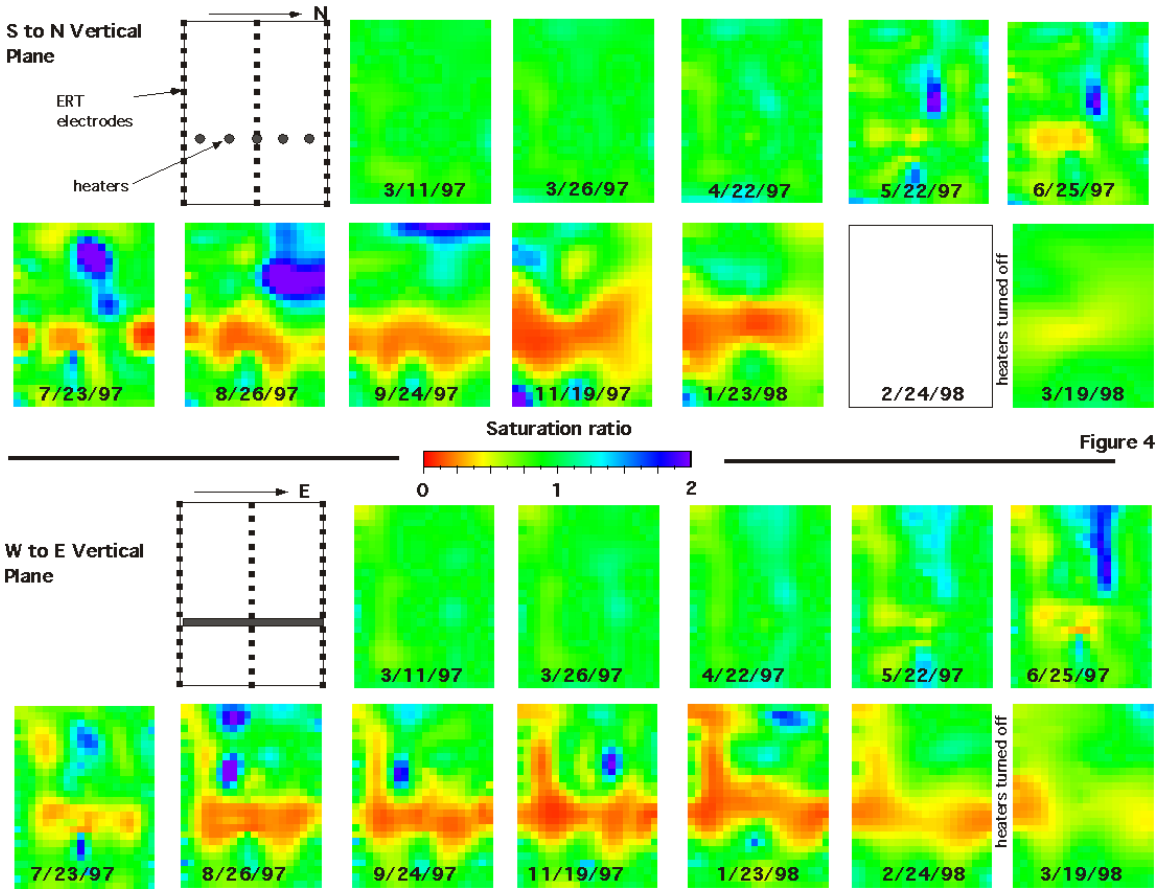

Figure 6.1.2.1-3. Distribution of Moisture Content in Two Vertical Planes in LBT

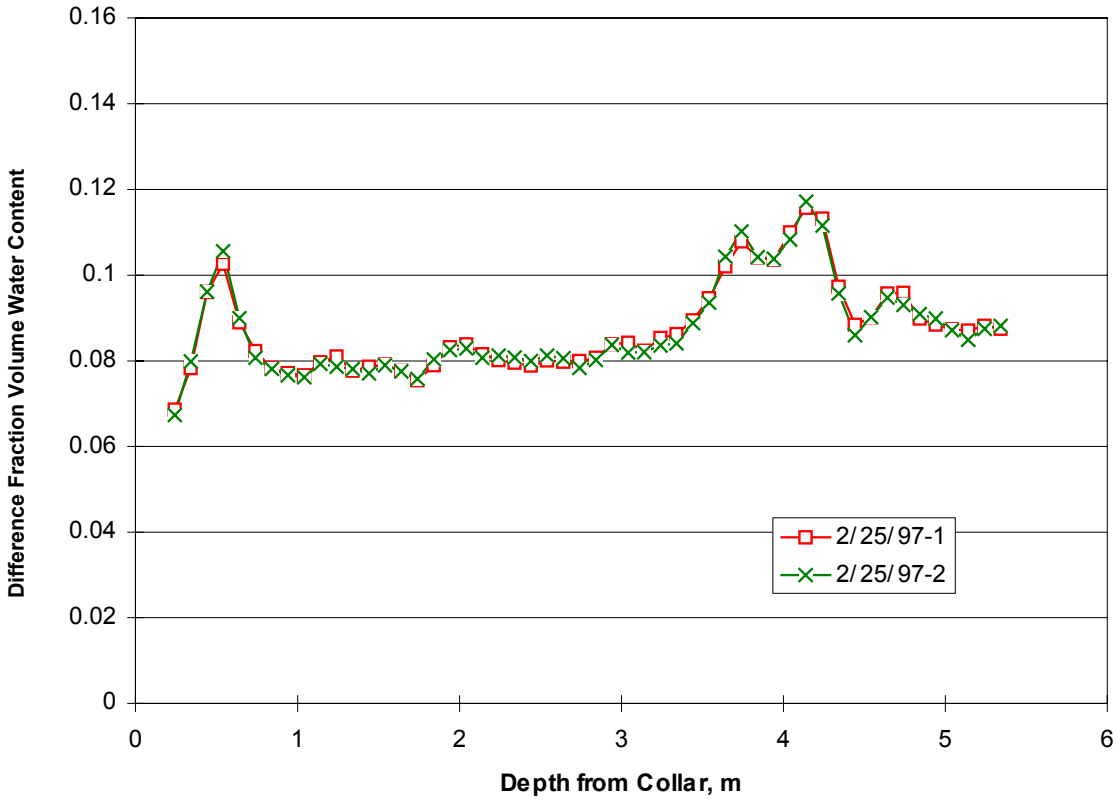

Figure 6.1.2.2-1. Difference Fraction Volume Water Content Measured in LBT Vertical Borehole TN3 using Neutron Logging (Pre-Heating/Baseline)

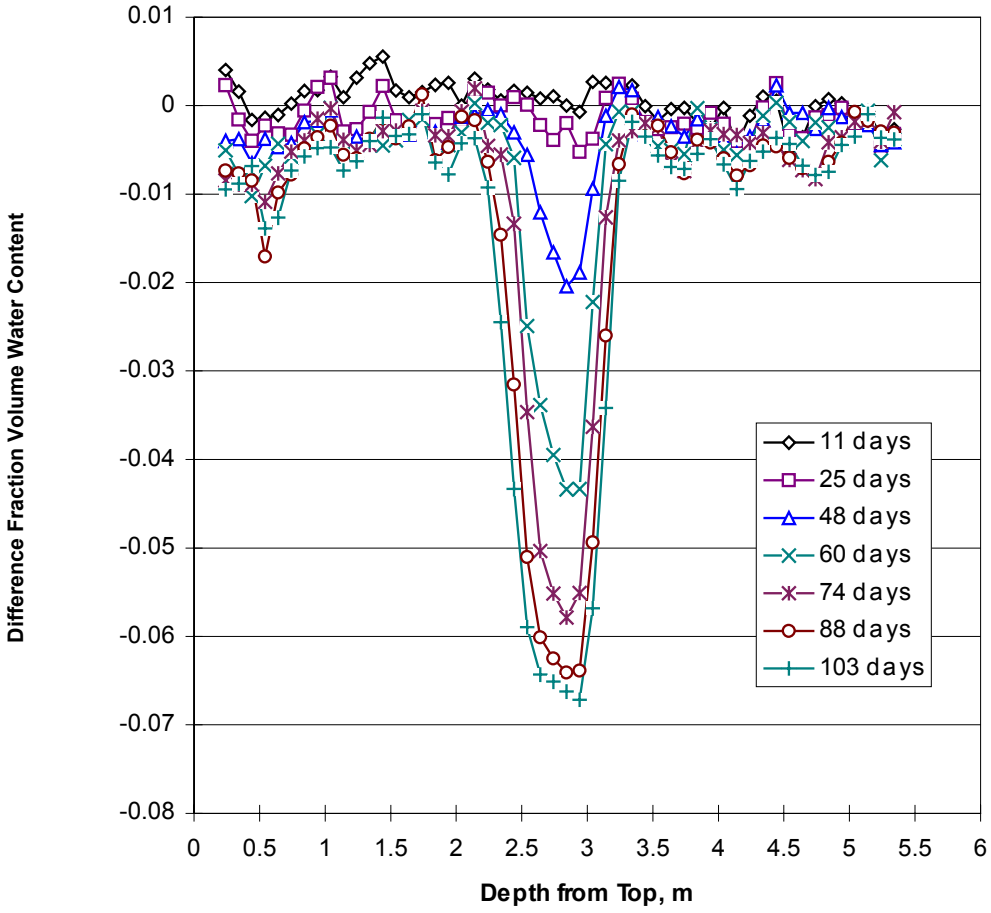

Figure 6.1.2.2-2. Difference Fraction Volume Water Content Measured in LBT Borehole TN3 using Neutron Logging (March 11 to June 11, 1997)

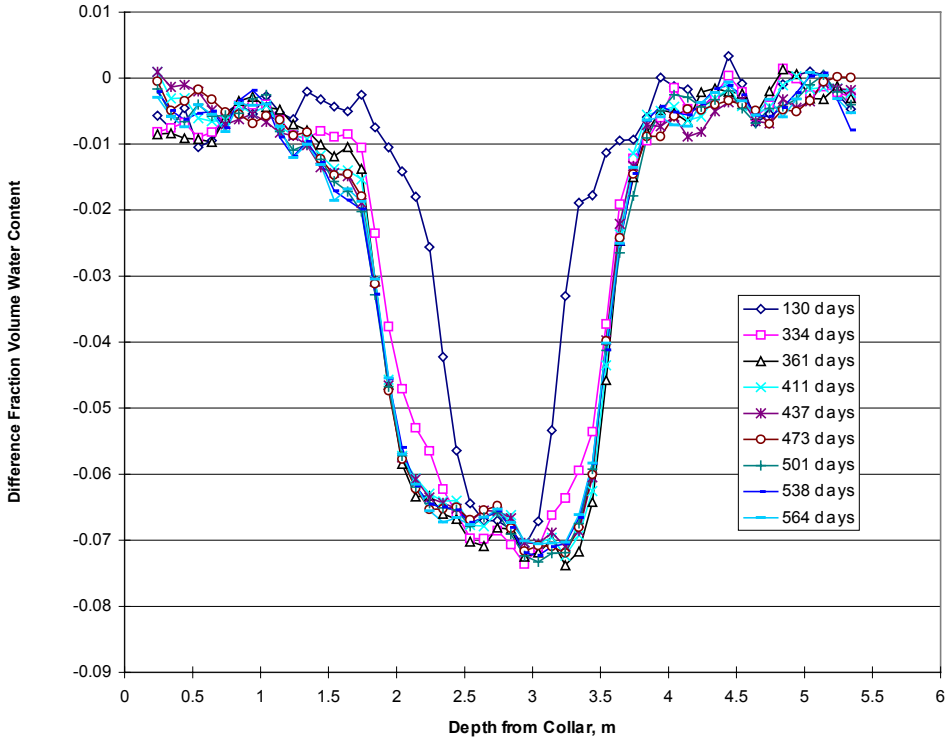

Figure 6.1.2.2-3. Difference Fraction Volume Water Content Measured in LBT Borehole TN3 using Neutron Logging (July 8, 1997, to September 15, 1998)

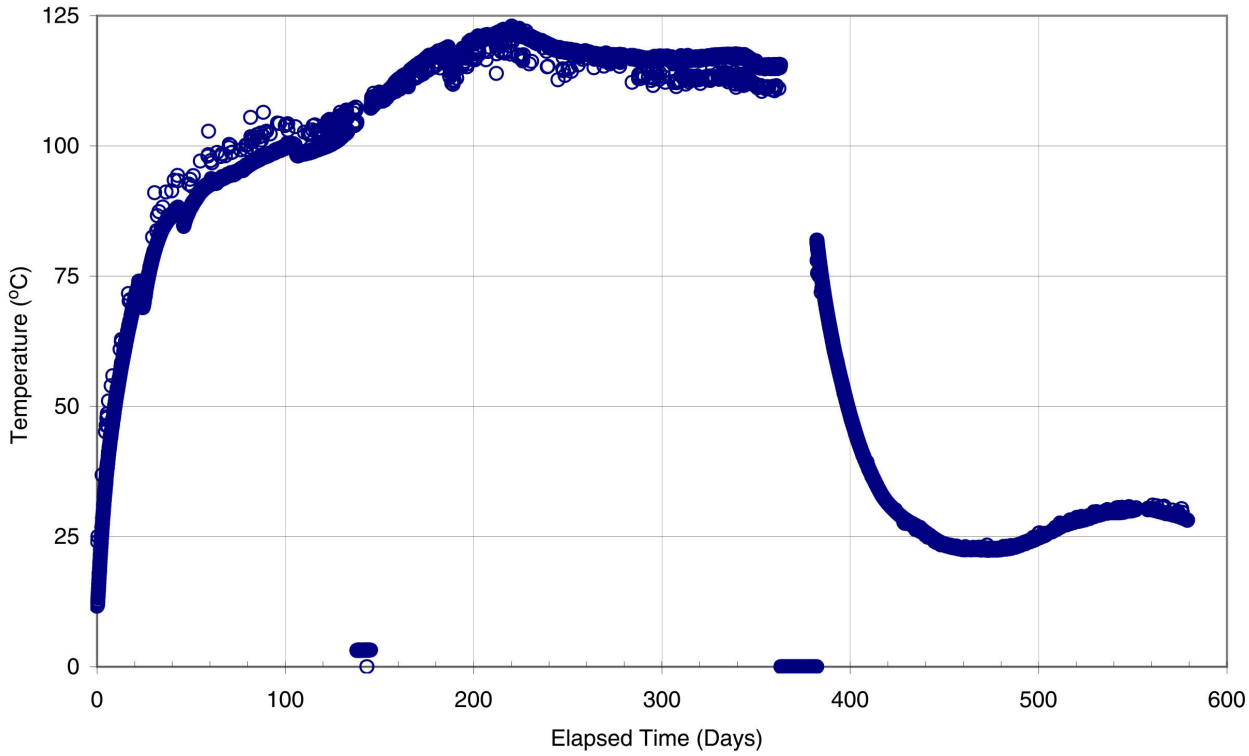

Figure 6.1.2.3-1. Temperature Measured in LBT Borehole WH-2 as a Function of Time

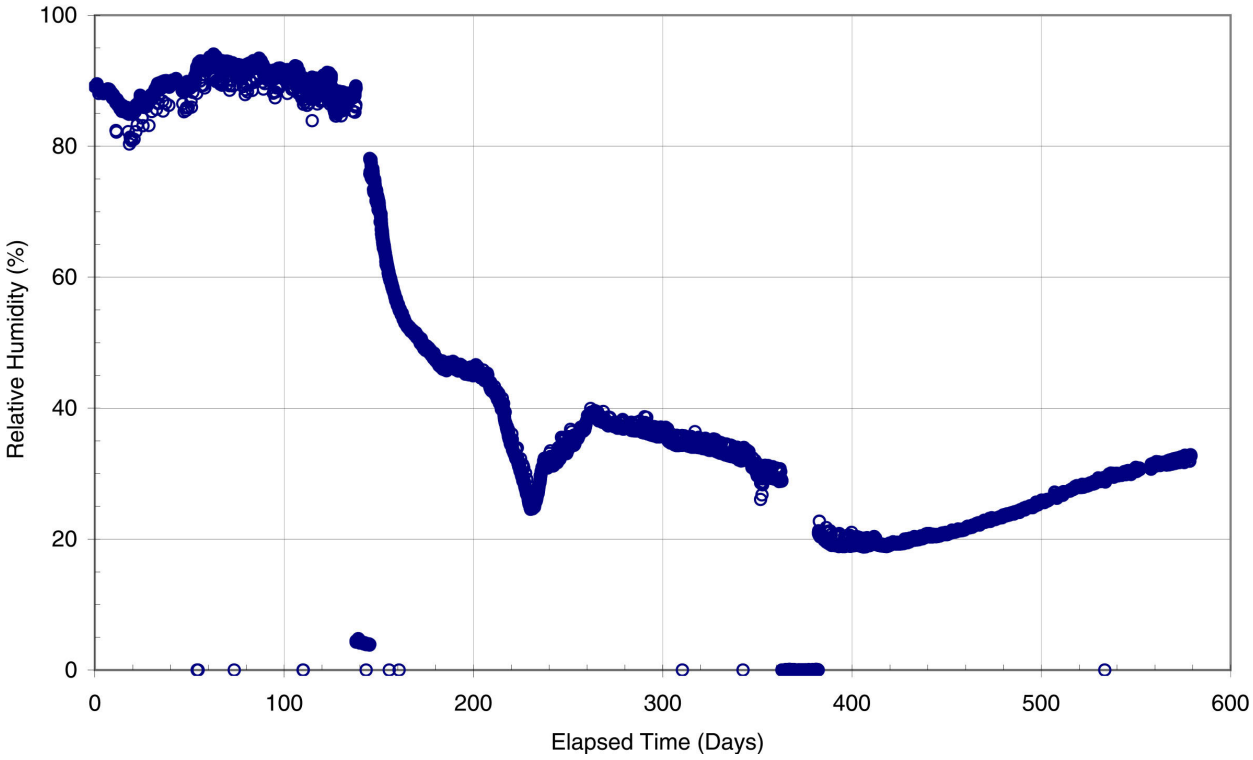

Figure 6.1.2.3-2. Relative Humidity Measured by the Humicap in LBT Borehole WH-2 as a Function of Time

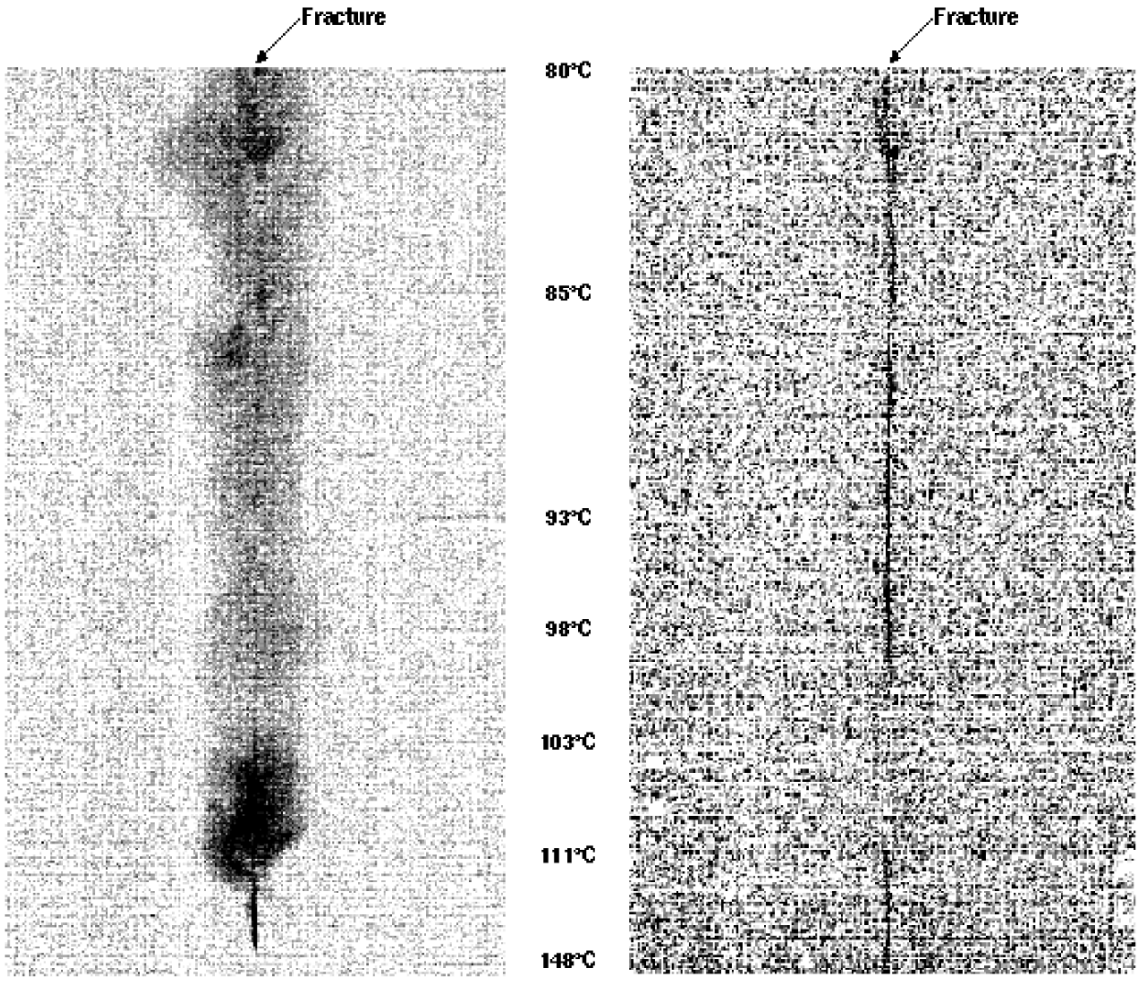

Figure 6.1.2.4-1. Images of Imbibition Under Thermal Gradient: (left) 0.26 m Water Head at 7.2 Hours and (right) 0.46 m Water Head at 0.67 Hours

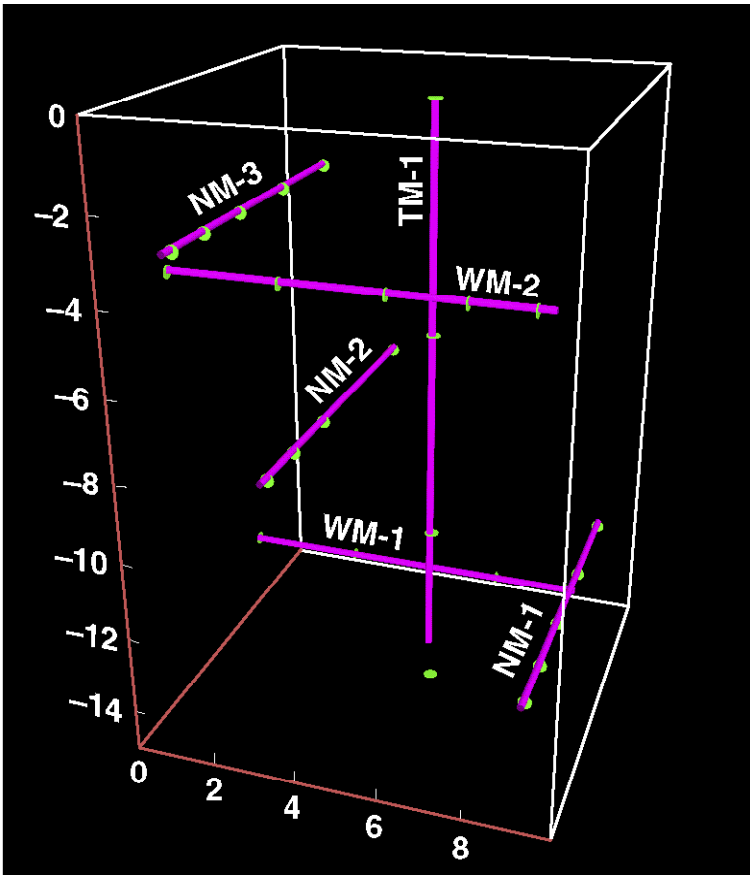

Figure 6.1.3.1-1. MPBX Borehole Locations, Viewed from the South Face

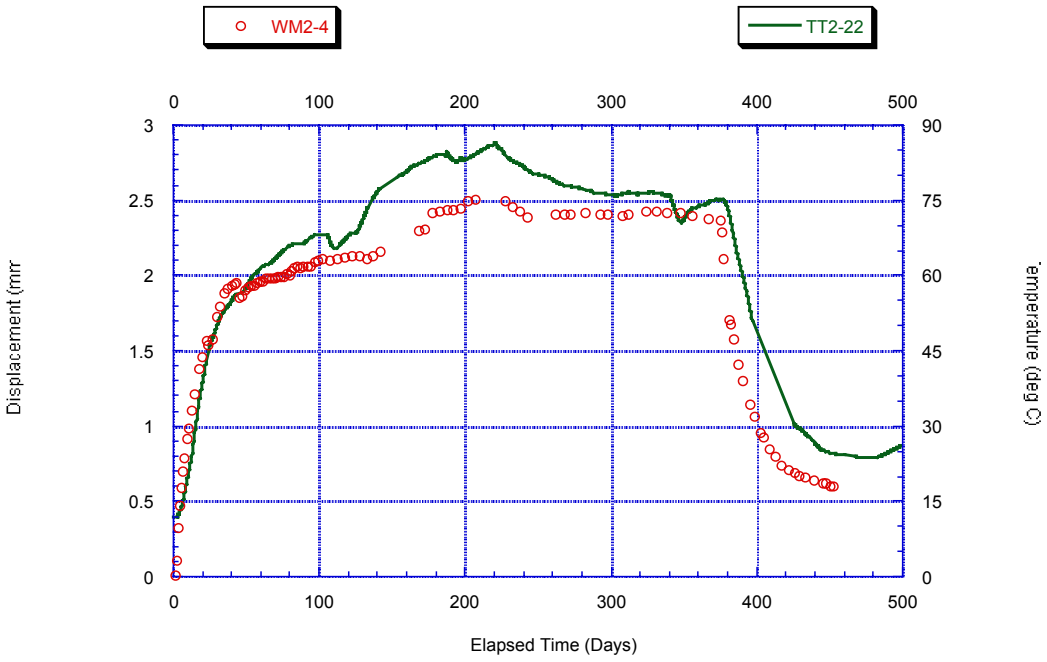

Figure 6.1.3.1-2. East-West Displacement for WM-2 Anchor 4 and Temperature at 1.2-m Depth

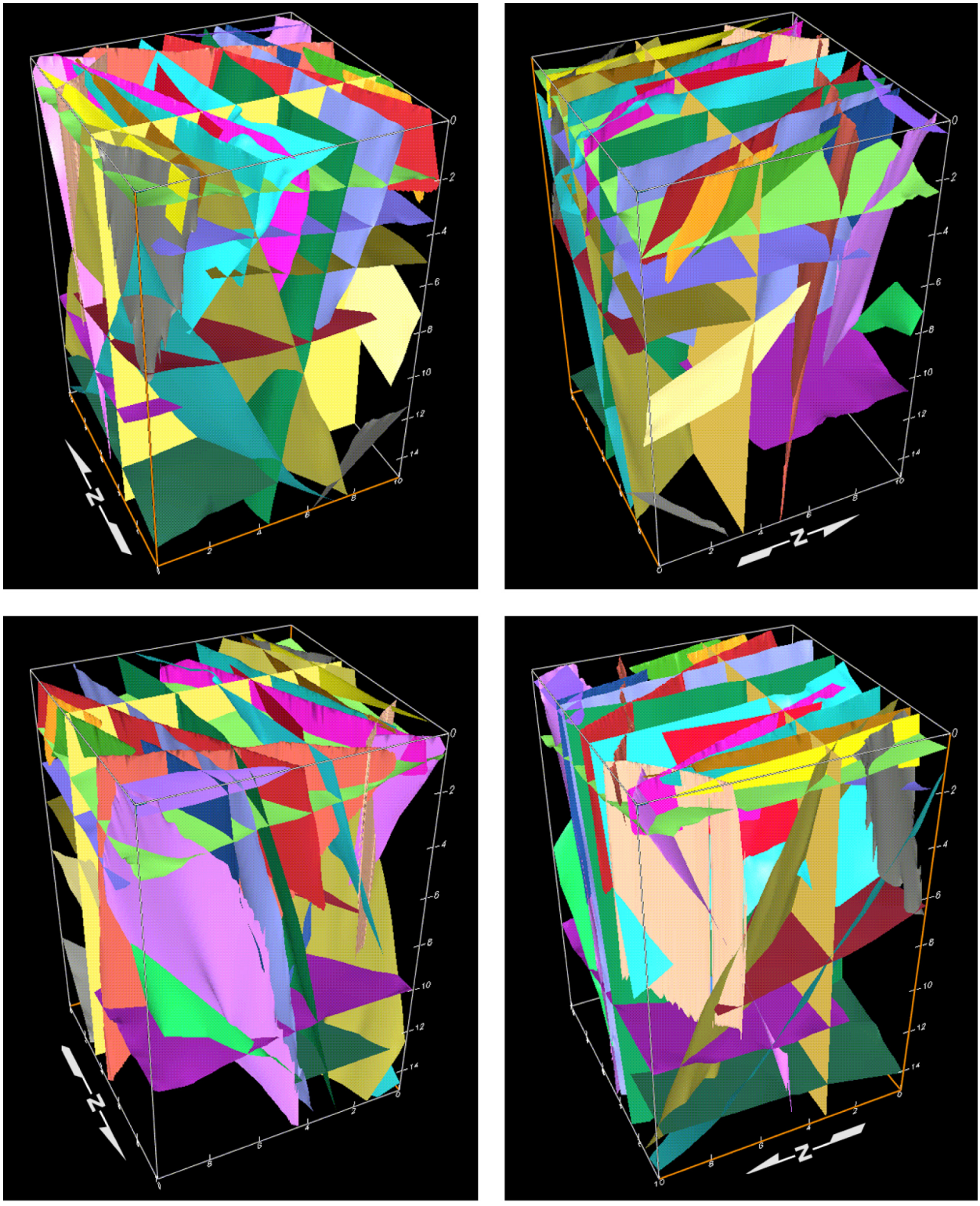

Figure 6.1.4.1-1. Three-Dimensional Depiction of the Major Mapped Fractures Cutting the LBT Block

INTENTIONALLY LEFT BLANK

Table 6.1-1. Output-DTNs along with Input-DTNs for the Large Block Test[1]

Input-DTN [DIRS]	Input-DTN Description	Input-DTN Text Location	Output-DTN	Output-DTN Description
LL980918904244.074 [135872]	Heater Power, Temperature, Relative Humidity, and Gas Pressure	6.1.1.1 6.1.1.2 6.1.2.3	LL020710523142.025	Heater Power, Temperature, and Displacement Data.
LL980919404244.076 [148630]	Rock Mass Displacements	6.1.3.1 6.1.3.2		
LL980913304244.072 [145385]	Electrical Resistance Tomograms	6.1.2.1	Unchanged-DTN	Unchanged-DTN
LL981001604244.079 [158261]	Electrical Resistivity	6.1.2.1	Unchanged-DTN	Unchanged-DTN
LL980919304244.075 [145099]	Neutron Logging	6.1.2.2	Unchanged-DTN	Unchanged-DTN
LL950812704242.017 [158237]	Porosity, Saturated and Dry Density	6.1.2.4	Unchanged-DTN	Unchanged-DTN
LL960905204244.022 [158244]	Laboratory Matrix Permeability	6.1.2.4	Unchanged-DTN	Unchanged-DTN
LL981208404244.092 [158263]	X-ray Radiography	6.1.2.4	Unchanged-DTN	Unchanged-DTN
LL960400404244.012 [158271]	Fracture Mapping	6.1.4.1	Unchanged-DTN	Unchanged-DTN
LL960400504244.013 [158274]	Fracture Mapping	6.1.4.1		
LL960400604244.014 [158275]	Fracture Mapping	6.1.4.1		
LL960400704244.015 [158276]	Fracture Mapping	6.1.4.1		
LL981202305912.004 [158270]	Bacterial Transport	6.1.4.3	Unchanged-DTN	Unchanged-DTN

NOTE: [1] DTNs: LA0106FH831151.002 [158230] and LA0106FH831151.003 [158229] provide access (Records Processing Center) to all thermal and mechanical data collected in LBT Data Collection System (original/electrical and converted/engineering units). These non-qualified DTNs also proves access (RPC) to pertinent measurement information such as scientific notebooks and calibration procedures.

Table 6.1-2. XYZ Coordinates of the Collar and Bottom of LBT Boreholes*

Borehole ID (Alt. ID)	X-Collar (m)	Y-Collar (m)	Z-Collar (m)	X-Bottom (m)	Y-Bottom (m)	Z-Bottom (m)	Borehole Type
eh1 (EH1)	3.05	0.30	-2.74	0.30	0.30	-2.74	Heater
eh2 (EH2)	3.05	0.91	-2.74	0.30	0.91	-2.74	
eh3 (EH3)	3.05	1.52	-2.74	0.30	1.52	-2.74	
eh4 (EH4)	3.05	2.13	-2.74	0.30	2.13	-2.74	
eh5 (EH5)	3.05	2.74	-2.74	0.30	2.74	-2.74	
e7 (TT1)	1.22	1.83	0.00	1.22	1.83	-5.51	RTD
e1 (TT2)	2.44	1.22	0.00	2.40	1.19	-5.38	
nt1 (NT1)	2.74	3.05	-2.44	2.74	0.30	-2.44	
nt2 (NT2)	0.91	3.05	-0.61	0.91	0.30	-0.61	
nt3 (NT3)	0.91	3.05	-3.20	0.91	0.30	-3.20	
nt4 (NT4)	0.30	3.05	-2.44	0.30	0.30	-2.44	
wt1 (WT1)	0.00	1.68	-0.76	2.74	1.68	-0.76	
wt2 (WT2)	0.00	1.68	-1.68	2.74	1.68	-1.68	
wt3 (WT3)	0.00	1.68	-3.05	2.74	1.68	-3.05	
tr1 (TR1)	1.27	1.32	0.00	1.27	1.32	-1.42	REKA
wr1 (WR1)	0.00	0.63	-1.86	1.75	0.63	-1.86	
wr2 (WR2)	0.00	0.91	-3.32	1.75	0.91	-3.32	
te1 (ERT)	1.52	1.37	0.00	1.52	1.37	-3.96	ERT
e5 (TN1)	1.22	0.61	0.00	1.18	0.57	-5.64	Neutron
e3 (TN2)	1.83	0.61	0.00	1.83	0.62	-3.75	
e6 (TN3)	1.22	1.22	0.00	1.21	1.16	-5.64	
e2 (TN4)	2.44	1.83	0.00	2.41	1.82	-5.44	
e8 (TN5)	1.22	2.44	0.00	1.21	2.45	-5.21	
nn1 (NN1)	2.13	3.05	-0.91	2.13	0.30	-0.91	
nn2 (NN2)	2.13	3.05	-1.98	2.13	0.30	-1.98	
nn3 (NN3)	2.13	3.05	-3.81	2.13	0.30	-3.81	
nn4 (NN4)	0.91	3.05	-0.91	0.91	0.30	-0.91	
nn5 (NN5)	0.91	3.05	-1.98	0.91	0.30	-1.98	
nn6 (NN6)	0.91	3.05	-3.81	0.91	0.30	-3.81	
wn1 (WN1)	0.00	2.13	-0.76	2.74	2.13	-0.76	
wn2 (WN2)	0.00	2.13	-1.68	2.74	2.13	-1.68	
wn3 (WN3)	0.00	1.68	-3.96	2.74	1.68	-3.96	
wn4 (WN4)	0.00	0.91	-1.68	2.74	0.91	-1.68	
n1 (TH1)	1.83	1.83	0.00	1.81	1.76	-4.01	Hydrology
nh1 (NH1)	0.00	3.05	-2.44	2.13	0.30	-2.44	
wh1 (WH1)	0.00	1.68	-1.22	2.74	1.68	-1.22	
wh2 (WH2)	0.00	1.68	-2.29	2.74	1.68	-2.29	
no1 (NO1)	2.13	3.05	-4.11	2.13	0.30	-4.11	Observation
no2 (NO2)	0.91	3.05	-4.11	0.91	0.30	-4.11	
eo3 (EO3)	3.05	2.74	-3.96	0.30	2.74	-3.96	
wo5 (WO5)	0.00	0.91	-3.96	2.74	0.91	-3.96	
n2 (TM1)	1.83	1.22	0.00	1.82	1.21	-4.05	Mechanical
n3 (TM2)	1.83	2.44	0.00	1.78	2.42	-4.09	
nm1 (NM1)	2.74	3.05	-3.81	2.74	0.30	-3.81	
nm2 (NM2)	0.91	3.05	-2.44	0.91	0.30	-2.44	
nm3 (NM3)	0.30	3.05	-0.91	0.30	0.30	-0.91	
wm1 (WM1)	0.00	2.13	-3.96	2.74	2.13	-3.96	
wm2 (WM2)	0.00	0.91	-1.22	2.74	0.91	-1.22	
wm3 (WM3)	0.00	0.91	-3.05	2.74	0.91	-3.05	

Table 6.1-2. XYZ Coordinates of the Collar and Bottom of LBT Boreholes* (continued)

Borehole ID (Alt. ID)	X-Collar (m)	Y-Collar (m)	Z-Collar (m)	X-Bottom (m)	Y-Bottom (m)	Z-Bottom (m)	Borehole Type
n4	1.52	3.05	0.00	1.52	3.05	-6.4	Rock bolt boreholes
n5	0	1.52	0	0	1.52	-6.4	
n6	1.52	0	0	1.52	0	-6.4	
n7	3.05	1.52	0	3.05	1.52	-6.4	
PTC#1	1.22	3.05	-2.29	1.22	0.00	-2.29	Post-cooling
PTC#2	1.22	3.05	-2.02	1.22	0.00	-1.48	
PTC#3	1.22	3.05	-2.56	1.22	0.00	-3.09	
PTC#4	1.22	3.05	-1.73	1.22	0.00	-0.62	
PTC#5	1.22	3.05	-2.84	1.22	0.00	-3.95	
PTC#6	1.22	3.05	-1.41	1.22	0.00	0.35	
PTC#7	1.22	3.05	-3.76	1.22	0.00	-6.70	
PTC#8	1.22	3.05	-1.01	1.22	0.00	1.55	
PTC#9	1.22	3.05	-2.29	2.53	0.00	-2.29	
PTC#10	0.00	1.83	-1.09	3.05	1.83	1.29	
PTC#11	0.00	1.83	-1.30	3.05	1.83	0.68	
PTC#12	0.00	1.83	-1.51	3.05	1.83	0.04	
PTC#13	0.00	1.83	-1.73	3.05	1.83	-0.62	
PTC#14	0.00	1.83	-1.91	3.05	1.83	-1.15	
PTC#15	0.00	1.83	-2.26	3.05	1.83	-2.21	
PTC#16	0.00	1.83	-2.55	3.05	1.83	-3.09	
PTC#17	0.00	1.83	-2.84	3.05	1.83	-3.95	
PTC#18	0.00	1.83	-3.35	3.05	1.83	-5.49	
PTC#19	0.00	1.83	-2.18	3.05	1.83	-1.97	
PTC#19a	0.00	1.83	-2.29	3.05	0.52	-2.29	
e10 (LBL1)	0.61	1.83	0.00	0.55	1.81	-4.00	Micro.
e9 (LBL2)	0.61	1.22	0.00	0.61	1.22	-3.98	

* Source: Large Block Final Report (Lin et al. 2001 [159069]).

Table 6.1.2.4-1. LBT Permeability Measurements on Intact Core Sample SPC00504573.4

Temperature (°C)	Confining Pressure (Mpa)	Differential Pressure (Mpa)	Permeability (μD)
23	5.06	1.92	0.12
25	5.07	2.47	0.14
53	5.06	2.42	0.11
53	5.06	1.91	0.15
91	5.06	2.17	0.14
92	5.06	1.60	0.14
154	5.06	1.61	0.09
130	5.05	1.46	0.13
130	5.05	2.04	0.11
83	5.06	2.02	0.17
26	5.06	2.59	0.67
26	5.06	2.61	0.20

Table 6.1.2.4-2. Density and Porosity of LBT Samples Determined by Gravimetric Method

Sample†	Sample ID	Depth (m)	Dry wt (g)	Wet wt (g)	Dry density (g/cm^3)	Wet density (g/cm^3)	Porosity
N1-6.3	0032079.3	1.92	1.5352	1.6111	2.23	2.35	0.110
N1-6.3A	0032079.3A	1.92	1.7890	1.8680	2.26	2.36	0.0997
N1-6.3B	0032079.3B	1.92	1.6358	1.7098	2.28	2.39	0.103
N1-11.0	0032081.3	3.35	1.6352	1.7181	2.25	2.37	0.114
N1-11.0A	0032081.3A	3.35	1.5920	1.6734	2.26	2.38	0.116
N1-11.0B	0032081.3B	3.35	1.6762	1.7525	2.30	2.41	0.105
N1-13.45	0032082.3	4.10	1.4982	1.5752	2.27	2.39	0.117
N1-13.45A	0032082.3A	4.10	1.7118	1.7951	2.27	2.38	0.110
N1-13.45B	0032082.3B	4.10	1.6954	1.7781	2.26	2.37	0.110
N1-16.9	0032083.3	5.15	1.6499	1.7522	2.20	2.33	0.136
N1-16.9A	0032083.3A	5.15	1.6094	1.6987	2.23	2.35	0.124
N1-16.9B	0032083.3B	5.15	1.6885	1.7670	2.27	2.38	0.106
N1-20.3	0032084.3	6.19	1.5438	1.6133	2.22	2.32	0.0998
N1-20.3A	0032084.3A	6.19	1.5567	1.6244	2.26	2.36	0.0982
N1-20.3B	0032084.3B	6.19	1.5109	1.5849	2.21	2.32	0.108
N4-11.6	0032104.3	3.54	1.5429	1.6036	2.26	2.34	0.0887
N4-11.6A	0032104.3A	3.54	1.6222	1.6864	2.24	2.33	0.0886
N4-11.6B	0032104.3B	3.54	1.6375	1.6969	2.27	2.35	0.0823
N5-4.9	0032107.3	1.49	1.6998	1.7687	2.25	2.34	0.0911
N5-4.9A	0032107.3A	1.49	1.6501	1.7104	2.28	2.37	0.0834
N5-4.9B	0032107.3B	1.49	1.8818	1.9569	2.31	2.40	0.0922
N5-20.4	0032111.3	6.22	1.5230	1.5909	2.22	2.32	0.0992
N5-20.4A	0032111.3A	6.22	1.4883	1.5593	2.21	2.32	0.106
N5-20.4B	0032111.3B	6.22	1.4765	1.5463	2.22	2.32	0.105
N6-4.75	0032112.3	1.43	1.7549	1.8228	2.25	2.33	0.0869
N6-4.75A	0032112.3A	1.43	1.6761	1.7374	2.29	2.37	0.0837
N6-4.75B	0032112.3B	1.43	1.7136	1.7755	2.27	2.35	0.0819
N6-14.2	0032116.3	4.33	1.6590	1.7398	2.26	2.37	0.110
N6-14.2A	0032116.3A	4.33	1.6869	1.7706	2.24	2.35	0.111
N6-14.2B	0032116.3B	4.33	1.6285	1.7137	2.23	2.35	0.117
N7-5.7	0032120.3	1.74	1.6161	1.7003	2.24	2.36	0.117
N7-5.7A	0032120.3A	1.74	1.6320	1.7051	2.29	2.39	0.102
N7-5.7B	0032120.3B	1.74	1.7091	1.7834	2.28	2.38	0.0991
N7-11.0	0032123.3	3.35	1.5850	1.6705	2.25	2.37	0.121
N7-11.0A	0032123.3A	3.35	1.6353	1.7171	2.26	2.38	0.113
N7-11.0B	0032123.3B	3.35	1.6318	1.7112	2.27	2.38	0.110
mean*	36 samples				2.25±0.03	2.36±0.02	0.104±0.013

Source: Roberts and Lin 1995 [159048]

NOTE: †Sample name consists of borehole designation followed by depth in feet below the template used to locate vertical boreholes.

*Statistical mean for 36 samples. Errors represent one standard deviation for all samples collectively.

6.2 SINGLE HEATER TEST (SHT)

The SHT was the first of several planned and conducted *in situ* thermal tests to investigate coupled processes in the local rock mass surrounding the potential repository. These coupled processes are thermally driven by heat released from an electrical heater that simulates heat from emplaced nuclear waste. The SHT is located in the same rock unit (Tptpmn) as the LBT, but the LBT block is from an outcrop while the SHT (and DST) are *in situ* or underground. More specifically, the SHT is located in Alcove 5 in the ESF as shown in Figure 6.2-1. The heating phase of the SHT started in August 1996 and continued for nine months until May 1997. The cooling phase continued for seven months until January 1998, at which time post-cooling characterization of the test block commenced. A detailed description of the SHT is in the *Single Heater Test Final Report* (CRWMS M&O 1999 [129261]).

The test block was characterized under ambient conditions prior to heater activation. Characterization included testing in the laboratory for thermal, mechanical, and hydrological properties, mineralogic-petrologic characteristics, as well as field measurements of permeabilities and fracture characteristics (CRWMS M&O 1996 [101428]).

SHT Input-DTNs and related information such as Q-status and respective locations in this report (figures, tables, and text) are tabulated in Table 4-2. SHT Output-DTNs are tabulated in Table 6.2-1.

A plan and cross section of the SHT are shown in Figure 6.2-2. The SHT block is approximately 12.9 m wide, 9.5 m deep and 5.5 m high. Forty-one boreholes with total length of 230 m are drilled into the block. Borehole 1 (shown in red in Figure 6.2-2) houses the single 5 m long heater capable of generating nominal 4 kW of heat. The other boreholes are installed with various equipment systems and sensors to monitor the thermal, mechanical, hydrological, and chemical responses of the rock as it was heated and cooled. Detailed description of the SHT as-built borehole locations is provided in Table 6.2-2. Coordinates of the various SHT sensors are provided in Appendix G of the *Single Heater Test Final Report* (CRWMS 1999 [129261]) and the respective Output-DTNs identified in Table 6.2-1. The origin of the SHT XYZ coordinate system is the center of the collar for the heater borehole. The X-axis is horizontal and positive to the right when facing the heater borehole, the Y-axis is also horizontal and follows the longitudinal direction of the heater borehole, and the Z-axis is vertical and positive in the upward direction. The borehole numbers in Figure 6.2-2 correspond to those in Table 6.2-2. Table 6.2-2 gives the sensor type or type of measurement for which any particular borehole is used. A total of 530 sensors were housed in the boreholes. Several boreholes were drilled for post-cooling characterization. The layout of the additional boreholes in the SHT block is shown in Table 6.2-3.

Most of the measurements made by the sensors were scanned and recorded by an automated Data Collection System (DCS). The central component of the DCS was a Geomation Model 2380 MCUs in NEMA-12 enclosure with a capacity of 640 channels. The DCS records the heater power and the readings of the thermocouples mounted on the heater itself every 15 minutes. The readings of the other sensors were recorded hourly. Certain measurements that were not recorded by the DCS included electrical resistivity tomography (ERT), neutron logging,

ground penetrating radar (GPR), Goodman Jack (borehole jack), pneumatic permeability, and infrared (IR) imaging.

The SHT DCS recorded thermal, hydrological (partial), and mechanical data, for the most part, on an hourly basis. The acquired data consists of both original (measured electronic values) and converted (engineering units). A package of data was submitted to the Records Processing Center (RPC) and a corresponding DTN: LA0002FH6001WP.001 [158278] was also obtained. This DCS-DTN is considered non-qualified because it is stored in the RPC but it does identify compact discs of identical qualified data that are distributed to the Thermal Test Team. These DCS-DTNs also identify scientific notebooks that provide details of SHT measurements including calibration information. These DCS-DTNs are reduced and re-structured and periodically submitted to the TDMS resulting in many of the Input-DTNs introduced below and listed in Table 4-2. As discussed in Section 1 and the introduction to Section 6, these Input-DTNs are further refined, reduced, and restructured before being resubmitted to the TDMS as Output-DTNs (see Table 6.2-1). In summary, the end user has access to three levels of data for SHT thermal, hydrological (partial), mechanical measurements: DCS-DTNs, Input-DTNs, and Output-DTNs. For most future applications, it is anticipated that end users will access the Output-DTNs because they are more user friendly.

6.2.1 SHT Thermal Measurements

Thermal measurements include the heater power and the temperatures at various locations in the test block. A detailed description of the thermal measurements discussed below can be found in Section 7.2 of the *Single Heater Test Final Report* (CRWMS M&O 1999 [129261]).

The Input-DTNs and Output-DTNs for SHT power and thermal measurements are listed in Tables 4-2 and 6.2-1, respectively.

6.2.1.1 Heater Power

The heater assembly for the SHT consisted of two single-ended 4,000-watt heating elements centered in a 5.4 cm (2.125 in.) diameter copper tube with a copper end cap at the bottom end. The two heating elements were contained in a nominally 2.5-cm (1-in.) diameter carbon-steel inner casing. The heating elements were made of nicrome and were each 5 m long, with a 180° bend at the bottom end. The design of the SHT heater allowed for one of the heating elements to act as a secondary heating source in the event that the other failed, or if additional heat needed to be added to the rock. The heater included a control loop that allowed for automatic switching from the primary element to the secondary element if the heater power dropped below a prescribed set point. Throughout the test, the heating elements were operated one at a time.

The heater power, voltage, and current were monitored using a Magtrol power monitor. The SHT called for the heater power to be nominally 4,000 watts for a period of nine months, followed by a cooldown period with the heater off completely. The cooldown period lasted approximately seven months.

The SHT power data may be found in Input-DTN SNF35110695001.008 [113812].

6.2.1.1.1 Results: Heater Power

The heater power history for the SHT over time periods of two weeks is illustrated in Figure 6.2.1.1-1. Power was applied to the heater starting on August 26, 1996, at 18:30:30 Universal Coordinated Time, time zero in Figure 6.2.1.1-1 showing the elapsed time from the activation of the heater. Between the time of activation and May 28, 1997, but omitting the anomalous data intervals and heater down times, the heater power output averaged approximately 3,800 watts.

The data indicate that the power output of the heater under normal operation declined by approximately 130 watts (3%) over the nine months that it was in operation. The heater was deactivated 275 days after being activated.

6.2.1.1.2 Measurement Uncertainty: Heater Power

The uncertainty in SHT power is similar to that discussed for the LBT in Section 6.1.1.1.2.

6.2.1.2 Temperatures

The thermocouple probes used in the SHT consist of Type-K thermocouples enclosed within 304 stainless steel, 0.64 cm (0.25 in.) diameter sheaths. The thermocouples within the sheaths were insulated from each other with magnesium oxide. Thermocouple probes were installed in seven boreholes in the rock mass around the heater to monitor temperature changes away from the heater. Three additional thermocouple probes were installed on the top, side, and bottom of the heater canister to monitor heater surface temperatures.

Five of the boreholes (boreholes 8–12) were drilled roughly parallel to the heater axis to a depth slightly exceeding the planned heater installation depth. Within these five boreholes, probes TMA-TC-1, TMA-TC-2, TMA-TC-3, TMA-TC-4, and TMA-TC-5 were located at nominal radial distances from the heater borehole of 0.4 m, 0.7 m, and 1.5 m, roughly corresponding to the numerically predicted temperature isotherms of 200°C, 150°C, and 100°C, respectively (CRWMS M&O 1996 [101375], pp. 3-2 and 3-5). Within each of these five boreholes, two thermocouple probes were installed. Two probes were required during test planning because the drift width was too narrow to allow installation of 8 m long thermocouple probes. Therefore, for each of these boreholes, two probes were used: one approximately 6 m long with ten Type-K thermocouple junctions spaced along its length (designated probe “A” for each borehole), and one approximately 2 m long with five Type-K thermocouple junctions spaced along its length (designated probe “B” for each borehole). The other two thermocouple probes (TMA-TC-6 and TMA-TC-7) were drilled perpendicular to the heater borehole from the Observation Drift and the Thermal-Mechanical Alcove Extension.

Temperatures were also measured on each of the free surfaces of the SHT block, using individual Type-K thermocouple junctions. Twelve individual thermocouples were installed on each face of the SHT block.

Temperatures were measured between the two layers of insulation on each of the three free surfaces of the SHT block, using individual thermistors. Five individual thermistors were installed between the layers of insulation on each face of the SHT block

The complete set of temperature data are provided in the Output-DTN identified in Table 6.2-1. The Output-DTN for the SHT temperature measured in the rock mass are organized into a series of EXCEL workbooks, one for each borehole, with temperatures sampled every fourteen days. Each of the workbooks contains two charts, with the data on an accompanying worksheet. The first chart shows the temperature history for thermocouples or RTDs. The second chart shows temperature profiles as a function of a spatial coordinate at various times during the SHT heating and cooling phases. The coordinates for borehole endpoints and corresponding sensors are also provided in the workbooks.

The SHT temperature data may be found in the Input-DTNs: SNF35110695001.008 [113812] and SNF35110695001.009 [113819].

6.2.1.2.1 Results: Temperatures

Because of the abundance of SHT temperature measurements, only representative discussion and graphics are provided below. All temperature data can be access in the Output-DTN identified in Table 6.2-1. Complete discussion of the SHT temperature data is documented in the *Single Heater Test Final Report* (CRWMS M&O 1999 [129261]).

The following discussion uses borehole 15 and borehole 1 to illustrate how temperature results are displayed in the output workbooks for individual boreholes. Borehole 15 is parallel to the x-direction and angles upward such that it extends above and beyond the heater as shown in Figure 6.2-2. Figures 6.2.1.2-1 and 6.2.1.2-2 present typical temperature history and temperature profile results for temperature sensors located in borehole 15. Figures 6.2.1.2-3 and 6.2.1.2-4 present the temperature history and temperature profile for borehole 1, respectively.

Expectedly, interruptions to heater power reduced the rock temperature but only slightly. When the heater was turned off after 275 days, the temperatures of the sensors dropped rapidly. The temperatures recorded by sensors closest to the center of the heater, which recorded the warmest temperatures, dropped more rapidly than the sensors further from the center of the heater. By 523 days after heater activation (after 248 days of cooling) the temperature recorded by the sensors in borehole 1 had cooled to between 23° and 32 °C.

6.2.1.2.2 Measurement Uncertainty: Temperatures

The uncertainty in SHT temperature measurements involves both RTDs and thermocouples. In general in the SHT, RTDs measured temperatures in the neutron boreholes and thermocouples measured temperatures in most other boreholes.

The RTD is accurate within 0.3^{o}C (Section 5.1 of the *Single Heater Test Status Report* (CRWMS M&O 1997 [101540])). With consideration of other factors, such as uncertainty in the location of the RTDs, the accuracy of the measured temperature in the SHT is estimated to be within 2°C. The RTD bundles were grouted in the boreholes, consequently some of the RTDs may not have had direct contact with the borehole wall. There may also have been some time delay between the temperature variations in the rock and that measured by the RTDs. But it is believed that this time delay was small because the rock mass was heated slowly. The thermocouple is accurate within 2.2^{o}C (Section 5.1 of the *Single Heater Test Status Report* (CRWMS M&O 1997

[101540])). With consideration of other factors, such as uncertainty in the location of the RTDs, the overall accuracy of the measured temperature in the SHT is estimated to be within 3.5°C.

6.2.1.3 Laboratory Thermal Conductivity

Four thermal conductivity tests and nine thermal expansion tests were performed (CRWMS M&O 1996 [101428]). The specimens tested represent Topopah Spring welded tuff specimens from the TSw2 thermal-mechanical unit and the Tptpmn lithostratigraphic unit. Cores from boreholes drilled into the SHT test block were used to prepare specimens for both mechanical and thermal properties testing in the laboratory.

The SHT Laboratory measured thermal conductivity may be found in the Input-DTN SNL22080196001.001 [109722].

6.2.1.3.1 Results: Laboratory Thermal Conductivity

Thermal conductivity data are tabulated in Table 6.2.1.3-1. The mean thermal conductivity and standard deviation about the mean are given at each temperature. It appears that temperature dependence on thermal conductivity is small. The sharp increase in thermal conductivity at 70°C reflects a change in instrumentation at that temperature.

6.2.1.3.2 Measurement Uncertainty: Laboratory Thermal Conductivity

Uncertainty in the laboratory measurement of thermal conductivity includes heterogeneity in the rock sample, temperature and insulator control, moisture determination, temperature effects, changes in instrumentation, and machine calibration. Most of these uncertainties are unquantifiable. In the case of machine calibration, if the error reached 4%, then it was recalibrated (CRWMS M&O 1996 [101428], p. 3-6).

6.2.2 SHT Hydrological Measurements

To assess the thermal-hydrologic processes in the SHT, the spatial distribution and the temporal variations of the moisture content in the rock mass were monitored. Electrical resistance tomography (ERT), ground penetrating radar (GPR), and neutron logging were used to monitor the moisture content. Air permeability was measured periodically to assess the changes in the fracture permeability during the test. Core samples collected from the SHT region were tested in the laboratory for some hydrological properties, such as porosity, density, and moisture retention curves. These will be presented in the following corresponding sections.

Detailed discussion of SHT hydrological measurements is documented in Sections 6.3 and 8 of the *Single Heater Test Final Report* (CRWMS M&O 1999 [129261]). Input-DTNs and Output-DTNs for SHT hydrological measurements are presented in Tables 4-2 and 6.2-1, respectively.

6.2.2.1 Electrical Resistance Tomography (ERT)

This section describes ERT surveys made during the SHT heating and cooling phases to map the changes in moisture content caused by heating. Of particular interest is the formation and movement of condensate within the fractured rock mass. Figure 6.2-2 in Section 6.2 shows the

relative position of the ERT (hydrological) boreholes in the SHT. Four inclined boreholes (24–27), forming a plane perpendicular to the heater axis, were used to position electrodes around the region of interest; this plane intersects the heater near its midpoint. Twenty-eight electrodes, equally spaced within the four boreholes, were used to conduct ERT surveys around the heater. The electrode spacing was about 30 cm with the electrodes grouted in the boreholes. Section 8.5 of the *Single Heater Test Final Report* (CRWMS M&O 1999 [129261]) presents the ERT in detail. All of the SHT ERT data can be found in the TDMS under the following Input-DTNs: LL970101004244.026 [158281], LL970505404244.031 [148609], LL971002904244.044 [158286], and LL980105204244.049 [148610].

6.2.2.1.1 Results: ERT

The discussion of the ERT data reduction can be found in Section 6.1.2.1.1. The saturation estimates produced by data reduction model 2, which assumes that the primary pathway of the electrical current is through the double layer (Section 6.1.2.1.1), are presented below. The interpretation of ERT results of the SHT are shown in Figures 6.2.2.1-1 and 6.2.2.1-2, for the heating phase and the cooling phase respectively. The drying and wetting regions in these figures are based on hand tracings made over the model 2 saturation estimates.

In general, the outline of the drying and wetting regions roughly coincide with saturations equal to 70% or less for the drying zone and 98% or more for the wetting zone. A significant region of drying is present around the heater. The dry zone is not centered on the heater and certainly is not symmetric about the heater. The pattern suggests a distribution of moisture that is strongly controlled by fractures. As time increases, the drying zone appears to propagate upward, especially after 219 days of heating; also, the minimum saturation estimate was near 10 percent. During the cooling phase, the dry zone around the heater appears to remain relatively stable; an exception to this observation is the result from September 25, 1997, which showed a change in the dry zone near the heater's location. At the end of the cooling phase, the image (December 17, 1997) still shows a clear dry zone around the heater and significant wetting regions on the lower left flank of the heater.

6.2.2.1.2 Measurement Uncertainty: ERT

Many factors may contribute to the uncertainty in the saturation changes in the rock mass estimated from ERT. The measurements of the voltage and current at the electrodes are fairly accurate. More importantly, the saturation estimates presented here are impacted by one or more of the following factors:

- The accuracy of the temperature maps in the vertical direction is limited by the sparse vertical coverage of the temperature sensors. Errors in the interpolated/extrapolated temperature maps will result in erroneous saturation estimates.

- The presence of metal in the SHT block such as the heater resulted in measurement interference.

- Other uncertainty factors that impact the ERT are similar to those listed in Section 6.1.2.1.3.

6.2.2.2 Ground Penetrating Radar (GPR)

This section describes the borehole radar tomography experiment conducted in the SHT block. In the borehole radar method, high frequency electromagnetic signals are transmitted from modified GPR antennas in one borehole through subsurface material to a receiving antenna in another borehole. Moisture content in the rock strongly influences the propagation of the signal, i.e., whether it travels at a high or low velocity or whether it is highly attenuated. The high dielectric permittivity of water—in contrast to dry rock—typically results in greatly reduced signal velocities. The cross-borehole transmitted signals may be represented as multiple raypaths crossing through the zone of interest. If sufficient raypaths are recorded, a tomographic image may be obtained through computer processing. The processed tomogram, containing the transit time (which depends on the wave velocity), and the amplitude (which depends on the wave attenuation), offers a high-resolution approach to monitoring the thermally induced spatial redistribution of the moisture content within the rock mass. The effect of temperature on radar measurements and its impact on moisture content estimation is included in the processing methodology.

The borehole radar field surveys were conducted in boreholes 15, 17, 22, and 23 (see Section 6.2, Figure 6.2-2). These same boreholes are used for neutron logging as discussed in the following Section 6.2.3. Boreholes 22 and 23 are collared from the Observation Drift and boreholes 15 and 17 are collared from the Thermal-Mechanical Alcove Extension. The boreholes are drilled several degrees off horizontal into the drift, cased with a Teflon liner and grouted into place. Each pair of boreholes defines a two-dimensional plane transverse to the heater assembly at mid-length and trending towards this assembly. In the case of boreholes 15 and 17, this plane actually extends across the strike of the heater. This is not the case with boreholes 22 and 23, which stop just short of the heater.

A pulse EKKO 100 radar system was used for the radar data acquisition in the SHT. Section 8.3 of the *Single Heater Test Final Report* (CRWMS 1999 [129261]) presents the GPR data acquisition in detail. Five separate surveys were performed using the borehole pairs. The first data set was acquired on August 22, 1996 before the heater was turned on (time = T0). Three data sets were acquired during heating: on January 15, 1997, 3 months after heating began (T1); on March 12, 1997, 5 months after heating began (T2); and on May 29, 1997, 9 months after heating and 1 day into cooling (T3). The fifth data set was acquired on January 7, 1998, a little over 7 months after the heater was turned off (T4). The complete set of GPR data for borehole pair 15 to 17[1] can be found in the TDMS under Input-DTN LB980901123142.003 [119016].

The crosshole radar data collection was performed using two acquisition modes. The first was a Zero Offset Profile (ZOP), in which the transmitter and receiver antennas were positioned within the boreholes at equal depths such that there was no vertical offset. The second was a Multiple Offset Profile (MOP), in which the receiving antenna remained at a fixed depth while the transmitter antenna was moved incrementally in the second borehole. Each multiple offset profile constitutes a “receiver gather.” In the SHT surveys, the transmitter and receiver intervals

[1] Radar data for the SHT started out as a scoping study to test out feasibility of the method. When the data from borehole pair 22 to 23 were found similar to that from borehole pair 15 to 17, data acquisition in the former pair was stopped after the first three surveys.

were located every 0.25 meters. Each of the necessary raypaths was collected and recorded for the subsequent tomographic processing.

Over the course of the heater experiment, the radar system was operated by using identical acquisition parameters for each of the five field surveys. No adjustments, filters, or gains were applied to the stored raw data. Therefore, data acquisition (and hence data repeatability) was the same regardless of who operated the system and when—so long as the antenna configuration was the same. Data repeatability is tantamount to successful tomographic differencing and interpretation. Small deviations in experimental methodology at such close spacing can result in large discrepancies in data processing.

Further, accurate travel times between the transmitter and receiver antennas must be obtained from the radar data to invert for the velocity structure between boreholes. Hence, it is important to know the precise time when the transmitter fires (known as zero time). An accurate measure of zero time throughout the surveys was obtained by direct airwave measurements (the signal from transmitter antenna to receiver antenna in air) with the antennas held together in air and at the borehole collars in air.

6.2.2.2.1 Results: GPR

The boreholes 15 and 17 are 0.785 meters apart at their collars at the alcove wall and deviate to approximately 4.0 meters at their endpoints while remaining in the same plane. Accurate coordinates for each transmitter and receiver point (which are at 0.25-meter intervals) were determined using the surveyed borehole coordinates. Each multiple offset profile constitutes a "receiver gather" (one receiver depth and many transmitter depths), and a series of these gathers are used to construct tomographic images.

Figure 6.2.2.2-1 shows two typical receiver gathers for the 15-17 borehole pair. The time scale along each trace is in nanoseconds. The travel times are picked at the moment of first arrival of energy, as marked for example in Figure 6.2.2.2-1. The input data (DTN LB980901123142.003 [119016]) on the TDMS consist of the XYZ coordinates of the transmitter (borehole 15) and receiver (borehole 17) and the respective picked travel times for each survey.

Figures 6.2.2.2-2A–D show the velocity (in a 4.25 m × 8.5 m field in the plane of boreholes 15 and 17) for the surveys taken 5, 7, 9, and 12 months after the start of heating.

Changes in moisture content (rather than the absolute moisture content) are of primary interest. Therefore, it is useful to subtract the velocity values between two tomograms since velocities relate directly to liquid saturation. The baseline velocity tomogram is subtracted from the four post-heating velocity tomograms, producing four velocity-difference tomograms: T1-T0, T2-T0, T3-T0, and T4-T0. The difference tomograms are shown in Figures 6.2.2.2-3A–D. The average absolute velocity value is about 0.1 m/ns, so a difference value of 0.01 m/ns is about a 10% change in velocity. The tomograms all show significant velocity increases and decreases. In general, radar velocities will decrease with temperature increase and increase with water content decrease. So an increase in velocity, as seen near the heater, shows that the velocity increase caused by drying (decrease in water content) is greater than the velocity decrease, associated with temperature increase.

The derived tomograms are submitted as output associated with this report under Output-DTN LB0208GPRSHTCP, as identified in Table 6.2-1.

6.2.2.2.2 Measurement Uncertainty: GPR

The uncertainties associated with data acquisition and processing were small and were discussed in the previous sections. They include:

- Relocation errors of the transmitters and receivers for each survey. The antenna were relocated to within one centimeter.

- Zero time shift. The methodology employed reduced zero time errors to less than 0.5 ns.

- Travel time picking errors less than one sample, or 0.2 ns. The travel times must be picked very accurately: due to the short distance between boreholes, small errors in geometry and travel-time picks can have a significant effect on the results. The accuracy and repeatability of the picks is better than one sample (0.2 ns) over a 20 ns travel time. Despite the low signal amplitudes, a sufficient number of travel times could be picked to obtain an estimate of the two-dimensional interborehole velocity structure, based on an inversion as described in Peterson (1986 [101698]). Any error in picking is dependent primarily on the zero time adjustment and the repeatability of transmitter/receiver locations. These are both quite accurate.

- Inversion errors, which can be calculated to be less than 0.03 ns.

Though the results presented here in terms of difference in velocities are quite accurate, converting these results to water content and liquid saturation would involve assumptions regarding porosity, temperature, and locations of the radar survey.

6.2.2.3 Neutron Logging

Neutron logging is used to determine moisture content in rocks and soils. Neutron logging was used to monitor moisture content in boreholes 15, 17, 22, and 23 (see Figure 6.2-2) during the SHT. The neutron probe used in this test is a Campbell Pacific Nuclear model 503DR. A 3.81 cm (1.5 in.) diameter probe (serial number H37067677) was used for the SHT. Under ambient conditions, the sampling volume surrounding the probe has a diameter of approximately 15 cm; this volume diameter increases as moisture content decreases.

For the SHT, a Teflon™ tube, with an RTD bundle mounted on its outside, was inserted into the boreholes and grouted into place. The Teflon™ tube permitted easy insertion, placement, and removal of the tool. Neutron counts were measured in each borehole at 10 cm intervals. Calibrations to known moisture contents were conducted for the neutron tool in a liner-RTD-grout assembly identical to that used in the SHT boreholes. Water content was calculated from the neutron counts using the calibration results.

The pre-heating neutron loggings were conducted on August 21, 1996, prior to initiation of heating (August 26, 1996). A total of eighteen neutron loggings were conducted in each of the

four neutron boreholes in the SHT. Section 8.6 of the Single Heater Test Final Report carries detailed descriptions of the neutron logging. The SHT neutron data can be found in the TDMS under Input-DTN LL980106904244.051 [118963].

6.2.2.3.1 Results: Neutron Logging

The neutron results are presented as the difference in water content between the heating/cooling measurements and the pre-heating baselines. Positive difference fraction volume water means gaining moisture content; negative difference fraction volume water means drying. To calculate water saturation, one can simply divide the fraction volume water content by the porosity. All of the neutron results were smoothed to remove some variations, but without changing their amplitudes very much.

As examples of the neutron results in the SHT, Figures 6.2.2.3-1 and 6.2.2.3-2 show the difference fraction volume water in borehole 15 as a function of depth from the collar, at the end of the heating phase and the end of the cooling phase, respectively. The shortest distance between the borehole and the heater is about 2.07 m, at approximately 5.75 m from the collar of the borehole. The peak temperature in this borehole before the heater was de-energized was approximately 62°C. The drying reached approximately 0.004 on May 21, 1997. During the cooling phase, the neutron results show a slight rewetting, especially at the closest point between the heater and the borehole.

The neutron logging in the SHT region displayed changes in the moisture content in the heated rock mass. The degree of drying seemed in good correlation with the temperatures in the rock. The decreases in water content for the drying regions were small, because the neutron logging boreholes were not close to the heater. Rewetting was observed at a few localized regions during the cooling phase. The amplitude of the rewetting was small.

6.2.2.3.2 Measurement Uncertainty: Neutron Logging

The uncertainty of the neutron logging itself is about 0.1% volume water content. For clarity, saturation refers to percent of moisture in air voids (porosity) and water content refers to fraction of rock volume occupied by moisture. Measurements are sensitive to the presence of elements, such as chlorine and boron, that have large neutron-capture cross sections. The uncertainty caused by those minerals is difficult to assess, but probably not significant in the tuff.

Under ambient conditions, the sampling volume surrounding the probe has a diameter of approximately 15 cm; this volume diameter increases as moisture content decreases. The neutron tool was calibrated to the exact liner-RTD bundle-grout, but variations in the grout volume along a borehole (possibly caused by changes in the borehole diameter, break-out regions, etc.) will introduce uncertainty in the measured results. It is assumed that the water content in the cured grout does not change during the course of the test. If the temperature causes the grout to de-hydrate, it will affect the neutron results, because the neutron tool is very close to the grout column.

6.2.2.4 Active Pneumatic Testing and Passive Hydrological Monitoring

Pre-Heating Air Injection

Characterization by means of air-injection tests, prior to the onset of heating, provides an estimate of the fracture permeability in the test block. Air-permeability testing in the SHT block was performed prior to the heating phase in boreholes 1–31 as shown in Figure 6.2-2. The pre-heating air injection data, which have been submitted under Input-DTN LB960500834244.001 [105587], contain 47 files of pressure, temperature, and flow data from each air-injection test, located in TDMS data tables S97535_001 through S97535_047. Data include the change in pressure from initial pressure in each borehole (ΔkPa), as well as columns of data containing the injection flow rate (SLPM for standard liters per minute), the barometric pressure (kPa), the relative humidity (%), and temperature (°C). Permeabilities estimated from injections tests performed in a short straddle packer in borehole 6 are found in TDMS data table S97535_048. Permeabilities estimated from injection tests performed in SHT boreholes isolated a single pneumatic packer at the collar of the borehole are found in TDMS data table S97535_049.

Heating/Cooling Air Injection and Passive Monitoring

During the heating and subsequent cooling phase, air-injection tests were periodically performed in boreholes 16 and 18 to provide information on the changes in flow arising from coupled thermal-hydrological processes. In boreholes 16 and 18 are strings of four pneumatically inflated packers to isolate the borehole into different instrumented intervals, numbered from the closest to the collar of the borehole, 1, to the deepest, 4. Behind each packer are relative humidity, temperature, and pressure transducers. The eight instrumented intervals are referred to by borehole number followed by the instrument interval number, i.e., 18-3 is the third instrument cluster from the collar in borehole 18. Injection tests were performed in three zones: (1) zone 1 between inflated packers 1 and 3 with packer 2 deflated, (2) zone 2 between inflated packers 2 and 4 with packer 3 deflated, and (3) zone 3 between inflated packer 4 and borehole bottom with all packers inflated. Measurement data associated with the quarterly injection tests were submitted to the TDMS under the following Input-DTNs: LB970100123142.001 [158287], LB980120123142.008 [158280], LB970500123142.001 [158293], LB0204SHAIRK3Q.001 [159543], and LB971000123142.001 [118965]. The heading of the data reports contains a description of the data in comma-separated format.

When air-injection testing was not in progress, the packers in boreholes 16 and 18 were left inflated, and pressure, temperature, and relative humidity sensors were used for passive monitoring of the heater test. Passive monitoring data from August 1996 through December 1997 can be found in the Input-DTN LB980901123142.002 [119009].

Post-cooling Air Injection Characterization and Tracer Tests

Post-cooling characterization by air injection was done during the third and fourth weeks of January 1998. Of the original 31 SHT boreholes, only boreholes 1, 3, 6, 7, and 19 were available for post-cooling air-injection testing. The other 26 boreholes contained grouted instrumentation and were not accessible. The post-cooling characterization strategy was to duplicate the pre-heating characterization test conditions when feasible. Therefore, inflatable packers were

installed near the collar of boreholes 3, 6, 7, and 19 to depths identical to those of their pre-heating characterization positions. The hydrology boreholes 16 and 18 were already equipped with packer strings for the duration of the SHT and were not modified for post-cooling characterization.

As part of the post-cooling characterization, gas tracer tests were conducted between borehole 1, the heater borehole, and boreholes 16 and 18. The purpose of the tracer tests was to gain a better understanding of the hydrological conditions that permitted rapid vapor transport from the heater borehole 1 vicinity into borehole 16 resulting in water accumulation in borehole 16. The gas tracer testing data, together with the post-cooling air-injection data, are located under the Input-DTN LB980901123142.001 [118999] in the TDMS.

The results of the pneumatic tests and passive monitoring data will be briefly summarized in Section 6.2.2.4.1. For a more detailed description and discussion of the measurements and results, readers are referred to Sections 8.1 and 8.2 of the *Single Heater Test Final Report* (CRWMS M&O 1999 [129261]), and the references therein. The Output-DTN is listed in Table 6.2-1.

6.2.2.4.1 Results: Active Pneumatic Testing and Passive Hydrological Monitoring

Estimated permeabilities from pre-heating air-injection tests have been calculated using Equation 5.1-1 and appear in Tables 6.2.2.4-1 and 6.2.2.4-2. The three-orders-of-magnitude range in the permeability values can be attributed to flow through fractures of hierarchical scales, with the microfractures accounting for the lower values, and longer fractures (a few meters in extent) responsible for the higher values.

Changes in the permeabilities for borehole 16 and 18 during heating and cooling are shown in Figure 6.2.2.4-1 as a ratio of transient permeabilities to pre-heating (baseline) value. For both 16-4 and 18-4, a decrease in permeability is shown after the initiation of heating, followed by an increase after heating has concluded. This decrease is interpreted as an increase in fracture liquid saturation, decreasing the relative gas-phase permeability. Similarly, the increase is attributed to the drainage of the water from the fractures. The increase between the baseline permeability and post-cooling estimates in the back zone of borehole 16 and 18 may result from lower fracture saturations after heating, because of the reduced saturation in the vicinity of the heater borehole, or to overall opening of fractures.

Pressure, temperature, and relative humidity in boreholes 16 and 18 were continuously monitored during heating and cooling. Figures 6.2.2.4-2, 6.2.2.4-3, and 6.2.2.4-4 show the temperature, humidity and pressure data, respectively. The pressure buildup in sensor 16-4 reflects accumulation of water in borehole 16 during the heating phase. A rise in pressure was discernable after only a few days of heating, indicating that water was rapidly mobilized from very near heater borehole 1 to 16-4. Each drop in pressure at 16-4 shown in Figure 6.2.2.4-4 data reflects the sampling of water that had accumulated in the borehole.

Post cooling site characterization activities began in January 1998. Table 6.2.2.4-3 shows the post-cooling air-permeability values of various injection zones estimated using Equation 5.2-1. Table 6.2.2.4-4 shows a comparison of permeability estimates from pre-heating and post-cooling

measurements using data from injections into boreholes 3, 6, 7, 16, 18, and 19. Direct comparison is possible in these boreholes because of the identical pre-heating and post-cooling packer configurations. The post-cooling and pre-heating permeability values in these boreholes have the same order of magnitude. Furthermore, a study of the cross-borehole steady-state pressure response show that they are also comparable under pre-heating and post-cooling conditions (i.e., the data do not reveal that the pneumatic connectivity between the boreholes tested had been significantly altered by heating and cooling). The ratios of post to pre-heating permeability values (Table 6.2.2.4-4), however, show that a consistent upward trend in the permeability values from pre-heating to post-cooling. This increase in permeability, ranging from about 20% to a factor of 3.5, may be attributed to opening of fractures from heating.

Post-cooling air-injection tests were also utilized to test the hypothesis that a fast path for vapor transport exists between heater borehole 1 and borehole 16, and that it was responsible for the accumulation of condensed water in borehole 16, zone 3. With this in mind, air-permeability tests were carried out in a multizone configuration for boreholes 1, 16, and 18. Specifically, injection was conducted in six consecutive zones in the heater borehole 1, and the cross-borehole pressure response in the zones behind the 4th packer (referred to as zone 3 earlier) in boreholes 16 and 18 were measured to identify plausible fast-path connections. Upon conclusion of air permeability tests, gas tracer tests were also performed between the heater borehole 1 and boreholes 16 and 18 to investigate the possible presence of fast paths for vapor transport.

For the gas tracer tests, zone 3, behind the 4^{th} packer in boreholes 16 and 18, has chosen as the tracer withdrawal interval, and borehole 1 was chosen as the tracer injection borehole. Based on the results of the post-cooling air-permeability tests, two intervals in borehole 1 that gave the largest cross-borehole pressure response were selected for gas tracer injections. The first interval, extending from 3.83 m to 4.42 m from the collar of the borehole, produced a strong pressure response in zone 3 of borehole 16 and a much weaker response in zone 3 of borehole 18. The second interval, between 5.05 m and 5.64 m as measured from (the collar of the borehole), produced a stronger response in zone 3 of borehole 18 than in zone 3 of borehole 16.

The perpendicular layout between borehole 1 and boreholes 16 and 18, which significantly complicates transport geometry, made the test results less amenable to detailed transport analysis. The purpose of the tracer testing was to gain an understanding of the rapid gas flux that gave rise to the observed presence of water (condensate) into the back of borehole 16, as opposed to borehole 18, from which no condensate had been sampled. Thus, it was determined to focus on the first arrival of tracer and only qualitatively examine the rate at which cumulative mass recovery occurred.

The results of five gas tracer tests are shown in Table 6.2.2.4-5. Tracer transport from zone 3 of borehole 1 to zone 3 of borehole 16 was extremely rapid, with 100% tracer recovery occurring within 30 minutes from injection. First arrival of tracer to zone 3 of borehole 18 took more than twice as long and 100% tracer recovery took approximately 15 hours. The differences in the transport times and recovery efficiencies suggests that the path between zone 3 of borehole 18 and borehole 1 is much more tortuous and indirect than the path between zone 3 of borehole 16 and borehole 1. This, together with the results of air-permeability tests, support the hypothesis of a direct fracture connection between borehole 1 and zone 3 of borehole 16 that allows for rapid

vapor transport. This direct fracture connection was subsequently confirmed by visual inspection of the over cores of borehole 16.

6.2.2.4.2 Measurement Uncertainty: Active Pneumatic Testing and Passive Hydrological Monitoring

Assumptions about the validity and accuracy of the acquired data of humidity, temperature, gas flowrate and pressure vary, depending on the sensor and the method by which the sensor is used to perform the measurement. Accuracy as used here is defined as combined nonlinearity, hysteresis, and nonrepeatability. The data acquisition equipment used to record the sensor signal can introduce an inaccuracy into the measurement of the sensor output. However, here the accuracy and repeatability of the acquisition system (Keithley model 2001 Digital Multimeters were used) far exceeds the limitations of the sensors being employed. The accuracy of the Keithley 2001 Digital Multimeter is approximately 25 ppm of the full scale output (FSO) for voltage measurements and 56 ppm of the FSO for resistance measurements. Limitations of the data acquisition systems can therefore be neglected in further discussion.

In the pre-heating and post-heating air-injection testing, pressure measurements were performed using Setra Model 204C pressure sensors. These sensors have an accuracy of 0.2% FSO. Borehole 16 and 18 sensors used Endevco Model 8520A-50 sensors, which also have an accuracy of 0.2% FSO. However, heating/cooling measurements of pressure by the eight Endevco sensors installed in the heated region indicated a significant thermal shift, ranging from 1% to 1.5% over the temperature range 10°C to 150°C. Vaisala Model HMP235-A humidity sensors were used to monitor temperature and relative humidity (RH) within boreholes 16 and 18. The humidity measurement has a tolerance of ±1.0% RH below 90% RH and an accuracy of ±2.0% RH above 90% RH. The temperature measurement performed with the HMP235-A has an accuracy of ±0.2°C. Sierra Instruments Model 840 Mass Flow Controllers (MFC) were used to monitor gas injection flow rates. Sierra Instruments specifies an accuracy of ±1.0% FSO. However, in thermal testing field conditions, the accuracy is derated to ±10.0% FSO. This derating of performance reflects the sensitivity of the MFC to the shock, vibration, and dust that it is subjected to during underground testing.

Short circuiting of gas flow caused by the high density of boreholes within the test block may increase the estimated permeability. The degree to which borehole short circuiting of fractures influences the estimated permeability is difficult to estimate. However, the range of values obtained here does not significantly differ from values obtained in the Drift Scale Test (Section 6.3.2.4) or from surface-based boreholes.

6.2.2.5 Laboratory Parameters—Saturation, Porosity, Density, Moisture Retention Curves

Pre-Heating

As part of the pre-heating characterization, laboratory measurements of saturation, porosity, bulk density, particle density, and gravimetric water content for cores from the SHT area were conducted. These studies aim to determine the amount of pore water available for evaporation and boiling during the heating phase. Hydrological laboratory measurements were carried out for

grab samples from wet excavation of the Observation Drift, and for cores, wrapped in sealed packets after coring from three wet-drilled boreholes (boreholes 1, 6, 5) in the SHT block. The grab samples, nominally 12" × 12" × 6" in size, were broken open with a jackhammer to retrieve samples (200 to 700 g in mass) from the interior regions away from drying surfaces. The results of these measurements have been submitted to the TDMS under DTN LB970500123142.003 [131500]. Detailed discussion of these measurements can be found in the *Single Heater Test Final Report* (CRWMS M&O 1999 [129261]).

In addition to the above parameters, moisture retention curves were also measured, at temperatures of 25.1°C, 49.6°C and 93.7°C for 11 SHT core samples from boreholes 20 (CHE-1) and 21 (CHE-2). Prior to the retention-curve measurements, the dry bulk density, the saturated bulk density and porosity of these samples were determined at room temperature. The results of these measurements are extracted from a report by Lin et al. (2002 [159099]). Data for 25.1°C before heating can be found in the TDMS under Input-DTN LL970709004244.035 [127312].

Post-cooling

A number of boreholes were dry-drilled following the termination of the cooling phase of the SHT for post-cooling characterization. In particular, protected (wrapped and sealed) cores from three dry-drilled boreholes (boreholes 199, 200, 201) were tested for porosity, density, and water content or liquid saturation. The locations of these protected cores (Table 6.2-3) were designed to pass through both the anticipated "dry-out" and "condensing" regions developing in the SHT block as a result of the heating. While the quantities measured and the methodology of these post-cooling laboratory measurements remain the same as their pre-heating counterparts, the focus here in the post-cooling effort is substantially different. In the pre-heating results, the intent is to estimate an average initial liquid saturation of the matrix cores; in the post-cooling results, the focus is on the change from their initial value as a result of thermal-hydrological coupled processes, and more importantly, the spatial location of the cores (with respect to the heater) where changes have occurred. The data have been submitted to the TDMS under the Input-DTN LB980901123142.006 [119029].

6.2.2.5.1 Results: Laboratory Parameters—Saturation, Porosity, Density, Moisture Retention Curves

Pre-Heating

The measurements of wet-drilled cores from boreholes 1, 6, and 5 of the SHT are shown in Table 6.2.2.5-1. These laboratory measurements were conducted following the Technical Implementation Procedure YMP-LBNL-TIP-AFT 2.0. Samples were placed in containers with tight-fitting lids and immediately weighed. The samples were subsequently oven-dried at a temperature between 100°C to 110°C, until they reached a constant weight (from several weighings). They were then placed in a desiccator, cooled, and weighed to determine the gravimetric water content. The samples were then water-saturated in a vacuum chamber, after which they were weighed following the method of Archimedes (i.e., immersed in air and water) to determine the weight under conditions of full saturation and the sample bulk volume. Knowledge of the dry weight, saturated weight, and sample bulk volume were used to calculate bulk density, porosity, and particle density.

Table 6.2.2.5-1 shows that saturation is approximately 95%. The variability of rock properties is evident. In the core processing procedure, any observation of factors potentially affecting the results is recorded. The abbreviated description for each core with abnormal features is included in the table footnotes. This "soft" information forms the basis for distinguishing cores that yield reliable weight measurement from cores that give potentially abnormal and inaccurate measurements. Large fractures with porous infill material generally introduce greater inaccuracy into the weight measurement. In the resaturation step needed to determine total pore volume with cores stored in water, debris is sometimes observed. Cyclic resaturation steps are used to quantify and to compensate for solid losses.

The data from two grab samples from the wet excavation of the Observation Drift near the SHT block are shown in Table 6.2.2.5-2. Five subsamples were tested.

One of the subsamples had an 81% saturation, while the saturation of the other four subsamples exceeded 94%. These measurements provide the only site-specific data for liquid saturation at the onset of the SHT. Consequently, those values resulted in using 92% initial saturation in modeling of the SHT.

Bulk density and porosity of the 11 core samples intended for moisture retention curves are shown in Table 6.2.2.5-3. These specimens have no obvious large cavities and inhomogeneous inclusions. The specimens were dried in a vacuum oven at a temperature of about 35°C until their weights became constant for several days. Dry bulk density was calculated by dividing the dry weight with the specimen volume. The specimens were than saturated with water under vacuum condition and remained in water until their weights were constant for several days. Saturated bulk density was calculated from the saturated weights. Porosity was calculated by subtracting the dry density from the saturated density, and dividing by the density of water. The average porosity for these samples is 11.1± 1.1%.

To start the moisture retention curve measurement in the wetting cycle at room temperature, the specimens were dried and placed in the relative humidity (RH) chamber at about 25°C and 20% RH. The sample weights were determined daily. When the weights reached a constant value for several days, it was assumed that equilibrium was established, and the sample weights were used to calculate the saturation level at that RH condition. Saturation was calculated by comparing the measured weights with dry weights and taking into account porosity. Then the RH was increased to 35%, and the procedures were repeated. This was repeated for the higher RH levels at 50, 65, 80, and 95%. After this, the RH was decreased according to the following steps: 80, 65, 50, 35, and 20% to start the measurements in the drying cycle at room temperature. The maximum saturation achieved at the highest RH was between 30% and 40% (see below). The process was then repeated for the drying portion of the measurement. This cycle of measurement was repeated at different temperatures, 50°C and 94ºC, without the measurements at 35 and 65% RH.

Moisture retention curves of the SHT specimens at a temperature of 25.1°C are shown in Figure 6.2.2.5-1. Only the "average" properties are shown for clarity. The averages are the mean saturation and matric potential of all 11 specimens. The error bars for saturation are the standard deviation from the average saturation at a matric potential level of all samples. There is very little hysteresis at all temperatures. The temperature cycle has a very small effect on moisture

retention: the post-temperature-cycle data show slightly smaller moisture retention than the first room-temperature data.

The moisture-retention curves are dependent on temperature. The effect is not significant between 25°C and 50°C, but seems to be significant between 50°C and 94°C. The temperature effect on the moisture-retention curves is always to decrease the level of saturation at a matric potential level with increasing temperature. The SHT samples show greater moisture retention than the DST samples (as shown in Section 6.3.2.5) at all temperatures. The difference decreases slightly with increasing temperature. The maximum saturation that can be reached in those samples depends on temperature. At 25.1°C, the maximum saturation achieved is about 36%. At 49.6°C, this increases to about 39%, but at 93.7°C it decreases to about 29%.

Post-cooling

Boreholes 199, 200, and 201 were dry drilled after cooling for the purpose of evaluating moisture movement. Figure 6.2.2.5-2 plots the liquid saturation of all cores tested, in their respective locations, in XZ view. Locations of the cores along the borehole are identified by the last two digits of their Sample Management Facility (SMF) ID, shown in the legend. The two dashed circles, with radius of 1 m and 3 m respectively from the heater, delineate the anticipated drying zone (approximately within the inner circle), and the wetting region (between the two circles). The radial symmetry does not account for gravity drainage of the condensate, hence borehole 201 was drilled at a steep angle in order to access rock at depth over 3 m below the heater horizon, with the intention of investigating the importance of condensate drainage via the fractures.

Table 6.2.2.5-4 presents laboratory-determined saturation, porosity, and particle density. Average porosity and particle density values are given at the end of the table. An average value for liquid saturation is not a meaningful parameter in these post-cooling cores, because liquid saturation of the cores reflects the thermal-hydrological processes that have taken place in the SHT, and their importance lies in their spatial variability with respect to the heat source. The porosity of three core samples (local ID H-1, H-22, H-27) is exceptionally high, and is attributed to visible evidence of fractures. In turn, the liquid saturation of these samples would be less reliable.

Saturation for cores along borehole 201 is relatively uniform. Excluding the two samples with large porosity, liquid saturation for all cores along borehole 201 is within 2% of their average 86%. For the cores along boreholes 199 and 200, note the following: (a) drying due to heat has occurred near the heater, as evidenced by the lower liquid saturation of cores within the 1 m radius from the heater; (b) the liquid saturations in the anticipated “condensing” zone between two circles are generally lower than those values in borehole 201; and (c) the liquid saturation seems to be higher below the heater horizon than above. These observations are consistent with a scenario stipulating that condensate is not held in the matrix (thus elevating its liquid saturation) but is drained through fractures of hierarchical scales. Drainage through the microscopic fractures account for the slightly drier cores above the heater horizon in borehole 199 than below the heater horizon in borehole 200. Drainage through larger fractures extending a few meters accounts for the overall wetter cores in borehole 201 than those in the “condensing” zones in boreholes 199 and 200.

6.2.2.5.2 Measurement Uncertainty: Laboratory Parameters—Saturation, Porosity, Density, Moisture Retention Curves

Saturation, Porosity, Bulk Density

Factors that can affect accuracy of laboratory measurements include

- Ability to account for all moisture in the rock sample because of the condensation of water on walls of core container. These are estimated by absorbing water from the container with a paper cloth and weighing the cloth.
- Large fractures and cores with infill material generally introduce greater inaccuracy in the weight measurements.
- Averages and standard deviations introduce a measure of data uncertainty.

Also, in Tables 6.2.2.5-1 and 6.2.2.5-2, observations of factors that may potentially affect the results are included in the table footnotes.

Moisture Retention Curves

A balance with a sensitivity of 0.01 mg calibrated to a traceable standard was used to weigh the samples. Saturation was calculated by comparing weights with dry weights and taking into account porosity. One difficulty was the establishment of steady weight values at the highest humidities, particularly at high temperatures. The reasons for this difficulty are that the RH is difficult to control at the highest settings and the weight of the samples is more sensitive to changes in RH at the highest settings. Refinement of the control parameters on the humidity chambers aided in solving this problem.

The measurement uncertainty involved in determining the moisture-retention curves include the measurements of weights, relative humidity, and sample size. The sample dimensions are used to determine sample wet and dry densities. It is estimated that the thickness of the sample can be determined to ± 0.005 mm and diameter to ± 0.05 mm. For the samples used here, this results in an error in sample volume of ~± 0.3%. The uncertainty in dry weight is estimated to be ~0.00002 g and for wet weight ~0.0001 g. The error in the wet weight is higher than that of the dry condition because of the difficulty in achieving and maintaining saturation levels of 100%. These uncertainties result in errors in dry and wet densities of ~0.3%.

When repetitive measurements are made on samples over a period of several days, such as the determination of weights at a specified RH, for example, the uncertainty in the measurement is often less than the statistical uncertainty in the mean of the measured parameter. In such cases, the error is taken as one standard deviation of the mean. The errors in saturation determined at specific temperature and RH are estimated to vary from ~0.07 to 0.5% water saturation which includes errors associated with dry and wet densities discussed above. Thus, the relative uncertainty is estimated to be between ~1 and 10%, with a 1–2% error most common.

The uncertainty in the relative humidity is approximately ± 2% RH. When propagated through Kelvin's equation to matric potential, the absolute uncertainties are fairly low, but the relative

uncertainties are high at the matric potentials closest to zero (as much as 200% at a matric potential of -1.36 ± 2.73 MPa).

6.2.3 SHT Mechanical Measurements

The discussion of mechanical data for the SHT has been divided into several subsections, based on the type of measurement:

- Multi-point borehole extensometer (MPBX) displacements were measured within the rock mass surrounding the SHT. These measurements were used to evaluate numerical models related to thermal-hydrological-mechanical coupling as well as to provide data for determination of rock mass thermal expansion.

- Wire and tape extensometer measurements were used to measure movement of the free surfaces of the SHT block.

- Borehole jack tests were performed to measure rock mass modulus at ambient and elevated temperatures.

- Rock bolt loading tests were performed to evaluate qualitatively the effects of elevated temperature on rock bolt performance.

- Laboratory properties/parameters such as elastic modulus, Poisson's ratio, and thermal expansion of the Tptpmn and the Invar rods used for the MPBXs were measured.

- Field properties/parameters—including rock-mass thermal expansion estimations from the MPBX displacement data, were measured.

Detailed descriptions of all SHT mechanical measurements may be found in Section 9 of the *Single Heater Test Final Report* (CRWMS M&O 1999 [129261]). Input-DTNs and Output-DTNs for SHT mechanical measurements are listed in Tables 4-2 and 6.2-1, respectively.

6.2.3.1 MPBX Displacements

Displacements were measured both within and on the surfaces of the SHT block. These measurements support numerical model evaluations related to thermal-mechanical-hydrological coupling and also provide data for determination of rock-mass thermal expansion. All displacements reported in this document follow the convention of extension positive. Four boreholes were instrumented with MPBXs: three boreholes drilled parallel to the heater axis and one borehole drilled perpendicular to the heater axis. The MPBXs include six or seven anchors spaced along the length of the borehole. Displacements were measured using high temperature linear variable differential transducers (LVDTs) and vibrating wire displacement transducers.

Wire extensometers and tape extensometer pins were installed on the three free surfaces of the SHT block (see Figures 6.2.3.1-1 and 6.2.3.1-2). Note that the legend for the abbreviations in these two figures is as follows: BX is multiple-point borehole extensometer, WX and WXM is wire extensometers, RB-LC is rockbolt load cell, and BJ is borehole jack. The wire extensometers consist of spring-loaded linear potentiometers mounted on brackets welded to

steel rebar segments. These segments are grouted into the rock near the top of the SHT block at six locations (two on each of the three free surfaces of the SHT block). These surface displacements are intended to augment the displacement data collected from the MPBXs and to provide qualitative "control" of the SHT free surfaces to support future modeling efforts.

Detailed discussion of the SHT displacements is presented in Section 9 and 11.2 of the *Single Heater Test Final Report* (CRWMS M&O 1999 [129261]). SHT displacement data can be found in the TDMS under the Input-DTNs: SNF35110695001.008 [113812], SNF35110695001.009 [113819], and LL980109904243.015 [158299]. Because of the abundance of SHT displacement data, only representative discussion and graphics are provided. All displacement data and graphics can be accessed in the Output-DTN identified in Table 6.2-1.

6.2.3.1.1 Results: MPBX Displacements

Only representative discussion and graphics are presented here. Figure 6.2.3.1-3 shows displacement data for MPBX-3, which is located approximately 1.5 m from the heater, above and to the right (south). The data from MPBX-3 show an increase in gage length (extension) for all anchor positions through about the first 70 days. From 70 to about 100 days, all anchors exhibit a gradual decrease in gage length. After about 100 days, all anchors except MPBX-3-1 reverse trend and increase extension through the second quarter of heating. Anchor MPBX-3-1 continues the relative compression from day 100 through about day 180, when it experiences a sudden extensional jump followed by continued extension throughout the fourth quarter of heating. The extensional jump at about day 180 is seen only in anchor MPBX-3-1; therefore, it is likely that it results from discrete movement along a fracture or system of fractures located between anchors MPBX-3-2 and MPBX-3-1. This region corresponds to similar presumed behavior near anchor MPBX-1-1 (MPBX-1) near day 210. The change in slope for most of the anchor responses after about 70 days may be the result of matrix thermal expansion closing existing fractures, thus limiting additional thermally driven displacements until a greater volume of rock is heated. Thus, three-dimensional confinement effects may influence the response of some anchors.

The cooldown data for MPBX-3 are also included in Figure 6.2.3.1-3 (cooling starts at day 275). Four gages in MPBX-3 are operational; gages MPBX-3-4 and MPBX-3-5 are suspected to have failed from unknown causes during heating. MPBX-3 exhibits step-wise decreases in all operational gages during cooldown. As with MPBX-1, this type of behavior may be suggestive of "stick-slip" type behavior resulting from normal and/or shear extension/compression of fractures in the cooling rock mass. This type of behavior should not be unexpected in a fractured rock mass.

Wire and tape extensometer pins were placed on the three free surfaces of the SHT block (see Figures 6.2.3.1-1 and 6.2.3.1-2). Because the measurements are made from short pins installed near the rock surface, they can be influenced by discrete block movement. All the wire extensometer stations show displacement changes of over several millimeters, with the exception of WX-4, which experienced displacements of less than 1 mm throughout the test. The data from the wire extensometers are provided in tabular form in Table 6.2.3.1-1. The wire extensometer data exhibit closure by the end of heating, with the exception of WX-2 (located on the west face of the SHT block, about 2 m to the left of the heater) which exhibits a small extension of less

than 1 mm through the end of heating. Other wire extensometer stations (such as WX-3 and WX-5, which are located on the south and north face of the block 3.7 mm from the Thermal-Mechanical Alcove) show over 20 mm of closure at the end of the fourth quarter.

The data from the manual tape-extensometer measurements are given in Table 6.2.3.1-2. The data show that the horizontal cross-drift measurements are largest for WXM-1, WXM-2, and WXM-3, with all measurements compressive (i.e., shortening of the gage length). In other words, the surface pins are moving away from the SHT block in all cases. These displacements are consistent with the gross displacements measured using the MPBXs. In addition, the tape extensometer results for WXM-2 are consistent with the large displacements measured by the wire extensometer station WX-2. This suggests gross surface displacements near the surface of the SHT block to the left of the heater. It is likely that either or both of the WXM-2 pins are located in a loose block of rock, which appears to have loosened almost immediately during the SHT. The subsequent data suggest that the block(s) stabilized somewhat, with only minor additional displacement after September 24, 1996.

6.2.3.1.2 Measurement Uncertainty: MPBX Displacements

There are several potential sources for measurement uncertainty in the displacement measurements presented in this section. These uncertainties, quantifiable and nonquantifiable, are listed below:

Quantifiable

- The accuracy of the instrumentation itself. The gage range and accuracy of SHT displacement-related instrumentation are presented in Table 6.2.3.1-3.

- The conversion of the electrical output to engineering units. The uncertainty from these equations and the round-off error inherent in the data conversion are negligible.

Non-quantifiable

- Electrical interference, such as spurious signals from power surges, can cause low-magnitude noise, unexplained meandering in the data, or high-magnitude spikes.

- Unidentified sensor or MPBX assembly stability issues, which have caused a few LVDTs or vibrating wire gages to either produce “bad” data for an extended period of time before returning "good" data, or to have an unexplained shift in magnitude while maintaining expected rates of behavior on both sides of the shift.

- The physical location of the gages in the test region are difficult to precisely determine. The location uncertainty is particularly important in regions of high temperature gradient, of which hydrological and thermal expansion behavior are thought to be strong functions for certain temperature ranges.

- The uncertainty related to the choice of method for computing thermal expansion of Invar rods, based on measured temperatures along MPBXs, is difficult to estimate. Piecewise linear discretization using average temperature values and a 4th-order

polynomial for thermal expansion as a function of temperature were used for the SHT. The choice of another method (e.g., an integral function along the length of the rods) requires different assumptions that may be as reasonable as the method chosen. The magnitude of any discretization error is likely not large enough to affect the general trends in thermal-mechanical deformation of the rock illustrated by the data.

- Instruments can degrade or fail.
- Anchors can slip (considered possible but unlikely).
- The temperature change near the anchor heads could affect LVDT calibration constants. This uncertainty is anticipated to be negligible.

6.2.3.2 Borehole Jack

Borehole jack tests were performed in ESF-TMA-BJ-1 (borehole 19). Detailed discussion of the borehole jack tests is presented in Sections 9.2 and 11.2 of the *Single Heater Test Final Report* (CRWMS M&O 1999 [129261]). Because the rock-mass modulus measured using the borehole jack is directional (perpendicular to the borehole), an estimate of horizontal modulus anisotropy was not possible. It is likely that some anisotropy in modulus exists locally because of differences in fracture stiffness for each set of fractures present in the SHT block. Also, it is likely that the rock mass modulus varies across the repository block. These measurements, which included 15 ambient and 10 elevated-temperature measurements, were taken at five locations within the testing borehole at nine different times during the heating and cooling phases of the SHT. Consequently, the effects of temperature on rock-mass modulus was examined.

Borehole jack data may be found in Input-DTN: SNF35110695001.010 [158300].

6.2.3.2.1 Results: Borehole Jack

The results from the borehole-jack testing show that the measured rock mass modulus ranges from about 3 to 23 Gpa where the higher values were generally associated with increases in temperature. The highest value is for the deepest measurement location in the borehole (~6.2 m from the collar). This location corresponds to roughly 0.33 m from the heater borehole, about 1.5 m from the end of the heater. Measurement at this location approximately 110 days before and 190 days after resulted in moduli of 8.5 Gpa and 9.2 Gpa, respectively. This anonymously high value of 23 GPa may be due to measurement error. All the other borehole-jack data are relatively low, less than 12 GPa.

These measured values at the SHT are considerably less than the intact modulus of about 32.4 GPa measured on intact samples of the Topopah Spring welded tuff. The data presented in Table 6.2.3.2-1 include italicized results in which the two LVDT readings (far and near) differ by slightly greater than 0.02 in. at the maximum test pressure. According to American Society for Testing and Materials (ASTM) D4971-89 (p. 3) these data should be discarded because of uneven loading. The fractured nature of the rock surrounding the borehole made it difficult in some cases to “set” the borehole jack at those locations. However, the data presented represent only slight deviation from the ASTM D4971-89 (p. 3) criteria and are presented to qualitatively

assess modulus difference along borehole BJ-1. The italicized data should not be used in calculations requiring rock mass modulus.

6.2.3.2.2 Measurement Uncertainty: Borehole Jack

Measurement uncertainties in SHT borehole-jack measurements include those associated with accuracy and precision as tabulated in Table 6.2.3.1-3 and proximity to fractures. The borehole jack is better suited for local regions that are intact rather than fractured rock. Also, elevated temperatures, especially near peak temperatures in the SHT block, may affect the performance of the borehole jack.

6.2.3.3 Rock-Bolt Load

Eight rock-bolt load cells were installed on Williams B7X Hollow Core rock bolts as part of the SHT mechanical testing program. The objective was to evaluate qualitatively the effects of elevated temperature on bolt performance by (1) monitoring load changes during the test, (2) evaluations of the bolt/grout/rock interface following heating and cooling, and (3) pull-testing selected bolts to failure after heating and subsequent cooling. Each rock bolt included one vibrating wire load cell (load washer) that was installed between cover plates and adjustable angled washers. This entire assembly was bolted to the Williams bolt on the cold side of the insulation.

Four of the rock bolts were installed on the heated side of the Thermal-Mechanical Alcove below the level of the heater. Another four rock bolts were installed on the opposite cold side of the Thermal-mechanical Alcove. The rock bolts and load cells were installed during July 1996. Initial readings were taken using a hand-held Geokon readout box, prior to connection to the DCS. The load cells each contain three strain gages, and the total load acting on the cell is calculated by averaging the measurements from all three. Post-cooling evaluation of bolt/grout interface was limited to the rock-bolt pull test because overcoring across these interfaces was unsuccessful.

The locations of the rock bolts instrumented with rock-bolt load cells (RBLCs) are shown in Figures 6.2.3.1-1 and 6.2.3.1-2. Four RBLCs were installed on the heated side of the west face of the SHT block (RB-1, RB-2, RB-3, and RB-4), and four were installed on the opposite ambient side of the Thermal-Mechanical Alcove (RB-5, RB-6, RB-7, and RB-8).

Detailed discussion of the SHT rock-bolt load testing is presented in Section 9.3 of the *Single Heater Test Final Report* (CRWMS M&O 1999 (129261]). SHT rock bolt data load data may be found in Input-DTN SNF35110695001.008 [113812].

6.2.3.3.1 Results: Rock-Bolt Load

The data are presented as load (lb) versus time from the start of heating, in tabular form in Table 6.2.3.3-1. The data show a general decline in load measured in all the RBLCs through the end of heating. Three of the four heated rock bolts (RB-2, RB-3, and RB-4) show an increase in load after the heater is turned off, and RB-1 exhibits a stabilization of the previously observed load decrease. The increase is to only up to 100 lb, or 0.7% of the load measured in the bolt. The load increase is likely caused by thermal-contraction effects in the bolt itself, which likely has a

higher thermal expansion/contraction coefficient than the rock mass surrounding it. The ambient rock bolts continue to experience a decrease in load throughout the reporting period.

Loads were measured in rock bolts installed on both the heated side of the SHT block and on the opposite ambient rib of the Thermal-Mechanical Alcove. The rock bolts were installed to evaluate the longer-term effects of elevated temperature on this type of rock anchorage. Results show that loads are decreasing in all load cells; however, the decrease is greatest in those rock bolts on the heated side of the SHT. Alternatively, there could also be some load loss caused by creep of the anchorage, which is composed of the steel bolt and mechanical anchor, the surrounding grout, and the rock itself. The fact that load decreases were about 1 –2% for all rock bolts, except RB-1 and RB-2, which decreased about 7% and 4% respectively, appears to indicate: (a) the influence of anchorage creep on all the bolts and (b) the effect of temperature on the creep of the rock bolts, because rock bolts with the highest temperatures had the most load decrease.

6.2.3.3.2 Measurement Uncertainty: Rock-Bolt Load

Measurement uncertainties in SHT rock-bolt measurements are similar to many of those discussed in Section 6.2.3.1.2. Additional uncertainties include those associated with accuracy and precision as tabulated in Table 6.2.3.1-3.

6.2.3.4 Laboratory Parameters—Thermal Expansion, Young's Modulus, Poisson's Ratio, and Peak Stress

The SHT includes pre-heating planning, test design, pre-heating analyses, pre-heating characterization, test implementation, heating-phase testing, cooling-phase testing, and post-cooling characterization and instrumentation/equipment evaluations. This section discusses the post-cooling characterization activities for mechanical processes after the cooling phase of the SHT was completed. Specifically, the activity described here is the use of post-cooling borehole and intact rock sample locations for laboratory determination of thermal-mechanical properties. A detailed discussion for all SHT laboratory mechanical parameters is presented in Section 6.2 of the *Single Heater Test Final Report* (CRWMS M&O 1999 (129261]) and Section 4 of the *Characterization of the ESF Thermal Test Area* (CRWMS M&O 1996 [101428]). SHT preheating and post-cooling laboratory parameter data may be found in the Input-DTNs: SNL22080196001.002 [158306] and SNL22080196001.003 [119042].

6.2.3.4.1 Results: Laboratory Parameters—Thermal Expansion, Young's Modulus, Poisson's Ratio, Peak Stress and Axial Strain at Peak Stress

The mean coefficients of thermal expansion (MCTEs) are summarized in Tables 6.2.3.4-1 and 6.2.3.4-2 for heating and cooling, respectively, during the first thermal cycle. Data are categorized as being either from within or outside the maximum extent of the 100°C isotherm, and either perpendicular or parallel to the heater. The mean MCTEs and standard deviations about each mean are given at each temperature for each category. Summary data for the entire test suite are given with standard deviations and 95% confidence limits at the bottom of each table. All specimens show steep increases in MCTE beginning at approximately 150–200°C and continuing until approximately 300°C. The steepest increases are between 250 and 300°C. This steep increase is

attributed to phase changes in the silica mineral phases. The MCTEs calculated over the temperature interval of 300–325°C decrease as the phase change is completed. The specimens with lower MCTEs are primarily from within the approximate maximum extent of the 100°C isotherm. The SHT pre-heating characterization data and data from within the approximate maximum extent of the 100°C isotherm continue to track one another and fall below the remaining data sets.

Fourteen specimens were tested in unconfined compression and the experimental data are summarized in Table 6.2.3.4-3. Mean values, standard deviations, and 95% confidence limits are given for Young's modulus, Poisson's ratio, peak stress, and axial strain at peak stress. Young's moduli ranged from 20.1 GPa to 37.0 Gpa, with a mean value of 31.6 GPa. The standard deviation was ±4.8 Gpa, and the 95% confidence limit was ±2.5 GPa. Poisson's ratio ranged from 0.12 to 0.39 with a mean value of 0.20. The standard deviation was ±0.07, and the 95% confidence limit was ±0.03. Peak stress ranged from 34 MPa to 246 Mpa, with a mean value of 134 MPa. The standard deviation was ±70 Mpa, and the 95% confidence limit was ±37 MPa. Axial strain at peak stress ranged from 0.11% to 0.89%, with a mean value of 0.47%. The standard deviation was ±0.25%, and the 95% confidence limit was ±0.13%.

6.2.3.4.2 Measurement Uncertainty: Laboratory Parameters—Thermal Expansion, Young's Modulus, Poisson's Ratio, and Peak Stress

The uncertainty in the uniaxial compressive testing of intact rock samples, which results in the measurement of Young's modulus, Poisson's ratio, and peak stress, includes the accuracy of the load cell, the accuracy of the LVDT, specimen alignment, square and parallel of the specimen ends, changes in the specimen cross section area during the test, specimen variation, and anisotropy of the rock. Among these factors, the greatest uncertainty is with the specimen variation. The heterogeneity in the rock mass will have significant effects on its compressive strength and moduli. Many of these uncertainties also apply to thermal expansion of intact samples. In addition, temperature control contributes to uncertainties in thermal expansion. Additional discussion of the uncertainties associated with these measurements can be found in Section 9 and 11.2 of the *Single Heater Test Final Report* (CRWMS M&O 1999 (129261]).

6.2.3.5 Field Parameters—Rock Mass Thermal Expansion

Rock-mass thermal expansion is calculated from the *in situ* heating cycle data, including temperature change for a given axial length from ambient, gage length, and measured thermal displacement over the gage length. The rock-mass thermal-expansion coefficient was calculated for the SHT using selected data from MPBX-1, MPBX-3, and MPBX-2. Only the data from these MPBXs with relatively uniform temperature were used. Discussion of the SHT rock mass classification is presented in Section 8 of the ESF Thermal Test Area (CRWMS M&O 1996 [101428]).

SHT displacement data may be found in Input-DTNs SNF35110695001.009 [113819] and LL980109904243.015 [158299].

6.2.3.5.1 Results: Rock Mass Thermal Expansion

The data presented in Table 6.2.3.5-1 are averaged values for each MPBX over the gage lengths shown. For MPBX-1, the mean value was 5.88×10^{-6}/°C; for MPBX-3, the mean value was 4.14×10^{-6}/°C; and for MPBX-2, the mean value was 2.36×10^{-6}/°C. The calculated values for rock mass thermal expansion are consistently lower than laboratory intact values, regardless of temperature and gage length. This is to be expected because of fractures that are present in the SHT test block. Also, the values presented in Table 6.2.3.5-1 are for the single orientation parallel to the heater (N72°W). It is possible that there could be some significant anisotropy in the rock mass thermal expansion coefficient because of differences in fracturing along different orientations.

6.2.3.5.2 Measurement Uncertainty: Rock Mass Thermal Expansion

Measurement uncertainty of the rock mass thermal expansion is dependent on the uncertainties of the original field measurements (MPBX displacements and temperatures), and in the discretization error associated with the available lengths over which to measure these values (primarily deviation from a constant temperature). Obviously the randomness of fracture spacing and size results in uncertainty that can be mitigated with numerous measurement locations along similar fractures patterns.

6.2.4 SHT Chemical Measurements

This section presents the results from geochemical studies of water samples collected during the SHT and mineralogical studies of pre-heating borehole cores and post-cooling overcores from the test block. The study of the geochemical composition of the water collected during the test provides insight into thermally driven geochemical processes. The mineralogical studies present information on the rock, providing a necessary starting point for the study of rock and water evolution with temperature and time. The aqueous geochemistry is discussed in Section 6.2.4.1. Mineralogical and petrologic studies are covered in Section 6.2.4.2.

A detailed description of SHT chemical measurements is documented in Sections 6.4 and 10 of the *Single Heater Test Final Report* (CRWMS M&O 1999 [129261]). Input-DTNs and Output-DTNs for SHT chemical measurements are listed in Tables 4-2 and 6.2-1, respectively.

6.2.4.1 Aqueous Chemistry

Samples of water were collected from borehole 16-4 (see Figure 6.2-2) on four occasions during the course of the SHT and were distributed for analysis. Water collected in the field was tested for pH, filtered to 0.45 μm, and splits for analyses were prepared for distribution. Each field sample was also given a unique identification number, which was tracked by the Sample Management Facility (SMF). Samples were designated for analysis of metals, anions, and, stable isotopes. The metals samples were stabilized by acidifying the water with HNO_3 and stored in polyethylene bottles. The anion samples were also stored in polyethylene, and the stable isotope samples were stored in glass. All bottles were filled to minimize headspace and tightly capped to reduce evaporation. The samples were maintained under refrigeration at the SMF until they were shipped.

Of the four sampling activities, the first one on November 25, 1996, was an unexpected opportunity. Consequently, the sample was collected without obtaining a pH measurement in the field, and neither the filtration nor the acidification procedure was performed; as a result, data in DTN: LL970409604244.030 [111481] are designated non-Q.

The cation analyses were performed at Lawrence Livermore National Laboratory (LLNL) by Inductively Coupled Plasma and Atomic Emission Spectroscopy (ICP/AES). Total dissolved metals of Al, B, Ca, Fe, Mg, Li, Na, K, S, Si, and Sr were measured. Anions were measured by Ion Chromatography (IC); anions measured included F^-, Cl^-, Br^-, NO_2^-, NO_3^-, PO_4^{3-}, and SO_4^{2-}. Bicarbonate (HCO_3^-) was computed by charge balance, using the measured pH to indicate actual hydrogen activity at the time of sampling. The analytical aqueous chemistry results are in the TDMS under DTNs LL970101004244.027 [158309], LL970409604244.030 [111481] (12/96 to 03/97), LL970703904244.034 [111482] (3/8/97 to 7/18/97) and LL971006604244.046 [148611]. In addition, as part of a scoping investigation, stable isotopes of oxygen and hydrogen, uranium, and strontium were analyzed by investigators at LLNL, Lawrence Berkeley National Laboratory (LBNL), and the U. S. Geological Survey (USGS) at Denver, Colorado.

6.2.4.1.1 Field Sampling

Among the boreholes instrumented with various monitoring systems shown in Figure 6.2-2, boreholes 20 (ESF-TMA-CHE-1) and 21 (ESF-TMA-CHE-2) were designed to collect aqueous chemical data from specific locations in the thermal test block. One borehole was instrumented with a suite of solid-state chemical sensors for *in situ*, real-time geochemical assessment of the contacting waters. Early in the SHT, however, the sensors' performance was inconsistent with the manufacturer's specifications. Subsequent laboratory testing demonstrated significant compositional dependencies; consequently, they were determined unsuitable for monitoring the water chemistry. The second borehole was fitted with absorbent pads that could be collected in the field and returned to the lab for analytical testing. Several pads were removed, examined, and found to be relatively dry. Nevertheless, an extraction process was developed in which pads were soaked in de-ionized water (dilution). The process was followed by sampling and filtering the solution. A clean-pad blank was also run to provide baseline corrections (per gram weight of fabric). The resulting solution chemistries were determined to be very dilute, with a high uncertainty arising from scatter in the background contributions as well as imprecise weight corrections.

Fortuitously, borehole 16 (ESF-TMA-NEU-2), which was drilled and instrumented for hydrology studies (See Sections 6.2.2.3 and 6.2.2.4) proved to be important to collecting SHT water for analysis. The borehole was instrumented with a string of high-temperature, inflatable packers, which isolated four open zones. The inflated packers, which straddled fractured regions, also provided a means of containing mobilized water entering an open zone. One zone in particular—zone 4 of borehole 16 (at a depth of 3 m)—yielded a significant and steady supply of water for chemical analyses starting in November 1996 and continuing throughout the heating phase of the SHT.

6.2.4.1.2 Results: Aqueous Chemistry

The results of chemical analyses for the four suites of SHT water are presented in Table 6.2.4.1-1 For comparative purposes, data from several relevant water sources (other than the SHT) have been included, and their respective sources are cited among the footnotes. The reported temperatures are those downloaded from the Data Acquisition System at time of sampling. The pH measurement is a field value taken at the time of sample collection. The one exception is for the initial sample (collected November 25, 1996); the pH value reported was for a sample measured about 30 days after collection.

Table 6.2.4.1-1 clearly shows that the SHT water is more dilute than other *in situ* waters from the general vicinity. Trends in the SHT water indicate Na and Si are the dominant metals, followed by Ca, with other cations and anions in considerably lower abundances. The same general patterns are observed in both saturated and unsaturated zone waters sampled from the region. Over time, the concentrations of Na, Ca, Mg, and Sr are seen to systematically decrease, whereas all other elements exhibit nonsystematic variation. SHT waters are slightly acidic with pH values between 6.2 and 6.9. These measured pH readings may have indicated elevated CO_2 partial pressures in equilibrium with the water in the packed-off interval.

Stable isotopic data (^{18}O and deuterium) are plotted as $\delta^{18}O$ relative to δD in Figure 6.2.4.1-1. The meteoric water line is plotted for reference. The scatter in the data for Suite 1 may reflect the fact that the first samples were collected during an unanticipated "window of opportunity" in a borehole not necessarily designed for chemical sampling. Consequently, standard collection procedures were not employed for these first waters sampled. Generally, data for Suites 2–4 were more tightly grouped and were broadly consistent with the other analyzed waters. There does not appear to be a clear distinction in the isotopic data among the various water sources represented here.

6.2.4.1.3 Measurement Uncertainty: Aqueous Chemistry

The borehole in which the four water samples were collected for chemical analysis was not designed for water sampling. In fact, the unanticipated first samples were collected prior to standard collection procedure being approved. This situation, however, was remedied so that the three subsequent water samples were collected, preserved, and stored appropriately. All the sample analyses were performed according to the existing quality procedures then in place.

6.2.4.2 Mineralogic and Petrologic Analyses

The SHT served as a prototype test for the larger DST. Here, techniques were developed to produce a quantitative inventory of natural minerals in the fracture network of the test block. Continuous characterization over meter-scale distances was essential to provide estimated mineral abundances of general validity as input to numerical geochemical models of thermal tests. Collection of data on this scale also would document the existence of variability in the mineral content of the fracture network. Data for natural-mineral abundances were obtained from cores drilled prior to heating. Data on stellerite abundance (fracture-surface coverage) in fractures have been submitted to the TDMS under the Input-DTN LA0009SL831151.001 [153485].

The ability to identify and document test-related mineralogic reactions was a key to assessing the reliability of computational models of coupled thermal-hydrologic-chemical processes. Two types of post-cooling (following heating and cooling) sampling were employed: overcoring of pre-heating boreholes and drilling of new continuously cored boreholes. Both coring and overcoring were performed after the field test was completed. Identification of pre-heating and post-cooling minerals was verified by X-ray diffraction analysis (XRD), scanning-electron microscopy (SEM), and energy-dispersive X-ray analysis (EDX). A summary of pre-heating fracture minerals and post-cooling products can be found in the TDMS under the Input-DTN LA0009SL831151.001 [153485].

6.2.4.2.1 Results: Mineralogy of the Pre-Heating Natural Fracture System

Time constraints precluded completion of an inventory for all fracture-coating minerals. Instead, a survey of stellerite abundance in macroscopically visible fractures was undertaken for pre-heating drill core MPBX-1 (borehole 2 as shown in Figure 6.2-2). Stellerite, a zeolite, was chosen because it can be identified with a high level of confidence based on stereomicroscopic examination. Visual-recognition criteria of crystal morphology, luster, and hardness were verified by XRD of typical deposits. Because stellerite is a major fracture-coating mineral in the SHT block, quantification of its abundance was especially useful input for geochemical modeling.

The survey was conducted piece-by-piece for the MPBX-1 core. For each fracture, the percent of fracture surface covered by stellerite was estimated by comparison with standard abundance diagrams like those of Compton (1962 [101588], pp. 332-333). The observed or calculated coverage of a fracture by stellerite is defined for this estimation as an attribute shared by the opposing surfaces of an intact fracture. For partly sealed fractures, the estimated percent stellerite coverage of nonsealed fracture area was treated as an attribute of the entire fracture. Matching fracture faces at the ends of adjacent core pieces count as a single fracture, with percent zeolite coverage equal to the higher of the values estimated for each face. The results of this inventory are presented in Table 6.2.4.2-1.

Additional natural-fracture minerals, as identified by XRD in two samples from drill core ESF-TMA-H-1 (borehole 1 as shown in Figure 6.2-2), include smectite, feldspar, and quartz (Tables 6.2.4.2-2 and 6.2.4.2-3).

6.2.4.2.2 Results: Evidence of Mineral Deposition

Alteration products of the SHT resulting from fluid/rock interaction have been identified in the overcores of borehole 16 (ESF-TMA-PTC-NEU-2) and borehole 2 (ESF-TMA-PTC-MPBX-1). The new mineral deposits are of three general varieties, described here from the occurrences in the ESF-TMA-PTC-NEU-2 borehole. This borehole was inclined upward from the surface of the test block, so that the “bottom” of the borehole was above the heater. Water that entered the borehole from fractures near the bottom flowed downslope along the wellbore. Small white mounds and patches, ≤1 mm across, of gypsum ± calcite ± opal-A are present on natural fracture surfaces and pre-heating borehole 16 surfaces near the bottom of the ESF-TMA-PTC-NEU-2 overcore. Some of the mounds are concentrated along the traces of very tight fractures intersecting the borehole or fracture surfaces on which the mounds were deposited. Glassy scale

deposits, mostly silica, are especially abundant on the bottom of the pre-heating borehole 2. Some scale deposits take the form of dried drip marks on the sides of the borehole.

Gypsum

The identification of gypsum is based on XRD of white deposits from pre-heating borehole surface and adjoining fractures in the 15.5–16.5 ft (4.72–5.03 m) interval of ESF-TMA-PTC-NEU-2. Only one core fragment contained enough material to collect about a milligram for XRD analysis. Smaller deposits on other core pieces are identified as gypsum on the basis of similar crystal morphology observed in SEM images and the Ca+S peaks in the energy-dispersive X-ray spectrum.

Opal-A and Other Silica

Opal-A in the white deposits from PTC-NEU-2 (pre-heating overcore borehole 16) was identified by a combination of XRD and SEM-EDX. A broad peak, characteristic of structurally amorphous material, was observed in the XRD pattern from the white deposits. SEM-EDX examination of the deposits revealed the presence of nearly pure silica (Si peak on the EDX spectrum) in portions of the deposits with no discernible crystal form.

Some opal-rich areas of the white mounds contain masses of minute silica tubules projecting up to about 5 μm from the surface of the deposit. A few tubules are straight, but most have variably tortuous shapes. Outside diameters of the tubules range from about 0.3 to 0.7 μm, whereas inside diameters vary from less than 0.1 to about 0.3 μm.

Deposits of glassy silica scale ≤0.2 mm thick were observed on the pre-heating wellbore surface of ESF-TMA-PTC-MPBX-1, a horizontal borehole close to the heater borehole. There is a 2–3 cm wide zone of silica deposition along what is inferred to be the bottom of the wellbore surface. In addition, silica scale deposits define elongate drip marks on the inferred lower half of the wellbore surface. The silica scale generally consists of two texturally distinct components. At the base of the deposits are aggregates of platy silica particles about 1 to 5 μm across, silica rods 1 to 2 μm across and up to about 15 μm long, and a few round particles 1 to 2 μm across. Overlying the silica particles are cracked silica sheets about 2 μm thick. The siliceous composition of the scale was documented by EDX).

Sampling the silica scale for mineralogic analysis was complicated by the small quantities of material and the difficulty in removing the scale from the wellbore surface while minimizing the incorporation of bedrock. Some of the thickest scale deposits were laid down on top of 0.1 mm thick fine particulate layers, to which the scale adheres. The milligram sample collected for XRD was estimated by visual examination to contain about 20% silica scale. Because of the high impurity content, identification of the scale mineralogy on the basis of XRD is very uncertain. Of the silica phases identified in the sample—cristobalite, quartz, tridymite, and opal-A—the opal-A (queried in Section 6.2.4.2-3 because its presence is uncertain) is most likely to be solely a test product. The ESF-TMA-MPBX-1 borehole (borehole 2), where this material was deposited, was heated to more than 150°C during the test. In comparison, the maximum temperature was slightly less than 80°C (SNF35110695001.008 [113812]) in borehole 16 where opal-A without platy morphology was deposited. Further mineralogic study might establish whether structural

differences exist between the silicas from the two boreholes and whether those differences might be related to the different thermal histories.

Calcite

Calcite has been documented by XRD as a constituent of the white mounds deposited on natural fracture surfaces and on the pre-heating borehole surface of overcore ESF-TMA-PTC-NEU-2 (borehole 16) in the 15.5–17.0 ft (4.72–5.18 m) interval. The mineral is also part of the thin, nearly invisible coatings present on the pre-heating wellbore surface in the same interval. A thin, brown particulate deposit on the bottom of the wellbore also contains calcite. In overcore ESF-TMA-PTC-MPBX-1, calcite occurs with silica scale, fine particulate deposits, or other deposits on the pre-heating wellbore. Discrete calcite crystals have not been documented by SEM-EDX studies of these deposits, due perhaps to spectroscopic interference from other calcium-rich phases such as gypsum and stellerite, or to overgrowths of other minerals.

6.2.4.2.3 Measurement Uncertainty: Mineralogic and Petrologic Analyses

A formal error analysis was not performed for the exploratory research technique employed to obtain the stellerite abundance in fractures presented in Table 6.2.4.2-1. The principal sources of error lie in estimating the percent zeolite coverage of a fracture and in estimating the portion of a fracture sealed by vapor-phase minerals. The loss of small amounts of core on account of nonrecovery or sample removal is an additional source of uncertainty not related to errors of measurement.

6.2.5 SHT Miscellaneous Measurements and Observations

This section discusses additional SHT measurements not covered in the prior four SHT sections. Specifically, fracture mapping, infrared imaging, and borehole video logging are discussed. Detailed discussion on these measurements is documented in the report entitled *Characterization of the ESF Thermal Test Area* (CRWMS M&O 1996 [101428]). Input-DTNs and Output-DTNs of applicable SHT miscellaneous measurements are listed in Tables 4-2 and 6.2-1, respectively.

6.2.5.1 Fracture Mapping

The objective of geologic mapping in the SHT area was to determine the vertical and horizontal variability of fracture networks, to characterize any faults and fault zones, to map the lithostratigraphic features of geologic subunits and the abundance and character of lithophysal zones, and to assist in selection of test locations. Two data collection techniques were used: full-periphery mapping and detailed line surveys.

Mapping in the Thermal Test Alcove was carried out by United States Geological Survey (USGS) and United States Bureau of Reclamation (USBR). It was done essentially to the same standards used in the ESF Main Drift, using Technical Procedure NWM-USGS-G-32, R0. From these procedures, the USGS/USBR used full-periphery mapping techniques and detailed line surveys to characterize the rock and fractures in the alcove.

Geologic mapping included recording lithostratigraphic and structural features on 1:125 scale drawings. Maps were developed in the full-periphery style, in which the tunnel walls were

unrolled to produce a flat map of the tunnel periphery. Discontinuities and lithostratigraphic contacts with trace lengths longer than 1 m were recorded on the field sheets. The orientation of geologic features was determined using a goniometer for strike azimuth and a Brunton compass for dip values. Discontinuity orientations were recorded using the right-hand rule, where dip direction is 90 degrees to the right (clockwise) of strike. Traces of lithostratigraphic and structural features were sketched onto the geologic drawings and later digitized with AutoCAD.

Detailed line surveys (DLS) were generally conducted along the right wall, one and a half meters above the floor of the drift. In the Thermomechanical Alcove and Thermomechanical Alcove Extension, the detailed line surveys were conducted along the left wall, which borders the SHT block and therefore the area of greatest interest. A metric measuring tape was affixed to the wall and discontinuities with trace lengths longer than 30 cm were reported on the survey. Discontinuities that intersect the wall within 30 cm above and below the tape were also considered. Strike azimuth, dip, discontinuity type, trace length, number of visible fracture terminations and types of terminations, aperture, roughness, infilling type, and thickness were recorded in the DLS notebook in tabular form. These data were then transferred to an Access database.

Detailed discussion, including full periphery geotechnical map for Alcove 5, is presented in Section 7 of the report entitled *Characterization of the ESF Thermal Test Area* (CRWMS M&O 1996 [101428]).

6.2.5.1.1 Results: Fracture Mapping

Thermal Test Alcove 5 was excavated at Station 28+27, near the base of the ESF North Ramp and at the beginning of the Main Drift. It was excavated in an easterly direction off the north-south trending Main Drift and at a downward angle of approximately 10 to 15 degrees.

The lithology of the unit consists of densely welded, devitrified tuff of rhyolitic composition, containing vapor-phase minerals and about 1% phenochrysts, chiefly feldspar and biotite. Lithophysae are rare (less than 1%), and range in size up to 80 mm, with vapor-phase minerals and very light gray (N8) rims and spots. Short (10–20 cm), discontinuous, subhorizontal vapor phase partings are present throughout the unit, while the more developed subhorizontal partings form bedding plane features on the order of meters apart.

Fractures in this unit are generally moderately to widely spaced (30 cm to 2 m), slightly to moderately continuous (1 m to 10 m), and slightly open to tight. A series of low-angle shears strike through the area of the alcove in an east-west direction and dip to the north. These shears form local subhorizontal breccia zones or wedges where they intercept the more predominant vapor phase partings and bedding planes.

Results of detailed line surveys indicated three prominent joint sets in the Thermal Test Facility. These joints sets correspond to similar sets observed in the Tptpmn in the Main Drift. Joint Set 1 (JS1) and Joint Set 2 (JS2) are both near vertical, relatively long (3–4 m in length), had relatively smooth surfaces (Brown 1981 [102003], pp. JRC 4–JRC 6), and relatively small variations in amplitudes normal to the joint surfaces (0.05–0.2 m). Joint apertures are typically 1 mm to 2 mm, open, and with little or no infilling. Joint Set 1 has a dip direction of approximately 40° and a dip

angle of 70° to 85°. Joint Set 2 has a dip direction of approximately 130° and a dip angle of 70° to 90°. Joint Set 1 and 2 are difficult to observe because their orientation was subparallel to the walls.

Joint Set 3 (JS3) is a relatively low-angle vapor-phase parting surface, with a dip direction of approximately 300° and a dip angle of 15° to 40°. Compared to Joint Set 1 and Joint Set 2, the parting surfaces of Joint Set 3 are generally shorter (1.0 m–1.3 m), have more irregular surfaces (Brown 1981 [102003], pp. JRC 10–JRC 16), and have larger variations in amplitudes normal to the joint surfaces (0.2 m–0.3 m). The apertures for Joint Set 3 are generally wider (3 m–5 m) and are filled with vapor-phase calcite and quartz and occasionally Fe-Mn oxides. The joint density is approximately seven fractures per cubic meter.

6.2.5.1.2 Measurement Uncertainty: Fracture Mapping

Uncertainty associated with SHT fracture mapping is similar to that discussed in Section 6.1.4.1.2.

6.2.5.2 Infrared Imaging

The objective of infrared imaging (IR) of rock surfaces prior to the onset of heating was to establish the initial conditions on the drift walls around the SHT region, specifically the temperature distributions at the outlets of potential pathways for fluids. During the heating period, thermally induced flow can change the temperature at and near the exits, and the hot spots can be detected.

Before the heating stage, the rock surface temperature depends on the heterogeneous pneumatic and hydrological characteristics in the fractured rock, the evaporative processes on the surfaces, and the drift conditions. Air with relative humidity substantially below 100%, maintained by the ventilation, can dry up the surfaces. The use of construction water during excavation and drilling, and in wall washing to suppress dust, can wet the surfaces. These construction and operation activities generally have larger impacts on the rock surface temperature than the intrinsic heterogeneous flow and heat transfer processes in the rock.

A set of reconnaissance surveys was conducted on April 11-12, 1996, after excavation of the drifts around the SHT region. For this set of reconnaissance IR surveys, a hand-held 1 m × 1 m aluminum frame was used against the wall above and below the spring line for reference and for aiding the focusing of the IR camera. The human body, with temperature hotter than the rock, introduced distortions to the IR images. The triangular-shaped aluminum foil marker at the lower left corner of the frame accentuates the high reflectivity, or low emissivity, of aluminum as an effective IR mirror. A ladder and nine spray paint cans identified in the muck pile also reflect the IR temperatures of the surroundings, including the air.

Similar images were taken on other walls surrounding the SHT region and on the ceilings. Additional surveys were also carried out in June 1996, with essentially uniform temperatures on the walls observed. These images were digitized and later compared with the images taken at the same location during and following the SHT heating phase. For the end wall of the alcove

extension, an aluminum grid was installed on the wall so that human body heat would not distort the IR images in later surveys.

Detailed discussion of SHT infrared imaging is presented in Section 9.2 of the *Characterization of the ESF Thermal Test Area* (CRWMS M&O 1996 [101428]) and Section 8.4 of the *Single Heater Test Final Report* (CRWMS M&O 1999 [129261]). SHT infrared images and accompanying data may be found in the following Input-DTNs: LB970100123142.002 [158288], LB970400123142.001 [158289], LB970700123142.002 [158295], LB971000123142.002 [158296], LB980120123142.001 [158297].

6.2.5.2.1 Results: Infrared Imaging

Wet (cool) surfaces appear in IR images near the invert where some remaining muck is piled against the wall. In the corresponding IR images, the muck pile is colder than the wall surface above. On the wall, there are slightly cooler areas corresponding to the apparently wet areas. "Hot" spots show up in the IR images of the SHT wall above and below the mid-height between the invert and the drift crown.

The "hot" spots in the rock could be associated with pathways through the rock masses behind the wall. The pneumatic pathways are likely along heterogeneous channels through the fracture network and exit at "spots."

6.2.5.2.2 Measurement Uncertainty: Infrared Imaging

Uncertainty in the infrared measurements include parallax changes to the images, subjective interpretation of temperature differences along the surface of the image, and natural variations along a surface.

6.2.5.3 Borehole Video Logging

The objective of borehole video logs was to provide descriptive visual information from boreholes in the DST block and to supplement other available characterization data. Borehole video logs were also used to help select appropriate depths for packer settings for air-permeability testing.

The borehole television camera consists of the downhole video camera system, monitor, and VCR. The TV/VCR was first configured to record, and then the camera was inserted into the borehole. The camera was paused as needed. The video tape was viewed to ensure visibility and adequacy. The process was repeated if the video information was inadequate. Any unusable entries or videos were identified as inadequate. The following information was recorded in the scientific notebook: borehole identifier, date, measuring and test equipment serial numbers if applicable, the location of the zero datum point, traceability between the notebook and the video, depth-correction measurements if applicable, and the total depth reached.

6.2.5.3.1 Results: Borehole Video Logging

Borehole video logs provide much visual information regarding fractures, including aperature size, fracture frequency, and fracture orientation. Video logs, which are documented by Mitchell (1996 [159518]), include visual descriptions of the boreholes in the SHT region.

6.2.5.3.2 Measurement Uncertainty: Borehole Video Logging

These observations are inherently subjective, and determination of orientation and location may be subjected to multiple interpretations.

INTENTIONALLY LEFT BLANK

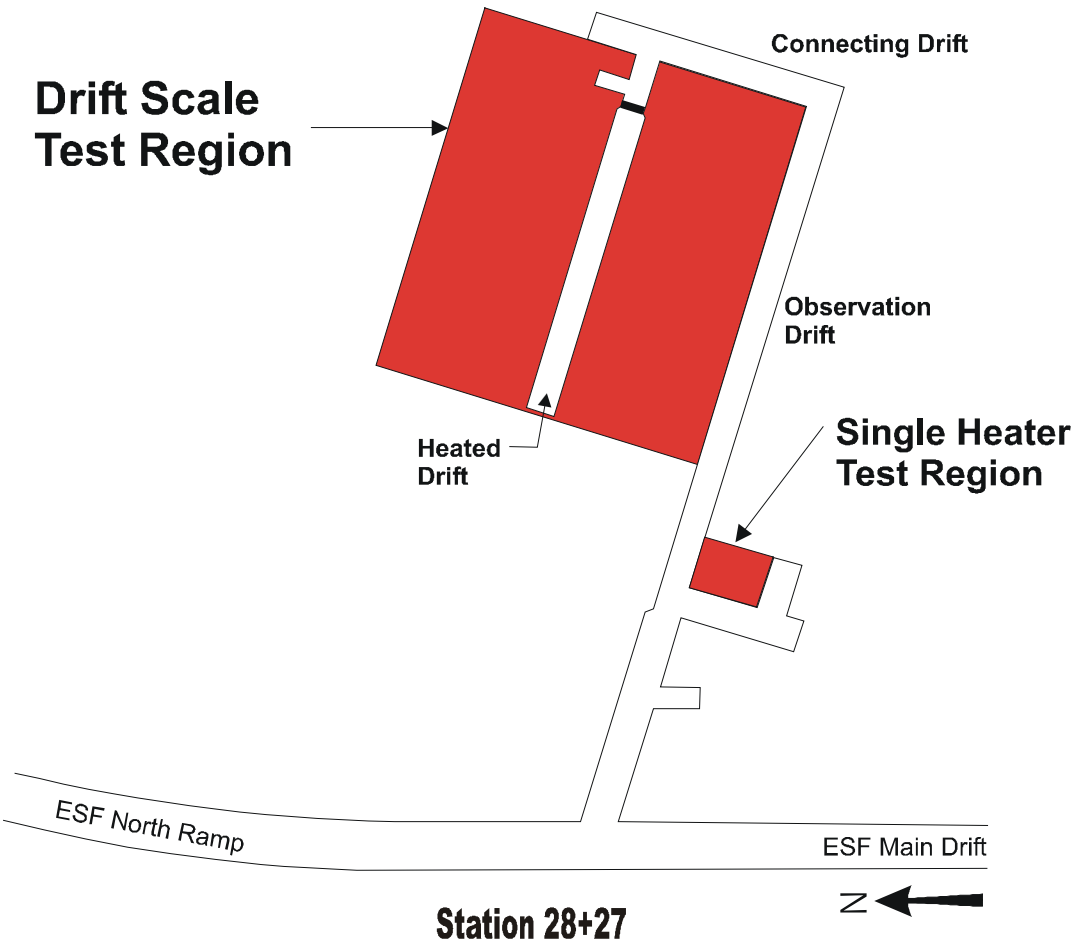

Figure 6.2-1. Schematic Plan View of ESF Thermal Test Facility Including the SHT

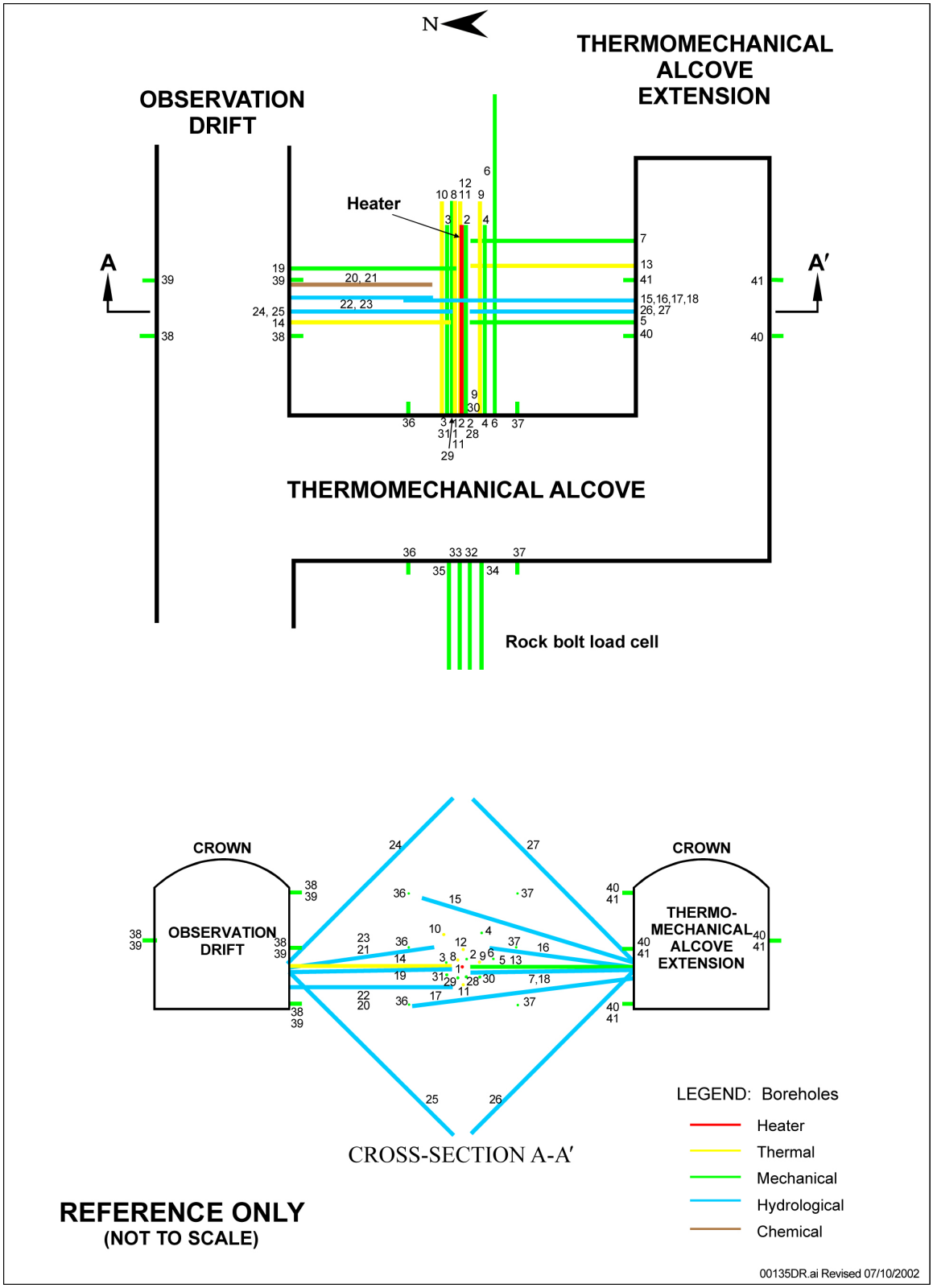

Figure 6.2-2. Schematic SHT Layout of the Instrumentation Boreholes

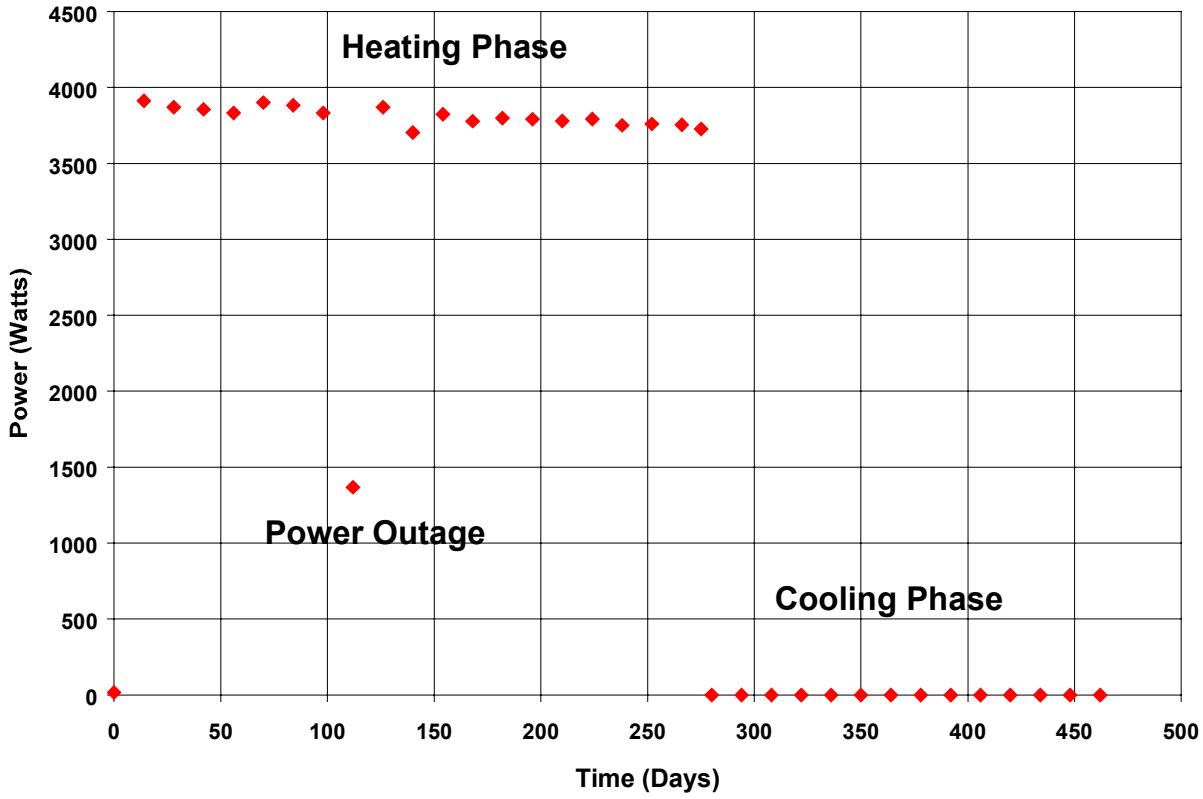

Figure 6.2.1.1-1. SHT Power History

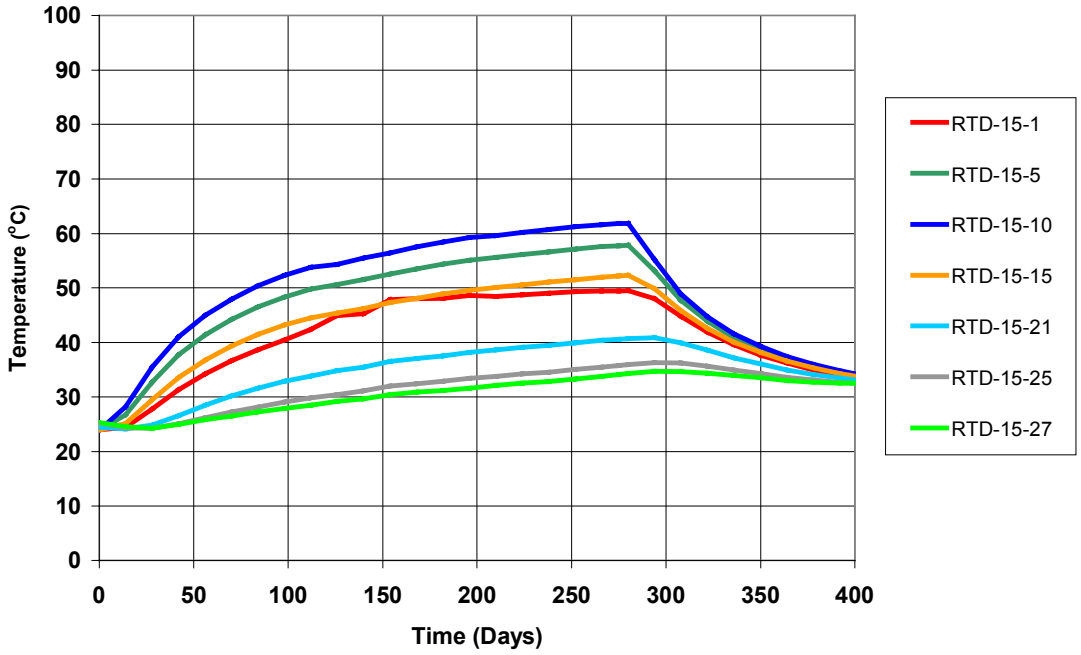

Figure 6.2.1.2-1. Temperature History for SHT Borehole 15 at Select Locations

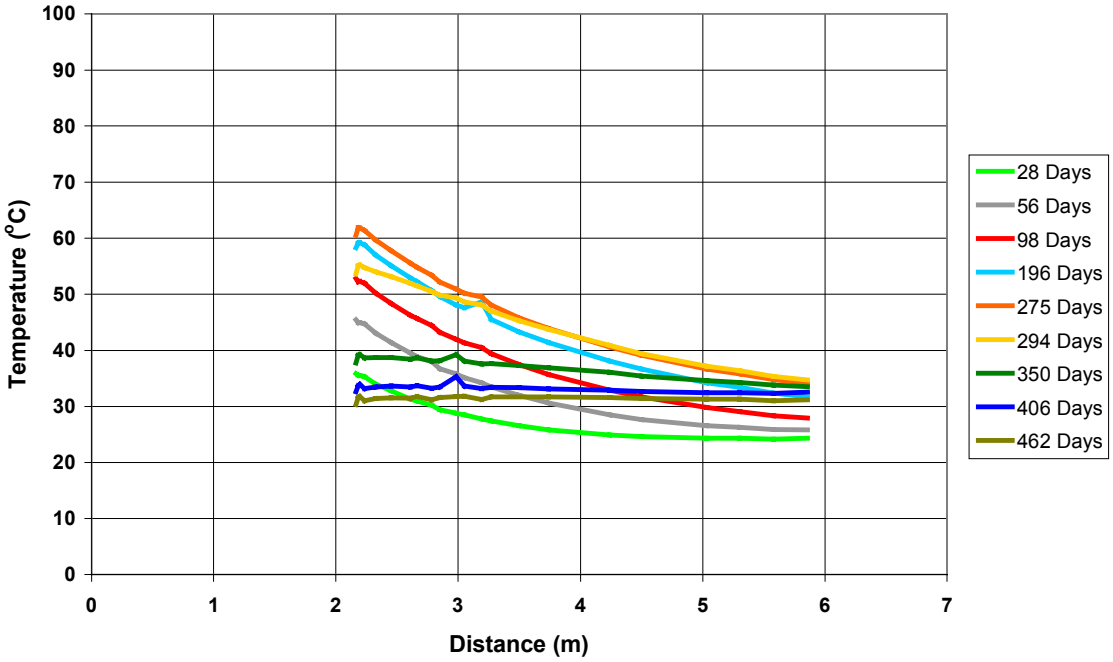

Figure 6.2.1.2-2. Temperature Profile for SHT Borehole 15 at Select Times

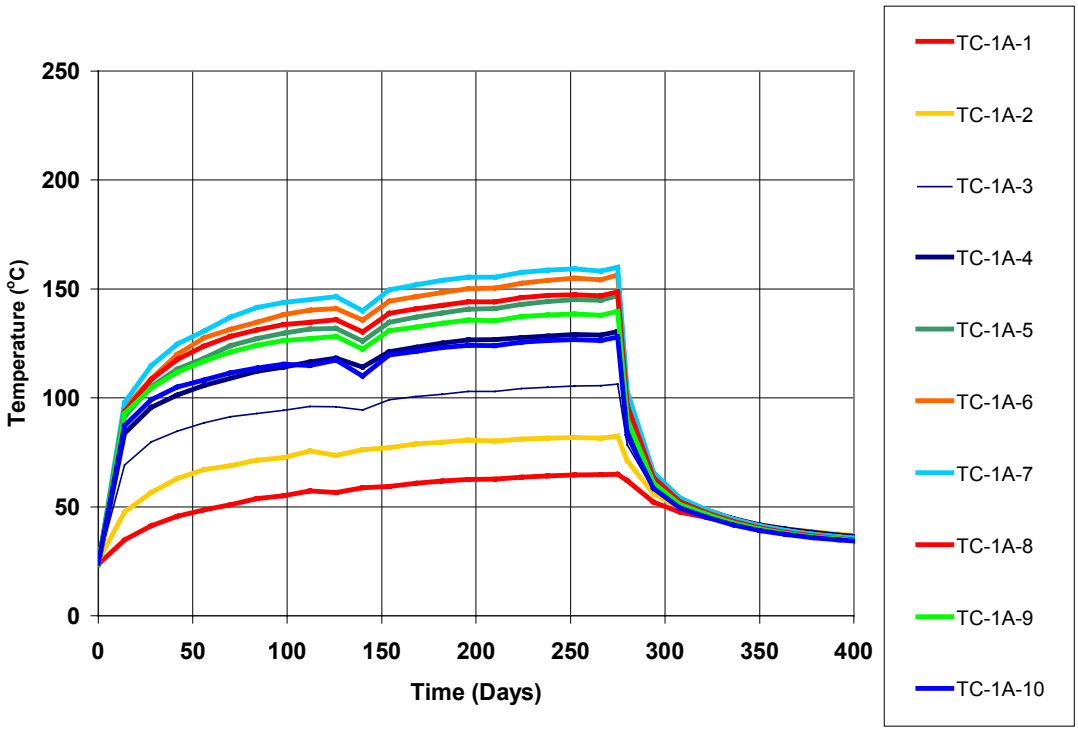

Figure 6.2.1.2-3. Temperature History for SHT Borehole 1 at Select Locations

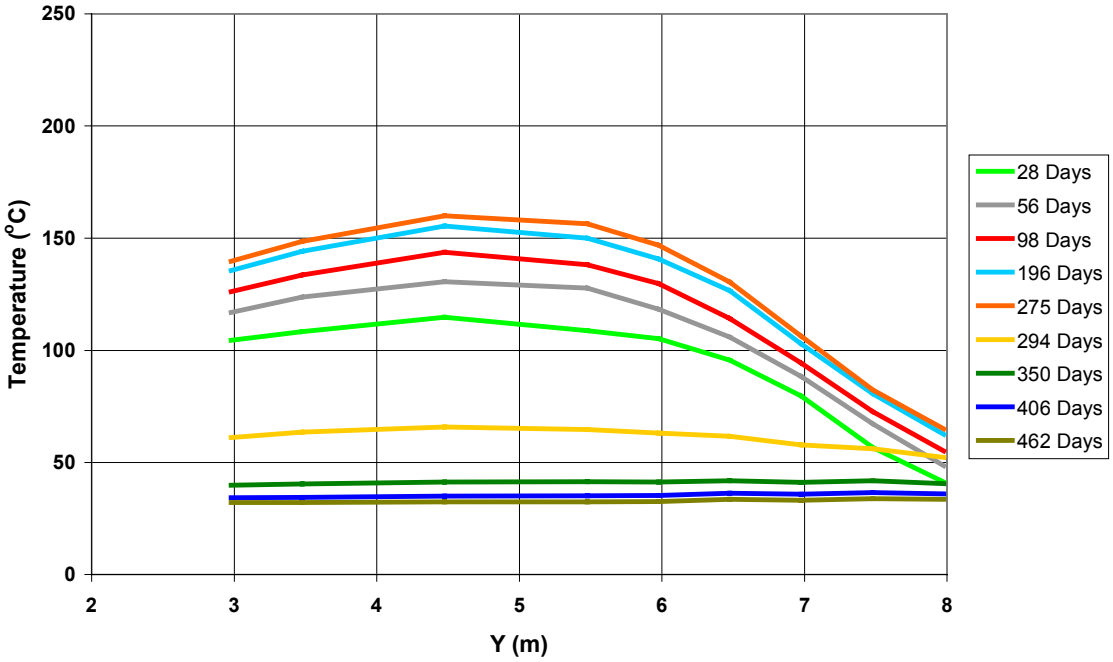

Figure 6.2.1.2-4. Temperature Profile for SHT Borehole 1 at Select Times

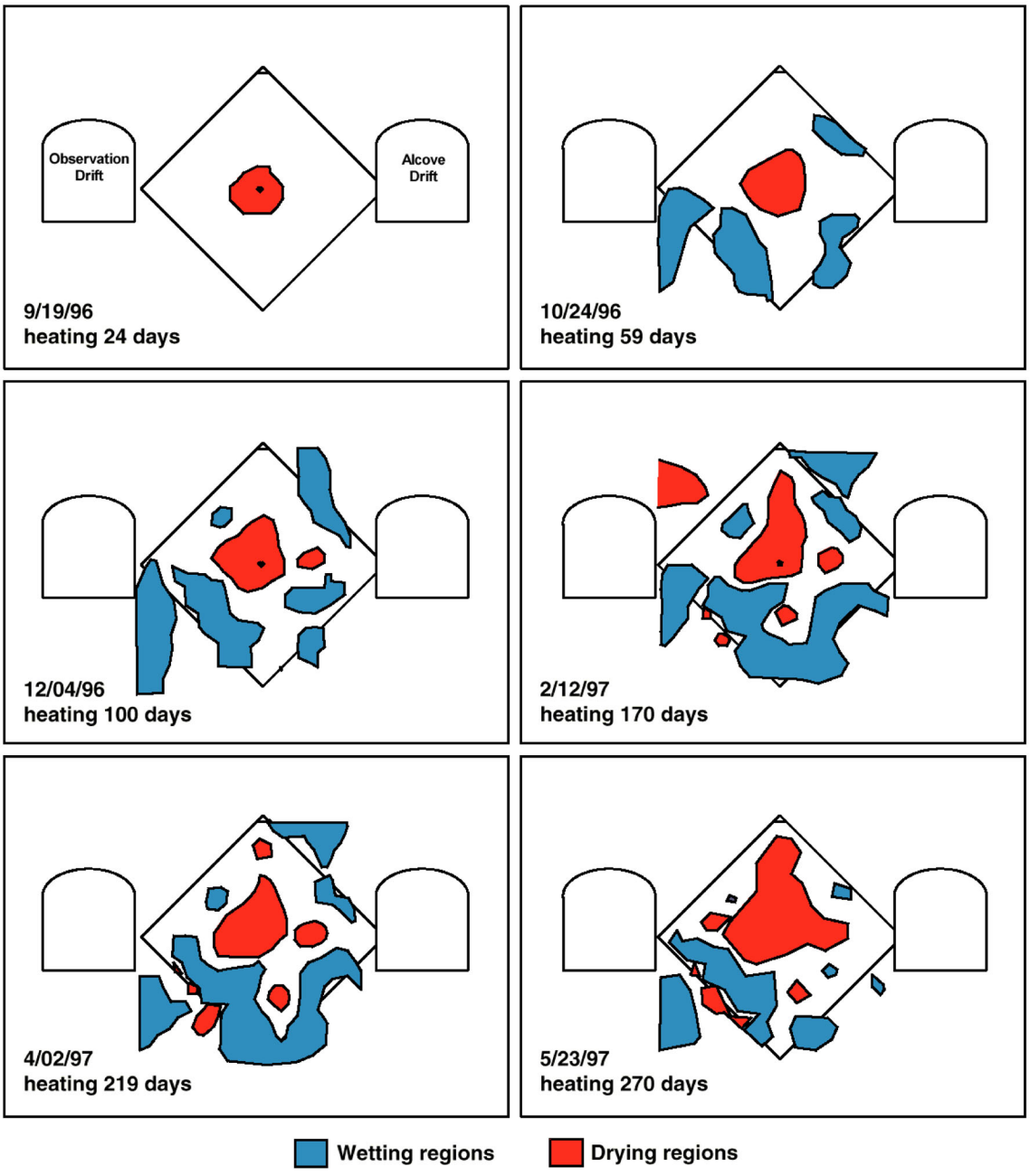

Figure 6.2.2.1-1. Interpretation of ERT Moisture Data during the SHT Heating Phase

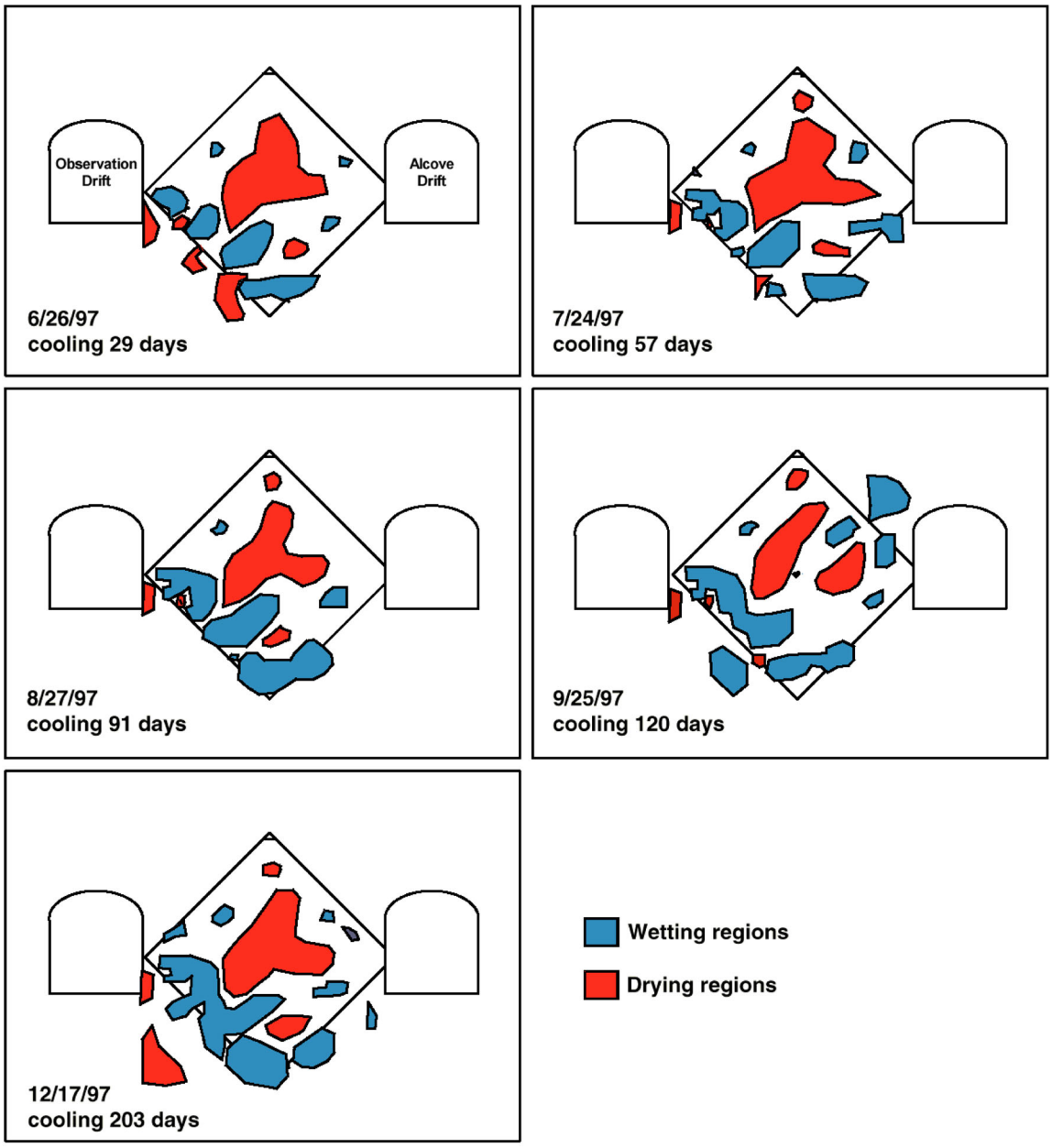

Figure 6.2.2.1-2. Interpretation of ERT Moisture Data during the SHT Cooling Phase

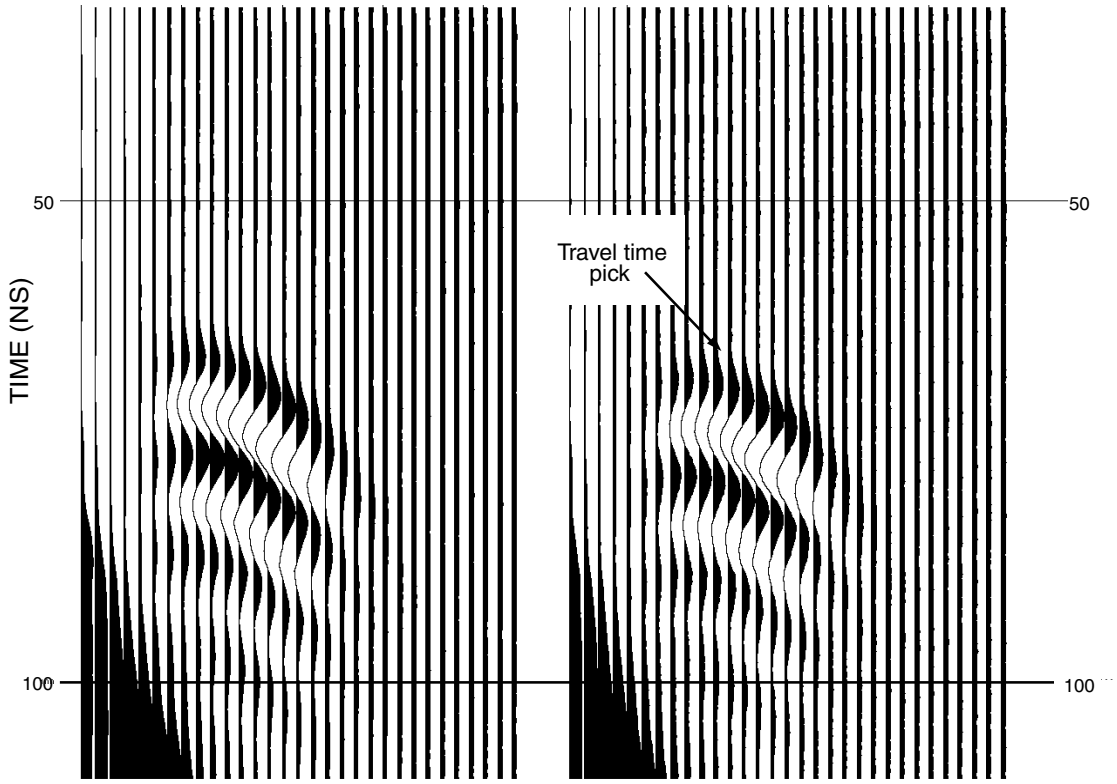

NOTE: Shown are gathers for receivers at 2.37and 2.61 meters down borehole 15.

Figure 6.2.2.2-1. Two Typical SHT GPR Receiver Gathers for the 15-17 Borehole Pair on January 16, 1997

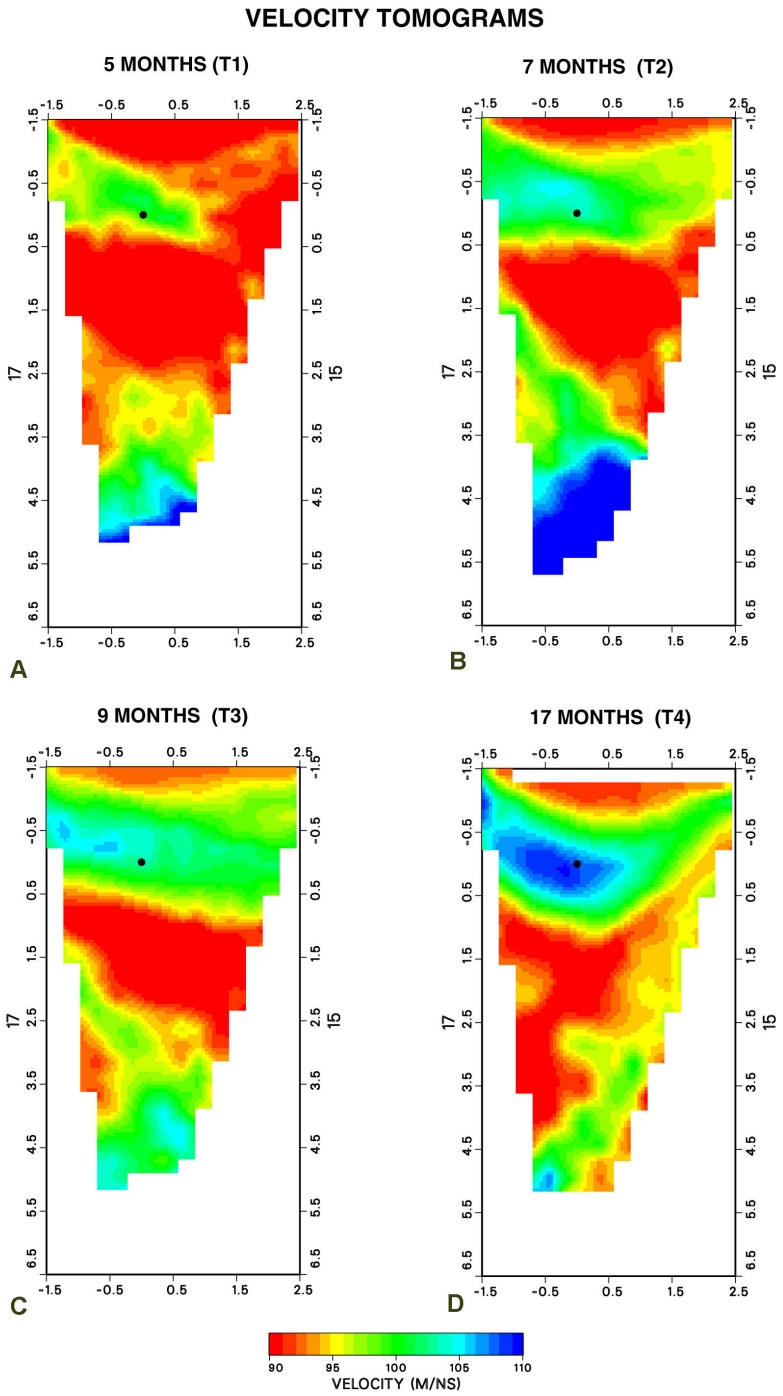

NOTE: a) Survey taken January 15, 1997, b) survey taken March 12, 1997, c) survey taken May 29, 1997, and d) survey taken January 7, 1998.

Figure 6.2.2.2-2. SHT GPR Velocity Tomograms for Borehole Pair 15-17

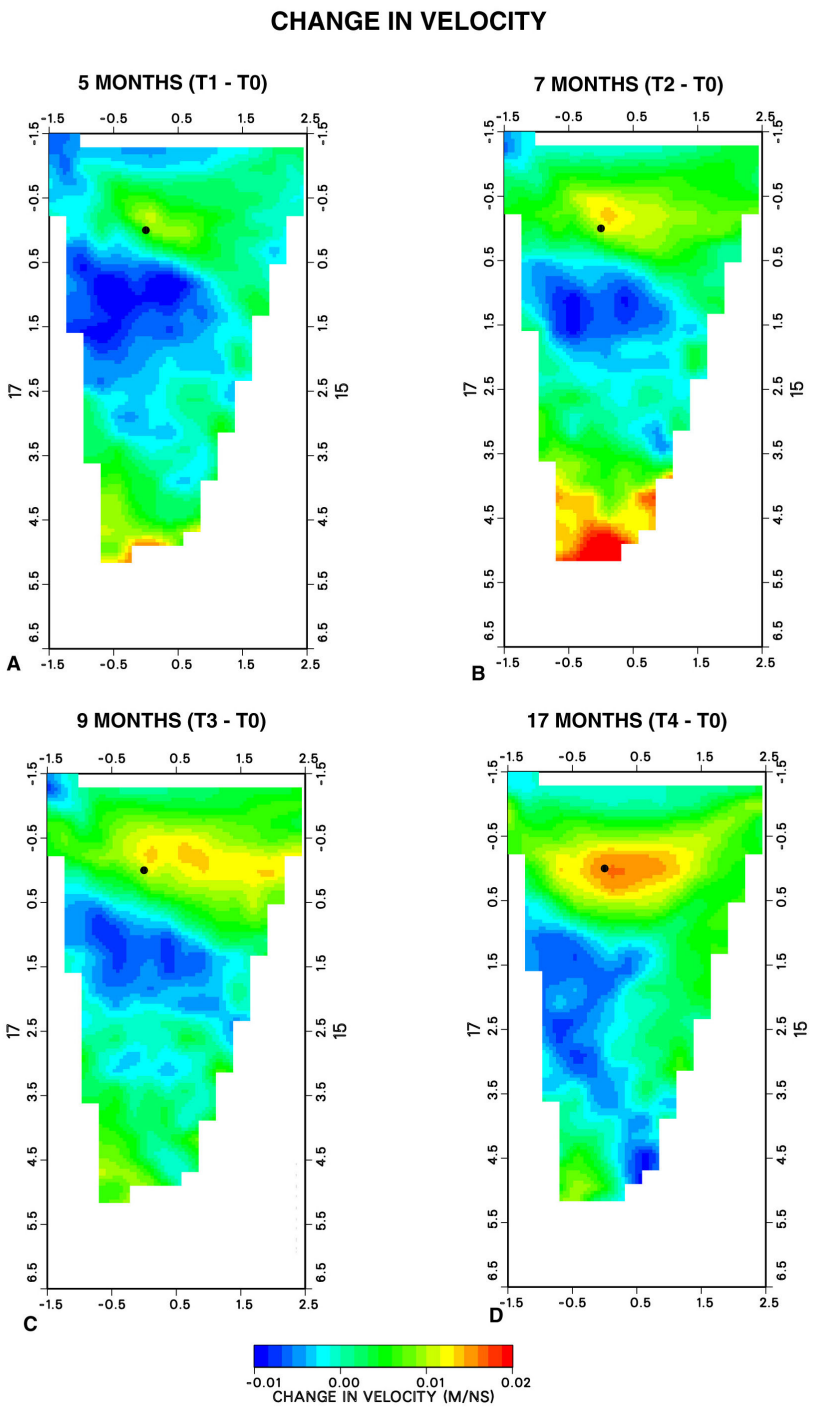

NOTE: Each tomogram is a difference from the baseline tomogram after a) 5 months, b) 7 months, c) 9 months, and d) 17 months.

Figure 6.2.2.2-3. SHT GPR Velocity Difference Tomograms for Borehole Pair 15-17

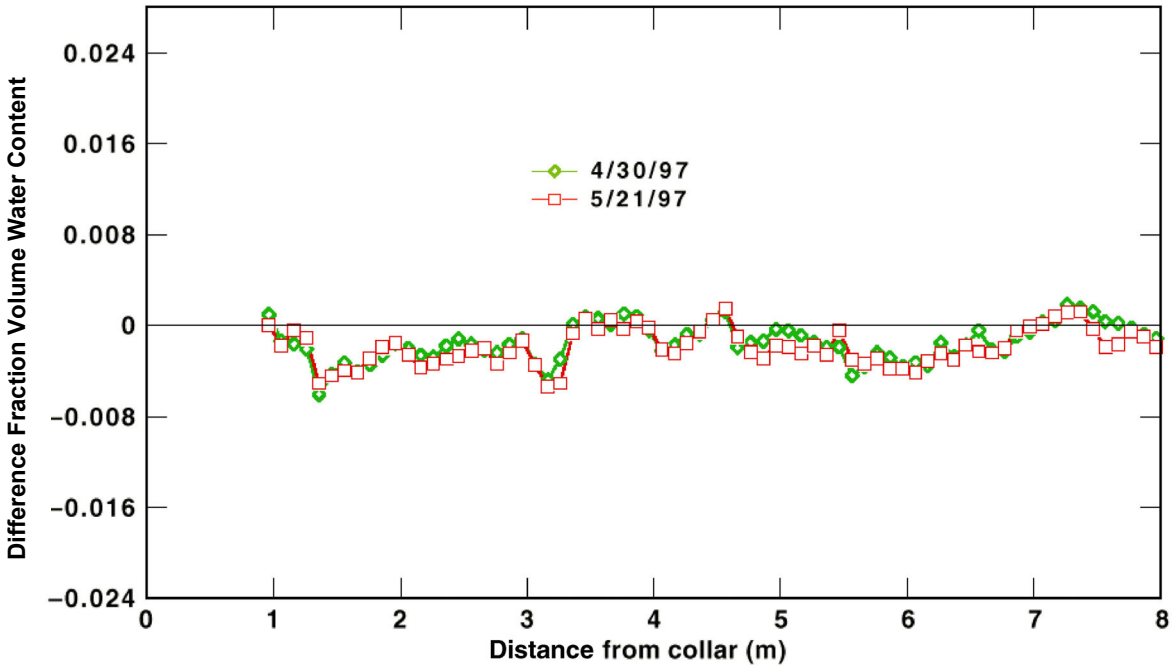

Figure 6.2.2.3-1. Smoothed Difference Fraction Volume Water Content Measured in SHT Borehole 15 using Neutron Logging (April 30 and May 21, 1997)

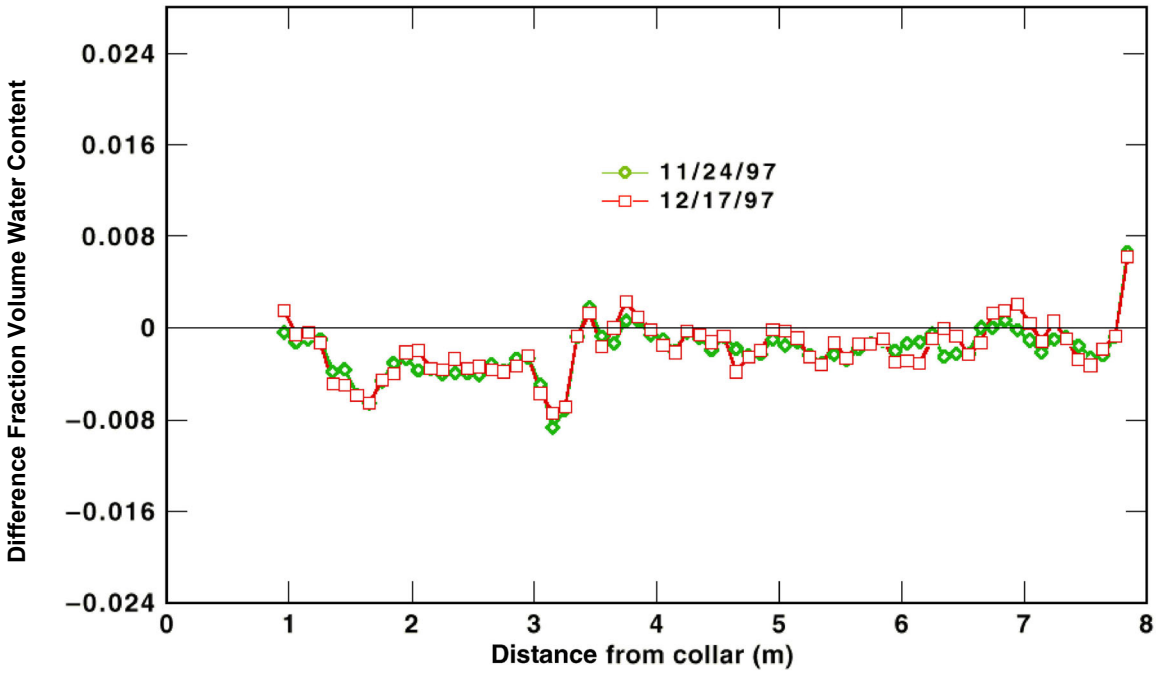

Figure 6.2.2.3-2. Smoothed Difference Fraction Volume Water Content Measured in SHT Borehole 15 using Neutron Logging (November 24 and December 17, 1997)

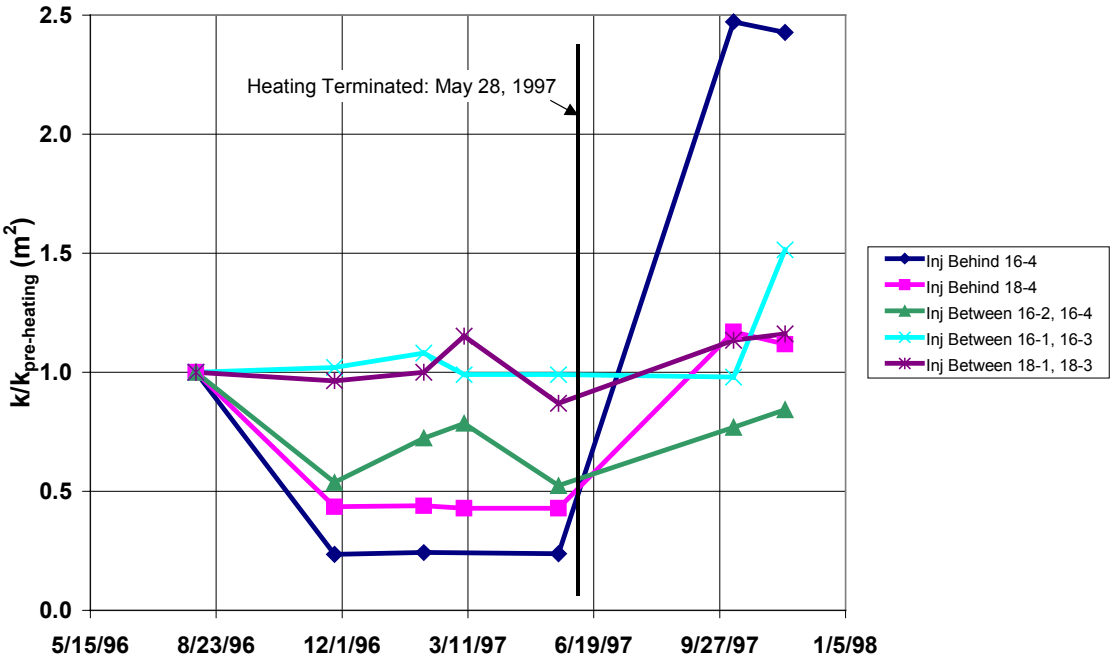

Figure 6.2.2.4-1. SHT Permeability Changes for Borehole 16 and 18 as a Ratio of Transient Permeabilities to the Baseline Permeability Estimate

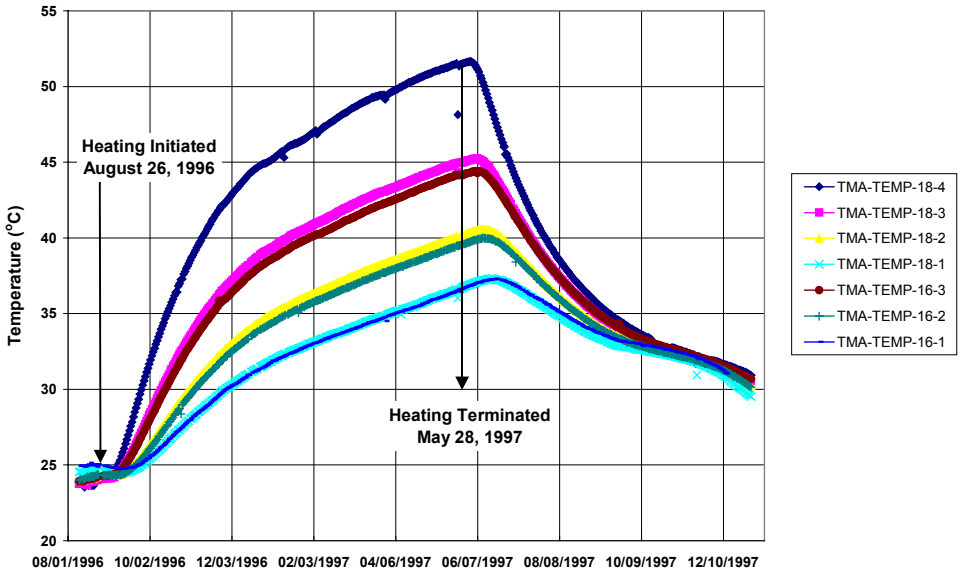

Figure 6.2.2.4-2. Passive Monitoring Temperature Data in SHT Boreholes 16 and 18

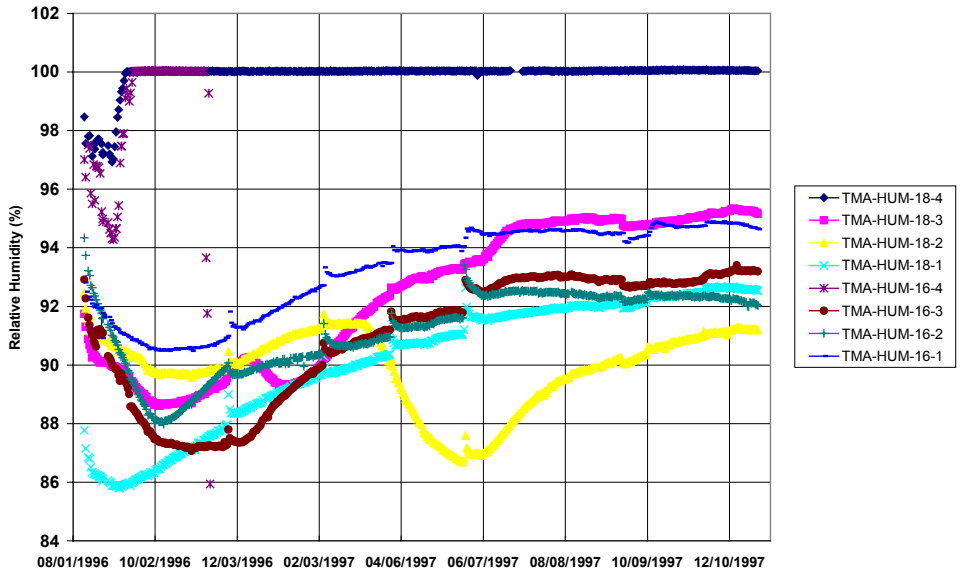

Figure 6.2.2.4-3. Passive Monitoring Relative Humidity Data in SHT Boreholes 16 and 18

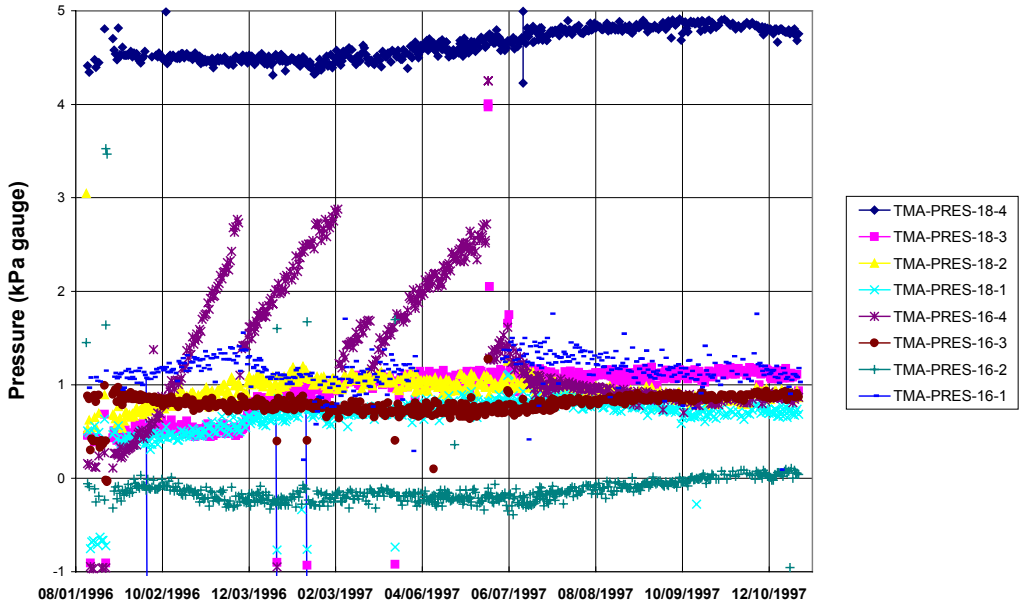

Figure 6.2.2.4-4. Passive Monitoring Pressure Data in SHT Boreholes 16 and 18

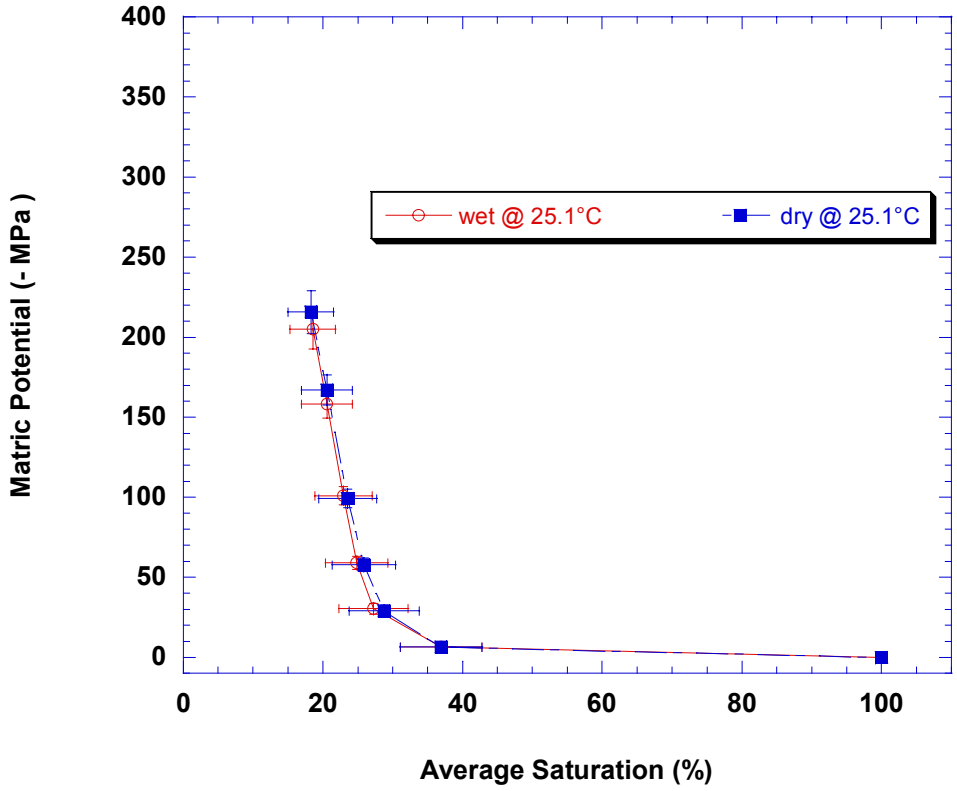

NOTE: Lines connect the points and do not represent curve fits. The point at 100% saturation is inferred.

Figure 6.2.2.5-1. Average Moisture Retention Curves for 11 SHT Samples at 25.1°C

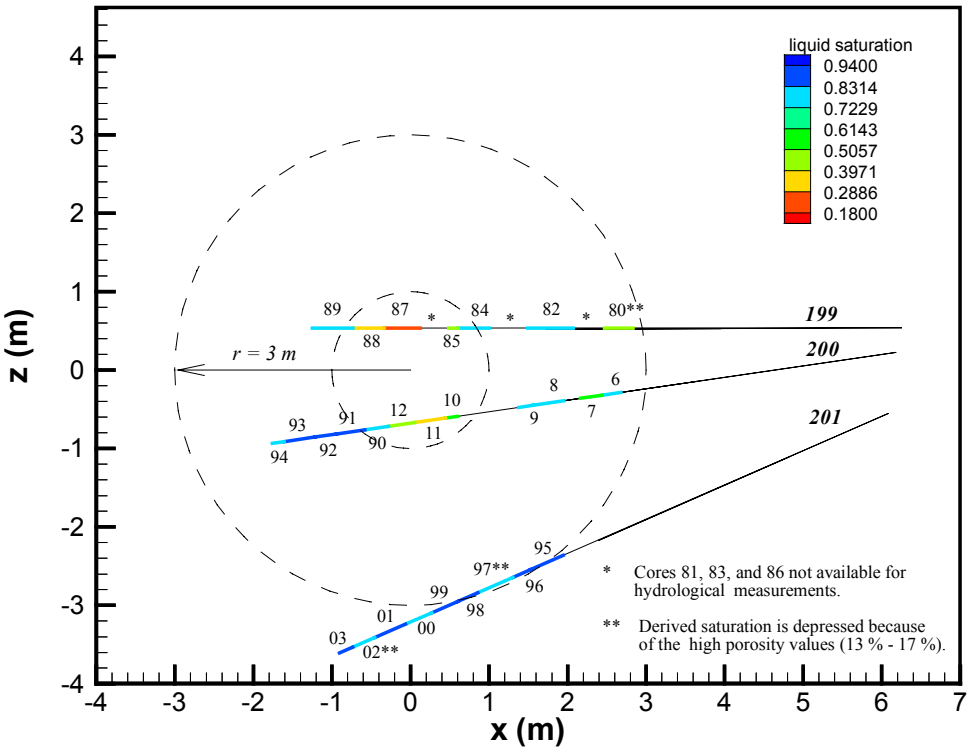

Figure 6.2.2.5-2. Percent Liquid Saturation of Cores from Boreholes 199, 200, 201, Dry-drilled after the Cooling Phase of the SHT

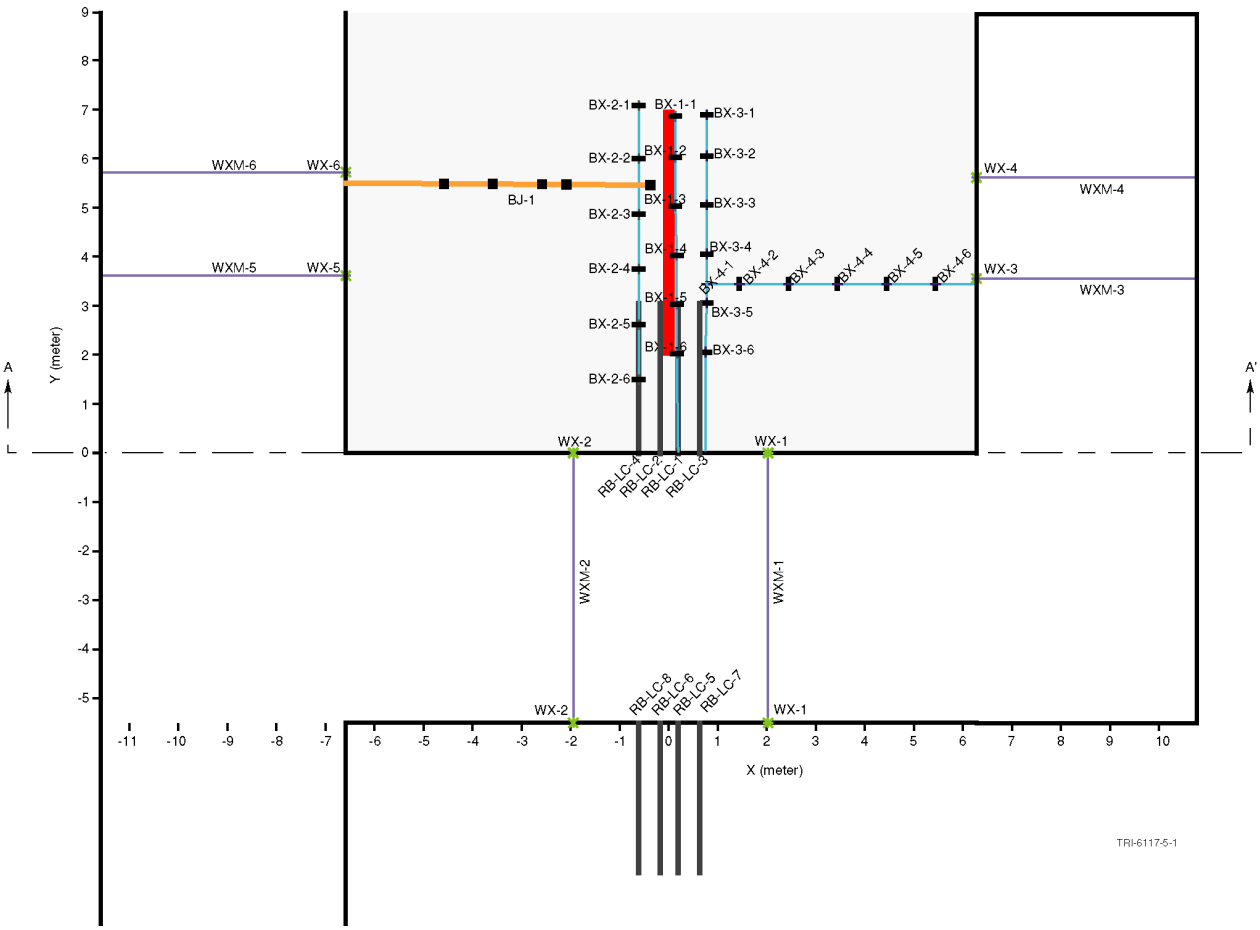

Figure 6.2.3.1-1. Plan View Showing Locations of the SHT Mechanical Boreholes

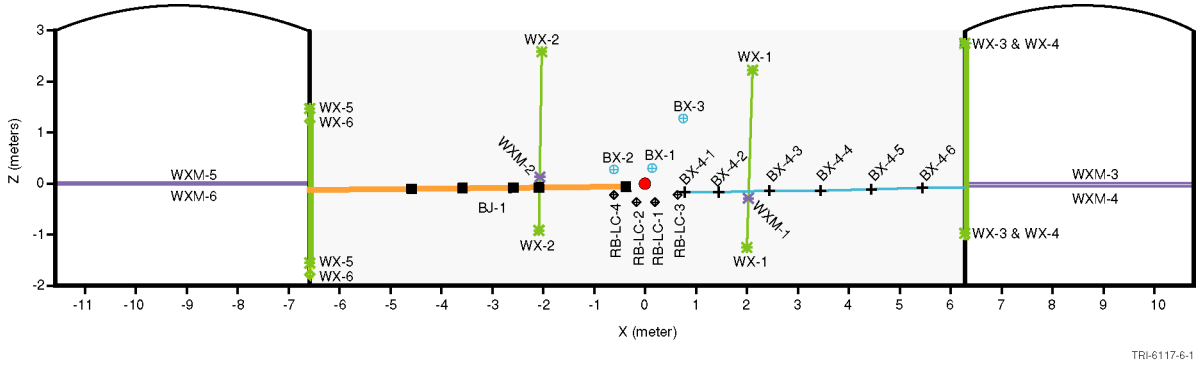

Figure 6.2.3.1-2. Cross-section Showing Locations of the SHT Mechanical Boreholes

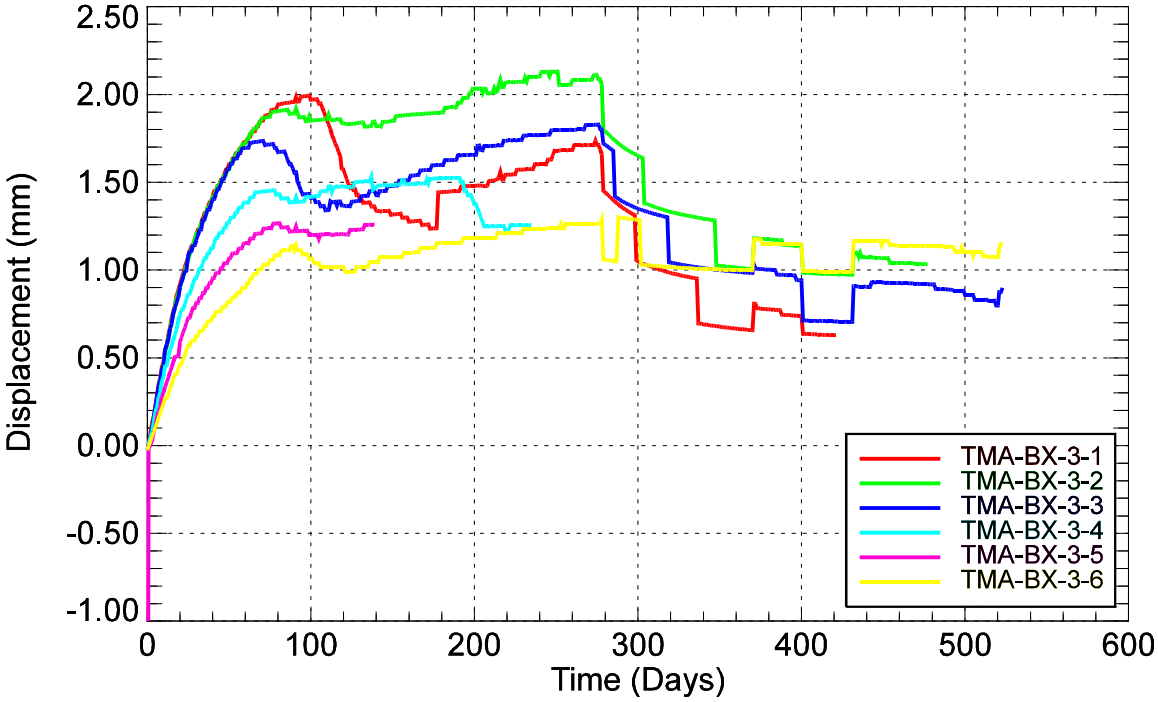

Figure 6.2.3.1-3. Displacement History for SHT MPBX-3 Borehole

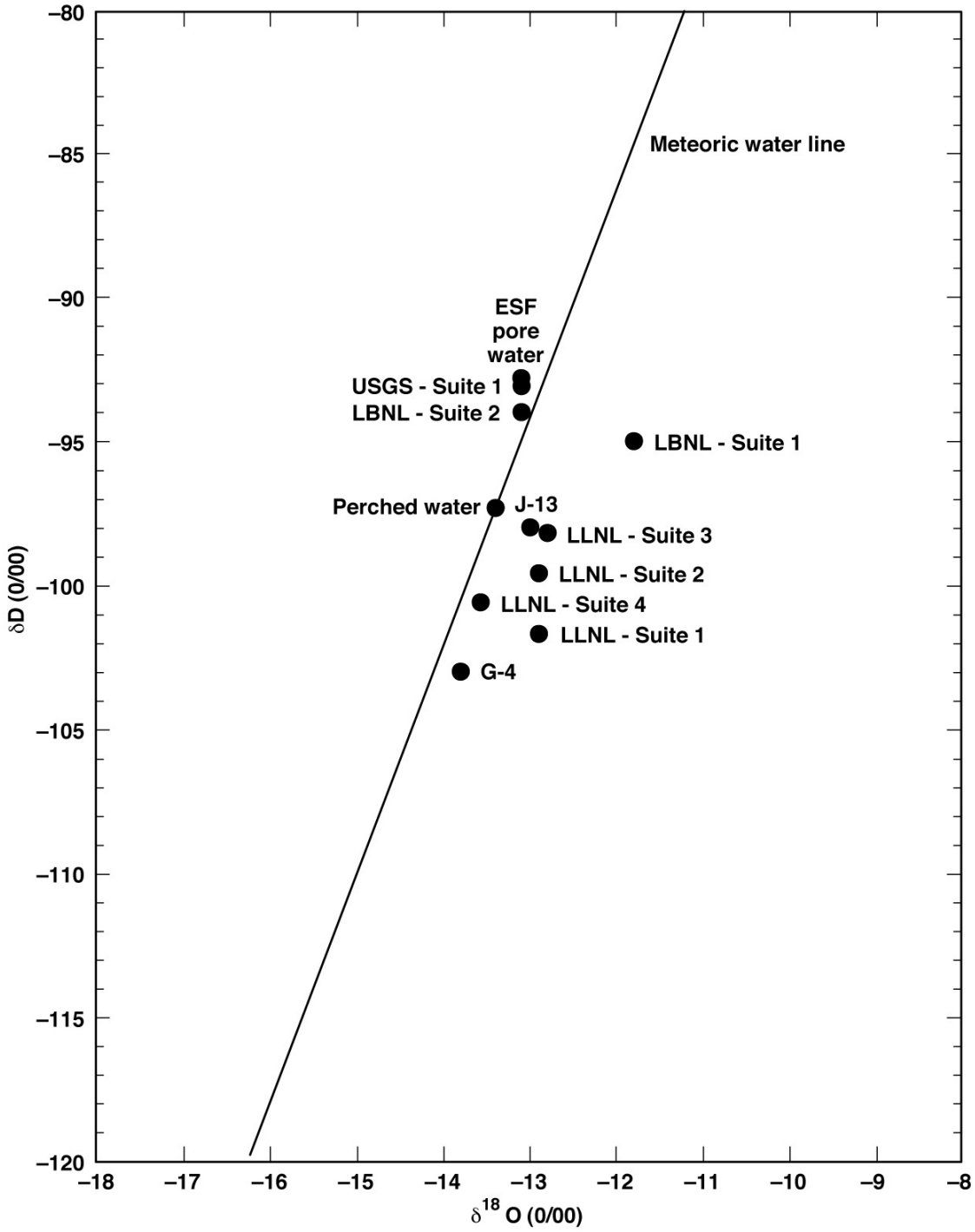

Figure 6.2.4.1-1. Stable Isotope Data for SHT Waters (Suite 1–4), Saturated-Zone Waters from Wells G-4 and J-13, UZ-14 Perched Water, and ESF Pore Water

Table 6.2-1. Output-DTNs along with Input-DTNs for the Single Heater Test

Input-DTN [DIRS]	Input-DTN Description	Input-DTN Text Location	Output-DTN	Output-DTN Description
SNF35110695001.001 [158315] and LL970805504244.043 [158313]	XYZ Coordinates of Boreholes and Sensors	6.2	Unchanged-DTN	Unchanged-DTN
SNF35110695001.008 [113812]	Heater Power	6.2.1.1	MO0208RESTRSHT.002	Power and Temperature Data
SNF35110695001.008 [113812]	Temperature – Heating and Initial Six Months of Cooling	6.2.1.2		
SNF35110695001.009 [113819]	Temperature – Last Two Months of Cooling	6.2.1.2		
SNL22080196001.001 [109722]	Thermal Conductivity	6.2.1.3	Unchanged-DTN	Unchanged-DTN
LL970101004244.026 [158281]	Electrical Resistance Tomography	6.2.2.1	LL020801823142.029	ERT Tomograms
LL970505404244.031 [148609]	Electrical Resistance Tomography	6.2.2.1		
LL971002904244.044 [158286]	Electrical Resistance Tomography	6.2.2.1		
LL980105204244.049 [148610]	Electrical Resistance Tomography	6.2.2.1		
LB980901123142.003 [119016]	Ground Penetrating Radar Data	6.2.2.2	LB0208GPRSHTCP.001	GPR Velocity Tomograms
LL980106904244.051 [118963]	Neutron Logging	6.2.2.3	Unchanged-DTN	Unchanged-DTN
LB960500834244.001 [105587]	Pre-Heating Air Injection	6.2.2.4	LB0208AIRKSHTC.001	Permeability Data (Boreholes 16 and 18)
LB980120123142.008 [158280]	Air Injections in Boreholes 16 and 18, Part 1 of 4	6.2.2.4		
LB970500123142.001 [158293]	Air Injections in Boreholes 16 and 18, Part 2 of 4	6.2.2.4		
LB0204SHAIRK3Q.001 [159543]	Air Injections in Boreholes 16 and 18, Part 3 of 4	6.2.2.4		
LB971000123142.001 [118965]	Air Injections in Boreholes 16 and 18, Part 4 of 4	6.2.2.4		
LB980901123142.001 [118999]	Post-Cooling Air Injection and Gas Tracer Testing	6.2.2.4	Unchanged-DTN	Unchanged-DTN
LB980901123142.002 [119009]	Temperature, Relative Humidity, Gauge Pressure (Passive Monitoring)	6.2.2.4	Unchanged-DTN	Unchanged-DTN
LB970500123142.003 [131500]	Pre-Heating Laboratory Saturation, Porosity, Bulk Density Gravimetric Water Content	6.2.2.5	Unchanged-DTN	Unchanged-DTN
LL970709004244.035 [127312]	Pre-Heating Laboratory Porosity, Relative Humidity, and Water Saturation	6.2.2.5	Unchanged-DTN	Unchanged-DTN

Table 6.2-1. Output-DTNs along with Input-DTNs for Single Heater Test (continued)

Input-DTN [DIRS]	Input-DTN Description	Input-DTN Text Location	Output-DTN	Output-DTN Description
LB980901123142.006 [119029]	Post-Cooling Laboratory Saturation, Porosity, Bulk Density Gravimetric Water Content	6.2.2.5	Unchanged-DTN	Unchanged-DTN
SNF35110695001.008 [113812]	Standard MPBX Displacements – Heating and Initial Six Months of Cooling	6.2.3.1	SN0208F3511695.011	Displacement Data
SNF35110695001.009 [113819]	Standard MPBX Displacements – Last Two Months of Cooling	6.2.3.1		
LL980109904243.015 [158299]	Optical MPBX Displacements	6.2.3.1	Unchanged-DTN	Unchanged-DTN
SNF35110695001.010 [158300]	Rock Mass Deformation Modulus – Borehole (Goodman) Jack	6.2.3.2	Unchanged-DTN	Unchanged-DTN
SNF35110695001.008 [113812]	Rock Bolt Load – Heating and Initial Six Months of Cooling	6.2.3.3	Unchanged-DTN	Unchanged-DTN
SNF35110695001.009 [113819]	Rock Bolt Load – Last Two Months of Cooling	6.2.3.3	Unchanged-DTN	Unchanged-DTN
SNL22080196001.001 [109722]	Laboratory Thermal Expansion	6.2.3.4	Unchanged-DTN	Unchanged-DTN
SNL22080196001.002 [158306]	Pre-Heating Laboratory Unconfined Compressive Strength, Dry Bulk Density, Poisson's Ratio, Young's Modulus, Saturated Bulk Density, Seismic Velocity	6.2.3.4	Unchanged-DTN	Unchanged-DTN
SNL22080196001.003 [119042]	Post-Cooling Laboratory Thermal Conductivity, Thermal Expansion, Unconfined Compressive Strength, Dry Bulk Density, Poisson's Ratio, Young's Modulus	6.2.3.4	Unchanged-DTN	Unchanged-DTN
SNF35110695001.008 [113812]	Rock Mass Thermal Expansion	6.2.3.5	Unchanged-DTN	Unchanged-DTN
LL970101104244.027 [158309]	Chemical Abundance Data	6.2.4.1	Unchanged-DTN	Unchanged-DTN
LL970409604244.030 [111481]	Chemical Abundance Data	6.2.4.1	Unchanged-DTN	Unchanged-DTN
LL970703904244.034 [111482]	Chemical Abundance Data	6.2.4.1	Unchanged-DTN	Unchanged-DTN
LL971006604244.046 [148611]	Chemical Abundance Data	6.2.4.1	Unchanged-DTN	Unchanged-DTN
LA0009SL831151.001 [153485]	Fracture Mineralogy	6.2.4.2	Unchanged-DTN	Unchanged-DTN
LB970100123142.002 [158288]	Infrared Images, Part 1 of 5	6.2.5.2	Unchanged-DTN	Unchanged-DTN
LB970400123142.001 [158289]	Infrared Images, Part 2 of 5	6.2.5.2	Unchanged-DTN	Unchanged-DTN
LB970700123142.002 [158295]	Infrared Images, Part 3 of 5	6.2.5.2	Unchanged-DTN	Unchanged-DTN
LB971000123142.002 [158296]	Infrared Images, Part 4 of 5	6.2.5.2	Unchanged-DTN	Unchanged-DTN
LB980120123142.001 [158297]	Infrared Images, Part 5 of 5	6.2.5.2	Unchanged-DTN	Unchanged-DTN

Table 6.2-2. SHT Borehole Information

Borehole Number	Borehole Identification	Primary Purpose	Collar Coordinates (meters)[1]			Bottom Coordinates (meters)[1]			Orientation Degree	Diameter (cm)	Length (m)	Volume (m^3)	Types and No. of Sensors										Comments
			X	Y	Z	X	Y	Z					Thermo-Couples	RTD	Thermistors	Load Call (Average)	Anchor in MPBX	Type/Wire Extensometer	Humidity Sensor	Pressure Transducer	Electrode Sensor (ERT)	Chemistry Absorbing Pad	
1	ESF-TMA-H-1	Heater	0.01	0.04	-0.03	0.00	6.97	-0.01	0.5	9.60	7.00	0.05	27										5 m Long Heater w/ Metallic Spring Centralizers
2	ESF-TMA-MPBX-1	MPBX - Rock Mass Displacement	0.18	0.08	0.27	0.14	6.99	0.28	0.5	7.57	7.00	0.03	9		1		6						Thermocouple Sensors between and at Anchors in MPBX
3	ESF-TMA-MPBX-2	MPBX - Rock Mass Displacement	-0.62	0.23	0.21	-0.62	7.25	0.25	0.5	7.57	7.00	0.03	13				7						Thermocouple Sensors between and at Anchors in MPBX
4	ESF-TMA-MPBX-3	MPBX - Rock Mass Displacement	0.75	0.10	0.24	0.78	7.00	1.29	0.5	7.57	7.00	0.03	9		1		6						Thermocouple Sensors between and at Anchors in MPBX
5	ESF-TMA-MPBX-4	MPBX - Rock Mass Displacement	6.43	3.50	-0.11	0.40	3.50	-0.21	0.5	7.57	6.20	0.03	12		1		6						Thermocouple Sensors between and at Anchors in MPBX
6	ESF-TMA-OMPBX-1	Optical MPBX	1.19	-0.05	0.28	1.21	11.99	0.13	-0.5	7.57	12.00	0.05											Laser Reflection MPBX System
7	ESF-TMA-OMPBX-2	Optical MPBX	6.20	6.49	-0.17	0.30	6.45	0.27	-0.5	7.57	6.20	0.03											Laser Reflection MPBX System
8	ESF-TMA-TC-1	Thermocouple	-0.18	0.15	0.28	-0.27	7.85	0.34	0.0	4.80	8.00	0.01	15										Thermocouple Probes Grouted in Borehole
9	ESF-TMA-TC-2	Thermocouple	0.63	0.06	0.21	0.62	8.15	0.26	0.0	4.80	8.00	0.01	15										Thermocouple Probes Grouted in Borehole
10	ESF-TMA-TC-3	Thermocouple	-0.75	0.23	1.26	-0.71	8.05	1.31	0.0	4.80	8.00	0.01	15										Thermocouple Probes Grouted in Borehole
11	ESF-TMA-TC-4	Thermocouple	-0.02	0.03	0.69	-0.09	5.49	-0.77	0.0	4.80	8.00	0.01	15										Thermocouple Probes Grouted in Borehole
12	ESF-TMA-TC-5	Thermocouple	0.00	0.16	0.65	-0.04	6.84	0.68	0.0	4.80	8.00	0.01	15										Thermocouple Probes Grouted in Borehole
13	ESF-TMA-TC-6	Thermocouple	6.26	5.49	-0.01	1.87	5.46	-0.04	0.0	4.80	6.20	0.01	10										Thermocouple Probes Grouted in Borehole
14	ESF-TMA-TC-7	Thermocouple	-6.59	3.46	-0.01	-0.34	3.43	-0.02	0.0	6.00	6.20	0.02	10										Thermocouple Probes Grouted in Borehole
15	ESF-TMA-NEU-1	Neutron Probe & Temp	6.10	4.29	0.33	-1.60	4.28	2.74	17.0	7.57	8.50	0.04		27									RTDs Grouted between Hole and Teflon Tube
16	ESF-TMA-NEU-2	Hydrology	6.10	4.30	0.04	1.14	4.32	0.71	7.5	7.57	5.50	0.02		4				4	4				Pressure, RTD & Humidity Sensors in Packer Systems
17	ESF-TMA-NEU-3	Neutron Probe & Temp	6.16	4.30	-0.45	-1.78	4.31	-1.47	-7.0	7.57	8.50	0.04		29									RTDs Grouted Between Borehole and Teflon Tube
18	ESF-TMA-NEU-4	Hydrology	6.17	4.29	-0.22	1.51	4.28	-0.28	-0.5	7.57	5.00	0.02		4				4	4				Pressure, RTD & Humidity Sensors in Packer Systems
19	ESF-TMA-BJ-1	Borehole Jack	-6.55	5.52	-0.14	-0.34	5.51	-0.07	0.5	7.57	6.20	0.03											Open Hole for Borehole Jack
20	ESF-TMA-CHE-1	Chemistry - SEAMIST	-6.64	4.91	-0.66	-1.51	4.93	-0.77	-0.5	7.57	5.00	0.02									50		SEAMIST System with Chemical Sensors, 45 Sensors Failed

INTENTIONALLY LEFT BLANK

Table 6.2-2. SHT Borehole Information (continued)

Borehole Number	Borehole Identification	Primary Purpose	Collar Coordinates (meters)[1]			Bottom Coordinates (meters)[1]			Orientation Degree	Diameter (cm)	Length (m)	Volume (m^3)	Types and No. of Sensors										Comments
			X	Y	Z	X	Y	Z					Thermo-Couples	RTD	Thermistors	Load Call (Average)	Anchor in MPBX	Type/Wire Extensometer	Humidity Sensor	Pressure Transducer	Electrode Sensor (ERT)	Chemistry Absorbing Pad	
21	ESF-TMA-CHE-2	Chemistry - SEAMIST	-6.59	5.01	-0.01	-1.06	5.10	0.63	7.5	7.57	5.50	0.02									50		SEAMIST System with Chemical Sensors, 45 Sensors Failed
22	ESF-TMA-HYD-1	Neutron Probe & Temp	-6.60	4.43	-0.66	-1.56	4.39	-0.74	-0.5	7.57	5.00	0.02		20									RTDs Grouted between Borehole and Teflon Tube
23	EFS-TMA-HYD-2	Neutron Probe & Temp	-6.57	4.43	0.00	-1.31	4.42	0.65	7.5	7.57	5.50	0.02		19									RTDs Grouted between Borehole and Teflon Tube
24	ESF-TMA-ERT-1	Electrical Resistivity Tomography	-6.56	3.89	0.12	-0.41	3.82	6.28	45.0	7.57	8.70	0.04								9			Electrical Resistivity Tomography, Electrode Sensor on 1 m Intervals
25	ESF-TMA-ERT-2	Electrical Resistivity Tomography	-6.57	3.91	-0.13	-0.29	4.07	-6.22	-45.0	7.57	8.70	0.04								9			Electrical Resistivity Tomography, Electrode Sensor on 1 m Intervals
26	ESF-TMA-ERT-3	Electrical Resistivity Tomography	6.25	3.89	-0.36	1.15	3.85	-5.71	-45.0	7.57	8.70	0.04								9			Electrical Resistivity Tomography, Electrode Sensor on 1 m Intervals
27	ESF-TMA-ERT-4	Electrical Resistivity Tomography	6.25	3.90	0.36	0.38	3.97	6.29	45.0	7.57	8.70	0.04								9			Electrical Resistivity Tomography, Electrode Sensor on 1 m Intervals
28	ESF-TMA-RB-1	Rock Bolt w/Load Cell	0.14	0.05	-0.38	0.26	4.21	-0.38	0.0	5.72	4.00	0.01			1	1							Vibrating Wire Load Cell on Head of Rock Bolt
29	ESF-TMA-RB-2	Rock Bolt w/Load Cell	-0.23	0.00	-0.35	-0.18	4.22	-0.42	0.0	5.72	4.00	0.01			1	1							Vibrating Wire Load Cell on Head of Rock Bolt
30	ESF-TMA-RB-3	Rock Bolt w/Load Cell	0.59	0.10	-0.31	0.60	4.03	-0.35	0.0	5.72	4.00	0.01			1	1							Vibrating Wire Load Cell on Head of Rock Bolt
31	ESF-TMA-RB-4	Rock Bolt w/Load Cell	-0.68	0.13	-0.29	-0.59	4.18	-0.23	0.0	5.72	4.00	0.01			1	1							Vibrating Wire Load Cell on Head of Rock Bolt
32	ESF-TMA-RB-5	Rock Bolt w/Load Cell	0.14	-5.37	-0.39	0.06	-9.47	-0.41	0.0	5.72	4.00	0.01			1	1							Vibrating Wire Load Cell on Head of Rock Bolt
33	ESF-TMA-RB-6	Rock Bolt w/Load Cell	-0.20	-5.45	-0.42	-0.21	-9.45	-0.42	0.0	5.72	40.00	0.01			1	1							Vibrating Wire Load Cell on Head of Rock Bolt
34	ESF-TMA-RB-7	Rock Bolt w/Load Cell	0.59	-5.49	-0.30	0.64	-9.60	-0.36	0.0	5.72	4.00	0.01			1	1							Vibrating Wire Load Cell on Head of Rock Bolt
35	ESF-TMA-RB-8	Rock Bolt w/Load Cell	-0.64	-5.38	-0.31	-0.73	-9.43	-0.45	0.0	5.72	4.00	0.01			1	1							Vibrating Wire Load Cell on Head of Rock Bolt
36	ESF-TMA-TE-1	Tape Extensometer Array 3	-2.00	0.00	Multiple				0.0	2.54	Up to 0.5							1					4-pin Tape Extensometer Array
37	ESF-TMA-TE-2	Tape Extensometer Array 3	2.00	0.00	Multiple				0.0	2.54	Up to 0.5							1					4-pin Tape Extensometer Array
38	ESF-TMA-TE-3	Tape Extensometer Array 3	-6.50	3.00	Multiple				0.0	2.54	Up to 0.5							1					4-pin Tape Extensometer Array
39	ESF-TMA-TE-4	Tape Extensometer Array 3	-6.50	5.10	Multiple				0.0	2.54	Up to 0.5							1					4-pin Tape Extensometer Array

INTENTIONALLY LEFT BLANK

Table 6.2-2. SHT Borehole Information (continued)

													Types and No. of Sensors									Comments
Borehole Number	Borehole Identification	Primary Purpose	Collar Coordinates (meters)[1]			Bottom Coordinates (meters)[1]			Orientation Degree	Diameter (cm)	Length (m)	Volume (m^3)	Thermo-Couples	RTD	Thermistors	Load Call (Average)	Anchor in MPBX	Type/Wire Extensometer	Humidity Sensor	Pressure Transducer	Electrode Sensor (ERT)	Chemistry Absorbing Pad	
			X	Y	Z	X	Y	Z															
40	ESF-TMA-TE-5	Tape Extensometer Array 3	6.50	3.00	Multiple				0.0	2.54	Up to 0.5							1					4-pin Tape Extensometer Array
41	ESF-TMA-TE-6	Tape Extensometer Array 3	6.50	5.00	Multiple				0.0	2.54	Up to 0.5							1					4-pin Tape Extensometer Array
	ESF-TMA-IN-THRM-1 through 15	Thermistors													15								5 Thermistors in the Insulation of Each Rib
	ESF-TMA-STC-1 through 36	Thermocouple											36										Surface Thermocouples Located on Each Rib
	ESF-ATC-1 through 3	Thermocouple											3										Surface Thermocouples Located on Each Rib
	ESF-TMA-WX-1 through 6	Wire Extensometer																6					6 Sets of Strain Measurements on Rib
										TOTAL	226.30	0.84	204	103	26	8	25	12	8	8	36	100	
										TOTAL NUMBER OF SENSORS (ALL TYPES):												530	

NOTE: [1] Borehole Coordinates are Referenced to a 0.0.0 Coordinate Located at the Center of the Collar for the Heater Borehole

INTENTIONALLY LEFT BLANK

Table 6.2-3. SHT Post-Testing Borehole Information*

Borehole Number	Borehole ID (ESF-TMA)	Primary Purpose	Collar Coordinates (Cartesian) [1]			Orientation	Hole Diameter	Hole Length*
			X	Y	Z			
			meters	meters	meters	azim/decline	cm	meters
194	PTC-H-1	Overcore Heater	0.00	0.00	0.00	az -288/ 0.5 deg	25.40	7.00
195 - Deleted	PTC-RB-1	Overcore Rock Bolt	0.18	0.00	-0.37	az -288/ 0.0 deg	15.24	4.00
196	PTC-MPBX-1	Overcore MPBX	0.18	0.00	0.29	az -288/ 0.5 deg	15.24	7.00
197	PTC-NEU-2	Overcore Hyd.	6.50	4.30	0.00	az 18/ 7.5 deg	15.24	6.00
198	PTC-TC-6	Overcore TC	6.50	5.50	0.00	az 18/ 0.0 deg	15.24	6.50
199	PTC-1	Observation	6.50	4.70	0.53	az 18/ 0.0 deg	7.57	7.50
200	PTC-2	Observation	6.50	4.70	0.26	az 18/ -7.94 deg	7.57	8.10
201	PTC-3	Observation	6.50	4.70	-0.28	az 18/ -22.68 deg	7.57	8.10
202	PTC-4	Observation	-0.31	0.00	0.18	az -288/ 0.0 deg	7.57	8.00
203	PTC-5	Observation	0.40	0.00	0.25	az -288/ 0.0 deg	7.57	8.00
204	PTC-6	Observation	1.14	0.00	0.50	az -288/ 9.8 deg	7.57	8.00

NOTES: * From field survey

[1] +X-direction azimuth = 18 degrees (N);
+Y-direction azimuth = 288 degrees (W);
+Z-direction azimuth = vertically.

Table 6.2.1.3-1. SHT Thermal Conductivity Laboratory Data for Four Specimens from Heater Borehole 1

Apparatus[(a)]	Temperature (°C)	Thermal Conductivity (W/(m-K))				Mean	Standard Deviation
		ESF-H1-0.6-B	ESF-H1-11.3-B	ESF-H1-11.6-B	ESF-H1-19.9-B		
LT	30	1.50	1.76	1.37	1.76	1.60	0.20
LT	50	1.52	1.79	1.40	1.77	1.62	0.19
LT	70	1.54	1.81	1.44	1.77	1.64	0.18
TCA	70	1.58	1.96	1.61	1.89	1.76	0.19
TCA	110	1.56	1.88	1.57	1.80	1.70	0.16
TCA	155	1.61	1.85	1.62	1.79	1.72	0.12
TCA	200	1.60	1.82	1.59	1.78	1.70	0.12
TCA	245	1.57	1.81	1.60	1.75	1.68	0.12
TCA	289	1.48	1.76	1.56	1.69	1.62	0.13
Mean		1.55	1.83	1.53	1.78	1.67	N/A
Standard Deviation		0.04	0.06	0.10	0.05	N/A	0.15

NOTE: (a) A low temperature (LT) device was used for testing at 70°C and below; a thermocouple apparatus (TCA) was used for 70°C and above.

Table 6.2.2.4-1. Parameters for the Estimation of Pre-Heating SHT Air-Permeability, k, around Injection Zones for Various Boreholes

Borehole and Data File ID	Borehole Length (m)	Borehole Radius (cm)	Packed Zone, L (m)	Constant Flow Rate, Q(SLPM)	P_2-P_1 (kPa)	Estimated Permeability k(m^2)
Borehole 1 (5/24-03)	7.00	4.8	1.73	53.	35.0	1.5E-13
Borehole 1 (5/28-08)	7.00	4.8	1.73	50.	32.5	1.5E-13
Borehole 1 (5/30-14)	7.00	4.8	2.70	22.	9.5	1.8E-13
Borehole 2 (5/28-06)	6.91	3.79	6.00	22.	13.4	7.2E-14
Borehole 3 (5/28-02)	7.02	3.79	6.11	100.	22.3	1.8E-13
Borehole 4 (5/28-03)	6.89	3.79	5.98	22.	77.0	9.2E-15
Borehole 6 (5/30-07)	11.99	3.79	11.07	40.	20.0	5.1E-14
Borehole 7 (5/31-01)	5.91	3.79	5.00	360.	10.7	1.7E-12
Borehole 7 (5/31-07)	5.91	3.79	2.26	500.	16.0	2.9E-12
Borehole 10 (5/24-02)	8.00	2.4	7.09	3.	10.6	1.2E-14
Borehole 11 (5/28-04)	6.80	2.4	5.89	300.	3.0	5.2E-12
Borehole 12 (5/28-05)	7.67	2.4	6.76	200.	37.0	2.1E-13
Borehole 13 (5/30-08)	5.95	3.79	5.04	22.	16.5	6.6E-14
Borehole 15 (5/29-14)	8.18	3.79	7.09	20.	48.0	1.4E-14
Borehole 16 (5/30-09)	5.18	3.79	3.94	11.	64.0	8.3E-15
Borehole 17 (5/28-07)	8.00	3.79	6.91	100.	1.5	2.8E-12
Borehole 18 (5/30-10)	4.86	3.79	3.59	21.	15.5	8.8E-14
Borehole 19 (5/31-04)	5.79	3.79	4.88	20.	6.6	1.6E-13
Borehole 22 (5/29-02)	5.00	3.79	4.09	1.	6.4	9.9E-15
Borehole 23 (5/29-01)	5.50	3.79	4.59	1.	11.0	5.0E-15
Borehole 24 (5/31-03)	8.71	3.79	7.44	5.	15.7	1.2E-14
Borehole 25 (5/31-02)	8.74	3.79	7.82	100.	7.8	4.6E-13
Borehole 26 (5/31-05)	8.70	3.79	7.73	200.	6.8	1.1E-12
Borehole 27 (5/30-13)	8.70	3.79	7.43	4.5	30.0	5.1E-15

Table 6.2.2.4-2. Input Parameters and Estimated Pre-heating Air Permeability, k(m^2) for Consecutive 0.69 Meter Zones from Injection Tests Between Straddle Packers in SHT Borehole 6

Borehole 6 Data File and Straddle Zone ID	Mid-zone Location from Collar (m)	Constant Flow Rate, Q(SLPM)	P_2-P_1 (kPa)	Permeability k(m^2)
(5/29-03) 3'-5'	1.22	1.03	47.00+	4.0E-15+
(5/29-04) 5'-7'	1.83	0.39	65.00	1.0E-15
(5/29-05) 7'-9'	2.44	0.62	57.20	1.9E-15
(5/29-06) 9'-11'	3.05	0.62	58.00	1.9E-15
(5/29-07) 11'-13'	3.66	0.62	*	*
(5/29-08) 13'-15'	4.27	2.04	*	*
(5/29-09) 15'-17'	4.88	2.01	58.00	6.1E-15
(5/29-10) 17'-19'	5.49	2.01	24.50	1.7E-14
(5/29-11) 19'-21'	6.10	2.01	28.00	1.4E-14
(5/29-12) 21'-23'	6.71	4.00	17.20	5.0E-14
(5/30-06) 23'-25'	7.32	4.02	8.00	1.1E-13
(5/29-13) 25'-27'	7.92	42.00	25.00	3.4E-13
(5/30-01) 25'-27'	7.92	40.50	25.20	3.3E-13
(5/31-06) 25'-27'	7.92	41.00	27.00	3.1E-13
(5/30-02) 27'-29'	8.53	2.00	6.20	7.3E-14
(5/30-03) 29'-31'	9.14	2.03	13.00	3.4E-14
(5/30-04) 31'-33'	9.75	2.03	14.00	3.1E-14
(5/30-05) 33'-35'	10.36	2.00	0.75	6.2E-13

* The pressure response to the constant injection flow rate is linear with time, indicative of injection into a nearly closed system, in other words, formation of a very low permeability.

Table 6.2.2.4-3. Post-cooling Air Permeability, k (m^2), for SHT Boreholes 1, 3, 6, 7, 16, 18, 19

Injection Zone and Datafile ID	Packed Zone L (m)	Constant Flowrate. Q(SLPM)	P_2-P_1 (kPa)	k(m^2) assuming T_f=30.6°C
Borehole 1-Zone 1 (Jan21-08)	0.59	1	1.62	1.5E-13
Borehole 1-Zone 2 (Jan21-09)	0.59	10	3.48	6.8E-13
Borehole 1-Zone 3 (Jan21-10)	0.59	10	2.3	1.0E-12
Borehole 1-Zone 4 (Jan21-11)	0.59	10	2.36	1.0E-12
Borehole 1-Zone 5 (Jan21-13)	0.59	10	0.46	5.2E-12
Borehole 1-Zone 6 (Jan21-12)	1.34	10	0.972	1.4E-12
Borehole 3 (21Jan03)	6.11	40	3.22	5.7E-13
Borehole 6 (21Jan04)	11.07	40	14.8	7.2E-14
Borehole 7 (21Jan05)	5.00	100	2.17	2.5E-12
Borehole 7-back zone (22Jan01)	2.43	100	2.15	4.5E-12
Borehole 16 Zone 3 (Jan2106)	2.10	1	2.71	3.9E-14
Borehole 18 Zone 3 (Jan2107)	1.55	10	4.9	2.7E-13
Borehole 19 (21Jan02)	4.88	20	3.37	3.3E-13

Table 6.2.2.4-4. Comparison of Pre-heating and Post-cooling Air Permeability Measurements for SHT Boreholes 3, 6, 7, 16, 18, 19

Pre-Heating Air Permeability (assume T_f=24.6°C)			Post-Cooling Air Permeability (assume T_f=30.6°C)			
Borehole and Datafile ID	**L (m)**	**k(m^2)**	**Borehole and Datafile ID**	**L (m)**	**k(m^2)**	**Post-Cooling/ Pre-Heating Ratio**
Borehole 3 (5/28-02)	6.11	1.8E-13	3 (21Jan-03)	6.11	5.7E-13	3.1
Borehole 6 (5/30-07)	11.07	5.1E-14	6 (21Jan-04)	11.07	7.2E-14	1.4
Borehole 7 (5/31-01)	5.00	1.7E-12	7 (21Jan-05)	5.00	2.5E-12	1.5
Borehole 7 (5/31-07)	2.26	2.9E-12	7 (22Jan-01)	2.43	4.5E-12	1.6
16 Zone 3 (Aug 7,8, 1996)	2.10	1.1E-14	16-Zone 3 (Jan21-06)	2.10	3.9E-14	3.5
18 Zone 3 (Aug 7,8, 1996)	1.55	2.3E-13	18-Zone 3 (Jan21-07)	1.55	2.7E-13	1.2
Borehole 19 (5/31-04)	4.88	1.6E-13	19 (21Jan-02)	4.88	3.3E-13	2.0

Table 6.2.2.4-5. SHT Gas Tracer Test Results

Tracer Injection (borehole 1, location w.r.t. collar)	Withdrawal Location Borehole Number - Zone	First Arrival Time	Mass Recovery (qualitative analysis)
3.93m – 4.42m	16-Zone 3	3 minutes	100% within 30 minutes
3.93m – 4.42m	16-Zone 3	3 minutes	100% within 30 minutes
3.93m – 4.42m	18-Zone 3	7 minutes	100% within 15 hours
5.05m – 5.64m	16-Zone 3	12 minutes	50% within 1 hour
5.05m – 5.64m	18-Zone 3	8 minutes	No analysis made

Table 6.2.2.5-1. SHT Pre-Heating Laboratory Hydrological Measurement of Wet-Drilled Cores

Borehole 1, ESF-TMA-H1					
Sample Location (m)	**Saturation (%)**	**Porosity (%)**	**Bulk Density (g/cc)**	**Particle Density (g/cc)**	**Gravimetric Water Content (g/g)**
1.0	89.46	10.66	2.25	2.51	0.043
2.5*	88.04	13.30	2.18	2.52	0.054
3.7	93.60	8.87	2.29	2.52	0.036
4.7	97.27	11.83	2.22	2.51	0.051
5.7	93.97	13.83	2.16	2.51	0.061
6.7	96.03	11.89	2.21	2.51	0.052

* contains small voids

Borehole 6, ESF-TMA-OMPBX-1					
Sample Location (m)	**Saturation (%)**	**Porosity (%)**	**Bulk Density (g/cc)**	**Particle Density (g/cc)**	**Gravimetric Water Content (g/g)**
0.2	94.82	11.00	2.24	2.51	0.047
2.4	94.75	10.43	2.25	2.51	0.044
4.4	93.58	10.18	2.26	2.51	0.042
7.5*	96.87	23.62	1.96	2.57	0.104
Subcore		20.44	2.02	2.53	
9.3	96.17	11.55	2.22	2.52	0.050
11.3	93.07	9.74	2.27	2.51	0.040

* split along axis during oven drying

Borehole 5, ESF-TMA-MPBX-4					
Sample Location (m)	**Saturation (%)**	**Porosity (%)**	**Bulk Density (g/cc)**	**Particle Density (g/cc)**	**Gravimetric Water Content (g/g)**
0.7*	95.85	17.03	2.05	2.48	0.079
2.1*	101.61	9.69	2.25	2.49	0.044
2.6#	102.17	13.33	2.17	2.50	0.063
3.8#	96.74	10.58	2.24	2.50	0.046
Subcore		10.44	2.24	2.50	
5.4	97.65	9.60	2.27	2.51	0.040

* contains open fractures and large vugs.
# received in fragments

Borehole Summary					
	Saturation (%)	**Porosity (%)**	**Bulk Density (g/cc)**	**Particle Density (g/cc)**	**Gravimetric Water Content**
SHT average:	95.39	12.53	2.20	2.51	0.053
standard deviation	3.56	3.89	0.09	0.02	0.017

Table 6.2.2.5-2. Pre-Heating Laboratory Hydrological Measurement of Grab Samples from Wet Excavation of the Observation Drift of the ESF Thermal Test Facility

Observation Drift Grab Samples					
Sample Location (m)	**Saturation (%)**	**Porosity (%)**	**Bulk Density (g/cc)**	**Particle Density (g/cc)**	**Gravimetric Water Content (g/g)**
30.0	99.00	8.60	2.26	2.47	0.038
Sub-sample	94.90	8.30	2.27	2.47	0.035
40.0	95.40	9.30	2.27	2.50	0.039
Sub-sample	93.80	10.10	2.24	2.49	0.042
Sub-sample	80.50	10.40	2.24	2.50	0.037
Observation Drift (OD) Grab Sample Summary					
	Saturation (%)	**Porosity (%)**	**Bulk Density (g/cc)**	**Particle Density (g/cc)**	**Gravimetric Water Content (g/g)**
OD Average	92.72	9.34	2.26	2.49	0.038
Standard Deviation	7.10	0.91	0.02	0.02	0.003

Table 6.2.2.5-3. SHT Bulk Densities and Porosity of Cores from Boreholes 20 and 21

Sample ID	Borehole	Depth (m)	Wet Bulk Density (g/cm^3)	Dry Bulk Density (g/cm^3)	Effective Porosity
0047525.2	CHE-1	0.7	2.348	2.247	0.102
0047525.2A	CHE-1	0.7	2.350	2.249	0.102
0047526.2	CHE-1	1.4	2.349	2.240	0.109
0047527.2	CHE-1	2.5	2.345	2.246	0.0998
0047528.2	CHE-1	3.8	2.331	2.224	0.107
0047529.2	CHE-1	4.3	2.344	2.235	0.109
0047530.2A	CHE-2	4.5	2.294	2.167	0.127
0047531.2	CHE-2	1.5	2.332	2.222	0.111
0047533.2	CHE-2	3.9	2.290	2.156	0.135
0047534.2	CHE-2	4.6	2.331	2.229	0.103
0047535.2	CHE-2	5.4	2.314	2.195	0.119
Mean*		11 samples	2.33±0.02	2.22±0.03	0.111±0.011

*Statistical mean for 11 samples; errors represent one standard deviation for all samples collectively

Table 6.2.2.5-4. SHT Laboratory Hydrological Measurements of Post-Cooling Dry-Drilled Cores

Sample ID	LBNL ID	Saturation	Porosity	Bulk Density (g/cc)	Particle Density (g/cc)	Gravimetric Water Content (g/g)
SPC01009880	H-1	0.50	0.169	1.96	2.36	0.043
SPC01009882	H-2	0.79	0.105	2.19	2.44	0.038
SPC01009884	H-3	0.75	0.115	2.16	2.44	0.040
SPC01009885	H-4	0.44	0.099	2.20	2.44	0.020
SPC01009887	H-5	0.19	0.101	2.18	2.42	0.009
SPC01009888	H-6	0.32	0.110	2.17	2.43	0.016
SPC01009889	H-7	0.80	0.104	2.19	2.45	0.038
SPC01009806	H-8	0.80	0.098	2.19	2.43	0.035
SPC01009807	H-9	0.61	0.099	2.19	2.43	0.027
SPC01009808	H-10	0.82	0.090	2.21	2.43	0.033
SPC01009809	H-11	0.78	0.092	2.20	2.42	0.033
SPC01009810	H-12	0.53	0.105	2.16	2.41	0.026
SPC01009811	H-13	0.38	0.097	2.19	2.43	0.017
SPC01009812	H-14	0.41	0.089	2.21	2.43	0.016
SPC01009890	H-15	0.76	0.090	2.21	2.43	0.031
SPC01009891	H-16	0.87	0.102	2.17	2.42	0.041
SPC01009892	H-17	0.89	0.101	2.18	2.42	0.041
SPC01009893	H-18	0.94	0.093	2.20	2.43	0.040
SPC01009894	H-19	0.83	0.106	2.17	2.43	0.041
SPC01009895	H-20	0.85	0.087	2.24	2.45	0.033
SPC01009896	H-21	0.89	0.082	2.22	2.42	0.033
SPC01009897	H-22	0.73	0.131	2.12	2.44	0.044
SPC01009898	H-23	0.86	0.104	2.17	2.42	0.041
SPC01009899	H-24	0.86	0.099	2.20	2.44	0.039
SPC01009900	H-25	0.82	0.117	2.15	2.44	0.045
SPC01009901	H-26	0.86	0.103	2.20	2.45	0.040
SPC01009902	H-27	0.77	0.143	2.09	2.44	0.053
SPC01009903	H-28	0.88	0.087	2.23	2.44	0.034
Average			0.104	2.18	2.43	
Standard Deviation			0.018	0.05	0.02	

Table 6.2.3.1-1. Wire Extensometer Data [a]

Gage	Days after Startup									
	0	**14**	**28**	**42**	**56**	**70**	**84**	**98**	**112**	**126**
TMA-WX-1	0	-0.1	0.08	0.02	0.03	0.27	0.2	0.33	0.49	0.47
TMA-WX-2	0	-0.14	-0.15	-0.12	3.16	3.21	3.26	3.27	3.29	3.27
TMA-WX-3	0	-0.03	-0.09	0.01	0.01	0.2	0.25	0.31	0.33	0.41
TMA-WX-4	0	-0.83	-0.78	-0.78	-0.78	-0.58	-0.49	-0.66	-0.63	-0.31
TMA-WX-5	0	-0.61	-0.66	-0.58	-0.52	-0.5	-0.44	-0.67	-0.4	-0.58
TMA-WX-6	0	-2.45	-2.46	-1.98	-1.88	-1.89	-1.83	-2.95	-2.97	-2.97
Gage	**Days after Startup**									
	140	**154**	**168**	**182**	**196**	**210**	**224**	**238**	**252**	**266**
TMA-WX-1	0.39	0.66	0.66	0.55	0.55	0.55	0.55	0.55	0.44	0.59
TMA-WX-2	3.17	3.52	3.51	3.51	3.51	3.5	3.5	3.5	3.41	3.38
TMA-WX-3	0.28	0.69	-23.92	-23.92	-23.84	-23.99	-24.08	-24.08	-24	-24.03
TMA-WX-4	-0.59	-0.2	-0.21	-0.04	-0.04	-0.09	-0.09	-0.1	-0.1	-0.12
TMA-WX-5	-0.89	-0.48	-0.59	-0.65	-0.78	-0.82	-0.82	-0.83	-0.81	-0.82
TMA-WX-6	-3.21	-2.75	-2.91	-2.74	-2.74	-3.06	-3.06	-3.06	-2.96	-2.92
Gage	**Days after Startup**									
		280	**294**	**308**	**322**	**336**	**350**	**364**	**378**	**392**
TMA-WX-1		0.46	0.22	0.01	-0.05	-5.89	-5.89	-6.4	-6.56	-6.63
TMA-WX-2		4.49	4.49	4.22	4.22	3.99	4.11	4.04	4.04	3.93
TMA-WX-3		-23.91	-24.16	-24.16	-23.91	-24.42	-24.42	-24.42	-24.68	-24.66
TMA-WX-4		-0.17	-0.17	-0.17	-0.17	-0.68	-0.42	-0.68	-0.90	-0.91
TMA-WX-5		-0.69	-0.69	-0.95	-0.95	-0.95	-1.2	-38.29	-38.61	-38.65
TMA-WX-6		-2.99	-3.25	-3.5	-3.5	-3.75	-3.75	-3.5	-3.77	-3.83
Gage	**Days after Startup**									
		406	**420**	**434**	**448**	**462**	**476**	**490**	**504**	**518**
TMA-WX-1		-6.40	-6.65	-3.93	-5.52	-5.54	-4.11	-2.31	-2.01	-2.39
TMA-WX-2		2.97	2.97	2.85	0.37	0.67	0.22	-21.04	-20.51	-20.89
TMA-WX-3		-24.67	-24.67	-24.72	-24.71	-24.65	-24.65	1.19	1.92	1.46
TMA-WX-4		-0.68	-0.68	-0.91	-0.91	-0.89	-0.87	-53.45	-53.42	-53.48
TMA-WX-5		-38.54	-38.54	-38.72	-38.76	-38.98	-38.99	1.72	1.55	-3.99
TMA-WX-6		-3.75	-3.50	-3.80	-3.79	-3.74	-3.71	-3.6	-3.42	-3.66

[a] Wire extensometer data given in mm. Extension is positive.

Table 6.2.3.1-2. Tape Extensometer Measurements for the SHT*

Gage No.	Initial Reading (m)	Displ. 9/24/96 (mm)	Displ. 10/21/96 (mm)	Displ. 12/19/96 (mm)	ΔDispl. 1/7/97 (mm)	Displ. 2/11/97 (mm)	Displ. 3/10/97 (mm)
WXM-1	5.40439	-0.48	-0.78	-0.86	-0.76	-1.14	-1.19
WXM-2	5.08585	-3.20	-3.20	-1.17	-3.71	-3.71	-3.71
WXM-3*		4.67249	0.33	erroneous	0.08	-1.93	2.24
WXM-4	4.33635	-0.46	-0.21	-0.56	-0.64	-0.84	erroneous
WXM-5	5.87639	-0.04	-0.32	-0.49	-0.57	-0.37	-0.82
WXM-6	5.83158	-0.29	-0.129	-0.17	-0.39	-0.72	-0.80
Gage No.		**Displ. 4/21/97 (mm)**	**Displ. 5/6/97 (mm)**	**Displ. 6/25/97 (mm)**	**Displ. 7/24/97 (mm)**	**Displ. 8/20/97 (mm)**	**Displ. 7/15/97 (mm)**
WXM-1		-1.27	-0.86	-1.39	-1.52	-1.34	-1.16
WXM-2		erroneous	-4.39	-4.21	-4.21	-4.21	-3.71
WXM-3**		0.26	0.31	-0.17	2.29	-0.07	0.26
WXM-4		-0.36	-0.18	-1.17	-1.22	-1.20	-1.50
WXM-5		-0.72	-0.79	-0.88	-0.95	-0.62	-0.60
WXM-6		-0.64	-0.31	-1.15	-0.95	-0.21	-0.64

Notes: * Extension is positive.
** WXM-3 initial reading suspect. Change in displacement from 9/24/96.

Table 6.2.3.1-3. Summary of SNL-Installed Measurement System Specifications

Measurement System	Manufacturer	Gage Accuracy, Range & Precision
Type-K Thermocouples (Chromel-Alumel)	STI (probes) Omega	±2.2°C max 1280°C
Vibrating Wire Displacement Transducers	GeoKon	1 in. full range Resolution: .02%
High-Temp LVDT	RDP	±0.5% of full range = ±19 mm @200°C
Wire Extensometer	Houston Scientific, Inc.	0.1% resolution 2-in. range
Vibrating Wire Load Cell	GeoKon	60,000 lb max ±0.5% full range
Tape Extensometer	GeoKon	±0.127 mm
Goodman Jack -Readout Box -Near LVDT -Far LVDT -Pressure Gage -Enerpak Pump	Sinco	Range: pressure: 0–10,000 psi displacement: -0.25 to +0.25 in. Accuracy: pressure: ±0.2% displacement: ±0.005 in.
Power Monitor	Magtrol	Volts (0.2% of reading +0.2% of range) 0–600 volts Amps (0.22% of reading +0.25% of range) 0–50 amps Watts (0.2% of reading +0.3% of range)
Thermistors	Omega	±0.2°C 100°C range

Table 6.2.3.2-1. Estimated Rock Mass Modulus in Borehole ESF-TMA-BJ-1 (Goodman/Borehole Jack)

Date	Distance from Collar				
	2.0 m	3.0 m	4.0 m	4.51 m	6.2 m
	Rock Mass Modulus-GPa (Temp °C)				
8/26/96	*6.9 (25)*	3.71 (25)	No test	No test	No test
10/10/96	10.3 (27.5)	10.3 (27.7)	*8.3 (30.2)*	6.0 (34)	No test
11/26/96	*Results discarded (31.1)*	10.2 (35.9)	*5.71 (46.4)*	*5.01 (55.4)*	8.4 (141.8)
3/18/97	*Results discarded (35)*	6.3 (41)	*10.3 (52)*	*5.7 (58.7)*	22.8 (143.1)
10/23/97 1st run	No test	No test	6.28 (Ambient)	Discarded	8.28 (Ambient)
10/23/97 2nd run	No test	No test	8.97 (Ambient)	7.1 (Ambient)	10.0 (Ambient)
1/29/98 1st run	5.47 (Ambient)	9.67 (Ambient)	8.28 (Ambient)	7.60 (Ambient)	Not calculated
1/29/98 2nd run	No test	No test	No test	No test	11.72 (Ambient)
1/29/98 3rd run	No test	No test	No test	No test	11.72 (Ambient)

NOTE: Italicized calculated moduli are based on field data in which the difference between the two borehole jack LVDT readings slightly exceeded the limits set in ASTM D 4971-89 1989 [101786]. The fractured nature of the rock made setting the jack difficult. Discarded results were for data that far exceeded ASTM D 4971-89 1989 [101786] limits.

Table 6.2.3.3-1. Rock Bolt Load Cells, Load Versus Time [a]

TMA RBLC	Days after Startup									
Gage	0	14	28	42	56	70	84	98	112	126
RB-LC-1-AVG	22662	22262.8	22158	21732.3	21537.1	21444.1	21407.5	21380.8	21340.3	21308.5
RB-LC-2-AVG	14859.4	14739.7	14708.6	14680.1	14643.7	14597	14559.8	14522.5	14496.5	14449.6
RB-LC-3-AVG	22428	22402.2	22378.7	22348.4	22317.5	22281	22262.3	22243.2	22231	22224.1
RB-LC-4-AVG	16663.9	16602.8	16580.3	16558.8	16522.1	16496.6	16467.4	16446.3	16424.2	16407.5
RB-LC-5-AVG	25971.9	25928.5	25887	25856.6	25829.3	25802.6	25783.4	25765.5	25748.7	25738.1
RB-LC-6-AVG	14642.7	14633.2	14632.7	14627.3	14619.4	14609.5	14601.2	14595.9	14589.2	14573.7
RB-LC-7-AVG	4932.6	4921.1	4919.7	4911.8	4904.3	4893.6	4890.9	4883.8	4877.5	4873
RB-LC-8-AVG	16862.8	16818.5	16783.6	16758.7	16738.7	16605	16592.7	16575.4	16566	16561.5
TMA RBLC	**Days after Startup**									
Gage	**140**	**154**	**168**	**182**	**196**	**210**	**224**	**238**	**252**	**266**
RB-LC-1-AVG	21279.7	21254.3	21206.3	21176.9	21161.2	21145.9	21127.1	21112.2	21100.9	21102.1
RB-LC-2-AVG	14422.7	14405.6	14389.9	14378.6	14369.9	14365.5	14353.4	14349	14342	14341.1
RB-LC-3-AVG	22214.2	22206.8	22201.1	22194.3	22189.6	22183.4	22176.4	22171.7	22165.3	22158.4
RB-LC-4-AVG	16394.3	16377.4	16361.5	16350.8	16340.4	16331	16320.2	16316.8	16312.1	16310.9
RB-LC-5-AVG	25728.1	25722.2	25714.1	25705.1	25698.3	25692.7	25683.1	25676	25665.6	25652
RB-LC-6-AVG	14567.1	14563.5	14562.3	14557.4	14553.9	14551.2	14549.3	14543.8	14543.4	14538.9
RB-LC-7-AVG	4866.9	4866.7	4867.2	4866.6	4868.2	4865.2	4863.2	4863.9	4864.1	4867.1
RB-LC-8-AVG	16552.8	16544.8	16538	16533.3	16528.6	16522.3	16516.4	16514	16503.2	16501.5
TMA RBLC	**Days after Startup**									
Gage		**280**	**294**	**308**	**322**	**336**	**350**	**364**	**378**	**392**
RB-LC-1-AVG		21090.8	21092.2	21097.1	21090.6	21081.3	21070.5	21066.3	21073.0	21072.7
RB-LC-2-AVG		14354.1	14380.2	14391.6	14396.8	14404.6	14409	14412.4	14416.8	14421.9
RB-LC-3-AVG		22160.3	22171.6	22179.8	22180.8	22182.1	22179.1	22180.2	22177.4	22179.1
RB-LC-4-AVG		16315.9	16332.3	16338.5	16340.7	16346.6	16348.2	16350.4	16354.0	16358.0
RB-LC-5-AVG		25641.1	25617.7	25604.4	25589.9	25581.9	25573.8	25571.5	25561.4	25555.1
RB-LC-6-AVG		14538.6	14538.2	14536.1	14534.8	14531.9	14531.1	14529.5	14528.5	14530.7
RB-LC-7-AVG		4865	4858.2	4857.6	4856.9	4851	4850.2	4850.1	4852.8	4853.3
RB-LC-8-AVG		16497.8	16491.7	16491.7	16488.4	16487	16484.6	16477.2	16480.8	16475.8
TMA RBLC	**Days after Startup**									
Gage		**406**	**420**	**434**	**448**	**462**	**476**	**490**	**504**	**518**
RB-LC-1-AVG		21080.6	21074.6	21058.0	21019.0	20999.9	20964.1	20943.1	20933.8	20928.1
RB-LC-2-AVG		14439.3	14435.0	14432.4	14419.5	14391.8	14352.8	14338.9	14347.6	14346.7
RB-LC-3-AVG		22183.0	22179.8	22177.4	22168.4	22150.2	22111.5	22097.6	22099.3	22096.8
RB-LC-4-AVG		16366.6	16360.9	16354.1	16345.6	16330.8	16282.0	16234.2	16268.6	16278.5
RB-LC-5-AVG		25548.7	25535.6	25525.3	25515.4	25496.9	25457.7	25444.7	25445.6	25445.2
RB-LC-6-AVG		14534.1	14533.1	14532.5	14528.0	14521.6	14503.0	14493.0	14492.2	14490.9
RB-LC-7-AVG		4856.6	4860.1	4858.9	4854.8	4842.0	4808.4	4796.1	4795.0	4680.1
RB-LC-8-AVG		16476.1	16468.7	16462.1	16454.2	16079.7	16060.3	16052.3	16056.2	16058.1

[a] Load cell data are for average load and are given in lbs.

Table 6.2.3.4-1. Mean Coefficients of Thermal Expansion during First Cycle Heating of Post-Cooling SHT Characterization Specimens

Specimen ID	Distance from collar (ft)	Max. Temp. (°C)	Mean CTE on Heat-up (10^{-6}/°C)											
			25-50	50-75	75-100	100-125	125-150	150-175	175-200	200-225	225-250	250-275	275-300	300-325
Perpendicular to Heater, Outside 100°C Isotherm														
PTC1-A 2.9-B	2.9	322	8.7	9.6	9.8	11.2	12.3	13.1	14.6	19.4	32.7	56.3	75.0	52.3
PTC1-A 16.8-B	16.8	321	9.1	11.0	9.6	10.4	11.3	12.5	12.3	15.8	20.3	33.2	62.1	49.8
PTC2-B 4.1-B	4.1	321	9.2	10.5	9.9	10.3	11.1	12.3	12.8	16.4	23.8	43.1	61.4	45.6
Compilation without		N[(a)] =	3	3	3	3	3	3	3	3	3	3	3	3
cooling outlier		Mean =	9.0	10.4	9.8	10.7	11.6	12.6	13.2	17.2	25.6	44.2	66.2	49.2
PTC1-A 2.9-B		STD[(a)] =	0.3	0.7	0.1	0.5	0.7	0.4	1.2	1.9	6.4	11.6	7.7	3.4
Perpendicular to Heater, Inside 100°C Isotherm														
PTC1-B19.0-B	19.0	322	9.0	10.1	8.9	9.4	10.8	12.9	13.5	16.0	20.4	30.6	51.4	54.0
Parallel to Heater, Outside 100°C Isotherm														
PTC4-A 4.6 B	4.6	321	8.8	10.0	8.3	9.5	10.5	11.9	11.2	13.9	20.1	34.1	81.4	69.0
PTC5-B 4.1-B	4.6	321	8.7	10.4	8.9	9.6	10.6	11.6	11.7	14.5	34.2	38.5	57.0	63.1
PTC5-B 24.4-B	4.6	321	8.9	10.5	8.6	9.4	10.2	11.2	11.1	14.1	17.9	26.7	47.5	52.9
PTC5-B 24.4-C	4.6	331	8.8	9.9	8.5	9.3	10.2	11.4	12.6	17.2	21.5	34.5	59.9	45.1
		N[(a)] =	4	4	4	4	4	4	4	4	4	4	4	4
		Mean =	8.8	10.2	8.6	9.5	10.4	11.5	11.7	14.9	23.4	33.5	61.5	57.5
		STD[(a)] =	0.1	0.3	0.3	0.1	0.2	0.3	0.7	1.5	7.3	4.9	14.3	10.6
Parallel to Heater, Inside 100°C Isotherm														
PTC4-A 6.8-B	6.8	318	7.9	8.8	9.1	9.4	10.5	11.1	12.4	15.4	24.3	38.0	70.2	73.0
PTC4-B 14.8-B	14.8	321	9.0	10.3	8.6	9.3	10.4	12.0	12.4	15.0	19.2	28.1	45.8	52.2
PTC4-A 19.0-B	19.0	319	8.1	8.9	8.9	9.2	10.1	11.1	12.4	14.5	17.5	28.0	51.0	56.9
PTC4-B 19.8-B	19.8	318	8.4	9.1	9.4	9.8	10.6	11.5	12.9	15.4	19.2	27.8	44.2	44.4
PTC H1-A 15.6-B	15.6	322	7.66	9.48	8.24	9.11	10.19	10.65	11.05	12.33	14.63	22.02	41.38	54.172
PTC MPBX1 14.2-B	14.2	322	8.51	9.64	8.49	9.04	9.86	11.50	11.82	15.29	20.75	28.98	50.49	55.86
		N[(a)] =	6	6	6	6	6	6	6	6	6	6	6	6
		Mean =	8.2	9.4	8.8	9.3	10.3	11.3	12.2	14.7	19.3	28.8	50.5	56.1
		STD[(a)] =	0.5	0.6	0.4	0.3	0.3	0.5	0.6	1.2	3.2	5.1	10.3	9.4
All Data Outside 100°C Isotherm														
		N[(a)] =	7	7	7	7	7	7	7	7	7	7	7	7
		Mean =	8.9	10.3	9.1	10.0	10.9	12.0	12.3	15.9	24.4	38.1	63.5	54.0
		STD[(a)] =	0.2	0.4	0.7	0.7	0.8	0.7	1.2	2.0	6.5	9.5	11.3	8.9
All Data Inside 100°C Isotherm														
		N[(a)] =	7	7	7	7	7	7	7	7	7	7	7	7
		Mean =	8.3	9.5	8.8	9.3	10.4	11.5	12.3	14.9	19.4	29.1	50.6	55.8
		STD[(a)] =	0.5	0.6	0.4	0.2	0.3	0.8	0.8	1.2	3.0	4.7	9.4	8.6
All Data														
		N[(a)] =	14	14	14	14	14	14	14	14	14	14	14	14
		Mean =	8.6	9.9	9.0	9.6	10.6	11.8	12.3	15.4	21.9	33.6	57.1	54.9
		STD[(a)] =	0.5	0.7	0.6	0.6	0.6	0.7	1.0	1.7	5.5	8.6	12.0	8.5
		95% [(a)]	0.2	0.3	0.3	0.3	0.3	0.4	0.5	0.9	2.9	4.5	6.3	4.5

[(a)] N = Number of samples; STD = Standard deviation; 95% = 95 Percent Confidence Limit
Lithostratigraphic Unit: Tptpmn; Thermal/mechanical Unit TSw2; Air dried.

Table 6.2.3.4-2. Mean Coefficients of Thermal Expansion during First Cycle Cooling of Post-Cooling SHT Characterization Specimens

Specimen ID	Distance from collar (ft)	Max. Temp. (°C)	Mean CTE on Cool-Down (10^{-6}/°C)											
			325-300	300-275	275-250	250-225	225-200	200-175	175-150	150-125	125-100	100-75	75-50	50-30
Perpendicular to Heater, Outside 100°C Isotherm														
PTC1-A 2.9-B	2.9	322	12.2	16.5	31.8	21.6	67.2	35.4	22.1	15.2	13.2	15.0	11.6	11.4
PTC1-A 16.8-B	16.8	321	16.1	30.2	42.1	39.5	26.3	19.2	15.1	12.9	12.1	10.7	10.2	9.7
PTC2-B 4.1-B	4.1	321	14.9	27.8	43.8	48.0	30.1	20.4	15.6	13.3	12.3	10.8	10.2	9.6
Compilation without		N[(a)] =	2	2	2	2	2	2	2	2	2	2	2	2
cooling outlier		Mean =	15.5	29.0	42.9	43.7	28.2	19.8	15.4	13.1	12.2	10.7	10.2	9.6
PTC1-A 2.9-B		STD[(a)] =	0.9	1.7	1.2	6.0	2.7	0.9	0.4	0.3	0.1	0.1	0.0	0.1
Perpendicular to Heater, Inside 100°C Isotherm														
PTC1-B19.0-B	19.0	322	18.8	32.2	38.3	32.9	22.9	18.0	15.0	12.7	12.3	10.3	10.2	9.1
Parallel to Heater, Outside 100°C Isotherm														
PTC4-A 4.6 B	4.6	321	14.2	29.3	50.7	53.8	29.6	20.7	15.8	13.7	12.6	11.5	10.4	10.4
PTC5-B 4.1-B	4.6	321	15.1	31.8	43.4	40.4	29.2	31.2	17.1	13.5	12.7	11.2	10.4	9.9
PTC5-B 24.4-B	4.6	321	19.1	29.9	35.9	32.0	21.9	16.6	14.0	11.9	11.5	10.2	9.7	9.1
PTC5-B 24.4-C	4.6	331	18.6	28.1	40.9	41.1	27.8	22.1	15.8	12.9	11.9	10.5	9.8	9.2
		N[(a)] =	4	4	4	4	4	4	4	4	4	4	4	4
		Mean =	16.8	29.8	42.7	41.8	27.1	22.7	15.7	13.0	12.2	10.8	10.1	9.7
		STD[(a)] =	2.5	1.5	6.1	9.0	3.6	6.2	1.3	0.8	0.6	0.6	0.4	0.6
Parallel to Heater, Inside 100°C Isotherm														
PTC4-A 6.8-B	6.8	318	12.2	26.6	39.0	45.8	33.5	26.0	17.5	14.0	12.2	11.9	10.4	9.8
PTC4-B 14.8-B	14.8	321	16.6	29.5	36.5	33.1	23.7	18.1	14.6	12.5	11.8	10.4	9.9	9.3
PTC4-A 19.0-B	19.0	319	16.9	29.2	38.3	34.6	23.4	17.5	13.7	12.3	11.2	9.7	9.7	10.0
PTC4-B 19.8-B	19.8	318	19.8	26.6	31.2	29.8	22.5	18.2	14.0	12.3	11.4	10.8	10.0	9.4
PTC H1-A 15.6-B	15.6	322	19.33	30.87	32.25	24.14	18.09	14.42	12.59	11.20	10.55	10.03	9.29	20.154
PTC MPBX1 14.2-B	14.2	322	17.89	30.67	39.41	33.88	23.31	18.80	15.12	12.42	11.60	10.27	9.79	8.99
		N[(a)] =	6	6	6	6	6	6	6	6	6	6	6	6
		Mean =	17.1	28.9	36.1	33.6	24.1	18.9	14.6	12.5	11.5	10.5	9.9	11.3
		STD[(a)] =	2.7	1.9	3.6	7.1	5.1	3.8	1.7	0.9	0.6	0.8	0.4	4.4
All Data Outside 100°C Isotherm (Without cooling outlier PTC1-A 2.9-B)														
		N[(a)] =	6	6	6	6	6	6	6	6	6	6	6	6
		Mean =	16.3	29.5	42.8	42.4	27.5	21.7	15.6	13.0	12.2	10.8	10.1	9.7
		STD[(a)] =	2.1	1.4	4.8	7.6	3.1	5.0	1.0	0.6	0.4	0.5	0.3	0.5
All Data Inside 100°C Isotherm														
		N[(a)] =	7	7	7	7	7	7	7	7	7	7	7	7
		Mean =	17.4	29.4	36.4	33.5	23.9	18.7	14.7	12.5	11.6	10.5	9.9	11.0
		STD[(a)] =	2.5	2.1	3.4	6.5	4.7	3.5	1.5	0.8	0.6	0.7	0.4	4.1
All Data (Without cooling outlier PTC1-A 2.9-B)														
		N[(a)] =	13	13	13	13	13	13	13	13	13	13	13	13
		Mean =	16.9	29.4	39.4	37.6	25.6	20.1	15.1	12.7	11.8	10.6	10.0	10.4
		STD[(a)] =	2.3	1.8	5.1	8.2	4.3	4.4	1.4	0.8	0.6	0.6	0.3	3.0
		95% [(a)]	1.3	1.0	2.8	4.4	2.3	2.4	0.7	0.4	0.3	0.3	0.2	1.6

[(a)] N = Number of samples; STD = Standard deviation; 95% = 95 Percent Confidence Limit
Lithostratigraphic Unit: Tptpmn; Thermal/mechanical Unit TSw2; Air dried.

Table 6.2.3.4-3. Summary Data: SHT Post-Cooling Characterization Unconfined Compression Tests

Specimen ID [a]	PTC4-B 9.2	PTC4-B 4.3	PTC4-B 6.6	PTC4 11.8	PTC4 17.4	PTC4 20.9	PTC4-B 26.0	PTC2-B 10.8	PTCH1 8.6
Date Tested	21-07-98	22-07-98	22-07-98	23-07-98	23-07-98	23-07-98	24-07-98	24-07-98	24-07-98
Thermal/Mechanical Unit	TSw2	TSw2	TSw2	TSw2	TSw2	TSw2	TSw2	TSw2	TSw2
Lithostratigraphic Unit	Tptpmn	Tptpmn	Tptpmn	Tptpmn	Tptpmn	Tptpmn	Tptpmn	Tptpmn	Tptpmn
Dry Bulk Density	2.25	2.27	2.26	2.32	2.30	2.32	2.31	2.21	2.30
Moisture Content (%)	1.1	1.0	0.8	0.9	1.1	1.1	1.1	1.0	1.0
Confining Pressure	0	0	0	0	0	0	0	0	0
Static Young's Modulus (GPa)	34.4	33.4	32.3	37.0	34.0	34.4	32.9	20.1	34.3
Static Poisson's Ratio	0.185	0.168	0.166	0.259	0.182	0.187	0.178	0.251	0.159
Peak Stress	175.4	34.3	113.9	144.9	240.5	245.7	191.4	51.8	80.5
Axial Strain at Peak Stress	0.005274	0.001138	0.003637	0.008941	0.007924	0.007909	0.006003	0.00213	0.002629

Test ID	SHTUC11	SHTUC13	SHTUC14	SHTUC15	SHTUC16	Statistical Summary [b]			
Specimen ID[a]	PTCH1 15.6	PTCH1 18.7	PTC1 12.5	PTC MPBX1-B 14.4	PTC1-B 15.7	Mean	Standard Deviation	Count	95% Confidence Limit
Date Tested	27-07-98	28-07-98	29-07-98	29-07-98	30-07-98				
Thermal/Mechanical Unit	TSw2	TSw2	TSw2	TSw2	TSw2				
Lithostratigraphic Unit	Tptpmn	Tptpmn	Tptpmn	Tptpmn	Tptpmn				
Dry Bulk Density	2.23	2.28	2.29	2.31	2.21				
Moisture Content (%)	1.3	0.9	1.1	0.9	0.9				
Confining Pressure	0	0	0	0	0				
Static Young's Modulus (GPa)	24.2	34.2	26.6	35.4	28.9	31.6	4.8	14	2.5
Static Poisson's Ratio	0.123	0.173	0.393	0.168	0.183	0.198	0.066	14	0.034
Peak Stress	38.7	137.0	78.7	183.5	159.2	134.0	70.2	14	36.8
Axial Strain at Peak Stress	0.002316	0.004349	0.001641	0.005806	0.005614	0.004665	0.002521	14	0.001321

[a] The distance from the borehole collar (in feet) is given as part of the specimen identification number.

[b] Tests SHTUC01, SHTUC12, and SHTUC17 were conducted on an aluminum specimen.

Table 6.2.3.5-1. Rock Mass Thermal Expansion Coefficients for Longest Available Gage Lengths Near Heating Cycle Culmination

MPBX Number	Anchor Numbers	Average α 10^{-6}/°C	Average Temperature (°C)	Gage Length (m)
TMA-MPBX-1	1 to 4	5.88	160.3	2.84
TMA-MPBX-3	2 to 6	4.14	70.07	4.0
TMA-MPBX-2	2 to 5	2.36	116.6	3.4

Table 6.2.4.1-1. Chemistry Analysis of SHT Borehole 16-4 Waters with Reported *In-Situ* Waters from the General Area

BH 16-4	SPC00521206 Suite 1	SPC00521245 Suite 2	SPC00521252 Suite 3	SPC00522238 Suite 4	Perched Water UZ-14 PT-4 [e]	SZ Ground-water J-13 [f]	Pore Water UZ-5-TP-4 [g]	Rainier Mesa Fracture Water [g]	SZ Ground-water G-4 [f]
Collection Date	11/25/96 *	02/04/97	02/27/97	05/22/97					
DCS Temp (°C)	NA	46.9	47.60	51.20					
	LLNL	LLNL	LLNL	LLNL					
Na (mg/L)	16	13.9	12.20	11.00	34.0	45.8	33	35	57
Si (mg/L)	16.8	17.4	14.50	15.20	32.1	28.5	99	25	21
Ca (mg/L)	13	9.76	8.65	7.70	27.0	13	58	8.4	13
K (mg/L)	2.5 2.69[a]	2.5	3.30	2.30	1.8	5	9	4.7	2.1
Mg (mg/L)	1.63	1.16	1.01	0.92	2.1	2.01	12	1.5	0.20
pH	6.2 [h]	6.9	6.80	6.55		7.4		7.5	
HCO_3 (mg/L) [d]	188				141.5	129		98	139
F^- (mg/L)	0.44	0.12	<0.5	<0.50		2.18		0.25	2.5
Cl^- (mg/L)	2.54 2.1 [b]	1.45	1.00	2.20	6.7	7.1	34	8.5	5.9
S (mg/L)	0.71		0.20	0.21					
SO_4^{2-} (mg/L)	1.83 1.5 [b]	0.42	<2	<2	14.1	18.4	39	15	19
PO_4^{3-} (mg/L)	<0.03	<0.4	<2	<2		<10			
NO_2^- (mg/L)	<0.01	0.15	<2	<2					
NO_3^- (mg/L)	1.1	<0.4	<2	<2	14.5	8.8			
Li (mg/L)	<0.03	<0.03	<0.01	<0.01		0.048			
B (mg/L)	0.37	0.74	0.66	0.93		0.134			
Al (mg/L)	<0.06	<0.06	<0.06	<0.06	0.0	0.02			
Fe (mg/L)	0.74	0.13	0.30	0.03			74		
Sr (mg/L)	0.2 0.1850 [a] 0.22 [c]	0.14	0.12	0.11		0.04	559		
Rb (mg/L)	0.0066 [a]								
Br^- (mg/L)	<0.02 0.008 [b]	<0.4	<2	<2	0.1				
δ D	–101.7 –95.00 [a] –93.1 [c]	–99.6 –94.0 [a]	–98.2	–100.6	–97.3	–98			–103
δ ^{18}O	–12.9 –11.80 [a] –13.1 [c]	–12.9 –13.1 [a]	–12.8	–13.57	–13.4	–13			–13.8
Tritium	0.44 ± 0.19 TU <0.3 TU [b]				0.0				
$^{87}Sr/^{86}Sr$	0.71243 [a] 0.71240 [c]								
U (mg/L)	1.013×10^{-1} [c]								
$^{234}U/^{238}U$	8.03200 [c]								

NOTE:
* This column contains non-Q data as discussed in text.
[a] LBNL data
[b] Los Alamos National Laboratory (LANL) data
[c] USGS data
[d] derived from charge balance
[e] Yang et al. 1996 [100194], p. 36, Table 6
[f] Harrar et al. 1990 [100814], p. 5.5, Table 5.1
[g] Harrar et al. 1990 [100814], p. 6.5, Table 6.1
[h] See text for description of pH measurement.

Table 6.2.4.2-1. SHT Stellerite Abundance on Fractures, Pre-heating Drill Core ESF-TMA-MPBX-1

Total number of fractures examined	75
Number of fractures with stellerite	58
Average percent coverage of fractures by stellerite	31%
Drill hole characteristics: 7 m long, 0.5º dip toward bottom of hole (eastward)	
Core interval examined: 0 to 4.33 m, minus 0.49 m unrecovered or removed for thermal/mechanical measurements	

Table 6.2.4.2-2. Summary Descriptions of SHT Natural-Fracture Mineral and Test-Product XRD Samples

Sample Identifier	Borehole	Depth (ft)	Description of sample
LANL 3052, p1	1	2.3-2.4	Natural fracture coating. Centimeter-scale vapor-phase pocket with zeolite-cemented breccia. Sample is mostly zeolite, with some brecciated tuff.
LANL 3054, p1	1	13.0-13.2	Natural fracture coating, ~0.1 mm thick, of microcrystalline zeolite, deposited directly on smooth, planar cooling-joint surface.
LANL 3006, p1	16	16.5-17.0	Test products, small white mounds on original borehole surface with minor bedrock impurities, orientation of sample unknown.
LANL 3004, SSL08p1	16	15.5-16.5	Post-test sample, outermost 0.5 mm of original borehole surface, orientation of sample site unknown.
LANL 3003	16	12.0-12.1	Test products, cohesive brownish particulate layer peeled from bottom of original pre-heating borehole.
LANL 3000, SSL02	2	2.9-3.4	Test products, silica scale, maximum thickness 0.2 mm, on bottom of original borehole surface. Impurities of bedrock and brownish particulates.

Table 6.2.4.2-3. Semiquantitative XRD Identification of SHT Natural-Fracture Minerals and Test Products

Sample Identifier	Borehole	Depth (ft)	Smectite	Zeolite	Amorphous	Calcite	Gypsum	Feldspar	Tridymite	Cristobalite	Quartz	Hematite	Other
Natural Fracture Minerals													
LANL 3052, p1	1	2.3-2.4	minor	major†	—	—	—	minor	—	—	major	—	—
LANL 3054, p1	1	13.0-13.2	trace	major†	—	—	—	—	—	—	—	—	—
Test Products													
LANL 3006, p1	16	16.5-17.0	—	minor	major§	major	minor	minor	—	—	trace	—	minor‡
LANL 3004, SSL08p1	16	15.5-16.5	minor	minor	—	minor	minor	major	—	major	major	trace	major Al metal
LANL 3003	16	12.0-12.1	trace	trace	—	minor	—	major	minor	major	major	—	—
LANL 3000, SSL02	2	2.9-3.4	minor	—	minor§	minor	—	major	minor	major	major	minor	minor mica

NOTES: Approximate limits of semiquantitative descriptors, all in weight %: major = >20%, minor = <20%, trace = <1%, "—" = not detected.
†Stellerite.
§Identified on the basis of XRD and SEM-EDX as opal-A.
‡Unidentified mineral, possibly a sulfate-bearing phase.

6.3 DRIFT SCALE TEST (DST)

The DST is the third and largest of several planned and conducted *in situ* thermal tests that investigate coupled processes in the local rock-mass surrounding the potential repository. These coupled processes are thermally driven by heat released from electrical heaters that simulate heat from emplaced nuclear waste. A block of rock, approximately 60 m wide, 50 m deep and 50 m high, includes 9 floor/canister heaters in a 5 m diameter drift and 50 wing heaters installed in horizontal boreholes drilled perpendicular to the drift into the rock. Numerous sensors located in the DST block measure thermal-hydrological-mechanical-chemical (T-H-M-C) behavior. The heating of the DST began on December 3, 1997 and continued through January 14, 2002. The test is on-going for a planned cooling phase of 4 years. A detailed description of the DST is provided in the following two reports, the *Drift Scale Test Design and Forecast Results* (CRWMS M&O 1997 [146917]) and *Drift Scale Test As-Built Report* (CRWMS M&O 1998 [111115]).

DST Input-DTNs and related information such as Q-status and respective locations (figures, tables, and text) are tabulated in Table 4-3. DST Output-DTNs are tabulated in Table 6.3-1.

The general layout and plan view of the Exploratory Studies Facility (ESF) Thermal Test Facility (TTF) and DST area are shown in Figures 6.2-1 and 6.3-1.

The configuration for the DST, as shown in Figure 6.2-1, includes a declining Observation Drift driven mostly east in a downward slope. The breakout, near the intersection of the ESF North Ramp and main drift, is 2,827 m from the North Ramp portal. The downward slope of the Observation Drift ensures a minimum 10 m of Tptpmn rock (Tertiary-Miocene (Age), Paintbrush (Group), Topopah Spring Tuff (Formation), Crystal-Poor (Member), Middle Nonlithophysal (Zone)) overlying the DST drifts. The Tptpmn represents one of the three geologic units targeted to host the potential repository. At the elevation of the DST crown, the Connecting Drift breaks out to the north from the Observation Drift (see Figure 6.2-1).

Figure 6.3-1 shows that the DST includes a 47.5 m long, 5 m diameter Heated Drift. The Heated Drift is complemented by an 11 m long entry from the Connecting Drift of similar diameter. Other components include plate loading and Data Collection System (DCS) niches. Figures 6.3-2 through 6.3-8 provide three-dimensional perspectives of the thermal, mechanical, hydrological, and chemical boreholes. Since some boreholes contain multiple types of sensors, only the primary usage of the borehole was highlighted. The boreholes are color coded to identify the wing heaters and the primary processes (T-M-H-C) measured in each of the 147 boreholes. The DST borehole numbering system begins at 42 because the initial 41 boreholes correspond to the Single Heater Test (which is co-located in the TTF).

The as-built locations of the 147 boreholes drilled into the DST block are listed in Table 6.3-2. All coordinates are based on a local right-hand coordinate system in which 0,0,0 is the center of the bulkhead on the cool side. The positive X, Y, Z-direction are generally northward (away from the Observation Drift), westward (away from the Connecting Drift), and upward, respectively. The last 12.5 meters of the Heated Drift (starting from Y = 35 m) is lined with concrete in order to evaluate the feasibility of concrete liner as ground support for waste emplacement drifts in the potential repository.

The DST DCS recorded thermal, hydrological (partial), and mechanical data, for the most part, on an hourly basis. The acquired data consists of both original (measured electronic values) and converted (engineering units). Four packages of data were submitted to the Records Processing Center (RPC) and corresponding DTNs (LA9908FH6001WP.001 [158319], LA0111FH831151.002 [158317], LA0208FH831151.001 [159515], and LA0208FH831151.002 [159308] were also obtained. These DCS-DTNs are considered non-qualified because they are stored in the RPC but they do identify CDs of identical qualified data that are distributed to the Thermal Test Team. These DCS-DTNs also identify Scientific Notebooks that provide details of measurements including calibration information. These DCS-DTNs are reviewed and re-structured and periodically submitted to the TDMS resulting in many of the Input-DTNs introduced below and listed in Table 4-3. As discussed in Section 1 and the introduction to Section 6, these Input-DTNs are further refined, reduced, and restructured and then resubmitted to the TDMS as Output-DTNs (see Table 6.3-1). As mentioned in Section 6.1, the end user has access to three levels of data for DST thermal, hydrological (partial), mechanical measurements: DCS-DTNs, Input-DTNs, and Output-DTNs. For most future applications, it is anticipated that end users will access the Output-DTNs because they are more user friendly.

6.3.1 DST Thermal Measurements

The following sections present discussions on the power and temperature histories of the DST during the four-year heating phase. Discussion includes measurements of heater power and rock-mass temperatures, as well as parameters derived from laboratory and field measurements.

Detailed discussion of DST power and thermal measurements is provided in Sections 6.2 and 8 of the *Drift Scale Test Design and Forecast Results Report* (CRWMS M&O 1997 [146917]), Sections 5.1.1, 6, and 9 of the *Drift Scale Test As-Built Report* (CRWMS M&O 1998 [111115]), and Sections 3 and 10.2 of the *Ambient Characterization of the Drift Scale Test Block* report (CRWMS M&O 1997 [101539]). The Input-DTNs and Output-DTN for DST power and thermal measurements are listed in Tables 4-3 and 6.3-1, respectively.

6.3.1.1 Heater Power

Heat was generated from 50 wing heaters and 9 floor (canister) heaters. These two types of electrical heaters had a combined power output of approximately 280 kW when operating at full capacity. The nine canister heaters were located in the center of the drift along a distance of approximately 47 m. The wing heaters were inserted in horizontal boreholes in the wall of the heated drift perpendicular to the longitudinal axis of the heated drift. These wing heaters were evenly distributed on 1.83 m spacings in boreholes located on both walls of the heated drift. Each wing heater had 10 m of heated length evenly divided between inner and outer heating elements of 1.145 kW and 1.719 kW capacity, respectively.

Each of the nine canister heaters in the Heated Drift had 60 heating elements in it, only 30 of which were switched on at any given time. (The other 30 elements were backups.) To estimate the power supplied to each canister, the current being supplied to all the heating elements in a given canister was summed and the result multiplied by the canister heater voltage. Note that for the first 20 days of the test, only 28 heating elements in canister #8 were active. A 29^{th} heating element was activated on day 20 and the 30^{th} heating element on day 40.

The DST wing heater, canister heater, and total power data may be found in the following Input-DTNs: MO9807DSTSET01.000 [113644], MO9810DSTSET02.000 [113662], MO9906DSTSET03.000 [113673], MO0001SEPDSTPC.000 [153836], MO0007SEPDSTPC.001 [153707], MO0012SEPDSTPC.002 [153708], MO0107SEPDSTPC.003 [158321], and MO0202SEPDSTTV.001 [158320].

6.3.1.1.1 Results: Heater Power

Because of the numerous DST power measurements, only representative discussion and graphics are provided. All DST power measurements and graphics can be accessed in the Output-DTNs identified in Table 6.3-1.

Figure 6.3.1.1-1 shows the total power applied to the wing heaters and the canister heaters, as a function of time. For the first 800 days, average total power to the wing heaters is approximately 135 kW, average total power to the canister heaters is approximately 52 kW, and average sum of the wing and canister power is approximately 186 kW. The voltage applied to the wing and canister heaters is also recorded. Average wing and canister heater voltages have been quite stable at approximately 212 and 189 volts, respectively.

For the first 820 days of the test, the power was nearly constant, dropping, from an initial value of approximately 188 kW to approximately 178 kW. On March 3, 2000, the first of five intentional interim power reductions were implemented to maintain drift wall temperature near 200^{o}C (see temperature plot at drift crown in Figure 6.3.1.1-1). The fifth and final interim power reduction occurred on August 22, 2001. After these five interim reductions, the total power was approximately 140 kW, or approximately 75% of its initial level. On January 14, 2002, all heaters to the drift scale test were reduced to zero power.

Of the 100 wing heater elements, 5 failed. Both elements of wing heater 29 failed after 185 days of heating, the outer element of wing heater 26 failed after 211 days of heating, the outer element of wing heater 9 failed after 412 days of heating, and the outer element of wing heater 16 failed after 622 days of heating.

6.3.1.1.2 Measurement Uncertainty: Heater Power

The accuracy of the watt transducers used in measuring the heater power is conservatively estimated to be within 2%. Refer to Section 6.1.1.1.2 for additional discussion of uncertainty related to heater power.

6.3.1.2 Temperatures

Temperatures of the rock in the DST were measured from approximately 1,950 resistivity temperature devices (RTDs). Temperatures elsewhere in the DST, including the Heated Drift, wing-heater boreholes, and MPBX boreholes, were measured with approximately 700 thermocouples as described in the *Drift Scale Test As-Built Report* (CRWMS M&O 1998 [111115]). Temperature boreholes in the DST were designed to ensure three-dimensional measurement of the thermal field. RTD sensors, which were used to measure rock-mass temperature, were bundled together with pre-determined spacing between sensor tips. The spatial density of sensors along an instrument borehole is higher in regions where greater thermal

gradients are expected. The spatial density is also higher in regions where transition between dryout and condensation is expected to develop during the tests.

The range of temperatures in the DST depended on the location of the measurement and the duration of heating. The highest temperatures were encountered in the vicinity of the heat sources (i.e., wing heaters). In these regions, the range of temperature varied from ambient to about 300°C. To properly cover the expected range of temperatures, sensors with the capability of measuring temperatures to at least 300°C were used. RTDs and thermocouples are commercially available, can cover the expected temperature range, and are reliable for long-term monitoring.

The heating-phase temperature data in the Output-DTN: for approximately 1,950 RTDs are organized into individual EXCEL workbook corresponding to each temperature borehole. Each workbook contains spreadsheets and charts. On one EXCEL spreadsheet, the data are organized with each RTD temperature history in each column in ten-day intervals for the duration of the heating phase. In general, there are approximately seventy RTDs for most of the temperature boreholes. Individual columns can be hidden or revealed for graphical display or usage. Another EXCEL spreadsheet in the workbook contains, for each temperature borehole, the coordinates for the respective temperature sensors. Two types of thermal graphs are developed in two separate charts. The first chart shows temperature history. The second chart shows temperature profiles as a function of a spatial coordinate at various times during the DST heating phase. These two types of graphics are intended to facilitate comparison with simulations for the validation of thermal-hydrological (TH) process models.

The DST temperature data may be found in the following Input-DTNs: MO9807DSTSET01.000 [113644], MO9810DSTSET02.000 [113662], MO9906DSTSET03.000 [113673], MO0001SEPDSTPC.000 [153836], MO0007SEPDSTPC.001 [153707], MO0012SEPDSTPC.002 [153708], MO0107SEPDSTPC.003 [158321], and MO0202SEPDSTTV.001 [158320].

6.3.1.2.1 Results: Temperatures

Because of the numerous DST temperature measurements, only representative discussion and graphics are provided. All DST temperature measurements and graphics can be accessed in the Output-DTN identified in Table 6.3-1.

Figure 6.3.1.1-1 presents the temperature response for a single thermocouple (TC-19) located near the center of the Heated Drift during the heating phase of the DST. The temperature response at the drift wall follows an expected response, in that temperatures initially rise rapidly in response to switching on the heaters over a period of approximately 50 days. As time passes, the temperatures rise gradually, then the rate of rise decreases and the temperatures tend to remain flat as a result of the five interim power reductions during the final two years of the heating phase. After all heaters are switched off, the drift surface temperature, including TC-19, decreases rapidly.

Figure 6.3.1.2-1 illustrates the temperature distribution near the end of the heating phase along the periphery of the Heated Drift. The contours are constructed from thermocouples installed on

the drift walls at the drift crown (roof) and at the ribs (elevation of the wing heaters). As expected, temperatures are lower near both ends of the heated drift and higher at the mid-length of the Heated Drift. For a given Y along the Heated Drift, temperature is higher at the wing-heater elevation (about 3.9 m from the drift crown). Boreholes 79 and 80 are parallel to the Heated Drift (Figure 6.3-3) and at an elevation of approximately 10 m from the centerline of the DST, above the horizontal boreholes that house the wing heaters. The temperature profiles for boreholes 79 and 80 are presented in Figures 6.3.1.2-2 and 6.3.1.2-3 respectively. These temperatures are higher over the central part of the DST and lower over the unheated portion (the 11 m entry into the bulkhead of the Heated Drift). Also, note that the temperatures in borehole 79 are somewhat higher than those in borehole 80. This is because the elevation of borehole 79 could not be maintained during drilling because of its extreme length, causing it to be closer to the wing heaters than planned.

There are two interesting thermal behaviors evident in borehole 79. The first is the tendency of the curves to flatten significantly at 96°C—the boiling point of water at this elevation. This phenomenon occurs because temperature rises pause temporally at the boiling point as the water in the rock vaporizes.

The other interesting thermal signature evident in borehole 79 is the temperature behavior near Y = 13 m (Figure 6.3.1.2-2). At sub-boiling temperatures, the rock near this location was substantially warmer than the rock on either side of it. Near the boiling point, the temperature profile was essentially constant, and at temperatures exceeding the boiling point, the rock near this location was somewhat cooler than the surrounding rock. This may be explained by the existence of a vertical fracture near this location. When the rock temperature was below boiling (i.e., the rock still contained liquid water), steam generated below this location (closer to the heater) may have been rising along the fracture, elevating the temperature of the rock near the fracture to levels exceeding those of adjacent rocks. At boiling, everything was isothermal for a while as water in the rock evaporated. After all the water in the rock had boiled off, the temperature of most of the rock started to increase again. Near the fracture, however, the temperature remained somewhat cooler than that of the surrounding rock. It may be that a lot of water condensed in this region when the temperature was sub-boiling, and additional heat was required to evaporate that water when the temperature in the vicinity of the fracture first reached and then exceeded the boiling temperature. Alternatively, the anomalous cool temperature near the fracture could reflect cool moisture flowing downward in the fracture toward the heated region.

The other thermal DST boreholes were drilled radially away from the heated drift centerline at a fixed Y station. Figures 6.3.1.2-4 through 6.3.1.2-7 present temperature histories and temperature profiles for boreholes 158 and 164, respectively. Borehole 158 is orientated vertically up in the crown of the heated drift near its midlength. Borehole 164 is a horizontal borehole that parallels the wing heater boreholes. The temperature distribution shows the boiling phenomenon discussed above, as well as comparatively high rock temperatures characteristic of rock-mass in close proximity to the wing heaters.

Figures 6.3.1.2-8 and 6.3.1.2-9 provide temperature contours after four years of heating in two respective planes: a vertical slice through the mid-length of the heated drift and a vertical slice through the longitudinal axis of the heated drift. These contours approximately describe the

dryout zone, where temperatures exceed 96ºC, surrounding the heated drift. The dryout zone is estimated to be 24,000 cubic meters at the end of the four-year heating phase. Also shown are the areal extents of the temperature distributions in the DST block. The formation of these temperature contours from the Input-DTNs included the application of AutoCAD software that evaluated temperature and location data at specific time intervals. Using this data, fitted curves or temperature contours were constructed for each point in time. Additional contours in these three planes for years one, two, and three are provided in the DST temperature Output-DTN.

6.3.1.2.2 Measurement Uncertainty: Temperatures

The uncertainty in DST temperature measurements involved both RTDs and thermocouples. Generally in the DST, the RTDs measured rock and air temperatures and the thermocouples measured heater temperatures.

The RTD was accurate within 0.3^{o}C (Section 5.1 of *Single Heater Test Status Report* (CRWMS M&O 1997 [101540])). With consideration of other factors, such as the location of the RTDs, measured temperature in the DST was estimated to be accurate within 2°C. The RTD bundles were grouted in the boreholes; consistently some of the RTDs might not have had direct contact with the borehole wall. There might have been some time delay between the temperature variations in the rock and that measured by the RTDs. But it is believed that this time delay was small because the rock-mass was heated slowly.

The thermocouple was accurate within 2.2^{o}C (Section 5.1 of the *Single Heater Test Status Report* (CRWMS M&O 1997 [101540])). With consideration of other factors, such as the location of the RTDs, the accuracy of the measured temperature in the DST was estimated to be within 3.5°C.

6.3.1.3 Laboratory Parameter: Thermal Conductivity

Thermal conductivity measurements on core samples were performed using the Guarded Heat Flow Meter test method (Brodsky et al. 1997 [100653], pp. 11-14) and the Section 3 of *Ambient Characterization of the Drift Scale Test Block* (CRWMS M&O 1997 [101539]). The apparatus functioned by placing a specimen between two heater plates controlled at different temperatures, producing heat flow through the specimen. A heat-flux transducer (HFT) located between the specimen and one heater plate measured heat flow. Since this heat-flux transducer is in series with the specimen and between both heater plates, the resulting temperatures on each side of the specimen, along with knowledge of the specimen thickness, allowed the thermal conductivity of the specimen to be determined.

Two series of tests were performed to measure thermal conductivity. In the first test series, samples recovered from the DST block were tested over the temperature range of 30°C to 300°C. The test specimens were placed between two heater plates controlled at different temperatures, and the heat flow was measured. Radial heat flow losses were minimized by using a cylindrical guard heater. Moisture contents were either air dry (as received), oven dry, vacuum saturated, or partially saturated (intermediate between air dry and vacuum saturated). The moisture contents of the specimens tested as received were not indicative of *in situ* conditions. Laboratory specimens were cored under water and dried out in storage. In a second series of tests, the relationship between thermal conductivity and saturation was determined (SNL 1998 [118788]).

Welded tuff was taken from Alcove 5 of the DST, and nonwelded tuffs from four lithostratigraphic units were obtained from three surface drillholes. Thermal conductivities were measured for six welded and six nonwelded specimens under dry, saturated, and approximately ten intermediate moisture conditions (SNL 1998 [118788]). All thermal conductivity tests were conducted at 30°C and at atmospheric pressure.

The DST thermal conductivity data may be found in the following Input-DTNs: SNL22100196001.006 [158213] and SN0203L2210196.007 [158322].

6.3.1.3.1 Results: Thermal Conductivity

A complete listing of DST thermal conductivity for different temperatures and saturation is provided in the Output-DTN identified in Table 6.3-1. A small subset is presented in Tables 6.3.1.3-1 and 6.3.1.3-2.

The thermal conductivity data over a range of temperatures from 30°C to 70°C are summarized in Table 6.3.1.3-1. Thermal conductivity values were relatively uniform throughout the sampling volume. The mean thermal conductivities and standard deviations about the mean are given at each temperature. No temperature dependence is observed. Thermal conductivities ranged from 1.9 to 2.3 W/(m-K) with an average thermal conductivity of 2.1 ± 0.1 W/(m-K) over this range of temperatures.

The distribution of thermal conductivity results obtained at 30°C provide a visual indication of the central tendency of the data. No analysis was performed to determine the best-fit distribution curve. Results show that the individual specimens with thermal conductivities farther than one standard deviation from the mean did not cluster in particular locations. The highest thermal conductivity, 2.3 W/(m-K), was obtained for HDFR197.5-C, which is from either the lower portion of the Tptpmn or upper portion of the Tptpll unit. The mean thermal conductivity for each individual borehole was 2.1 W/(m-K).

Results for the second series of tests in which thermal conductivities were determined for a range of saturation are illustrated in Table 6.3.1.3-2. A linear and commonly used nonlinear curve were fitted to the data and the goodness of fit determined. The linear relationship provides a better fit to the data, as indicated by the sum of the squared errors.

6.3.1.3.2 Measurement Uncertainty: Thermal Conductivity

The uncertainty in DST thermal conductivity is similar to that discussed for the SHT in Section 6.2.1.3.2.

6.3.1.4 Field Parameters (REKA–Thermal Conductivity and Thermal Diffusivity)

A thermal probe was developed at the University of Nevada, Reno, to determine *in situ* thermal conductivity and thermal diffusivity. The probe is called **r**apid **e**stimation of thermal conductivity (**k**) and thermal diffusivity (**a**lpha), or REKA. REKA is a self-contained probe consisting of a heat source and 16 temperature sensors. During measurements, a small amount of heat, about 2 watts, was transferred to the rock, and temperature differences were measured. Assembled, a REKA probe is a rigid cylinder approximately 0.5 cm in diameter and about 60 cm

in length. The REKA probe was grouted in a borehole of approximately 1.2 cm in diameter. The borehole had to be sufficiently straight to allow probe insertion.

For characterization during the pre-heating phase, five locations were selected based on the competency of the wall rock at this site, including minimal fracturing, sufficient separation from rock bolts, and similarity of density (as determined by drilling rate). All five locations chosen for analysis appear to have similar characteristics based on these criteria. The boreholes were drilled in random directions to average the effects of unseen physical phenomena (faulting, stress relief, etc.). Detailed discussion of the REKA measurements and methodology can be found in the following reports: *Ambient Characterization of the DST Block* (CRWMS M&O 1997 [101539], pp. 10-4 – 10-8) and Danko and Mousset-Jones (1993 [134360]).

During the heating phase, measurements were made in boreholes 151, 152, and 153 (see Table 6.3-2). The REKA–thermal conductivity and thermal diffusivity data during the heating phase may be found in the following Input-DTNs: LL980411004244.060 [159107], LL980411104244.061 [159111], LL980902104244.070 [159109], UN0106SPA013GD.003 [159115], UN0106SPA013GD.004 [159116], UN0109SPA013GD.005 [159117], UN0112SPA013GD.006 [159118], UN0201SPA013GD.007 [159119].

6.3.1.4.1 Results: Field Thermal Conductivity and Thermal Diffusivity

Results of thermal conductivity and thermal diffusivity measurements using the REKA probe during the pre-heating phase are taken from Section 10.2 of CRWMS M&O 1997 ([101539]) and presented in Table 6.3.1.4-1 and Table 6.3.1.4-2. These results are shown for corroborative purposes to compare with the laboratory measurements presented in the previous Section 6.3.1.3. Table 6.3.1.4-1 shows the REKA evaluation results assuming that the rock-mass temperature is only affected by the REKA probe's heater during the 12-hour measurement period; therefore, no rock-mass background temperature correction was performed. Table 6.3.1.4-2 shows the REKA results assuming that the rock-mass temperature changes with time during the 12-hour measurement period because of both the REKA probe's heater, and some other heating or cooling effect, such as a change in the ambient temperature.

We note that the values of thermal conducting in Tables 6.3.1.4-1 and 6.3.1.4-2 fall within the same range as that observed in the laboratory measurement presented in 6.3.1.3.

6.3.1.4.2 Measurement Uncertainty: Field Thermal Conductivity and Thermal Diffusivity

The REKA probe assumes the rock will behave in a homogenous, isotropic manner, which may not be the case. Nonetheless, its application is valid, since more sophisticated measurement devices do not exist and historical correlation of predicted and measured temperatures, using *in situ* thermal properties, is good (CRWMS M&O 1997 [146917]). The temperature measurement for the REKA probes over the temperature range in the DST is estimated to be within 1^{o}C. The drift of the thermocouple measurement will affect the accuracy of the calculated thermal conductivity and thermal diffusivity. The drift in the thermocouples was estimated to be less than 1% of the temperature. REKA measurements pertain to a small volume, with an estimated radius of 0.1 m.

6.3.2 DST Hydrological Measurements

To assess the thermal-hydrologic processes in the DST, the spatial distribution and the temporal variations of the moisture content in the rock-mass were monitored. Electrical resistance tomography (ERT), ground penetrating radar (GPR), and neutron logging were used to monitor the moisture content. Air permeability was measured periodically to assess the changes in the fracture permeability during the test. Core samples collected from the DST region were tested in the laboratory for some hydrologic properties, such as porosity, density, and moisture retention curves, and electrical properties, such as resistivity and relative permittivity. These will be presented in the following corresponding sections.

6.3.2.1 Electrical Resistance Tomography (ERT)

This section describes ERT surveys made during the DST heating phase to map the changes in moisture content caused by heating. Of particular interest is the formation and movement of condensate within the fractured rock-mass. Figure 6.3-8 in Section 6.3 shows the location of the ERT boreholes in the DST. The ERT in the DST was conducted in four imaging planes: two vertical cross sections from the Observation Drift to the Heated Drift and two vertical planes along the axis of the Heated Drift. The two vertical cross sections from the Observation Drift to the Heated Drift are located at Y = 4.6 m, formed by boreholes 45 and 46, and at Y = 24.7 m, formed by boreholes 62 and 63. Borehole lengths are about 40 m. The two vertical planes along the axis of the Heated Drift include: one in the crown of the Heated Drift formed by boreholes 135, 145, 166, and 176; and one in the invert of the Heated Drift formed by boreholes 136, 146, 167, and 177. The two vertical planes along the axis of the Heated Drift cover a length of the drift from Y = 2.7 m to 39.3 m. The borehole lengths are about 20 m in the crown and about 16 m in the invert. The electrode spacing in the DST ERT is about 1 m. The electrodes were grouted in the boreholes.

Near the end of the heating phase, the vertical cross section image plane at Y = 24.7 m malfunctioned because of the increased contact impedance between the electrodes and the rock. Otherwise, the ERT has been functioned well. All of the DST ERT data can be found in the TDMS under the following Input-DTNs: LL000804023142.009 [158325], LL990702704244.099 [113872], LL980808604244.065 [113791], LL980406404244.057 [113782], and LL980108804244.052 [158332].

6.3.2.1.1 Results: ERT

The saturation estimates produced by data reduction model 2 (as presented in Section 6.1.2.1.1), which assumes that the primary pathway of the electrical current is through the double layer, are presented in here. As examples of the DST ERT results, Figures 6.3.2.1-1 and 6.3.2.1-2 show the resistivity image as measured on January 10, 2002, at of the end of the heating phase, and the saturation image produced from it, respectively. Images are presented as a ratio to the pre-heating baseline values. The vertical image planes along the longitudinal axis of the Heated Drift started at about 2.7 m from the bulkhead. The vertical cross section imaging plane intersects the Heated Drift at about 4.6 m from the bulkhead. These figures are examples of the ERT results in the DST. The rest of the ERT results can be found in the TDMS under the Input-DTNs listed above. As shown in Figure 6.3.2.1-2, the drying of rock started in regions near the heaters.

Tomograms for the different vertical planes along the Heated Drift indicate that the end effect is apparent at the bulkhead at Y = 0, but not as obvious at the far end of the Heated Drift. Aside from the end effects, the drying along the Heated Drift was fairly uniform. Some localized increases of moisture were observed in regions both above and below the Heated Drift, but seemed to be more profound in the region below the Heated Drift. The vertical extent of the drying region near the wing heater seemed to be greater than that near the floor heaters in the Heated Drift. This was probably a result of the greater heating effects in the wing heater plane than in the Heated Drift.

6.3.2.1.2 Measurement Uncertainty: ERT Saturation Changes

There are many factors that could contribute to the uncertainty in the estimated saturation changes in the rock-mass by using ERT. The measurements of the voltage and current at the electrodes are fairly accurate. More importantly, saturation changes, estimated by ERT, are impacted by the following uncertainties:

- The accuracy of the temperature maps in the vertical cross section imaging planes near the Observation Drift is limited by the sparse coverage of the temperature sensors. Errors in the extrapolated temperature maps will result in erroneous saturation estimates.

- The other uncertainty factors that impact the ERT in general can be found in Section 6.1.2.1.3.

6.3.2.2 Ground Penetrating Radar (GPR)

The feasibility of the cross-hole radar profiling method to monitor the saturation changes due to thermal hydrological processes was proven for the Single Heater Test and discussed in Section 6.2.2.2. The same data acquisition and data analysis method discussed in 6.2.2.2 were applied to the Drift Scale Test. Detailed discussion of the data acquisition and data processing specific to Drift Scale Test can also be found in three Level 4 Milestone reports (Peterson and Williams 1998 [159128]; 1998 [159120]; Williams and Peterson 1998 [159121]).

The radar data were acquired in ten boreholes (47-51, 64-68) as shown in Figure 6.3-6. These boreholes are collared from the Observation Drift and are the same boreholes used for neutron logging. These ten boreholes form two arrays of five boreholes each in two vertical planes. Cross-hole tomographic data were collected between adjacent borehole pairs using two acquisition modes: the Zero Offset Profile (ZOP) and Multiple Offset Profile (MOP) as discussed previously in Section 6.2.2.2. The severity of the borehole inclination in the well pairs 47-48 and 64-65, however, limited the data acquired between these boreholes to ZOP data only. Full MOP data coverage, necessary for subsequent tomographic processing, could not be accomplished. Since these well pairs represent data coverage that is far enough away from the Heated Drift intersection that few thermally induced changes in the radar data were anticipated, the impact of data acquisition limitation is minimal.

GPR data were acquired according to the schedule shown in Table 6.3.2.2-1.

After acquisition of Phase 1, the borehole temperatures became so great that the cables used in the measurements melted. It took many months to redesign and manufacture cables that were more heat resistant for Phase 2. Furthermore, owing to the extreme heat encountered in borehole 67 (due to its proximity to a wing heater), accurate measurements could no longer be taken. Hence, all data acquisition for well pairs involving this borehole (66-67 and 67-68) was halted after phase 5. However, because of the similarity in spatial positioning of the well pairs, the data acquired between well pairs 49-50 and 50-51 acted as sufficient proxy for the well pairs 67-68 and 66-67.

The primary data recorded are the radar waveforms. Data in the form of the transmitter and receiver stations, and the respective wave travel times, have been submitted to the TDMS periodically over the course of the experiment. The DTNs (referenced according to the phase numbers—PRE (Pre-heating); P1 (Phase 1 of heating)) are listed as follows: LB990630123142.005 [129274] (PRE, P1, P2, P3), LB000121123142.004 [158338] (P4), LB000718123142.004 [153354] (P5), LB0101GPRDST01.001 [158346] (P6), LB0108GPRDST05.001 [158440] (P7), and LB0203GPRDSTEH.001 [158350] (P8, P9, P10). The XYZ coordinates of the transmitter and receiver positions were determined from the borehole collar and bottom as-built coordinates are in the Input-DTN: LB990630123142.005 [129274].

6.3.2.2.1 Results: GPR

To perform the travel-time inversion, a 40 m x 40 m field in each plane of boreholes was divided into a grid of 160 x 160 pixels producing a pixel dimension of 0.25 x 0.25 m, which corresponds to the antenna-station spacing of 0.25 meters. The multiplicity of source and receivers resulted in a dense sampling of the inter-borehole area; over 4,000 arrival times were available for each tomographic inversion. The inverted times produce the velocity fields for each of the 11 surveys (PRE, and P1 through P10).

The velocity differences are highlighted by subtracting the travel time values between two successive surveys and inverting these differenced data. The P1 values are differenced from the PRE values, the P2 values are differenced from the P1 values, and so on, until P10 is differenced from the P9 travel times. Difference tomograms for the 51-50 and 50-49 well pairs are shown in Figure 6.3.2.2-1. The average absolute velocity value is about 0.1 m/ns, so a difference value of 0.01 m/ns is about a 10% change in velocity. The scale of the graphs is from ±0.008 m/ns, which is about an 8% change in velocity. The tomograms all show significant velocity increases and decreases. In general, radar velocities will decrease with temperature increase, and increase with water-content decrease. So an increase in velocity, as seen near the Heated Drift and the wing heaters, shows that the velocity increase resulting from the decrease in water content is greater than the velocity decrease resulting from the increase in temperature so near the heater. The amount of drying can also be observed as a ring around the heat source expanding with each survey.

The derived tomograms are submitted as output associated with this report under Output-DTN: LB0208GPRDSTHP.001, as identified in Table 6.3-1.

6.3.2.2.2 Measurement Uncertainty: GPR

Data uncertainty associated with picking the travel times and inversion errors are as discussed in Section 6.2.2.2.2 for SHT.

6.3.2.3 Neutron Logging

Neutron logging is used to determine moisture content in rocks and soils. Neutron logging was conducted to monitor moisture content in boreholes 47-51, 64-68, and 79-80 (see Figure 6.3-6) during the DST. For the DST, a Teflon™ tube, with an RTD bundle mounted on its outside, was inserted into the boreholes 79 and 80, and grouted into place. In the other neutron boreholes (47-51 and 64-68) the Teflon tube was grouted in the boreholes, without the RTD. The Teflon tube permits easy insertion, placement, and removal of the tool. The neutron probe used for the pre-heating baseline measurements and the very early in-heat measurements of the DST was a Campbell Pacific Nuclear model 503DR, serial number H37067677, 3.81 cm (1.5 in.) diameter probe. Starting from February 1998, when a probe (Comprobe model 1905-07EF, serial number 4751, 4.13 cm (1.625 in) diameter), designed for operating at temperatures up to 200°C, became available, it was used in the DST through the remainder of the DST heating phase. To evaluate the possible impact of changing tools, the baseline measurement in borehole 47 conducted on October 27, 1997, using the Campbell Pacific tool, was compared with the Comprobe measurement in the same borehole on February 17, 1998. As shown in Figure 6.3-6, borehole 47 was one of the farthest neutron boreholes from the heaters. No moisture-content change was expected in this borehole at this early stage of the heating. A relationship of Comprobe count = 0.11387 x CPN count was established to convert the Campbell Pacific counts to Comprobe counts. The DST neutron data can be found in the TDMS under the DTN: LL020710223142.024 [159551].

6.3.2.3.1 Results: Neutron Logging

A very small subset of the DST neutron results that reside at the TDMS are presented here. The neutron results are shown as the difference in fraction volume water content between the heating phase measurements and the pre-heating baselines. Therefore, in the following figures, a positive difference fraction volume water means gaining moisture content; and a negative difference fraction volume water means drying. To calculate water saturation, one can simply divide the fraction volume water content by the porosity. All of the neutron results were smoothed to remove some variations, but did not change their amplitudes much.

As an example of the DST neutron logging results, Figure 6.3.2.3-1 shows the difference fraction volume water in borehole 66 as a function of depth from the collar during the heating phase. Borehole 66 extends from the Observation Drift to above the Heated Drift at about 26.5 m from the bulkhead. This borehole is near the crown of the Heated Drift, but not close to the wing heaters. Figure 6.3.2.3-1 shows four snapshots of the difference fraction volume water content at about one, two, three, and four years of heating. The water content was virtually not changed at the end of the first two years of heating. During the third year of heating, the drying was most significant, both in spatial extent and amount of moisture loss. During the fourth year of heating, the moisture content in the dry region did not change much, but the dry region extended significantly. This is consistent with the neutron logging in the LBT and SHT.

Neutron logging results in the DST showed that the moisture content in boreholes 47, 48, 64, and 65 did not change significantly during the four-year heating phase. The drying in a neutron borehole was a strong function of its distance to the heaters (either to the wing heaters or to the floor heaters in the Heated Drift.

Figure 6.3.2.3-2 shows the relationship between volume water content and temperature based on neutron measurements from borehole 79 and 80. This plot shows that the water content in the rock remains nearly constant within 8–14% until temperatures near boiling are reached. Thereafter, significant reduction in water content occurs between 90°C and 105°C where it nears 1%. Water content in the rock continues to decrease as it approaches zero at approximately 150°C. Although some anomalously low volume water content is measured in the sub-boiling regime, most of the volume water content is reasonably consistent for the range of temperatures considered (25–190°C).

6.3.2.3.2 Measurement Uncertainty: Moisture Content Determined by Neutron Logging

The neutron tool was calibrated to the liner-grout and liner-RTD bundle-grout systems as used in the DST borehole. However, variations in the grout volume along a borehole, possibly caused by changes in the borehole diameter, break-out regions, etc., will introduce uncertainty in the measured results. One particularly severe case was in borehole 80, where the pre-heating baseline measurements were conducted before grouting and after grouting. The baseline measurements showed that the deepest 6 m section of the borehole was not grouted. Calibration results without grout were used for reducing the data in the ungrouted section of the borehole. But the amount of grout in the region between the grouted and the ungrouted sections of the borehole (between 50 and 53 m from the collar) was unknown. Therefore, the moisture content in that portion of the borehole is associated with a greater degree of uncertainty.

The other factors that contribute to measurement uncertainty associated with neutron logging are as discussed in Section 6.2.2.3.2.

6.3.2.4 Active Pneumatic Testing and Passive Hydrological Monitoring Measurements

Pre-Heating Air Injection

Pre-heating characterization by air-permeability tests were performed in DST boreholes as they became available for testing. The pre-heating air-injection tests provide an estimate of the fracture permeability in the test block and establish baseline values for tracking changes arising from thermally driven coupled processes. Single-hole air-permeability tests were performed in November - December 1996, and in February - March 1997, in 14 boreholes (boreholes 45-48, 51-53, 56-57, 69-70, 73, 75, and 78). Locations of these boreholes in the test block are shown in Figures 6.3-4, 6.3-6, 6.3-7, and 6.3-8. Pressure and flow data for these tests can be found in DTN: LB970600123142.001 [105589] and are documented in Tsang and Cook (1997 [100646]). In addition, 24 boreholes were tested in July 1997. These are boreholes 158–167, 170–174, and 176–177 (Figure 6.3-3) intended for temperature measurements, and several wing heater boreholes (boreholes 98–100, 115–118). Pressure and flow data for the July 1997 tests can be found in DTN: LB980120123142.005 [114134] and are documented in Tsang and Freifeld (1998 [159097]).

Heating Phase Air Injection

For each of the 12 hydrology boreholes (57-61, 74-78, and 185-186, as shown in Figure 6.3-4), a string of custom-designed high-temperature packers were installed to divide the 40 m long borehole typically into four isolated zones of approximately 8 m each. For boreholes 58 and 77, only a string of three packers could be installed because of obstruction caused by fallen rocks from the fractures and lithophysal cavities. After installation of the pneumatic packer strings in the baseline, air-permeability measurements were performed in the 46 isolated intervals. Air was injected at a constant flow rate in a zone isolated either by two packers or by a packer and the bottom of borehole, while the pressure responses in this and all other packed-off zones were monitored. The air-injection pressure and flow data from the hydrology boreholes prior to initiation of heating can be found in DTN: LB980120123142.004 [105590] and are documented in Tsang and Freifeld (1998 [105774]). After the collection of the initial DST pre-heating air-injection data, the entire process of selecting injection intervals was automated, using computer-controlled gas delivery manifolds installed near the collars of each cluster of boreholes. The new combination of hardware and software makes the entire process of air-permeability measurement fully automated, allowing for more consistent collection of data with minimum need for on-site field personnel to oversee the testing. Detailed information on the setup of the air-injection equipment can be found in Freifeld and Tsang (1998 [159098]).

The DST active hydrologic testing program consists of periodic (approximately quarterly) air-injection tests conducted in these same 46 isolated intervals in the 12 hydrology boreholes. These tests are to monitor the changes in the fracture permeability as a result of coupled processes.

Periodic air-injection test data containing measured pressures and flow rates collected during the heating have been submitted to the TDMS under the following DTNs: LB980420123142.002 [113706], LB981016123142.002 [129245], LB990630123142.001 [129247], LB000121123142.002 [158337], LB000718123142.002 [158341], LB0101AIRKDST1.001 [158345], LB0108AIRKDST5.001 [158438], and LB0203AIRKDSTE.001 [158348].

Passive Hydrological Monitoring Data of Pressure,Temperature, and Humidity

In addition to active air-injection tests, passive monitoring of pressure, temperature and humidity is being conducted on an hourly basis by the Data Collection System (DCS). Locations (XYZ coordinates) of these sensors can be found in the DTN: MO0002ABBLSLDS.000 [147304]. Because of the slow rate of change for these parameters, the data is parsed to 4 points per day by the DCS manager. This reduced data set is then reviewed and submitted in three data reports, containing time-stamped pressure, temperature, and humidity data. Each file contains a sequential list of data for all 46 monitored locations within the DST hydrology boreholes. Passive monitoring data for the heating phase of the DST can be found under eight Input-DTNs: LB980420123142.001 [113696], LB980715123142.001 [113733], LB981016123142.001 [158353], LB990630123142.002 [158355], LB000121123142.001 [158335], LB000718123142.001 [158340], LB0101H2ODST01.001 [158347], LB0108H2ODST05.001 [158441], and LB0203H2ODSTEH.001 [158351]. The Output-DTN is as listed in Table 6.3-1.

Gas Tracer Tests

Tracer tests were performed in boreholes 75 and 76 to estimate fracture porosity in the test block. The gas tracer data can be found in DTN: LB980420123142.002 [113706]. Estimated fracture porosity from the gas tracer data can be found in DTN: LB980912332245.002 [105593]. Detailed discussion of testing are presented in Freifeld and Tsang (1998 [159098]).

Tracer tests were performed with the hardware and software used for performing DST quarterly air-injection tests, with additional hardware to perform the mixing of a tracer gas into the air-injection stream and to control and analyze gas withdrawn from an extraction interval. A Quadrupole Mass Spectrometer Gas Analyzer was set up in the field to perform in real time the quantitative analysis of tracer gas concentration.

6.3.2.4.1 Results: Active Pneumatic Testing and Passive Hydrological Monitoring

Pre-Heating Air Injection

Steady-state analysis of the data was performed using Equation 5.1-1. Estimated permeability values from pre-heating characterizations conducted in November-December 1996 and February-March 1997 are shown in Table 6.3.2.4-1. Estimated permeability values for the 24 boreholes tested in July 1997 are shown in Table 6.3.2.4-2. Estimated pre-heating baseline permeabilities for the 46 isolated intervals tested in November 1997 are shown in Table 6.3.2.4-3.

Heating Phase Air Injection

The air-injection test data collected during the heating phase that was submitted to the TDMS contained measured pressures and flow rates only. Pressure data appeared as absolute pressure. To estimate permeability for the injection interval, the pressure values measured prior to the start of the injection, and the steady-state value obtained late in the injection period, are used in Equation 5.1-1. An example analysis of an air-injection test is illustrated by the pressure and flow data for an injection in borehole 185-2, as shown in Figure 6.3.2.4-1. Note that the near zero flowrate at the end of this injection test was set to zero for Figures 6.3.2.4-1, 6.3.2.4-5, and 6.3.2.4-6. This particular test can be found in DTN LB000718123142.002 [158341]. Data needed to apply Equation 5.2-1 included the borehole zone length (8.54 m), obtained from Table 6.3.2.4-3, along with the steady-state pressure change (20.5 kPa) and injection flow rate (100 SLPM) as shown in Figure 6.3.2.4-1. The estimated permeability using these values is 1.64×10^{-13} m^2. Throughout the heating phase, changes in permeability as a ratio to baseline permeability estimates could be used to indicate changes in fracture liquid saturation. These are shown in Figures 6.3.2.4-2, 6.3.2.4-3, and 6.3.2.4-4 for boreholes 57-61, 74-78, and 185-186, respectively. Permeability ratio as a function of time through the heating phase for the packed-off zones in the hydrology boreholes as shown in these Figures are the content of the Output-DTN LB0208AIRKDSTH.001.

Changes in the borehole 185-2 permeability can be used to demonstrate the use of these figures in interpreting changes in fracture saturation throughout the DST. As shown in Figure 6.3.2.4-4, the borehole 185-2 permeability gradually declined from its baseline value. This decrease in air

permeability indicates a gradual build-up in fracture liquid saturation during the heating phase of the DST.

As heating of the test block continued, many air-injection tests showed responses that were considered anomalous. Most of the unusual behavior was attributable to two-phase processes, such as vapor condensation or evaporation. An example of an anomalous response to an air injection is shown in Figure 6.3.2.4-5, for air injection in borehole 60-3. The odd-shaped response was attributed to the injection of cool dry air into a saturated hot environment. In these cases, the data cannot be used for the estimation of formation permeability, because no meaningful steady-state values are obtained.

Another type of anomalous response is shown in Figure 6.3.2.4-6, an air injection into 78-4. In this test, borehole zones 78-1, 78-2, and 78-3 all show decreases in pressure. This is counter-intuitive, since mass is being added to the system and pressure should increase. However, the observed pressure declines are the result of cold gas being transported in the 78-4 injection tube which needs to go through the sealed-off packer intervals 78-1, 78-2, and 78-3. This cooling can lead to condensation of vapor in these zones and thereby reduces pressure during the injection test.

The failure of some of the pneumatic packers as heating progresses is another factor affecting analysis of the DST air-injection tests. Because a deflated packer changes the injection interval length, the data collected from the zones before and after the packer deflates were not amenable to comparison with the baseline data. Hence, the estimated permeabilities for zones next to deflated packers were not amenable to comparison with baseline permeability values. The deflated packers and dates that they became deflated are shown in Table 6.3.2.4-4.

Passive hydrological monitoring data of pressure, temperature, and humidity

For this report, the passively monitored hydrology data for the heating phase from December 1997 through January 14, 2002, were assembled by appending the data files from each data submittal together and collecting a subsample of data points. These are submitted as output to this Scientific Analysis Report under Output-DTN LB0208H2ODSTHP.001. As an example, Figure 6.3.2.4-7 shows the temperature data for the sensors located in borehole 75.

Gas Tracer Tests

Three convergent weak-dipole flow field tracer tests were performed between boreholes 75 and 76 in the DST. Air with a sulfur hexafluoride tracer was injected into borehole 76, and gas was withdrawn from borehole 75 for analysis. Gas tracer tests in the DST area were conducted in borehole 75 and 76, zones 2 and 4. Two different-strength dipoles were used in zone 2, 10:1 and 30:1. A 10:1 dipole was used to test zone 4. The strength of the dipole refers to the ratio of withdrawal gas flux to injected gas flux. The flow rates for each test and the borehole geometries are listed in Table 6.3.2.4-5.

The injection air and withdrawal gas flow rates and zone pressures were monitored prior to the injection of any tracer to ensure that a steady-state flow field was achieved. After a steady-state pressure field was obtained, the air-injection flow rate was reduced to 0.90 of the original value. A make-up gas stream of tracer equal to 0.10 of the original injection air stream was added from

a 10,000 PPM cylinder of SF_6. The final injection gas stream had a concentration of 1,000 PPM SF_6. After a limited injection period, the injection of tracer was halted, and the injection air stream was returned to its original flux rate. Throughout the entire duration of the experiment, the withdrawal gas stream was maintained at a steady flux rate, and SF_6 concentration measurements were performed by the mass spectrometer every 30 seconds. Figure 6.3.2.4-8 shows the mass breakthrough curve for one weak-dipole tracer test, as well as the cumulative mass recovery. Estimates for porosity using the plug-flow analysis procedure outlined in Section 5.3 are given in Table 6.3.2.4-6.

6.3.2.4.2 Measurement Uncertainty: Active Pneumatic Testing and Passive Hydrological Monitoring Measurements

Since the same type of measurements were performed for the SHT, readers are referred to the discussion for the SHT in Section 6.2.2.4.2. Measurement uncertainty in analysis has been considered. For example, although the estimate of air permeability may not be as accurate as desired because of the assumptions involved, restricting the use of only the ratio of permeability to its respective pre-heating value, while keeping all other experimental parameters identical throughout the test, minimizes the impact of measurement uncertainty.

6.3.2.5 Laboratory Hydrological Parameters

Laboratory test results of saturation, porosity, bulk density, particle density, and gravimetric water content were conducted for both dry drilled cores and wet drilled cores from the DST block at Alcove 5 of the ESF. The measurements were carried out according to the Technical Implementation Procedure (TIP) YMP-LBNL-TIP/AFT 2.0 identical to those described in Section 6.2.2.5. Data can be found on TDMS under DTN: LB970500123142.003 [131500].

Similar to that discussed in Section 6.2.2.5 for the SHT, moisture retention curves were measured at elevated temperatures to about 94°C for samples taken from the DST block. In preparation for the moisture retention measurements, the dry bulk density, saturated bulk density and porosity for these samples were determined. The moisture retention curves and the related densities and porosity data measurements have been documented in Lin et al. (2002 [159099]).

In addition to the above, electrical resistivity and relative permittivity were also measured as a function of water saturation at 35, 50, 70, and 95°C, over a range of frequency from 10^{-2} to 10^{6} Hz. These properties are useful for the processing of geophysical imaging data. The measurements were made using either a HP4274A LCR meter, a HP4284A LCR meter, or a Solartron 1260 frequency response analyzer. Measurements made over a range of frequencies verify measurements made at a single frequency and provide additional information about conduction mechanisms and microstructural parameters. The electrical property data can be found in the TDMS under DTNs: LL981109904242.072 [118959] and LL020502523142.020 [159105]. Reporting can be found in Section 11.1 of the *Drift Scale Test As-Built Report* (CRWMS M&O 1998 [111115]).

6.3.2.5.1 Results: Laboratory Hydrological Parameters

Saturation, Porosity, Density, and Gravimetric Water Content

The data from two sets of core measurements are tabulated in Table 6.3.2.5-1 for the dry-drilled cores and in Table 6.3.2.5-2 for the wet-drilled cores from the DST area. Summaries of the averages and standard deviations of the measured values are presented at the end of each table to facilitate comparison between different data sets. The first data set in Table 6.3.2.5-1 are based on the cores from boreholes 182, 183 and 184 dry drilled from an elevated platform at the end of the Connecting Drift across from the DST block. Included in the second set in Table 6.3.2.5-2 are wet-drilled cores from boreholes 52, 53, 56, and 81 within the DST block.

The data in Tables 6.3.2.5-1 and 6.3.2.5-2 indicate that the liquid saturation of the wet-drilled cores can differ from that of the dry drilled cores by 10%. The discrepancy is in part a result of the different drilling methods and may in part arise from spatial heterogeneity. There are obvious differences from the cores from the dry-drilled cores away from the Heated Drift in Table 6.3.2.5-1 and wet-drilled cores near the Heated Drift in Table 6.3.2.5-2. The two most notable differences between the two batches are (1) the samples are less fractured or crumbled in the dry drilled cores, and (2) the core surfaces and core containers of dry-drilled cores are relatively drier. The statistics of the two batches suggest that the competent rocks have more uniform properties and less spatial variability or heterogeneity. Less competent rocks have more heterogeneous variations, containing porous packets interlaced with highly fractured rock blocks.

The average saturation value compiled from all surface-based boreholes for Topopah Spring crystal-poor middle nonlithophysal tuff (266 samples) is 85 ± 12% (Flint 1996 [100673]). Here, the average value for the dry-drilled cores is 84%, and that for the wet-drilled cores is 93%. The corresponding surface-based borehole porosity value is 11 ± 2%, as compared to the average values from 11% for dry cores to 13% for wet cores. Therefore, the 10% difference in liquid saturation between the dry-drilled and the wet-drilled data sets in the thermal test area is within the standard deviation of 12% for all the surface-based samples.

Moisture Retention Curves

Identical to the procedures discussed in Section 6.2.2.5, moisture retention curves were measured for core samples taken from boreholes 52 (CHE-1), 53 (CHE-2), 56 (CHE-5), 69 (CHE-6), 70 (CHE-7), and 73 (CHE-10), whose locations are shown in Figure 6.3-6. In preparation for the moisture-retention measurements, hydrological properties were measured.

Moisture-retention curves of the DST samples were performed at temperatures of 25.1ºC, 49.6ºC, and 93.7ºC. Similar to the SHT data (Section 6.2.2.5), there is very little hysteresis observed between the wetting and drying curves at all temperatures. The temperature cycle has a very small effect on moisture retention: the post-temperature-cycle room-temperature data show a slightly smaller moisture retention than the initial room-temperature data.

The DST samples show less moisture retention than the SHT samples (Section 6.2.2.5) at all temperatures. However, they show greater moisture retention than that of USW G-4 (Roberts and Lin 1995 [159100]; 1995 [159048]) and the Fran Ridge samples (Section 6.1.2.5). The data of

the DST samples are at the high end of the results of the USW H-1 samples (Section 6.1.2.5). The data of the DST samples are at the lower bound of that shown by Flint (1998 [100033]).

Electrical Resistivity and Relative Permittivity

Resistivity measurements are reported for one frequency, 1 kHz, because this frequency was determined to be free of electrode contamination (contact impedance) and represents the electrical properties of the material. Relative permittivity measurements are reported at 1 MHz, the highest frequency in the measurements. Samples were prepared from cores obtained from chemistry boreholes 69, 70, and 73 of the DST (Figure 6.3-6). Samples with obvious large cavities and inhomogeneous inclusions were avoided. Prior to the electrical property measurement, hydrological properties were obtained. Table 6.3.2.5-3 shows the sample ID, borehole, depth, wet and dry densities, and properties of the samples used. The samples are disk-shaped, with a diameter to thickness aspect ratio of 10:1 (dime shaped). The diameter of the samples is ~5.1 cm. All samples were prepared with the bedding direction perpendicular to the direction of measurement.

Electrical measurements began on samples that were dry. Water from well J-13 was added to the samples in small amounts and allowed to distribute throughout the sample. The length of time for this to occur was typically 3 to 4 hours, as verified by examining the resistivity of a sample as a function of time. Saturations were determined by weighing the samples immediately after electrical measurements were completed. Each sample was placed in a custom built holder made of Lucite or Lexan and separated from the atmosphere by an o-ring seal. Despite these precautions, water was sometimes lost from samples when measurements at relatively high saturations were attempted at high temperatures. The holders were placed in a standard oven and allowed time to equilibrate to the temperature (typically overnight). Upon reaching maximum saturation, the drying portion of the measurements began. The maximum saturation achieved was between 95% and 100%. Some samples were damaged (chipping and cracking) because of the cooling and heating, and the handling. Those samples were reshaped when necessary and the holders modified to accept the new shape. Samples were no longer used when indicators, such as noise in the data or mechanical flaws, demonstrated that the electrical-properties measurements were unreliable.

Figure 6.3.2.5-1 shows the electrical resistivity of the DST samples as a function of water saturation in the drying cycle at 50°C. This is just one example to illustrate the variation of electrical resistivity with water saturation. The rest of the resistivity data can be found in the TDMS. The characteristics of the variation of resistivity with water saturation at other temperatures are similar. This type of resistivity saturation dependence is similar to that observed for other tuff samples. For all temperatures, the dry resistivity is between 10^7 and 10^8 Ωm and drops rapidly to between approximately 3,000 and 1,000 Ωm (depending on temperature) as saturation increases. This is interpreted as an indication that the adsorption of water and surface conduction dominates this region of saturation. At approximately 30% saturation, there is a change in the slope of log σ versus saturation. Between 30% and 100% saturation, the resistivity decreases by only ½ to one order of magnitude.

A small amount of hysteresis is observed between wetting and drying cycles. There are small increases in resistivity during the wetting phase, similar to previous measurements utilizing distilled water as the saturating fluid (Roberts and Lin 1997 [101710]).

Figure 6.3.2.5-2 shows the relative permittivity of the DST samples as a function of water saturation in the drying cycle at 50ºC. This example illustrates the variation of the relative permittivity with water saturation. The rest of the permittivity data can be found in the TDMS under the DTNs listed above. At low saturations, permittivity is insensitive to temperature. The dry samples all have a dielectric constant (relative permittivity) between five and six. The near-saturated samples have a range of values between 22 and 26. This range of relative permittivity values at one temperature is fairly typical above approximately 40% saturation for all temperatures. The scatter in the data increases as temperature increases and is particularly bad for the 70°C wetting cycle above approximately 60% saturation. It is not known why this run shows this scatter. One possible explanation is that capacitance measurement noise at the highest frequencies of measurement (up to 1 MHz) increases with temperature.

6.3.2.5.2 Measurement Uncertainty: Laboratory Hydrological Parameters

Saturaton, Porosity, Density and Gravimetric Water Content

The main source of error for saturation measurement is in the estimate of the weight of water condensed in the walls of the core container. This is evaluated by absorbing the water from the container with a paper cloth and weighing the cloth. When large amounts of fragments and powder are observed on the surfaces of the container, this measurement overestimates the water loss because it includes the weight of fine solids. Although the reason for this physically meaningless value of saturation over 100% is understood, there is no clearly better measurement to arrive at a more accurate value. In Tables 6.3.2.5-1 and 6.3.2.5-2, observations of factors that may potentially affect the results are included in footnotes. This “soft” information forms the basis for distinguishing cores that yield reliable weight measurements from cores that give potentially abnormal and inaccurate measurement. For example, the footnote concerning the crumbled core with two open fractures, a “crushed” zone and a porous, calcitic-like intrusion, for the particular data point with saturation over 100%, from borehole 81 in Table 6.3.2.5-2, gives reason to question the validity of this high value.

Discussions in Section 6.3.2.5.1 also indicate that the liquid saturation of the wet-drilled cores can differ from that of the dry-drilled cores by 1-%. The difference can be attributed in part to different drilling methods and in part to spatial heterogeneity.

Moisture Retention Curves

Readers are referred to Section 6.2.2.5.2 for a discussion of the measurement accuracy and data uncertainty in moisture-retention measurements.

Electrical Properties

The accuracy of the instruments for the electrical property measurement was very high, usually better than 5% at the highest impedance limits (>100 MΩ). Each instrument was checked using a set of 1% tolerance resistors and capacitors. The instruments were found to yield consistent

results. Sample variations, as can be seen on the data, are greater than the instrument error. There were some uncertainties in the water saturation level during the measurement, especially at elevated temperatures and high saturation levels. Anisotropy in the electrical properties was not assessed for the DST samples. During the measurements, the path of the electric current was perpendicular to the bedding plane of the rock, which was not well established. Obvious heterogeneity in the test samples was avoided. The heterogeneity may cause great variation in electrical properties.

6.3.2.6 Heat and Mass Flow through the Bulkhead

The following discussion involves in-depth and unplanned investigations of heat and mass flow through the DST bulkhead. The subject matter was discussed in a white paper entitled "Heat and Mass Flow Through the Bulkhead in the Drift Scale Test" (Pannell 2001 [159514]). The white paper satisfied an agreement (TEF 2.1) reached between DOE and NRC at the January 2001 Technical Exchange on Thermal Effects on Flow. The discussion in that white paper covers both measurements and modeling. A brief summary pertaining to only the measurement aspect will be presented here. These measurements were conducted for informative and complementary purposes and were never intended to be a requisite for the understanding of heat and mass loss through the bulkhead.

The bulkhead separating the hot side of the Heated Drift from the unheated section is not perfectly sealed because bundles of power cable and instrument-wiring pass through the bulkhead (CRWMS M&O 1998 [111115], pp. 8-2 and 8-5). The unsealed bulkhead acting as an open boundary for unmonitored heat and mass flow introduces an artifact in the test.

The issue of heat and mass loss through the DST bulkhead has been ongoing since the design of the DST, a design in which the primary purpose of the bulkhead was to act as a thermal barrier (CRWMS M&O 1996 [101375], pp. 3-17 and 3-18) that includes safety considerations. Pre-heating numerical simulations of the DST resulted in concerns about unmonitored heat and mass loss through the thermal bulkhead (Buscheck and Nitao 1995 [100657]). Recommendations included isolating the DST Heated Drift from direct pneumatic interference with the ESF tunnel system. This precaution was in itself problematic, since safety concerns would develop if the pressure within the DST heated drift were allowed to increase.

On December 3, 1997, the heating of the DST was initiated. Within 40 days of the start of heating, moisture started to flow out of the bulkhead, as evidenced by condensation on various surfaces on the cool side of the bulkhead. This behavior was consistent with the heating of a large volume of rock that is highly fractured and approximately 90% saturated. As water in the rock boiled and turned to steam, the vapor moved under pressure gradient into cooler rocks, as well as into the Heated Drift and through the bulkhead. Also, the observed wetting on the cool side of the bulkhead alternated with drier conditions, with the latter coinciding with low relative humidity readings in the Heated Drift. Upon investigation, it appeared that barometric pumping was the cause for the intermittent wetting. Gas-phase flow from the rock to the Heated Drift is driven by pressure gradient. Superimposed on the positive pressure gradient from the rock to the Heated Drift is the barometric pressure fluctuations. Therefore, as barometric pressure decreased, more vapor flowed from the rock into the Heated Drift and out the permeable bulkhead, increasing the relative humidity in the Heated Drift. Conversely, as the barometric pressure

increased, less vapor flowed from the rock into the Heated Drift and the relative humidity decreased. Indeed, the relative humidity measurements in the Heated Drift vary inversely with the barometric pressure.

Between July 1998 and May 1999, several measurements of conductive and convective heat loss through the bulkhead were performed (CRWMS M&O 1998 [159512], p. 3-1; 1999 [154585]; 1999 [159513]). A summary listing of field efforts to address the issue of mass and heat loss through the bulkhead is provided below:

(1) Determination of conductive heat flux by applying a heat-flux meter to seven locations on the bulkhead (five measurement locations were steel and two were glass)

(2) Estimation of convective heat loss by considering how much water vapor was removed from a small-diameter pipe in the bulkhead during a 60-minute sampling period

(3) Attempt to utilize the relative humidity data in the cool side of the bulkhead from the Moisture Monitoring Program to estimate the moisture loss from the DST. However, the operational ventilation flow rates (between 50 and 150 million liters per hour) imposed just outside of the Heated Drift were too large to allow a direct measurement of changes in the monitored humidity data.

As mentioned above, these measurements were conducted for informative and complementary purposes. For example, these measurements provided much insight into the difficulty of obtaining useful measurements of conductive and convective losses. Problems with obtaining an accurate measurement of conductive losses as attempted in item (1) involved the irregular and multiple-material surface of the bulkhead. Complications with measuring convective heat losses in items (2) and (3) mainly stemmed from the intrinsic difficulty of measuring a highly heterogeneous moisture and heat flux from a diffuse source. Also, considerable uncertainty was involved in item (2) because it was not possible to reasonably estimate the fraction of moisture loss captured in the measurement system as a result of the inherent leakage through bundles of power cables and instrument-wiring pathways.

After the white paper, which references measurements (1) and (2) above, was prepared, the thermal test team initiated a final field experiment to determine whether a heat and mass measurement was feasible. The basic approach involves measuring the temperature and the relative humidity, on the cool side of the Heated Drift, as a function of time and discrete spatial locations. Then the integral moisture increase in the drift volume on the cool side of the bulkhead was used to estimate the mass loss from DST convective heat flow. This measurement is nontrivial because of the substantial ventilation on the cool side of the bulkhead and the limitations of relative humidity measuring devices. In the July 2001 scoping study, the measured temperature and relative humidity in 38 installed Rotronic HygroClip® relative humidity temperature sensors were used to estimate the changes in vapor mass and energy. The preliminary estimates of heat loss (for “nonrepresentative” conditions because the airflow from the ventilation system was necessarily reduced) yielded a total heat loss of ~ 0.5 to 2.6 kW. This is at least one order of magnitude less than what was expected from the numerical modeling of

the DST. This final experiment demonstrated that the vapor loss through the bulkhead of the Heated Drift was too complex to measure directly.

6.3.3 DST Mechanical Measurements

The discussion of mechanical measurements for the Drift Scale Test has been divided into several subsections based on the type of measurement:

- Multi-point borehole extensometer (MPBX) displacement data
- Cross-drift extensometers (CDEX, or "pogo-sticks")
- Strains measured on the inner surface of the cast-in-place liner
- Acoustic emission
- Laboratory parameters such as elastic modulus, Poisson's ratio, and thermal expansion for intact rock and concrete
- Plate loading test
- Additional measurements, including rock scaling and acoustic emissions

Detailed discussion of the mechanical measurements is documented in Section 6.3 in the *Drift Scale Test Design and Forecast Results Report* (CRWMS M&O 1997 [146917]), in Section 5.1.2 of the *Drift Scale Test As-Built Report* (CRWMS M&O 1998 [111115]), and in Sections 4 and 8 of the *Ambient Characterization of the Drift Scale Test Block* report (CRWMS M&O 1997 [101539]). Input-DTNs and Output-DTNs for DST mechanical measurements are listed in Tables 4-3 and 6.3-1, respectively.

6.3.3.1 Multi-Point Borehole Extensometers (MPBX)

Figure 6.3.3.1-1 shows the layout of the MPBX boreholes. The as-built location coordinates of the collars and anchors are provided in Table 6.3-2. Displacements reported in this document followed the convention of extension being positive. Displacements were measured within the rock-mass surrounding the Heated Drift and between the Heated Drift and the Observation Drift. These measurements were used to evaluate numerical models related to T-H-M coupling as well as to provide data for determination of rock-mass thermal expansion. Multi-point borehole extensometers (MPBXs) were installed in 17 boreholes both within and outside the Heated Drift to monitor rock-mass movement during the DST.

Two of the MPBXs (designated ESF-HD-81-MPBX1 and ESF-HD-82-MPBX2, with 81 and 82 referring to the borehole numbers) were installed in two long horizontal boreholes drilled parallel to the Heated Drift from the connecting drift. Twelve MPBXs (MPBX3 through MPBX14) were installed in three four-borehole arrays (numbers 147-150, 154-157, and 178-181) drilled into the surrounding rock-mass from within the Heated Drift itself. The array containing MPBXs 3, 4, 5, and 6 (boreholes 147-150) is located in the Heated Drift at Y = 13.7 m; the array with MPBXs 7, 8, 9, and 10 (boreholes 154-157) is located at Y = 21.0 m; and the array with MPBXs 11, 12, 13,

and 14 (boreholes 178-181) is located at Y = 41.1 m, in the concrete liner test section of the Heated Drift. For the three MPBXs in each array collared in the crown of the drift, the four anchors for each were located nominally at 1, 2, 4, and 15 m from the collar. For the fourth MPBX in each array, which was collared at the top of the invert, the anchors were installed so as to put them in the same relative position in the surrounding rock-mass as the other MPBXs (i.e., approximately 2.2, 3.2, 5.2, and 16.2 m from the collar).

The remaining three borehole MPBXs were drilled for sequential drift mine-by monitoring. These MPBXs were installed in November-December 1996 in boreholes 42, 43, and 44, drilled slightly downward from the Observation Drift toward the Heated Drift. Boreholes 42, 43, and 44 are located at Heated Drift stations 0+13.7, 0+20.8, and 0+32.2 m, respectively (each station refers to the Y-axis distance from the heated drift bulkhead). Refer to Section 5.2 for discussion related to the approach used to "smooth" the MPBX measurements.

The displacement data may be found in the following Input-DTNs: SNF39012298002.002 [159114], SN0203F3912298.033 [158361], SNF39012298002.010 [158367], SN0001F3912298.014 [153841], SN0007F3912298.018 [158374], SN0101F3912298.024 [158400], SN0107F3912298.029 [158408], and SNF39012298002.006 [158419]. The displacement data corrected for thermal expansion may be found in the following Input-DTNs: SNF39012298002.012 [153840], SNF39012298002.008 [153839], SN0203F3912298.035 [158363], SN0001F3912298.016 [153842], SN0007F3912298.020 [158388], SN0101F3912298.026 [158402], SN0107F3912298.031 [158413], SNF39012298002.004 [153837].

6.3.3.1.1 Results: MPBX Displacements

Because of the abundance of DST MPBX displacements, only representative discussion and graphics are provided. All MPBX displacement data and graphics can be accessed in the Output-DTN identified in Table 6.3-1.

The following discussion provides a cross section of MPBX measurements of displacements within the DST block. The displacement plots have been smoothed by the procedure discussed above, with each plot representing the maximum (or minimum) over a 10-day period.

MPBX1 is located in borehole 81, which runs parallel to and is collared outside the Heated Drift. This borehole is on the north side of the drift (the anchor is located in the Data Acquisition System niche). A time-history plot of smoothed, temperature-corrected displacement is shown in Figure 6.3.3.3-2. The overall performance of this MPBX1 is very good; there is very little noise, and the data for the heating phase of the DST show thermomechanical responses consistent with elastic model predictions. Some of the temperature data indicate the possibility of steam fronts or fracture flow paths in the borehole; the sharp temperature rise at 400 days for TC-6 is a primary example. There is very little indication of potential fracture slippage in the displacement data from this borehole.

MPBX7 is located at Y = 21.0 m in borehole 154 anchored in the crown of the Heated Drift, and angled 30° from the vertical towards the north (away from the Observation Drift). A time-history plot of smoothed, temperature-corrected displacement is shown in Figure 6.3.3.1-3. The overall

quality of the data from MPBX7 is good, although the data are very noisy because of the temperature oscillations from moisture recirculation. The level and frequency of noise make this data useable only for evaluating general thermomechanical behavior, and not determination of specific events. Two interesting observations may be made about the displacement data: (1) the displacement at anchor 3 is much less than might be expected from elastic analyses; and (2) the displacements shown for anchors 1 (1 m from the collar) and 4 (15 m from the collar) are much closer to each other than would have been expected.

MPBX8 is located at Y = 21.0 m in borehole 155, anchored in the crown of the Heated Drift, and angled 30° from the vertical towards the south (towards the Observation Drift). A time-history plot of smoothed, temperature-corrected displacement is shown in Figure 6.3.3.1-4. The overall quality of the displacement data from MPBX 8 is good. The biggest disappointment for this borehole was the loss of its TC-1, which required using the corresponding TC-1 from MPBX9 for the reference temperature. (MPBX9 is vertically up, whereas MPBX7 is located at the mirror position opposite MPBX8. The thermocouple from MPBX9 was originally chosen because its data were cleaner than MPBX7, and the typical values were about the same.) There are two sources of moisture-induced noise: (1) temperature fluctuations in borehole 155 (days 300-500), for which the displacement data reflect real thermal-mechanical response; and (2) at later times (after day 800), fluctuations of MPBX9-TC-1, which introduce artificial noise into the conversion and thermal correction of MPBX8 data. Some evidence of moisture-related temperature oscillation is seen at other TCs for MPBX8. A large temperature perturbation event for all the TCs at days 475-545 (3/23/1999-6/1/1999) is similar in nature and timing to temperature events for MPBX9, as well as farthest sections of MPBX12 and 13, located 20 m further down the drift. This event may indicate connectivity between these four boreholes. The LVDT for Anchor 3 apparently failed on day 1247 (5/2/2001).

MPBX9 is located at Y=21.0 m in borehole 156 anchored in the crown of the Heated Drift, and angled vertically upward. A time-history plot of smoothed, temperature-corrected displacement is shown in Figure 6.3.3.1-5. The displacement data from anchors 2, 3, and 4 of MPBX9 are good. The displacement data from anchor 3 level off unexpectedly (that is, when compared with an elastic model) at around 500 days. The biggest surprise is the onset of large-scale moisture-induced temperature perturbations, which eventually affect all the TCs except those already near boiling. MPBX10 is located at Y=21.0 m, anchored in the top of the invert of the Heated Drift, and angled vertically downward. A time-history plot of smoothed, temperature-corrected displacement is shown in Figure 6.3.3.1-6. The displacement data for MPBX10 are anomalous for all the anchors: anchor 1 failed early in the test; anchor 2 is erratic for the first year, then looks good for the remainder of the test; anchor 3 is erratic throughout the entire test; and anchor 4 has regions of good data interspersed with large-sale noise that is not moisture-induced (because the TCs are clean throughout the test). Because of the erratic nature of the MPBX10 data, it is hard to identify any events that may be related to microseismic phenomena.

6.3.3.1.2 Measurement Uncertainty: MPBX Displacements

The uncertainty of the DST MPBX measurements are similar to comparable SHT MPBX measurements, as discussed in Section 6.2.3.1.2. as shown in Table 6.3.3.1-1, the gauge range and accuracy of the LVATs for the MPBXs are ± 25.4 mm and 0.5% respectively.

6.3.3.2 Cross-Drift Extensometers

Two cross-drift extensometers (CDEXs) were installed in the section of the Heated Drift with a cast-in-place concrete liner to measure cross-drift convergence. Often referred to as "pogo-sticks," these convergence meters CDEX-1 and CDEX-2 were located nominally at approximately Y=42.3m, between the eighth and ninth canister heaters. CDEX-1 measures vertical closure, and it is anchored in the top of the invert of the Heated Drift and to the crown of the liner. CDEX-2 measures horizontal closure and is anchored to the liner on each rib. As for the MPBXs, displacements from the CDEXs reported in this document follow the convention of extension being positive.

The cross-drift extensometer data may be found in the following Input-DTNs: SNF39012298002.002 [159114], SN0203F3912298.033 [158361], SNF39012298002.010 [158367], SN0001F3912298.014 [153841], SN0007F3912298.018 [158374], SN0101F3912298.024 [158400], SN0107F3912298.029 [158408], and SNF39012298002.006 [158419]. The cross-drift extensometer data corrected for thermal expansion may be found in the following Input-DTNs: SNF39012298002.012 [153840], SNF39012298002.008 [153839], SN0203F3912298.035 [158363], SN0001F3912298.016 [153842], SN0007F3912298.020 [158388], SN0101F3912298.026 [158402], SN0107F3912298.031 [158413], SNF39012298002.004 [153837].

6.3.3.2.1 Results: Cross-Drift Extensometers

The thermocouple and anchor locations, as well as the quality of the data from CDEX-1 and CDEX-2, are listed in Table 6.3.3.2-1; a time-history plot of smoothed, temperature-corrected displacement is shown in Figure 6.3.3.2-1. In general, ovalization takes place during the heating phase in which horizontal closure and vertical extension occurs. This deformation reflects increasing horizontal stresses as temperatures increase during the heating phase. Vertical stresses tend to remain constant during heating, since in an elastic regime their magnitudes are limited by the overburden.

6.3.3.2.2 Measurement Uncertainty: Cross-Drift Extensometers

There are several potential sources for measurement uncertainty in the displacement measurements presented in Section 6.3.3.1.2 and 6.2.3.1.2 for the MPBXs. Much of that same discussion pertains as well to the CDEXs. The only exception to that discussion would be any effects caused by being inside a borehole, which obviously the CDEXs are not. The gage range and accuracy of CDEX-related instrumentation are presented in Table 6.3.3-6 in Section 6.3.3.1.

6.3.3.3 Strains

Strain gages were installed on the surface of the cast-in-place (CIP) concrete sections located at the west end of the Heated Drift to monitor the concrete behavior during heating and cooling of the DST. A total of 45 four-inch-long Karma foil resistive strain gages were installed in fifteen rosettes (three gages per rosette) in a circumferential-axial-45º pattern at three Y stations. The five strain gage rosettes at each station were located at the crown, to the left and right above the springline, and to the left and right near the concrete invert; this layout is shown in Figure 6.3.3.3-1. The rosette strain gages are designated by rosette number and orientation (AXL=axial,

CIR=circumferential, DIA=diagonal); for example, ESF-HD-RSG-5-AXL is the axial strain gage for rosette number 5. In addition to the 45 strain gages (15 rosettes) bonded to the CIP liner, there were five additional strain gages bonded to concrete and 304 stainless steel "coupons" placed near Canister Heater 8 in the Heated Drift. These "coupons" are prisms of concrete and steel that are used to provide baseline data on the strain-gage response and some indication of unconstrained concrete material response. Gage and anchor locations (as-builts) for strain-gage measurements made for the DST are presented in DTN: SNF38040197001.001 [159130]. Refer to Section 5.2 regarding the approach used to "smooth" the strain measurements.

The strain data may be found in the following Input-DTNs: SN0203F3912298.034 [158362], SNF39012298002.011 [158368], SNF39012298002.007 [158365], SN0001F3912298.015 [158372], SN0007F3912298.019 [158387], SN0101F3912298.025 [158401], SN0107F3912298.030 [158409], SNF39012298002.003 [158417]. The strain data corrected for thermal expansion may be found in the following Input-DTNs: SN0203F3912298.036 [158364], SNF39012298002.009 [158366], SNF39012298002.013 [158369], SN0001F3912298.017 [158373], SN0007F3912298.021 [158391], SN0101F3912298.027 [158407], SN0107F3912298.032 [158414], SNF39012298002.005 [158418].

6.3.3.3.1 Results: Strains

Because of the abundance of DST strain data, only representative discussion and graphics are provided. All strain data and graphics can be accessed in the Output-DTN identified in Table 6.3-1.

Figure 6.3.3.3-2 shows a time history plot of the strains measured by the axial, circumferential, and diagonal strain gages on the liner surface, respectively. The strain gages placed on the concrete liner and on unconstrained concrete samples (not shown here) in the Heated Drift indicate the combined effects of thermal expansion, dehydration-induced shrinkage, and mechanical stress imposed by the interaction of the concrete with the heated rock surrounding the drift. The results from the strain gages on the unconstrained samples exhibit behavior indicative of drying shrinkage caused by dehydration, a phenomenon seen elsewhere in engineering literature.

The circumferential, or hoop, strains begin as compressive strains, as the surrounding rock expands inward and compresses the liner. The axial and diagonal strains are nearly always in extension, because there is far less interference with thermal expansion of the liner in the axial direction. All of the strain gages on the liner surface went into extension by approximately day 325 on account of combined thermal and mechanical effects. A mechanical component of the strain can be estimated by subtracting the strains measured from the unconstrained coupons (the thermal component) from the total strains. The mechanical component of the circumferential strain gages on the liner consistently shows that the crown of the liner is in compression, while the rest of the liner experiences smaller magnitudes of compression and tension. Note in the strain plots the beginning of the creep degradation of the epoxy beginning at around 950 days.

Thermal expansion coefficients for T>96°C have been estimated for the unconstrained concrete coupons that lay on the floor of the Heated Drift. The coupons reveal some very interesting information regarding the thermal expansion of concrete at elevated temperatures. The data seem

to reveal four distinct temperature regimes, each with its own characteristics for the thermal expansion coefficient α:

1. T<100°C, fast temperature rise : 8–12 με/°C
2. T<100°C, slow temperature rise : ~0 due to coincident drying shrinkage
3. 100°C<T<165°C : 10–14 με/°C
4. T>165°C: 31–37 με/°C

This behavior is within the same range as to the laboratory thermal expansion data for SHT and DST intact rock samples (SNL 1997 [117471]). When the strain for each coupon is plotted as a function of temperature, the coupons all exhibit a precipitous change in slope (i.e., thermal expansion) at about 165°C. In another interesting development, hysteresis in the strain data can be observed when temperature drops due to power outages. These data may be very important to the repository designers should concrete liners once again become part of the design plan.

6.3.3.3.2 Measurement Uncertainty: Strains

The following list includes all the known sources of measurement uncertainty for the strain data:

Quantifiable

- The accuracy of the instrumentation itself. The gage range and accuracy of strain gage-related instrumentation are presented in Table 6.3.3.3-1.

- The conversion of the electrical output to engineering units. The uncertainty from these equations, and the computational (round-off) error inherent in the DCS data conversion software, are negligible.

Non-quantifiable

- Electrical interference, such as spurious signals from power surges, can cause low-magnitude noise, unexplained meandering in the data, or high-magnitude spikes.

- Problems caused by elevated temperature leading to epoxy degradation.

6.3.3.4 Acoustic Emission

Passive seismic monitoring was used to monitor changes in acoustic emission (AE) activity and wave propagation characteristics. Microseismic events can be attributed to cracking of the rock or movement along pre-existing fractures or joints from thermal expansion. The methods, concepts, and instrumentation that were developed and tested in the early 1980 at the Climax Stock spent fuel test (Majer and McEvilly 1985 [159101]) were closely followed here for the DST. The microseismic monitoring measurements were governed by the Technical Implementing Procedure YMP-LBNL-TIP/TT 4.0, Rev. 1 Mod. 0). Detailed discussions of experimental set-up and data processing can be found in three level 4 milestones (Peterson and Williams 1998 [159102]; Williams et al. 1998 [159104]; Williams and Peterson 1998 [159121]).

Sixteen accelerometers were placed in DST boreholes 138-140, 142-144, 159-161, 163-165, 171, 172, 174, and 175 (see Table 6.3-2). There were two different types of sensors depending on maximum temperature rating: Wilcoxin Research Model 793-6 (rated to 150°C) and Model 728-T (rated to 125°C). These were selected based on anticipated temperatures from pre-heating modeling. All ratings are at least 20°C higher than the maximum temperature anticipated. The sensors were connected to the Data Collection Shed by high-temperature (Teflon) coaxial wire so that sensor measurements could be recorded. The desired bandwidth was in the 1,000 to 10,000 Hz range. The numbering, location, serial number, and model number of the sixteen accelerometer are listed in Table 6.3.3.4-1. Data recording the microseismic activity in the test block have been submitted to the TDMS periodically over the course of the heating phase under the following Input-DTNs: LB980120123142.007 [158352] (for background measurements), LB980420123142.004 [113717] (for time period 01/1998 to 04/1998), LB990630123142.004 [158360] (for time period 04/1998 to 06/1999), LB000121123142.005 [158339] (for time period 06/1999 to 01/2000), LB000718123142.005 [158343] (for time period 01/2000 to 07/2000), LB0101ACEMDST1.001 [158344] (for time period 07/2000 to 01/2001), and LB0108ACEMDST5.001 [158437] (for time period 01/2001 to 08/2001).

6.3.3.4.1 Results: Acoustic Emissions

Although the monitoring system was designed to operate continuously over the duration of the experiment, numerous problems occurred. Because of high-voltage noise spikes conducted along the accelerometer coaxial connections, the acquisition system initially was plagued by false triggering memory buffer errors. Efforts to reduce these problems were finally completed by December 1998, a full year after initiation of the heating phase. Enhancements to the recording system (bandpass filters) resulted in greatly improved data quality (i.e., increased signal/noise) starting in late December 1998. From this period until late October 2000, the system recorded microseismic events at a roughly uniform rate. After October 2000, however, a period of very low activity followed. Although deterioration in accelerometer sensitivities (resulting from thermal exposure, corrosive, fluids, etc.) may be one potential cause for the decrease in recorded activity, the system was judged to be operating properly during this time, according to the accelerometer and recording system check procedures detailed in YMP-LBNL-TIP/TT 4.0, Rev. 1, Mod. 0. A histogram of microseismic events with time are shown in Figure 6.3.3.4-1.

The data recorded in the seismic monitoring consist of the microseismic waveform and the time and date that it was recorded. To determine the location of the source of energy causing the seismic event, the data were processed as follows. The first-arrival times were picked by determining when the initial burst of energy arrived at each of the 16 monitoring station. After the first-arrivals times are picked, the location of the seismic energy source can be estimated by inversion. Figure 6.3.3.4-2 shows the locations of all the seismic events (collapsed to the yz plane) through the heating phase. The data in the TDMS contain the following:

EVENT#: Represents the sequential order in which the acoustic emission/microseismic event was recorded by the recording system

DATE: Represents the date on which the event was recorded

TIME: Represents the time when the event was recorded

X(M): Represents the 'X' coordinate for the located event

Y(M): Represents the 'Y' coordinate for the located event

Z(M): Represents the 'Z' coordinate for the located event

OTIME(MS): Represents the origin or "zero" time or first-arrival time of the event by the recording system

ERROR: Root Mean Square (RMS) error in travel time

AMPLITUDE: Represents the amplitude of the recorded event

An initial comparison between MPBX displacements and acoustic emissions was based on the time period of 12/21/1998 to 6/1/1999. A total of 76 AE events and 60 MPBX events were identified for comparison. Events were then eliminated due to lack of temporal or spatial correlation with other events. After all of this, only one pair of events was identified as a potential event captured by both AE and MPBX. The AE event identified in Table 6.3.3.4-2 produced perhaps the strongest signal of any event registered by the AE equipment. Although the two data points correlate reasonably well, this alone is not proof that they correlate to the same mechanical event. Furthermore, since only one correlation was found, there is little evidence to support the possibility that the MPBX and AE data would indeed register the same event.

Usually, one of two conditions was met to indicate that an AE event did not correspond with an MPBX event. The first condition was to have an AE event that was reasonably close to either a specific MPBX borehole or close to the plane in which an array of MPBX boreholes was located. For these events, although a spatial correlation was possible, there were no MPBX events from those boreholes within a reasonable time (i.e., less than 24 hours) after the AE event. Secondly, an AE event might have occurred at the same time as an MPBX event, but the two events were so far apart spatially, and without any corroborating events in locations between them, that they were considered to be unrelated.

Eventually, AE data collected through 3/21/2000 (296 AE data points) were available for comparison with MPBX data. The only potential correlation is between a series of microseismic events on 7/1/1999 and 7/2/1999 (days 574–575) and several discontinuities in SDM-MPBX3. Because of the small number of potential matches, and the nature of the two types of measurements, this comparison of AE and MPBX events did not yield any significant findings that showed a correlation between these data.

After the rock scaling events were first noticed in late summer 2001, more recent AE data were evaluated to determine if any correlations exist between these events. The following conclusions were drawn from this latest comparison:

- There is no apparent temporal correlation between AE data and rockfall events.
- AE data indicates several significant "pops" in the drift crown at earlier times, which may or may not indicate the stress relief that caused the rockfall.

- Rock spalling itself probably does not generate enough signal to register in AE data; the signal is weak, and the high local temperatures degrade the signal.

6.3.3.4.2 Measurement Uncertainty: Acoustic Emissions

Hammer blows to the wall of the Observation Drift are periodically recorded during the experiment. These data are included with transmittals to the TDMS and represent the primary means by which system repeatability and, in a sense, measurement error is assessed. Because the hammer blows always occur at the same location along the Observation Drift wall, the post-processing of the hammer "event" should result in the proper spatial locating of this event. However, given the greatly elevated accuracy of locating events *within* the array of accelerometers, the hammer blows are not an ideal means of measurement error assessment: the hammer blow occurred outside of the array. Therefore, comparing the location of the hammer blow events over time should result in consistent locations within some reasonable error envelope. The acceptable envelope was determined to be a 2 x 2 x 2-meter region. The actual microseismic events should have a much higher degree of accuracy because they fall within the array boundaries. Post-processing of the microseismic events also results in the determination of a RMS error in the seismic-wave travel times. This error may be used to assess the accuracy of the resulting microseismic event location.

6.3.3.5 Laboratory Mechanical Parameters

Several pre-heating laboratory investigations were done to gather intact rock mechanical and thermomechanical properties/parameters of the TSw2 middle nonlithophysal tuff in the DST area, and to assess the concrete used in the invert and liner in the Heated Drift. This section describes the results of the following four suites of laboratory testing of parameters.

- Thermal expansion of intact rock (Input-DTN: SN0203L2210196.007 [158322])
- Elastic constants and strength properties of intact rock (Input-DTN: SNL02100196001.001 [158420])
- Elastic constants and strength properties of concrete samples (Input-DTN: SNL23030598001.001 [158370])
- Creep testing of cast-in-place concrete (Input-DTN: SNL23030598001.003 [158422]).

Detailed discussions of rock parameters are presented in Section 4 of the *Ambient Characterization of the Drift Scale Test Block* (CRWMS M&O 1997 [101539]).

6.3.3.5.1 Results: Thermal Expansion

The mean coefficients of thermal expansion (MCTEs) are summarized in Tables 6.3.3.5-1 and 6.3.3.5-2 for heating and cooling, respectively, during the first thermal cycle. The mean MCTEs and standard deviations about the mean are given at each temperature for each borehole. Summary data for the entire test suite are given with standard deviations and 95% confidence limits at the bottom of each table. The data obtained during the first heating cycle show similar behavior for most MCTEs. With the exception of three, most specimens show steep increases in MCTE, beginning at approximately 200°C and continuing until approximately 300°C. This steep increase is attributed to phase changes in the silica mineral phases because of the presence of

cristobolite and tridymite. The increase in MCTE at elevated temperatures is not attributed to thermally induced fracturing or differential expansion, since these behaviors would not be significant during the second heating phase. The test data indicates sharp increases for both sets of heating/cooling cycles. The decrease in MCTE at 300°C suggests that the phase changes have been completed. Also, hystereses are linked with phase changes. The three specimens showed behavior different from the remainder of the suite partly because of different concentrations of cristobolite and tridymite. These minerals vary substantially from their respective mean values for two of the three samples that exhibited anomalous behavior. Two of these specimens (MPBX2-85.0-B and MPBX1-40.4) appeared to initiate phase changes below 200°C, and one specimen (HDFR1-97.9-B) appeared to undergo essentially no phase change.

6.3.3.5.2 Results: Elastic Constants and Strength Parameters of DST Intact Rock

The experimental data for the 16 specimens tested in unconfined compression are summarized in Table 6.3.3.5-1. Mean values, standard deviations, and 95% confidence limits are given in Table 6.3.3.5-1 for Young's modulus, Poisson's ratio, unconfined compressive strength, and axial strain at peak stress. One specimen, MPBX1-1.0-A (test UCDST001), was unloaded after force began to drop at approximately 53 MPa. The specimen was later reloaded (test UCDST017) to a peak stress of 179 MPa. Data from the first loading of this specimen were used to calculate the mean elastic moduli to be consistent with the other tests. Data from the second loading were used in calculations of mean unconfined compressive strength and mean axial strain at peak stress.

Young's modulus ranged from 28.9 GPa to 43.1 GPa, with a mean value of 36.8 GPa. The standard deviation was ± 3.5 Gpa, and the 95% confidence limit was ± 1.7 GPa. The high Young's modulus value (43.1 GPa) corresponds to the first loading of MPBX1-1.0-A. Because this specimen was unloaded at a low stress difference, the modulus was calculated over a lower stress range than for the other specimens.

Poisson's ratio ranged from 0.17 to 0.34, with a mean value of 0.20. The standard deviation was ± 0.04, and the 95% confidence limit was ± 0.02. The three specimens with the highest Poisson's ratios were the only specimens that had pre-existing open fractures.

Strengths ranged from 71 MPa to 324 MPa, with a mean value of 176 MPa. The standard deviation was ± 66 Mpa, and the 95% confidence limit was ± 32 MPa. The highest and lowest strengths were obtained on specimens from MPBX2 that were in relatively close proximity (4 m apart). Neither specimen had notable surface features that might indicate anomalous behavior. No analyses were performed to determine the best-fitting distribution curves for Young's modulus, Poisson's ratio, or unconfined compressive strength.

6.3.3.5.3 Results: Elastic Constants and Strength Properties of Cast-in-Place Concrete Samples

Six concrete specimens were tested to failure in unconfined compression, and four specimens were cycled to approximately 40% of the failure strength. Mean values and standard deviations of unconfined compressive strength, Young's modulus, and Poisson's ratio are given in Tables 6.3.3.5-2 and 6.3.3.5-3 for reinforced and nonreinforced concretes, respectively. Separate Poisson's ratio values are given for the two (0° and 90°) radial gages. Average failure strengths

were 56.6 ± 3.2 MPa for reinforced concrete and 54.3 ± 13.8 MPa for nonreinforced concrete. When an outlier was removed, the failure strength for nonreinforced concrete was increased to 62.2 ± 0.9 MPa. Mean Young's modulus (determined during all loading cycles) was 33.3 ± 2.1 GPa for the reinforced concrete and 38.8 ± 3.9 GPa for the nonreinforced concrete. Mean Poisson's ratio (also determined during all loading cycles) was 0.25 ± 0.03 for the reinforced concrete and 0.24 ± 0.04 for the nonreinforced concrete.

6.3.3.5.4 Results: Creep Testing of Cast-In-Place Concrete

Creep strains versus time for all tests are given in Figure 6.3.3.5-1. The average strains, as measured by the two LVDTs, are shown because of the shrinkage exhibited by the strain-gage bonding agent. Compression is negative, and so all specimens show axial compression occurring at a decreasing rate with increasing time. Three specimens with low steel fiber content were tested. One of these was tested at low stress and low temperature (CIP02A), one at low stress and high temperature (CIP01A), and one at high stress, high temperature (CIP04A). As expected, except for small perturbations or noise in the curves, the strains measured for CIP02A were lowest and those measured for CIP01A were highest at any given time.

Four specimens with high steel fiber content were tested. CIP19A Stage 1 was run at low stress and low temperature, CIP19A Stage 2 was run at high stress and low temperature, CIP16A and CIP20A were both run at low stress and high temperature, and CIP15A was run at high stress and high temperature. It was anticipated that CIP19A Stage 1 would exhibit the lowest strains, CIP15A would exhibit the highest strains, and the other tests would provide intermediate results. The data basically followed this pattern, except that the two nominally identical tests (CIP16A and CIP20A), gave distinctly different results. Also, at early times (<15 days) CIP16A shows lower strain than CIP19A Stage 1.

6.3.3.5.5 Measurement Uncertainty: Laboratory Mechanical Parameters

The uncertainty in the uniaxial compressive test of rock and concrete includes the accuracy of the load cell, the accuracy of the LVDT, specimen alignment, square and parallel of the specimen ends, changes in the specimen cross section area during the test, specimen variation, and anisotropy of the rock. Among these factors, the greatest uncertainty is with the specimen variation. The heterogeneity in the rock-mass will have significant effects on its compressive strength and moduli. Many of these uncertainties also apply to thermal expansion and creep testing of intact samples. In addition, temperature and stress control contribute to uncertainties in thermal expansion and creep testing, respectively.

6.3.3.6 Field Mechanical Parameters

The following mechanical field measurements are presented:

- Plate loading test
- *In situ* stress
- Fracture mapping
- Rock-mass classification
- Rock-mass thermal expansion.

6.3.3.6.1 Results: Plate Loading Test

The Plate Loading Tests (PLT) was conducted as part of the DST. The purpose of the PLT was to obtain rock-mass elastic-modulus measurements under ambient and hot conditions for the middle nonlithophysal tuff. Two earlier tests were conducted in 1998, after which design changes were made to ensure a stiffer loading frame for improved measurements. These improved measurements, from the October 2000 test, are summarized in Table 6.3.3.6-1. A detailed discussion of the setup, testing procedure, raw test data, and rock-mass modulus calculation from the raw data may be found in the documentation for two Output-DTNs: Plate Loading Test PLT Test (2000) Displacement and Pressure Data (SN0011F3912298.022 [158392]) and PLT Test (2000) Rock-mass Modulus Data (SN0011F3912298.023 [158399]).

6.3.3.6.2 Results: *In Situ* Stress Measurements

A series of five successful hydraulic fracturing tests, used to determine *in situ* stress states, were conducted. Test number 4, centered at 19.2 m from the collar of the borehole, yielded the typical pressure-time signature obtained during hydraulic fracturing of intact test intervals. The other test results showed signs of possible pre-existing fracturing, probably induced during drilling. In addition, two tests conducted at approximately 10 m from the alcove may also have been within the zone of influence of that excavation.

Thus, the most reliable hydraulic fracturing results were obtained in test number 4. Based on these results, and on the average vertical hydraulic fracture strikes in all tests, the estimate of the *in situ* stress state around borehole ESF-AOD-HDFR#1 is:

σ_h = 1.7 (±0.1) MPa acting in the N 75° W (+14°)
σ_H = 2.9 (±0.4) MPa acting in the N 15° E (+14°)

The measured *in situ* stress state is small, which is consistent with the dominant local normal faults. The north-northeastern maximum horizontal stress direction is subparallel to the average strike of these faults and is supported by previous measurements in the Yucca Mountain area. Detailed discussion is presented in a report by SNL (1997 [117471]) and in Section 10.4 of the *Ambient Characterization of the DST Block* (CRWMS M&O 1997 [101539]).

6.3.3.6.3 Results: Rock-Mass Classification

Rock-mass quality assessments were performed in all of the thermal testing excavations using line mapping surveys and are reported in both the Q rating system (Barton et al. 1974 [101541]) and the Rock Mass Rating (RMR) system (Bieniawski 1974 [101567]), using Schmidt Hammer Rebound Index Testing as a non-qualified activity. The rock-mass quality data concerning the DST have been submitted under DTN: SNF32020196001.015 [158434]. Related data surrounding the SHT have been submitted under DTN: SNF32020196001.010 [158314]. Rock-mass quality assessment was performed in satisfaction of Level 4 Milestone SP5140M4 (Lum 1997 [159132]).

While some structural variations within the heated drift were observed, the Q and RMR indices were found to be relatively consistent with those found from the repository horizon TSw2 and

did not display any significant systematic variation relative to location. The Q and RMR indices are presented in Tables 6.3.3.6-2 and 6.3.3.6-3, respectively. Note that these tables include data that were previously presented as part of the SHT block characterization (CRWMS M&O 1996 [101428], pp. 8-1 and 8-8), specifically the observation drift from station 5 to station 60, the SHT thermomechanical alcove, and the SHT thermomechanical alcove extension.

Surrounding the DST block, Q indices ranged from 0.761 to 621.875, while RMR indices ranged from 51.1 to 97. Note that the Q value of 621.875 is anomalously high. Both Q and RMR indices were relatively constant through the TTF, with relatively little scatter in values. The range in Q and RMR indices from the TTF was relatively limited compared to that observed from the main drift.

Examining the Q and RMR values from the DST block shows that the observed variation falls within the range observed for TSw2 in the main drift. The average RMR and standard deviation for the DST block is 74.1 ± 9.1, as compared to 63.7 ± 7.0 for the TSw2 unit in the main drift (Table 6.3.3.6-4). This indicates that no significant difference exists in RMR values determined from the DST block and TSw2 main drift. Similarly, Q and RMR indices calculated for the SHT block also fall within the range observed for TSw2 main drift (DTNs: SNF32020196001.010 [158314] and SNF32070996001.005 [109620]).

6.3.3.6.5 Results: Rock-Mass Thermal Expansion

Rock-mass thermal expansion has been calculated from the DST *in situ* heating phase data, including temperature change for a given axial length from ambient, gage length, and measured thermal displacement over the gage length. The rock-mass thermal-expansion coefficient was calculated for the DST using selected data from displacement measurement boreholes 81 and 82. These boreholes run roughly parallel to the Heated Drift, and extend over a distance of 45 m. Much of that distance is in a high-temperature region of relatively constant temperature.

Table 6.3.3.6-5 lists the rock-mass thermal-expansion coefficients calculated from the DST MPBX data from boreholes 81 and 82. It also lists *in situ* rock values taken from DST and SHT samples for comparison. Below boiling, the rock-mass coefficient ranges from 2.0 to 4.5×10^{-6}/°C; these values are approximately half of the intact values. As the temperatures approach 200°C, the rock-mass coefficient values approach the *in situ* values, with a maximum rock-mass coefficient of 12.55×10^{-6}/°C in the highest temperature range. The calculated values for rock-mass thermal expansion are, as expected, lower than the values from intact laboratory specimens, because of the ubiquitous presence of vertical fractures in the Tptpmn tuff. The fractures would tend to accommodate some of the thermal expansion in the joint stiffness, particularly during early heating, because the thermal displacement would be insufficient to mechanically close fractures. Also, the 3-D effects of heated rock bounded by lower-temperature rock would decrease the net effect of thermal expansion by resisting the thermal displacements in adjacent volumes of rock.

6.3.3.6.6 Measurement Uncertainty: Field Mechanical Parameters

Measurement uncertainties are numerous because measured uncertainty of the various types of measurements. Specifically, data monitoring of original field measurements (temperature and

MPBX displacements), subjective interpretations, high-pressure complications, fracture spacing, fracture aperture, and inelastic time-dependent deformation represent primary uncertainties. In many cases, these uncertainties can be mitigated with repetitive measurements.

6.3.3.7 Scaling along the Roof of the Heated Drift

The following discussion on scaling along the roof of the Heated Drift is an in-depth, unplanned investigation involving mostly observations and measurements. Limited scaling was initially observed in the roof of the Heated Drift in four zones, each covering an area less than two square meters. Associated with each of these scaling zones are small pieces of rock on the floor that have dropped through the 7.5 cm x 7.5 cm openings in the welded wire fabric of the ground support system. These scaling zones have been contained by the existing ground support system in the manner designed. The scaling behavior is summarily discussed herein in terms of background, observations, and conclusions. Observations of the progression of scaling are ongoing during the cooling phase of the DST. A white paper was prepared with detailed discussion on this subject (Williams 2001 [159516]).

6.3.3.7.1 Background

As shown in the *Drift Scale Test As-Built Report* (CRWMS M&O 1998 [111115], pp. 8-2 and 8-5), the Heated Drift is isolated from workers and visitors with a bulkhead to provide safety from the high temperatures and to isolate the test from external conditions. The planned thermal management strategy includes maintaining the drift wall temperature at approximately 200°C. This temperature behavior is representative for most of the Heated Drift because of the effectiveness of radiation.

The ground support system for the roof consists of rock bolts and welded wire fabric through the first 35 m of the Heated Drift. The support system for the remaining 12.5 m consists of a concrete liner, which covers the rockbolts and welded wire fabric, and extends to the far end of the Heated Drift (see Figures 6.3.3.7-1 and 6.3.3.7-2, showing layout sketch and pre-heating conditions, respectively).

6.3.3.7.2 Observations

Visual observations documented on November 16, 1999 indicated the presence of small rock chips on the floor located 5 to 20 m from the bulkhead. This observation triggered further investigation with the DST remote camera. Although small rock chips were present on the floor, there was no evidence of accumulated larger rock fragments retained in the welded wire fabric.

During a subsequent cleaning and re-installation of the DST bulkhead windows (April 23, 2001), loose rock was observed at several locations above the welded wire fabric attached to the roof of the Heated Drift. Cables from two instrumented boreholes located 2.7 m and 11.9 m from the bulkhead along the longitudinal axis of the Heated Drift were observed to have pulled loose from the welded wire fabric. These cables were originally fastened to the wire fabric during installation and remained fastened during prior video imaging in October 2000. This suggests that much of the scaling had occurred since then. To better characterize the extent of the loose rock, remote video imaging of the inside of the Heated Drift was scheduled for the following week.

On May 2, 2001, the extent of scaling along the roof of the Heated Drift was further examined. Video images were recorded with the DST's remote video camera and with an additional video unit mounted at the bulkhead. In addition, photographs were taken using a 35 mm camera with a telephoto lens. The 7.5 cm squares in the welded wire fabric provide a usable reference scale in the images. The camera door in the bulkhead was opened and the video equipment prepared. The insulated camera box, which contains two video cameras, successfully traveled the full length of the rail mounted to the roof of the Heated Drift (see Figure 6.3.3.7-2). One of the cameras recorded roof, wall, and floor images by rotating the lens about the longitudinal axis of the Heated Drift. However, this camera did not image most of the scaling zones because the camera's blind spot (created by rotational limitations of 320^{o} does not allow it to view that part of the roof. The second remote camera is forward looking. It was not intended to record images along the roof of the Heated Drift. At the far end of the Heated Drift (35-47.5 m from the bulkhead), the drift periphery is covered with a concrete liner. The traveling remote camera clearly showed that this concrete liner remained intact, with no evidence of fractures or damage from heating.

From the observations, sketches of the scaling zones along the roof were developed. Most of these observations were made from the viewing window located on the lower left side of the bulkhead. Figure 6.3.3.7-1 shows four zones of observed scaling that were mapped by estimating the number of welded wire fabric squares that held loose rock. The three zones closest to the bulkhead showed scaling concentrated along the drift crown (i.e., the apex). A fourth zone was located about at the 2 o'clock position relative to the crown, about 13 m into the Heated Drift. For the scaling zone closest to the bulkhead (about 3 m from the bulkhead), the elongated area is estimated to be 1.0 m^2 (see Figure 6.3.3.7-3). The existing ground support system consists of 3 m long Super Swellex rockbolts installed on a one m square pattern and 3 x 3 x W1.9 x W1.9 welded wire fabric (see Figures 6.3.3.7-2 and 6.3.3.7-3). This ground support was installed above the springline of the excavation and continues to perform as designed. For the scaling zone located about 7 m from the bulkhead, the lens-shaped area is estimated to be 0.7 m^2. At 12.5 m from the bulkhead, a somewhat circular zone is estimated to cover an area of about 1.6 m^2. Located close to the collar or instrument head of a multi-point borehole extensometer referred to as MPBX-3 (see Section 6.3.3.1), the fourth scaling zone covers an area of approximately 0.6 m^2. The loose rock fragments appear to have thickness between 2-5 cm. The ground support is expected to retain the scaling.

Other scaling zones may exist further from the bulkhead; however, observation and characterization was hindered because of distance and lighting constraints in these zones. Small chips of rock observed along the floor suggest that additional scaling zones exist. Even the characterization of the two scaling zones located at 12 m and 13 m from the bulkhead was difficult because of the distance from the viewing window and poor illumination.

The ground support system that was installed during the Heated Drift excavation approximately fours years ago, is functioning as designed. There is not any evidence of failed components or deep fractures. Pieces of rock that were held by the welded wire fabric varied in diameter from about 5 cm (silver dollar size) to about 20 cm (dinner plate size). The loose rock fragments, which were mostly flattened shapes, were indicative of rock scaling.

In addition to the remote video run, the YMP project photographer set up digital video and still photography equipment on the door platform for the remote camera. From that vantage point, high-resolution images of the loose rocks held by the rockbolts and welded wire fabric at several of the zones described above were obtained. Photographs of the roof suggest that most of the observed scaling zones are associated with uneven surfaces or ridges left by the alpine mining machine during excavation of the Heated Drift. This observation is not surprising, since these irregular ridges should experience higher stress concentrations and thus more failure than smoother surfaces along the drift periphery.

6.3.3.7.3 Conclusions

The occurrence of limited scaling from four small zones along the roof of the Heated Drift of the DST is not unexpected. The middle nonlithophysal rock (Tptpmn) is highly fractured, and additional fractures were likely created during the drift construction process. This altered zone around the drift, especially above the Heated Drift, is also exacerbated by:

- Uneven surfaces generated by the alpine miner during drift excavation
- Aggressive heating that is estimated to be 6 and 12 times the areal thermal loading associated with the current design and alternative low-temperature designs, respectively
- Transient reversal of the maximum principal stress from a vertical (ambient) to horizontal (heating) orientation. More simply stated, the changing stress differences along the room periphery as a result of DST heating
- Proximity of instrumentation and rock-bolt holes to the observed scaling zones.

The addition of heat increases the circumferential stresses around the Heated Drift, creating conditions that would lead to small amounts of rock scaling from the roof. The fallen rocks are shaped like flat plates, which is consistent with the development of circumferential fractures by a thermally induced biaxial stress state.

The amount of fallen rock observed is relatively small, which would indicate that rock damage is superficial. This conclusion is further supported by mechanical (MPBX) measurements, which do not indicate large-scale, deeply penetrating rock movements, but rather that the effects of scaling are limited to the surface of the Heated Drift.

The existing ground support system comprised mostly of rock bolts and welded wire fabric continues to perform as designed. Despite the appearance of inelastic deformation, onsite personnel who have much experience assessing ground support systems believe that the welded wire fabric and rock bolts remain competent and will continue to support the existing loose rock in the observed scaling zones.

Given the superficial nature of the observed scaling zones, adverse consequences of these scaling zones are expected to minimally impact the performance of the DST. To date, test equipment, instrumentation, and sensors have not been damaged. Ground support of rock bolts and welded wire fabric has functioned as expected for controlling and containing this type of rock behavior. The occurrence of the observed scaling zones does not appear to affect conceptual understanding

of the thermal-mechanical behavior of the rock-mass involving pre-closure and post-closure performance of the potential repository.

6.3.4 DST Chemical Measurements

This section presents chemical data that have been collected from the DST and intended for the validation of thermal-hydrological-chemical processes by numerical modeling. The following subsections will discuss, respectively, aqueous chemistry (6.3.4.1), gas chemistry and isotopic compositions (6.3.4.2), mineralogical and petrologic analyses (6.3.4.3), strontium and uranium isotopic compositions of water samples (6.3.4.4), and special investigations of waters with high fluoride concentrations (6.3.4.5).

6.3.4.1 DST Aqueous Chemistry

Periodically, during the heating phase, water samples have been collected from multiple locations throughout the DST block and analyzed in the laboratory for concentrations of metals, anions, and certain isotopes. Aqueous sampling is conducted from boreholes, instrumented to include water and gas sampling capabilities. The boreholes are (by design) drilled to intersect regions of the thermally perturbed rock that would be undergoing different thermal-hydrological-chemical processes (boiling, drying, condensing, dissolving and precipitating) at different times. For pre-heating baseline data, pore water was obtained from centrifuged cores of boreholes 182–184 (ESF-HD-PERM1–PERM3) on the other side of the Connecting Drift across from the DST block. The concentrations of inorganic ions have been measured and reported. Otherwise, all of the analytical data reported in this section are from samples derived during heating from boreholes constructed for water sampling within the DST block.

A series of boreholes equipped with two types of fluid sampling systems was installed into the DST. First, ten boreholes were instrumented with FLUTe™ liners (Flexible Liner Underground Technologies, Ltd.) designed specifically for sampling water and gas for chemical analyses. (Liners installed into the different thermal field tests were manufactured by both SEAMIST™ and by FLUTe.™ Although FLUTe™ provided all of the liners used in the DST, in some documents they continued to be referred to as SEAMIST™ liners. (e.g., Section 5.1.4 of the *Drift Scale Test As-Built Report* (CRWMS M&O 1998 [111115])). These are the chemistry boreholes, ESF-HD-CHE-(1-10) (or boreholes 52-56 and 69-73, as shown in Figure 6.3-7). Second, boreholes instrumented with inflatable packer strings were designed with air-permeability testing as the primary function (see Section 6.3.2.4). Observations during the SHT (see Section 6.2.4.1) demonstrated how the system could be effectively implemented in fluid sampling. These are the hydrology boreholes, ESF-HD-HYD-(1-12) (or boreholes 57-61, 74-78, 185-186, shown in Figure 6.3-4).

Both the chemistry and the hydrology boreholes were expected to provide opportunities for water collection throughout thermal testing. The chemistry boreholes, with proper spacing of high absorbency pads, would yield good spatial and temporal coverage of geochemical data even with small volumes of water. The hydrology boreholes, with inflated packers that straddle highly fractured regions of rock, would potentially accumulate water as moisture entered along the 5–10 m of opening. Generally, although both systems employed proven technology, the high

temperatures of the DST would place somewhat unusual requirements on materials used for their construction.

For the FLUTe™ liners, a high-temperature silicon rubber was selected to ensure flexibility and durability for the often-repeated liner installation and retrieval processes. Unfortunately, the liners themselves never performed to expectations, either under the thermal load of the DST or with sufficient strength to survive repeated manipulations against the irregular and sharp features of the borehole walls. For the inflatable packers, two high-temperature rubbers were selected. Among the cooler regions of rock, a neoprene rubber was employed, and in the hottest boreholes, a fluorocarbon rubber was employed. Both proved to be mechanically sound, but not chemically inert in the hotter boreholes. In this section, the geochemistry of water samples that have been collected in the DST will be discussed. Although attempts were made to salvage the installed liner systems of the chemistry boreholes, those attempts proved to be unsuccessful. Consequently, the aqueous sampling role of the hydrology boreholes has been critical, and the analyses of waters collected from them form the aqueous geochemistry database of the DST.

The field measurement data are identified with data in DTNs: MO0207AL5WATER.001 [159300], MO0101SEPFDDST.000 [153711] and SN0203F3903102.001 [159133].

Analytical data acquired by Inductively Coupled Plasma and Atomic Emission Spectroscopy (ICP/AES) and Ion Chromatography (IC) for metals and anions respectively are performed under the control of the technical implementation procedures, TIP-AC-02 for metal concentrations and TIP-AC-03 for anion analyses. The standard metals suite includes: Al, B, Ca, Fe, K, Li, Mg, Na, S, Si, and Sr; trace metals analyses are available upon request. The standard anion suite includes the following: F, Cl, Br, NO_2, NO_3, PO_4, and SO_4. The analytical results are in the TDMS identified with data in the following DTNs: MO0005PORWATER.000 [150930], LL001100931031.008 [153288], LL001200231031.009 [153616], LL020302223142.015 [159134], and LL020405123142.019 [159307].

6.3.4.1.1 Sampling Procedures

In this section, water sampling in the hydrology boreholes is described. The 12 hydrology boreholes instrumented with strings of inflatable packers were located in three arrays sketched in Figure 6.3.4.1-1. (The angles of inclination are exaggerated; black markers identify the packer locations along the borehole lengths.) When inflated, the packers formed isolated open intervals that are referred to as test zones. Test zone 1 for a given borehole is defined to be the interval between the packer closest to the Observation Drift, and the next closest packer. All the zones continue to be numbered sequentially, with the deepest zone (zone 3 or 4) defined by the deepest packer and the borehole bottom. To implement the packer system as a water collection device in the DST, the air-injection lines used in the air-permeability testing become the sampling tubes to pump water out into the Observation Drift. The air-injection tubing opens to the lowest elevation of each zone. If fluids enter the zone by fracture flow, they would potentially drain to the bottom, where access to the tube opening would be possible. The provisions for water capture and retention, however, would be somewhat dubious, since the boreholes would be expected to act as capillary barriers to liquid flow. Nevertheless, experience in the SHT demonstrated that fluid would enter into some of the intervals, collect in the lowest end, and remain until pumping could

be conducted. Water samples obtained from these zones, were potentially derived from the entire open interval, a length of ~5–10 m.

Water sampling has been conducted by peristaltic pumping of individual zones on a regular and on an as-needed basis. The zones that have produced water samples during water collection activities in the DST heating stage are indicated in Figure 6.3.4.1-1. In addition, a couple of opportunities to collect DST borehole waters presented themselves to other thermal test personnel; water samples collected opportunistically were done so without the benefit of standard sampling instrumentation, analytical field testing, and field preservation. These miscellaneous waters are not represented in Figure 6.3.4.1-1 or in the compilation of field data to follow. During water sampling activities, all zones are pumped for at least five minutes. Thus, zones that may be well above the boiling temperature, ~96ºC, are pumped along with lower-temperature zones. An important observation has been the collection of water from some of the highest temperature zones. In these boreholes, heated *water vapor* that was pumped through the sample tubing condensed as it was pulled away from the hot sampled area to the cooler vicinity of the Observation Drift. The condensed water vapor was then collected in the field as a sample of water. The intervals that have produced condensed water vapor are indicated in the same diagram.

Water sampling from boreholes in the relatively dry host rock of the DST precludes practices that are common to sampling in saturated formations from an essentially unlimited water supply. Water volumes typically collected from a borehole zone are ~100–1500 mL. As a consequence, conservation measures are generally followed to maximize the information that may be gained from analytical tests. To collect water from individual zones in the hydrology boreholes, a peristaltic pump located in the Observation Drift was connected to an air-injection line through a manifold located outside each borehole array. Before sampling a zone, the peristaltic pump was prepared with clean sample tubing for the intake and the output lines, or the installed tubing might be thoroughly flushed with de-ionized water. Pumping was initiated once the hose from the pump to the manifold and from the pump to the collection vessel were in place. An optional vacuum gauge might be inserted into the intake line. (Gauge readings could then be used to indicate whether the air-injection line from the borehole was submersed in water or is open.)

The collected samples were designated for field-testing and various analytical suites; samples designated for analyses were prioritized based on acquired sample volumes. Field-testing included temperature and temperature-dependent measurements of pH, total dissolved solids (TDS), electrical conductivity (EC). When sufficient sample was available, an alkalinity titration could be performed. From the measured alkalinity, the sample's carbonate, bicarbonate, and hydroxide concentrations could be calculated. Samples designated for laboratory analysis were filtered in the field (≤ 0.45 μm), collected into certifiably clean sample bottles, and preserved. The samples to be collected for analysis may included: (1) a metals sample filtered into a polyethylene bottle and acidified to pH ≤ 2 using Ultrapure nitric acid; (2) an anion sample filtered, collected in a polyethylene bottle, and preserved in cold storage; (3) isotope samples for Sr and U analyses filtered into plastic bottles and acidified to pH < 2 using Ultrapure nitric acid; and (4) stable-isotopes sample (C, H, and O), filtered and collected in glass sample bottles.

The DST aqueous sampling and field characterization has evolved with the practical experience gained. After the first year, the sampling protocol and field-testing were reviewed. Members of

the thermal test team participated to recommend and draft the new field procedure, TIP-NF-33, which has remained the governing procedure for water sampling activities. As part of that effort, expanded field geochemistry was incorporated (requiring the purchase of additional supplies and test equipment), and priorities were placed upon the analyses to be performed. Limited sample volumes have and will continue to be the single factor restricting chemical characterization of DST waters. Upon completion of field activities, samples have been delivered to the SMF and stored under refrigeration until further instruction, or the collected samples shipped directly to individual principal investigators.

6.3.4.1.2 Results: Aqueous Chemistry

Field Measurements and Observations

Aqueous samples collected for chemical analyses have been acquired from several hydrology boreholes during the four years of heating. The first samples were collected six months after heating began, with subsequent sampling activities about every two to three months (more or less frequently as indicated). A summary of the water samples, the field data, and important observations for samples collected up to January 14, 2002 is presented in Table 6.3.4.1-1. Samples are reported and tracked by the Sample Management Facility (SMF) code assigned in the field—an 8-digit number, generally preceded by "SPC." Although the assigned SMF codes are formally used for sample and data traceability, for written and oral communication among the thermal test team, reference to a sample is generally by "borehole location and zone" and "collection date." The borehole numbers that are used in the Table 6.3.4.1-1 are the sequentially numbered DST boreholes (Figure 6.3-4).

Each row in Table 6.3.4.1-1 is a tabulation of relevant information recorded for a single sample. The information may include collection date, start and stop pumping times, total approximate volume, location by borehole number and zone (BH# - zone), field data, sample number (SMF ID), sample temperature (measured in the field at time of collection), comments and observations. The information represented derives from different personnel (with varying degrees of experience), different field-test equipment, and differences in working instrumentation and supplies. The table does not present sampling efforts in which no water was collected.

In Table 6.3.4.1-1, temperature entries represent those values measured in the field during sampling and do not represent the *in situ* borehole temperatures (which are recorded by the DST Data Collection System). Furthermore, the temperature-dependent field properties, (i.e., pH, TDS, and EC) were determined for the measured temperature reported. A multi-parameter field-test meter measures and automatically compensates for temperature, using the known thermal sensitivity of the glass electrode. The pumping start and stop times are included whenever the information was noted. The stated pumping times by themselves are not important, but, together with the estimated volume, they give an approximate sample flow rate. It has been observed that zones with accumulated water exhibited generally higher flow rates than ones that, for example, were produced by steam condensing in the sampling line (cf. Figure 6.3.4.1-1: Water vapor collection zones compared to liquid water collection zones). Finally, although alkalinity is a field measurement, it is incorporated with the table of analytical results that follow. Measured alkalinity was an important addition incorporated in the revised sampling procedure, but the

titration requires ~100 mL of sample. Consequently, for zones that produce low water volumes, alkalinity is not generally measured because of insufficient sample volumes.

Finally, in reviewing Table 6.3.4.1-1, an attempt to interpret the *lack* of water from different borehole zones, as suggested by gaps in the data, should be avoided. Field personnel generally allowed several minutes pumping time from each interval. However, the fact that no water was acquired does not necessarily indicate a dry zone; it may also reflect a failed packer seal (see Table 6.3.2.4-4 for list of failed packers), clogged sampling tube, or inadequate pump pressure.

Laboratory Analyses

Water samples collected from the hydrology boreholes are prioritized for several analytical tests including major ion chemistry and certain isotope analyses. Metal and anion concentrations measured by ICP/AES and IC, respectively, are reported in this section. The major ion data compiled for the samples analyzed are presented in Table 6.3.4.1-2; values for pH and HCO_3 (measured in the field) are included for convenience.

In Table 6.3.4.1-2, the SMF sample identifications are traceable to the field activities recorded in Table 6.3.4.1-1. (The exception is for baseline water acquired from pore water centrifuged from boreholes 182 (ESF-HD-PERM1) through 184 (ESF-HD-PERM3). Different conventions have been followed for assigning the unique SMF identification number used in both tables. Water samples are pumped during a sampling trip, and collected into different bottles designated for analyses. Entries in Table 6.3.4.1-2 reflect two conventions that have been followed: First, in a given sampling trip all sample bottles filled from one zone have been assigned a single SPC#; additional descriptions may record a date and time that the sample was acquired for distinguishing the order. Second, a unique SMF identifier is assigned to each of the bottles collected from a single zone, and the relevant date and time are recorded. It is worth noting that samples for metal and anion analyses identified with the same SPC# are not more closely related than samples identified with different SPC# (entries in Table 6.3.4.1-2 might appear to suggest otherwise). This is important because several samples collected one after another have exhibited increasingly dilute chemistries with continued pumping. Similar evidence is also observed in field data when multiple samples from a zone are tested and recorded.

Chemical analyses have been reported from water samples collected from each of the three borehole arrays (see Figure 6.3.4.1-1) and from boreholes located both above and below the Heated Drift. Most of the aqueous samples collected and analyzed would appear to fall into two main groups: (1) Water samples for which chemistries have been consistent with mineral/water interactions, particularly fracture lining minerals such as silica polymorphs and calcium carbonate. Intervals from which these waters derive are below and up to boiling (~96°C) temperatures. (2) Very dilute water samples obtained from intervals near or above boiling that were consistent with derivation from condensed moisture in the sampling line. From the beginning, these samples were not considered to add value to the aqueous geochemistry study and were thought unnecessary for collection. However, it has been up to individual field personnel working in concert with the aqueous sampling procedure, whether to collect and save the samples. Generally, all zones were pumped during the field collection trips, and no distinctions were made for samples derived from condensed water vapor.

Some trends may be observed among the first group of samples. First, measured pH values range from ~6.1 to 8.3. Concentrations for specific analytes were variable, but the trends were similar. In general, SO_4 and Cl were the dominant anions; Si is the principal metal, followed by Ca and Na (having similar concentrations to each other). Present, but in lower concentrations, were K, Mg, Sr, and NO_3. (These data were different from chemistry of the baseline pore water samples and were unrelated to construction water, which had a bromide tracer of ~20 ppm.) This class included a small number of water samples with very distinctive, concentrated water. Borehole 59-4 (11/98 and 01/99) in particular appeared to exhibit evaporatively concentrated water, and boreholes 59-2 (08/99) and 76-3 (10/99) had somewhat higher concentrations of the principal analytes observed.

Some samples could be recognized in the field and by laboratory analyses as deriving from condensed vapor and generally showing little or no water/rock interaction. The samples generally had lower pH values (approximately 4.0 – 6.0) and low TDS and EC. These samples were collected from hotter boreholes, at boiling temperatures and higher. The analytical results from the samples indicate the compositions are consistent with relatively pure water. (These analyses were generally of little interest; they were therefore not routinely submitted to the TDMS.) On the other hand, condensates from the highest temperature intervals (>140°C) exhibited lower pH values (<4.0) than might be expected from the effect of CO_2-bearing steam condensation alone. These samples also exhibit values of TDS and EC that are not negligible and have unusually high fluoride concentrations (5–66 mg/L). Further field-testing was carried out to investigate the cause of the unexpected fluoride concentration for these water samples. These investigations are discussed in detail in Section 6.3.4.5.

6.3.4.1.3 Measurement Uncertainty: Aqueous Chemistry

Field Sampling

The procedures developed for use in the field were intended to support the analytical data that ultimately would derive from the collected samples. Measures included obtaining field values for some unstable properties on calibrated instruments (e.g., pH, EC, TDS, and alkalinity) and appropriately treating and preserving specific samples (e.g., filtering, acidifying, and storing in appropriate bottles). Every effort was made to accomplish these goals during each sampling trip. However, occasionally, for reasons outside the field technician's control (e.g., a meter battery was out, replacement bottles and supplies had not arrived before the sampling trip.), the protocol could not be followed in its entirety. In those cases, samples were collected (the most important objective) and deviations were described in field notes. These types of issues were not considered to have significant impact on the actual data. Although attempts were made to minimize the time between collection and analysis, delays in getting samples delivered from the SMF were regularly encountered. When redrafting the protocol after the first year of heating, many of the issues were addressed.

The use of peristaltic pumping to acquire water from the hydrology boreholes is generally considered a suitable method for obtaining a representative, *in situ* DST water sample. However, certain conditions inherent to the thermal test environment may introduce uncertainty into some geochemical parameters. First, because of the relatively dry host rock, most water accumulations are insufficient to achieve and maintain water-filled lines during the sample collection process.

(In the field, this is evidenced by air bubbles in the sample tubing.) Potentially, water passing through the tubing may equilibrate with air in the line and thereby affect the concentrations of dissolved gases (CO_2 for example). Another issue previously mentioned is important when water is pumped to sequentially fill multiple bottles. Water samples clearly marked as to the order in which they become filled (see time notations in Tables 6.3.4.1-1 and corresponding analyses in Table 6.3.4.1-2) may exhibit increasingly dilute concentrations with time. This suggests that as the standing water in the borehole is depleted, the heated vapors present condense and dilute water in the line. This effectively becomes a problem because (for example) if the initial sample is designated and preserved for metals testing, the second sample is designated for anions, and the final sample is used for field measurements (pH, EC, and bicarbonate), then a charge balance calculation and a check of the electrical neutrality would indicate inconsistency. This condition taken to its extreme gives rise to samples derived solely from condensed vapor.

Laboratory Analyses

For both ICP/AES and IC, method detection limits (MDL) are determined for each analyte. The MDL represents the minimum concentration that can be identified, measured, and reported with 99% confidence that the analyte concentration is greater than zero. Generally, reportable concentrations (as established by laboratory chemists) are required to be greater than 3–5 times the MDL. For the concentrations reported in Table 6.3.4.1-2, values determined to be less than the "reportable limit" are indicated as nondetected (therefore, no distinction is made for analytes that are present at some very low level and those with no measurable concentration).

An additional uncertainty that may be introduced into analytical results occurs for samples that require some level of dilution. Samples may need to be diluted when concentrations exceed the measurement range for analytes of interest; or, if the total sample volume is very small, reagent grade water may be added to extend the sample. In such cases, the concentration measured, as well as the limits of detection, are multiplied by the dilution ratio. The result is that very small errors are exaggerated.

Holding times are another source of uncertainty (and might just as easily be considered in the field-sampling section as in the analytical results). Ideally, all sample analyses should be performed as soon after sample collection as possible to ensure that the analyses are representative of the *in situ* water chemistry. The EPA has established maximum hold times, which are almost universally recognized for drinking water analyses. As guidance for the DST borehole water samples, the EPA hold times, which typically ranged from 2 to 25 days, were suggested in the protocol (TIP-AC-03). The guidelines have generally been met, with the exception of the holding time recommendations for NO_3, NO_2, and PO_4. The measured concentrations for these less stable anions may be impacted as a result.

Quality control in the analytical laboratories is maintained using reagent blanks, laboratory control samples, and matrix spiked samples submitted in duplicate with sample batches (~10 samples or less). Analytical precision is assessed using the duplicate analyses of both the laboratory control and matrix spiked samples (typically prepared with analyte concentrations approximately midpoint of that expected for the samples). Acceptance limits for measured concentrations in the control samples are ± 10% of the known true value. The accuracy of the results is based upon the percent recoveries for each analyte in the control and matrix spiked

samples; the total recoveries of method analytes in the control sample and matrix spiked sample must be within 80–120% to be acceptable.

6.3.4.2 Gas Chemistry

Gas samples were periodically collected from the hydrology boreholes (see Figure 6.3-4) during the heating phase from December 3, 1997, through January 14, 2002. The purpose of these samples was to measure the concentration and carbon isotope ratio of CO_2 and the hydrogen and oxygen isotope ratios of water vapor. The concentration and isotopic composition of CO_2 in the Heated Drift and the Observation Drift were also measured during the test. In addition, to provide data on the background concentration and isotopic composition of CO_2 in the rock, two gas samples were collected in August 1997 from borehole 182 (one of the ambient testing boreholes drilled on the opposite side of the Connecting Drift across from the DST block). The CO_2 concentrations and isotope compositions for both the gas samples and the condensate samples collected in 16 sampling trips through the heating phase are in the TDMS under the following DTNs: LB980420123142.005 [111471], LB980715123142.003 [111472], LB981016123142.004 [113278], LB990630123142.003 [111476], LB000121123142.003 [146451], LB000718123142.003 [158342], LB0102CO2DST98.001 [159306], LB0108CO2DST05.001 [156888], LB0203CO2DSTEH.001 [158349], LB0206C14DSTEH.001 [159303].

6.3.4.2.1 Gas Sampling

Gas samples were pumped from the 12 hydrology boreholes (57-61, 74-78, and 185-186). Each hydrology borehole was separated into three or four intervals by strings of high-temperature, inflatable packers. High-temperature plastic tubes (that function as conduits for both air injection in permeability measurements and fluid sampling) led from each interval in the boreholes to the Observation Drift. For gas sampling, the tube leading to the interval to be sampled was isolated and connected to a diaphragm pump with a moisture trap. For higher-temperature intervals (greater than ~50°C), a 4°C gas chiller unit was placed before the pump to condense the water vapor from the gas before collection.

After purging the interval and sample tubing for 4–5 minutes, the gas samples were collected in 1-liter Tedlar® bags from the outlet of the diaphragm pump. The normal pumping speed for the pump is 60 L/min, however, airflow rates during sampling varied considerably, depending on factors such as the permeability of the interval, the temperature, and the air moisture content. In particular, when the temperature in an interval was near the boiling temperature or above, water vapor constituted the major component of the gas phase (>98%). Since most of the water vapor was being stripped from the gas before it entered the pump, the flow of noncondensable gas out of the pump was very low (to <1 L/min).

The water vapor condensed in the chiller trap was sampled for oxygen and hydrogen isotope measurements. The condensate in the water trap was comprised of all of the water vapor that condensed in the trap throughout the pumping period, including the time during which the sampling interval was being purged. Sampling times for the vapor condensates ranged from approximately 20 minutes for cooler intervals (up to about 80°C) to as little as 5 minutes for the higher-temperature intervals, resulting from the high vapor contents of the intervals near the

boiling point. After each sample was collected, the chiller trap was thoroughly dried, and the chiller unit was purged with dry tunnel air for at least 5 minutes before collection of the next sample was begun.

Air samples from the Observation Drift were collected using the diaphragm pump to fill a 3-liter Tedlar® bag. Samples of the Heated Drift were collected by attaching the pump to a 0.25 inch stainless steel tube leading to approximately the mid-point of the drift. The sample was taken after purging the tube for ~5 minutes. To determine the initial concentration and isotopic composition of CO_2 in the rock, two gas samples from borehole 182 were collected during August 1998. To take these samples, an inflatable packer was installed approximately 20 m into the borehole. The first sample was collected after the borehole was purged for approximately 5 minutes. The second sample was taken after the interval had been pumped for almost 24 hours.

6.3.4.2.2 Results: CO_2 Concentration

The CO_2 and isotopic compositions are given in Table 6.3.4.2-1. The CO_2 concentrations in the gas samples were measured using two different instruments. Initially, the laboratory measurements of the CO_2 concentrations for these samples were only intended to gain an estimate of the amount of CO_2 that should be produced during separation of the CO_2 from the samples intended for isotopic analyses. The CO_2 concentrations in the rock were supposed to be analyzed *in situ* with a Columbus Instruments Model 180C Gas Analyzer. However, because of problems with the sampling technique for the *in situ* measurements and the gas analyzer, the only CO_2 concentration data from the first 3 years of heating are the laboratory data for the samples listed in Table 6.3.4.2-1. Starting in January 2001, the CO_2 concentrations of the isotope samples were analyzed using the Columbus Instrument gas analyzer at the site calibrated with qualified standards. Both the laboratory and field analytical techniques are outlined below, and a comparison of the data for samples analyzed by both methods is presented.

For the first 3 years of the DST, the samples were transported back to a labratory for analysis. The CO_2 concentrations in the samples are measured using an infrared analyzer (Li-Cor®) in the Amundson Laboratory at the University of California, Berkeley. For analyses, 5 cc of gas was injected into the CO_2 analyzer and compared to a 500 ppm standard. At low concentrations ($\leq$2,000 ppm or 0.2% v/v), the precision of this technique was approximately ± 1% of the measured value. At higher concentrations, the analyses were out of the range of the standard used to calibrate the instrument, and the precision is not as good (see discussion below).

Beginning in January 2001, samples were also analyzed using the Columbus Instruments Model 180C Gas Analyzer at the ESF. For these analyses, approximately 250 cc of gas was fed into the instrument and analyzed after calibration with a qualified standard gas. For samples with lower concentrations ($\leq$1% v/v), the analyses were done using the low-range sensor calibrated with a 0.504% CO_2 standard. These analyses are accurate to approximately ±0.05%. Higher concentration samples (>1% v/v) were measured with the high-range sensor calibrated with a 4.995% CO_2 standard, with accuracy of ± 0.3%.

For comparison between the two instruments, Table 6.3.4.2-2 shows analyses using both techniques on January 2001 samples. At the lower end (less than 0.05%), the Li-Cor analyses tend to be a bit higher than the Columbus Instruments analyses. For this case, the Li-Cor data are

probably better, since the standard used for comparison on this instrument was a 0.05% standard. At higher concentrations, the Li-Cor data are consistently lower than Columbus Instruments data. For these samples, the Columbus Instruments data are more reliable, because they were measured using calibration gases in the same range of concentration. The data for samples with CO_2 concentrations greater than 0.2% are plotted on Figure 6.3.4.2-1. As would be expected, there is a strong linear correlation between the data measured with the Li-Cor and the data measured with the Columbus Instruments analyzer. In general, for samples with CO_2 concentrations greater than 0.2%, the Li-Cor measurements are low by approximately 16%.

6.3.4.2.3 Results: Isotopic Composition of CO_2

After measuring the CO_2 concentration in the gas samples, the CO_2 was cryogenically separated from the samples for isotopic analyses. The CO_2 isotopic compositions are also given in Table 6.3.4.2-1. For large enough yields of CO_2 (>30 μmoles), two aliquots of CO_2 were collected. The stable carbon ($\delta^{13}C$ value) and oxygen ($\delta^{18}O$ value) isotope ratios aliquot was analyzed according to the YMP Technical Implementing Procedure YMP-LBNL-TIP/TT-7.0, *Extraction and Analysis of the Stable Isotopic Compositions of CO_2 in Gas Samples for Isotopic Analyses*. If there were problems with the first analysis, then the split was used for a second stable isotope analysis. If there were no problems, then the splits were catalogued and stored for possible radiocarbon (^{14}C) analysis.

6.3.4.2.4 Results: Isotopic Analyses of Vapor Condensate Samples

The hydrogen and oxygen isotope compositions of the vapor-condensate samples were measured to gain an estimate of the isotopic composition of the pore water in the rock (Table 6.3.4.2-3). The hydrogen isotope ratios (δD values) were measured following YMP Technical Implementing Procedure YMP-LBNL-TIP/TT-9.0, *Hydrogen Isotope Analyses of Water*. The oxygen isotope ratios ($\delta^{18}O$ values) were measured following YMP Technical Implementing Procedure YMP-LBNL-TIP/TT-10.0, *Analysis of the Oxygen Isotopic Composition of Water Samples Using the Isoprep 18*. The isotopic composition of the pore water can be calculated from the isotopic composition of the vapor (Horita and Wesolowski 1994 [159108]), assuming that the pore water is in isotopic equilibrium with the vapor in the gas samples at the temperature of the rock. This information can provide valuable insights into the degree of dryout in the rock and the extent of vapor transport.

6.3.4.2.5 Measurement Uncertainty: Concentration and Isotopic Ratios

CO_2 Concentration

Besides the uncertainties associated with the measurements, there were a number of other factors that affected the measured CO_2 concentrations. These are listed below, together with an assessment of the potential impact on the measured CO_2 concentrations:

1. Removal of water vapor from the samples–Condensing the water vapor from the samples will lead to measurement of high CO_2 concentrations in the gas relative to the actual concentrations of pore gas in the rock. This is very significant in intervals at or above the

boiling point. However, the magnitude of this effect can be calculated by assuming that the gas in the rock was saturated with water vapor at the temperature of the rock.

2. Small leaks in the sampling apparatus–This could lead to some contamination of the samples with air from the Observation Drift. This was probably not significant except in samples where the gas flow rates were very low (e.g., those intervals with high vapor contents in the gas). In those instances, the measured concentrations could be diluted by as much as 50% relative to the actual concentrations.

3. Other tests using the hydrology boreholes–The hydrology boreholes were used for a variety of other measurements, including air-permeability tests and sampling of water. The impact of water sampling was probably minimal, but the air-permeability measurements (which consisted of injecting N_2 gas into the intervals) could significantly dilute the CO_2. As much as possible, gas sampling was scheduled just before any air-permeability tests were performed to minimize the effects of the air-permeability measurements on the CO_2 measurements.

4. Deflated packers–Over time, several packers in the hydrology boreholes developed leaks and deflated (see Table 6.3.2.4-4 for a list of deflated packers and the dates they became deflated). This was especially prevalent in the higher-temperature intervals. Even when deflated, the packers still formed a barrier between the intervals (their deflated diameter is only slightly less than the diameter of the borehole). However, it is likely that samples taken from intervals with deflated packers contained some gas from the intervals on the other side of the deflated packers. After April 2000 (when the problem became more prevalent), investigators began noting which samples were collected from intervals with deflated packers by including the adjacent intervals in the sample name. For instance, when the packer between interval 3 and 4 in borehole 57 was deflated and a sample was collected from interval 3, the sampling interval was noted as 57-3/4 indicating that the sample was taken from borehole 57, interval 3, but may contain input from interval 4. Several of the packers began leaking before April 2000 and were deflated (most notably in borehole 77), but this was not indicated by the sampling interval.

5. Refer to precision and accuracy discussion in Section 6.3.4.2.2.

Isotopic Composition of Pore Water Estimated from That of Condensate

There are a number of uncertainties that limit the reliability of these measurements for that purpose:

1. Temperature uncertainties–The temperature can vary significantly within an interval, making it difficult to determine the temperature to use for calculating the isotopic composition of the water.

2. Condensation in sample tubing–During sampling, the water vapor moves from the hot temperatures in the rock to the cooler temperatures in the Observation Drift. This can lead to significant condensation of water vapor in the tubing prior to the chiller unit. This effect is believed to have been minimal because of the large volume of air flushed through the tubing and the increase in the temperature of the tubing during sampling.

However, this still may account for some loss of vapor prior to the chiller unit. Since the δD and $\delta^{18}O$ values of the vapor are lower than those of the liquid, this will cause the isotopic composition of the water vapor that reaches the condensate trap to be lower than the composition of the water vapor in the rock.

3. Inefficient trapping by the chiller unit–The chiller unit used for this sampling was not capable of completely cooling high-temperature water vapor (>80°C) to 4°C. As a result, a fraction of the water vapor in the higher-temperature samples passed through the chiller unit. The water vapor that does not condense in the trap will have lower δD and $\delta^{18}O$ values than the water in the trap, which will lead to high values for the condensate. To minimize this effect, any water in the pump trap (generally <10 ml) after the chiller unit was mixed back into the water in the chiller trap. Altogether, the amount of water vapor loss is believed to be less than 5%. For this amount of loss, the net effect on the δD values will be <3‰; on the $\delta^{18}O$ values it will be <0.5‰. It should also be noted that this shift and any shift caused by #2 above would offset each other.

6.3.4.3 DST Mineralogic and Petrologic Analyses

Mineralogic characterization data provide quantitative information on mineral distribution and abundance in the pre-heating rock under ambient conditions. Mineralogic changes while the test is in process are also documented. These data support the coupled thermal-hydrologic-chemical modeling effort.

Expectedly, detectable mineralogic changes from the test were restricted to the natural fracture system and the surfaces of pre-heating boreholes that function as preferential fluid-flow paths. Mineralogic changes within the rock matrix were expected to be undetectably minute. These expectations were supported by qualitative examination of the SHT post-cooling overcores (see Section 6.2.4.2) and by quantitative X-ray diffraction (XRD) of pre- and post-testing crushed TSw2 samples from a hydrothermal column test (Lowry 2001 [157900], p. 29). These studies found no detectable mineralogic alteration of the rock matrix at the conclusion of the hydrothermal tests. Evidence of mineralogic alteration was limited to fractures and borehole surfaces of the SHT and to crushed-tuff fragment surfaces from the column test.

Mineralogic characterization of the natural rock-fracture surfaces was accomplished by study of pre-heating drill core from the DST block. A decision was made to employ stereoscopic examination of fracture surfaces, supplemented by scanning electron microscope (SEM) and XRD, for mineralogic analysis, so as to characterize as much fracture surface as possible. Compared to the exclusive use of microanalytical techniques, this strategy sacrifices achievable precision and accuracy, but maximizes the representativeness of the data because more fracture surface is examined. The end product is a quantitative mineralogic inventory of the fracture system that can be input to modeling. Mineral abundances of stellerite, manganese minerals, crystalline silica and feldspar, clay, and calcite on the fracture surfaces are in the TDMS under the Input-DTN LA9912SL831151.002 [146449].

Investigators learned from the SHT that mineralogic sampling while a test is in progress would be more valuable than collecting samples only after the test is finished. To realize this goal for the DST, a sidewall-sampling tool was designed and built to provide an in-progress sampling

capability. The tool operates within existing boreholes, targeting intervals of fractured rock that were identified from borehole video recordings. Two coring sessions have been conducted during the transition from heating to cooling phases of the test.

In November 2000, the sidewall coring tool was used to collect six sidewall cores from inclined boreholes ESF-HD-CHE-2 and ESF-HD-CHE-3 (boreholes 53 and 54 in Figure 6.3-7). In June 2001, eight samples were collected from the two previously sampled boreholes plus borehole ESF-HD-CHE-9 (borehole 59 in Figure 6.3-7). The sidewall cores from these boreholes have provided information on mineralogic changes in the boiling zone. The elemental abundances and chemical, textural, and mineralogic characteristics of core samples from borehole 54 are in the TDMS under the Input-DTN LA0201SL831225.001 [158426].

6.3.4.3.1 Results: Mineralogy of the Pre-Heating Natural Fracture System

Systematic data on natural, pre-heating fracture-mineral coverage were collected from the drill core of borehole ESF-HD-TEMP-2 (borehole 80 in Figure 6.3-3), a horizontal borehole that runs parallel to the Heated Drift. The drill core is 195.6 ft (59.62 m) long, but the first 25 ft (7.62 m) of the core are well outside the Heated Drift and were excluded from study. The number of fractures in the relevant length of core was too large for all to be included in the characterization. Therefore, a conceptual model of fracture attributes was developed to guide the selection of a subset of fractures for mineralogic analysis. The conceptual model is based on a major simplification of the criteria used to define subzones of the middle nonlithophysal zone (Buesch and Spengler 1998 [101433], pp. 18, 20).

The rock traversed by ESF-HD-TEMP-2 consists of intervals dominated by vapor-phase features and intervals where vapor-phase features are not prominent. As seen in the drill core, the dominant vapor-phase features are vapor-phase partings and vapor-phase stringers that dip eastward at low angles parallel to the rock foliation. Both partings and stringers are fractures lined with crystalline silica and feldspar fracture coatings, commonly called vapor-phase minerals. In intervals where vapor-phase partings and stringers and associated vapor-phase cavities (lithophysae) are common, the rock-matrix color is light brownish gray. Rock-matrix color in the intervals with only rare vapor-phase features is grayish orange pink to light brown.

Reconnaissance examination of the drill core suggested that the fracture coatings are different in the vapor-phase and nonvapor-phase intervals, an observation that was confirmed by detailed study. Based on this observation, detailed fracture-mineral studies were performed in two core sections of approximately equal length representing each type of interval. Mineral abundances on the fracture surfaces were determined for stellerite, manganese minerals, crystalline silica and feldspar (combined), clay (probably also including minor mordenite), and calcite. The results are presented in Table 6.3.4.3-1. For the minerals included in the inventory, differences in abundance of crystalline silica plus feldspar, and in calcite between the vapor-phase and nonvapor-phase intervals, were documented. The greater abundance of crystalline silica plus feldspar in the vapor-phase interval is expected because these minerals are among the defining characteristics of vapor-phase void spaces.

Additional natural minerals observed in very small quantities or in local concentrations by SEM of pre-heating core include mordenite, pyrite, and possible hematite. Other minerals are also present and will be characterized based on their importance for modeling the test results.

6.3.4.3.2 Results: Evidence of Mineral Deposition

Sidewall cores collected during the test revealed new mineral deposits on borehole surfaces and on the surfaces of fractures that intersect the boreholes. New mineral deposits are common on the borehole surfaces because the boreholes act as preferential pathways for fluid flow. Deposits are less common and quantities of new minerals less abundant on the natural fractures within the core samples.

Mineral deposition within the boiling zone is documented by samples from borehole ESF-HD-CHE-3 (borehole 54). The three products observed so far are tentatively identified as amorphous silica, gypsum, and calcite (DTN LA0201SL831225.001 [158426]). The tentative identifications of gypsum and calcite are based on identifications of these phases by XRD as products of the SHT (DTN LA0009SL831151.001 [153485]). The silica deposits exhibit considerable textural heterogeneity, perhaps because some were deposited when the collection site was in the condensation zone and others deposited when boiling-zone dryout conditions were reached.

Examples of possible condensation zone silica deposition above the Heated Drift have been identified. In one example, a fracture surface is completely coated by terrace-like silica deposits up to a few micrometers thick. In another example, several discoid silica deposits (up to about 20 micrometers across) rest on a surface of earlier-deposited discs cemented and largely obscured by silica particles about one or two micrometers across. In both examples, the deposits were built up during multiple episodes of silica deposition, perhaps during the passage of numerous pulses of silica-saturated water.

Very thin (less than 0.5 micrometer thick), curled silica sheets may be products of final dryout in the boiling zone. There is no textural evidence of successive buildup in the silica sheets. Also lying atop the earlier silica deposits or on pre-heating fracture surfaces are scattered deposits of prismatic gypsum and rounded mounds of calcite.

6.3.4.3.3 Results: Evidence of Mineral Dissolution

Studies of pre-heating core from the SHT showed that some of the natural fracture minerals have experienced dissolution caused by ancient or ongoing geochemical processes. This complicates the effort to document mineral dissolution resulting specifically from the DST. To provide documentation of natural alteration, samples of pre-heating drill core from approximately the same locations as sidewall samples were examined by SEM. Images of the typical morphologies of natural fracture-coating minerals and rock-fracture surfaces were recorded. The majority of such documentation was devoted to stellerite because it is the single most abundant fracture-coating mineral.

The natural stellerite fracture coatings in pre-heating samples did not show clear evidence of dissolution. Stellerite in the sidewall core samples also showed no evidence of dissolution. The lone exception occured on one fracture from the 66.5-ft (20.27-m) depth in borehole ESF-HD-CHE-3. In this location, a highly corroded stellerite crystal, several slightly to moderately

corroded stellerite crystals, and a moderately corroded silica crystal were adjacent to or within a lobate deposit of amorphous silica (DTN LA0201SL831225.001 [158426]). At the time of sample collection, this sample came from within the boiling zone. However, the sampled rock volume had previously been within the condensation zone before the boiling zone moved to its farthest position away from the heaters. It is possible that the observed mineral dissolution and, perhaps, deposition, occurred when the rock volume was in the condensation zone.

6.3.4.3.4 Measurement Uncertainty: Mineralogic and Petrologic Analyses

Estimates of fracture coverage by minerals are the principal numerical data derived from these studies. No formal analysis of the errors of estimation has been performed. It is likely that mineral coverages estimated to be 10% or less have relative errors of 50–100% (e.g., the estimated 2% coverage by a mineral could be in the 1–3% range). Estimated mineral coverages greater than 10% probably have estimated relative errors of 20% or less. Uncertainties of these magnitudes are considered adequate for current modeling purposes.

6.3.4.4 Strontium and Uranium in Water Samples

This section discusses strontium and uranium isotopic data obtained from a subset of water samples collected from the DST during the heating phase (Section 6.3.4.1). Measurements of strontium and uranium concentrations and isotopic compositions in water samples may provide information on mineral reactions and water flow paths occurring as the block is heated during the test. In addition, isotopic analyses can provide unequivocal evidence of interaction of test-produced water with the engineered materials introduced into the test block during construction. This section discusses data obtained from waters sampled from five boreholes: 60, 186, 59, 76, and 80. Data were acquired at the USGS in Denver under Technical Procedures NWM-USGS-GCP-03 and NWM-USGS-GCP-12. Uranium and strontium concentrations were determined by isotope dilution mass spectrometry. Uranium and strontium isotopic ratios were determined by thermal-ionization mass spectrometry. The data have been submitted to the TDMS under two Input-DTNs: GS011108312322.008 [159136] and GS011108312322.009 [159137].

6.3.4.4.1 Results: Strontium and Uranium in Water Samples

Figure 6.3.4.4-1 shows uranium concentrations and $^{234}U/^{238}U$ activity ratios in DST waters, as well as values obtained for pore water from upper lithophysal and middle nonlithophysal units of the Topopah Spring Tuff (Tptp) and values for water perched in the base of the Tptp. Uranium concentrations in DST samples vary from 0.003 to 0.65 µg/L and are typically lower than concentrations observed in pore water extracted by ultracentrifugation from the same units. The $^{234}U/^{238}U$ activity ratios (AR) in DST samples vary from 1.14 to 5.68, and unlike U concentrations, typically overlap the $^{234}U/^{238}U$ AR values observed in pore water. Samples from individual DST sites obtained at different times during the heating phase of the test have uranium concentrations that show a fairly systematic decrease with time (Figure 6.3.4.4-2). Zone 60-3 water shows a 10-fold decrease in U concentration between 6/4/98 and 5/25/99 to a value of 0.01 µg/L. Zone 59-3 water shows an even greater decrease from 0.015 to 0.0003 µg/L. Temporal changes in $^{234}U/^{238}U$ are not as systematic. Zone 60-3 water decreases significantly from values of 3.6 to 4.1 in 1998, to a value of 1.4 in May 1999. In contrast, the sample collected from borehole 80 in October 1999 has substantially higher $^{234}U/^{238}U$ AR than samples collected in

April of the same year. Samples from 59-2 collected between October 1999 and January 2001 show nearly constant $^{234}U/^{238}U$ AR.

The general trends of decreasing U concentration with time are consistent with increasing proportions of condensate mixed in with pore water that was mobilized during the DST heating phase. The wide range in U concentrations observed in Tptp pore waters makes it difficult to estimate the amount of condensate added; however, all but two samples with U concentrations >0.15 µg/L appear to contain at least some condensate. Samples with U concentrations <0.01 µg/L probably consist of more than 90% condensate. Even though these samples are particularly susceptible to contamination, most still have $^{234}U/^{238}U$ AR within the range of observed porewater. Only four DST samples have $^{234}U/^{238}U$ AR outside the expected range. Water from 60-3 collected on 5/25/99 has a low U concentration as well as a $^{234}U/^{238}U$ AR of 1.425. Contamination with rock or anthropogenic material is likely to add U with a $^{234}U/^{238}U$ AR near secular equilibrium value of 1.0. This same sample also shows evidence of contamination of strontium (see below). In addition, three samples collected at different distances in borehole 80 on April 20, 1999, have $^{234}U/^{238}U$ AR between 1.14 and 1.24. The $^{234}U/^{238}U$ AR for these three samples is substantially lower than the 2.70 value obtained from a sample from the same borehole collected 10/27/99. Although it is not clear if the latter sample is devoid of all contamination, the material causing the anomalously low $^{234}U/^{238}U$ values in the 4/20/99 sampling was largely eliminated from the later sample.

Similar to uranium, the strontium concentrations in the test waters approach the values estimated for pore water and decrease with time. Borehole 60-3 water reached a strontium concentration of 0.2 µg/L in June 1999, about 1,000 times less strontium than this zone produced initially. Figure 6.3.4.4-3 shows the variation of strontium isotopic compositions in the test waters compared to various reservoirs of strontium in the DST block. The orange and red bands show the strontium isotopic compositions of the Topopah Spring Tuff (middle nonlithophysal and upper lithophysal zones) today and at the time of their deposition, respectively. The green band is the range of $^{87}Sr/^{86}Sr$ in pore water; these data are from borehole USW SD-9, which is the closest vertical borehole to the DST block. Grout introduced into the DST block during emplacement of borehole instrumentation has also been measured and is shown by the black line at an $^{87}Sr/^{86}Sr$ value of 0.7086. The grout contains over 800 ppm strontium, providing a potentially important added source.

Most of the water obtained during the DST to date has $^{87}Sr/^{86}Sr$ values within the range of pore water. A very dilute sample obtained from borehole 60-3 falls outside the range of pore water. The most significant deviations from pore water are exhibited by water from borehole 80. These samples, obtained from this neutron borehole, apparently have interacted with the grout used to emplace the liner in this borehole. This statement is conclusive evidence of contamination based on the known isotopic compositions of the grout and the natural system; the chemistry of these samples should be used only as an example of water that has interacted with the engineered materials. It is notable that the chemistry of these waters does not show additional evidence of interaction with grout. Further studies of the sampling materials may be warranted for verification that the contamination occurred *in situ* rather than during sampling.

Borehole 59, zone 4 was sampled in November 1998 and showed a very unusual chemistry, as reported in Table 6.3.4.1-2 (approximately 1,200 mg/L chloride) that was initially interpreted as

probable contamination. This sample was analyzed for strontium isotopic composition, and the result plots in the field of pore water (Figure 6.3.4.4-3). Similarly, the $^{234}U/^{238}U$ AR for this sample is in the range of observed porewaters and higher than other samples from borehole 59 (Figure 6.3.4.4-1) unlike samples with low $^{234}U/^{238}U$ suspected of contamination. Based on these results, the 59-4 sample is not likely contaminated with grout or other anthropogenic materials. Rather, this sample may represent pore water that has become isolated and evaporated either through natural processes or enhanced by the heat during the test. This is a potentially important sample because it exhibits high sulfate and fluoride and thus could be more corrosive to engineered materials than more typical pore water or condensate-pore water mixtures.

6.3.4.4.2 Measurement Uncertainty: Strontium and Uranium in Water Samples

The accuracy of the isotopic dilution concentration measurements is maintained within the analytical precision by the analysis of known concentration standards; the precision of strontium concentrations is about 1% and the precision of uranium concentrations varies from less than 1% to about 10%, depending on the amount of uranium present. The accuracy of the isotopic measurements is maintained by the frequent analysis of standards with known or assumed isotopic compositions. For uranium, this standard is a material in which the isotopes are in secular equilibrium. For strontium, a standard with a ratio equivalent to modern seawater is analyzed; all $^{87}Sr/^{86}Sr$ ratios are relative to a value of 0.70920 for modern seawater. Absolute precisions at 95% confidence are 0.00005 for $^{87}Sr/^{86}Sr$ and from 0.02 to 0.3 for $^{234}U/^{238}U$.

6.3.4.5 Investigation of Waters with High Fluoride Concentrations

Certain water samples acquired from superheated (>140°C) zones within DST hydrological boreholes (see Table 6.3.4.1-2) show relatively high fluoride concentrations (9–74 ppm) and low pH (3.1–3.5) values relative to background values (sub-ppm fluoride and pH greater than 4.5). In these high-temperature regions of the rock, water is present as superheated vapor only—liquid water is formed during the sampling process by cooling. The compositions of these condensed steam samples show near-stoichiometric balance of hydrogen and fluoride ions, suggesting dissolution of hydrogen fluoride (HF) gas into the aqueous phase. Since HF can be corrosive, it could have deleterious effects on the performance of the waste package if it originated from the rock. If the source of the HF is from introduced materials, the source can be eliminated through use of alternative materials. Field and multiple laboratory tests were initiated to identify the source of the HF gas in the DST.

Several water samples were collected in the DST to determine whether the HF results from the degradation of materials originally introduced to facilitate measurements, or whether the HF could have been derived from fluoride-bearing minerals in the host rock. The materials introduced in this test include fluoroelastomer (abbreviated “FKM”) synthetic rubber manufactured by Seaquest Rubber company (similar in composition to Viton™ manufactured by DuPont) and Teflon™. The fluoroelastomer was used in making pneumatic packers to isolate test zones, while the Teflon™ tubing was used to draw water and steam from the test zones.

Analyses of water samples taken both before and after the introduction of materials to a previously clean borehole in the DST demonstrate clearly that the source of the fluoride is the introduced materials. Data from the field tests were submitted to the TDMS with the following

Input-DTNs: SN0203F3903102.001 [159133] and LL020405123142.019 [159307]. More detailed discussion of this investigation has been documented in a white paper (YMP 2002 [158176]).

6.3.4.5.1 Background

One important objective of the DST was to acquire and study samples of water from the hydrology boreholes over time. Condensed steam samples, however, were never the focus of chemical analysis because they do not represent water within the rock. Rather, such samples condensed in the sampling tube as relatively dilute water, with some dissolved CO_2 yielding pH in the 4-6 range. In general, the condensed steam samples contain very low dissolved solids, indicating minimal reaction of water with minerals present in the rock. A fringe of mobilized pore water, which provided almost all of the high-temperature water samples in the early stages of the DST, was driven ahead of the expanding dry-out zone around the Heated Drift and the wing heaters. Once the dry-out zone passed the boreholes, however, the only moisture present in the above-boiling rock regions was water vapor (steam) passing through the fracture system. The condensed vapor samples, drawn from sampling intervals of the hydrology boreholes that reached or exceeded temperatures about 40° above the boiling temperature, showed lower pH and higher dissolved solids. The chemical compositions of these condensed steam samples are not characteristic of the slightly carbonated water condensed from steam in some of the lower-temperature (but still above boiling) boreholes.

As shown in Figure 6.3.4.5-1, the hottest hydrologic boreholes (60, 77, and 186) in the DST were drilled from the Observation Drift to a length of about 40 m to pass under the Heated Drift. These boreholes slope downward, passing within a meter of the wing-heater boreholes, finally terminating below and beyond the Heated Drift. The hydrologic boreholes required the use of pneumatic packers, to isolate test zones and multiple Teflon™ tubes that passed through the packers, allowing access to accumulated water or steam. The packers in these boreholes were made of fluoroelastomer synthetic rubber manufactured by the Seaquest Rubber Company from unvulcanized raw materials provided by Burton Rubber Processing, Inc. Fluoroelastomer was chosen as the most suitable packer material because it was reported by the manufacturer to withstand temperatures up to 200°C.

6.3.4.5.2 Field Testing Strategy

Recognizing that water samples acquired from superheated (>140°C) zones within hydrological boreholes of the DST show relatively high fluoride concentrations (9–74 ppm) and low pH (3.1–3.5) values, the Thermal Test Team devised an appropriate strategy to resolve the question as to the origin of the HF contamination. The planned field investigations would test two competing hypotheses: (1) that the source of the fluoride in the samples is introduced materials, or (2) that the source is the host rock itself. The proposed plan was to remove the potential source of contamination (the packer material) from boreholes 60 and 77 and introduce the suspected contaminants into relatively clean test zones. Sampling of the boreholes would have to be done before the introduction of the materials to characterize the uncontaminated system, and then after the materials were introduced to see if a high fluoride signal was generated.

The best candidate boreholes for introducing the potential source of contamination (packer materials) were considered to be in arrays adjacent to the hydrology borehole arrays and to be intersecting essentially the same temperature field. For this reason, boreholes 72 and 55, both from the FLUTe™-instrumented (a.k.a. SEAMIST) chemical arrays, were selected. These boreholes were nearly parallel to 77 and 60, respectively, and they were in close proximity to wing heaters (Figure 6.3.4.5-1). Details of the FLUTe™ system are provided in Section 6.3.4.1. Except for a few chips of silicon rubber liner, the FLUTe™ system from borehole 72 was extracted in spring of 2001 to allow for sidewall drilling operations. What materials remained were pushed to the bottom of the borehole by the sidewall drill bit.

6.3.4.5.3 Experimental Methods

The HF field experiment included characterizing boreholes 55 and 72 to locate accessible sample collection zones with temperatures above 140°C, while allowing enough vapor to be drawn and condensed as sufficient water samples for analyses. On November 8, 2001, borehole 72 was characterized using a thermocouple and Tygon™ sampling tube clamped to a 6 ft length of titanium pipe to form a probe. Beginning from the collar, temperatures were recorded at 6 ft intervals. The temperature along borehole 72 were found to be comparable with those measured in borehole 60. Borehole 72 also produced abundant water vapor within the elevated temperature zone. This characterization confirmed that borehole 72 was a good candidate for further experimentation. The hottest zone, with temperatures above 170°C, was found to be in the 78–84 ft depth interval. As the probe was positioned there, a 50 mL sample of condensed steam was collected through the Tygon™ tubing in about 25 minutes. Previously, on June 28, 2001, a similar method had been used to collect a sample from borehole 72, although no direct temperature measurements had been taken within the borehole. Analytical results of condensed steam samples collected from this borehole are discussed below and included in Table 6.3.4.5-1.

Characterization of borehole 55 encountered several setbacks, including blockage of the temperature probe from torn FLUTe™ liner, temperatures along the boreholes not exceeding the desired 140°C, and difficulty in obtaining water condensate from the borehole. For these reasons, the decision was made to use borehole 55 only as a control interval. All sampling of borehole 55 was in parallel with that conducted in borehole 72, and all samples were submitted for laboratory analyses.

After the initial field survey to establish background values of F-content, the next activity was preparation of the apparatus used to introduce fluoroelastomer and Teflon™-bearing samples into borehole 72. An apparatus was developed that employed a rigid push rod to position a Teflon™ sampling tube and various fluoroelastomer samples at a predetermined depth in the highest temperature zone. Threaded rods, couplings, and 16-gage wire milled from C276 alloy were procured. Alloy C276 was chosen because it is less reactive to corrosive environments relative to other metals and would be much less likely to attenuate any HF signal that developed, as might occur with the use of conventional stainless steel or titanium. The various fluoroelastomer samples are: (1) aged fluoroelastomer sections cut from a borehole 60 packer, following the removal of the entire packer assembly from borehole 60; (2) sections from an unused SHT packer; and (3) test batch sections of fluoroelastomer (obtained prior to the full production run for the DST). These were wired to a 12 ft long section of C276 alloy push rod.

Before the fluoroelastomer sample string was installed, a baseline water sample was acquired from borehole 72 by means of a Teflon™ sampling tube. Then field measurements were performed on the water sample to quantify pH, temperature, and electrical conductivity (EC). The push rods and sampling tube were then removed in preparation for installation of the fluoroelastomer sample string. The sampling string was installed in borehole 72 along with six additional 12 ft C276 alloy rods. The sampling port was located at a depth of 23.8 m. Two mechanical borehole plugs were installed at the borehole collar to reduce the exchange of air with the DST Observation Drift.

For sampling in borehole 55, a 0.375-inch O.D. C276 alloy steel tube was employed. The end of the tube, or sampling port, was located at a depth of 71.75 ft. A pump was connected to steel alloy tubing at the collar that drew only 20 mL of water in about 2 hours. Field measurements of pH, temperature, and conductivity were also obtained. Three days following the first sampling, on November 29, 2001, samples were again collected from both boreholes. It only took about 10 minutes to flush the line in borehole 72 with 100 mL of condensed water. This borehole continued to produce abundant sample. Field measurements were performed on the 100 mL sample, and the equipment was moved to borehole 55. In this borehole, once again, the rate of water collection was extremely slow. Only a 13 mL sample was collected after 3 hours of pumping. More samples were collected on December 5, 2001, with a similar outcome. Borehole 72 produced 500 mL of water in less than an hour, while borehole 55 remained comparatively dry. Final samples were collected on January 9, 2002, before the removal of the sampling string from borehole 72.

6.3.4.5.4 Results: Fluoride Contents of "Condensates"

The components of focus from this field study are those parameters collected in the field that are indicative of high fluoride concentrations (e.g., pH, and electrical conductivity/total dissolved solids) and the fluoride concentration measured by ion chromatography (IC) in the laboratory. Field parameters were obtained for each sample with sufficient sample volume (>10 mL). Values reported for pH, and electrical conductivity (EC)/total dissolved solids (TDS) are those measured at the temperature of sample collection (ranging from 20 to 50°C) and documented in sample collection summaries.

The summary of field (pH, TDS, EC) and laboratory analyses (fluoride) for borehole 72 and borehole 55 (control samples) are compiled in Table 6.3.4.5-1. Additional data for borehole 72 (collection dates: 06/28/01 and 11/8/01) and borehole 55 (collection dates: 11/15/01 and 11/21/01) are provided from sampling activities that predate the HF field study.

6.3.4.5.5 Conclusion

Analytical results from the first attempt at characterization of borehole 55 on 11/15/01 and again on 11/21/01 strongly suggest that the test zone was contaminated with the FLUTe™ still remaining in the borehole. The water collected from borehole 55 at this time shows elevated concentrations of chloride and sulfate, suggesting contamination by small amounts of various salts left in the FLUTe™. Similar high chloride and sulfate values have not been observed in any of the other HF-contaminated boreholes. The small sample volumes collected during both pre-test events made it difficult to thoroughly flush the Tygon™ tubing, undoubtedly contributing

to the chances of field contamination and measurement uncertainty. The baseline sample recorded on 11/26/02 was relatively clean, so borehole 55 offered a viable test zone from which to collect control samples.

The evidence that the introduced materials are responsible for the HF in the DST includes the following observations. Water samples collected from borehole 72 at high temperatures (~170°C) prior to introduction of any fluoroelastomer or Teflon™ show pH values in the range 4.8 to 5.5 and fluoride concentrations well below 1 ppm over a period of six months. These characteristics are typical of condensing DST steam that contains only some dissolved carbon dioxide generated by water-mineral-gas reactions in the rock. In addition, the low fluoride content of these fluids is similar to background values found for lower-temperature samples collected throughout the duration of the DST. After the introduction of the fluoroelastomer packer materials and Teflon™ sampling tube in borehole 72 on November 26, 2001, however, the pH of the water samples dropped to 3.8 and fluoride rose to 2.4 ppm within three days. Nine days after introduction of the fluoroelastomer and Teflon™ in BH72, fluoride concentrations reached as high as 7.6 ppm for a sample with a pH of 3.4.

Laboratory tests were implemented to provide confirmation of the results of the field test and, if possible, to determine which of the introduced materials was responsible for the HF in the DST. Results from this investigation will be presented in a revision to this report.

In summary, the results of the field test confirm the hypothesis that the source of the elevated fluoride and low pH in high-temperature (>140°C) samples from the DST is the introduced test materials.

6.3.5 DST Miscellaneous Measurements

This section discusses additional DST measurements not covered in the prior four DST sections. Specifically, fracture mapping and borehole video logging are discussed. Detailed discussion of these measurements is documented in the report entitled *Ambient Characterization of the Drift Scale Test Block* (CRWMS M&O 1997 [101539]). Input-DTNs and Output-DTNs are listed in Tables 4-3 and 6.3-1, respectively.

6.3.5.1 Fracture Mapping

The objective of geologic mapping in the DST block was to determine the vertical and horizontal variability of fracture networks and lithophysal zones and to identify values for parameters to be used for rock-mass classification.

Mapping was done essentially to the same standards used in the ESF Main Drift, using technical procedure NWM-USGS-G-32 (see DTN: GS970608314224.006 [158429]). From these procedures, the USGS/USBR used full-periphery mapping techniques and detailed line surveys (DLSs) to characterize the rock and fractures in the DST area.

6.3.5.1.1 Results: Fracture Mapping

Full-periphery geotechnical maps for the DST Connecting Drift are presented in Figures 7-1 through 7-3, and Figures 7-4 through 7-6 for the DST Heated Drift in the *Ambient*

Characterization of the Drift Scale Test Block Report (CRWMS M&O 1997 [101539]). The lithology of the unit consists of densely welded, devitrified tuff of rhyolitic composition, containing vapor-phase minerals and about 1% phenochrysts, chiefly feldspar and biotite. Matrix colors are a variable mixture of reddish purple (5RP5/2) or pale red (5R4/2) and light brown (5YR5/6) with wisps of very light gray (N8). Pumice (less than 5%) is mostly less than 20 mm, spherulitic, and grayish brown (5YR3/2) to very light gray (N8). Volcanic lithics (1–2%) are light gray (N8), less than 10 mm in size, and locally have very light gray (N8) rims. Lithophysae are rare (less than 1%) and range in size up to 80 mm, with vapor-phase minerals and very light gray (N8) rims and spots. Short (10–20 cm), discontinuous, subhorizontal vapor phase partings are present throughout the unit, while the more developed subhorizontal partings from bedding-plane features are on the order of meters apart.

6.3.5.1.2 Measurement Uncertainty: Fracture Mapping

Uncertainty associated with DST fracture mapping is similar to that discussed in Section 6.1.4.1.2.

6.3.5.2 Borehole Video Logging

The objective of borehole video logs was to provide descriptive visual information from boreholes in the DST block and to supplement other available characterization data. Borehole video logs were also used to help select appropriate depths for packer settings for air-permeability testing.

6.3.5.2.1 Results: Borehole Video Logging

Borehole video logs provide much visual information regarding fractures, including aperture size, fracture frequency, and fracture orientation. Videos can be acquired by referring to the Input-DTN cited in Table 4-3 (DTN: LARO831422AQ97.002 [158431]).

6.3.5.2.2 Measurement Uncertainty: Borehole Video Logging

These observations are inherently subjective, which results in unquantifiable uncertainty. Also, determination of orientation and location of the video monitor may be flawed.

6.3.5.3 Waste Package Materials

Coupons of candidate waste package materials (at the time the DST heating phase was started) were placed at strategic locations such as hot/dry locations near heaters and warm/wet regions in the condensation zones in hydrological boreholes and in the heated drift. These coupons consisted of one of three materials (Alloy-22, carbon steel, and Monel-400). The coupons were tested before the heating phase and will be tested after the cooling phase to evaluate their corrosion potential. Also included in the hydrological boreholes were concrete samples which are not considered waste package materials. Slight corrosion is anticipated in these waste package materials during the DST.

Discussions of these non-qualified corrosion measurements of waste package materials are included in this report for completeness.

6.3.5.4 Microbiological Investigations

The potential significance of the microbial activity on the chemical evolution of a radioactive waste repository, waste package lifetime, and radionuclide transport are not understood well enough to determine their significance. The purpose of including the microbial experiments in the DST is to obtain complex process level information about survival and migration of microbes in an environment analogous to a radioactive waste repository. It is considered advantageous to evaluate microbiological response in terms of thermal, hydrological, mechanical and chemical behavior. With the goal of understanding the significance of microbial survival and migration in this geological repository environment, the following tests were designed:

1. Survival/migration test: borehole emplacement of labeled microbes
2. Survival/migration test: heated drift emplacement of labeled microbes
3. Survival/material-microbe-rock interaction test: carbon steel-microbe-rock and carbon steel-microbe-concrete
4. Sterile collection and freezing of pre-heating rock sample.

All tests were conducted with microbes that are indistinguishable from the microbes that are present in the rock surrounding the DST block. A non-altering label was added to the microbes that acts as a tracking device to monitor their progress. The microbes are not pathogenic and have been collected and isolated for the Yucca Mountain Project during the excavation of the ESF.

The total number of microbes that have been installed are far less than the number of microbes that have been unintentionally introduced during the construction of the DST. Locations of installation points include the heated drift and select borehole locations.

For completeness, discussions of these non-qualified measurements of microbial behavior are included in this report.

INTENTIONALLY LEFT BLANK

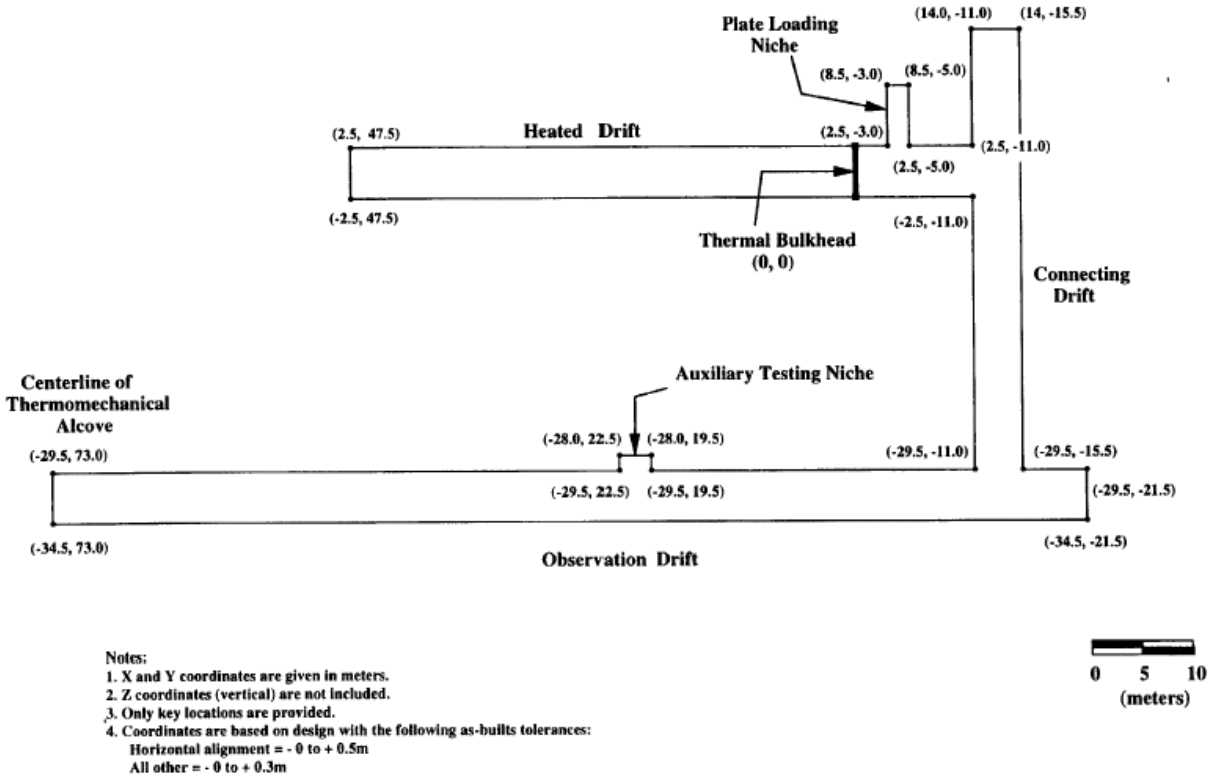

Figure 6.3-1. DST As-Built Plan View with Two-Dimensional Coordinates of Key Locations

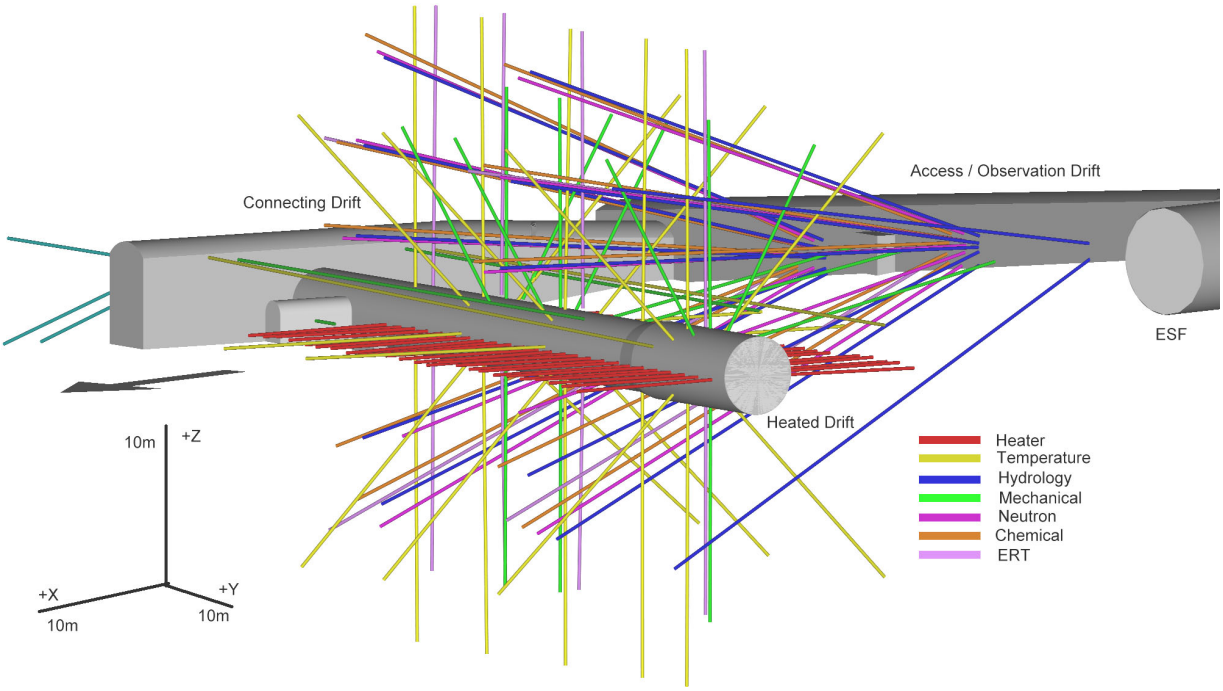

Figure 6.3-2. Perspective View Showing Drifts and Boreholes of the DST

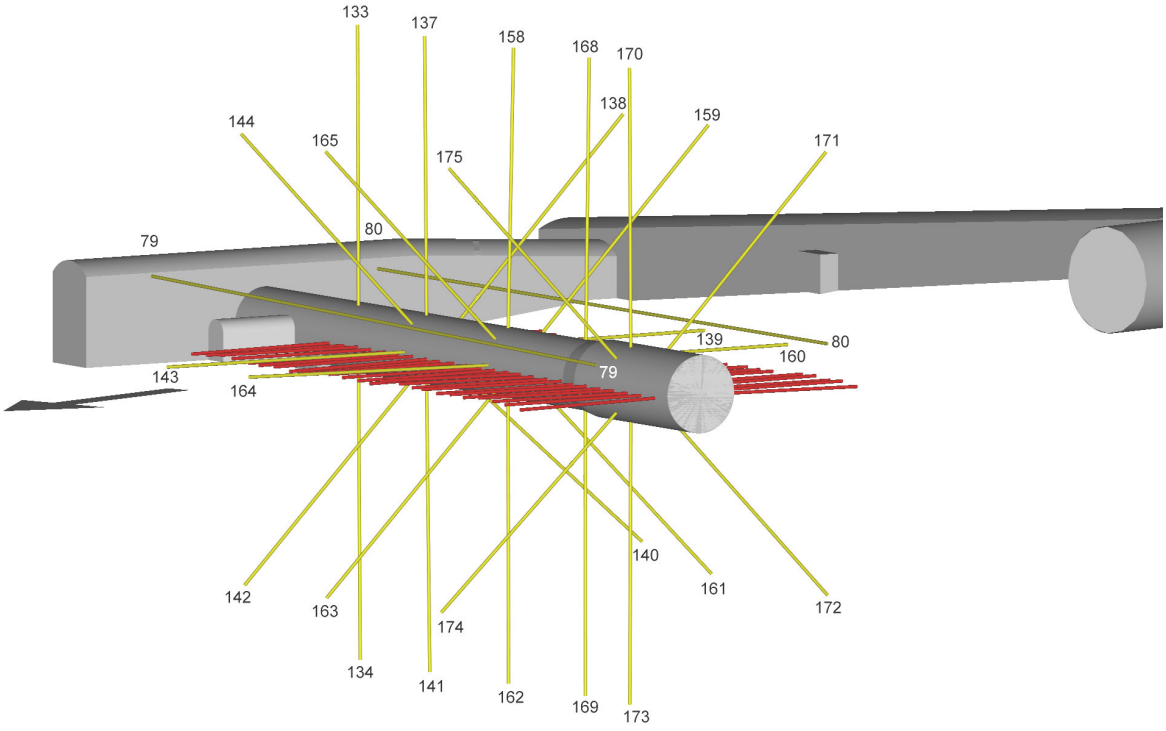

Figure 6.3-3. Perspective View Showing Temperature (RTD) Boreholes of the DST

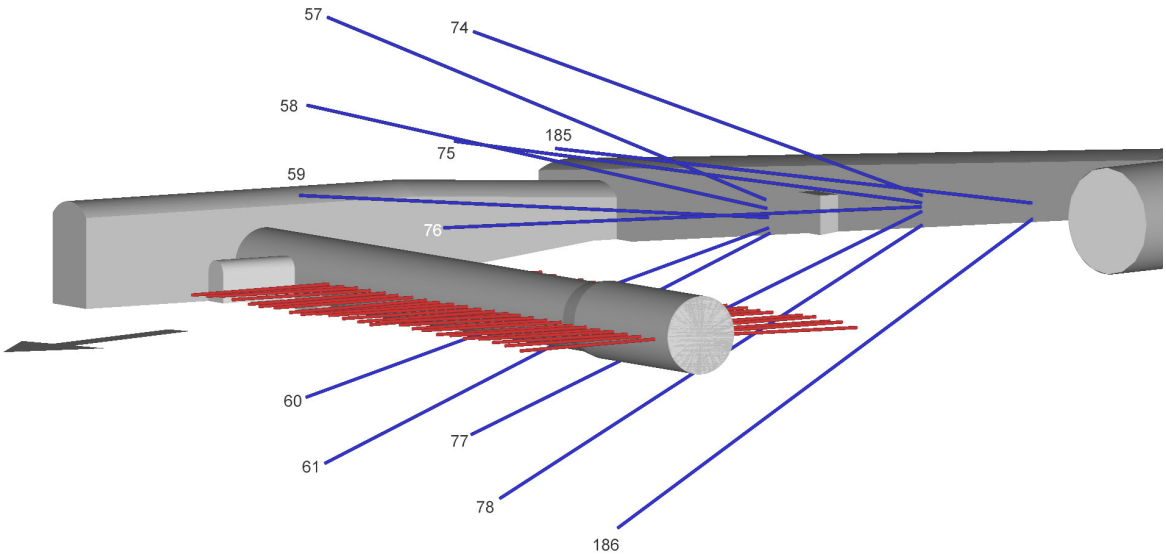

Figure 6.3-4. Perspective View Showing Hydrology Boreholes of the DST

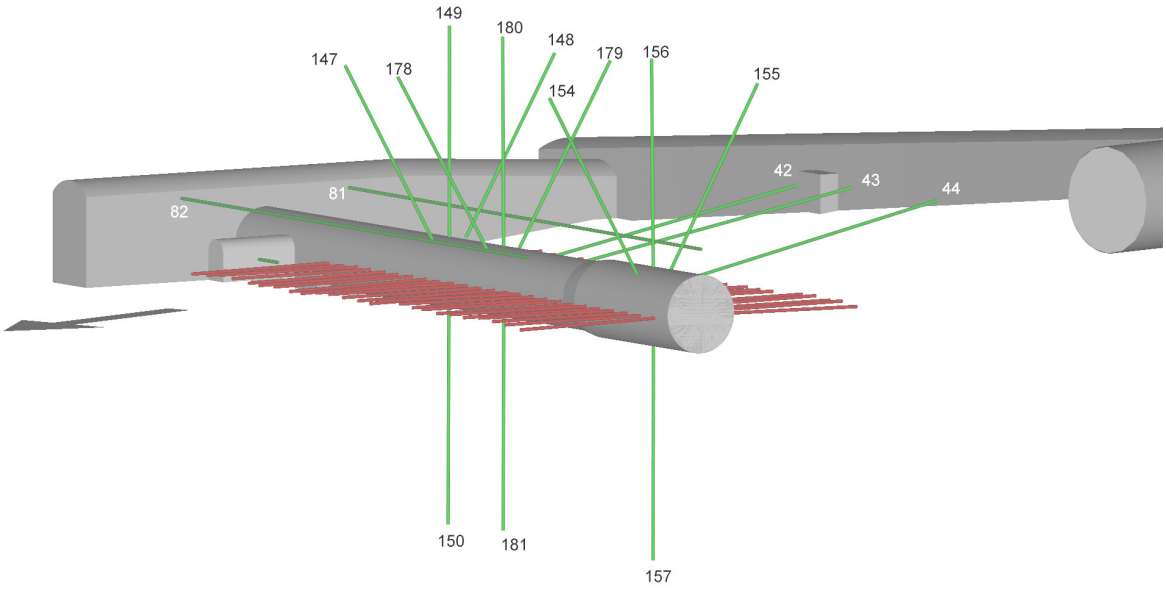

Figure 6.3-5. Perspective View Showing Mechanical (MPBX) Boreholes of the DST

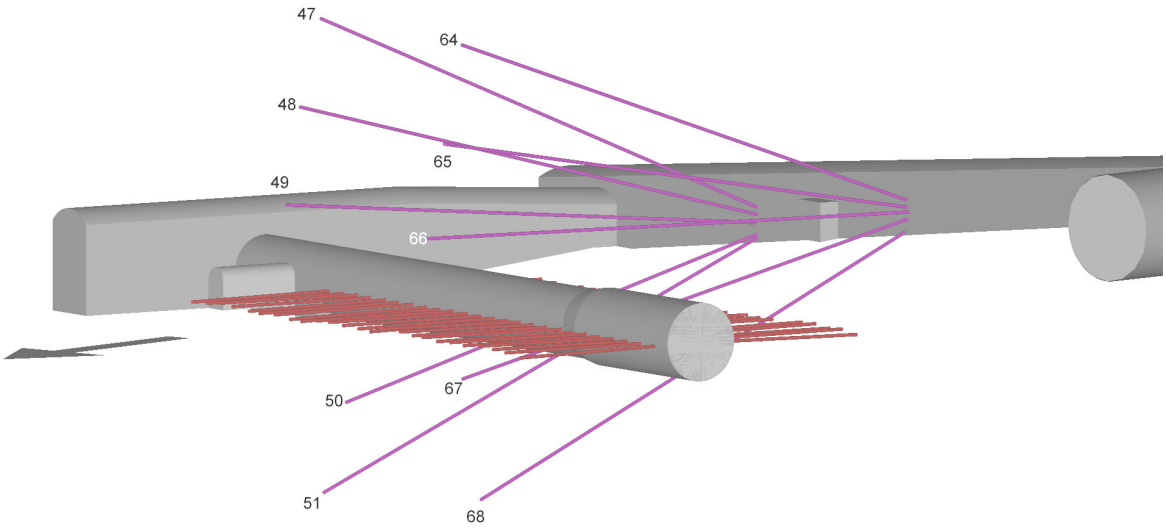

Figure 6.3-6. Perspective View Showing Neutron GPR Boreholes of the DST

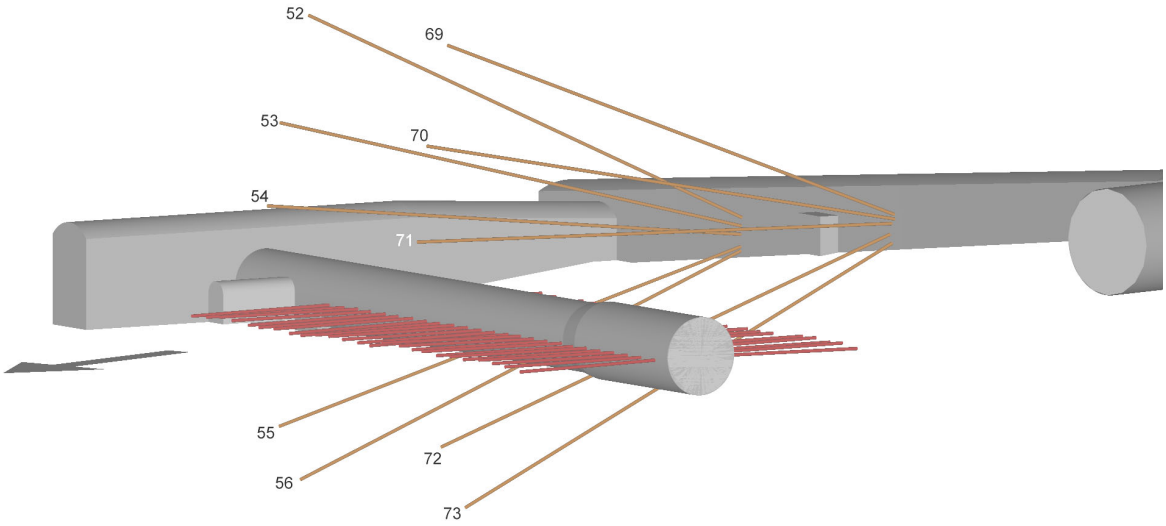

Figure 6.3-7. Perspective View Showing Chemical (SEAMIST) Boreholes of the DST

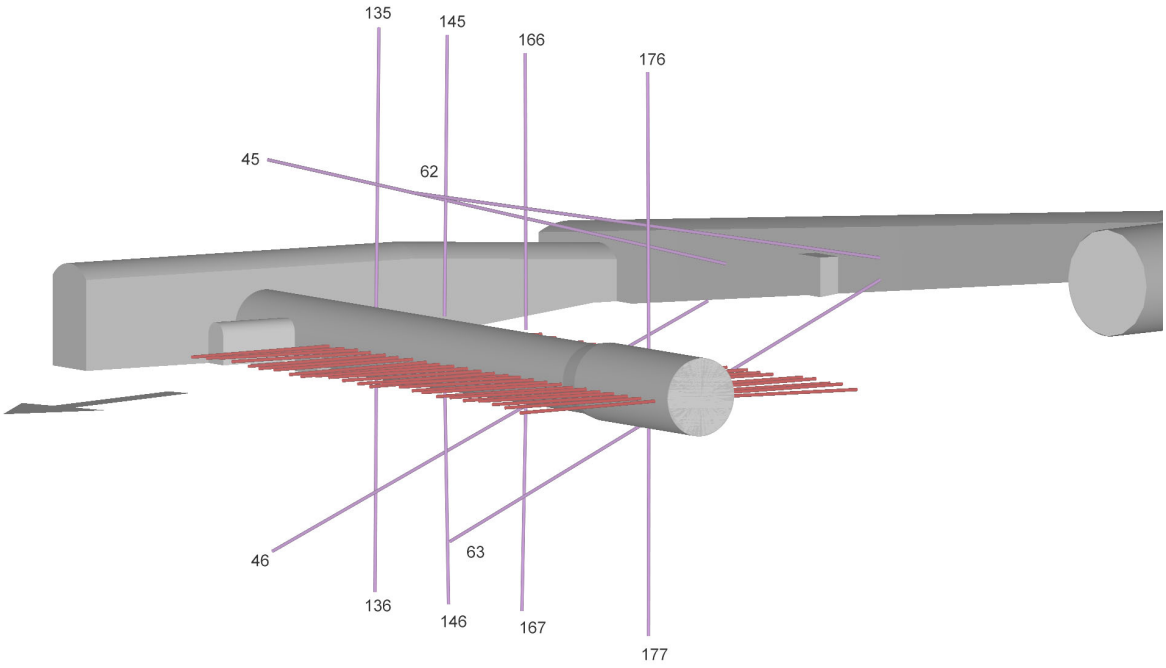

Figure 6.3-8. Perspective View Showing ERT Boreholes of the DST

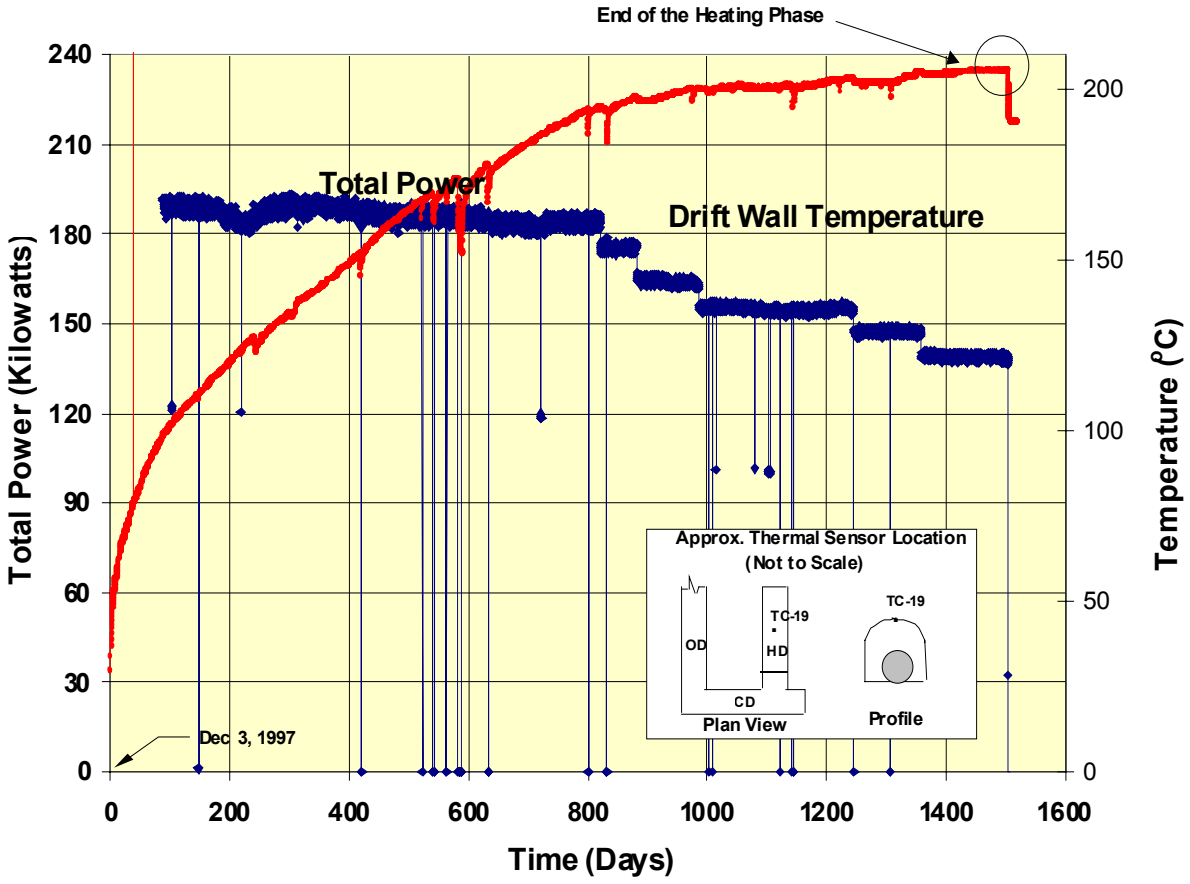

Figure 6.3.1.1-1. Total Power and Representative Drift Wall Temperature (TC-19) during the DST Heating Phase

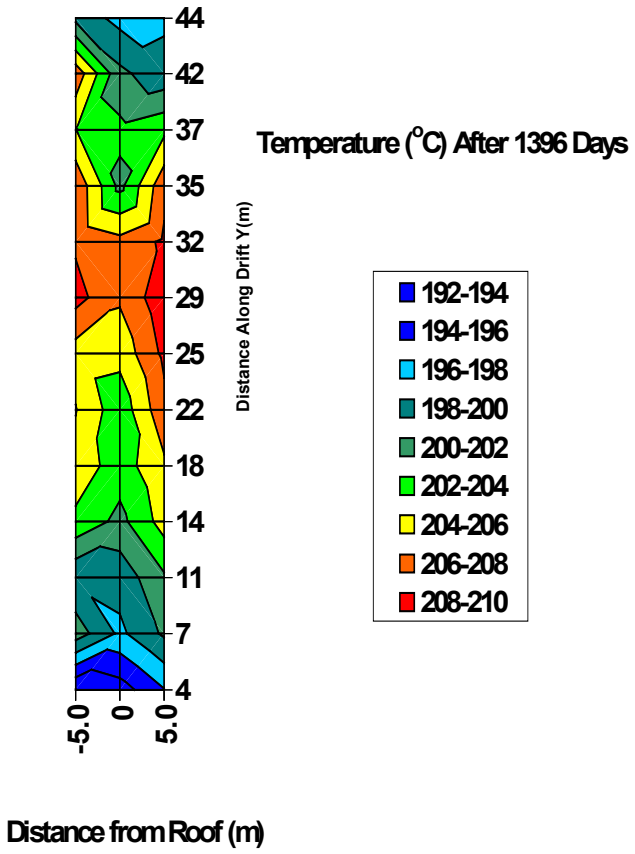

Figure 6.3.1.2-1. Measured Temperature Distribution along the Periphery of the DST Heated Drift Near End of DST Heating Phase

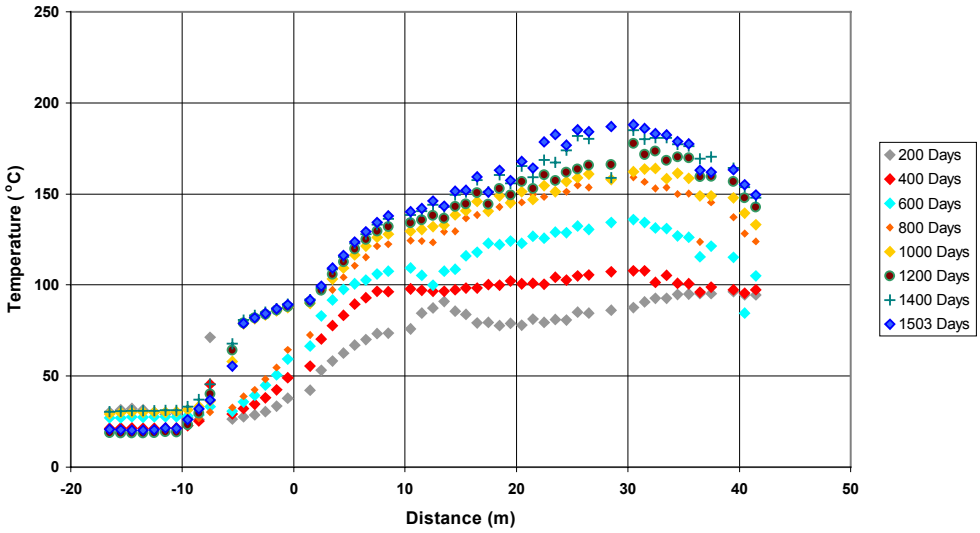

Figure 6.3.1.2-2. Temperature Profile along DST Borehole 79 at Select Times

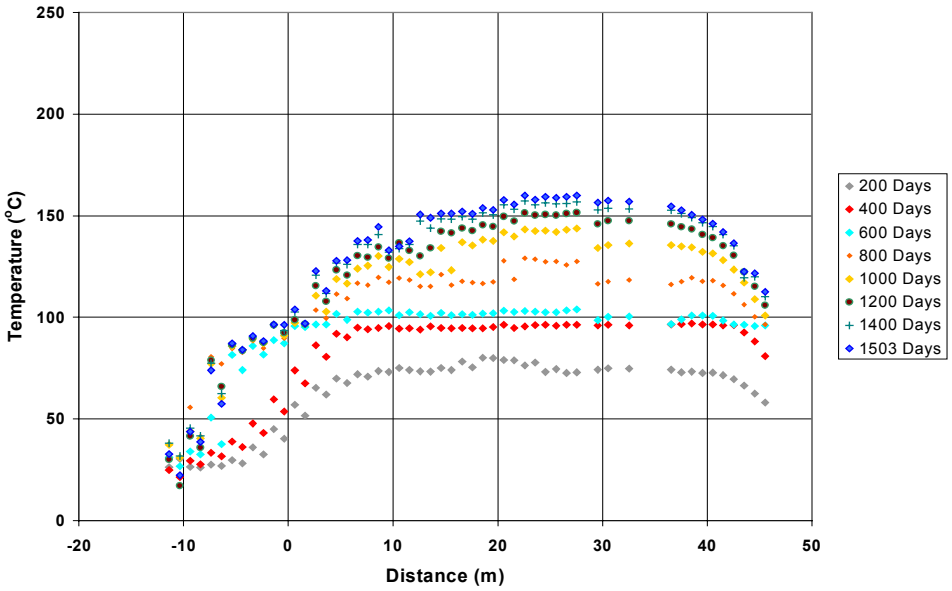

Figure 6.3.1.2-3. Temperature Profile along DST Borehole 80 at Select Times

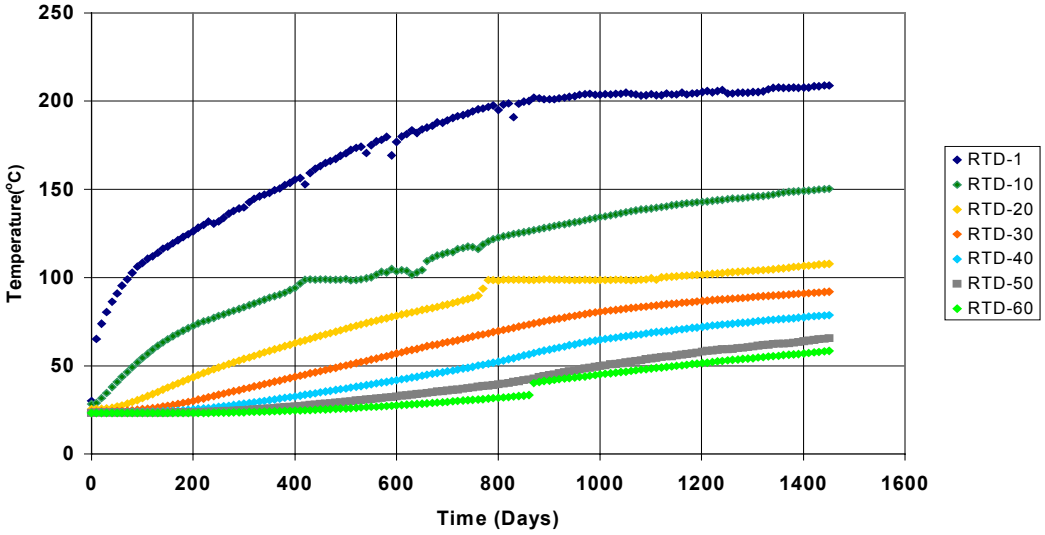

Figure 6.3.1.2-4. Temperature Histories for DST Borehole 158 at Selected Locations

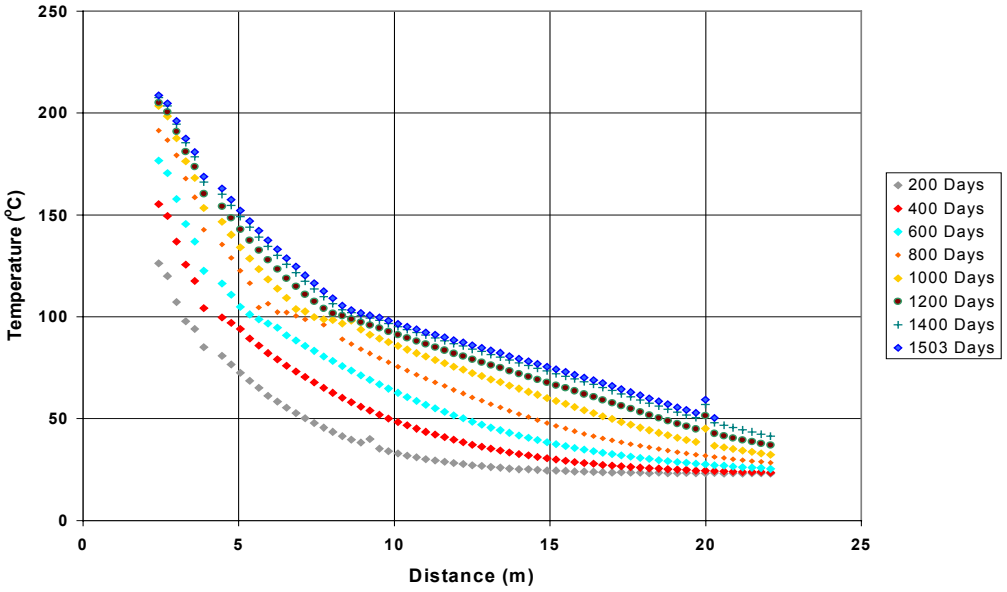

Figure 6.3.1.2-5. Temperature Profile along DST Borehole at Select Times

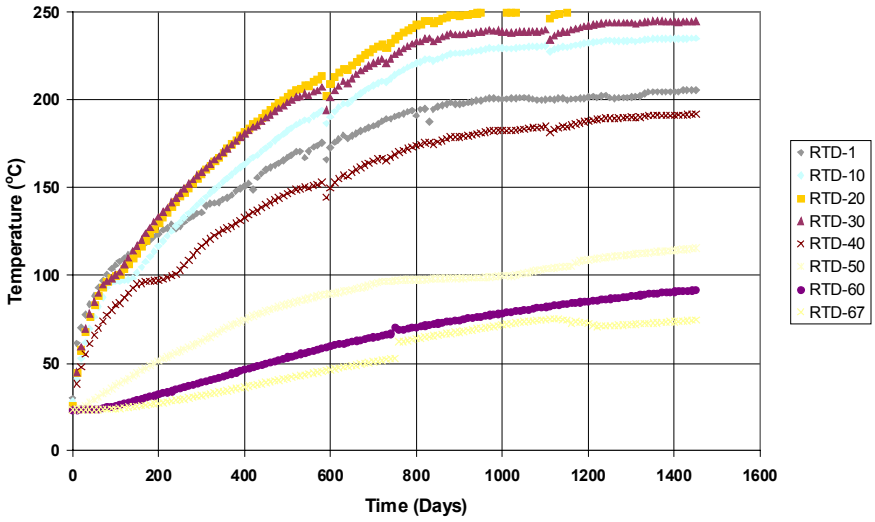

Figure 6.3.1.2-6. Temperature Histories for DST Borehole 164 at Select Locations

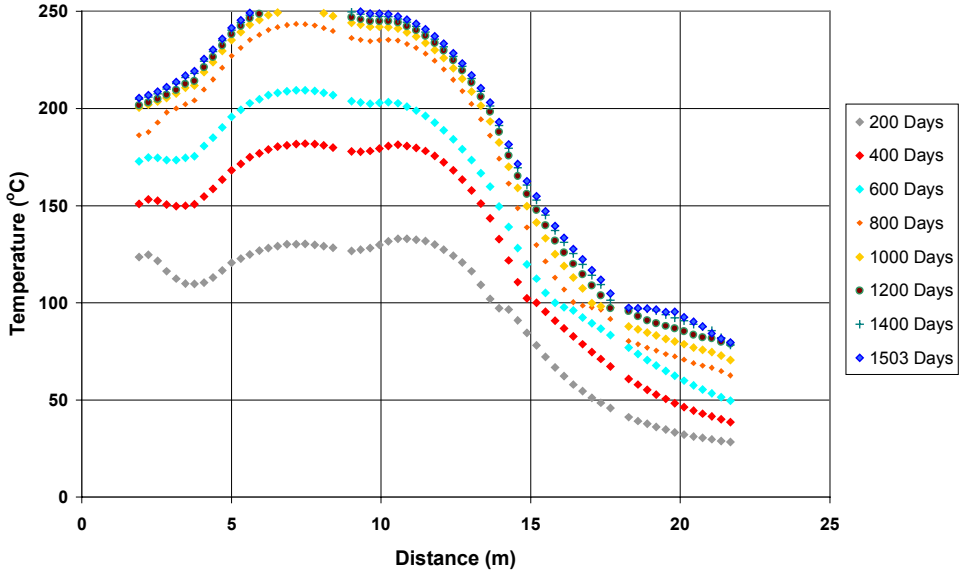

Figure 6.3.1.2-7. Temperature Profile along DST Borehole 164 at Select Times

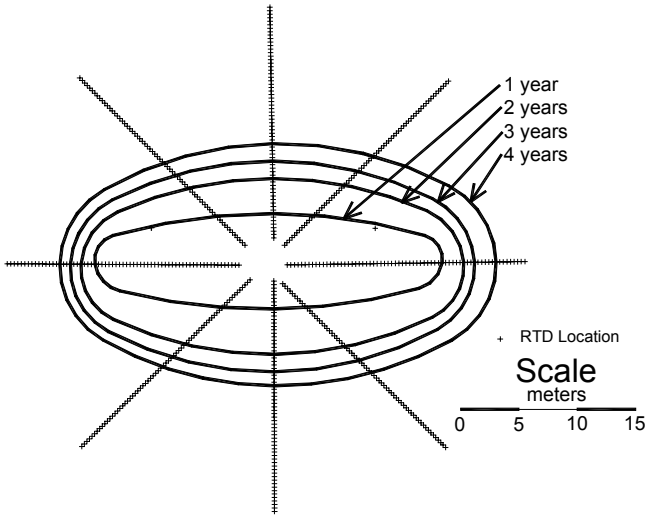

Figure 6.3.1.2-8. Vertical Slice Through the Mid-Length of the DST Heated Drift Showing 95 ^{0}C Temperature Contours after 1, 2, 3, and 4 Years of Heating

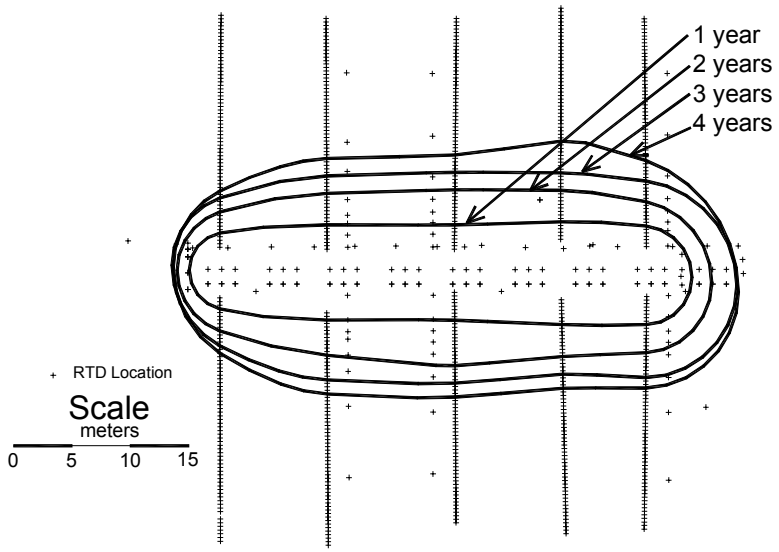

Figure 6.3.1.2-9. Vertical Slice Through the Longitudinal Axis of the DST Heated Drift Showing 95 ^{0}C Temperature Contours after 1, 2, 3, and 4 Years of Heating

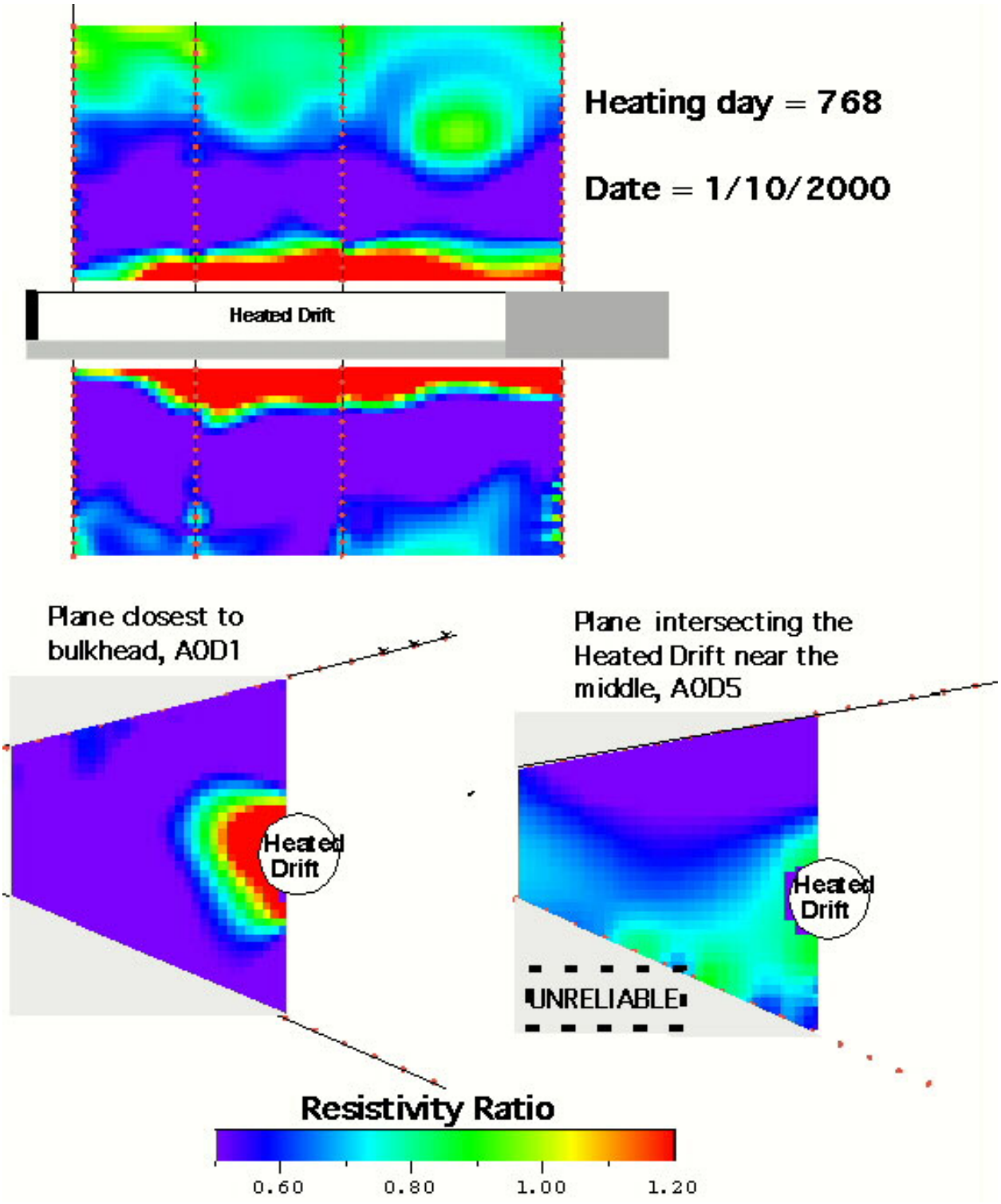

Figure 6.3.2.1-1. The DST ERT Resistivity Ratios of the 1/10/00 Measurement to the Pre-Heating Measurement

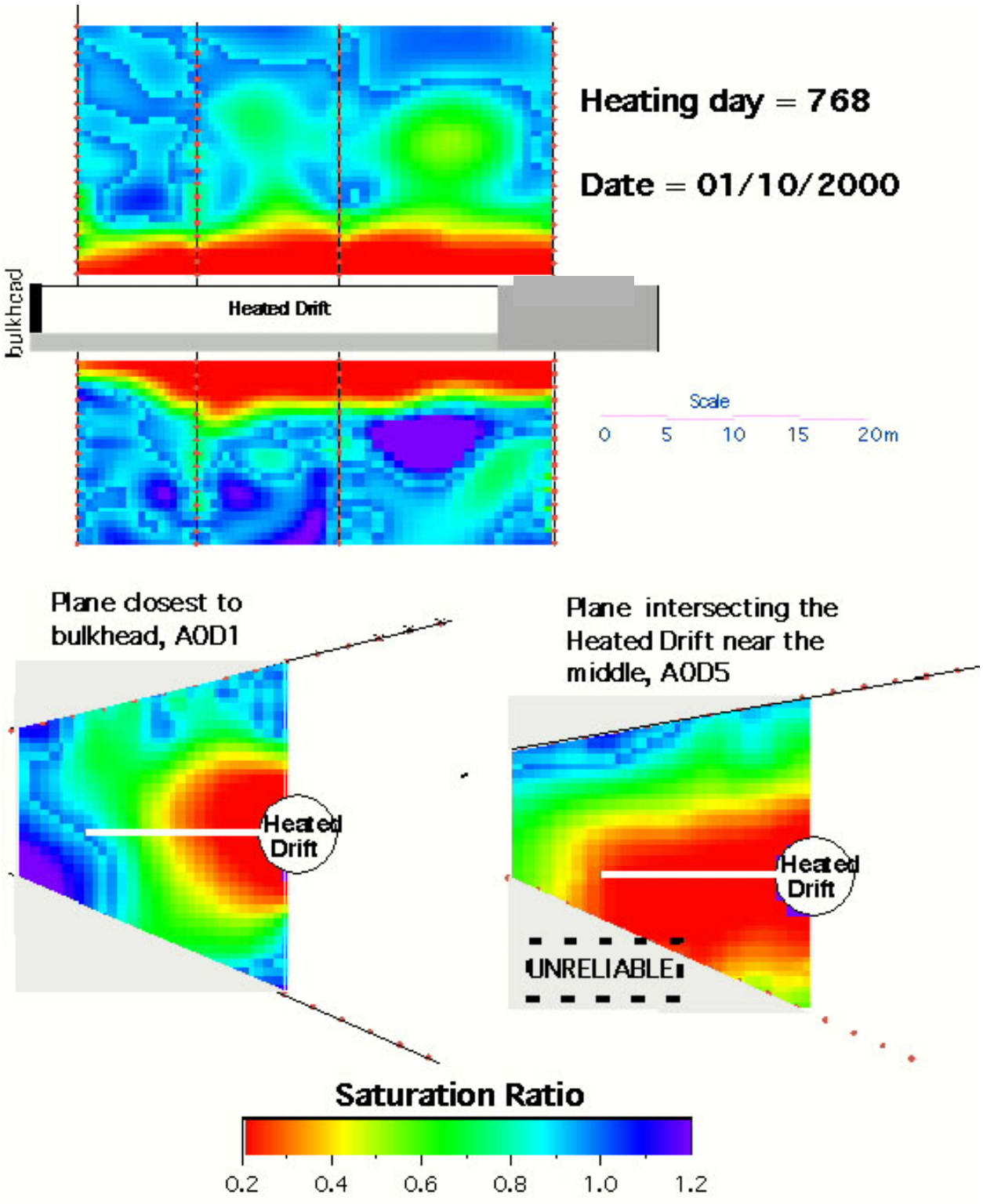

Figure 6.3.2.1-2. The DST Saturation Ratio Calculated from the 1/10/00 Resistivity Ratio

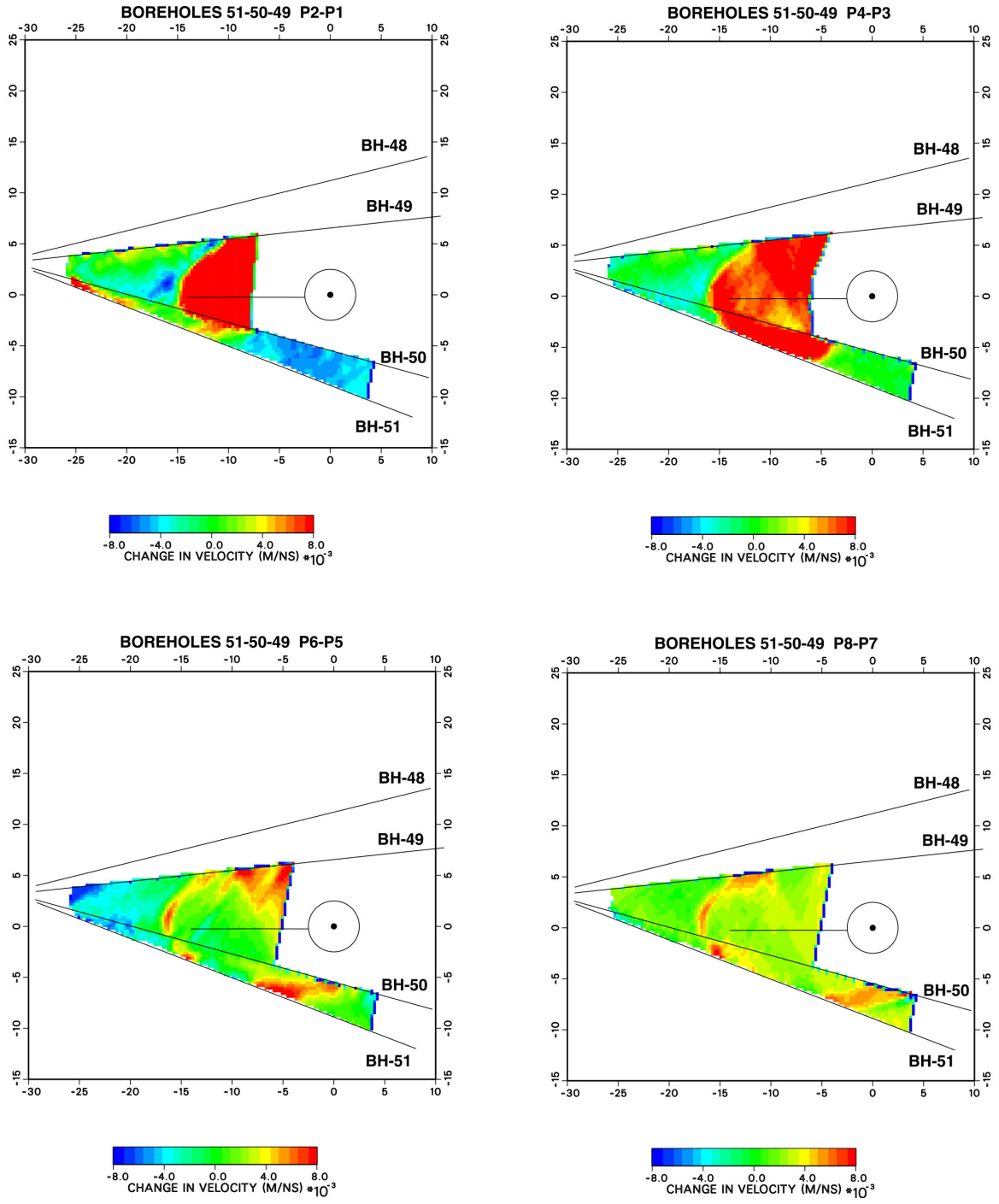

Figure 6.3.2.2-1. GPR Difference Velocity Tomograms for DST Borehole Pairs 51-50 and 50-49

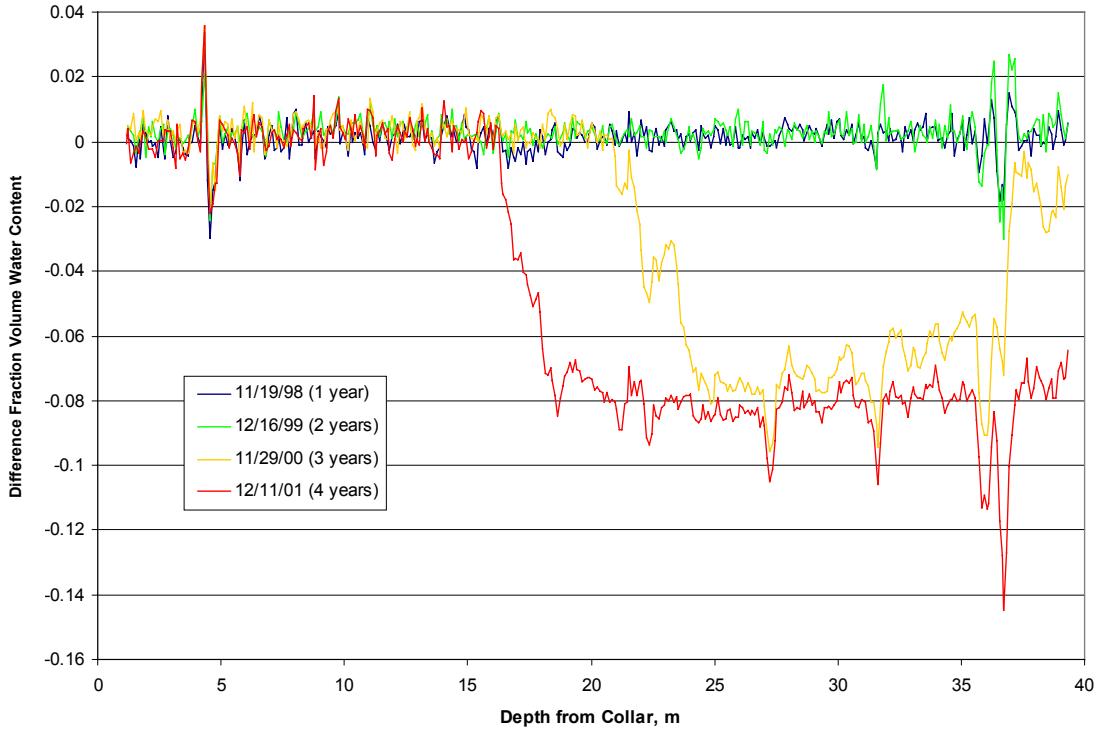

Figure 6.3.2.3-1. Difference Fraction Volume Water Content Measured in DST Borehole 66 using Neutron Logging (November 19, 1998, to December 11, 2001)

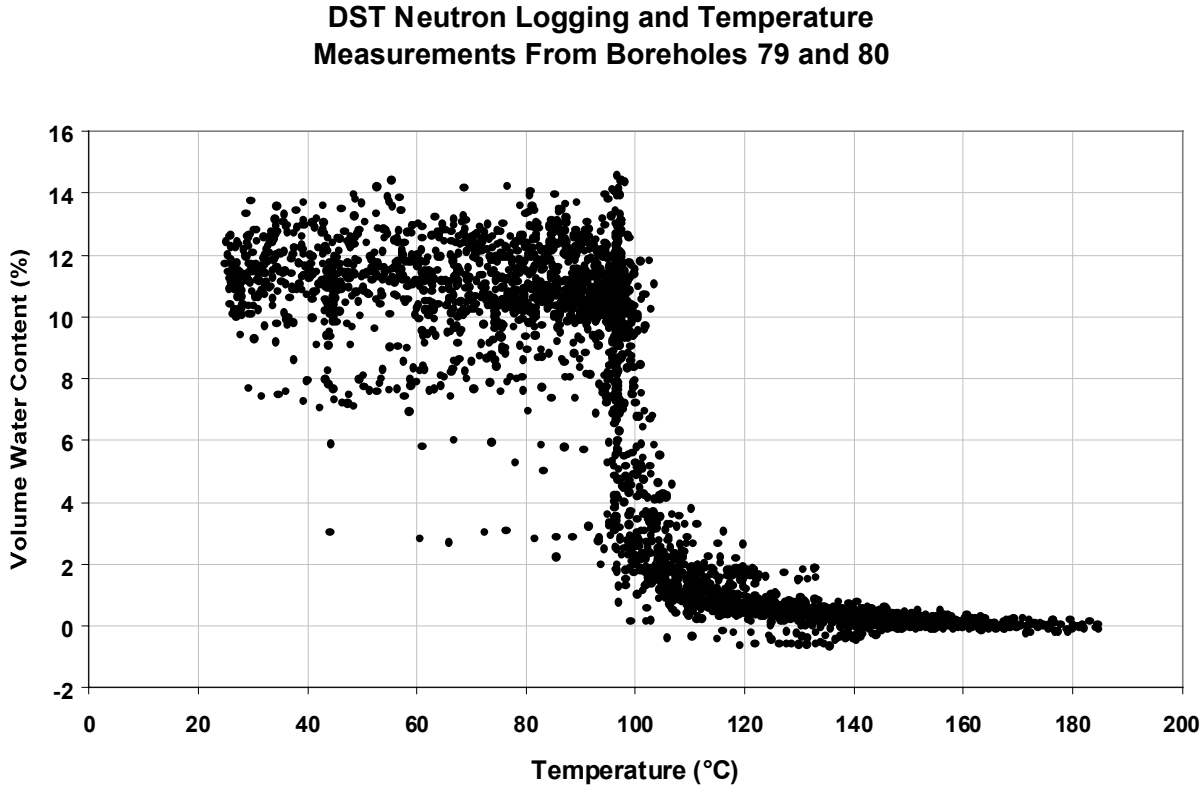

Figure 6.3.2.3-2. Rock Moisture Content as a Function of Temperature as Measured from Neutron Logging of Boreholes 79 and 80 during the DST Heating Phase

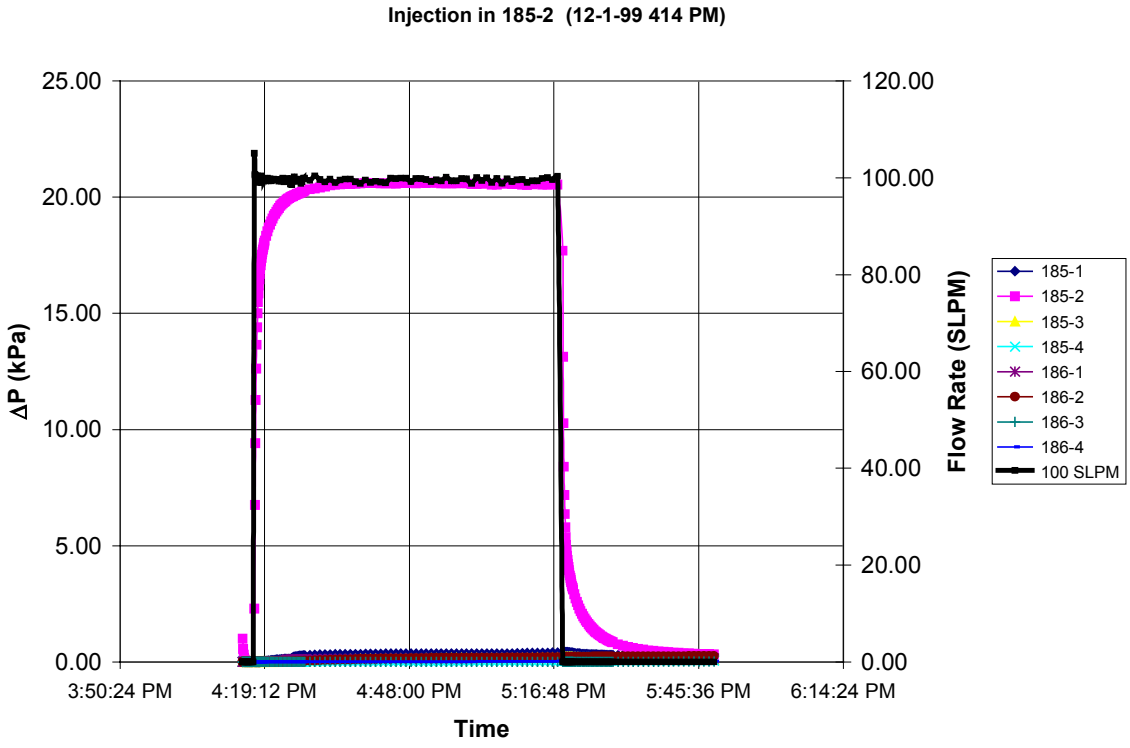

NOTE: Much smaller pressure responses are observable in nearby observation intervals.

Figure 6.3.2.4-1. Air-injection Test in DST Borehole 185-2 Showing Flowrate and Pressure in the Injection Zone on 12/1/99

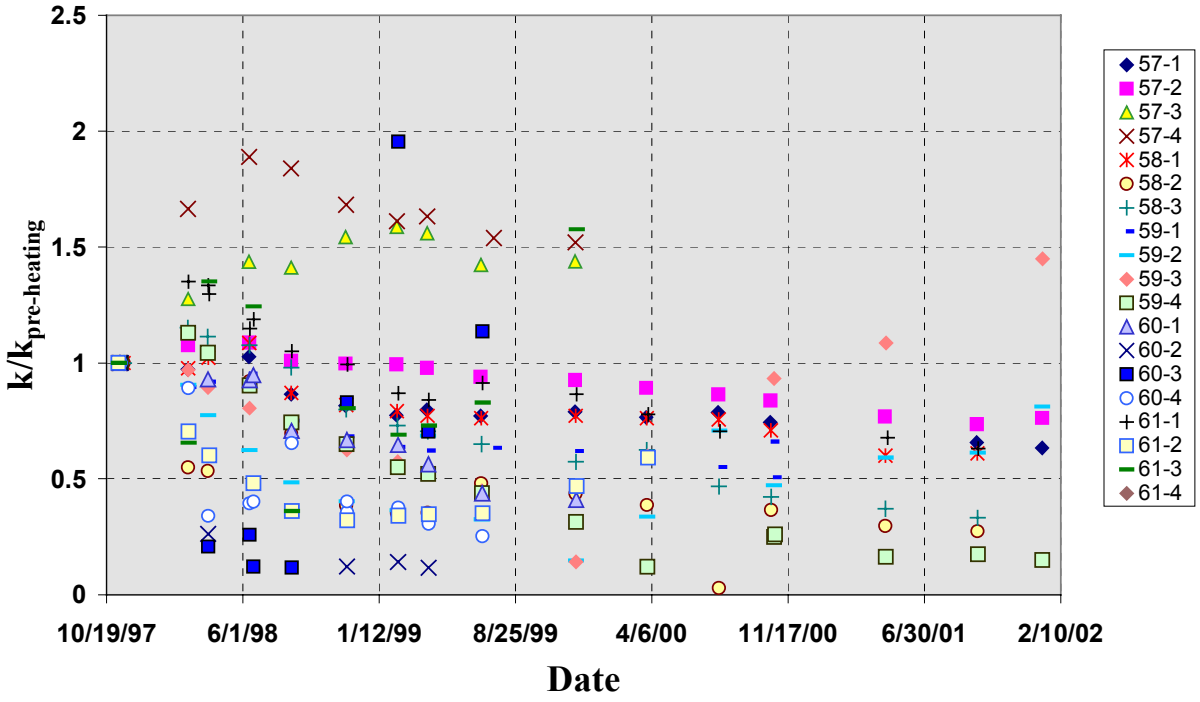

Figure 6.3.2.4-2. Changes In Permeability Displayed as a Ratio to the Pre-Heating Permeability Estimate for DST Boreholes 57–61

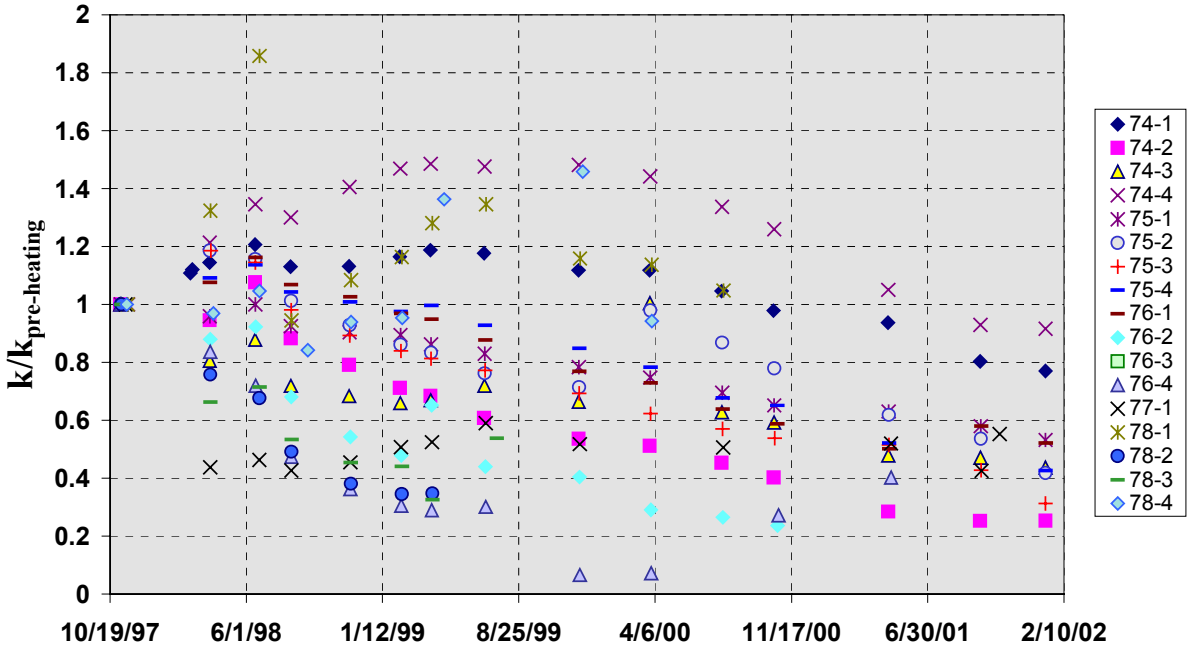

Figure 6.3.2.4-3. Changes In Permeability Displayed as a Ratio to the Pre-Heating Permeability Estimate for DST Boreholes 74–78

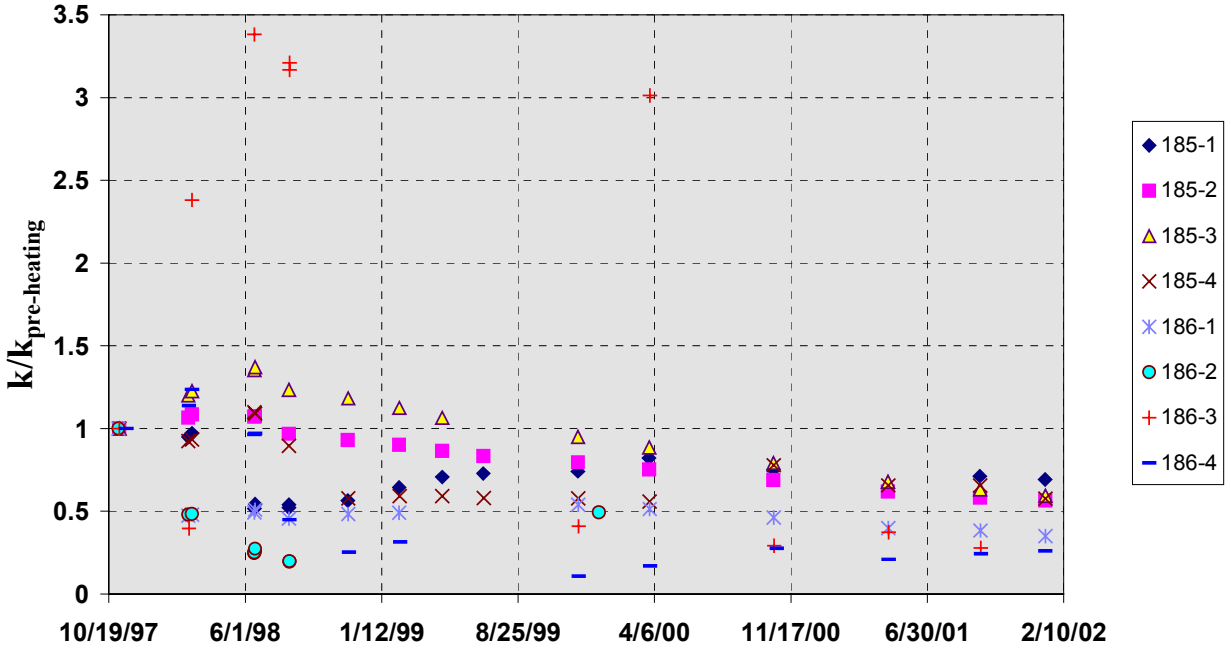

Figure 6.3.2.4-4. Changes In Permeability Displayed as a Ratio to the Pre-Heating Permeability Estimate for DST Boreholes 185–186

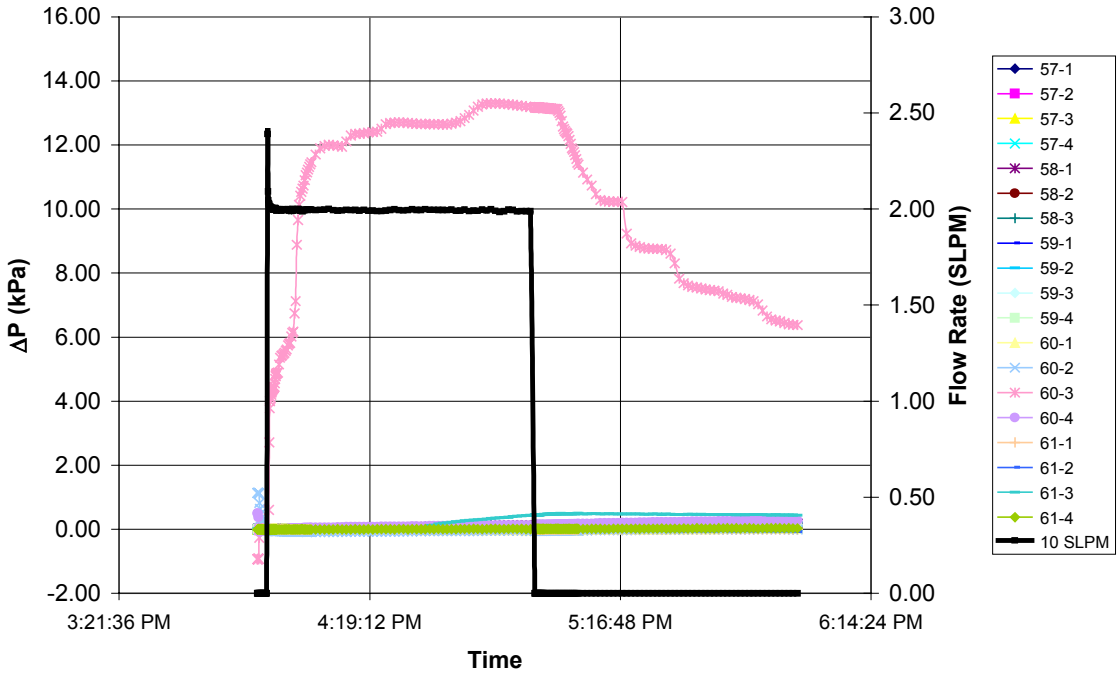

Figure 6.3.2.4-5. An Injection Test in DST Borehole 60-3 Showing Anomalous Response Attributed to Two-Phase Flow Processes on 4/2/99

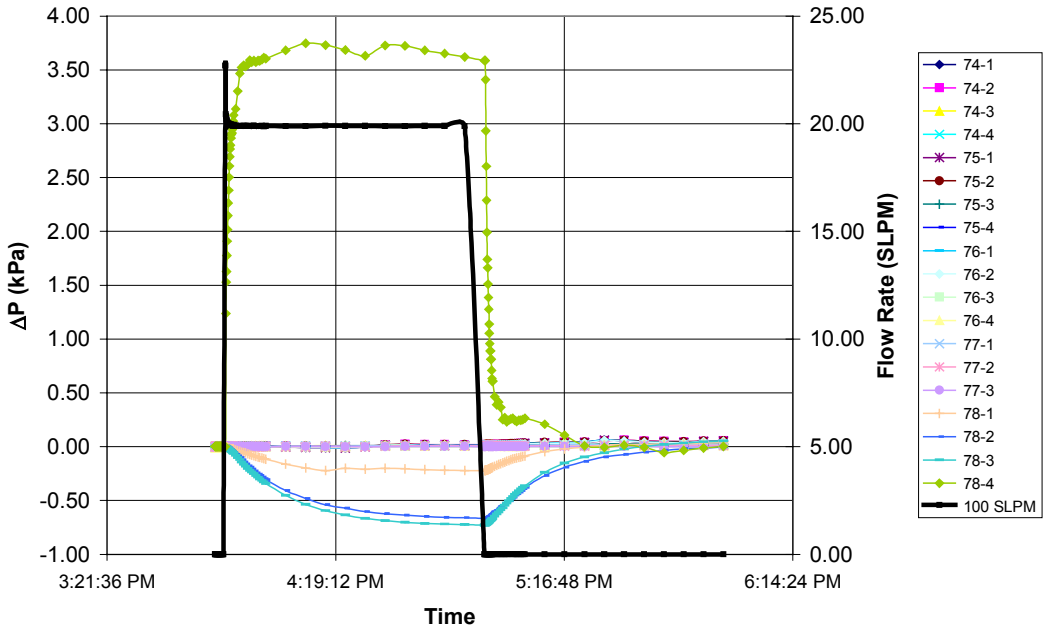

NOTE: The reductions in pressure measured in DST Borehole 78-1, 78-2 and 78-3 are attributed to effects of cool injection gas being transported in the injection tube for 78-4 through the sealed off intervals.

Figure 6.3.2.4-6. An Anomalous Response to Air Injection into DST Borehole 78-4 during the Heating Phase of the DST on 4/22/99

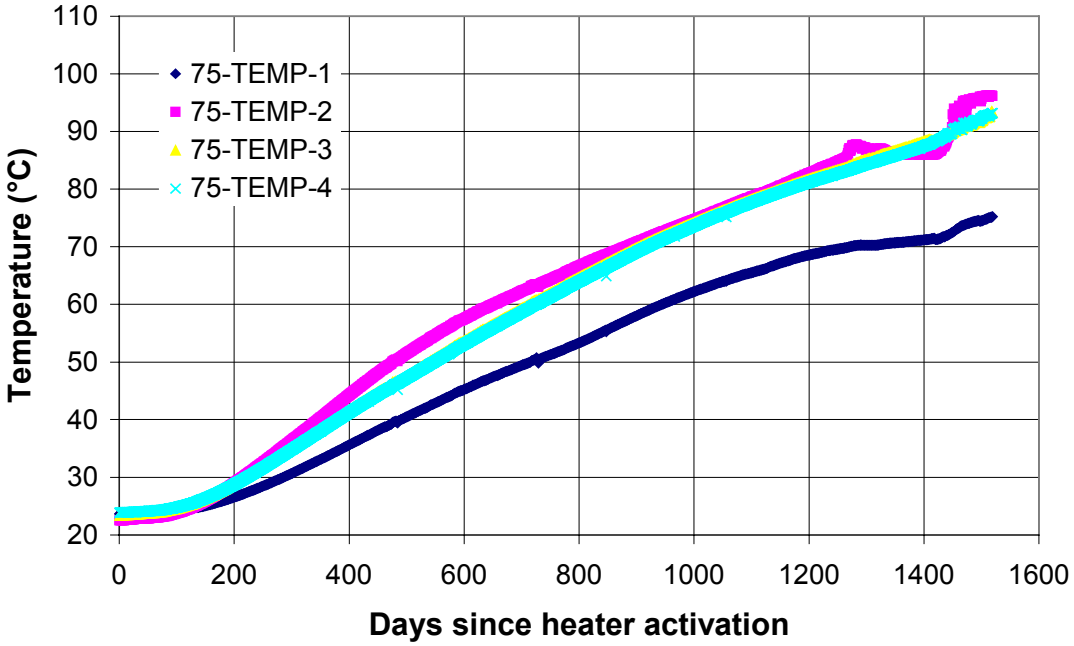

Figure 6.3.2.4-7. Passive Monitoring Temperature Data for DST Borehole 75

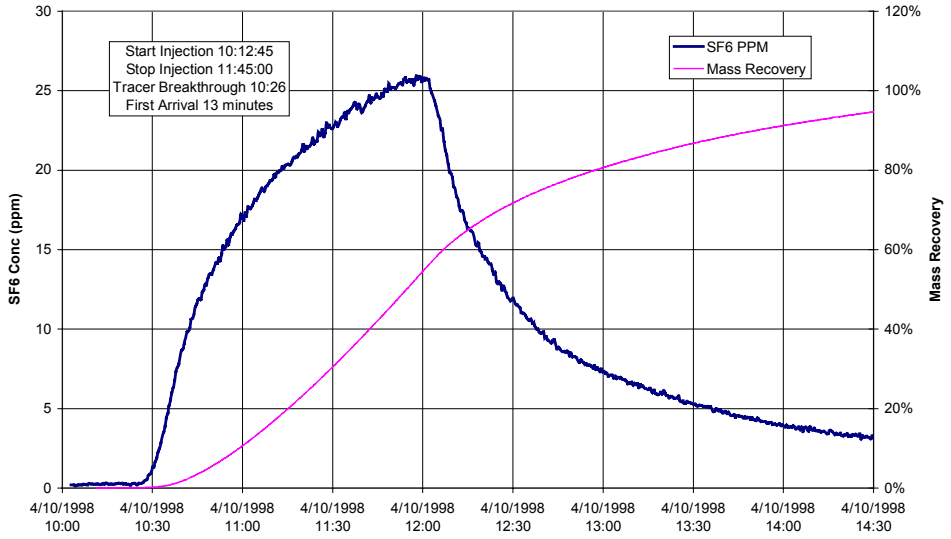

Figure 6.3.2.4-8. Mass Breakthrough Curve and Cumulative Mass Recovery for DST Borehole 76-2 from 30:1 Gas Tracer Test

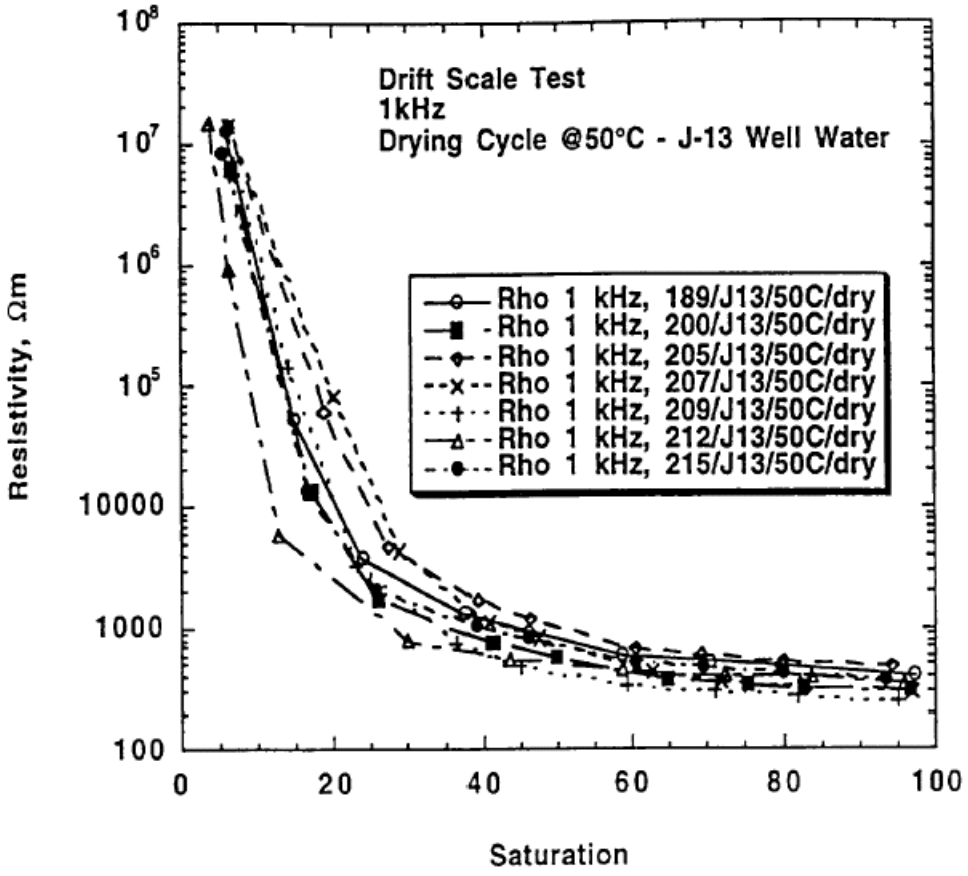

Figure 6.3.2.5-1. Electrical Resistivity of DST Samples as Function of Saturation in the Drying Cycle at 50°C

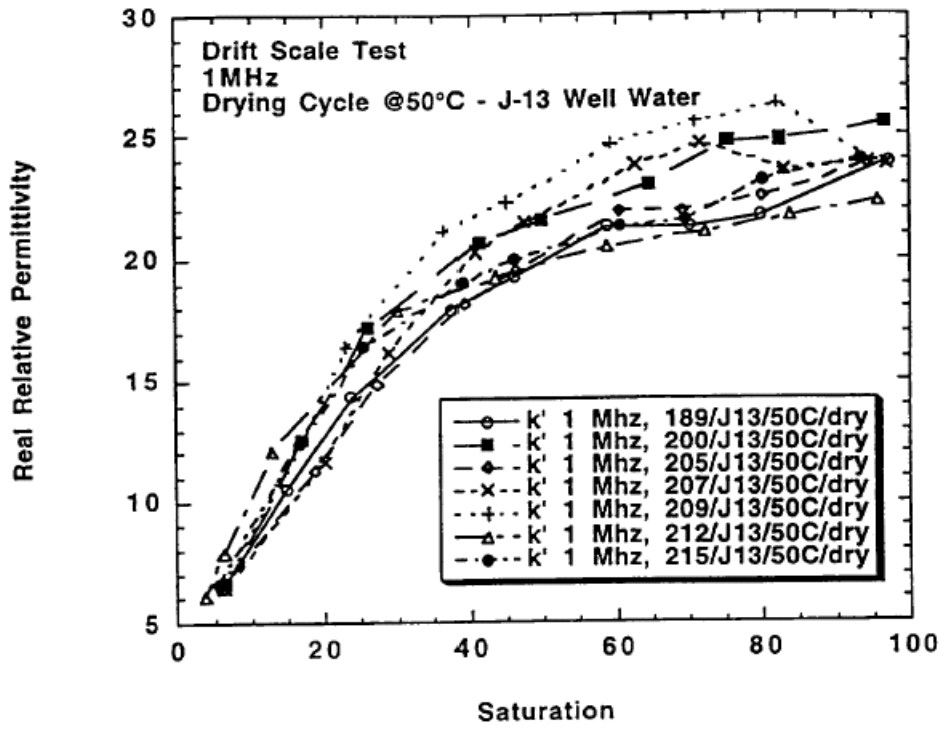

Figure 6.3.2.5-2. The Relative Permittivity of the DST Samples as a Function of Saturation in the Drying Cycle at 50°C

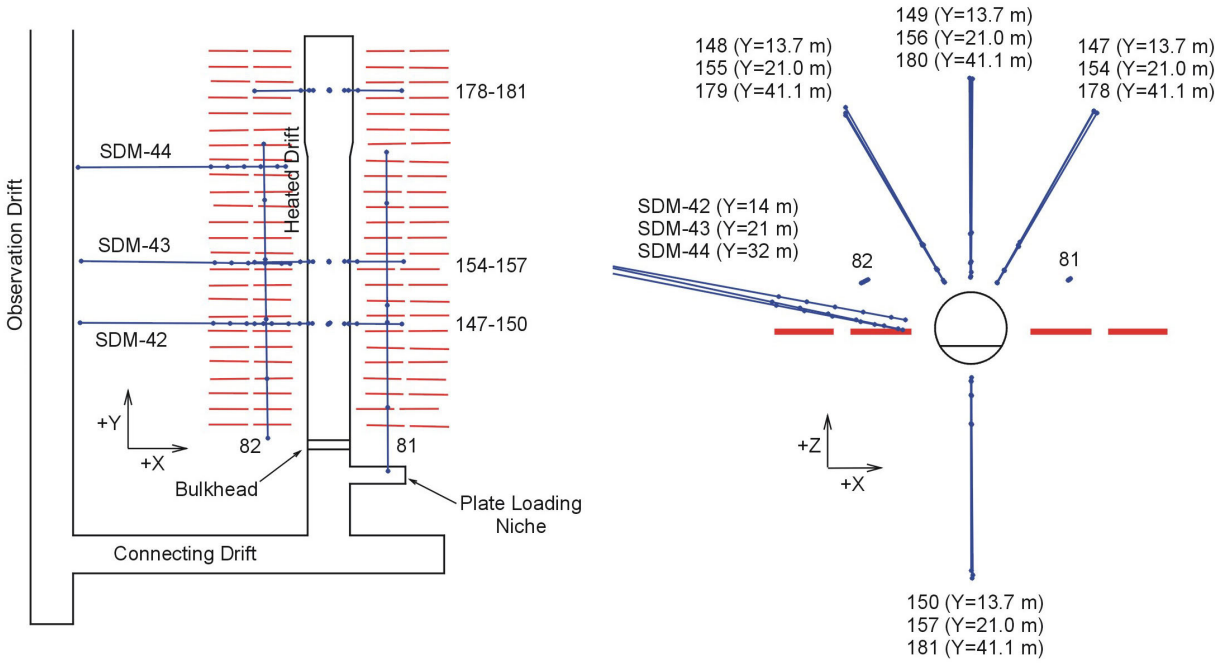

Figure 6.3.3.1-1. DST MPBX Layout

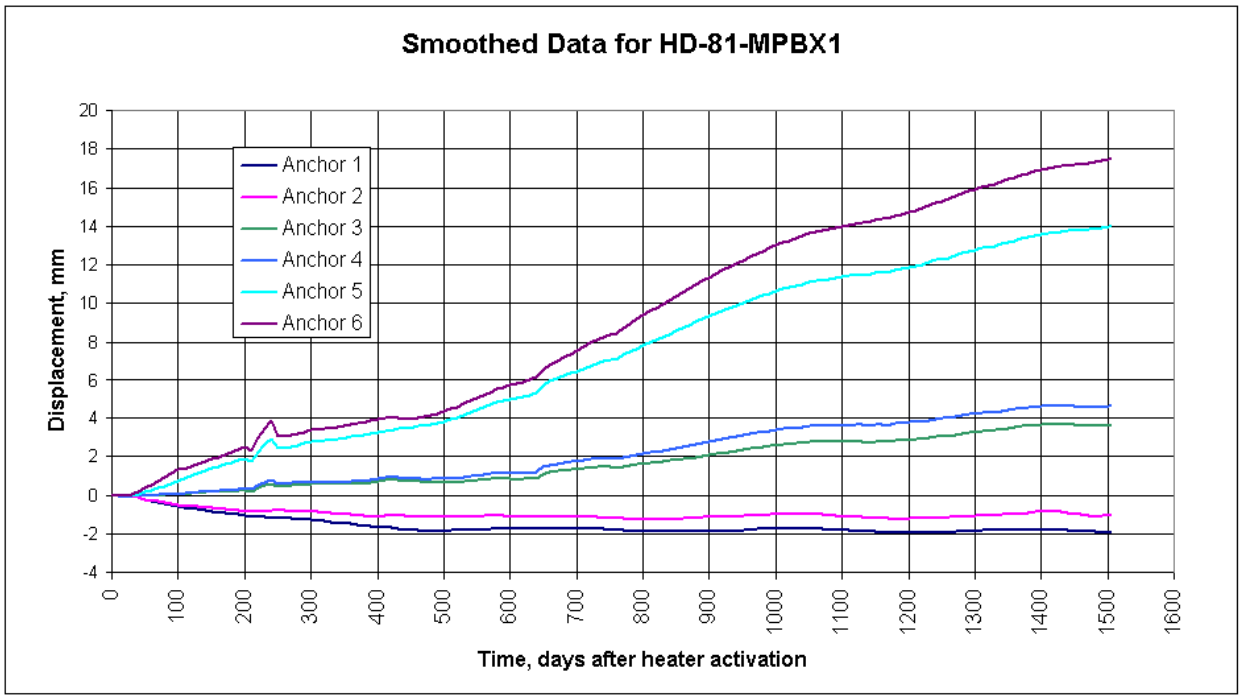

Figure 6.3.3.1-2. DST Displacements from Borehole 81 (MPBX1)

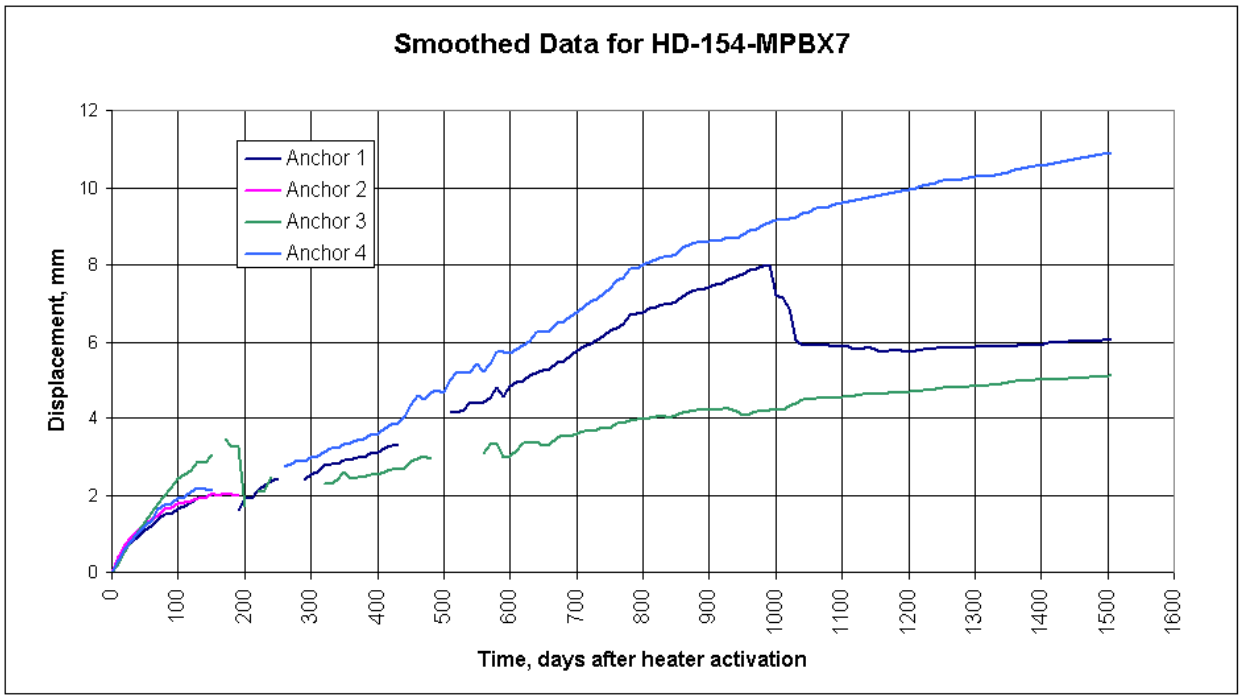

Figure 6.3.3.1-3. DST Displacements from Borehole 154 (MPBX7)

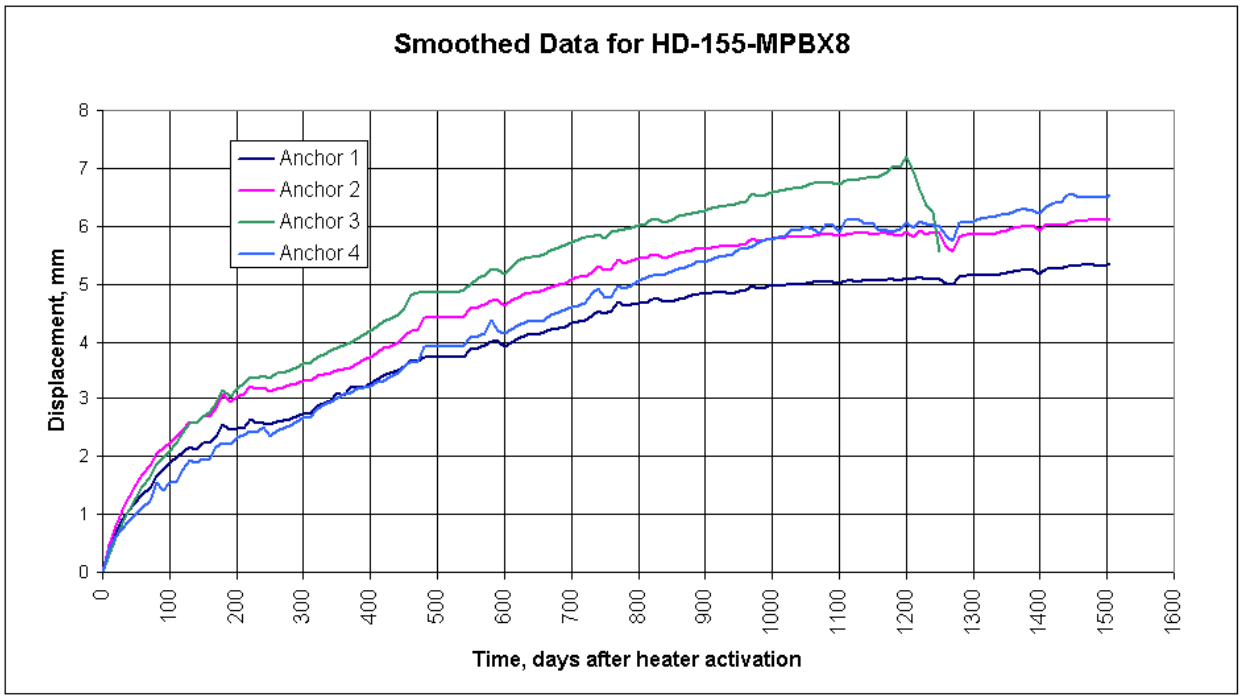

Figure 6.3.3.1-4. DST Displacements from Borehole 155 (MPBX8)

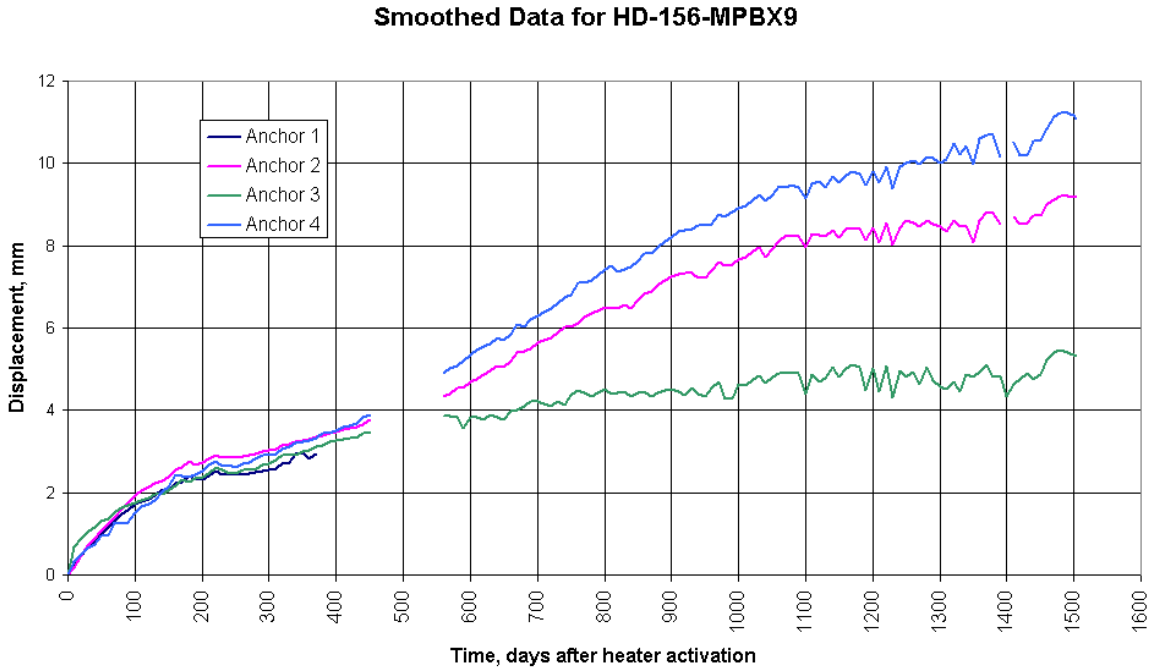

Figure 6.3.3.1-5. DST Displacements from Borehole 156 (MPBX9)

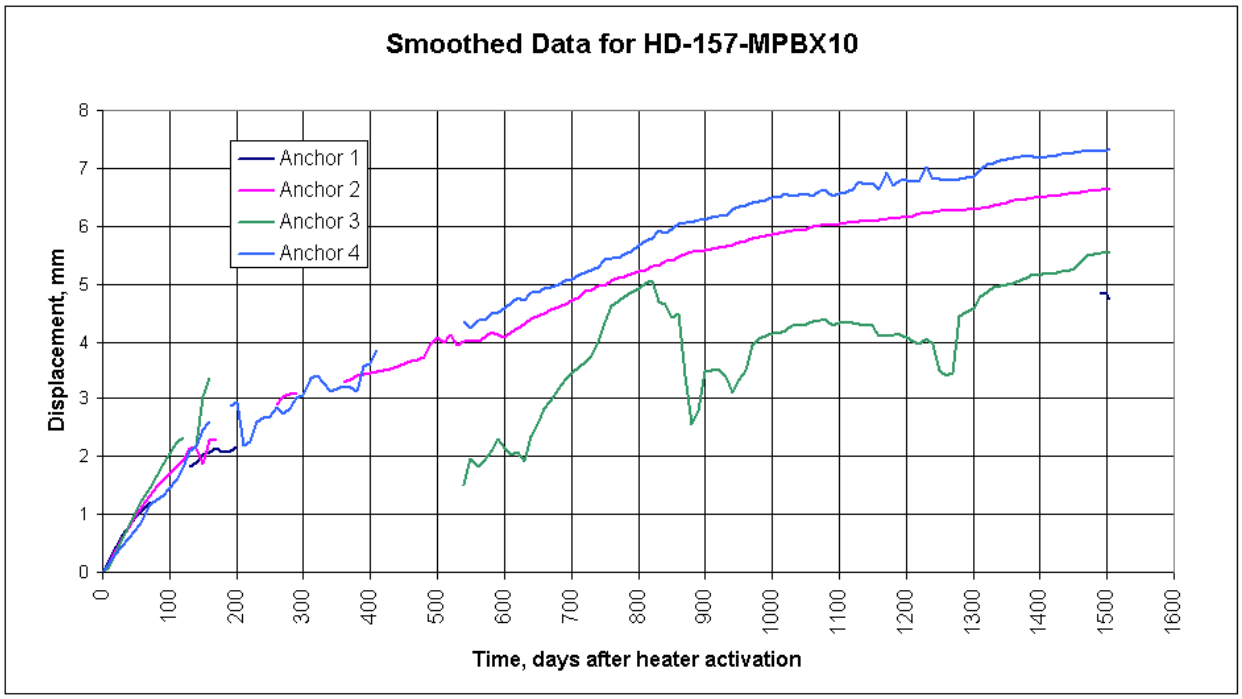

Figure 6.3.3.1-6. DST Displacements from Borehole 157 (MPBX10)

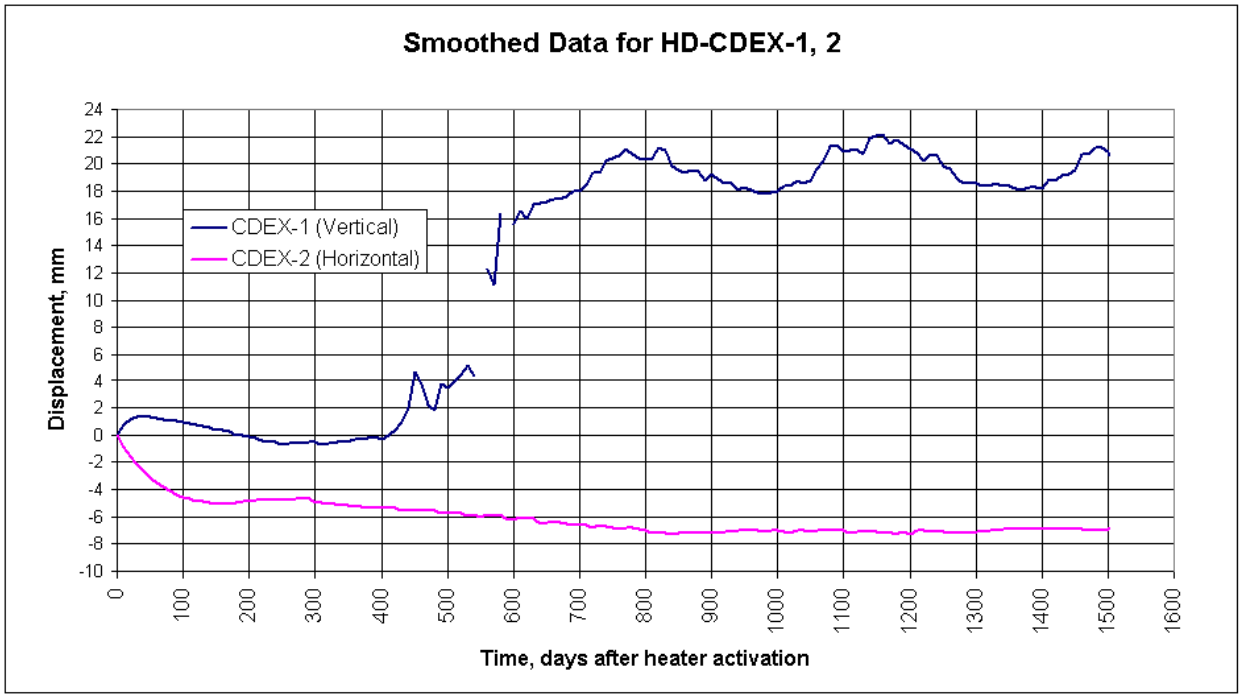

Figure 6.3.3.2-1. DST Displacements from CDEX-1 and CDEX-2

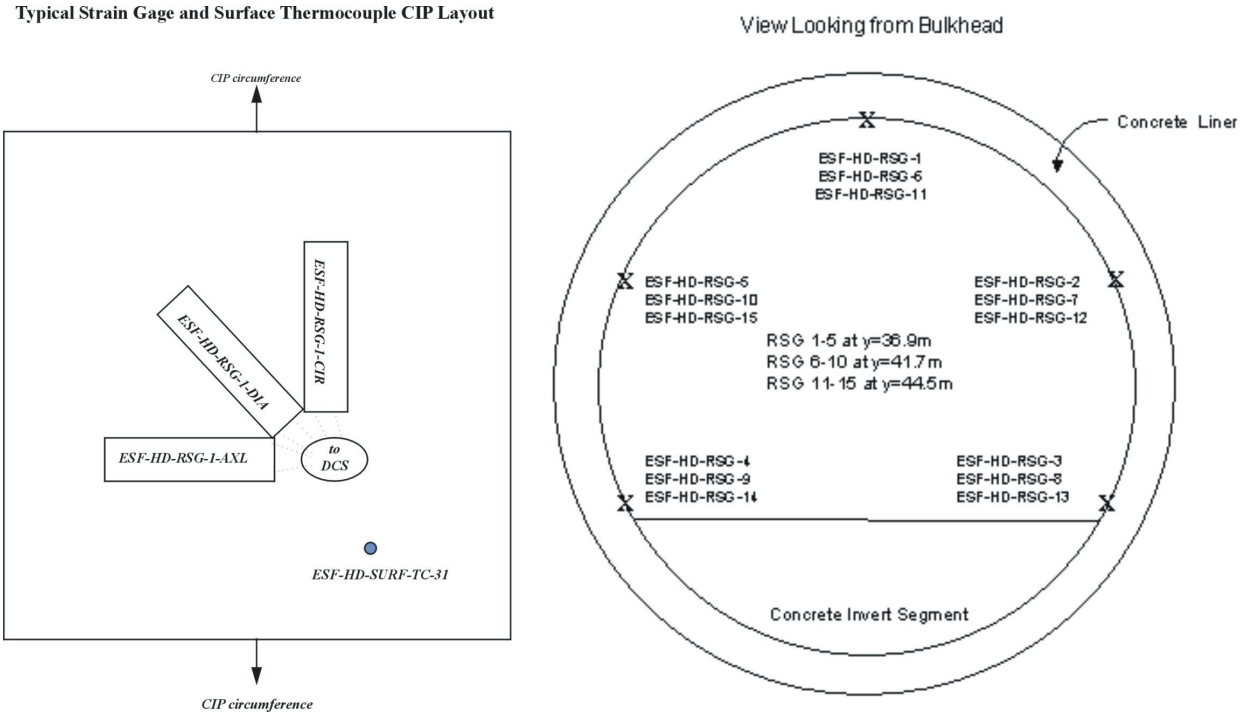

Figure 6.3.3.3-1. Layout and Location of DST Strain Gage Rosettes on the Concrete Liner

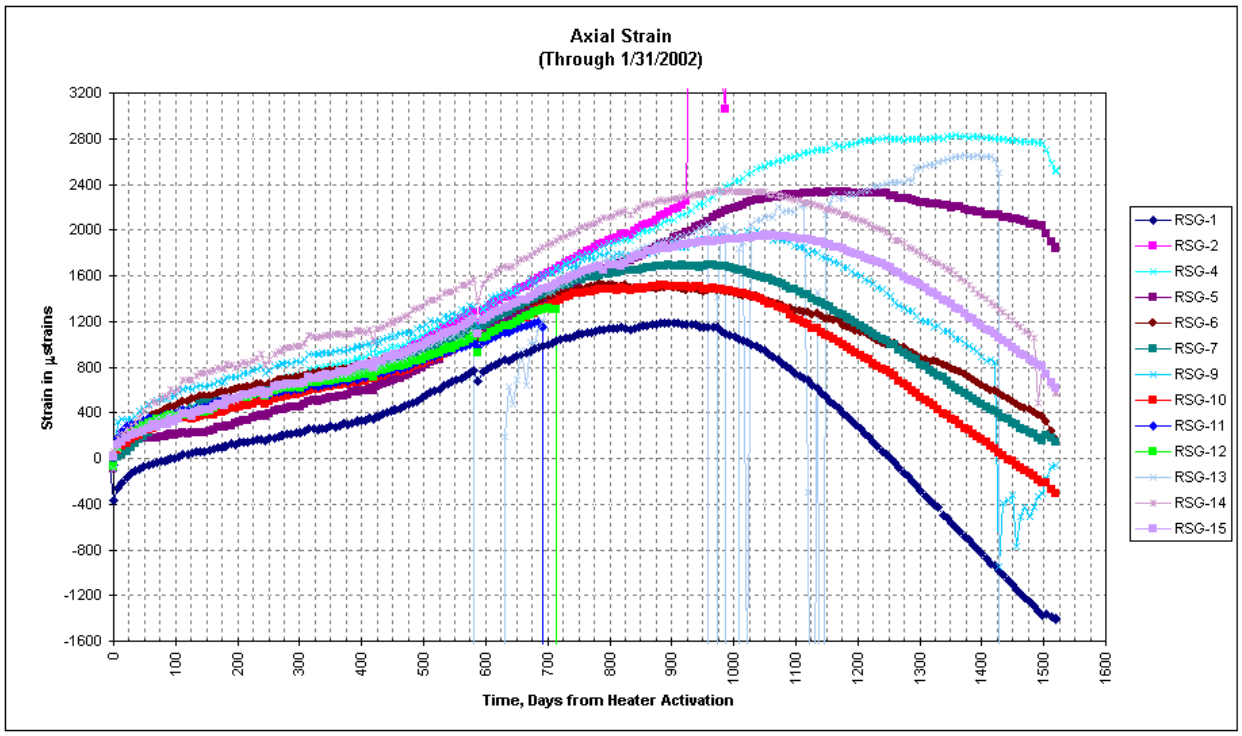

Figure 6.3.3.3-2. Axial Strains Measured by the Strain Gages on the DST Concrete Liner

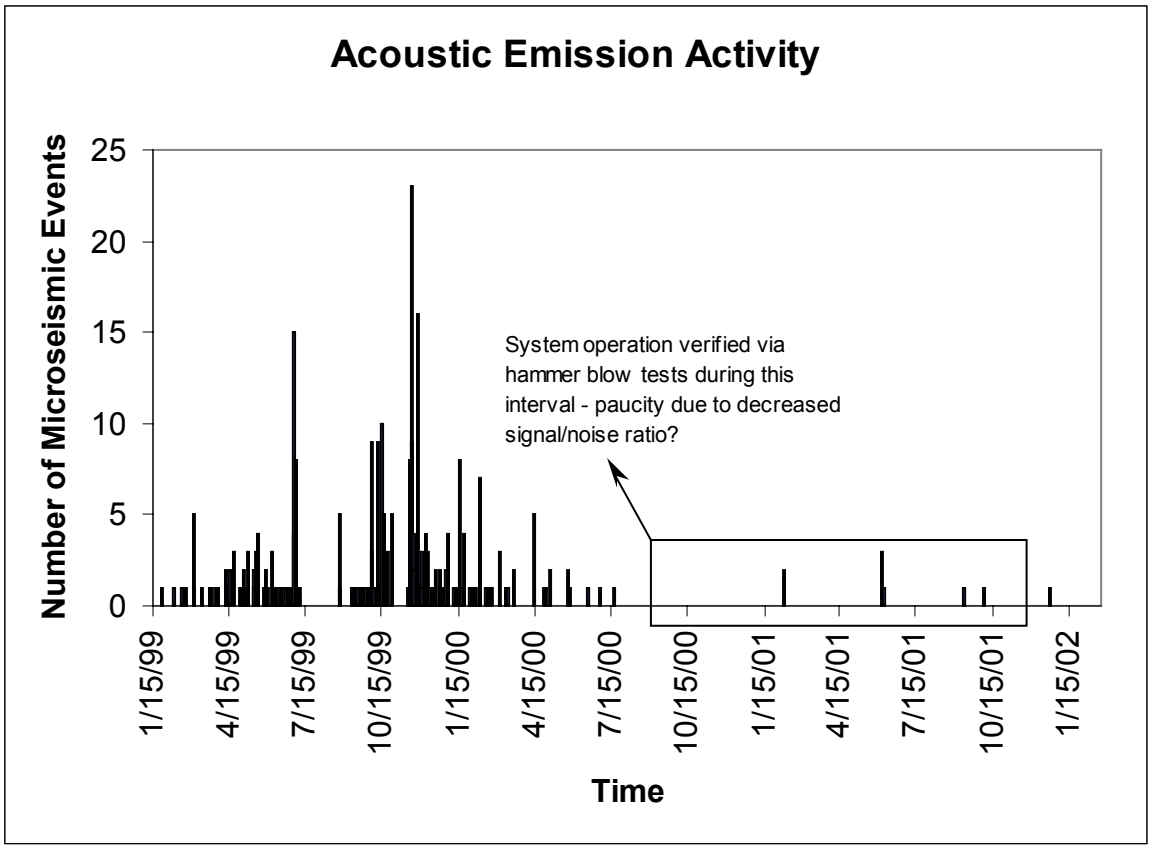

Figure 6.3.3.4-1 Histogram of DST Microseismic Activity (Acoustic Emission)

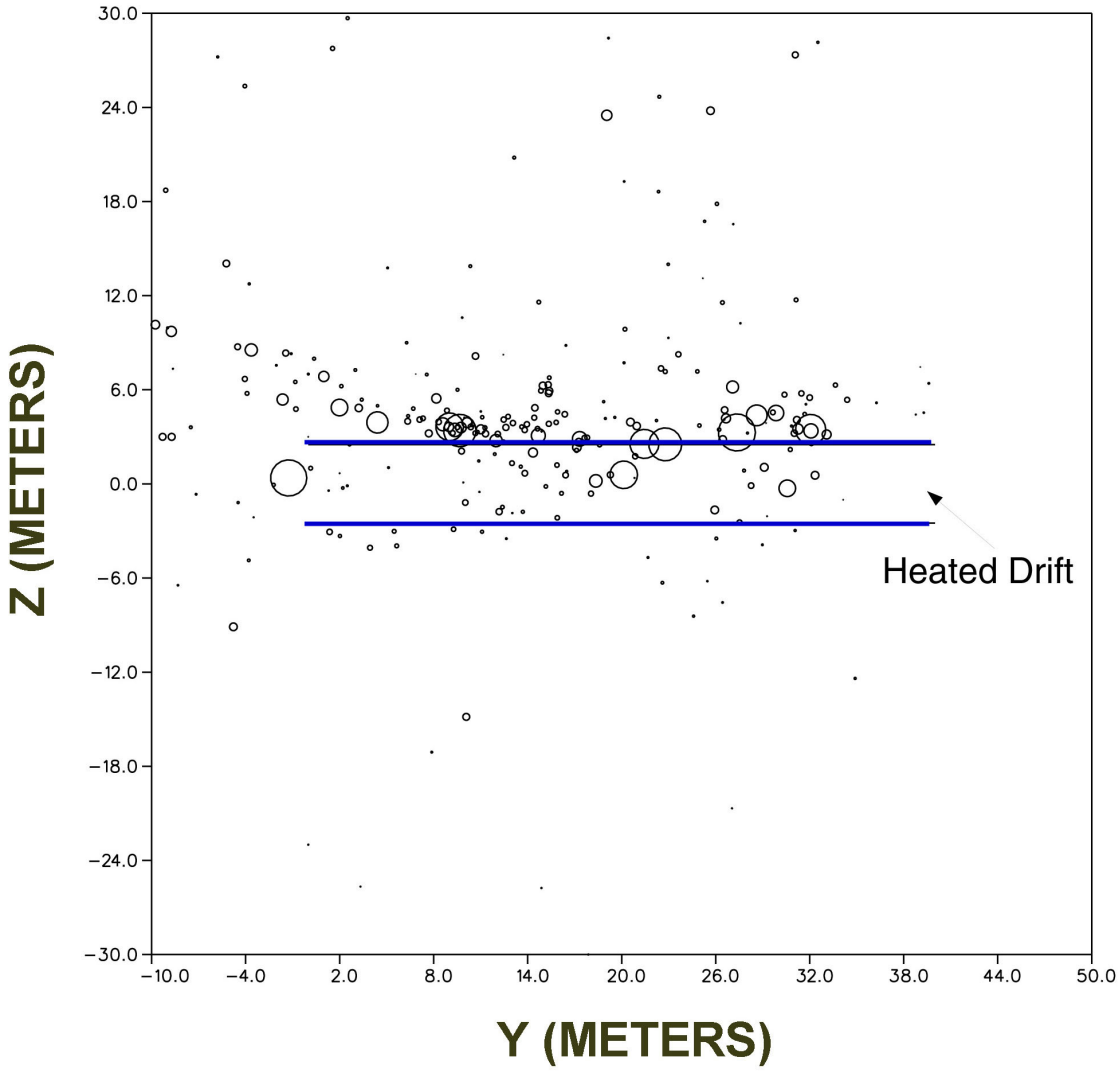

Figure 6.3.3.4-2 Location of DST Microseismic Activity (Acoustic Emissions) between January 1, 1999 and October 15, 2001

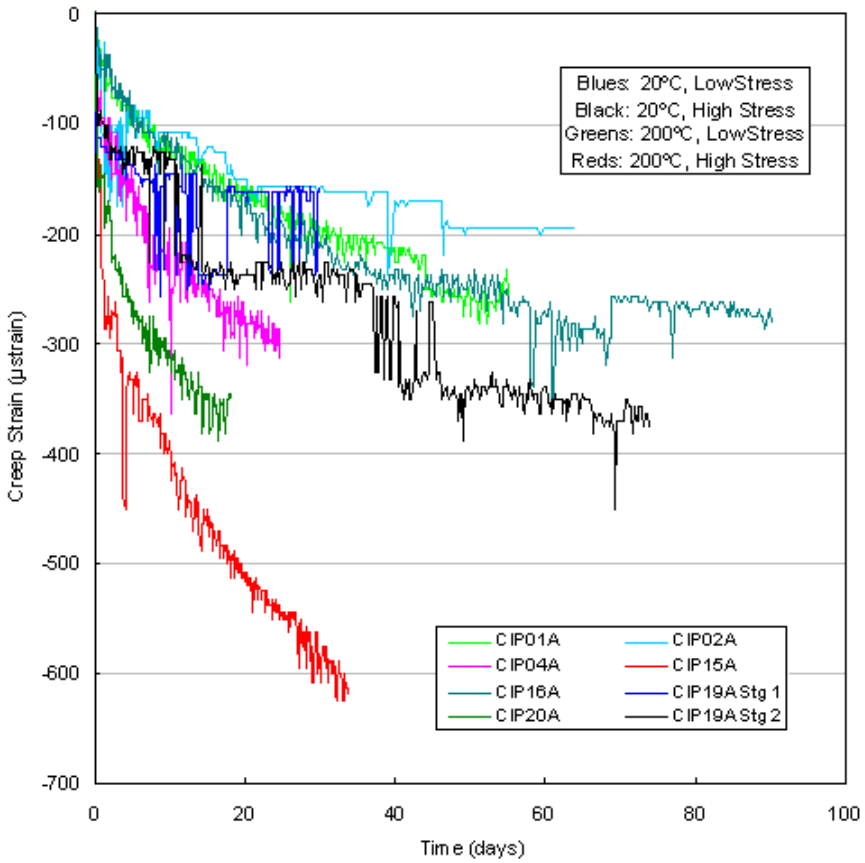

Figure 6.3.3.5-1. Strain-Versus-Time Curves for DST Creep Tests of Cast-in-Place Concrete

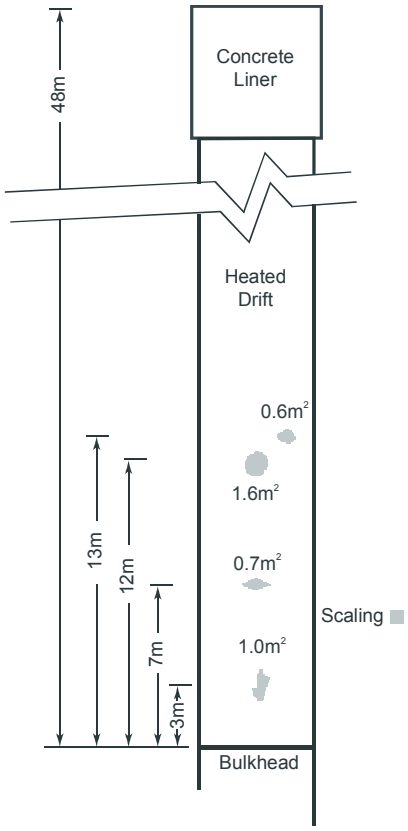

Figure 6.3.3.7-1. Locations of Four Scaling Zones in the Roof of the DST Heated Drift

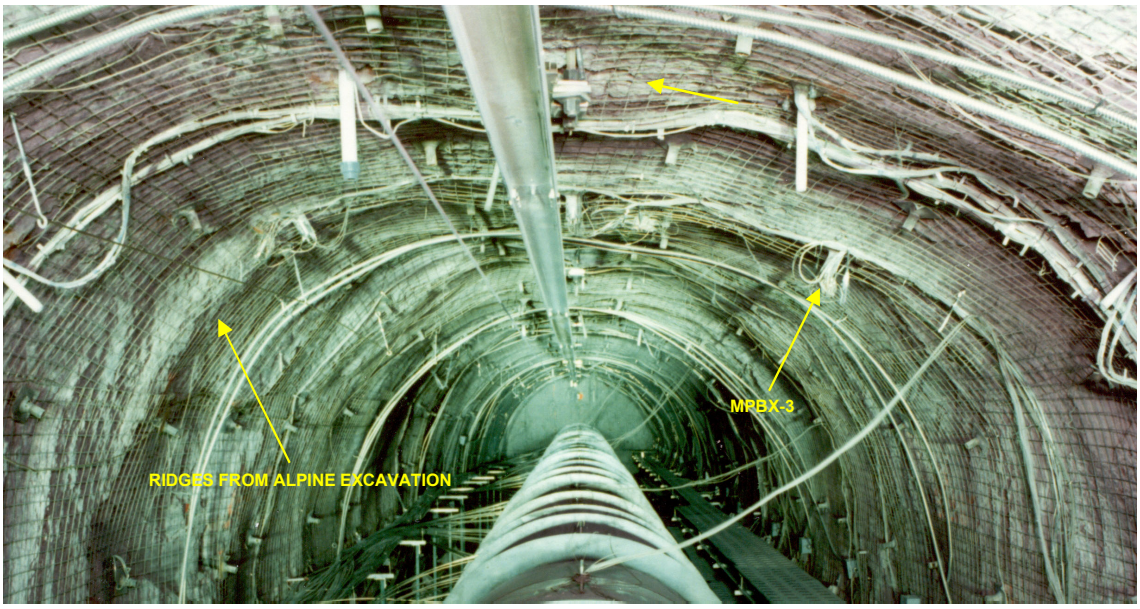

NOTE: Several distinct ridges along the roof of the Heated Drift appear to coincide with observed scaling zones.

Figure 6.3.3.7-2 View of the DST Prior to Heater Activation

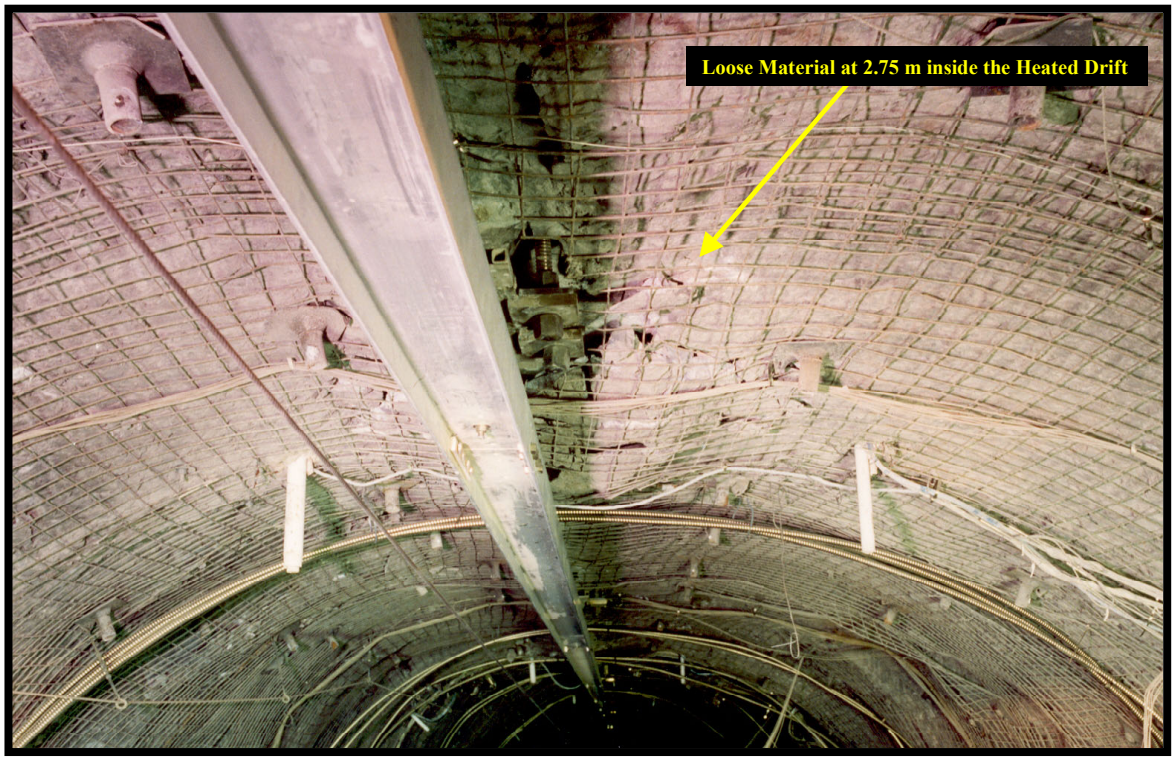

Figure 6.3.3.7-3. View of Roof Scaling Located 3 m From the DST Bulkhead and Retained in the Ground Support System Comprised of Rock Bolts and Welded Wire Fabric

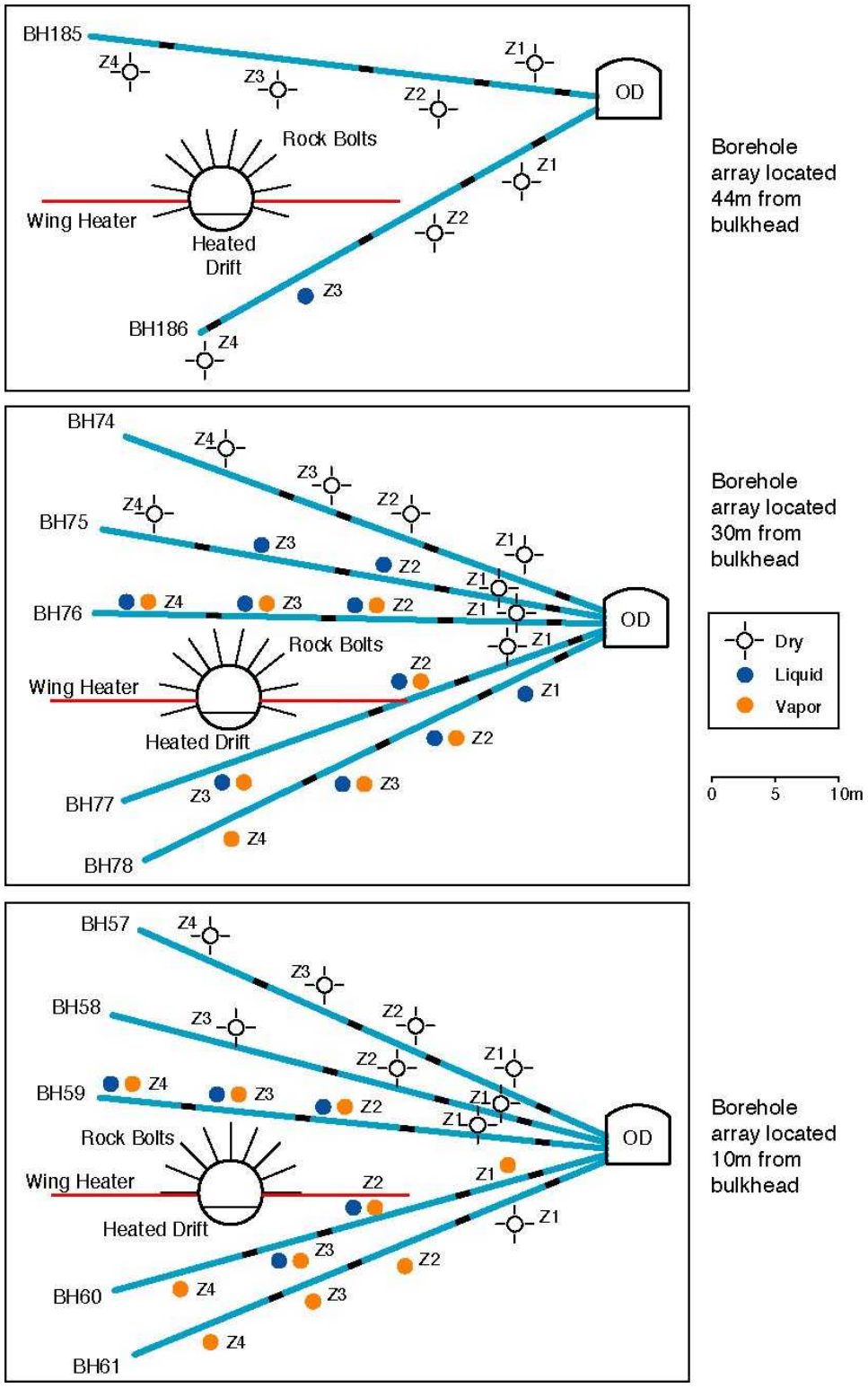

Figure 6.3.4.1-1. Three Arrays of DST Hydrology Boreholes Showing Relative Packer Positions and Fluid Sampling Zones

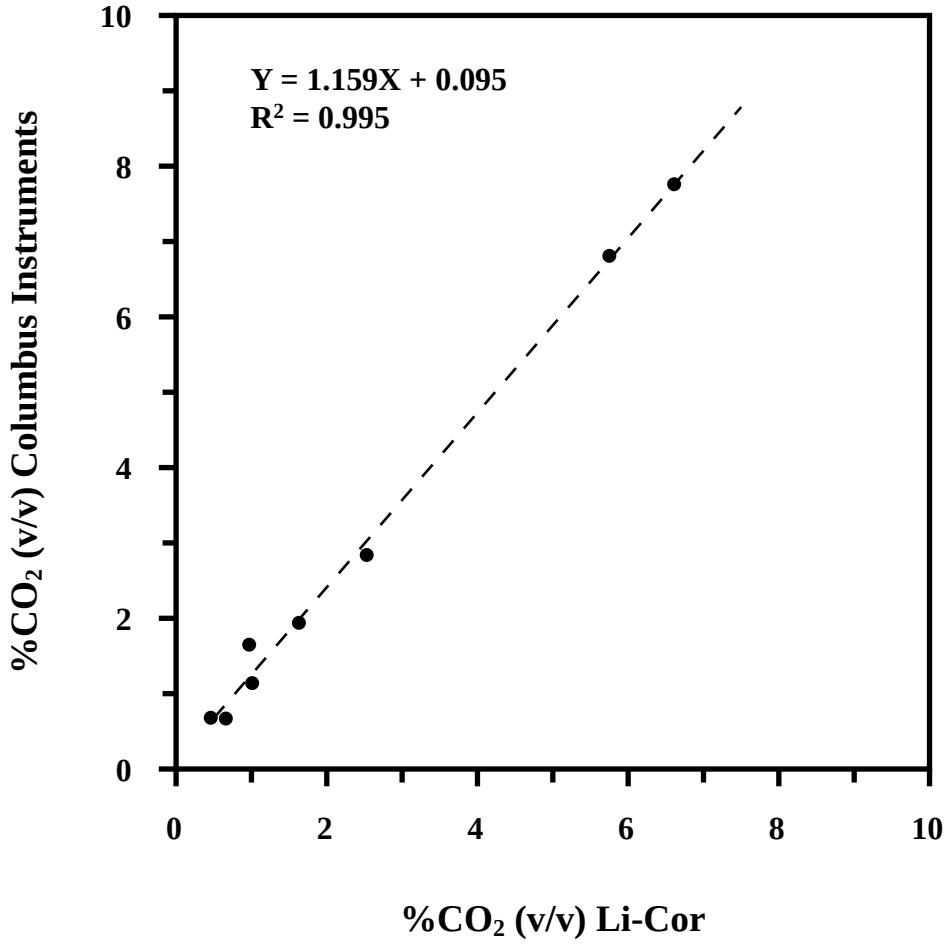

Figure 6.3.4.2-1. Comparison of CO_2 Concentrations >0.2% Measured with the Li-Cor in the Amundson Lab at UC Berkeley and the Columbus Instruments Analyzer at the ESF (January, 2001)

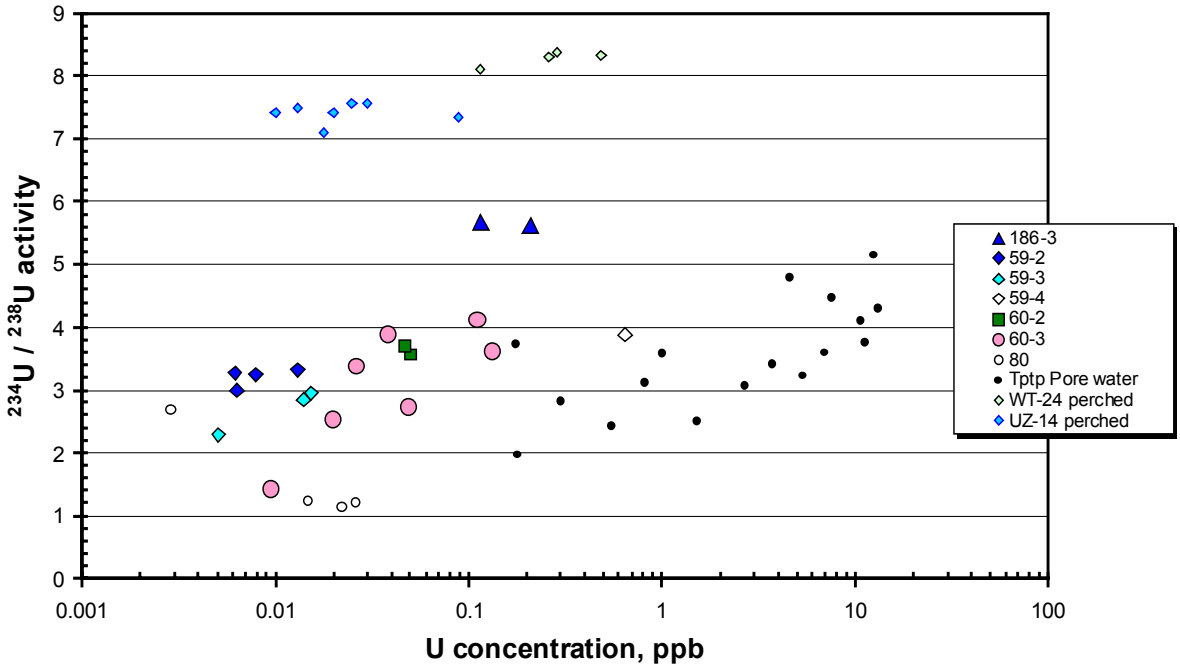

NOTE: Analytical errors are typically smaller than the size of the symbols. Pore waters and perched waters shown for comparison.

Figure 6.3.4.4-1. Uranium Concentrations and Isotopic Compositions of Water Samples Collected from the DST

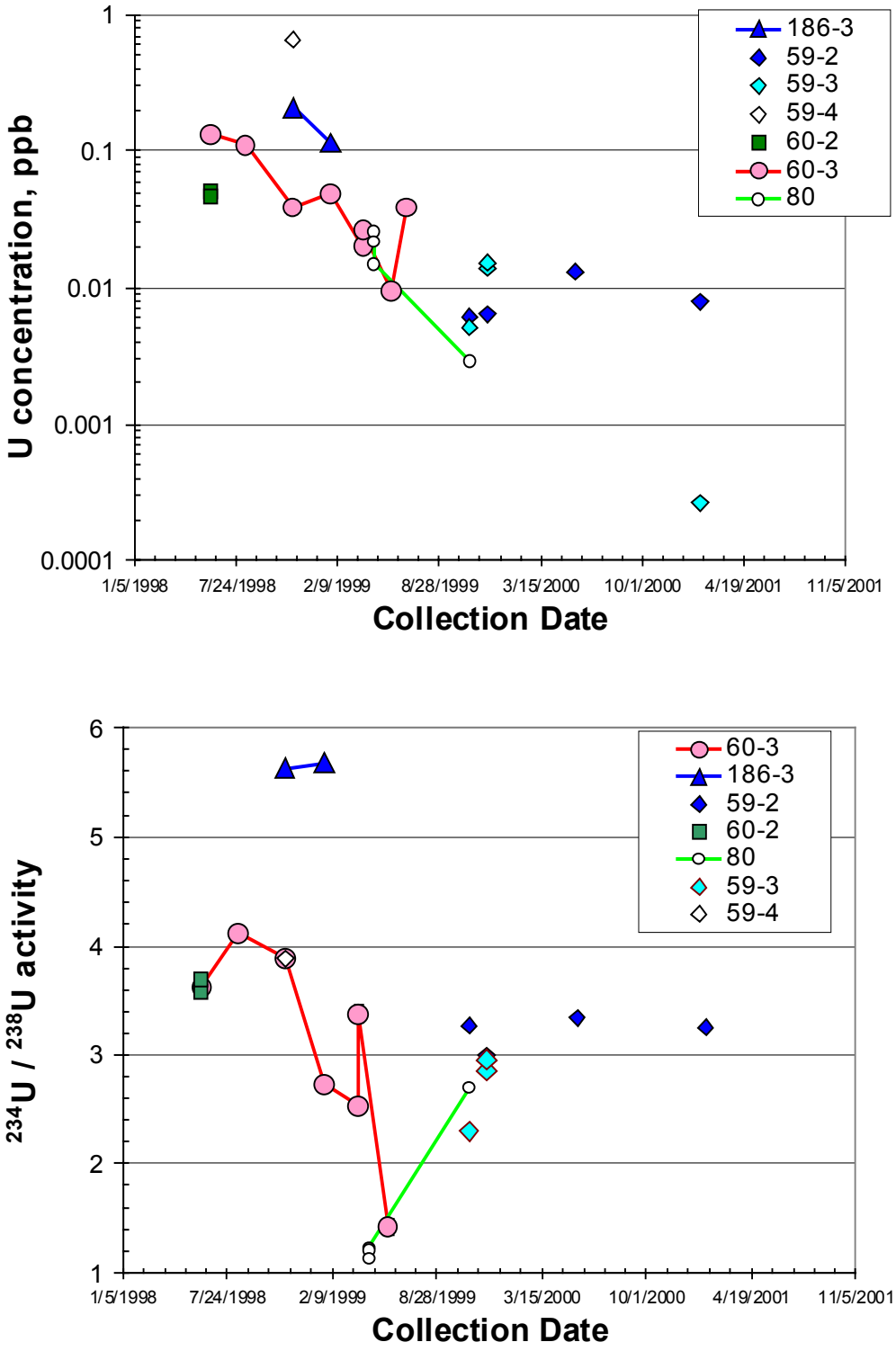

Figure 6.3.4.4-2 U Concentration (upper) and $^{234}U/^{238}U$ Activity Ratios (lower) in DST Samples Plotted versus Collection Date

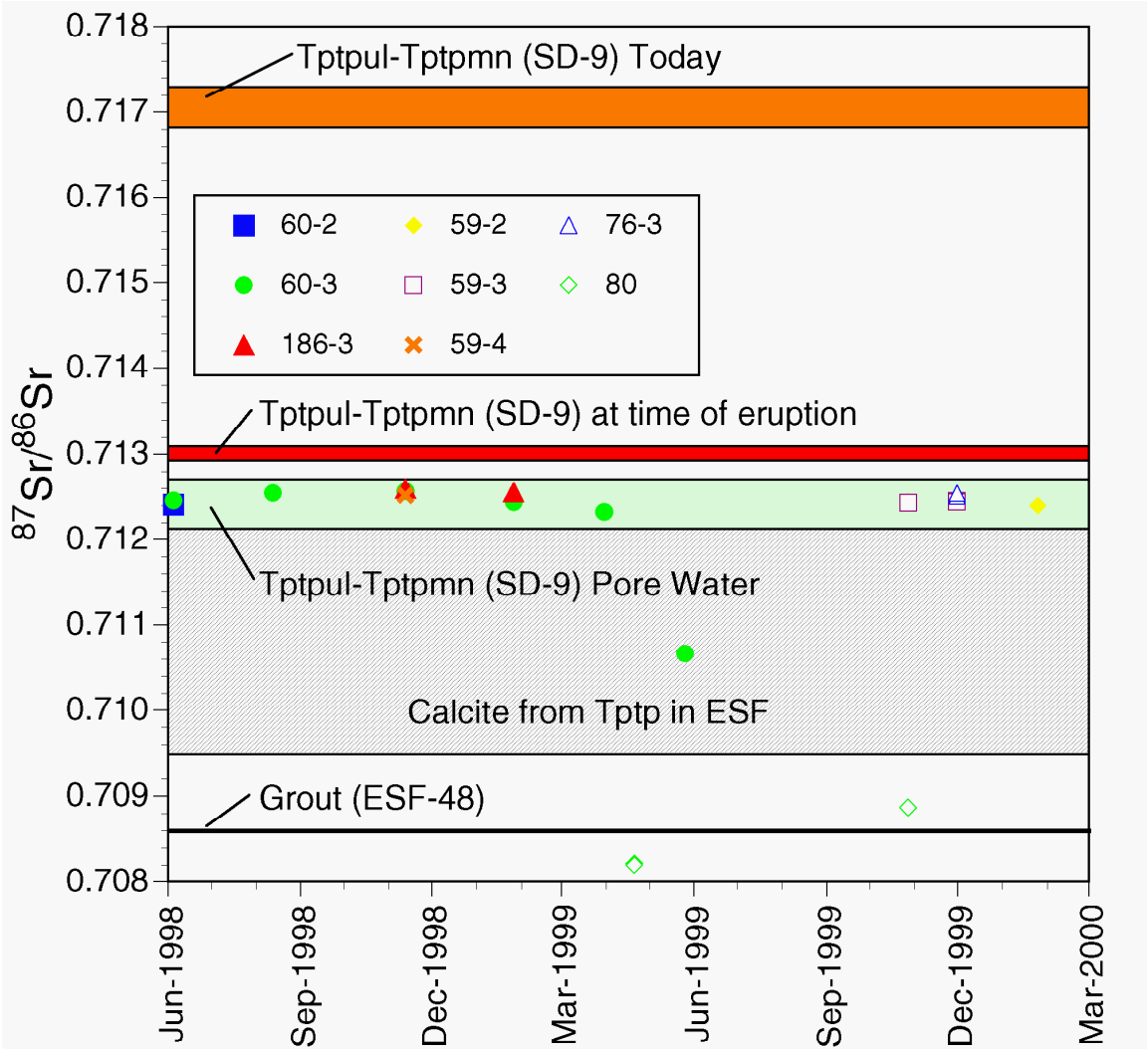

NOTE: The calcite field should extend to overlap the pore water field.

Figure 6.3.4.4-3. Strontium Isotope Ratio Compositions of Water Samples Collected from DST Boreholes Compared to Compositions of Pore Water, Rock, Calcite, and Grout

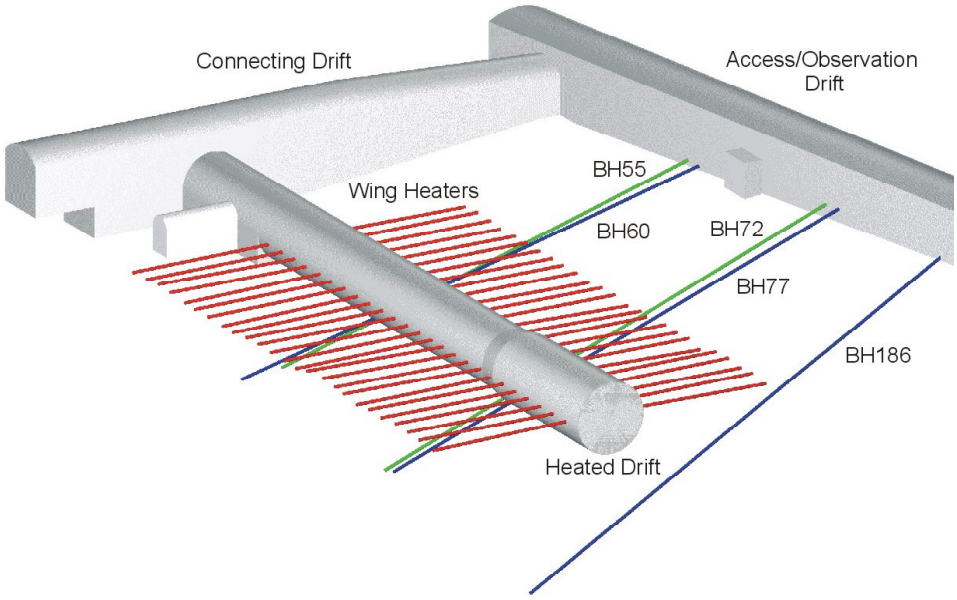

Figure 6.3.4.5-1. Three-Dimensional View of the DST Showing the Hydrology Boreholes (blue) that Contain Fluoroelastomer Packers, Wing Heater Boreholes (red), and FLUTe™ (Chemistry or SEAMIST™) Boreholes (green)

INTENTIONALLY LEFT BLANK

Table 6.3-1. Output-DTNs along with Input-DTNs for the Drift Scale Test

Input-DTN [DIRS]	Input-DTN Description	Input-DTN Text Location	Output-DTN	Output-DTN Description
MO0002ABBLSLDS.000 [147304]	XYZ Coordinates of Boreholes and Sensors	6.3	MO0208RESTRDST.002	Heater Power and Temperature Data
MO9807DSTSET01.000 [113644]	Heater, Power, Current, Voltage, Temperature: November 7, 1997 – May 1998	6.3.1.1 6.3.1.2		
MO9810DSTSET02.000 [113662]	Heater, Power, Current, Voltage, Temperature: June 1998 – August 1998	6.3.1.1 6.3.1.2		
MO9906DSTSET03.000 [113673]	Heater, Power, Current, Voltage, Temperature: September 1998 – May 1999	6.3.1.1 6.3.1.2		
MO0001SEPDSTPC.000 [153836]	Heater, Power, Current, Voltage, Temperature: June 1999 – October 1999	6.3.1.1 6.3.1.2		
MO0007SEPDSTPC.001 [153707]	Heater, Power, Current, Voltage, Temperature: November 1999 – May 2000	6.3.1.1 6.3.1.2		
MO0012SEPDSTPC.002 [153708]	Heater, Power, Current, Voltage, Temperature: June 2000 – November 2000	6.3.1.1 6.3.1.2		
MO0107SEPDSTPC.003 [158321]	Heater, Power, Current, Voltage, Temperature: December 2000 – May 2001	6.3.1.1 6.3.1.2		
MO0202SEPDSTTV.001 [158320]	Heater, Power, Current, Voltage, Temperature: June 2001 – January 14, 2002	6.3.1.1 6.3.1.2		
SNL22100196001.006 [158213]	Thermal Conductivity as Function of Saturation	6.3.1.3	Unchanged-DTN	Unchanged-DTN
SN0203L2210196.007 [158322]	Thermal Expansion Thermal Conductivity DST Specimens	6.3.1.3	Unchanged-DTN	Unchanged-DTN
LL980411004244.060 [159107]	DST Baseline REKA Probe Measurements. Temperature Measurements using REKA Probes: 11/14/97 - 7/31/98.	6.3.1.4	Unchanged-DTN	Unchanged-DTN
LL980411104244.061 [159111]	DST Baseline REKA Probe Measurements for Thermal Conductivity and Diffusivity. VA Supporting Data	6.3.1.4	Unchanged-DTN	Unchanged-DTN
LL980902104244.070 [159109]	DST Baseline REKA Probe Measurements for Thermal Conductivity and Diffusivity. Probe 1 from Borehole #153, Probe 2 from Borehole #152, Probe 3 from Hole #151.	6.3.1.4	Unchanged-DTN	Unchanged-DTN

Table 6.3-1. Output-DTNs along with Input-DTNs for the Drift Scale Test (continued)

Input-DTN [DIRS]	Input-DTN Description	Input-DTN Text Location	Output-DTN	Output-DTN Description
UN0106SPA013GD.003 [159115]	DST REKA Probe Acquired Data for Thermal Conductivity and Diffusivity: 05/01/1998 to 04/30/2001	6.3.1.4	Unchanged-DTN	Unchanged-DTN
UN0106SPA013GD.004 [159116]	DST REKA Probe Developed Data for Thermal Conductivity and Diffusivity: 05/01/1998 to 04/30/2001	6.3.1.4	Unchanged-DTN	Unchanged-DTN
UN0109SPA013GD.005 [159117]	DST Rapid Evaluation of K and Alpha (REKA) Probe Acquired Data for Thermal Conductivity and Diffusivity: 05/01/2001 to 08/31/2001	6.3.1.4	Unchanged-DTN	Unchanged-DTN
UN0112SPA013GD.006 [159118]	DST REKA Probe Acquired Data for Thermal Conductivity and Diffusivity: 09/01/2001 to 12/31/2001	6.3.1.4	Unchanged-DTN	Unchanged-DTN
UN0201SPA013GD.007 [159119]	DST REKA Probe Developed Data for Thermal Conductivity and Diffusivity: 05/01/2001 to 12/31/2001	6.3.1.4	Unchanged-DTN	Unchanged-DTN
LL000804023142.009 [158325]	Water Saturation	6.3.2.1	LL020801723142.028	ERT Tomograms
LL980108804244.052 [158332]	Electrical Resistivity	6.3.2.1		
LL980406404244.057 [113782]	Electrical Resistance Tomography	6.3.2.1		
LL990702704244.099 [113872]	Electrical Resistivity	6.3.2.1		
LL980808604244.065 [113791]	Electrical Resistance Tomography	6.3.2.1.		
LB990630123142.005 [129274]	Ground Penetrating Radar Data	6.3.2.2	LB0208GPRDSTHP.001	GPR Velocity Tomograms
LB000121123142.004 [158338]	Ground Penetrating Radar Data	6.3.2.2		
LB000718123142.004 [153354]	Ground Penetrating Radar Data	6.3.2.2		
LB0101GPRDST01.001 [158346]	Ground Penetrating Radar Data	6.3.2.2		
LB0108GPRDST05.001 [158440]	Ground Penetrating Radar Data	6.3.2.2		
LL020710223142.024 [159551]	Neutron Logging	6.3.2.3	Unchanged-DTN	Unchanged-DTN
LB970600123142.001 [105589]	Active DST Pre-Heating Air Injection, Part 1 of 2	6.3.2.4	LB0208AIRKDSTH.001	Permeability Data
LB980120123142.005 [114134]	Active DST Pre-Heating Air Injection, Part 2 of 2	6.3.2.4		
LB980120123142.004 [105590]	Active Baseline Air Injections in Boreholes 57-61, 74-78, 185-186	6.3.2.4		

Table 6.3-1. Output-DTNs along with Input-DTNs for the Drift Scale Test (continued)

Input-DTN [DIRS]	Input-DTN Description	Input-DTN Text Location	Output-DTN	Output-DTN Description
LB980420123142.002 [113706]	Active Hydrology Testing for Boreholes 57-61, 74-78, 185-186; Air Injection and Gas Tracer Tests	6.3.2.4	LB0208AIRKDSTH.001 (continued)	Permeability Data (continued)
LB980715123142.002 [113742]	Active Hydrology Testing Data (Air Injection) Collected from 12 Hydrology Boreholes: March 1998 to May 1998	6.3.2.4		
LB981016123142.002 [129245]	Active Hydrology Testing for Boreholes 57-61, 74-78, 185-186; Air Injection Tests: June 1998 to August 1999	6.3.2.4		
LB990630123142.001 [129247]	Active Hydrology Testing by Air Injection: September 1998 to May 1999	6.3.2.4		
LB000121123142.002 [158337]	Active Hydrology Testing by Air Injection: June 1999 to October 1999	6.3.2.4		
LB000718123142.002 [158341]	Active Hydrology Testing Data (Air Injection) Collected from 12 Hydrology Holes: November 1, 1999 to May 31, 2000	6.3.2.4		
LB0101AIRKDST1.001 [158345]	Active Hydrology Testing Data (Air Injection) Collected from 12 Hydrology Boreholes: June 1, 2000 to November 30, 2000	6.3.2.4		
LB0108AIRKDST5.001 [158438]	Active Hydrology Testing Data (Air Injection) Collected from 12 Hydrology Boreholes: December 1, 2000 to May 31, 2001	6.3.2.4		
LB0203AIRKDSTE.001 [158348]	Active Hydrology Testing Data (Air Injection) Collected from 12 Hydrology Boreholes: June 1, 2001 to January 2002	6.3.2.4		
LB980420123142.001 [113696]	Passive Monitoring Data for Boreholes 57-61, 74-78, 185-186: Nov 1997 to Feb 1998	6.3.2.4	LB0208H2ODSTHP.001	Passive Hydrological Monitoring Data of Temperature, Relative Humidity and Pressure in the Hydrology Boreholes
LB980715123142.001 [113733]	Passive Monitoring Data Collected from 12 Hydrology Boreholes: March 1998 to May 1998	6.3.2.4		
LB981016123142.001 [158353]	Passive Monitoring Data for Boreholes 57-61, 74-78, 185-186 Taken from June 1998 to Aug 1998, 3rd Quarter	6.3.2.4		

Table 6.3-1. Output-DTNs along with Input-DTNs for the Drift Scale Test (continued)

Input-DTN [DIRS]	Input-DTN Description	Input-DTN Text Location	Output-DTN	Output-DTN Description
LB990630123142.002 [158355]	Passive Monitoring Data (Relative Humidity, Pressure, Temperature): September 1998 to May 1999	6.3.2.4	LB0208H2ODSTHP.001 (continued)	Passive Hydrological Monitoring Data of Temperature, Relative Humidity and Pressure in the Hydrology Boreholes (continued)
LB000121123142.001 [158335]	Passive Monitoring Data (Relative Humidity, Pressure, Temperature): June 1 through October 31, 1999	6.3.2.4		
LB000718123142.001 [158340]	Passive Monitoring Data Collected from 12 Hydrology Boreholes Test: November 1, 1999 to May 31, 2000	6.3.2.4		
LB0101H2ODST01.001 [158347]	Passive Monitoring Data Collected from 12 Hydrology Boreholes: June 1, 2000 to November 30, 2000	6.3.2.4		
LB0108H2ODST05.001 [158441]	Passive Monitoring Data Collected from 12 Hydrology Boreholes: Dec. 1, 2000 to May 31, 2001	6.3.2.4		
LB0203H2ODSTEH.001 [158351]	Passive Monitoring Data Collected from 12 Hydrology Boreholes: June 1, 2001 through end of Heating Phase Jan. 14, 2002	6.3.2.4		
LB980912332245.002 [105593]	Gas Tracer Test and Estimated Porosity	6.3.2.4	Unchanged-DTN	Unchanged-DTN
LB970500123142.003 [131500]	Laboratory Saturation, Porosity, Bulk Density, Particle Density, Gravimetric Water Content Data from Dry Drilled and wet drilled Cores in the DST and SHT	6.3.2.5	Unchanged-DTN	Unchanged-DTN
LL970709004244.035 [127312]	Laboratory Moisture Retention and Porosity	6.3.2.5	Unchanged-DTN	Unchanged-DTN
LL020502523142.020 [159105]	Laboratory Measured Electrical Properties of the DST Samples as a Function of Saturation at 95ºC	6.3.2.5	Unchanged-DTN	Unchanged-DTN
LL981109904242.072 [118959]	Saturated and Dry Bulk Density Permitivity	6.3.2.5	Unchanged-DTN	Unchanged-DTN
SNF39012298002.002 [159114]	Measurements of Displacement Data for the Drift Scale Test (with results from 11/1/1997 through 5/31/1998)	6.3.3.1 6.3.3.2	Unchanged-DTN	Unchanged-DTN

Table 6.3-1. Output-DTNs along with Input-DTNs for the Drift Scale Test (continued)

Input-DTN [DIRS]	Input-DTN Description	Input-DTN Text Location	Output-DTN	Output-DTN Description
SNF39012298002.006 [158419]	MPBX and CDEX Displacement June 1998 – August 1998	6.3.3.1 6.3.3.2	SN0207F3912298.037 and SN0208F3912298.039	Smoothed Displacement Data and Rock Mass Thermal Expansion
SNF39012298002.010 [158367]	MPBX and CDEX Displacement September 1998 – May 1999	6.3.3.1 6.3.3.2		
SN0001F3912298.014 [153841]	MPBX and CDEX Displacement June 1999 – October 1999	6.3.3.1 6.3.3.2		
SN0007F3912298.018 [158374]	MPBX and CDEX Displacement November 1999 – May 2000	6.3.3.1 6.3.3.2		
SN0101F3912298.024 [158400]	MPBX and CDEX Displacement June 2000 – November 2000	6.3.3.1 6.3.3.2		
SN0107F3912298.029 [158408]	MPBX and CDEX Displacement December 2000 – May 2001	6.3.3.1 6.3.3.2		
SN0203F3912298.033 [158361]	MPBX and CDEX Displacement June 2001 – January 14, 2002	6.3.3.1 6.3.3.2		
SNF39012298002.004 [153837]	MPBX and CDEX Displacement Corrected for Thermal Expansion November 9 1997 – May 1998	6.3.3.1 6.3.3.2		
SNF39012298002.008 [153839]	MPBX and CDEX Displacement Corrected for Thermal Expansion June 1998 – August 1998	6.3.3.1 6.3.3.2		
SNF39012298002.012 [153840]	MPBX and CDEX Displacement Corrected for Thermal Expansion September 1998 – May 1999	6.3.3.1 6.3.3.2		
SN0001F3912298.016 [153842]	MPBX and CDEX Displacement Corrected for Thermal Expansion June 1999 – October 1999	6.3.3.1 6.3.3.2		
SN0007F3912298.020 [158388]	MPBX and CDEX Displacement Corrected for Thermal Expansion November 1999 – May 2000	6.3.3.1 6.3.3.2		
SN0101F3912298.026 [158402]	MPBX and CDEX Displacement Corrected for Thermal Expansion June 2000 – November 2000	6.3.3.1 6.3.3.2		
SN0107F3912298.031 [158413]	MPBX and CDEX Displacement Corrected for Thermal Expansion December 2000 – May 2001	6.3.3.1 6.3.3.2		

Table 6.3-1. Output-DTNs along with Input-DTNs for the Drift Scale Test (continued)

Input-DTN [DIRS]	Input-DTN Description	Input-DTN Text Location	Output-DTN	Output-DTN Description
SN0203F3912298.035 [158363]	MPBX and CDEX Displacement Corrected for Thermal Expansion June 2001 – January 14, 2002	6.3.3.1 6.3.3.2	SN0207F3912298.037 and SN0208F3912298.039 (continued)	Smoothed Displacement Data and Rock Mass Thermal Expansion (continued)
SNF38040197001.001 [159130]	Strain-gage and Anchor Locations	6.3.3.3	Unchanged	Unchanged
SNF39012298002.003 [158417]	Ground Support System Strain: November 9, 1997 – May 1998	6.3.3.3	SN0208F3912298.038	Smoothed Strain Data
SNF39012298002.007 [158365]	Ground Support System Strain: June 1998 – August 1998	6.3.3.3		
SNF39012298002.011 [158368]	Ground Support System Strain: September 1998 – May 1999	6.3.3.3		
SN0001F3912298.015 [158372]	Ground Support System Strain: June 1999 – October 1999	6.3.3.3		
SN0007F3912298.019 [158387]	Ground Support System Strain: November 1999 – May 2000	6.3.3.3		
SN0101F3912298.025 [158401]	Ground Support System Strain: June 2000 – November 2000	6.3.3.3		
SN0107F3912298.030 [158409]	Ground Support System Strain: December 2000 – May 2001	6.3.3.3		
SN0203F3912298.034 [158362]	Ground Support System Strain: June 2001 – January 14, 2002	6.3.3.3		
SNF39012298002.005 [158418]	Ground Support System Strain Corrected for Thermal Expansion: November 9, 1997 – May 1998	6.3.3.3		
SNF39012298002.009 [158366]	Ground Support System Strain Corrected for Thermal Expansion: June 1998 – August 1998	6.3.3.3		
SNF39012298002.013 [158369]	Ground Support System Strain Corrected for Thermal Expansion: September 1998 – May 1999	6.3.3.3		
SN0001F3912298.017 [158373]	Ground Support System Strain Corrected for Thermal Expansion: June 1999 – October 1999	6.3.3.3		
SN0007F3912298.021 [158391]	Ground Support System Strain Corrected for Thermal Expansion: November 1999 – May 2000	6.3.3.3		

Table 6.3-1. Output-DTNs along with Input-DTNs for the Drift Scale Test (continued)

Input-DTN [DIRS]	Input-DTN Description	Input-DTN Text Location	Output-DTN	Output-DTN Description
SN0101F3912298.027 [158407]	Ground Support System Strain Corrected for Thermal Expansion: June 2000 – November 2000	6.3.3.3	SN0203F3912298.038 (continued)	Smoothed Strain Data (continued)
SN0107F3912298.032 [158414]	Ground Support System Strain Corrected for Thermal Expansion: December 2000 – May 2001	6.3.3.3		
SN0203F3912298.036 [158364]	Ground Support System Strain Corrected for Thermal Expansion: June 2001 – January 14, 2002	6.3.3.3		
LB980120123142.007 [158352]	Acoustic Emissions: Baseline and Heating	6.3.3.4	LB0208ACEMDSTH.001	Acoustic Emissions: Baseline and Heating
LB980420123142.004 [113717]	Acoustic Emissions: Baseline and Heating	6.3.3.4		
LB990630123142.004 [158360]	Acoustic Emissions: Baseline and Heating	6.3.3.4		
LB000121123142.005 [158339]	Acoustic Emissions: Baseline and Heating	6.3.3.4		
LB000718123142.005 [158343]	Acoustic Emissions: Baseline and Heating	6.3.3.4		
LB0101ACEMDST1.001 [158344]	Acoustic Emissions: Baseline and Heating	6.3.3.4		
LB0108ACEMDST5.001 [158437]	Acoustic Emissions: Baseline and Heating	6.3.3.4		
SNL23030598001.003 [158422]	Creep Testing of Concrete Liner	6.3.3.5	Unchanged-DTN	Unchanged-DTN
SN020312210196.007 [158322]	Laboratory Thermal Expansion	6.3.3.5	Unchanged-DTN	Unchanged-DTN
SNL02100196001.001 [158420]	Elastic Constants and Strength Properties	6.3.3.5	Unchanged-DTN	Unchanged-DTN
SNL23030598001.001 [158370]	Elastic Constants and Strength of Concrete	6.3.3.5	Unchanged-DTN	Unchanged-DTN
SN0011F3912298.022 [158392]	Rock Mass Displacement Pressure Data Plate Load Test October 16-17 2000	6.3.3.6	Unchanged-DTN	Unchanged-DTN
SN0011F3912298.023 [158399]	Rock Mass Displacement Pressure Data in Modulus October 16-17 2000	6.3.3.6	Unchanged-DTN	Unchanged-DTN
GS970608314224.007 [158430]	Rock Mass Rating and Rock Mass Quality	6.3.3.6	Unchanged-DTN	Unchanged-DTN
SNF32020196001.010 [158314]	Rock Mass Quality	6.3.3.6	Unchanged-DTN	Unchanged-DTN
SNF32020196001.015 [158434]	Rock Mass Quality	6.3.3.6	Unchanged-DTN	Unchanged-DTN

Table 6.3-1. Output-DTNs along with Input-DTNs for the Drift Scale Test (continued)

Input-DTN [DIRS]	Input-DTN Description	Input-DTN Text Location	Output-DTN	Output-DTN Description
MO0207AL5WATER.001 [159300]	Water Sampling in Alcove 5 (Results from 2/4/1997 through 4/20/1999).	6.3.4.1	SN0208F3903102.002	Field Water Sampling and Chemistry
MO0101SEPFDDST.000 [153711]	Field Measured Data of Water Samples from the Drift Scale Test	6.3.4.1		
SN0203F3903102.001 [159133]	Drift Scale Test Water Sampling (with Results from 4/17/2001 through 1/14/2002)	6.3.4.1		
MO0005PORWATER.000 [150930]	Perm-Sample Pore Water Data	6.3.4.1	Unchanged-DTN	Unchanged-DTN
LL001100931031.008 [153288]	Aqueous Chemistry of Water Sampled from Boreholes of the Drift Scale Test (DST)	6.3.4.1	LL020709923142.023*	Water Chemistry
LL001200231031.009 [153616]	Aqueous Chemistry of Water Sampled from Boreholes of the Drift Scale Test (DST)	6.3.4.1		
LL020302223142.015 [159134]	Aqueous Geochemistry of DST Samples Collected from HYD Boreholes.	6.3.4.1		
LL020405123142.019 [159307]	Aqueous Geochemistry of Condensed Fluids Collected During Studies of Introduced Materials	6.3.4.1		
LB980420123142.005 [111471]	Isotope Data for CO_2 from Gas Samples Collected from DST: February 1998	6.3.4.2	LB0208ISODSTHP.001	Gas Chemistry (CO_2 Concentration and Isotopic Data)
LB980715123142.003 [111472]	Isotope Data for CO_2 from Gas Samples Collected from DST: June 4, 1998	6.3.4.2		
LB981016123142.004 [113278]	Isotope Data for CO_2 from Gas and Water Samples: June 1998 to September 1998	6.3.4.2		
LB990630123142.003 [111476]	Isotope Data for CO_2 from Gas and Water Samples: September 1998 to May 1999.	6.3.4.2		
LB000121123142.003 [146451]	Isotope Data for CO_2 Gas Samples Collected from the Hydrology Boreholes: August 9, 1999 Through November 30, 1999	6.3.4.2		
LB000718123142.003 [158342]	Isotope Data for CO_2 Gas Samples Collected from the Hydrology Boreholes: April 18, 2000 Through April 19, 2000.	6.3.4.2		

Table 6.3-1. Output-DTNs along with Input-DTNs for the Drift Scale Test (continued)

Input-DTN [DIRS]	Input-DTN Description	Input-DTN Text Location	Output-DTN	Output-DTN Description
LB0102CO2DST98.001 [159306]	Concentration and Isotope Data for CO_2 and H_20 from Gas Samples Collected from Hydrology Boreholes: May and August 1999, April 2000, January and April 2001	6.3.4.2	LB0208ISODSTHP.001 (continued)	Gas Chemistry (CO_2 Concentration and Isotopic Data) (continued)
LB0108CO2DST05.001 [156888]	Concentration and Isotope Data for CO_2 and H_20 from Gas Samples Collected from Hydrology Boreholes: May and August 1999, April 2000, January and April 2001	6.3.4.2		
LB0203CO2DSTEH.001 [158349]	Concentration/Isotope Data for CO_2/H_20 from Gas Samples Collected from Hydrology Boreholes up to End of Heating	6.3.4.2		
LB0206C14DSTEH.001 [159303]	Carbon 14 Isotope Data from CO_2 Gas Samples Collected from DST	6.3.4.2		
LA9912SL831151.002 [146449]	Percent Coverage By Fracture-Coating Minerals in Core ESF-HD-TEMP-2	6.3.4.3	Unchanged-DTN	Unchanged-DTN
LA0201SL831225.001 [158426]	Chemical, Textural, and Mineralogical Characteristics of Sidewall Samples from the Drift Scale Test.	6.3.4.3	Unchanged-DTN	Unchanged-DTN
LA0009SL831151.001 [153485]	Fracture Mineralogy of the ESF Single Heater Test Block, Alcove 5	6.3.4.3	Unchanged-DTN	Unchanged-DTN
LA0201SL831225.001 [158426]	Chemical, Textural, and Mineralogical Characteristics of Sidewall Samples from the Drift Scale Test.	6.3.4.3	Unchanged-DTN	Unchanged-DTN
GS011108312322.008 [159136]	Uranium Concentrations and 234u/238u Activity Ratios Analyzed Between February 1, 1999 and August 1, 2001 for Drift-Scale Heater Test Water Collected Between June 1998 and April 2001, and Pore Water Collected Between March 1996 and April 1999.	6.3.4.4	Unchanged-DTN	Unchanged-DTN
GS011108312322.009 [159137]	Strontium Isotope Ratios and Strontium Concentrations in Water Samples from the Drift Scale Test Analyzed from March 16, 1999 to June 27, 2001.	6.3.4.4	Unchanged-DTN	Unchanged-DTN

Table 6.3-1. Output-DTNs along with Input-DTNs for the Drift Scale Test (continued)

Input-DTN [DIRS]	Input-DTN Description	Input-DTN Text Location	Output-DTN	Output-DTN Description
SN0203F3903102.001 [159133]	Drift Scale Test Water Sampling (With Results from 4/17/2001 Through 1/14/2002)	6.3.4.5	SN0208F3903102.003	Field Hydrogen Fluoride (HF) Data
LL020405123142.019 [159307]	Aqueous Geochemistry of Condensed Fluids Collected During Studies of Introduced Materials.	6.3.4.5		
LARO831422AQ97.002 [158431]	DST Borehole Video Logging	6.3.5.2	Unchanged-DTN	Unchanged-DTN

NOTE: * This data set was submitted as non-Q because of the preliminary status of a subset of data. That subset of data should only be used for corroborative purposes.

Table 6.3-2. DST As-Built Borehole, Sensor, and Heater Information[1]

Borehole Number	Borehole Identification	Primary Purpose	Collar Coordinates (meters) [2] x meters	y meters	z meters	Bottom Coordinates (meters) [2] x meters	y meters	z meters	Orientation Degree	Diameter cm	Length [3] meters	Volume m^3	Types and No. of Sensors: Thermo-Couples	RTD	Thermistors	REKA	Mech. MPBX, RSG	Neutron	Humidity Sensor	Pressure Transducer	Electrode [5] Sensor (ERT)	Chemical	Electrical Amps.
BOREHOLES																							
42	ESF-SDM-MPBX-1	MPBX - Rock Mass Displacement	-29.304	13.820	4.631	-3.555	13.688	-0.371	-11.0	7.57	26.23	0.12	14		1		6						
43	ESF-SDM-MPBX-2	MPBX - Rock Mass Displacement	-29.166	21.062	5.073	-3.424	20.743	0.356	-10.4	7.57	26.17	0.12	14		1		6						
44	ESF-SDM-MPBX-3	MPBX - Rock Mass Displacement	-29.539	32.079	5.137	-3.600	32.192	-0.372	-12.0	7.57	26.52	0.12	14		1		6						
45	ESF-HD-ERT-1	Electrical Resistivity Tomography	-28.875	4.577	4.118	9.565	4.674	13.693	14.0	7.57	39.62	0.18									41		
46	ESF-HD-ERT-2	Electrical Resistivity Tomography	-27.408	4.572	1.533	9.093	4.533	-14.333	-23.5	7.57	39.80	0.18									41		
47	ESF-HD-NEU-1	Neutron Probe / GPR	-29.114	6.385	4.636	7.166	6.338	21.099	24.4	7.57	39.84	0.18						1					
48	ESF-HD-NEU-2	Neutron Probe / GPR	-29.051	6.391	4.042	9.515	6.260	13.545	13.8	7.57	39.72	0.18						1					
49	ESF-HD-NEU-3	Neutron Probe / GPR	-29.039	6.377	3.435	10.841	6.703	7.714	6.1	7.57	40.11	0.18						1					
50	ESF-HD-NEU-4	Neutron Probe / GPR	-29.012	6.395	2.558	9.680	6.419	-8.126	-15.4	7.57	40.14	0.18						1					
51	ESF-HD-NEU-5	Neutron Probe / GPR	-28.993	6.414	2.254	8.072	6.687	-11.996	-21.0	7.57	39.71	0.18						1					
52	ESF-HD-CHE-1	Chemistry - SEAMIST	-29.211	8.247	4.540	7.405	8.293	20.070	23.0	9.60	39.77	0.29										11	
53	ESF-HD-CHE-2	Chemistry - SEAMIST	-29.232	8.258	4.014	9.415	8.702	13.889	14.3	9.60	39.89	0.29										6	
54	ESF-HD-CHE-3	Chemistry - SEAMIST	-29.139	8.227	3.434	10.332	8.375	6.906	5.0	9.60	39.62	0.29										13	
55	ESF-HD-CHE-4	Chemistry - SEAMIST	-29.233	8.224	2.583	5.087	7.976	-7.547	-16.4	9.60	35.78	0.26										12	
56	ESF-HD-CHE-5	Chemistry - SEAMIST	-29.223	8.248	2.322	7.264	8.456	-13.833	-23.9	9.60	39.90	0.29										12	
57	ESF-HD-HYD-1	Hydrology	-28.841	10.054	4.748	7.773	9.825	19.805	22.4	7.57	39.59	0.18		4					4	4			
58	ESF-HD-HYD-2	Hydrology	-28.951	10.017	4.114	9.567	9.961	13.627	13.9	7.57	39.68	0.18		3					3	3			
59	ESF-HD-HYD-3	Hydrology	-29.071	10.044	3.453	10.248	10.045	7.227	5.5	7.57	39.50	0.18		4					4	4			
60	ESF-HD-HYD-4	Hydrology	-29.107	10.003	2.707	9.213	9.259	-7.328	-14.7	7.57	39.62	0.18		4					4	4			
61	ESF-HD-HYD-5	Hydrology	-29.193	10.062	2.337	8.215	10.184	-12.022	-21.0	7.57	40.07	0.18		4					4	4			
62	ESF-HD-ERT-3	Electrical Resistivity Tomography	-29.238	24.703	6.307	10.095	24.853	13.169	9.9	7.57	39.93	0.18									41		
63	ESF-HD-ERT-4	Electrical Resistivity Tomography	-29.284	24.690	4.730	7.004	25.015	-11.927	-24.7	7.57	39.93	0.18									41		
64	ESF-HD-NEU-6	Neutron Probe / GPR	-29.311	26.519	6.639	8.073	26.437	20.795	20.7	7.57	39.97	0.18						1					
65	ESF-HD-NEU-7	Neutron Probe / GPR	-29.341	26.524	6.310	9.937	26.650	13.715	10.7	7.57	39.97	0.18						1					
66	ESF-HD-NEU-8	Neutron Probe / GPR	-29.118	26.506	5.999	10.682	26.580	6.890	1.3	7.57	39.81	0.18						1					
67	ESF-HD-NEU-9	Neutron Probe / GPR	-28.974	26.489	5.222	8.262	25.877	-7.953	-19.5	7.57	39.50	0.18						1					
68	ESF-HD-NEU-10	Neutron Probe / GPR	-29.116	26.550	4.588	6.847	26.856	-12.272	-25.1	7.57	39.72	0.18						1					
69	ESF-HD-CHE-6	Chemistry - SEAMIST	-29.199	28.368	6.842	8.312	28.683	20.044	19.4	7.57	39.77	0.18										10	
70	ESF-HD-CHE-7	Chemistry - SEAMIST	-29.261	28.373	6.315	10.024	29.034	13.092	9.8	7.57	39.87	0.18										11	
71	ESF-HD-CHE-8	Chemistry - SEAMIST	-29.393	28.345	5.964	10.664	27.898	6.244	0.4	9.60	40.06	0.29										13	
72	ESF-HD-CHE-9	Chemistry - SEAMIST	-29.289	28.385	5.467	8.353	28.822	-8.300	-20.1	9.60	40.08	0.29										12	
73	ESF-HD-CHE-10	Chemistry - SEAMIST	-29.062	28.375	4.546	6.628	28.542	-12.589	-25.6	7.57	39.59	0.18										11	
74	ESF-HD-HYD-6	Hydrology	-29.380	30.194	6.811	8.168	30.068	20.601	20.2	7.57	40.00	0.18		4					4	4			
75	ESF-HD-HYD-7	Hydrology	-29.306	30.215	6.303	10.024	30.485	12.913	9.5	7.57	39.88	0.18		4					4	4			
76	ESF-HD-HYD-8	Hydrology	-29.295	30.177	6.002	10.731	30.178	6.737	1.1	7.57	40.03	0.18		4					4	4			
77	ESF-HD-HYD-9	Hydrology	-29.331	30.210	5.672	8.268	29.906	-8.208	-20.3	7.57	40.08	0.18		3					3	3			
78	ESF-HD-HYD-10	Hydrology	-29.376	30.191	4.702	6.165	30.379	-12.850	-26.3	7.57	39.64	0.18		4					4	4			
79	ESF-HD-TEMP-1	Temperature/Neutron	9.460	-11.022	3.752	9.459	48.478	2.706	-1.0	9.60	59.51	0.43		60									
80	ESF-HD-TEMP-2	Temperature/Neutron	-9.486	-11.059	3.228	-9.903	48.570	3.162	-0.1	9.60	59.63	0.43		60									
81	ESF-HD-MPBX-1	MPBX - Rock Mass Displacement	6.994	-11.130	3.463	6.781	34.945	3.326	-0.2	7.57	46.08	0.21	19				6						
82	ESF-HD-MPBX-2	MPBX - Rock Mass Displacement	-7.028	-10.958	3.451	-7.675	35.252	3.128	-0.4	7.57	46.22	0.21	20				6						
83	ESF-HD-WH-1	Wing Heater	-2.483	1.837	-0.259	-14.005	1.848	-0.325	-0.3	9.60	11.52	0.08	5										
84	ESF-HD-WH-2	Wing Heater	-2.488	3.645	-0.239	-14.030	3.676	-0.182	0.3	9.60	11.54	0.08	5										
85	ESF-HD-WH-3	Wing Heater	-2.470	5.498	-0.248	-14.050	5.529	-0.255	0.0	9.60	11.58	0.08	5										
86	ESF-HD-WH-4	Wing Heater	-2.491	7.310	-0.251	-13.908	7.190	-0.353	-0.5	9.60	11.42	0.08	5										
87	ESF-HD-WH-5	Wing Heater	-2.605	9.154	-0.251	-13.963	9.334	-0.233	0.1	9.60	11.36	0.08	5										
88	ESF-HD-WH-6	Wing Heater	-2.567	10.984	-0.242	-14.007	10.946	-0.249	0.0	9.60	11.44	0.08	5										
89	ESF-HD-WH-7	Wing Heater	-2.778	12.816	-0.239	-14.001	12.881	-0.270	-0.2	9.60	11.22	0.08	5										
90	ESF-HD-WH-8	Wing Heater	-2.517	14.602	-0.269	-14.088	14.507	-0.381	-0.6	9.60	11.57	0.08	5										
91	ESF-HD-WH-9	Wing Heater	-2.512	16.482	-0.234	-13.791	16.640	-0.188	0.2	9.60	11.28	0.08	5										

INTENTIONALLY LEFT BLANK

Table 6.3-2. DST As-Built Borehole, Sensor, and Heater Information[1] (continued)

Borehole Number	Borehole Identification	Primary Purpose	Collar Coordinates (meters) [2]			Bottom Coordinates (meters) [2]			Orientation	Diameter	Length [3]	Volume	Types and No. of Sensors										
			x meters	y meters	z meters	x meters	y meters	z meters	Degree	cm	meters	m^3	Thermo-Couples	RTD	Thermistors	REKA	Mech. MPBX, RSG	Neutron	Humidity Sensor	Pressure Transducer	Electrode [5] Sensor (ERT)	Chemical	Electrical Amps.
92	ESF-HD-WH-10	Wing Heater	-2.537	18.280	-0.260	-14.051	18.171	-0.342	-0.4	9.60	11.51	0.08	5										
93	ESF-HD-WH-11	Wing Heater	-2.447	20.108	-0.274	-13.970	20.104	-0.475	-1.0	9.60	11.52	0.08	5										
94	ESF-HD-WH-12	Wing Heater	-2.475	21.958	-0.246	-13.928	22.088	-0.237	0.0	9.60	11.45	0.08	5										
95	ESF-HD-WH-13	Wing Heater	-2.575	23.777	-0.253	-14.065	23.777	-0.293	-0.2	9.60	11.49	0.08	5										
96	ESF-HD-WH-14	Wing Heater	-2.603	25.617	-0.278	-14.092	25.653	-0.550	-1.4	9.60	11.49	0.08	5										
97	ESF-HD-WH-15	Wing Heater	-2.541	27.451	-0.234	-14.051	27.619	-0.350	-0.6	9.60	11.51	0.08	5										
98	ESF-HD-WH-16	Wing Heater	-2.445	29.241	-0.238	-13.642	29.156	-0.254	-0.1	9.60	11.20	0.08	5										
99	ESF-HD-WH-17	Wing Heater	-2.584	31.126	-0.260	-14.038	31.267	-0.263	0.0	9.60	11.45	0.08	5										
100	ESF-HD-WH-18	Wing Heater	-2.466	32.933	-0.247	-13.995	33.022	-0.311	-0.3	9.60	11.53	0.08	5										
101	ESF-HD-WH-19	Wing Heater	-2.715	34.732	-0.262	-14.062	34.660	-0.281	-0.1	9.60	11.35	0.08	5										
102	ESF-HD-WH-20	Wing Heater	-2.595	36.571	-0.283	-14.000	36.407	-0.621	-1.7	9.60	11.41	0.08	5										
103	ESF-HD-WH-21	Wing Heater	-2.597	38.409	-0.246	-14.167	38.457	-0.160	0.4	9.60	11.57	0.08	5										
104	ESF-HD-WH-22	Wing Heater	-2.613	40.230	-0.250	-14.133	40.306	-0.099	0.8	9.60	11.52	0.08	5										
105	ESF-HD-WH-23	Wing Heater	-2.588	42.092	-0.272	-14.109	42.233	-0.246	0.1	9.60	11.52	0.08	5										
106	ESF-HD-WH-24	Wing Heater	-2.590	43.875	-0.239	-14.109	43.911	-0.155	0.4	9.60	11.52	0.08	5										
107	ESF-HD-WH-25	Wing Heater	-2.567	45.734	-0.260	-14.150	45.795	-0.384	-0.6	9.60	11.58	0.08	5										
108	ESF-HD-WH-26	Wing Heater	2.593	45.737	-0.278	14.083	45.805	-0.489	-1.1	9.60	11.49	0.08	5										
109	ESF-HD-WH-27	Wing Heater	2.581	43.876	-0.251	14.099	43.790	-0.302	-0.3	9.60	11.52	0.08	5										
110	ESF-HD-WH-28	Wing Heater	2.582	42.065	-0.258	14.106	42.121	-0.216	0.2	9.60	11.52	0.08	5										
111	ESF-HD-WH-29	Wing Heater	2.586	40.216	-0.236	14.099	40.278	-0.133	0.5	9.60	11.51	0.08	5										
112	ESF-HD-WH-30	Wing Heater	2.561	38.385	-0.262	14.178	38.316	-0.269	0.0	9.60	11.62	0.08	5										
113	ESF-HD-WH-31	Wing Heater	2.576	36.561	-0.245	14.141	36.476	-0.212	0.2	9.60	11.57	0.08	5										
114	ESF-HD-WH-32	Wing Heater	2.850	34.787	-0.273	14.325	34.970	-0.276	0.0	9.60	11.48	0.08	5										
115	ESF-HD-WH-33	Wing Heater	2.593	32.913	-0.232	14.115	32.667	-0.194	0.2	9.60	11.52	0.08	5										
116	ESF-HD-WH-34	Wing Heater	2.668	31.081	-0.254	13.903	31.031	-0.229	0.1	9.60	11.24	0.08	5										
117	ESF-HD-WH-35	Wing Heater	2.646	29.228	-0.241	13.813	29.165	-0.129	0.6	9.60	11.17	0.08	5										
118	ESF-HD-WH-36	Wing Heater	2.609	27.420	-0.207	14.168	27.390	-0.048	0.8	9.60	11.56	0.08	5										
119	ESF-HD-WH-37	Wing Heater	2.498	25.603	-0.256	14.100	25.657	-0.406	-0.7	9.60	11.60	0.08	5										
120	ESF-HD-WH-38	Wing Heater	2.509	23.775	-0.267	13.979	23.831	-0.377	-0.5	9.60	11.47	0.08	5										
121	ESF-HD-WH-39	Wing Heater	2.451	21.940	-0.272	14.077	21.945	-0.299	-0.1	9.60	11.63	0.08	5										
122	ESF-HD-WH-40	Wing Heater	2.482	20.114	-0.249	14.082	20.122	-0.232	0.1	9.60	11.60	0.08	5										
123	ESF-HD-WH-41	Wing Heater	2.490	18.287	-0.248	14.050	18.275	-0.297	-0.2	9.60	11.56	0.08	5										
124	ESF-HD-WH-42	Wing Heater	2.529	16.434	-0.273	14.025	16.280	-0.514	-1.2	9.60	11.50	0.08	5										
125	ESF-HD-WH-43	Wing Heater	2.509	14.643	-0.288	13.977	14.678	-0.523	-1.2	9.60	11.47	0.08	5										
126	ESF-HD-WH-44	Wing Heater	2.511	12.801	-0.245	14.145	12.865	-0.342	-0.5	9.60	11.63	0.08	5										
127	ESF-HD-WH-45	Wing Heater	2.578	10.949	-0.272	14.056	10.705	-0.441	-0.8	9.60	11.48	0.08	5										
128	ESF-HD-WH-46	Wing Heater	2.515	9.141	-0.260	14.012	9.212	-0.419	-0.8	9.60	11.50	0.08	5										
129	ESF-HD-WH-47	Wing Heater	2.612	7.313	-0.245	14.069	7.108	-0.272	-0.1	9.60	11.46	0.08	5										
130	ESF-HD-WH-48	Wing Heater	2.561	5.504	-0.230	14.011	5.350	-0.177	0.3	9.60	11.45	0.08	5										
131	ESF-HD-WH-49	Wing Heater	2.567	3.672	-0.277	14.078	3.705	-0.326	-0.2	9.60	11.51	0.08	5										
132	ESF-HD-WH-50	Wing Heater	2.648	1.816	-0.264	14.000	1.583	-0.444	-0.9	9.60	11.36	0.08	5										
133	ESF-HD-TEMP-3	Temperature	0.749	2.736	2.397	0.878	2.834	22.465	89.5	7.57	20.07	0.09		67									
134	ESF-HD-TEMP-4	Temperature	0.736	2.734	-1.603	0.635	2.787	-22.938	-89.7	7.57	21.34	0.10		67									
135	ESF-HD-ERT-5	Electrical Resistivity Tomography	-0.763	2.709	2.397	-0.957	2.756	22.399	89.4	7.57	20.00	0.09									21		
136	ESF-HD-ERT-6	Electrical Resistivity Tomography	-0.758	2.740	-1.615	-0.707	2.625	-17.953	-89.6	7.57	16.34	0.07									17		
137	ESF-HD-TEMP-5	Temperature	0.775	11.918	2.510	0.880	11.840	22.463	89.6	7.57	19.95	0.09		67									
138	ESF-HD-TEMP-6	Temperature	-1.983	11.880	1.958	-15.960	11.516	15.926	45.0	7.57	19.76	0.09		67									
139	ESF-HD-TEMP-7	Temperature	-2.569	11.891	-0.017	-22.536	11.953	0.149	0.5	7.57	19.97	0.09		67									
140	ESF-HD-TEMP-8	Temperature	-1.911	11.907	-1.599	-17.366	11.791	-14.661	-40.2	7.57	20.24	0.09		67									
141	ESF-HD-TEMP-9	Temperature	0.764	11.893	-1.637	0.570	12.034	-22.973	-89.4	7.57	21.34	0.10		67									

INTENTIONALLY LEFT BLANK

Table 6.3-2. DST As-Built Borehole, Sensor, and Heater Information[1] (continued)

Borehole Number	Borehole Identification	Primary Purpose	Collar Coordinates (meters) [2]			Bottom Coordinates (meters) [2]			Orientation	Diameter	Length [3]	Volume	Types and No. of Sensors										
			x meters	y meters	z meters	x meters	y meters	z meters	Degree	cm	meters	m^3	Thermo-Couples	RTD	Thermistors	REKA	Mech. MPBX, RSG	Neutron	Humidity Sensor	Pressure Transducer	Electrode [5] Sensor (ERT)	Chemical	Electrical Amps.
142	ESF-HD-TEMP-10	Temperature	1.617	11.912	-1.639	16.017	11.903	-15.924	-44.8	7.57	20.28	0.09		67									
143	ESF-HD-TEMP-11	Temperature	2.665	11.890	-0.008	22.513	11.918	0.022	0.1	7.57	19.85	0.09		67									
144	ESF-HD-TEMP-12	Temperature	2.009	11.915	1.982	16.394	12.063	16.351	45.0	7.57	20.33	0.09		67									
145	ESF-HD-ERT-7	Electrical Resistivity Tomography	-0.757	11.892	2.579	-0.899	12.019	22.667	89.5	7.57	20.09	0.09									21		
146	ESF-HD-ERT-8	Electrical Resistivity Tomography	-0.757	11.894	-1.613	-1.065	11.929	-18.014	-88.9	7.57	16.40	0.07									17		
147	ESF-HD-MPBX-3	MPBX - Rock Mass Displacement	1.284	13.706	2.213	8.682	13.653	15.233	60.4	7.57	14.98	0.07	8				4						
148	ESF-HD-MPBX-4	MPBX - Rock Mass Displacement	-1.390	13.725	2.387	-8.864	13.700	15.172	59.7	7.57	14.81	0.07	8				4						
149	ESF-HD-MPBX-5	MPBX - Rock Mass Displacement	-0.028	13.697	2.484	-0.097	13.608	17.594	89.6	7.57	15.11	0.07	8				4						
150	ESF-HD-MPBX-6	MPBX - Rock Mass Displacement	0.006	13.693	-1.639	0.145	13.807	-18.008	-89.4	7.57	16.37	0.07	8				4						
151	ESF-HD-REKA-1	Thermal Conductivity and Diffusivity	-0.027	17.352	2.669	-0.049	17.348	12.705	89.9	4.80	10.04	0.02				1							
152	ESF-HD-REKA-2	Thermal Conductivity and Diffusivity	-2.437	17.359	0.017	-12.528	17.234	0.078	0.3	4.80	10.09	0.02				1							
153	ESF-HD-REKA-3	Thermal Conductivity and Diffusivity	-1.603	17.359	-1.603	-9.199	17.241	-9.312	-45.4	4.80	10.82	0.02				1							
154	ESF-HD-MPBX-7	MPBX - Rock Mass Displacement	1.285	21.020	2.186	8.867	21.011	15.099	59.6	7.57	14.97	0.07	8				4						
155	ESF-HD-MPBX-8	MPBX - Rock Mass Displacement	-1.317	21.006	2.270	-9.016	20.919	15.268	59.4	7.57	15.11	0.07	8				4						
156	ESF-HD-MPBX-9	MPBX - Rock Mass Displacement	-0.013	21.001	2.504	0.028	20.944	17.482	89.7	7.57	14.98	0.07	8				4						
157	ESF-HD-MPBX-10	MPBX - Rock Mass Displacement	-0.004	21.037	-1.624	0.031	21.014	-17.820	-89.9	7.57	16.20	0.07	8				4						
158	ESF-HD-TEMP-13	Temperature	0.757	22.847	2.565	0.412	23.021	22.599	88.9	7.57	20.04	0.09		67									
159	ESF-HD-TEMP-14	Temperature	-1.949	22.876	1.931	-16.007	22.892	16.157	45.3	7.57	20.00	0.09		67									
160	ESF-HD-TEMP-15	Temperature	-2.502	22.871	-0.004	-22.615	22.956	0.107	0.3	7.57	20.11	0.09		67									
161	ESF-HD-TEMP-16	Temperature	-1.607	22.883	-1.605	-16.040	23.241	-15.875	-44.7	7.57	20.30	0.09		67									
162	ESF-HD-TEMP-17	Temperature	0.769	22.850	-1.623	0.828	23.004	-22.820	-89.6	7.57	21.20	0.10		67									
163	ESF-HD-TEMP-18	Temperature	1.515	22.828	-1.597	15.772	22.510	-15.913	-45.1	7.57	20.21	0.09		67									
164	ESF-HD-TEMP-19	Temperature	2.489	22.869	0.016	22.586	23.017	0.299	0.8	7.57	20.10	0.09		67									
165	ESF-HD-TEMP-20	Temperature	1.862	22.845	1.882	16.004	22.754	16.020	45.0	7.57	20.00	0.09		67									
166	ESF-HD-ERT-9	Electrical Resistivity Tomography	-0.735	22.845	2.566	-0.558	23.020	22.390	89.3	7.57	19.83	0.09									21		
167	ESF-HD-ERT-10	Electrical Resistivity Tomography	-0.772	22.810	-1.637	-0.458	22.747	-17.522	-88.8	7.57	15.89	0.07									17		
168	ESF-HD-TEMP-21	Temperature	-0.071	31.952	2.451	-0.335	31.978	22.650	89.2	7.57	20.00	0.09		67									
169	ESF-HD-TEMP-22	Temperature	-0.003	32.007	-1.629	0.259	32.435	-22.894	-88.6	7.57	21.20	0.10		67									
170	ESF-HD-TEMP-23	Temperature	0.751	39.306	2.488	0.746	39.115	22.604	89.5	7.57	20.12	0.09		67									
171	ESF-HD-TEMP-24	Temperature	-1.853	39.313	1.817	-15.619	39.292	15.716	45.3	7.57	19.56	0.09		67									
172	ESF-HD-TEMP-25	Temperature	-1.581	39.291	-1.571	-16.011	38.870	-16.010	-45.0	7.57	20.42	0.09		67									
173	ESF-HD-TEMP-26	Temperature	0.758	39.324	-1.623	0.715	39.104	-22.887	-89.4	7.57	21.27	0.10		67									
174	ESF-HD-TEMP-27	Temperature	1.584	39.306	-1.586	16.413	38.942	-15.444	-43.1	7.57	20.30	0.09		67									
175	ESF-HD-TEMP-28	Temperature	1.880	39.320	1.843	15.914	39.177	16.275	45.8	7.57	20.13	0.09		67									
176	ESF-HD-ERT-11	Electrical Resistivity Tomography	-0.750	39.296	2.463	-0.779	39.120	22.462	89.5	7.57	20.00	0.09									21		
177	ESF-HD-ERT-12	Electrical Resistivity Tomography	-0.739	39.327	-1.623	-0.749	39.263	-17.823	-89.8	7.57	16.20	0.07									17		
178	ESF-HD-MPBX-11	MPBX - Rock Mass Displacement	1.297	41.138	2.249	8.693	41.103	15.341	60.5	7.57	15.04	0.07	8				4						
179	ESF-HD-MPBX-12	MPBX - Rock Mass Displacement	-1.319	41.143	2.279	-8.785	41.067	15.433	60.4	7.57	15.13	0.07	8				4						
180	ESF-HD-MPBX-13	MPBX - Rock Mass Displacement	0.010	41.134	2.597	0.121	41.079	17.687	89.5	7.57	15.09	0.07	8				4						
181	ESF-HD-MPBX-14	MPBX - Rock Mass Displacement	0.035	41.194	-1.658	0.083	41.211	-18.122	-89.8	7.57	16.46	0.07	8				4						
182	ESF-HD-PERM-1	Ambient Characterization	11.616	-15.677	2.284	11.954	-34.533	-4.367	-19.4	7.57	20.00	0.09											
183	ESF-HD-PERM-2	Ambient Characterization	10.716	-15.649	3.045	10.861	-35.731	3.003	-0.1	7.57	20.08	0.09											
184	ESF-HD-PERM-3	Ambient Characterization	8.853	-15.678	2.298	8.856	-34.504	-4.376	-19.5	7.57	19.97	0.09											
185	ESF-HD-HYD-11	Hydrology	-29.488	44.728	7.563	10.084	44.145	13.613	8.7	7.57	40.04	0.18		4					4	4			
186	ESF-HD-HYD-12	Hydrology	-29.609	44.774	6.470	5.008	44.352	-13.781	-30.3	7.57	40.11	0.18		4					4	4			
187	ESF-PL-MPBX-1	MPBX - Rock Mass Displacement	5.500	-5.000	-0.270	5.500	-7.500	-0.270	0.0	7.57	2.50	0.01	8				4						
188	ESF-PL-MPBX-2	MPBX - Rock Mass Displacement	5.500	-3.000	-0.270	5.500	-0.500	-0.270	0.0	7.57	2.50	0.01	8				4						

INTENTIONALLY LEFT BLANK

Table 6.3-2. DST As-Built Borehole, Sensor, and Heater Information[1] (continued)

Borehole Number	Borehole Identification	Primary Purpose	Collar Coordinates (meters) [2]			Bottom Coordinates (meters) [2]			Orientation	Diameter	Length [3]	Volume	Types and No. of Sensors										
			x meters	y meters	z meters	x meters	y meters	z meters	Degree	cm	meters	m^3	Thermo-Couples	RTD	Thermistors	REKA	Mech. MPBX, RSG	Neutron	Humidity Sensor	Pressure Transducer	Electrode [5] Sensor (ERT)	Chemical	Electrical Amps.
HEATERS																							
	ESF-HD-CAN1[4]	Floor Heater	-0.144	0.565	-0.218	-0.144	5.213	-0.218	NA	NA	NA	NA	9										60
	ESF-HD-CAN2[4]	Floor Heater	-0.156	5.848	-0.237	-0.156	10.496	-0.237	NA	NA	NA	NA	9										60
	ESF-HD-CAN3[4]	Floor Heater	-0.139	11.013	-0.236	-0.139	15.661	-0.236	NA	NA	NA	NA	9										60
	ESF-HD-CAN4[4]	Floor Heater	-0.177	16.305	-0.250	-0.177	20.953	-0.250	NA	NA	NA	NA	9										60
	ESF-HD-CAN5[4]	Floor Heater	-0.165	21.544	-0.251	-0.165	26.192	-0.251	NA	NA	NA	NA	9										60
	ESF-HD-CAN6[4]	Floor Heater	-0.176	26.892	-0.246	-0.176	31.540	-0.246	NA	NA	NA	NA	9										60
	ESF-HD-CAN7[4]	Floor Heater	-0.167	32.077	-0.237	-0.167	36.725	-0.237	NA	NA	NA	NA	9										60
	ESF-HD-CAN8[4]	Floor Heater	-0.148	37.375	-0.225	-0.148	42.023	-0.225	NA	NA	NA	NA	9										60
	ESF-HD-CAN9[4]	Floor Heater	-0.163	42.664	-0.235	-0.163	47.312	-0.235	NA	NA	NA	NA	9										60
	ESF-HD-83-WH1	Wing Heater	-4.263	1.839	-0.269	-14.093	1.848	-0.326	NA	NA	NA	NA											2
	ESF-HD-84-WH2	Wing Heater	-4.208	3.650	-0.231	-14.038	3.676	-0.182	NA	NA	NA	NA											2
	ESF-HD-85-WH3	Wing Heater	-4.250	5.503	-0.249	-14.080	5.529	-0.255	NA	NA	NA	NA											2
	ESF-HD-86-WH4	Wing Heater	-4.081	7.293	-0.265	-13.910	7.190	-0.353	NA	NA	NA	NA											2
	ESF-HD-87-WH5	Wing Heater	-4.175	9.179	-0.249	-14.004	9.335	-0.233	NA	NA	NA	NA											2
	ESF-HD-88-WH6	Wing Heater	-4.137	10.979	-0.243	-13.967	10.946	-0.249	NA	NA	NA	NA											2
	ESF-HD-89-WH7	Wing Heater	-4.348	12.825	-0.243	-14.178	12.882	-0.270	NA	NA	NA	NA											2
	ESF-HD-90-WH8	Wing Heater	-4.267	14.588	-0.286	-14.096	14.507	-0.381	NA	NA	NA	NA											2
	ESF-HD-91-WH9	Wing Heater	-4.292	16.507	-0.227	-14.121	16.645	-0.187	NA	NA	NA	NA											2
	ESF-HD-92-WH10	Wing Heater	-4.237	18.264	-0.272	-14.066	18.171	-0.342	NA	NA	NA	NA											2
	ESF-HD-93-WH11	Wing Heater	-4.127	20.107	-0.303	-13.955	20.104	-0.475	NA	NA	NA	NA											2
	ESF-HD-94-WH12	Wing Heater	-4.035	21.976	-0.245	-13.864	22.087	-0.237	NA	NA	NA	NA											2
	ESF-HD-95-WH13	Wing Heater	-4.255	23.777	-0.259	-14.085	23.777	-0.293	NA	NA	NA	NA											2
	ESF-HD-96-WH14	Wing Heater	-4.233	25.622	-0.317	-14.060	25.653	-0.549	NA	NA	NA	NA											2
	ESF-HD-97-WH15	Wing Heater	-3.691	27.468	-0.246	-13.519	27.611	-0.345	NA	NA	NA	NA											2
	ESF-HD-98-WH16	Wing Heater	-4.115	29.228	-0.240	-13.945	29.154	-0.254	NA	NA	NA	NA											2
	ESF-HD-99-WH17	Wing Heater	-4.184	31.146	-0.260	-14.013	31.267	-0.263	NA	NA	NA	NA											2
	ESF-HD-100-WH18	Wing Heater	-4.186	32.946	-0.257	-14.015	33.022	-0.311	NA	NA	NA	NA											2
	ESF-HD-101-WH19	Wing Heater	-4.215	34.722	-0.265	-14.045	34.660	-0.281	NA	NA	NA	NA											2
	ESF-HD-102-WH20	Wing Heater	-4.204	36.548	-0.331	-14.029	36.407	-0.622	NA	NA	NA	NA											2
	ESF-HD-103-WH21	Wing Heater	-4.267	38.416	-0.234	-14.097	38.457	-0.161	NA	NA	NA	NA											2
	ESF-HD-104-WH22	Wing Heater	-4.313	40.241	-0.228	-14.142	40.306	-0.099	NA	NA	NA	NA											2
	ESF-HD-105-WH23	Wing Heater	-4.018	42.109	-0.269	-13.847	42.230	-0.247	NA	NA	NA	NA											2
	ESF-HD-106-WH24	Wing Heater	-4.260	43.880	-0.227	-14.090	43.911	-0.155	NA	NA	NA	NA											2
	ESF-HD-107-WH25	Wing Heater	-4.267	45.743	-0.278	-14.096	45.795	-0.383	NA	NA	NA	NA											2
	ESF-HD-108-WH26	Wing Heater	4.263	45.747	-0.309	14.091	45.805	-0.489	NA	NA	NA	NA											2
	ESF-HD-109-WH27	Wing Heater	4.211	43.864	-0.258	14.041	43.790	-0.302	NA	NA	NA	NA											2
	ESF-HD-110-WH28	Wing Heater	4.202	42.073	-0.252	14.032	42.121	-0.216	NA	NA	NA	NA											2
	ESF-HD-111-WH29	Wing Heater	4.226	40.225	-0.221	14.055	40.278	-0.133	NA	NA	NA	NA											2
	ESF-HD-112-WH30	Wing Heater	4.311	38.375	-0.263	14.141	38.316	-0.269	NA	NA	NA	NA											2
	ESF-HD-113-WH31	Wing Heater	4.296	36.548	-0.240	14.126	36.476	-0.212	NA	NA	NA	NA											2
	ESF-HD-114-WH32	Wing Heater	4.450	34.813	-0.273	14.279	34.969	-0.276	NA	NA	NA	NA											2
	ESF-HD-115-WH33	Wing Heater	4.233	32.878	-0.227	14.060	32.668	-0.194	NA	NA	NA	NA											2
	ESF-HD-116-WH34	Wing Heater	4.018	31.075	-0.251	13.848	31.031	-0.229	NA	NA	NA	NA											2
	ESF-HD-117-WH35	Wing Heater	3.946	29.221	-0.228	13.775	29.165	-0.129	NA	NA	NA	NA											2
	ESF-HD-118-WH36	Wing Heater	4.219	27.416	-0.185	14.048	27.390	-0.050	NA	NA	NA	NA											2
	ESF-HD-119-WH37	Wing Heater	4.268	25.611	-0.279	14.097	25.657	-0.406	NA	NA	NA	NA											2
	ESF-HD-120-WH38	Wing Heater	4.009	23.782	-0.281	13.838	23.830	-0.376	NA	NA	NA	NA											2
	ESF-HD-121-WH39	Wing Heater	4.251	21.941	-0.276	14.081	21.945	-0.299	NA	NA	NA	NA											2
	ESF-HD-122-WH40	Wing Heater	3.162	20.114	-0.248	12.992	20.121	-0.234	NA	NA	NA	NA											2
	ESF-HD-123-WH41	Wing Heater	4.130	18.285	-0.255	13.960	18.275	-0.297	NA	NA	NA	NA											2
	ESF-HD-124-WH42	Wing Heater	4.328	16.410	-0.311	14.155	16.278	-0.517	NA	NA	NA	NA											2
	ESF-HD-125-WH43	Wing Heater	4.299	14.648	-0.325	14.127	14.678	-0.526	NA	NA	NA	NA											2
	ESF-HD-126-WH44	Wing Heater	4.131	12.810	-0.259	13.960	12.864	-0.340	NA	NA	NA	NA											2
	ESF-HD-127-WH45	Wing Heater	4.287	10.913	-0.297	14.114	10.704	-0.442	NA	NA	NA	NA											2
	ESF-HD-128-WH46	Wing Heater	4.115	9.151	-0.282	13.944	9.212	-0.418	NA	NA	NA	NA											2
	ESF-HD-129-WH47	Wing Heater	3.922	7.290	-0.248	13.750	7.114	-0.271	NA	NA	NA	NA											2
	ESF-HD-130-WH48	Wing Heater	4.161	5.482	-0.223	13.990	5.350	-0.177	NA	NA	NA	NA											2
	ESF-HD-131-WH49	Wing Heater	3.067	3.673	-0.279	12.897	3.702	-0.321	NA	NA	NA	NA											2

INTENTIONALLY LEFT BLANK

Table 6.3-2. DST As-Built Borehole, Sensor, and Heater Information[1] (continued)

Borehole Number	Borehole Identification	Primary Purpose	Collar Coordinates (meters) [2]			Bottom Coordinates (meters) [2]			Orientation	Diameter	Length [3]	Volume	Types and No. of Sensors										
			x meters	y meters	z meters	x meters	y meters	z meters	Degree	cm	meters	m^3	Thermo-Couples	RTD	Thermistors	REKA	Mech. MPBX, RSG	Neutron	Humidity Sensor	Pressure Transducer	Electrode [5] Sensor (ERT)	Chemical	Electrical Amps.
	ESF-HD-132-WH50	Wing Heater	4.287	1.782	-0.290	14.114	1.581	-0.446	NA	NA	NA	NA											2
MISC.																							
	ESF-HD-BHSF	Bulkhead	NA	NA	NA	NA	NA	NA	NA	NA	NA	NA	9										
	ESF-HD-CDEX-MPBX-1	Cross Extensometer	0.427	42.357	2.510	0.409	42.357	-1.250	NA	NA	NA	NA	3				1						
	ESF-HD-CDEX-MPBX-2	Cross Extensometer	2.547	42.268	-0.019	-2.547	42.277	0.011	NA	NA	NA	NA	3				1						
	ESF-HD-SURF	Surface Monitor	NA	NA	NA	NA	NA	NA	NA	NA	NA	NA	50				50						
	ESF-HD-AIR	Air Monitor	NA	NA	NA	NA	NA	NA	NA	NA	NA	NA		12					2	5			1
	ESF-HD-RACK	Type K TC in Rack	NA	NA	NA	NA	NA	NA	NA	NA	NA	NA	26										
	ESF-HD-CAN-CBL-RTD	RTD in Power Cable Tray	NA	NA	NA	NA	NA	NA	NA	NA	NA	NA		7									
	ESF-HD-CAN	TCO Power Monitor Panel in CD	NA	NA	NA	NA	NA	NA	NA	NA	NA	NA											8
	ESF-HD-WH-CBL-RTD	RTD in Power Cable Tray	NA	NA	NA	NA	NA	NA	NA	NA	NA	NA		7									
	ESF-HD-WH	TCO Power Monitor Panel in CD	NA	NA	NA	NA	NA	NA	NA	NA	NA	NA											8
	ESF-HD-SIG-CBL-RTD	RTD in Signal Cable Tray	NA	NA	NA	NA	NA	NA	NA	NA	NA	NA		6									
	ESF-HD-TOTAL	Total Volt.,Amp.,Pwr.	NA	NA	NA	NA	NA	NA	NA	NA	NA	NA											9
	ESF-HD-OFF	1000 ohm / 4-wire RTD	NA	NA	NA	NA	NA	NA	NA	NA	NA	NA		4									6
	ESF-HD-CHEM-PAD-REF	Ref. Monitor of Absorbing Pad	NA	NA	NA	NA	NA	NA	NA	NA	NA	NA										11	1
	SYS-1,2,3,4-VXI	Thermistor in Cabinets	NA	NA	NA	NA	NA	NA	NA	NA	NA	NA			108								
	VXI-EXH-TEMP	Thermal Monitor	NA	NA	NA	NA	NA	NA	NA	NA	NA	NA	15										
										Total	3247.77	17.18	630	1944	111	3	138	10	48	51	316 [5]	122	673

Total Number of Sensors (All Types) : 3730

Notes:

1. Technical Data Management System Numbers: TDIF: 309730, DTN: MO0002ABBLSLDS.000 [147304].
2. Borehole Coordinates are Referenced to a 0,0,0 Coordinate Located at the Center of the Bulkhead in the Heated Drift.
3. Borehole Length is Calculated Using the Surveyed X,Y,Z Coordinates.
4. Canister Heater Coordinates are for the Approximate Longitudinal Centerline of the Two Ends. It was Estimated Based on Its Dimensions of Length (4.6482 m) and Diameter (1.6764 m).
5. Not Considered an Individual Sensor

INTENTIONALLY LEFT BLANK

Table 6.3.1.3-1. Summary of Thermal Conductivity Data for Saturated Specimens from the DST Block

		Thermal Conductivity (W/m-K)					
Distance from collar (ft)	**Max. Temp. (°C)**	**30°C**	**50°C**	**70°C**	**Mean**	**STD[(a)]**	**N[(a)]**
ESF-SDM-MPBX1-C							
1.0	70	2.2	2.2	2.2	2.2	0.0	3
32.1	70	2.2	2.2	2.1	2.2	0.0	3
40.6	70	2.1	2.1	2.1	2.1	0.0	3
62.0	70	2.2	2.2	2.2	2.2	0.0	3
80.5	70	2.15	2.1	2.1	2.1	0.0	3
N[(a)] =		5	5	5			
Mean =		2.2	2.2	2.1			
STD[(a)] =		0.1	0.0	0.0			
ESF-SDM-MPBX2-C							
13.0	70	2.1	2.1	2.1	2.1	0.0	3
29.0	70	2.1	2.1	2.1	2.1	0.0	3
48.4	70	2.0	2.0	2.0	2.0	0.0	3
71.5	70	2.3	2.3	2.3	2.3	0.0	3
84.6	70	2.0	2.0	2.1	2.0	0.1	3
N[(a)] =		5	5	5			
Mean =		2.1	2.1	2.1			
STD[(a)] =		0.1	0.1	0.1			
ESF-SDM-MPBX3-C							
3.0	70	1.9	1.9	1.9	1.9	0.0	3
17.7	70	2.1	2.1	2.1	2.1	0.0	3
38.7	70	2.2	2.2	2.2	2.2	0.0	3
72.0	70	2.2	2.2	2.2	2.2	0.0	3
85.3	70	2.1	2.1	2.1	2.1	0.0	3
N[(a)] =		5	5	5			
Mean =		2.1	2.1	2.1			
STD[(a)] =		0.1	0.1	0.1			
ESF-AOD-HDFR1-C							
8.6	70	2.0	2.0	2.0	2.0	0.0	3
32.2	70	2.1	2.1	2.1	2.1	0.0	3
48.7	70	1.9	1.9	2.0	1.9	0.0	3
68.8	70	2.1	2.1	2.0	2.1	0.0	3
97.5	70	2.3	2.3	2.3	2.3	0.0	3
N[(a)] =		5	5	5			
Mean =		2.1	2.1	2.1			
STD[(a)] =		0.2	0.1	0.1			
All Drift Scale Test Characterization Boreholes							
N[(a)] =		20	20	20			
Mean =		2.1	2.1	2.1			
STD[(a)] =		0.1	0.1	0.1			
All Specimens, All Temperatures							
N[(a)] =		60					
Mean =		2.1					
STD[(a)] =		0.1					

NOTE: Air dried. Lithostratigraphic unit: Tptpmn, except for HDFR1-97.5-C, which may be from Tptpll (see Section 3.2).
[(a)] N = Number of samples; STD = Standard deviation

Table 6.3.1.3-2. Thermal Conductivity as a Function of Saturation State[a]

Lithostratigraphic Unit	Number of Specimens	Linear Fit[b]: $K=K_d+Slope \cdot S_l$				Fit[b] to $K=K_d+(K_w-K_d)\cdot\sqrt{S_l}$		
		Intercept or K_d W/(m-K)	Slope	K_w W/(m-K)	Sum of Squared Errors	K_d W/(m-K)	K_w W/(m-K)	Sum of Squared Errors
Tptpmn	6	1.79	0.414	2.20	0.46	1.71	2.14	0.53
Tac4	1	0.52	0.54	1.06	0.007	0.42	0.98	0.011
Tac3	1	0.53	0.55	1.08	0.004	0.43	1.00	0.013
Tac2	2	0.52	0.59	1.11	0.020	0.39	1.03	0.056
Tacbs	2	0.71	0.59	1.31	0.007	0.59	1.21	0.062

NOTE: [a] Refer to SNL 1998 [118788] and DTN cited in Table 4-3.
[b] K_w: Thermal Conductivity for Saturated Specimen
K_d: Thermal Conductivity for Oven-Dried Specimen
S_l: Liquid Saturation

Table 6.3.1.4-1. REKA Results with No Background Temperature Correction

REKA Location	Thermal Conductivity, K (W/(m-C))	Thermal Diffusivity, Alpha (m^2/s)
1	1.69	0.76×10^{-6}
2	1.95	0.77×10^{-6}
3	1.86	0.91×10^{-6}
4	1.88	0.82×10^{-6}
5	1.70	0.85×10^{-6}

Source: CRWMS M&O 1997 ([101539], Section 10.2)

NOTE: Values in this table derived from *in situ* measurements are used for corroborative purposes with laboratory measurements discussed in Section 6.3.1.3.
Error of fit is the Root Mean Square between the simulated and measured temperature fields, all having 35 readings with time and 6 readings along the length of the REKA probe.

Table 6.3.1.4-2. REKA Results with Background Temperature Correction

REKA Location	Thermal Conductivity, K (W/(m-C))	Thermal Diffusivity, Alpha (m^2/s)
1	1.72	0.93×10^{-6}
2	1.92	0.90×10^{-6}
3	1.89	1.04×10^{-6}
4	1.93	1.09×10^{-6}
5	1.76	0.97×10^{-6}

Source: CRWMS M&O 1997 ([101539], Section 10.2)

NOTE: Values in this table derived from *in situ* measurements are used for corroborative purposes with laboratory measurements discussed in Section 6.3.1.3.
Error of fit is the Root Mean Square between the simulated and measured temperature fields, all having 35 readings with time and 6 readings along the length of the Sierra Science REKA probe.

Table 6.3.2.2-1 DST GPR Measurement Schedule

Acquisition	Date	Heating Days	Borehole Pairs
PRE	10/29/97	-33.0	51-50, 50-49, 68-67, 67-66, 66-65, 65-64
PHASE 1	02/13/98	74.0	51-50, 50-49, 68-67, 67-66, 66-65, 65-64
PHASE 2	01/26/99	421.0	51-50, 50-49, 68-67, 67-66, 66-65
PHASE 3	04/15/99	533.0	51-50, 50-49, 68-67, 67-66, 66-65
PHASE 4	10/26/99	694.0	51-50, 50-49, 68-67, 67-66, 66-65
PHASE 5	04/13/00	864.0	51-50, 50-49, 68-67, 66-65
PHASE 6	09/28/00	1032.0	51-50, 50-49, 66-65, 65-64
PHASE 7	02/06/01	1163.0	51-50, 50-49, 66-65, 65-64
PHASE 8	06/20/01	1330.0	51-50, 50-49, 66-65, 65-64
PHASE 9	10/30/01	1429.0	51-50, 50-49, 66-65
PHASE 10	01/10/02	1501.0	51-50, 50-49, 66-65, 65-64

Table 6.3.2.4-1. Estimated Local Permeability for 41 Packed-off Zones in 14 Boreholes During DST Pre-Heating (Nov/Dec 1996 and Feb/Mar 1997)

Borehole ID	k(m^2) in zone 1	k(m^2) in zone 2	k(m^2) in zone 3
45 ESF-HD-ERT- 1	5.8E-14	2.4E-14	4.5E-13
46 ESF-HD-ERT-2	4.1E-15	6.2E-15	9.0E-14
47 ESF-HD-NEU-1	6.1E-14	4.4E-13	4.7E-13
48 ESF-HD-NEU-2	2.4E-14	3.5E-14	3.4E-13
51 ESF-HD-NEU-5	8.8E-16	4.4E-13	4.1E-14
52 ESF-HD-CHE-1	1.0E-13	1.2E-13	2.0E-12
53 ESF-HD-CHE-2	1.1E-13	1.3E-12	N/A
56 ESF-HD-CHE-5	1.9E-15	3.4E-14	4.8E-13
57 ESF-HD-HYD-1	2.7E-13	6.1E-14	1.4E-13
69 ESF-HD-CHE-6	2.IE-13	9.5E-15	4.9E-13
70 ESF-HD-CHE-7	1.9E-14	4.5E-14	4.2E-13
73 ESF-HD-CHE-l0	6.6E-14	6.8E-15	1.0E-13
75 ESF-HD-HYD-7	4.9E-13	1.4E-13	3.0E-13
78 ESF-HD-HYD-10	15.5E-14	1.1E-14	7.8E-14

Table 6.3.2.4-2. Parameters Used in Equation 5.2-1 for the Estimation of Local Permeability During DST Pre-Heating (July 1997)

Borehole ID_Data File	L (m)	Q (SLPM)	P_2-P_1 (kPa)	P_1 (kPa)	k (m^2)
177_02JUL19	12.822	10	30.67	89.24	7.01E-15
158_02JUL08	16.076	99	16.68	90.14	1.12E-13
159_02JUL07	16.062	99	8.48	89.38	2.33E-13
160_01JUL03	16.012	499	0.83	89.45	1.26E-11
160_01JUL04	12.964	499	4.20	89.52	2.89E-12
161_01JUL01	16.312	299	11.09	89.52	5.22E-13
161_01JUL02	13.264	199	15.99	89.45	2.79E-13
162_01JUL01	17.822	54	27.01	89.45	3.32E-14
163_02JUL01	16.312	99	32.60	89.38	5.29E-14
164_02JUL02	16.012	299	15.99	89.45	3.59E-13
164_02JUL03	12.964	299	17.99	89.52	3.76E-13
165_02JUL05	16.012	299	16.61	89.52	3.44E-13
166_02JUL06	16.038	99	21.36	89.59	8.63E-14
167_01JUL06	12.822	199	35.56	89.52	1.17E-13
170_02JUL21	16.012	99	5.38	89.72	3.72E-13
171_02JUL20	16.012	99	22.88	89.45	8.02E-14
172_02JUL18	16.312	99	6.34	89.45	3.10E-13
173_02JUL17	17.822	21	33.15	89.52	1.02E-14
174_02JUL16	16.312	21	21.50	89.45	1.79E-14
176_02JUL22	16.012	199	5.72	89.38	7.05E-13
100_02JUL15	7.512	99	7.37	93.24	4.61E-13
115_02JUL12	7.512	99	4.69	93.17	7.36E-13
116_02JUL11	7.512	199	6.68	93.24	1.03E-12
117_02JUL10	7.512	299	12.13	93.31	8.26E-13
118_02JUL09	7.512	299	8.13	93.17	1.26E-12
98_02JUL13	7.512	499	1.17	93.24	1.51E-11
99_02JUL14	7.512	299	4.62	93.24	2.26E-12

Table 6.3.2.4-3. Parameters Used in Equation 5.2-1 for the Estimation of Local DST Permeability During Pre-Heating (Nov 1997)

Borehole-Zone (data file ID)	L(m)	Q(SLPM)	(P_2-P_1) (kPa)	P_1 (kPa)	k (m^2)
57-1 (11797544PM)	8.84	20	4.58	89.2	1.46E-13
57-2 (11897401AM)	6.10	100	18.5	89.5	2.26E-13
57-3 (11897218PM)	7.62	2	39.9	89.3	1.58E-15
57-4 (119971235AM)	10.55	200	12.6	89.7	4.37E-13
58-1 (111697133AM)	6.10	20	5.12	90.2	1.74E-13
58-2 (1116971151AM)	8.54	20	3.18	90.4	2.15E-13
58-3 (1116971008PM)	17.98	171	3.74	89.9	8.45E-13
59-1 (111097610PM)	10.06	100	22.1	86.9	1.27E-13
59-1 (111097610PM)	10.06	20	4.25	86.9	1.45E-13
59-2 (111197427AM)	7.62	100	8.95	90.8	4.04E-13
59-3 (111197244PM)	8.54	100	10.8	88.0	3.11E-13
59-4 (111297101AM)	7.19	200	7.8	91.6	9.69E-13
60-1 (111097101PM)	5.49	20	2.75	88.8	3.62E-13
60-1 (111097101PM)	5.49	100	21.2	88.8	2.13E-13
60-2 (1110971118PM)	10.67	100	5.8	87.7	4.98E-13
60-3 (111197936AM)	5.49	2	7.2	88.5	1.35E-14
60-4 (111197753PM)	11.19	20	45.5	89.5	9.85E-15
61-1 (117971235PM)	7.01	200	34	89.5	2.04E-13
61-1 (117971235PM)	7.01	100	14.6	89.5	2.61E-13
61-2 (117971052PM)	8.54	100	3.85	88.8	8.99E-13
61-3 (11897909AM)	6.10	20	16.3	100.0	4.68E-14
61-4 (11897727PM)	12.63	100	26.9	89.4	8.23E-14
74-1 (11497749PM)	10.37	100	10.6	90.0	2.65E-13
74-2 (114971139PM)	6.71	20	12.9	90.3	6.12E-14
74-3 (11597330AM)	4.27	20	8.04	90.4	1.44E-13
74-4 (111797308PM)	14.09	100	17.3	90.9	1.21E-13
75-1 (11597140PM)	8.23	100	11.3	91.4	2.95E-13
75-2 (11597450PM)	7.32	100	23.7	90.8	1.46E-13
75-3 (115978PM)	10.67	100	17.3	89.9	1.53E-13
75-4 (111797129PM)	8.48	100	4.68	90.8	7.24E-13
76-1 (116971106AM)	7.93	100	13.1	90.0	2.64E-13
76-2 (11697216PM)	8.54	20	5.27	89.8	1.29E-13
76-3 (11697526PM)	8.54	20	9.89	89.0	6.76E-14
76-4 (11697836PM)	10.00	20	6.82	90.5	8.62E-14
77-1 (111597825PM)	8.84	100	21.5	91.0	1.40E-13

Table 6.3.2.4-3. Parameters Used in Equation 5.2-1 for the Estimation of Local DST Permeability During Pre-Heating (Nov 1997) (continued)

Borehole-Zone (data file ID)	L(m)	Q(SLPM)	(P_2-P_1) (kPa)	P_1 (kPa)	k (m^2)
77-1 (11697351PM)	8.84	20	1.87	90.6	3.57E-13
77-1 (111397341PM)	8.84	20	1.72	89.9	3.91E-13
77-2 (111697642AM)	5.49	20	21.2	90.0	4.21E-14
77-2 (11697701PM)	5.49	20	33.1	89.3	2.56E-14
77-2 (111397828PM)	5.49	20	31.4	88.7	2.74E-14
77-2 (110797729AM)	5.49	20	31.1	89.4	2.75E-14
77-3 (111697459PM)	22.70	100	3.83	90.5	3.94E-13
78-1 (1117971013AM)	6.10	20	4.4	90.4	2.02E-13
78-2 (11797419AM)	8.23	20	14.3	90.4	4.64E-14
78-3 (11797554AM)	5.79	20	16	89.9	5.49E-14
78-4 (1115971008AM)	14.49	20	4	91.1	1.09E-13
185-1 (115971204PM)	5.79	20	2.75	89.5	3.46E-13
185-2 (11597315PM)	8.54	100	15.6	89.4	2.07E-13
185-3 (11597625PM)	15.24	100	20.9	90.2	9.26E-14
185-4 (11597935PM)	6.65	20	4.18	89.6	2.01E-13
186-1 (11497553PM)	5.79	20	2.47	90.4	3.80E-13
186-2 (11497944PM)	8.54	20	22.1	93.9	2.71E-14
186-3 (11597134AM)	13.11	20	51.9	89.9	7.34E-15
186-4 (1117971151AM)	5.09	2	11.4	90.6	8.68E-15

Table 6.3.2.4-4. Date of Pneumatic Packer Deflation in the DST Hydrology Boreholes

Packer Location	Date
57-4	March 22, 2000
59-1	February 6, 2001
60-1	November 14, 2001
60-2	January 1, 2000
60-3	November 30, 1999
60-4	August 27, 1999*
61-2	November 7, 2001
61-3	July 24, 2000
61-4	February 6, 2001
76-3	December 24, 2000
77-3	January 7, 1998
78.2	December 24, 2000
78.3	December 1, 1999
78.4	September 9, 2000

* Reinflated February 16, 2000, deflated again August 15, 2000

Table 6.3.2.4-5. DST Tracer Testing Locations and Parameters

Test Name	Injection Location	Withdrawal Location	Q_{inject} (SLPM)	$Q_{withdraw}$ (SLPM)	Tracer Injection Duration (min)	Average Zone Separation (m)
76-2 10:1	76-2	75-2	3	30	87	2.78
76-2 30:1	76-2	75-2	2	20	276	5.64
76-4 10:1	76-4	75-4	1	30	93	2.78
Huff-puff	76-2	76-2	10	20	20	N/A

Table 6.3.2.4-6. DST Plug-Flow Tracer Analysis of Cross-Hole Tracer Data

Tracer Test	Zone length (m)	t_{50} (min)	$\phi_{fracture}$
76-2-75-2 10:1	7.93	67	.010
76-2-75-2 30:1	7.93	56	.006
76-4-75-4 10:1	9.12	294	.009

Table 6.3.2.5-1. Laboratory Measurement of Dry-Drilled Cores from DST Permeability Boreholes (182, 183, 184)

Borehole #182, ESF-HD-PERM-1					
sample location	**saturation**	**porosity**	**bulk density**	**particle density**	**gravimetric water content**
(m)	**(%)**	**(%)**	**(g/cc)**	**(g/cc)**	**(g/g)**
5.5	86.67	9.61	2.27	2.51	0.037
9.9	89.67	11.02	2.24	2.52	0.044
15.5	85.08	10.27	2.25	2.51	0.039
19.8	86.72	10.27	2.25	2.51	0.039

Borehole #183, ESF-HD-PERM-2					
sample location	**saturation**	**porosity**	**bulk density**	**particle density**	**gravimetric water content**
(m)	**(%)**	**(%)**	**(g/cc)**	**(g/cc)**	**(g/g)**
5.2	83.84	9.62	2.27	2.51	0.035
10.1	82.86	12.02	2.21	2.51	0.045
15.3	76.61	13.35	2.19	2.53	0.046
19.9	79.21	10.89	2.24	2.51	0.038

Borehole #184, ESF-HD-PERM-3					
sample location	**saturation**	**porosity**	**bulk density**	**particle density**	**gravimetric water content**
(m)	**(%)**	**(%)**	**(g/cc)**	**(g/cc)**	**(g/g)**
5.1	81.40	9.87	2.25	2.50	0.035
10.0	86.61	10.91	2.24	2.51	0.042
15.5	85.80	9.43	2.27	2.51	0.035
18.9	81.76	10.17	2.26	2.52	0.037

Borehole Summary					
	saturation	**porosity**	**bulk density**	**particle density**	**gravimetric water content**
	(%)	**(%)**	**(g/cc)**	**(g/cc)**	**(g/g)**
average	83.85	10.62	2.25	2.51	0.039
standard deviation	3.67	1.14	0.02	0.01	0.004

Table 6.3.2.5-2. Laboratory Measurement of Wet-Drilled Cores from DST Boreholes (81, 52, 53, 56)

Borehole #81, ESF-HD-MPBX-1					
sample location (m)	saturation (%)	porosity (%)	bulk density (g/cc)	particle density (g/cc)	gravimetric water content (g/g)
4.6#	96.43	10.15	2.25	2.50	0.043
6.8	84.97	9.73	2.27	2.51	0.036
12.3**	96.02	10.16	2.26	2.52	0.043
17.8##	96.80	9.46	2.26	2.49	0.040
20.8*	103.77	15.34	2.14	2.53	0.073
24.1	94.10	8.77	2.28	2.50	0.036
32.0	95.42	9.67	2.28	2.52	0.040
35.1^	92.97	11.81	2.21	2.51	0.050
39.4	92.82	10.31	2.26	2.52	0.042
45.3	94.57	9.27	2.28	2.51	0.038

* two open fractures + "crushed zone" + porous looking calcite inclusion
# entire surface of core was wet
^ large open fracture down center of upper half
** closed vertical fracture along core axis
two fractures with small aperture

Borehole #52, ESF-HD-CHE-1					
sample location (m)	saturation (%)	porosity (%)	bulk density (g/cc)	particle density (g/cc)	gravimetric water content (g/g)
15.3^	87.56	11.73	2.22	2.52	0.046
18#	95.91	17.32	2.09	2.52	0.079
26.5^	87.89	11.04	2.24	2.51	0.043
29.9*	97.32	13.98	2.16	2.51	0.063
35.0	96.98	18.19	2.07	2.53	0.085
38.2**	98.58	16.57	2.11	2.53	0.077

* contains large open vug on side surface
# large fracture exposed on surface
^ water drop loss during transfer
** contains fracture on side surface

Borehole #53, ESF-HD-CHE-2					
sample location (m)	saturation (%)	porosity (%)	bulk density (g/cc)	particle density (g/cc)	gravimetric water content (g/g)
10.7#	95.31	11.67	2.22	2.51	0.050
16.7#	96.84	12.94	2.19	2.51	0.057
22.2	94.96	11.52	2.22	2.51	0.049
28.2*	74.03	15.62	2.11	2.50	0.055
36.5*	95.47	12.80	2.21	2.53	0.055

* large amount of water condensed in container
# contains fracture on side surface

Table 6.3.2.5-2. Laboratory Measurement of Wet-Drilled Cores from DST Boreholes (81, 52, 53, 56) (continued)

Borehole #56, ESF-HD-CHE-5					
sample location (m)	saturation (%)	porosity (%)	bulk density (g/cc)	particle density (g/cc)	gravimetric water content (g/g)
10.6	94.99	14.57	2.15	2.52	0.064
18.0*	94.34	12.33	2.20	2.51	0.053
23.2	95.58	16.02	2.11	2.51	0.072
29.6	92.79	15.91	2.14	2.54	0.069
35.7	86.21	11.65	2.21	2.51	0.045
38.9	82.40	10.09	2.25	2.51	0.037

* contains fracture on side surface

Borehole Summary					
	saturation (%)	porosity (%)	bulk density (g/cc)	particle density (g/cc)	gravimetric water content (g/g)
average	93.15	12.54	2.20	2.51	0.053
standard deviation	5.93	2.75	0.06	0.01	0.015

Table 6.3.2.5-3. DST Samples Prepared for Electrical Properties Measurements

Sample ID	Borehole	Depth (m)	Wet Density (g/cm^3)	Dry Density (g/cm^3)	Porosity
01002189-2	CHE-6	13.2 - 13.4	2.362	2.271	0.0914
01002190-2	CHE-6	19.4 - 19.6	2.361	2.276	0.0850
01002194-2	CHE-6	30.2 - 30.4	2.338	2.231	0.107
01002200-2	CHE-7	24.2 - 24.5	2.372	2.284	0.0883
01002205-2	CHE-7	38.9 - 39.1	2.382	2.296	0.0862
01002206-1	CHE-10	4.8 - 4.9	2.359	2.258	0.101
01002207-1	CHE-10	8.3 - 8.5	2.370	2.282	0.0876
01002209-1	CHE-10	22.9 - 23.1	2.373	2.258	0.114
01002212-2	CHE-10	27.8 - 28.0	2.354	2.214	0.140
01002215-2	CHE-10	37.6 - 37.8	2.330	2.248	0.0825
Mean*		10 Samples	2.36 ± 0.02	2.26 ± 0.03	0.098 ± 0.018

* Statistical mean for 10 samples. Errors represent one standard deviation for all samples collectively.

Table 6.3.3.1-1. Summary of SNL-Installed Measurement System Specifications for the DST

Measurement System	Manufacturer	Gage Range, Accuracy	Comments
Type-K Thermocouples	Watlow ARI, Inc. (probes)	Range: max 1280ºC Accuracy: ± 2.2ºC	Chromel-Alumel
Vibrating Wire Displacement Transducers	GEOKON	1 in. (± 25.4 mm) full range Accuracy: 0.02% of full range	
High Temperature LVDTs (Heated Drift)	RDP Electrosense, Inc.	± 1 in. (± 25.4 mm) full range Accuracy of 0.5% linearity full range (linear within range; i.e. 0.5% of measured value) calibrated from ambient to 350ºC	AC-LVDT's

Table 6.3.3.2-1. Location and Quality Information for CDEX-1 and CDEX-2

Instrument ID	X (m)	Y (m)	Z (m)	General Quality of Data
ESF-HD-CDEX-1 (vertical)	0.425	42.357	2.01	Good data until Day 450 (2/26/1999); unexplainable rise in displacement through Day 650 (9/14/1999) which may or may not be real; oscillating high level of displacement (17.5-20.5 mm) through heater turn-off which is probably bad data; observation by Tim Vogt (M&O) that time-averaged oscillation matches annual climatic cycle.
ESF-HD-CDEX-2 (horizontal)	2.047	42.269	-0.016	Occasional electrical noise – overall very good

Table 6.3.3.3-1. Summary of SNL-Installed Strain Gage Specifications for the DST

Measurement System	Manufacturer	Gage Range, Accuracy
CIP Strain Gages	BLH Electronics	Karma Foil 4-in gages with gage factor of 2 Temperature range limited by bonding epoxy and extension wire

Table 6.3.3.4-1. Description of DST AE Accelerometers

Channel	Borehole Number	S/N	Model	X (m)	Y(m)	Z(m)	Distance from Borehole Collar
1	163	3032	728-T	9.24	22.66	-9.35	10.95
2	171	3034	728-T	-9.47	39.30	9.50	10.82
3	139	2019	793-6	-21.87	11.95	0.14	19.30
4	161	2890	728-T	-8.54	23.05	-8.46	9.75
5	175	3037	728-T	10.23	39.23	10.43	11.98
6	140	2883	728-T	-10.12	11.85	-8.54	10.75
7	144	2886	728-T	9.26	11.98	9.23	10.25
8	159	2889	728-T	-9.67	22.88	9.74	10.98
9	142	2884	728-T	9.78	11.91	-9.74	11.50
10	164	2022	793-6	12.49	22.94	0.16	10.00
11	138	2881	728-T	-9.06	11.70	9.03	10.00
12	143	2020	793-6	21.71	11.92	0.02	19.05
13	160	2021	793-6	-11.99	22.91	0.05	9.49
14	165	3033	728-T	10.36	22.79	10.38	12.01
15	172	3035	728-T	-8.47	39.09	-8.47	9.75
16	174	3036	728-T	9.80	39.10	-9.27	11.25

Table 6.3.3.4-2. Corresponding AE and MPBX Events

		DST Coordinate System			Days after heater activation	Date/Time (UTC)
Data Type	Occurrence	X	Y	Z		
AE	6_1	-1.340	22.780	2.520	442.39	02/19/1999 04:03
MPBX	HD-156-MPBX9-2	-0.007	20.993	4.604	442.98	02/19/1999 18:06

Table 6.3.3.5-1. Summary of Thermal Expansion Data for Specimens from the DST Block for the First Heating Cycle

		MCTE on Heat-up (10^{-6}/°C)											
	Temp. (°C)	25-50	50-75	75-100	100-125	125-150	150-175	175-200	200-225	225-250	250-275	275-300	300-325
N[(a)] =		17	17	17	17	17	17	17	17	17	17	17	13
Mean =		7.34	8.99	9.73	10.22	10.91	12.20	14.74	22.31	27.34	33.88	54.13	52.28
STD[(a)] =		0.57	0.47	0.54	0.58	0.79	1.04	4.79	18.09	15.70	6.94	12.18	13.42
95% [(a)]		0.27	0.22	0.26	0.28	0.38	0.49	2.28	8.60	7.46	3.30	5.79	7.29

[(a)]N = Number of samples; STD = Standard deviation; 95% = 95 percent confidence limit.

Table 6.3.3.5-2. Summary of the Mean Thermal Expansion Coefficients for Specimens from DST Block for the First Cooling Cycle

	Mean CTE on Cool-Down (10^{-6}/°C)											
Temp. (°C)	325-300	300-275	275-250	250-225	225-200	200-175	175-150	150-125	125-100	100-75	75-50	50-30
N(a) =	13	17	17	17	17	17	17	17	17	17	16	15
Mean =	15.74	24.07	35.63	36.01	26.50	24.19	18.30	14.14	12.36	11.05	10.24	9.67
STD(a) =	1.88	5.70	8.39	8.32	4.69	9.82	7.37	2.61	1.76	0.84	1.24	0.66
95% (a)	1.02	2.71	3.99	3.96	2.23	4.67	3.50	1.24	0.84	0.40	0.61	0.33

(a) N = Number of samples; STD = Standard deviation

Table 6.3.3.5-3. Tabulation of DST Unconfined Compression Tests

	Statistical Summary (a)			
All specimens TSw2, Tptpmn	Mean	Standard Deviation	Count	95% Confidence Limit
Static Young's Modulus (GPa)	36.8	3.5	16	1.7
Static Poisson's Ratio	0.201	0.040	16	0.020
Unconfined Compressive Strength (MPa)	176.4	65.8	16	32.3
Axial Strain at Peak Stress	0.005209	0.002048	16	0.001004

Test Conditions: Nominally 38.1 mm in diameter, 76.2 mm in length, ambient temperature and pressure, nominal strain rate of 10^{-5} s^{-1}.

NOTE: (a) Test specimen ESF-SDM-MPBX1-1.0-A was tested twice. Mean Young's modulus and mean Poisson's ration were calculated using data from the first loading only (UCDST001). Mean unconfined compressive strength was calculated using data from the second loading only (UCDST017).

Table 6.3.3.5-4. Summary of Results for DST Reinforced Concrete

	Strength (MPa)	Young's Modulus (GPa)		Poisson's Ratio (0°)		Poisson's Ratio (90°)	
		Loading	Unloading	Loading	Unloading	Loading	Unloading
Tests to Failure							
CIP11	58.2	31.4		(a)		0.197	
CIP13	58.6	37.3		0.293		0.253	
CIP17	52.9	34.4		0.247		0.233	
Cyclic Loading Tests							
CIP14							
Cycle 1:		31.3	34.9	0.301	0.276	0.292	0.267
Cycle 2:		32.2	34.4	0.254	0.281	0.244	0.274
Cycle 3:		31.5	34.1	0.254	0.278	0.242	0.269
Cycle 4:		31.7	33.3	0.252	0.250	0.238	0.217
CIP18							
Cycle 1:		32.3	34.5	0.222	0.208	0.261	0.261
Cycle 2:		35.2	34.3	0.228	0.210	0.255	0.266
Cycle 3:		35.3	32.8	0.230	0.205	0.255	0.257
Mean		33.3	34.0	0.253	0.244	0.247	0.259
Standard Deviation		2.1	0.7	0.027	0.036	0.024	0.019
No. of Measurements		10	7	9	7	10	7
Mean (All Data)	56.6	33.6		0.249		0.252	
Standard Deviation	3.2	1.7		0.031		0.022	
No. of Measurements	3	17		16		17	

(a) Radial gage did not function properly so data are omitted.

Table 6.3.3.5-5. Summary of Results for Nonreinforced Concrete

	Strength (MPa)	Young's Modulus (GPa)		Poisson's Ratio (0°)		Poisson's Ratio (90°)	
		Loading	Unloading	Loading	Unloading	Loading	Unloading
Tests to Failure							
CIP7	62.89	36.8		(a)		0.210	
CIP8	61.60	36.8		(a)		0.235	
CIP10	38.33	45.0 (b)		0.153		0.288	
Cyclic Loading Tests							
CIP9							
Cycle 1:		38.4	38.6	0.252	0.236	0.243	0.260
Cycle 2:		41.7	41.1	0.272	0.256	0.278	0.284
Cycle 3:		42.2	42.2	0.297	0.264	0.306	0.289
Cycle 4:		42.3	42.8	0.274	0.271	0.271	0.307
CIP3							
Cycle 1:		32.0	34.5	0.226	0.238	0.179	0.177
Cycle 2:		36.2	34.3	0.239	0.242	0.205	0.171
Cycle 3:		36.5	32.5	0.233	0.231	0.206	0.180
Mean		38.8	38.0	0.243	0.248	0.242	0.238
Standard Deviation		3.9	4.2	0.043	0.016	0.042	0.060
No. of Measurements		10	7	8	7	10	7
Mean (All Data)	54.3	38.5		0.246		0.241	
Standard Deviation	13.8	3.9		0.032		0.049	
No. of Measurements	3	17		15		17	

(a) Radial gage did not function properly so data are omitted.

(b) CIP10 had a lower strength than CIP7 and CIP8. Because moduli are calculated between 50 microstrain and 40% of the failure strength, the moduli for CIP10 were determined over a lower stress range than CIP7 and CIP8

Table 6.3.3.6-1. DST PLT Results from October 2000

	Maximum Displacement (mm)	Secant Moduli (GPa)	Elastic Moduli (GPa)
Ambient Side			
Deep Anchor	1.69	17.3	41.0
Medium Anchor	1.49	19.6	49.5
Shallow Anchor	1.21	24.2	59.4
Elevated Temp.			
Deep Anchor	LVDT malfunctioned	LVDT malfunctioned	LVDT malfunctioned
Medium Anchor	.68	43	62.5
Shallow Anchor	.55	53.2	99.0

NOTE: Maximum pressure equals 31.75 MPa.

Table 6.3.3.6-2. Rock Mass Rating Q for the Thermal Test Facility

Start Station	End Station	Record Number	Revision Number	Stratigraphic Unit	RQD	Jn	Jr	Ja	Jw	SRF	Q	
Observation Drift												
5	10	1	0	Tptpmn	88.6	12	4.0	1.0	1	5.0	5.907	
10	15	11	0	Tptpmn	81.8	12	4.0	1.0	1	5.0	5.453	
15	20	2	0	Tptpmn	89.1	12	4.0	1.0	1	5.0	5.940	
20	25	3	0	Tptpmn	87.7	6	4.0	1.0	1	5.0	11.693	
25	30	4	0	Tptpmn	95.7	12	4.0	1.0	1	1.0	31.900	
30	35	5	0	Tptpmn	71.2	12	4.0	4.0	1	5.0	1.187	
35	40	6	0	Tptpmn	73.9	12	4.0	4.0	1.	5.0	1.232	
40	45	7	0	Tptpmn	63.8	12	4.0	1.0	1	5.0	4.253	*
45	50	8	0	Tptpmn	92.6	12	4.0	3.0	1	5.0	2.058	*
50	55	9	0	Tptpmn	94.3	12	4.0	3.0	1	5.0	2.096	*
55	60	10	0	Tptpmn	92.7	12	4.0	3.0	1	5.0	2.060	*
60	65	12	0	Tptpmn	85.6	12	4.0	3.0	1	5.0	1.902	
65	70	13	0	Tptpmn	87.6	12	4.0	3.0	1	5.0	1.947	
70	75	14	0	Tptpmn	91.7	15	3.3	3.0	1	5.0	1.345	**
75	80	15	0	Tptpmn	75.7	12	4.0	3.0	1	5.0	1.682	**
80	85	16	0	Tptpmn	97.6	6	2.3	3.0	1	5.0	2.494	**
85	90	17	0	Tptpmn	73.0	12	4.0	3.0	1	5.0	1.622	**
90	95	18	0	Tptpmn	83.7	20	4.0	3.0	1	5.0	1.116	**
95	100	19	0	Tptpmn	99.0	20	4.0	3.0	1	5.0	1.320	**
100	105	20	0	Tptpmn	92.7	12	4.0	3.0	1	7.5	1.373	**
105	110	21	0	Tptpmn	49.5	6	4.0	3.0	1	7.5	1.467	**
110	115	22	0	Tptpmn	79.5	12	2.4	3.0	1	7.5	0.707	**
115	120	23	0	Tptpmn	87.2	12	4.0	3.0	1	7.5	1.292	**
120	125	24	0	Tptpmn	88.7	20	4.0	3.0	1	7.5	0.788	**
125	130	25	0	Tptpmn	67.7	6	4.0	3.0	1	7.5	2.006	**
130	135	26	0	Tptpmn	51.4	12	4.0	3.0	1	7.5	0.761	

* Interval adjacent to the single heater block.
** Interval adjacent to the heated drift.
RQD Rock Quality Designation
Jn Joint Set Number
Jr Joint Roughness Number
Ja Joint Alteration Number
Jw Joint Water Reduction Factor
SRF Stress Reduction Factor
Q Rock Mass Quality Indices

Table 6.3.3.6-3. Rock Mass Rating RMR for the Thermal Test Facility

Start Station	End Station	Record Number	Revision Number	Stratigraphic Unit	RQD-1	C	Js	Jc	Jw	JOA	RMR	
Observation Drift												
5	10	1	0	Tptpmn	17	12	15	21.1	15	-5	75.1	
10	15	11	0	Tptpmn	17	12	15	21.1	15	-5	75.1	
15	20	2	0	Tptpmn	17	12	15	22.4	15	-5	76.4	
20	25	3	0	Tptpmn	17	12	15	23.6	15	-5	77.6	
25	30	4	0	Tptpmn	20	12	15	23.6	15	-5	80.6	
30	35	5	0	Tptpmn	13	12	8	24.9	15	-5	67.9	
35	40	6	0	Tptpmn	13	12	8	23.6	15	-5	66.6	
40	45	7	0	Tptpmn	13	12	15	21.1	15	-5	71.1	*
45	50	8	0	Tptpmn	20	12	10	22.4	15	-5	74.4	*
50	55	9	0	Tptpmn	20	12	10	22.4	15	-5	74.4	*
55	60	10	0	Tptpmn	20	12	15	22.4	15	-5	79.4	*
60	65	12	0	Tptpmn	17	12	15	21.1	15	-5	75.1	
65	70	13	0	Tptpmn	17	12	15	22.4	15	-5	76.4	
70	75	14	0	Tptpmn	20	12	20	20.1	15	-12	75.1	**
75	80	15	0	Tptpmn	17	12	15	21.1	15	-5	75.1	**
80	85	16	0	Tptpmn	20	12	20	20.1	15	-12	75.1	**
85	90	17	0	Tptpmn	13	12	10	22.4	15	-12	60.4	**
90	95	18	0	Tptpmn	17	12	15	21.1	15	-5	75.1	**
95	100	19	0	Tptpmn	20	12	20	21.1	15	-12	76.1	**
100	105	20	0	Tptpmn	20	12	8	20.1	15	-12	63.1	**
105	110	21	0	Tptpmn	8	12	8	20.1	15	-12	51.1	**
110	115	22	0	Tptpmn	17	12	8	21.3	15	-12	61.3	**
115	120	23	0	Tptpmn	17	12	15	20.1	15	-5	74.1	**
120	125	24	0	Tptpmn	17	12	15	21.1	15	-5	75.1	**
125	130	25	0	Tptpmn	13	12	5	22.4	15	-12	55.4	**
130	135	26	0	Tptpmn	13	12	10	21.1	15	-5	66.1	

* Interval adjacent to the single heater block.
** Interval adjacent to the heated drift.
RQD Rock Quality Designation Rating
C Intact Rock Strength Rating
Js Joint Spacing Rating
Jc Joint Condition Rating
Jw Ground Water Rating
JOA Joint Orientation Adjustment
RMR Rock Mass Rating

Table 6.3.3.6-4. RMR Indices for Topopah Spring Middle Non-Lithophysal Zone (TSw2)

	RMR (Average)	RMR (Standard Deviation)	N (Number of Samples)
Thermal Test Facility	74.1	9.1	33
Main Drift	63.7	7.0	718

Table 6.3.3.6-5. Rock Mass Thermal Expansion Coefficients from DST MPBX Data

		Thermal expansion coefficients in μstrain/°C						
	T_{max}, °C	25°C-50°C	50°C-75°C	75°C-100°C	100°C-125°C	125°C-150°C	150°C-175°C	175°C-200°C
DST MPBX data through 1/14/2002								
HD-81-MPBX1 Anc 4-Anc 5	178.02	1.94	3.27	4.61	3.98	7.02	9.47	12.55
HD-81-MPBX1 Anc 5-Anc 6	171.74	3.65	1.19	0.46	4.37	7.04	10.34	
HD-82-MPBX2 Anc 2-Anc 3	158.24	0.48	2.78	6.84	4.89	7.21	8.40	
HD-82-MPBX2 Anc 3-Anc 4	163.03	2.82	1.36	4.52	6.12	8.15	10.23	
HD-82-MPBX2 Anc 4-Anc 5	168.72	0.55	3.31	4.66	6.17	7.81	9.79	
HD-82-MPBX2 Anc 5-Anc 6	171.48	2.76	2.57	4.03	0.85	7.38	10.60	
Avg., DST MPBX		2.03	2.41	4.19	4.40	7.43	9.80	12.55
Std. Dev., DST MPBX		1.29	0.93	2.07	1.95	0.46	0.80	
Avg., DST MPBX (no outliers)		2.03	2.41	4.45	5.11	7.43	9.80	12.55
Std. Dev., DST MPBX (no outliers)		1.29	0.93	0.29	1.00	0.46	0.80	
SHT Pre-Heating Heat. (TDIF 305593)	300	7.47	8.88	9.64	10.01	10.72	11.26	12.78
SHT Post-Cooling 1st Heat. (TDIF 307112)	322	8.6	9.9	9.0	9.6	10.6	11.8	12.3
SHT Post-Cooling 2nd Heat. (TDIF 307112)	323	8.5	9.7	9.0	10.2	11.1	12.2	14.1
DST Pre-Heating 1st Heat. (TDIF 306127)	327	7.34	8.99	9.73	10.22	10.91	12.20	14.74
DST Pre-Heating 2nd Heat. (TDIF 306127)	328	7.22	8.87	9.63	10.24	11.28	13.22	19.37

Table 6.3.4.1-1. Summary of DST Water Samples, the Field Data, and Important Observations through January 14, 2002

Date	Approx. Start Time	Approx. Finish Time	Est. Volume (mL)	Collection Hole/Zone	pH	Electrical Conductivity (mS/cm)	Total Dissolved Solids (ppm)	Sample Number	Solution Temp. (°C)	Comments
06/04/98	9:30		500	60/2	7.5			SPC00527968		anion
06/04/98	9:30		500	60/2	7.5			SPC00527969		metals
06/04/98	9:30		500	60/2	7.5			SPC00527970		O, H, & C
06/04/98	9:30		500	60/2	7.5			SPC00527971		Tritium
06/04/98	9:30		500	60/2	7.5			SPC00527972		U, Sr
06/04/98	9:30		500	60/2	7.5			SPC00527973		U, Sr
06/04/98	9:30		500	60/2	7.5			SPC00527974		^{36}Cl
06/04/98	9:30		2200	60/2	7.5			SPC00527975		Surplus H_2O
06/04/98	10:45		250	60/3	7.7			SPC00527977		
08/12/98	8:23	8:50	125	60/2	6.9			SPC00527915		
08/12/98	8:51	9:10	900	60/3	6.8			SPC00527916		
08/12/98	9:49	10:07	200	77/3	5.5			SPC00527917		
11/12/98	9:53	10:04	100	59/4	6.6			SPC00541803	25	Color noted as yellow by lab report
11/12/98	10:22	11:42	4000	60/3	6.9			SPC00541804	26.5 - 49.6	
11/12/98	13:37	14:04	3000	186/3	6.8			SPC00541805	34.3 - 35.1	
01/26/99	10:20	10:29	25	59/4				SPC00504397		Not Filtered
01/26/99	9:11	9:14	2000	60/3	7.36-7.44		140-141	SPC00504396	52	est. 3.5 L pumped, not filtered
01/26/99	11:33	11:50	800	186/3	7.24-7.17		320	SPC00527961		Not Filtered
03/30/99	9:50	10:10	700	60/3	8.0			SPC00529637		
03/30/99	12:40		200	77/3	7.0			SPC00529634	31	
04/20/99	9:00	9:32	175	60/3	4.19-4.50		30	SPC00551100	32-41	
04/20/99	12:00	13:45	500	60/3	4.8		10	SPC00551103	40	
04/20/99	9:15	10:07	375	BH80	6.39-6.72		30-50	SPC00551102	64	
05/10/99	10:20		40*	60/3	4.78-4.80	12.4	7.98	SPC00551104	21.1-24.0*	
05/10/99	10:24		40*	60/3	4.68	11.37	7.09	SPC00551105	34.8-36.3*	
05/10/99	10:10	10:29	175*	60/3	4.68-4.80*			SPC00551106	21.1-36.3*	100 mL used for alkalilinity
05/10/99	11:04		40*	60/3	4.84	9.67-8.72	6.01-5.38	SPC00551107	35.3-41.3*	Conductivity & TDS represent pre - post filtration
05/25/99	9:40		40*	60/3	4.75	11.74	7.43	SPC00551111	26.4-27.3*	
05/25/99	9:23		40*	60/3	4.68	16.07	10.18	SPC00551110	24.1-25.6*	
05/25/99	9:10	9:50	150*	60/3	4.68-4.75*			SPC00551151	24.1-27.3*	100 mL used for alkalilinity
05/25/99	10:04		40*	60/3	4.75	9.37	5.92	SPC00551112	24.8*	
06/24/99	9:17		40*	60/3	5.02	8.84		SPC00551154	27.5*	
06/24/99	9:25	9:55	170*	60/3	5.08*			SPC00551157	28.9*	100 mL used for alkalilinity
06/24/99	9:25	9:27	40*	60/3	5.08			SPC00551156	28.9*	
10/27/99	12:54		150*	59/2	5.93	113.4		SPC00557028*	43.4*	
10/27/99	13:03		50*	59/2	6.08	110.2		SPC00557029*	52*	
10/27/99	13:27		250*	59/3	6.64	203.1		SPC00557035*	60.2*	
10/27/99	13:45		40*	59/3	6.81	192.3	118.1	SPC00557036*	62.3*	
10/27/99	14:27		50*	76/3	6.14-6.46			SPC00557039*	28.7*	
11/30/99	10:21		50*	59/2	7.53	80.8	52.84	SPC00557082*	39.5*	
11/30/99	10:24		150*	59/2	7.24	69.14	43.9	SPC00557080*	46.6*	
11/30/99	10:30			59/2	6.8	67.04	42.3			
11/30/99	10:38		40*	59/2		70.3	44.36	SPC00557083*	55.9*	
11/30/99	10:47		50*	59/3	7.06	105.2	65.86	SPC00557042*	47.3*	
11/30/99	10:50		150*	59/3	7.27	106.8	65.4	SPC00552575*	60*	
11/30/99	10:55		40*	59/3	7.47	112	63.8	SPC00557043*	68.4*	

Table 6.3.4.1-1. Summary of DST Water Samples, the Field Data, and Important Observations through January 14, 2002 (continued)

Date	Approx. Start Time	Approx. Finish Time	Est. Volume (mL)	Collection Hole/Zone	pH	Electrical Conductivity (mS/cm)	Total Dissolved Solids (ppm)	Sample Number	Solution Temp. (°C)	Comments
11/30/99	11:59		50*	76/3	7.04	307.2	198.6	SPC00552577*	37.7*	
11/30/99	12:03		150*	76/3	6.91	312.3	201.3	SPC00557085*	48.9*	
11/30/99	12:10		125*	76/3	6.86	317.7	199.4	SPC00552576*	57.9*	
11/30/99	12:20		40*	76/3	6.94	326.2	207.3	SPC00552579*	53.2*	
11/30/99	13:10		50*	77/3	4.68	156.4	9.99	SPC00557084*	45.2*	Reported conductivity and TDS values are suspect.
01/25/00	9:30		150*	59/2	7.43	104.7	67.1	SPC00550668*	27.1*	
01/25/00	9:33		150*	59/2	7.07	62.03	39.35	SPC00550669*	38.5*	
01/25/00	9:36		150*	59/2	6.85	63.01	39.31	SPC00550671*	51.5*	
01/25/00	9:45			59/2	6.68	61.21	37.89		57.5*	
01/25/00	11:35		50*	77/2	4.63	61.24	40.24	SPC00550672*	37*	
01/25/00	12:00		50*	77/3	3.47	224.9	145.5	SPC00550674*	36.8*	
05/23/00	11:58		150*	59/2	6.96	96.13	61.27	SPC00550680*	30.5*	
05/23/00	12:00		150*	59/2	6.95	98.55	61.91	SPC00550682*	42.6*	
05/23/00	12:15			59/2	6.96	99.73	61.76		60.4*	
05/23/00	12:26		120*	59/3	5.19	5.2	3.14	SPC00550687*	46.4*	
05/23/00	9:11		160*	76/3	6.92-6.96	134.8	86.86	SPC00550697*	21-40.8*	
06/29/00	11:20			59/2	6.81-6.92	100.3	62.73		47.2*	
06/29/00	11:24			59/2	7	111.7	68.4		58.4*	
06/29/00	11:27			59/2	6.99-7.08	79.9	49.12		50.9*	
06/29/00	11:45			59/3	5.39	4.39	2.74		40.4*	
06/29/00	11:50			59/3	5.6	4.7	2.91		45.9*	
06/29/00	12:00			59/4	4.6	13.72	8.48		50.2*	
06/29/00	12:03			59/4	4.74	14.83	9.21		49.2*	
06/29/00	9:35			76/3	5.75	13.81	8.64		35.8*	
06/29/00	9:46			76/4	4.74-4.77	12.85	7.99		34.4*	
06/29/00	10:10			78/2	4.12	35.64	20.44		32.8*	
06/29/00	10:18			78/3	4.22	28.54	17.78		42.1*	
08/21/00	10:46	10:52	20*	76/3	6.27-5.04					
08/21/00	10:52	11:02	15*	76/4	5.01-4.99					
08/21/00	11:03	11:10	10*	78/3	5.05-5.21					
01/23/01	12:00	12:03	100*	59/2				SPC00530399*		Ultrameter problem, no pH, TDS
01/23/01	12:00	12:03	100*	59/2				SPC00529636*		Ultrameter problem, no pH, TDS
01/23/01	12:00	12:03	100*	59/2				SPC00529635*		Ultrameter problem, no pH, TDS
01/23/01	12:00	12:03	90*	59/2				SPC00530398*		Ultrameter problem, no pH, TDS
01/23/01	12:13	12:15	60*	59/3				SPC00530316*		Ultrameter problem, no pH, TDS
01/23/01	12:13	12:15	60*	59/3				SPC00530314*		Ultrameter problem, no pH, TDS
01/23/01	12:13	12:15	60*	59/3				SPC00530313*		Ultrameter problem, no pH, TDS
01/23/01	12:13	12:15	60*	59/3				SPC00530397*		Ultrameter problem, no pH, TDS
01/23/01	12:30	12:35	30*	60/4				SPC00530318*		Ultrameter problem, no pH, TDS
04/17/01	10:10	10:25	120	59/2	4.9	6.6	10.4	SPC00559467	32	Preserved with HNO_3
04/17/01	10:10	10:25	100	59/2	5.3	6.7	4.2	SPC00559468	35	Preserved with HNO_3
04/17/01	10:40	10:50	200	59/3	6.0	54.2	34.7	SPC00559463	30	Preserved with HNO_3
04/17/01	10:40	10:50	100	59/3	5.8	30.6	19.0	SPC00559465	38	Preserved with HNO_3
04/17/01	11:15	11:30	200	59/4	5.2	9.8	6.1	SPC00559466	33	Preserved with HNO_3

Table 6.3.4.1-1. Summary of DST Water Samples, the Field Data, and Important Observations through January 14, 2002 (continued)

Date	Approx. Start Time	Approx. Finish Time	Est. Volume (mL)	Collection Hole/Zone	pH	Electrical Conductivity (mS/cm)	Total Dissolved Solids (ppm)	Sample Number	Solution Temp. (°C)	Comments
04/17/01	12:40	12:45	200	76/2	5.7	40.1	25.8	SPC00559460	29	
04/17/01	12:45	12:50	500	76/2	7.7	41.5	25.8	SPC00559464	43	Preserved with HNO_3
04/17/01	12:50	12:55	500	76/2	7.9	40.2	24.8	SPC00559461	48	
04/17/01	12:55	13:00	500	76/2	8.1	38.9	24.7	SPC00559462	33	
04/17/01	13:00	13:09	500	76/2	8.2	38.4	24.4	SPC00559459	29	
04/17/01	13:09	13:20	250	76/2	8.2	37.8	24.1	SPC00559458	30	
04/17/01	13:20	13:25	120	76/2	8.3	33.5	22.5	SPC00559456	33	
04/17/01	13:25	13:33	120	76/2	8.3	37.3	24.0	SPC00559457	31	
06/26/01			10	76/3	5.3		3.7		32	
06/26/01	11:40	11:55	80	76/4	5.5	11.2	6.7	SPC00559493	42	
06/26/01	12:10	12:20	25	78/2	5.3	5.2	3.2	SPC00559494	44	
06/26/01	12:25	12:35	25	78/3	5.0	5.2	3.4	SPC00559495	47	
06/26/01	12:40	12:50	25	78/4	5.0	6.7	4.0	SPC00559496	44	
06/27/01	10:40	10:50	240	59/2	5.2	6.1	3.6	SPC00559497	57	Preserved with HNO_3
06/27/01	10:50	11:25	500	59/2	5.1	4.5	2.6	SPC00559498	58	
06/27/01	11:25	12:10	500	59/2	5.2	4.2	2.5	SPC00559499	56	
06/27/01	12:10	12:40	100	59/2	5.6	6.4	3.8	SPC00559471	49	
06/27/01	12:40	13:15	500	59/2	5.1	4.6	2.7	SPC00559472	54	
06/27/01	13:15	13:35	25	59/2	5.5	4.5	3.1	SPC00559473	48	
06/27/01	13:35	14:20	500	59/2	5.2	4	2.4	SPC00559474	42	
06/28/01	12:30	12:50	100	59/3	4.9	8.3	5.1	SPC00559476	44	
06/28/01	9:20	12:00	400	BH-72	4.8	14.6	8.9	SPC00559475	55	Using flex-tubing and rods
06/28/01	13:30	13:50	40	60/3	3.3	189	115.0	SPC00559477	35	
06/28/01	13:55	14:05	10	60/4	5.1	10.5	8.8		39	
08/07/01			5	76/3	5.2	4.1	2.5		48	
08/07/01	11:55	12:05	60	76/4	5.4	7.8	4.7	SPC00559454	61	
08/07/01	11:55	12:05	15	76/4	5.4	7.8	4.7	SPC00575214	61	
08/07/01	12:15	12:25	100	77/2	3.3	284	173.0	SPC00559455	61	
08/07/01	12:15	12:25	15	77/2	3.3	284	173.0	SPC00575218	61	
08/07/01	12:35	12:45	60	77/3	3.3	231	138.0	SPC00559484	60	
08/07/01	12:35	12:45	15	77/3	3.3	231	138.0	SPC00575213	60	
08/07/01	12:55	13:05	30	78/2	4.5	8.8	5.2	SPC00559485	47	
08/07/01			5	78/3	5.2	9.1	5.6		40	
08/07/01			10	78/4	5.5	14.3	8.8		38	
08/08/01	10:30	10:50	500	59/2	5.4	2.2	1.3	SPC00559486	38	
08/08/01	10:30	10:50	15	59/2	5.4	2.2	1.3	SPC00575215	38	
08/08/01	11:00	11:40	200	59/3	4.9	6	3.6	SPC00559487	58	
08/08/01	11:00	11:40	15	59/3	4.9	6	3.6	SPC00575212	58	
08/08/01	11:50	12:05	200	59/4	5.1	2.8	1.6	SPC00559488	51	
08/08/01	11:50	12:05	15	59/4	5.1	2.8	1.6	SPC00575217	51	
08/08/01			5	60/1	4.8	25	15.0		35	
08/08/01	12:20	12:35	100	60/2	3.1	309	194.0	SPC00559490	52	
08/08/01	12:20	12:35	15	60/2	3.1	309	194.0	SPC00575216	52	
08/08/01	13:30	13:50	15	60/3	3.4	186	114.0	SPC00559491	56	
08/08/01	13:55	14:05	10	60/4	4.4	14.5	8.8		41	
10/22/01	10:30	10:40	50	76/3	5.2	8.4	5.1	SPC00575220	42	
10/22/01	10:45	10:55	30	76/4	5.1	5.2	3.0	SPC00575222	62	
10/22/01	11:05	11:15	100	77/2	3.1	403	245.0	SPC00575226	53	
10/22/01	11:20	11:30	30	77/3	3.2	344	208.0	SPC00575223	58	
10/22/01			5	78/1	4.2	11.6	6.9		57	

Table 6.3.4.1-1. Summary of DST Water Samples, the Field Data, and Important Observations through January 14, 2002 (continued)

Date	Approx. Start Time	Approx. Finish Time	Est. Volume (mL)	Collection Hole/Zone	pH	Electrical Conductivity (mS/cm)	Total Dissolved Solids (ppm)	Sample Number	Solution Temp. (°C)	Comments
10/22/01			5	78/2	4.8	5.6	3.3		52	
10/22/01			10	78/3	5.0	7.7	4.5		59	
10/22/01			10	78/4	5.4	10	6.0		53	
10/22/01	10:30	10:50	100	59/2	4.9	8.5	5.2	SPC00575227	52	
10/22/01			10	59/3	5.0	5.2	3.0		57	
10/22/01			10	59/4	4.9	6	3.5		61	
10/22/01	12:50	13:00	80	60/2	3.2	406	252.0	SPC00575225	56	
10/22/01	13:10	13:20	30	60/3	3.5	151	90.0	SPC00575221	56	
10/22/01	13:25	13:35	40	60/4	3.8	63	38.0	SPC00575224	49	
10/22/01			5	61/1	4.4	14.6	8.7		51	
10/22/01			10	61/3	4.9	7.9	4.8		45	
10/22/01			10	61/4	5.0	7.1	4.3		52	
11/08/01	14:45	15:10	50	BH 72	5.1	20.0	12.5	SPC00575228	28	HF Experiment
11/08/01				BH 72	5.5	17.5	10.8		27	HF Experiment
11/15/01	11:00	12:15	20	BH 55	7.5	279.0	176.0	SPC00575231	23	HF Experiment
11/21/01			100					SPC00559482		HF Exp., rinse of flex tubing
11/21/01			4	BH 55				SPC00559483		HF Experiment-not filtered
11/26/01	9:50	10:30	100	BH 72	5.3	13.8	8.6	SPC00575219	25	HF Experiment
11/26/01	13:10	15:10	20	BH 55	5.0	20.5	12.8	SPC00575229	24	HF Experiment
11/29/01	10:30	11:00	100	BH 72	3.8	39.7	24.3	SPC00559478	39	HF Experiment
11/29/01	10:30	11:00		BH 72	3.8	41.4	25.3		40	HF Experiment
11/29/01	11:30	14:30	13	BH 55	5.2			SPC00559479		HF Experiment
12/05/01	12:00	13:00	200	BH 72	3.5	111.5	70.6	SPC01016065	21	HF Experiment
12/05/01	12:00	13:00		BH 72	3.4	167.3	106.0		32	HF Experiment
12/05/01	12:00	13:00	500	BH 72	3.4	135.0	85.4	SPC01016066	20	HF Experiment
12/05/01	11:00	15:10	10	BH 55				SPC01016067		HF Experiment
01/07/02			2	BH 55				SPC01016084		HF Experiment
01/07/02	11:30	11:40	500	76/2	7.8	30.2	18.0	SPC01016082	52	
01/07/02	11:30	11:40	15	76/2	7.8	30.2	18.0	SPC01014151	52	
01/07/02	11:40	11:50	50	76/3	4.9	7.3	4.3	SPC01016076	56	
01/07/02	11:40	11:50	15	76/3	4.9	7.3	4.3	SPC01014154	56	
01/07/02	11:50	12:00	30	76/4	4.8	5.5	3.2	SPC01016074	55	
01/07/02	11:50	12:00	15	76/4	4.8	5.5	3.2	SPC01016071	55	
01/07/02	12:15	12:25	30	78/2	5.1	4.9	2.9	SPC01016075	44	
01/07/02	12:15	12:25	15	78/2	5.1	4.9	2.9	SPC01016070	44	
01/07/02	12:25	12:35	30	78/3	4.9	5.1	3.1	SPC01016078	43	
01/07/02	12:25	12:35	15	78/3	4.9	5.1	3.1	SPC01014147	43	
01/07/02	12:40	12:50	40	78/4	4.9	5.4	3.2	SPC01016072	40	
01/07/02	12:40	12:50	15	78/4	4.9	5.4	3.2	SPC01014149	40	
01/07/02	13:05	13:20	400	59/2	5.2	3.3	2.0	SPC01016083	30	
01/07/02	13:05	13:20	15	59/2	5.2	3.3	2.0	SPC01014150	30	
01/07/02	13:20	13:35	250	59/3	5.3	2	1.2	SPC01016079	34	
01/07/02	13:20	13:35	15	59/3	5.3	2	1.2	SPC01014153	34	
01/07/02	13:40	13:50	40	59/4	4.8	5.7	3.5	SPC01016073	35	
01/07/02	13:40	13:50	15	59/4	4.8	5.7	3.5	SPC01014152	35	
01/07/02	14:00	14:10	50	61/2	5.5	6.5	4.0	SPC01016081	32	
01/07/02	14:00	14:10	15	61/2	5.5	6.5	4.0	SPC01014148	32	
01/07/02	14:15	14:25	40	61/3	5.2	4.8	2.9	SPC01016080	28	
01/07/02	14:15	14:25	15	61/3	5.2	4.8	2.9	SPC01016068	28	

Table 6.3.4.1-1. Summary of DST Water Samples, the Field Data, and Important Observations through January 14, 2002 (continued)

Date	Approx. Start Time	Approx. Finish Time	Est. Volume (mL)	Collection Hole/Zone	pH	Electrical Conductivity (mS/cm)	Total Dissolved Solids (ppm)	Sample Number	Solution Temp. (°C)	Comments
01/07/02	14:30	14:40	50	61/4	5.1	7.7	4.5	SPC01016077	33	
01/07/02	14:30	14:40	15	61/4	5.1	7.7	4.5	SPC01016069	33	
01/09/02	9:30	9:50	120	77/2	3.7	49.8	30.6	SPC01014156	41	
01/09/02	9:30	9:50	15	77/2	3.7	49.8	30.6	SPC01014159	41	
01/09/02	10:00	10:20	100	77/3	3.4	176	106.0	SPC01014155	54	
01/09/02	10:00	10:20	15	77/3	3.4	176	106.0	SPC01014158	54	
01/09/02	10:20	10:50	150	BH 72	3.3	85.8	54.9	SPC01014157	16	HF Exp. F.A. done on 1/16/02
01/09/02	10:20	10:50	15	BH 72	3.3	85.8	54.9	SPC01014160	16	HF Exp. F.A. done on 1/16/02

NOTES: 1) A single set of field measurements, in conjunction with multiple samples from a single borehole/zone, indicates that samples were split.
2) Volumes and temperatures listed are included for information only.
3) Small fluid volumes (<10mL) were depleted after conducting field measurements and not saved as samples.
4) Blank cell indicates no measurement recorded.
5) Asterisk indicates information source from Cho 2001 [159473].

Table 6.3.4.1-2. Chemical Analyses of DST Borehole Water Samples

SMF No. (SPC0…)	1002488	1002586	1002525	0527969[9]	0527968[9]	0527977[9]	0527915[9]	0527916[9]	0527917[9]
Collection Date	Pre-Htng.	Pre-Htng.	Pre-Htng.	06/04/98	06/04/98	06/04/98	08/12/98	08/12/98	08/12/98
Collection Time									
Sample ID	PERM-1[4]	PERM-2[4]	PERM-3[4]	BH 60-2	BH 60-2	BH 60-3	BH 60-2	BH 60-3	BH 77-3
Field pH[2]	7.79	8.32	8.31	7.5	na	7.7	6.9	6.8	5.5
Metals / Cations									
Na (mg/L)	60.5	61.0	61.5	20.0	na	24.0	20.4	17.2	2.4
Si (mg/L)	37	31	35	56	na	41	51.8	43.5	1.48
Ca (mg/L)	98.17	106.17	96.67	20	na	25	19.9	18.7	2.09
K (mg/L)	6.0	7.0	9.0	6.0	na	4.5	5.4	4.5	1.4
Mg (mg/L)	25.65	16.55	17.35	2.9	na	5.7	1.21	4.0	0.21
Al (mg/L)	< 0.06	< 0.06	< 0.06	0.12	na	0.017[5]	< 0.06	0.003[5]	< 0.06
B (mg/L)	3.05	2.75	2.75	1.2	na	0.92	1.84	1.14	0.13
S (mg/L)	42.25	38.6	38.65	5.5	na	9.2	4.5	5.2	1.4
Fe (mg/L)	< 0.02	< 0.02	< 0.02	0.04	na	< 0.02	0.02	0.12	< 0.02
Li (mg/L)	0.1	0.45	0.05	0.07	na	0.07	0.03	0.040	< 0.01
Sr (mg/L)	1.4	1	1.05	0.18	na	0.34	0.11	2.21	0.05
Anions									
HCO_3 (mg/L)[3]				na	na	na	na	na	na
F (mg/L)	0.36	0.96	0.76	na	1.00	0.82	0.71	0.43	0.41
Cl (mg/L)	122.73	109.93	123.13	na	10	16	6.14	5.52	2.15
Br (mg/L)	0.6	0.76	1.2	na	0.84	0.73	0.05	0.21	0.03
SO_4 (mg/L)	124.18	111.38	119.78	na	17	30	4.88	8.81	1.86
PO_4 (mg/L)	< 0.07	< 0.07	< 0.07	na	< 0.07	< 0.07	0.25	0.16	1.06
NO_2 (mg/L)	< 0.04	< 0.04	< 0.04	na	< 0.01	< 0.01	< 0.04	< 0.04	< 0.04
NO_3 (mg/L)	21.72	2.52	10.40	na	3.00	3.6	0.46	0.60	0.22

SMF No. (SPC0…)	0541803[9]	0541803[6,9]	0541804[9]	0541804[6,9]	0541805[9]	0541805[6,9]	0504397[9]	0504396[9]	0527961[9]
Collection Date	11/12/98	11/12/98	11/12/98	11/12/98	11/12/98	11/12/98	01/26/99	01/26/99	01/26/99
Collection Time									
Sample ID	BH 59-4	BH 59-4	BH 60-3	BH 60-3	BH 186-3	BH 186-3	BH 59-4	BH 60-3	BH 186-3
Field pH[2]	6.63	6.63	6.92	6.92	6.83	6.83	na	7.4	7.2
Metals / Cations									
Na (mg/L)	22.6	135	10.1	20.3	105	17.0	219	19.1	25.9
Si (mg/L)	33.5	44.2	60.0	53.8	16.0	27.2	12.0	65.0	49.3
Ca (mg/L)	476	450	15.3	13.9	11.5	20.2	429	5.93	2.92
K (mg/L)	29.5	37.8	8.7	7.8	3.5	3.9	29.7	4.1	5.9
Mg (mg/L)	64.1	83.9	3.35	3.00	5.1	5.68	164	1.17	6.32
Al (mg/L)	0.01[5]	< 0.06	0.033[5]	0.033[5]	< 0.003[5]	< 0.003[5]	0.086[5]	< 0.06	< 0.06
B (mg/L)	4.47	4.13	1.58	1.41	0.51	0.58	6.68	1.75	0.84
S (mg/L)	50.7	64.8	11.6	10.5	8.47	9.42	109	6.4	7.9
Fe (mg/L)	< 0.02	< 0.02	0.02	< 0.02	0.02	< 0.02	< 0.02	< 0.02	0.09
Li (mg/L)	0.21	0.20	0.040	0.040	0.05	0.05	0.33	0.02	0.05
Sr (mg/L)	4.02	3.71	0.22	0.20	0.30	0.34	5.84	0.09	0.37
Anions									
HCO_3 (mg/L)[3]	na	na	na	na	na	na	na	41	116
F (mg/L)	0.8	4.3	0.49	0.50	0.56	0.62	0.51	1.27	1.20
Cl (mg/L)	1,130	1,250	19.5	19.6	18.7	18.6	1,160	10.3	23.3
Br (mg/L)	1.13	< 0.07	0.6	0.51	0.67	0.60	1.51	0.15	0.32
SO_4 (mg/L)	226	213	30.6	30.8	26.3	26.2	240	13.5	21
PO_4 (mg/L)	< 5	< 0.2	< 0.2	< 0.2	< 0.2	< 0.2	< 0.5	< 0.05	< 0.1
NO_2 (mg/L)	< 3	< 10	< .10	< .10	< .1	< .1	< .3	< .03	< 0.05
NO_3 (mg/L)	3.12	7.81	3.38	3.17	7.47	7.27	11.6	2.56	6.73

Table 6.3.4.1-2. Chemical Analyses of DST Borehole Water Samples (continued)

SMF No. (SPC0…)	0529637-#1[9]	0529637-#2[9]	0529637-#3[9]	0529634[9]	0551100[9]	0551103[9]	0551104[9]	0551105[9]	0551106[9]
Collection Date	03/30/99	03/30/99	03/30/99	03/30/99	04/20/99	04/20/99	05/10/99	05/10/99	05/10/99
Collection Time	9:50 AM	9:55 AM	10:10 AM		9:32 AM	1:45 PM	10:20 AM	10:24 AM	
Sample ID	BH 60-3	BH 60-3	BH 60-3	BH 77-3	BH 60-3	BH 60-3	BH 60-3	BH 60-3	BH 60-3
Field pH[2]	8.0	na	na	4.8	4.19-4.50	4.77	4.78-4.80	4.68	na
Metals / Cations									
Na (mg/L)	11.2	11.0	2.2	< 0.2	0.14	< 0.05	1.8	2.5	0.15
Si (mg/L)	62.8	59.8	12.1	1.03	0.7	< 0.5	1.1	1.2	0.6
Ca (mg/L)	2.06	2.27	1.22	0.41	0.14	0.10	0.14	0.09	0.22
K (mg/L)	2.4	2.4	0.5	< 0.5	< 0.5	< 0.5	< 0.5	< 0.5	< 0.5
Mg (mg/L)	0.27	0.26	0.01	0.02	< 0.005	< 0.005	< 0.005	< 0.005	< 0.005
Al (mg/L)	0.36, 0.27[5]	0.36, 0.27[5]	0.08, 0.07[5]	0.005[5]	< 0.2	< 0.2	< 0.2	< 0.2	< 0.2
B (mg/L)	2.10	2.11	1.23	0.09	1.7	1.0	2.3	2.6	0.9
S (mg/L)	1.83	1.82	0.42	< 0.02	< 0.5	< 0.5	< 0.5	< 0.5	< 0.5
Fe (mg/L)	< 0.02	< 0.02	< 0.02	0.05	0.02	0.01	< 0.01	< 0.01	< 0.01
Li (mg/L)	0.02	< 0.01	< 0.01	< 0.01	< 4	< 4	< 4	< 4	< 4
Sr (mg/L)	0.02	0.02	0.01	< 0.01	< 0.05	< 0.05	< 0.05	< 0.05	< 0.05
Anions									
HCO_3 (mg/L)[3]	25.0	na	na	1.25	na	na	na	na	8.1
F (mg/L)	1.02	0.97	0.11	0.01	< 0.005	< 0.005	< 0.005	< 0.005	< 0.005
Cl (mg/L)	4.15	3.92	0.72	0.3	0.05	0.08	0.06	0.05	0.11
Br (mg/L)	< 0.04	< 0.04	< 0.04	< 0.04	< 0.03	< 0.03	< 0.03	< 0.03	< 0.03
SO_4 (mg/L)	3.83	3.75	0.79	0.13	0.1	0.09	0.09	0.09	0.08
PO_4 (mg/L)	< 0.05	< 0.05	< 0.05	< 0.05	< 0.02	< 0.02	0.92	0.84	0.62
NO_2 (mg/L)	< 0.03	< 0.03	< 0.03	< 0.03	< 0.007	< 0.007	< 0.007	< 0.007	< 0.007
NO_3 (mg/L)	0.92	0.84	0.17	0.065	< 0.02	< 0.02	< 0.02	< 0.02	< 0.02

SMF No. (SPC0…)	0551107	0551110[9]	0551111[9]	0551154[9]	0551155[9]	0551159[9]	0551160[9]	0551169[9]	0557029[9]
Collection Date	05/10/99	05/25/99	05/25/99	06/24/99	06/24/99	08/09/99	08/09/99	08/10/99	10/27/99
Collection Time	11:04 AM	9:23 AM	9:40 AM	9:17 AM	9:23 AM				
Sample ID	BH 60-3	BH 60-3	BH 60-3	BH 60-3	BH 60-3	BH 59-2(AC)	BH 59-2(BC)	BH 61-3	BH 59-2
Field pH[2]	4.84	4.68	4.75	5.02	na	na	na	na	na
Metals / Cations									
Na (mg/L)	2.8	1.8	1.6	1.87	2.26	30	24	19	na
Si (mg/L)	1.4	2.1	0.7	6.30	3.22	78	81	67	na
Ca (mg/L)	0.15	0.13	0.09	0.69	0.23	47	39	14	na
K (mg/L)	< 0.5	< 0.5	< 0.5	0.5	< 0.5	8	6	5	na
Mg (mg/L)	< 0.005	< 0.005	< 0.005	0.012	< 0.005	13	11	3.2	na
Al (mg/L)	< 0.2	< 0.2	< 0.2	< 0.04	< 0.04	< 0.2	< 0.2	< 0.2	na
B (mg/L)	2.8	2.0	1.9	0.62	1.85	0.8	0.6	1.5	na
S (mg/L)	< 0.5	< 0.5	< 0.5	< 0.1	< 0.1	22	17	3.1	na
Fe (mg/L)	0.31	< 0.01	< 0.01	< 0.01	< 0.01	0.41	0.32	1.2	na
Li (mg/L)	< 4	< 4	< 4	< 1	< 1	< 4	< 4	< 4	na
Sr (mg/L)	< 0.05	< 0.05	< 0.05	< 0.01	< 0.01	0.54	0.45	0.14	na
Anions									
HCO_3 (mg/L)[3]	na	8.6	8.6	na	na	na	na	na	23.5
F (mg/L)	< 0.005	< 0.005	< 0.005	0.685	0.195	0.725	0.575	0.835	0.27
Cl (mg/L)	0.09	0.20	0.06	0.615	0.305	88.3	71.0	24.1	9.5
Br (mg/L)	< 0.03	< 0.03	< 0.03	< 0.03	< 0.03	0.515	0.46	0.35	0.61
SO_4 (mg/L)	0.12	0.09	0.07	< 0.03	0.325	64.2	53.5	9.13	6.2
PO_4 (mg/L)	< 0.02	0.69	0.33	< 0.02	< 0.02	< 0.02	< 0.02	< 0.02	< 0.02
NO_2 (mg/L)	< 0.007	< 0.007	< 0.007	< 0.007	< 0.007	< 0.007	< 0.007	< 0.007	< 0.007
NO_3 (mg/L)	< 0.02	< 0.02	< 0.02	na	< 0.02	3.79	2.83	0.825	1.32

Table 6.3.4.1-2. Chemical Analyses of DST Borehole Water Samples (continued)

SMF No. (SPC0…)	0557032	0557033[9]	0557036[9]	0557038[9]	0557040[9]	0557080	0557081	0557083	0552575	0557043
Collection Date	10/27/99	10/27/99	10/27/99	10/27/99	10/27/99	11/30/99	11/30/99	11/30/99	11/30/99	11/30/99
Collection Time										
Sample ID	BH 59-2	BH 59-2	BH 59-3	BH 59-3	BH 76-3	BH 59-2	BH 59-2	BH 59-2	BH 59-3	BH 59-3
Field pH[2]	5.93	6.08	na	6.64	6.14-6.46	6.86	7.24	na	7.47	na
Metals / Cations										
Na (mg/L)	9.2	9.2	na	19.3	64.5	6.6	7.7	na	15.6	na
Si (mg/L)	44.5	44.9	na	84.2	133.4	38.0	39.9	na	92.5	na
Ca (mg/L)	7.53	7.47	na	13.2	59.5	4.33	5.63	na	2.86	na
K (mg/L)	3.4	3.6	na	5.6	13.4	2.6	3.0	na	3.9	na
Mg (mg/L)	1.81	1.72	na	1.49	13.8	1.02	1.38	na	0.29	na
Al (mg/L)	0.033[7]	0.033[7]	na	0.040	0.010	0.030	0.030	na	0.071	na
B (mg/L)	0.27	0.21	na	0.86	2.38	0.14	0.17	na	1.06	na
S (mg/L)	2.52	2.50	na	14.48	34.55	0.76	1.33	na	3.25	na
Fe (mg/L)	0.20	0.19	na	< 0.02	< 0.02	0.09	0.14	na	< 0.02	na
Li (mg/L)	0.16	0.01	na	0.02	0.13	0.01	0.01	na	0.02	na
Sr (mg/L)	0.11	0.08	na	0.13	0.78	0.06	0.08	na	0.03	na
Anions										
HCO_3 (mg/L)[3]	na	23.5	12.4	12.4	na	na	na	22.3	na	20.7
F (mg/L)	na	0.27	0.64	0.73	1.11	na	na	0.35	na	1.3
Cl (mg/L)	na	9.1	12.9	12.9	81.9	na	na	5.0	na	8.8
Br (mg/L)	na	0.58	0.89	0.51	0.97	na	na	< 0.03	na	< 0.03
SO_4 (mg/L)	na	6.3	40.7	40.3	94.6	na	na	2.8	na	8.2
PO_4 (mg/L)	na	< 0.02	< 0.04	< 0.04	< 0.02	na	na	< 0.02	na	< 0.02
NO_2 (mg/L)	na	< 0.007	< 0.01	< 0.01	< 0.007	na	na	< 0.007	na	< 0.007
NO_3 (mg/L)	na	1.40	3.06	3.05	6.42	na	na	< 0.02	na	2.4

SMF No. (SPC0…)	0552578	0552579	0557081[9]	0557084[9]	0557022	0550671	0550673	0550698[9]	0550674[9]	0550674[9]
Collection Date	11/30/99	11/30/99	11/30/99	11/30/99	01/25/00	01/25/00	01/25/00	01/25/00	01/25/00	01/25/00
Collection Time										
Sample ID	BH 76-3	BH 76-3	BH 77-3	BH 77-3	BH 59-2	BH 59-2	BH 59-2	BH 77-2	BH 77-3	BH 77-3
Field pH[2]	6.94	na	na	4.68	7.07	6.68	na	4.63	3.47	na
Metals / Cations										
Na (mg/L)	28.2	na	na	0.6	8.1	6.6	na	< 0.3	< 0.3	na
Si (mg/L)	92.8	na	na	2.45	42.8	41.7	na	2.0	2.5	na
Ca (mg/L)	22.3	na	na	1.27	7.54	2.89	na	0.17	< 0.005	na
K (mg/L)	7.4	na	na	< 0.2	3.6	2.8	na	< 0.2	< 0.2	na
Mg (mg/L)	4.71	na	na	0.19	1.78	0.72	na	0.01	< 0.005	na
Al (mg/L)	0.031	na	na	0.334	< 0.05	0.043	na	0.049	0.023	na
B (mg/L)	0.81	na	na	0.09	0.29	0.21	na	0.05	0.04	na
S (mg/L)	9.46	na	na	0.24	6.44	0.65	na	< 0.05	< 0.05	na
Fe (mg/L)	0.10	na	na	0.37	0.07	< 0.02	na	0.25	0.07	na
Li (mg/L)	0.04	na	na	< 0.01	< 0.01	< 0.01	na	< 0.01	< 0.01	na
Sr (mg/L)	0.26	na	na	0.02	0.091	0.036	na	< 0.005	< 0.005	na
Anions										
HCO_3 (mg/L)[3]	na	82.3	na	na	na	na	22.8	na	na	na[8]
F (mg/L)	na	1.3	15	na	na	na	0.73	6.7	19.9	20.8[8]
Cl (mg/L)	na	19	3.5	na	na	na	3.8	0.6	0.8	0.29[8]
Br (mg/L)	na	< 0.03	< 0.03	na	na	na	< 0.1	< 0.1	< 0.1	< 0.1[8]
SO_4 (mg/L)	na	26.0	1.6	na	na	na	1.8	0.39	< 0.1	< 0.1[8]
PO_4 (mg/L)	na	< 0.02	< 0.02	na	na	na	0.62	0.64	4.0	2.9[8]
NO_2 (mg/L)	na	< 0.007	< 0.007	na	na	na	< 0.05	< 0.05	< 0.05	< 0.06[8]
NO_3 (mg/L)	na	2.5	< 0.02	na	na	na	0.77	< 0.1	0.20	0.18[8]

Table 6.3.4.1-2. Chemical Analyses of DST Borehole Water Samples (continued)

SMF No. (SPC0…)	0550681	0550682	0550684	0550687	0550697	0550679	0550693	0550694	0550691
Collection Date	05/23/00	05/23/00	05/23/00	05/23/00	05/23/00	05/23/00	06/29/00	06/29/00	06/29/00
Collection Time									
Sample ID	BH 59-2	BH 59-2	BH 59-2	BH 59-3	BH 76-3	BH 76-4	BH 59-2	BH 59-2	BH 59-2
Field pH [2]	6.96	6.96	6.95	5.19	6.92-6.96	na	6.99-7.08	6.99-7.08	7.00
Metals / Cations									
Na (mg/L)	17	18	17	< 2.4	29	< 2.4	16	15	< 4.8
Si (mg/L)	59.4	59.2	59.3	< 0.46	96.0	3.4	62.7	57.5	36.3
Ca (mg/L)	4.7	4.4	4.5	< 0.17	7.1	1.5	4.3	3.8	2.0
K (mg/L)	4.3	4.4	4.4	< 0.095	6.5	0.70	4.7	4.2	2.5
Mg (mg/L)	1.1	1.1	1.1	< 0.042	1.4	0.14	1.1	1.0	0.54
Al (mg/L)	< 0.053	< 0.053	< 0.053	< 0.053	< 0.053	< 0.053	< 0.053	< 0.053	< 0.11
B (mg/L)	na	na	na	na	na	na	na	na	na
S (mg/L)	na	na	na	na	na	na	na	na	na
Fe (mg/L)	< 0.038	< 0.038	< 0.038	< 0.038	< 0.038	< 0.038	< 0.038	< 0.038	< 0.076
Li (mg/L)	0.021	0.022	0.021	< 0.0007	0.045	0.0037	0.019	0.018	0.010
Sr (mg/L)	< 0.013	< 0.013	< 0.013	< 0.013	< 0.013	< 0.013	< 0.013	< 0.013	< 0.026
Anions									
HCO_3 (mg/L) [3]	31.4	31.4	31.4	na	na	na	na	na	na
F (mg/L)	0.58	0.55	0.49	0.15	0.76	0.13	na	na	na
Cl (mg/L)	10.15	10.6	10.15	0.07	14.5	2.75	na	na	na
Br (mg/L)	< 0.1	0.38	< 0.1	< 0.1	< 0.1	< 0.1	na	na	na
SO_4 (mg/L)	2.9	3.18	3.1	< 0.1	4.98	2.24	na	na	na
PO_4 (mg/L)	< 0.2	< 0.2	< 0.2	< 0.2	< 0.2	< 0.2	na	na	na
NO_2 (mg/L)	< 0.06	< 0.06	< 0.06	< 0.06	< 0.06	< 0.06	na	na	na
NO_3 (mg/L)	0.56	0.54	0.71	0.38	1.47	0.85	na	na	na

SMF No. (SPC0…)	0550689	0550690	0550685	0550686	0530300	0530302	0550678	0530303	0550688
Collection Date	06/29/00	06/29/00	06/29/00	06/29/00	06/29/00	06/29/00	06/29/00	06/29/00	06/29/00
Collection Time									
Sample ID	BH 59-2	BH 59-2	BH 59-4	BH 59-3	BH 76-3	BH 76-3	BH 76-4	BH 76-4	BH 78-2
Field pH [2]	na	na	4.60-4.74	5.60	5.75	5.75	4.74-4.77	na	4.12
Metals / Cations									
Na (mg/L)	na	na	< 2.4	< 2.4	na	< 2.4	< 2.4	na	< 2.4
Si (mg/L)	na	na	< 0.46	< 0.46	na	3.1	< 0.46	na	< 0.46
Ca (mg/L)	na	na	< 0.17	< 0.17	na	< 0.17	< 0.17	na	0.5
K (mg/L)	na	na	< 0.095	< 0.095	na	< 0.095	< 0.095	na	< 0.095
Mg (mg/L)	na	na	< 0.042	< 0.042	na	0.29	< 0.042	na	< 0.042
Al (mg/L)	na	na	< 0.053	< 0.053	na	0.17	0.18	na	< 0.053
B (mg/L)	na	na	na	na	na	na	na	na	na
S (mg/L)	na	na	na	na	na	na	na	na	na
Fe (mg/L)	na	na	< 0.038	< 0.038	na	< 0.038	< 0.038	na	< 0.038
Li (mg/L)	na	na	< 0.0007	< 0.0007	na	< 0.0007	< 0.0007	na	< 0.0007
Sr (mg/L)	na	na	< 0.013	< 0.013	na	< 0.013	< 0.013	na	< 0.013
Anions									
HCO_3 (mg/L) [3]	29.4	29.4	na	na	na	na	na	na	na
F (mg/L)	0.18	0.15	na	na	< 0.007	na	na	< 0.007	0.11
Cl (mg/L)	0.90	0.32	na	na	0.67	na	na	0.94	2.79
Br (mg/L)	0.62	0.48	na	na	0.47	na	na	0.57	1.15
SO_4 (mg/L)	0.5	0.42	na	na	1.54	na	na	< 0.1	< 0.1
PO_4 (mg/L)	< 0.2	< 0.2	na	na	< 0.2	na	na	< 0.2	< 0.2
NO_2 (mg/L)	< 0.06	< 0.06	na	na	< 0.06	na	na	< 0.06	< 0.06
NO_3 (mg/L)	0.65	0.48	na	na	0.49	na	na	< 0.09	< 0.09

Table 6.3.4.1-2. Chemical Analyses of DST Borehole Water Samples (continued)

SMF No. (SPC0…)	0550642	0530398	0530316	0530318	0559467	0559463	0559466	0559464	0559458
Collection Date	06/29/00	01/23/01	01/23/01	01/23/01	04/17/01	04/17/01	04/17/01	04/17/01	04/17/01
Collection Time									
Sample ID	BH 78-3	BH 59-2	BH 59-3	BH 60-4	BH 59-2	BH 59-3	BH 59-4	BH 76-2	BH 76-2
Field pH [2]	4.22	na	na	na	4.87	5.96	5.20	7.68	8.22
Metals / Cations									
Na (mg/L)	< 2.4	29	< 2.4	< 2.4	< 2.4	6	< 2.4	9	9
Si (mg/L)	2.3	84.5	< 0.46	46.1	5.2	< 0.46	< 0.46	42.6	44.1
Ca (mg/L)	1.1	7.8	< 0.17	0.68	0.6	3.5	0.57	1.3	1.1
K (mg/L)	0.2	5.8	< 0.053	< 0.095	0.33	0.35	< 0.095	1.6	1.6
Mg (mg/L)	0.15	1.8	< 0.042	< 0.042	0.14	1.40	< 0.042	0.27	0.22
Al (mg/L)	0.31	< 0.053	< 0.053	< 0.053	< 0.053	< 0.053	< 0.053	0.42	0.43
B (mg/L)	na	na	na	na	na	na	na	na	na
S (mg/L)	na	na	na	na	na	na	na	na	na
Fe (mg/L)	< 0.038	< 0.038	< 0.038	< 0.038	< 0.038	< 0.038	< 0.038	0.40	0.40
Li (mg/L)	< 0.0007	0.033	< 0.0007	< 0.0007	< 0.0007	< 0.0007	< 0.0007	0.0098	0.010
Sr (mg/L)	< 0.013	< 0.013	< 0.013	< 0.013	< 0.013	< 0.013	< 0.013	< 0.013	< 0.013
Anions									
HCO_3 (mg/L) [3]	na	na	na	na	na	na	na	na	na
F (mg/L)	< 0.007	0.78	< 0.007	0.35	na	na	na	na	0.38
Cl (mg/L)	1.39	25.20	0.26	0.55	na	na	na	na	1.9
Br (mg/L)	0.79	< 0.1	< 0.1	< 0.1	na	na	na	na	< 0.1
SO_4 (mg/L)	< 0.1	9.5	< 0.1	0.57	na	na	na	na	0.89
PO_4 (mg/L)	< 0.2	< 0.2	< 0.2	< 0.2	na	na	na	na	< 0.2
NO_2 (mg/L)	< 0.06	< 0.06	< 0.06	0.59	na	na	na	na	< 0.06
NO_3 (mg/L)	< 0.09	0.99	< 0.09	0.54	na	na	na	na	< 0.09

SMF No. (SPC0…)	0559456	0559481	0559477	0559455	0559455	0559484	0559484	0559490	0559491
Collection Date	04/17/01	06/28/01	06/28/01	08/07/01	08/07/01	08/07/01	08/07/01	08/08/01	08/08/01
Collection Time									
Sample ID	BH 76-2	BH 60-3	BH 60-3	BH 77-2	BH 77-2	BH 77-3	BH 77-3	BH 60-2	BH 60-3
Field pH [2]	8.29	3.3	3.30	3.3	3.3	3.3	3.3	3.1	3.4
Metals / Cations									
Na (mg/L)	9	< 2.4	na	< 2.4	na	< 2.4	na	< 2.4	< 2.4
Si (mg/L)	45.6	4.9	na	10.7	na	17.4	na	22.7	5.3
Ca (mg/L)	1.3	< 0.17	na	< 0.17	na	< 0.17	na	< 0.17	0.7
K (mg/L)	1.9	< 0.095	na	< 0.095	na	< 0.095	na	< 0.095	0.35
Mg (mg/L)	0.23	< 0.042	na	< 0.042	na	< 0.042	na	< 0.042	< 0.042
Al (mg/L)	0.45	0.67	na	1.0	na	2.2	na	2.5	0.8
B (mg/L)	na	na	na	na	na	na	na	na	na
S (mg/L)	na	na	na	na	na	na	na	na	na
Fe (mg/L)	0.39	0.15	na	0.20	na	0.19	na	1.6	< 0.038
Li (mg/L)	0.0076	< 0.0007	na	< 0.0007	na	< 0.0007	na	< 0.0007	< 0.0007
Sr (mg/L)	< 0.013	< 0.013	na	< 0.013	na	< 0.013	na	< 0.013	< 0.013
Anions									
HCO_3 (mg/L) [3]	na	na	na	< 5	< 5	< 5	< 5	< 5	< 5
F (mg/L)	0.47	na	17.7	41.0	50.0	50	57.8	66	8.77
Cl (mg/L)	1.71	na	0.90	< 0.05	0.77	< 0.05	1.12	0.76	0.82
Br (mg/L)	< 0.1	na	< 0.1	< 0.1	< 0.2	< 0.1	< 0.1	< 0.1	< 0.1
SO_4 (mg/L)	0.85	na	< 0.1	< 0.1	0.42	< 0.1	< 0.1	< 0.1	< 0.1
PO_4 (mg/L)	< 0.2	na	< 0.2	< 0.2	< 0.3	< 0.2	< 0.2	< 0.2	< 0.2
NO_2 (mg/L)	< 0.06	na	< 0.06	< 0.06	< 0.1	< 0.06	< 0.06	< 0.06	< 0.06
NO_3 (mg/L)	< 0.09	na	< 0.09	0.60	0.69	0.48	0.21	< 0.09	< 0.09

Table 6.3.4.1-2. Chemical Analyses of DST Borehole Water Samples (continued)

SMF No. (SPC0…)	0575227	0575225	0575221	0575224	0575222	0575226	0575223	1016082	1014156	1014155
Collection Date	10/22/01	10/22/01	10/22/01	10/22/01	10/22/01	10/22/01	10/22/01	01/07/02	01/09/02	01/09/02
Collection Time										
Sample ID	BH 59-2	BH 60-2	BH 60-3	BH 60-4	BH 76-4	BH 77-2	BH 77-3	BH 76-2	BH 77-2	BH 77-3
Field pH [2]	4.9	3.2	3.5	3.8	5.1	3.1	3.2	7.8	3.7	3.4
Metals / Cations										
Na (mg/L)	< 2.4	< 2.4	< 2.4	< 2.4	na	< 2.4	< 2.4	na	na	na
Si (mg/L)	1.7	10.3	10.9	22.9	na	3.6	2.60	na	na	na
Ca (mg/L)	0.49	< 0.17	< 0.17	0.54	na	0.36	< 0.17	na	na	na
K (mg/L)	< 0.095	< 0.095	< 0.095	< 0.095	na	0.25	< 0.095	na	na	na
Mg (mg/L)	< 0.042	< 0.042	< 0.042	< 0.042	na	< 0.042	< 0.042	na	na	na
Al (mg/L)	< 0.053	0.41	0.22	< 0.053	na	0.3	0.25	na	na	na
B (mg/L)	na	na	na	na	na	na	na	na	na	na
S (mg/L)	na	na	na	na	na	na	na	na	na	na
Fe (mg/L)	< 0.038	0.34	< 0.038	0.047	na	0.18	0.16	na	na	na
Li (mg/L)	<0.0007	<0.0007	<0.0007	<0.0007	na	<0.0007	<0.0007	na	na	na
Sr (mg/L)	< 0.013	< 0.013	< 0.013	< 0.013	na	< 0.01	< 0.013	na	na	na
Anions										
HCO_3 (mg/L) [3]	< 5	< 5	< 5	< 5	< 5	< 5	< 5	< 5	< 5	< 5
F (mg/L)	0.27	74	na	na	<0.007	51	62	0.4	4.85	19
Cl (mg/L)	< 0.05	2.29	na	na	0.41	0.75	0.7	2.75	0.63	0.89
Br (mg/L)	< 0.1	< 0.1	na	na	< 0.1	< 0.1	< 0.1	< 0.2	< 0.2	< 0.2
SO_4 (mg/L)	0.16	0.08	na	na	0.4	< 0.1	< 0.1	1.02	0.5	0.40
PO_4 (mg/L)	< 0.2	< 0.2	na	na	< 0.2	< 0.2	< 0.2	< 0.3	< 0.3	< 0.3
NO_2 (mg/L)	< 0.06	< 0.06	na	na	< 0.06	< 0.06	< 0.06	< 0.2	< 0.2	< 0.2
NO_3 (mg/L)	< 0.09	< 0.09	na	na	0.06	< 0.09	0.50	< 0.2	< 0.2	0.30

NOTE: [1] na = not available; < = not detected (less than "practical reporting limit"); Field chemistry of samples for high fluoride study (11/8/01 to 12/5/01) are reported in Tble 6.3.4.5-1

[2] see entry in Table 6.3.4.1-1 for temperature of pH measurements

[3] HCO3 - field measurement

[4] pore water samples (baseline): sample ultracentrifuged from borehole core

[5] low detection limit analysis - sample filtered to 0.10 mm and acidified

[6] sample filtered in the field and laboratory (LLNL) prior to analyses

[7] sample ID SPC0057028 submitted for low detection for Al analysis

[8] anion sample analyzed two different times

[9] analytical results are corroborating data (as defined in Section 3.6 of AP-SIII.3Q) and non-qualified

Table 6.3.4.2-1. Concentration and Isotopic Compositions of CO_2 in Gas Samples Collected during the DST Heating Phase

Sample Interval[1] (BH-Zone)	YMP Tracking Number	Date Sampled	$^{2}CO_2$ (v/v-%)[2]	$\delta^{13}C$ (‰)[3]	$\delta^{18}O$ (‰)[4]	^{14}C (fraction modern carbon)
57-3	SPC 0052 7911	2/10/98	0.094	-13.8	31.2	
59-3	SPC 0052 7900	2/09/98	0.078	-10.3	31.9	
60-3[5]	SPC 0052 7906	2/09/98	0.093	-8.0	22.9	
61-3	SPC 0052 7914	2/10/98	0.103	-11.6	30.2	
74-4	SPC 0052 7903	2/09/98	0.058	-11.2	32.9	
77-3	SPC 0052 7901	2/09/98	0.596	-5.5	48.3	
77-3[5]	SPC 0052 7902	2/10/98	0.596	-7.4	24.1	
78-3	SPC 0052 7913	2/10/98	0.225	-11.3	30.7	0.400
Heated Drift	SPC 0052 7909	2/10/98	0.037	-10.3	32.3	
Observation Drift	SPC 0052 7907	2/10/98	0.040	-10.3	40.0	
57-3	SPC 0052 7978	6/04/98	0.170	-16.6	29.5	
58-3	SPC 0052 7979	6/04/98	0.189	-12.0	29.1	
59-3	SPC 0052 7980	6/04/98	0.222	-9.7	26.6	
59-4	SPC 0052 7988	6/04/98	0.538	-8.9	25.8	
74-3	SPC 0052 7981	6/04/98	0.143	-13.6	30.1	
75-3	SPC 0052 7982	6/04/98	0.189	-11.8	29.0	0.416
76-3	SPC 0052 7983	6/04/98	0.687	-5.5	25.2	0.214
77-3	SPC 0052 7984	6/04/98	0.621	-5.5	21.1	
78-3	SPC 0052 7986	6/04/98	1.494	-8.7	23.4	0.210
185-3	SPC 0052 7987	6/04/98	0.160	-14.7	22.0	
Observation Drift	SPC 0052 7989	6/04/98	0.046	-10.6	36.4	
57-3	SPC 0052 7278	8/06/98	0.152	-15.4	29.5	
58-3	SPC 0052 7279	8/06/98	0.234	-9.3	28.3	
59-3	SPC 0052 7281	8/06/98	0.342	-7.7	25.4	
60-3	SPC 0052 7283	8/06/98	14.160	-0.5	24.2	
61-3	SPC 0052 7285	8/06/98	2.986	-3.7	23.9	
74-3	SPC 0052 7267	8/05/98	0.133	-12.1	29.9	
75-3	SPC 0052 7270	8/05/98	0.222	-10.4	29.4	
76-3	SPC 0052 7269	8/05/98	0.949	-3.5	24.5	
77-3	SPC 0052 7271	8/05/98	3.330	-4.3	24.0	
78-3	SPC 0052 7273	8/05/98	2.474	-7.2	23.4	0.156
185-3	SPC 0052 7275	8/06/98	0.186	-12.7	28.8	
186-2	SPC 0052 7277	8/06/98	1.497	-8.4	25.8	
182 (56')	SPC 0052 7276	8/06/98	0.092	-13.1	33.0	
182 (64')	SPC 0052 7266	8/05/98	0.054	-11.9	32.4	
Observation Drift	SPC 0052 7287	8/06/98	0.038	-9.8	38.0	
57-3	SPC 0052 7288	10/07/98	0.189	-16.0	29.2	0.492
58-3	SPC 0052 7289	10/07/98	0.414	-7.5	28.0	
59-3	SPC 0052 7290	10/07/98	0.633	-5.1	22.7	0.200
61-3	SPC 0052 7293	10/07/98	5.335	-2.1	22.6	0.125
74-3	SPC 0052 7295	10/07/98		-	-	
75-3	SPC 0052 7994	10/07/98	0.374	-10.3	27.6	0.322
76-3	SPC 0052 7296	10/07/98	1.611	-3.1	21.3	0.140
77-3	SPC 0052 7990	10/08/98	0.216	-5.1	25.1	
78-3	SPC 0052 7992	10/08/98	2.702	-3.9	22.1	0.105
185-3	SPC 0052 7995	10/08/98	0.264	-10.5	-	0.369
186-2	SPC 0052 7996	10/08/98	2.239	-7.5	24.0	

Table 6.3.4.2-1. Concentration and Isotopic Compositions of CO_2 in Gas Samples Collected during the DST Heating Phase (continued)

Sample Interval[1] (BH-Zone)	YMP Tracking Number	Date Sampled	$^{2}CO_2$ (v/v-%)[2]	$\delta^{13}C$ (‰)[3]	$\delta^{18}O$ (‰)[4]	^{14}C (fraction modern carbon)
Observation Drift	SPC 0052 7998	10/08/98	0.046	-10.8	37.6	
Heated Drift	SPC 0052 7999	10/08/98	0.044	-9.5	30.0	
57-1	SPC 0054 1258	12/16/98	0.068	-9.8	31.2	
57-2	SPC 0054 1259	12/16/98	0.191	-7.9	29.3	
57-3	SPC 0054 1260	12/16/98	0.220	-16.5	28.7	
57-4	SPC 0054 1261	12/16/98	0.130	-12.8	29.5	
58-3	SPC 0054 1262	12/16/98	0.392	-6.1	28.0	
59-1	SPC 0054 1263	12/16/98	0.087	-7.9	28.0	
59-3	SPC 0054 1264	12/16/98	0.501	-4.1	22.4	
59-4	SPC 0054 1267	12/16/98	1.562	-4.2	24.1	
60-2	SPC 0054 1269	12/16/98	0.099	-5.5	23.7	
61-1	SPC 0054 1271	12/16/98	0.051	-3.9	32.0	
61-2	SPC 0054 1272	12/16/98	0.083	-4.4	24.8	
61-4	SPC 0054 1274	12/16/98	0.331	-	-	
74-1	SPC 0054 1236	12/14/98	0.047	-10.0	29.8	
74-2	SPC 0054 1235	12/14/98	0.084	-	-	
74-3	SPC 0054 1234	12/14/98	0.220	-12.3	29.8	
74-4	SPC 0054 1233	12/14/98		-	-	
75-3	SPC 0054 1232	12/14/98	0.495	-9.3	27.8	
76-1	SPC 0054 1231	12/14/98	0.058	-9.6	30.6	
76-2	SPC 0054 1237	12/15/98	0.308	-5.2	24.5	
76-3	SPC 0054 1239	12/15/98	1.430	-2.7	20.9	
76-4	SPC 0054 1241	12/15/98	2.164	-3.5	23.6	
77-3	SPC 0054 1243	12/15/98	0.115	-	-	
78-1	SPC 0054 1245	12/15/98	0.100	-11.4	29.1	
78-2	SPC 0054 1246	12/15/98	2.188	-3.8	24.6	
78-3	SPC 0054 1248	12/15/98	2.370	-1.5	23.2	0.081
78-4	SPC 0054 1250	12/15/98	0.358	-11.7	28.1	
185-1	SPC 0054 1252	12/15/98	0.159	-13.2	29.5	
185-2	SPC 0054 1253	12/15/98	1.387	-10.7	28.6	
185-3	SPC 0054 1254	12/15/98	0.293	-10.3	27.9	
185-4	SPC 0054 1255	12/15/98	0.136	-12.4	28.8	
186-2	SPC 0054 1256	12/15/98	2.043	-6.6	23.5	
Observation Drift	SPC 0054 1266	12/16/98	0.038	-9.3	39.2	
Heated Drift	SPC 0054 1276	12/16/98	0.040	-9.7	26.5	0.988
57-3	SPC 0055 0611	3/02/99	0.277	-16.5	26.4	
58-3	SPC 0055 0612	3/02/99	0.552	-5.7	25.8	
59-3	SPC 0055 0613	3/02/99	0.746	-3.3	20.1	
60-2	SPC 0055 0616	3/02/99	0.087	-5.9	22.5	
61-2	SPC 0055 0618	3/02/99	0.097	-3.5	21.5	
74-1	SPC 0054 1278	3/01/99	0.046	-	-	
74-2	SPC 0054 1279	3/01/99	0.110	-10.9	27.9	
74-3	SPC 0054 1280	3/01/99	0.437	-11.2	27.1	
74-4	SPC 0054 1281	3/01/99	0.302	-11.0	27.6	
75-3	SPC 0054 1282	3/01/99	1.051	-7.9	25.5	
76-1	SPC 0054 1283	3/01/99	0.055	-7.9	33.9	
76-2	SPC 0054 1285	3/01/99	0.324	-4.6	22.7	

Table 6.3.4.2-1. Concentration and Isotopic Compositions of CO_2 in Gas Samples Collected during the DST Heating Phase (continued)

Sample Interval[1] (BH-Zone)	YMP Tracking Number	Date Sampled	$^{2}CO_2$ (v/v-%)[2]	$\delta^{13}C$ (‰)[3]	$\delta^{18}O$ (‰)[4]	^{14}C (fraction modern carbon)
76-3	SPC 0054 1287	3/01/99	1.860	-3.0	19.9	
76-4	SPC 0055 0600	3/01/99	4.987	-3.0	20.1	
77-3	SPC 0055 0603	3/02/99	0.119	-6.3	20.5	
78-1	SPC 0054 1284	3/02/99	0.090	-9.0	28.4	
78-3	SPC 0055 0605	3/02/99	4.409	-1.8	18.8	
185-2	SPC 0055 0607	3/02/99	2.020	-9.5	26.1	0.197
185-3	SPC 0055 0608	3/02/99	0.331	-9.8	25.7	0.314
186-2	SPC 0055 0609	3/02/99	2.455	-5.8	20.1	
Observation Drift	SPC 0055 0602	3/01/99	0.039	-7.8	33.9	
57-3	SPC 0055 1123	5/25/99	0.333	-15.0	30.7	0.467
58-3	SPC 0055 1121	5/25/99	0.681	-3.5	30.2	
59-3	SPC 0055 1119	5/25/99	1.101	-1.0	23.5	
60-2	SPC 0055 1115	5/25/99	0.074	-6.9	26.4	
60-3	SPC 0055 1113	5/25/99	0.072	-9.3	31.5	
61-2	SPC 0055 1117	5/25/99	0.073	-4.7	27.3	
74-1	SPC 0055 1124	5/25/99	0.047	-	-	
74-2	SPC 0055 1125	5/25/99	0.129	-10.2	29.1	
74-3	SPC 0055 1126	5/25/99	0.639	-9.9	28.7	0.277
74-4	SPC 0055 1127	5/25/99	0.406	-9.6	29.5	
75-3	SPC 0055 1128	5/25/99	1.374	-6.3	27.9	0.178
76-1	SPC 0055 1130	5/26/99	0.058	-	-	
76-2	SPC 0055 1131	5/26/99	0.535	-2.2	24.8	
76-3	SPC 0055 1133	5/26/99	3.112	-2.0	20.0	0.139
76-4	SPC 0055 1135	5/26/99	13.077	-1.3	22.7	
77-3	SPC 0055 1137	5/26/99	0.187	-0.2	28.9	
78-3	SPC 0055 1139	5/26/99	0.288	-0.1	23.1	0.243
185-2	SPC 0055 1142	5/26/99	2.311	-3.5	36.9	
185-3	SPC 0055 1143	5/26/99	0.426	-8.6	27.1	
186-2	SPC 0055 1141	5/26/99	0.041	-9.5	37.5	
Observation Drift	SPC 0055 1144	5/26/99	0.042	-	-	
57-2	SPC 0055 1145	8/09/99	0.362	-4.7	26.7	
57-3	SPC 0055 1146	8/09/99	0.330	-15.1	27.7	
57-4	SPC 0055 1147	8/09/99	0.173	-6.4	35.2	
58-3	SPC 0055 1148	8/09/99	1.209	-4.3	25.5	
59-2	SPC 0055 1161	8/09/99	1.016	-0.3	19.6	
59-3	SPC 0055 1163	8/09/99	1.273	-1.0	18.6	0.120
59-4	SPC 0055 1165	8/09/99	6.573	-2.5	22.4	
60-3	SPC 0055 1167	8/10/99	0.332	-5.5	22.5	
74-2	SPC 0055 1170	8/10/99	0.158	-10.2	27.6	
74-3	SPC 0055 1171	8/10/99	0649	-10.1	27.3	
74-4	SPC 0055 1172	8/10/99	0.328	-9.0	30.3	
75-3	SPC 0055 1173	8/10/99	1.315	-7.1	25.1	
76-3	SPC 0055 1175	8/10/99	2.658	-2.1	21.5	
77-3	SPC 0055 1177	8/10/99	0.152	-	-	
78-3	SPC 0055 1179	8/10/99	0.123	-2.5	20.6	
185-2	SPC 0055 1182	8/10/99	3.214	-7.4	26.3	
185-3	SPC 0055 1183	8/10/99	0.496	-6.2	29.7	

Table 6.3.4.2-1. Concentration and Isotopic Compositions of CO_2 in Gas Samples Collected during the DST Heating Phase (continued)

Sample Interval[1] (BH-Zone)	YMP Tracking Number	Date Sampled	$^{2}CO_2$ (v/v-%)[2]	$\delta^{13}C$ (‰)[3]	$\delta^{18}O$ (‰)[4]	^{14}C (fraction modern carbon)
186-3	SPC 0055 1184	8/10/99	0.613	-8.2	23.5	
Observation Drift	SPC 0055 1181	8/10/99	0.038	-8.2	38.3	
57-3	SPC 0055 1186	11/29/99	0.431	-11.5	31.4	0.427
57-4	SPC 0055 1187	11/29/99	0.275	-7.3	32.1	
58-3	SPC 0055 1188	11/29/99	1.210	-3.0	26.3	
59-4	SPC 0055 1191	11/29/99	9.016	-1.6	14.8	
61-4	SPC 0055 1194	11/29/99	3.551	-3.8	19.9	
74-3	SPC 0055 1197	11/29/99	1.330	-8.6	26.0	
74-4	SPC 0055 1198	11/29/99	0.698	-8.7	26.4	
75-3	SPC 0055 1199	11/29/99	2.779	-5.5	23.1	0.129
76-3[7]	SPC 0055 7071	11/30/99	0.594	-3.0	19.6	0.182
76-4	SPC 0055 7058	11/30/99	6.861	-0.1	14.7	
77-3	SPC 0055 7060	11/30/99	0.220	-4.3	22.6	
78-3	SPC 0055 7062	11/30/99	0.619	-0.3	24.1	
78-4	SPC 0055 7064	11/30/99	1.059	-4.6	25.7	
185-2	SPC 0055 7067	11/30/99	5.208	-6.3	25.7	0.133
185-3	SPC 0055 7068	11/30/99	0.895	-6.8	24.4	0.190
186-3	SPC 0055 7069	11/30/99	1.796	-7.4	22.6	0.206
Heated Drift	SPC 0055 1196	11/30/99	0.043	-9.9	20.1	
Observation Drift	SPC 0055 7066	11/30/99	0.040	-8.8	37.5	
57-3	SPC 0055 9314	4/19/00	0.383	-8.8	29.2	
58-3	SPC 0055 9315	4/19/00	1.672	-4.1	22.0	
59-3	SPC 0055 9317	4/19/00	0.210	-2.5	24.0	
60-4	SPC 0055 9319	4/19/00	0.132	-9.7	37.0	
0.75	SPC 0055 9321	4/19/00	0.075	-	-	
61-4	SPC 0055 9323	4/19/00	6.308	-3.3	21.8	
74-3	SPC 0055 9304	4/18/00	1.291	-8.1	23.3	
74-4	SPC 0055 9305	4/18/00	0.724	-7.3	25.7	
75-3	SPC 0055 9306	4/18/00	2.430	-3.6	21.8	
77-3	SPC 0055 9308	4/18/00	0.156	-6.7	21.0	
78-3	SPC 0055 9310	4/18/00	0.353	-0.5	21.6	0.185
78-4	SPC 0055 9312	4/18/00	1.657	-4.5	22.5	
185-2	SPC 0055 9300	4/18/00	3.877	-5.8	23.7	
185-3	SPC 0055 9301	4/18/00	0.823	-5.6	22.7	
186-3	SPC 0055 9302	4/18/00	1.418	-3.1	35.2	
Heated Drift	SPC 0055 9326	4/19/00	0.042	-10.7	13.7	
Observation Drift	SPC 0055 9325	4/19/00	0.042	-	-	
57-3/4	SPC 0055 9328	8/21/00	0.605	-8.4	15.3	0.201
58-3	SPC 0055 9329	8/21/00	3.262	-3.0	12.1	
59-3	SPC 0055 9331	8/21/00	0.108	-4.0	17.4	
60-2/3/4	SPC 0055 9333	8/21/00	0.077	-8.3	18.7	
61-3/4	SPC 0055 9335	8/21/00	0.056	-8.0	16.6	
74-3	SPC 0055 9337	8/22/00	1.179	-7.1	13.4	0.154
74-4	SPC 0055 9338	8/22/00	0.978	-5.8	14.7	
75-3	SPC 0055 9339	8/22/00	1.573	-2.2	10.7	
76-3	SPC 0055 9341	8/22/00	0.082	-5.2	16.4	

Table 6.3.4.2-1. Concentration and Isotopic Compositions of CO_2 in Gas Samples Collected during the DST Heating Phase (continued)

Sample Interval[1] (BH-Zone)	YMP Tracking Number	Date Sampled	$^{2}CO_2$ (v/v-%)[2]	$\delta^{13}C$ (‰)[3]	$\delta^{18}O$ (‰)[4]	^{14}C (fraction modern carbon)
77-2/3	SPC 0055 9343	8/22/00	0.095	-7.0	13.7	
78-2/3	SPC 0055 9346	8/22/00	0.355	-2.4	10.9	
185-2	SPC 0055 9348	8/22/00	5.115	-5.2	14.1	
185-3	SPC 0055 9350	8/22/00	1.405	-4.5	13.0	
186-3	SPC 0055 9352	8/22/00	4.408	-3.0	11.0	
Heated Drift	SPC 0055 9354	8/22/00	0.046	-	-	
Observation Drift	SPC 0055 9345	8/22/00	0.040	-9.7	27.2	
57-3/4	SPC 0055 9395	1/22/01	0.67	-7.6	25.8	0.170
58-3	SPC 0055 9397	1/22/01	2.84	-3.4	20.5	
59-3	SPC 0055 9399	1/22/01	0.11	-5.0	27.4	
60-3/2/4	SPC 0055 9401	1/22/01	0.11	-10.4	24.0	
61-3/2	SPC 0055 9403	1/22/01	0.54	-7.2	26.4	
74-3	SPC 0055 9406	1/23/01	1.14	-6.3	23.4	0.144
75-3	SPC 0055 9408	1/23/01	1.65	2.7	32.9	0.166
76-3/2	SPC 0055 9410	1/23/01	0.19	-1.6	-	0.296
77-3/2	SPC 0055 9412	1/23/01	0.09	-7.9	22.2	
78-3/2/4	SPC 0055 9414	1/23/01	0.68	1.3	35.3	
185-2	SPC 0055 9416	1/23/01	6.68	-4.8	24.6	
185-3	SPC 0055 9418	1/23/01	1.94	-4.3	23.2	
186-3	SPC 0055 9420	1/23/01	7.76	-3.1	20.8	
Observation Drift 1	SPC 0055 9394	1/22/01	0.04	-10.4	37.6	
Observation Drift 2	SPC 0055 9422	1/23/01	0.04	-9.8	37.7	
57-3/4	SPC 0055 9357	4/17/01	0.784	-6.5	26.1	
58-3	SPC 0055 9359	4/17/01	3.467	-3.7	19.9	
59-3	SPC 0055 9361	4/17/01	0.108	-3.2	27.8	
60-3/2/4/1	SPC 0055 9363	4/17/01	0.080	-10.7	26.3	
61-3/2/4	SPC 0055 9365	4/17/01	0.068	-6.8	24.7	
74-3	SPC 0055 9367	4/18/01	1.139	-5.6	22.8	
75-3	SPC 0055 9369	4/18/01	0.941	-0.1	24.8	
76-3/2	SPC 0055 9371	4/18/01	0.178	-2.7	20.9	
77-3/2	SPC 0055 9373	4/18/01	0.102	-8.2	23.1	
78-3/2/4/1	SPC 0055 9375	4/18/01	0.795	-4.9	20.9	0.187
185-2	SPC 0055 9378	4/18/01	7.855	-3.9	25.9	
185-3	SPC 0055 9380	4/18/01	2.284	-4.6	21.6	
186-3	SPC 0055 9382	4/18/01	6.413	-2.8	18.7	
Heated Drift	SPC 0055 9384	4/18/01	0.046	-	-	
Observation Drift	SPC 0055 9377	4/18/01	0.038	-9.1	38.1	

Table 6.3.4.2-1. Concentration and Isotopic Compositions of CO_2 in Gas Samples Collected during the DST Heating Phase (continued)

Sample Interval[1] (BH-Zone)	YMP Tracking Number	Date Sampled	$^{2}CO_2$ (v/v-%)[2]	$\delta^{13}C$ (‰)[3]	$\delta^{18}O$ (‰)[4]	^{14}C (fraction modern carbon)
57-3/4	SPC 0055 9385	8/07/01	1.011	-	-	0.240
58-3	SPC 0055 9387	8/07/01	6.342	-3.1	20.0	
59-3/4	SPC 0055 9389	8/08/01	0.178	-	-	
60-3/2/4/1	SPC 0055 9391	8/07/01	0.096	-10.3	27.6	
61-3/2/4	SPC 0055 9393	8/07/01	0.557	-5.8	25.6	
74-3	SPC 0055 9431	8/08/01	0.643	-1.1	35.1	0.326
75-3	SPC 0055 9433	8/08/01	0.821	-3.1	23.7	0.233
76-3/2	SPC 0055 9435	8/08/01	0.130	-4.5	21.4	0.456
77-3	SPC 0055 9437	8/08/01	0.090	-4.1	31.9	
78-3/2/4	SPC 0055 9439	8/08/01	1.966	1.2	29.3	0.192
185-2	SPC 0055 9424	8/07/01	11.522	-4.1	23.1	0.080
185-3	SPC 0055 9426	8/07/01	4.427	-4.7	21.9	0.080
186-3	SPC 0055 9428	8/07/01	8.039	-1.2	21.7	
Heated Drift	SPC 0055 9356	8/07/01	0.039	-10.0	17.7	0.982
Observation Drift	SPC 0055 9430	8/07/01	0.034	-8.9	38.8	
57-3/4	SPC 0101 6517	11/27/01	0.88	-7.0	22.8	
58-3	SPC 0101 6519	11/27/01	2.50	-	-	
59-3/4	SPC 0101 6522	11/28/01	0.08	-3.4	33.2	
61-3/2/4	SPC 0101 6524	11/28/01	0.27	-3.6	24.0	
74-3	SPC 0101 6501	11/27/01	0.64	-	-	
75-3	SPC 0101 6504	11/27/01	0.85	-	-	
76-1	SPC 0101 6511	11/27/01	0.37	-4.9	24.1	
76-3/2	SPC 0101 6509	11/27/01	0.92	-0.1	18.9	
76-4	SPC 0101 6507	11/27/01	0.07	-6.5	32.3	
77-3	SPC 0101 6513	11/27/01	0.06	-	-	
78-3/2/4	SPC 0101 6515	11/27/01	0.71	-8.5	35.5	
185-1	SPC 0055 9448	11/26/01	0.69	-4.4	26.4	
185-2	SPC 0055 9445	11/26/01	4.83	-4.5	23.5	
185-3	SPC 0055 9443	11/26/01	2.90	-	-	
185-4	SPC 0055 9450	11/26/01	1.49	-6.6	24.0	
186-3	SPC 0101 6526	11/28/01	7.70	-	-	
Heated Drift	SPC 0101 6528	11/26/01	0.06	-9.8	36.4	
Observation Drift	SPC 0055 9452	11/26/01	0.07	-6.9	33.4	

Table 6.3.4.2-1. Concentration and Isotopic Compositions of CO_2 in Gas Samples Collected during the DST Heating Phase (continued)

Sample Interval[1] (BH-Zone)	YMP Tracking Number	Date Sampled	$^{2}CO_2$ (v/v-%)[2]	$\delta^{13}C$ (‰)[3]	$\delta^{18}O$ (‰)[4]	^{14}C (fraction modern carbon)
57-3/4	SPC 0101 6546	1/08/02	0.90	-5.5	26.6	
59-3/4	SPC 0101 6400	1/08/02	0.15	-	-	
61-3/2/4	SPC 0101 6402	1/08/02	0.63	3.1	43.8	
74-3	SPC 0101 6538	1/07/02	1.08	-4.6	24.2	
75-3	SPC 0101 6540	1/07/02	6.65	-1.5	19.4	
76-3/2	SPC 0101 6542	1/07/02	0.77	-0.7	17.9	
78-3/2/4	SPC 0101 6544	1/07/02	0.79	-4.8	19.7	
185-2	SPC 0101 6532	1/07/02	7.50	-4.5	23.5	
185-3	SPC 0101 6534	1/07/02	3.43	-4.4	22.5	
186-3	SPC 0101 6536	1/07/02	3.45	-	-	
Heated Drift	SPC 0101 6531	1/07/02	0.05	-9.2	25.9	
Observation Drift	SPC 0101 6530	1/07/02	0.06	-10.1	37.3	

[1] Sample interval indicates the DST borehole followed by the interval within the borehole from which the sample was collected. Where more than one interval is noted, that means the sample was taken from the first interval given, but the packers between that interval and the others listed were deflated (e.g., 57-3/4 indicates the sample was taken from DST borehole 57, interval 3, but the packer between intervals 3 and 4 was deflated). Heater Drift samples were taken from Heater Drift gas sampling port #2 (by the bulkhead) and AO Drift samples were air samples taken from the Access Observation.

[2] CO_2 concentrations reported for samples collected during February of 1997 through August of 2000 and from April of 2001 through August of 2001 were measured using the Li-Cor in the Amundson laboratory on the UC Berkeley campus. Data reported for samples collected during January of 2001 and November of 2001 through January of 2002 were measured on the Columbus Instruments Gas Analyzer at the ESF.

[3] Stable carbon isotope ratios are given as part per thousand or per mil (‰) variations in the ratio of ^{13}C to ^{12}C relative to carbon isotope ratio of VPDB (Vienna PeeDee Belemnite), an internationally accepted standard for reporting carbon isotope data.

[4] Stable oxygen isotope ratios are given as part per thousand or per mil (‰) variations in the ratio of ^{18}O to ^{16}O relative to oxygen isotope ratio of VSMOW (Vienna Standard Mean Ocean Water), an internationally accepted standard for reporting oxygen isotope data.

[5] Samples collected in 150-cc metal canisters (as opposed to Tedlar® bags).

Table 6.3.4.2-2. CO_2 Concentrations in DST Gas Samples Collected during January, 2001

Borehole interval	Tracking Number	UC Berkeley Amundson Lab Li-Cor (%-volume)	Columbus Instruments Field Gas Analyzer (%-volume)
57-3/4	SPC 00559395	0.66	0.67
58-3	SPC 00559397	2.53	2.84
59-3	SPC 00559399	0.10	0.11
60-3/2/4	SPC 00559401	0.11	0.11
61-3/2	SPC 00559403	0.06	0.05
74-3	SPC 00559406	1.01	1.14
75-3	SPC 00559408	0.97	1.65
76-3/2	SPC 00559410	0.18	0.19
77-3/2	SPC 00559412	0.09	0.09
78-3/2/4	SPC 00559414	0.46	0.68
185-2	SPC 00559416	5.75	6.81
185-3	SPC 00559418	1.63	1.94
186-3	SPC 00559420	6.61	7.76
Observation Drift Air#1	SPC 00559394	0.04	0.04
Observation Drift Air#2	SPC 00559422	0.04	0.04

Table 6.3.4.2-3. Hydrogen (δD) and Oxygen ($\delta^{18}O$) Isotope Compositions of Steam Condensed from Gas Samples Collected During the DST Heating Phase

Sample Interval[1]	YMP Tracking #	Date Sampled	Isotope Composition	
			Hydrogen δD (‰)	[2] Oxygen $\delta^{18}O$ (‰)
77-3	SPC 0052 7985	6/04/98	-95	-13.2
58-3	SPC 0052 7280	8/06/98	-128	-18.1
59-3	SPC 0052 7282	8/06/98	-132	-18.6
60-3	SPC 0052 7284	8/06/98	-110	-16.1
61-3	SPC 0052 7286	8/06/98	-152	-21.0
76-3	SPC 0052 7270	8/05/98	-122	-17.5
77-3	SPC 0052 7272	8/05/98	-103	-14.1
78-3	SPC 0052 7274	8/05/98	-127	-18.6
59-3	SPC 0052 7291	10/07/98	-126	-18.3
76-3	SPC 0052 7299	10/07/98	-126	-18.1
77-3	SPC 0052 7991	10/08/98	-86	-10.6
78-3	SPC 0052 7993	10/08/98		-18.1
186-2	SPC 0052 7997	10/08/98	-126	-17.9
59-3	SPC 0054 1265	12/16/98	-122	-18.0
59-4	SPC 0054 1268	12/16/98	-119	-16.9
60-2	SPC 0054 1270	12/16/98	-90	-12.2
61-2	SPC 0054 1273	12/16/98	-106	-16.1
61-4	SPC 0054 1275	12/16/98	-119	-16.9
76-2	SPC 0054 1238	12/15/98	-131	-17.6
76-3	SPC 0054 1240	12/15/98	-127	-18.5
76-4	SPC 0054 1242	12/15/98	-110	-16.6
77-3	SPC 0054 1244	12/15/98	-83	-10.1
78-2	SPC 0054 1247	12/15/98	-110	-16.8
78-3	SPC 0054 1249	12/15/98	-132	-18.5
78-4	SPC 0054 1251	12/15/98	-116	-17.2
186-2	SPC 0054 1257	12/15/98	-140	-20.3
Heated Drift 2	SPC 0054 1277	12/16/98	-64	-7.5
59-3	SPC 0055 0614	3/02/99	-118	-17.2
60-2	SPC 0055 0617	3/02/99	-87	-10.9
60-3	SPC 0055 0615	3/02/99	-101	-13.8
61-2	SPC 0055 0619	3/02/99	-95	-14.4
76-2	SPC 0054 1286	3/01/99	-138	-19.0
76-3	SPC 0054 1288	3/01/99	-126	-18.2
76-4	SPC 0055 0601	3/01/99	-110	-16.1
77-3	SPC 0055 0604	3/02/99	-82	-8.2
78-3	SPC 0055 0606	3/02/99	-122	-17.7
186-2	SPC 0055 0610	3/02/99	-130	-19.4
60-2	SPC 0055 1116	5/25/99	-85	-11.2
60-3	SPC 0055 1114	5/25/99	-86	-19.4
61-2	SPC 0055 1118	5/25/99	-91	-11.1
59-3	SPC 0055 1120	5/25/99	-104	-11.0
58-3	SPC 0055 1122	5/25/99	-124	-12.2
75-3	SPC 0055 1129	5/25/99	-128	-17.4
76-2	SPC 0055 1132	5/26/99	-140	-17.1

Table 6.3.4.2-3. Hydrogen (δD) and Oxygen ($\delta^{18}O$) Isotope Compositions of Steam Condensed from Gas Samples Collected During the DST Heating Phase (continued)

Sample Interval[1]	YMP Tracking #	Date Sampled	Isotope Composition	
			Hydrogen δD (‰)	[2] Oxygen $\delta^{18}O$ (‰)
76-3	SPC 0055 1134	5/26/99	-111	-12.5
76-4	SPC 0055 1136	5/26/99	-110	-11.0
77-3	SPC 0055 1138	5/26/99	-83	-12.8
78-3	SPC 0055 1140	5/26/99	-117	-18.4
58-3	SPC 0055 1149	8/09/99	-126	-17.6
59-2	SPC 0055 1162	8/09/99	-112	-17.1
59-3	SPC 0055 1164	8/09/99	-109	-15.9
59-4	SPC 0055 1166	8/09/99	-107	-16.1
60-3	SPC 0055 1168	8/10/99	-86	-12.1
75-3	SPC 0055 1174	8/10/99	-119	-16.8
76-3	SPC 0055 1176	8/10/99	-122	-17.7
77-3	SPC 0055 1178	8/10/99	-89	-11.2
78-3	SPC 0055 1180	8/10/99	-114	-17.1
186-3	SPC 0055 1185	8/10/99	-94	-13.8
58-3	SPC 0055 1189	11/29/99	-122	-17.4
59-3	SPC 0055 1190	11/29/99	-103	-14.3
59-4	SPC 0055 1192	11/29/99	-125	-18.9
61-3	SPC 0055 1193	11/29/99	-101	-14.2
61-4	SPC 0055 1195	11/29/99	-113	-16.3
75-3	SPC 0055 7056	11/29/99	-121	-17.5
76-3	SPC 0055 7072	11/30/99	-107	-16.3
76-4	SPC 0055 7059	11/30/99		-12.6
77-3	SPC 0055 7061	11/30/99	-81	-9.9
78-3	SPC 0055 7063	11/30/99	-104	-13.7
78-4	SPC 0055 7065	11/30/99	-107	-15.8
186-3	SPC 0055 7070	11/30/99	-93	-13.2
58-3	SPC 0055 9316	4/19/00	-117	-17.3
59-3	SPC 0055 9318	4/19/00	-89	-12.0
60-4	SPC 0055 9320	4/19/00	-87	-11.8
61-3	SPC 0055 9322	4/19/00	-101	-14.3
61-4	SPC 0055 9324	4/19/00	-121	-18.3
75-3	SPC 0055 9307	4/18/00	-117	-16.5
77-3	SPC 0055 9309	4/18/00	-83	-11.0
78-3	SPC 0055 9311	4/18/00	-92	-11.6
78-4	SPC 0055 9313	4/18/00	-101	-16.5
186-3	SPC 0055 9303	4/18/00	-90	-13.7
58-3	SPC 0055 9330	8/21/00		-17.2
59-3	SPC 0055 9332	8/21/00	-90	-10.9
60-3/2/4	SPC 0055 9334	8/21/00	-89	-12.0
61-3/4	SPC 0055 9336	8/21/00	-89	-12.0
75-3	SPC 0055 9340	8/22/00	-118	-17.1
76-3	SPC 0055 9342	8/22/00	-101	-13.4
77-3/2	SPC 0055 9344	8/22/00	-85	-10.7
78-3/2	SPC 0055 9347	8/22/00	-95	-13.0

Table 6.3.4.2-3. Hydrogen (δD) and Oxygen ($\delta^{18}O$) Isotope Compositions of Steam Condensed from Gas Samples Collected During the DST Heating Phase (continued)

Sample Interval[1]	YMP Tracking #	Date Sampled	Isotope Composition	
			Hydrogen δD (‰)	[2] Oxygen $\delta^{18}O$ (‰)
185-2	SPC 0055 9349	8/22/00	-139	-17.3
185-3	SPC 0055 9351	8/22/00	-132	-18.1
186-3	SPC 0055 9353	8/22/00	-123	-15.0
57-3/4	SPC 0055 9396	1/22/01	-128	-17.9
58-3	SPC 0055 9398	1/22/01	-126	-19.4
59-3	SPC 0055 9400	1/22/01	-86	-11.2
60-3/2/4	SPC 0055 9402	1/22/01	-81	-11.1
61-3/2	SPC 0055 9404	1/22/01	-88	-11.0
74-3	SPC 0055 9407	1/23/01	-122	-17.4
75-3	SPC 0055 9409	1/23/01	-121	-17.1
76-3/2	SPC 0055 9411	1/23/01	-90	-12.5
77-3/2	SPC 0055 9413	1/23/01	-90	-11.0
78-3/2/4	SPC 0055 9415	1/23/01	-95	-12.8
185-2	SPC 0055 9417	1/23/01	-139	-18.4
185-3	SPC 0055 9419	1/23/01	-132	-18.1
186-3	SPC 0055 9421	1/23/01	-135	-19.1
57-3/4	SPC 0055 9358	4/17/01	-123	-18.0
58-3	SPC 0055 9360	4/17/01	-129	-19.6
59-3	SPC 0055 9362	4/17/01	-85	-11.1
60-3/2/4/1	SPC 0055 9364	4/17/01	-81	-10.1
61-3/2/4	SPC 0055 9366	4/17/01	-86	-11.3
74-3	SPC 0055 9368	4/18/01	-123	-17.7
75-3	SPC 0055 9370	4/18/01	-112	-16.8
76-3/2	SPC 0055 9372	4/18/01	-92	-13.0
77-3/2	SPC 0055 9374	4/18/01	-91	-11.7
78-3/2/4/1	SPC 0055 9376	4/18/01	-91	-12.9
185-2	SPC 0055 9379	4/18/01	-137	-18.2
185-3	SPC 0055 9381	4/18/01	-133	-18.5
186-3	SPC 0055 9383	4/18/01	-111	-16.2
57-3/4	SPC 0055 9386	8/07/01	-121	-17.7
58-3	SPC 0055 9388	8/07/01	-129	-20.1
59-3/4	SPC 0055 9390	8/08/01	-87	-11.3
60-3/2/4/1	SPC 0055 9392	8/07/01	-74	-8.8
61-3/2/4	SPC 0055 9355	8/07/01	-59	-10.7
74-3	SPC 0055 9432	8/08/01	-126	-17.8
75-3	SPC 0055 9434	8/08/01	-115	-16.9
76-3/2	SPC 0055 9436	8/08/01	-100	-13.2
77-3	SPC 0055 9438	8/08/01	-89	-11.6
78-3/2/4	SPC 0055 9440	8/08/01	-84	-10.1
185-2	SPC 0055 9425	8/07/01		-18.6
185-3	SPC 0055 9427	8/07/01	-117	-18.4
186-3	SPC 0055 9429	8/07/01	-112	-16.2

Table 6.3.4.2-3. Hydrogen (δD) and Oxygen ($\delta^{18}O$) Isotope Compositions of Steam Condensed from Gas Samples Collected During the DST Heating Phase (continued)

Sample Interval[1]	YMP Tracking #	Date Sampled	Isotope Composition	
			Hydrogen δD (‰)	[2] Oxygen $\delta^{18}O$ (‰)
57-3/4	SPC 0101 6518	11/27/01	-116	-16.9
58-3	SPC 0101 6520	11/27/01	-124	-18.3
59-3/4	SPC 0101 6523	11/28/01	-78	-10.2
61-3/2/4	SPC 0101 6525	11/28/01	-60	-11.5
74-3	SPC 0101 6502	11/27/01	-130	-18.1
75-3	SPC 0101 6505	11/27/01	-114	-16.1
76-1	SPC 0101 6512	11/27/01	-134	-18.2
76-3/2	SPC 0101 6510	11/27/01	-143	-12.6
76-4	SPC 0101 6508	11/27/01	-79	-11.3
77-3	SPC 0101 6514	11/27/01	-95	-12.3
78-3/2/4	SPC 0101 6516	11/27/01	-88	-11.5
185-1	SPC 0055 9449	11/26/01	-133	-17.4
185-2	SPC 0055 9446	11/26/01	-138	-18.3
185-3	SPC 0055 9444	11/26/01	-122	-18.4
185-4	SPC 0055 9451	11/26/01	-149	-17.7
186-3	SPC 0101 6500	11/26/01	-100	-14.2
186-3(II)	SPC 0101 6527	11/28/01	-113	-16.2
57-3/4	SPC 0101 6547	1/08/02	-81	-17.7
58-3	SPC 0101 6549	1/08/02	-84	-18.5
59-3/4	SPC 0101 6401	1/08/02	-79	-10.5
61-3/2/4	SPC 0101 6403	1/08/02	-85	-11.2
74-3	SPC 0101 6539	1/07/02	-117	-17.1
75-3	SPC 0101 6541	1/07/02	-114	-17.0
76-3/2	SPC 0101 6543	1/07/02	-88	-11.9
78-3/2/4	SPC 0101 6545	1/07/02	-82	-10.7
185-2	SPC 0101 6533	1/07/02	-131	-17.3
185-3	SPC 0101 6535	1/07/02	-132	-18.5
186-3	SPC 0101 6537	1/07/02	-109	-15.4

[1] Field # corresponds to intervals in hydrology boreholes

[2] Stable oxygen isotope ratios are given as part per thousand or per mil (‰) variations in the ratio of ^{18}O to ^{16}O relative to oxygen isotope ratio of VSMOW (Vienna Standard Mean Ocean Water), an internationally accepted standard for reporting oxygen isotope data

Table 6.3.4.3-1. Mineral Coverage on Fractures, Drill Core ESF-HD-TEMP-2

Section 1, 25.0-29.3 ft, Non-Vapor-Phase Interval				
Stellerite	**Manganese Minerals**	**Crystalline Silica/Feldspar**	**Clay**	**Calcite**
42.3%	1.5%	1.0%	4.3%	0%
Section 2, 62.15-66.45 ft, Vapor-Phase Interval				
Stellerite	**Manganese Minerals**	**Crystalline Silica/Feldspar**	**Clay**	**Calcite**
41.6%	2.0%	3.5%	4.7%	2.2%

Table 6.3.4.5-1. Field Measurements and Fluoride Content of "Condensates" from HF Field Tests

Sample Identification	SMF Number	Collection Date	Field pH	E.C. / TDS (µS/cm) / (ppm)	F (mg/L)
BH 72 (pre-test)*	SPC00559475	6/28/2001	4.8	15 / 9	nd < 0.007
BH 72 (pre-test)*	SPC00575228	11/8/2001	5.1 – 5.5	19 / 12	0.15
BH 72 baseline*	SPC00575219	11/26/2001	5.3	14 / 9	nd < 0.007
Fluoroelastomer (FKM) and Teflon installed 11/26/2001					
BH 72 (FKM, PTFE)	SPC00559478	11/29/2001	3.8	41 / 25	2.39
BH 72 (FKM, PTFE)	SPC01016065	12/5/2001	3.4 – 3.5	139 / 88	7.60
BH 72 (FKM, PTFE)	SPC01016066	12/5/2001	3.44	135 / 85	7.23
Fluoroelastomer (FKM) and Teflon removed 1/9/2002					
BH 55 (pre-test)*	SPC00575231	11/15/2002	7.5	279/176	0.52
BH 55 (pre-test)*	SPC00559483	11/21/2002	NA	NA	8.56 ***
BH 55 baseline**	SPC00575229	11/26/2001	5.0	21 / 13	1.34
BH 55**	SPC00559479	11/29/2001	5.2	NA	0.35
BH 55**	SPC01016067	12/5/2001	NA	NA	0.08

* sample acquired with Tygon tubing

** sample acquired using C276 alloy tubing

*** sample likely contaminated, refer to Section 6.3.4.5.5

7. SUMMARY

As mentioned in Section 1, the purpose of this Scientific Analysis Report is to document, in one report, the comprehensive set of measurements taken within the Yucca Mountain Site Characterization Project (YMP) Thermal Testing Program since its inception in 1996. This documentation is intended to make data collected readily usable to end users. Only brief discussions are provided for different data sets. These are intended to impart a clear sense of applicability of data, so that they will be used properly within the context of measurement uncertainty. This approach also keeps this report to a manageable size, an important constraint since massive amounts of measurements for three long-term thermal tests are addressed. Furthermore, thermal testing data currently residing in the TDMS have been reorganized and reformatted, as applicable, from often cumbersome Input-DTNs into a new set of more user-friendly Output-DTNs.

Based on the above discussion, which indicates this report focuses only on measurements, and guidance provided in Attachment 3 of AP-SIII.9Q, the following discussion is a summary rather than a conclusion of a scientific analysis. The scientific analysis, which is broadly defined in Section 3.13 of AP-SIII.9Q, as applied in this report mostly involves the definition and investigation of thermal-hydrological-mechanical-chemical measurements, including laboratory and field characterization of the respective test blocks, from three thermal tests (LBT, SHT, and DST). This scientific analysis contrasts typical scientific analysis in other reports which tend to focus on numerical analyses and subsequent interpretations of findings that lead to a set of conclusions.

The summary of this work, which addresses massive amounts of diverse measurements collected in the YMP Thermal Testing Program over the past six years, can be grouped into the following two categories:

- The preparation of a single, comprehensive document that provides ready access to key material related to the myriad of thermal testing measurements from each of the three thermal tests.

- The development of user-friendly Output-DTNs that will facilitate the usage of thermal testing data.

Discussion of key material regarding thermal testing measurements associated with the YMP Thermal Testing Program is presented in Section 6. This discussion is organized by the four processes (thermal, hydrological, mechanical, and chemical) for each of the three thermal tests (LBT, SHT, and DST). Documentation includes an introduction and description, a cross section of behavior for each type of measurement (laboratory and field) for the two main testing phases (characterization and testing), a listing of Input-DTNs that contain the measurements, discussion of corresponding measurement uncertainties, and a set of germane references that provide much additional detail regarding the measurements. In addition, summaries of three in-depth investigations are provided: (1) heat and mass loss through the DST bulkhead, (2) scaling along the roof of the DST Heated Drift, and (3) investigation of DST water samples with high fluoride concentrations. Output-DTNs have also been restructured, as needed, to be more functional and

user-friendly than corresponding Input-DTNs. These Output-DTNs for the LBT, SHT, and DST are listed in Tables 6.1-1, 6.2-1, and 6.3-1, respectively. The improved structure of the Output-DTNs facilitates the review, understanding, and usage of the thermal testing measurements by providing improved data layout including: consolidation of incremental test data into a single set, graphical descriptions, and coordinates of boreholes and sensors.

Any uncertainties related to measurements are described in the previous sections and no restrictions within the described parameters are necessary for subsequent use.

8. INPUTS AND REFERENCES

The following is a list of the references cited in this document. Column 1 represents the unique six digit numerical identifier, which is placed in the text following the reference callout (e.g., BSC 2002 [159051]). The purpose of these numbers is to assist the reader in locating a specific reference. Within the reference list, multiple sources by the same author (e.g., BAC 2002) are sorted alphabetically by title.

8.1 CITED DOCUMENTS

101786 ASTM D 4971-89. 1989. *Standard Test Method for Determining the In Situ Modulus of Deformation of Rock Using the Diametrically Loaded 76-mm (3-in.) Borehole Jack*. Philadelphia, Pennsylvania: American Society for Testing and Materials. TIC: 245311.

101541 Barton, N.; Lien, R.; and Lunde, J. 1974. "Engineering Classification of Rock Masses for the Design of Tunnel Support." *Rock Mechanics, 6*, (4), 189-236. New York, New York: Springer-Verlag. TIC: 219995.

101567 Bieniawski, Z.T. 1974. "Geomechanics Classification of Rock Masses and its Application in Tunneling." *Proceedings of the Third International Congress on Rock Mechanics.* Volume II, part A. 27-32. Washington, D.C.: National Academy of Sciences. TIC: 217640.

100653 Brodsky, N.S.; Riggins, M.; Connolly, J.; and Ricci, P. 1997. *Thermal Expansion, Thermal Conductivity, and Heat Capacity Measurements for Boreholes UE25 NRG-4, UE25 NRG-5, USW NRG-6, and USW NRG-7/7A*. SAND95-1955. Albuquerque, New Mexico: Sandia National Laboratories. ACC: MOL.19980311.0316.

102003 Brown, E.T., ed. 1981. *Rock Characterization Testing & Monitoring, ISRM Suggested Methods*. New York, New York: Pergamon Press. TIC: 209865.

159051 BSC (Bechtel SAIC Company) 2002. *Technical Work Plan for: Unsaturated Zone Sections of License Application Chapters 8 and 12*. TWP-NBS-HS-000003 REV 01. Las Vegas, Nevada: Bechtel SAIC Company. ACC: MOL.20020613.0192.

158190 BSC (Bechtel SAIC Company) 2002. *Test Plan for: Drift Scale Test*. SITP-02-UZ-012 REV 00. Las Vegas, Nevada: Bechtel SAIC Company. ACC: MOL.20020204.0143.

101433 Buesch, D.C. and Spengler, R.W. 1998. "Character of the Middle Nonlithophysal Zone of the Topopah Spring Tuff at Yucca Mountain." *High-Level Radioactive Waste Management, Proceedings of the Eighth International Conference, Las Vegas, Nevada, May 11-14, 1998*. Pages 16-23. La Grange Park, Illinois: American Nuclear Society. TIC: 237082.

100657 Buscheck, T.A. and Nitao, J.J. 1995. *Thermal-Hydrological Analysis of Large-Scale Thermal Tests in the Exploratory Studies Facility at Yucca Mountain*. UCRL-ID-121791. Livermore, California: Lawrence Livermore National Laboratory. ACC: MOL.19960501.0392.

159473 Cho, J. 2001. ESF TCO Field Notebook #2 - Borehole Water Collection at ALCOVE 5. Scientific Notebook SN-LANL-SCI-183-V1. ACC: MOL.20010531.0102.

101588 Compton, R.R. 1962. *Manual of Field Geology*. New York, New York: John Wiley and Sons. TIC: 209518.

101428 CRWMS M&O (Civilian Radioactive Waste Management System Management and Operating Contractor) 1996. *Characterization of the ESF Thermal Test Area*. B00000000-01717-5705-00047 REV 01. Las Vegas, Nevada: CRWMS M&O. ACC: MOL.19970116.0187.

101375 CRWMS M&O 1996. *Test Design, Plans and Layout Report for the ESF Thermal Test*. BAB000000-01717-4600-00025 REV 01. Las Vegas, Nevada: CRWMS M&O. ACC: MOL.19970114.0166.

101539 CRWMS M&O 1997. *Ambient Characterization of the Drift Scale Test Block*. BADD00000-01717-5705-00001 REV 01. Las Vegas, Nevada: CRWMS M&O. ACC: MOL.19980416.0689.

146917 CRWMS M&O 1997. *Drift Scale Test Design and Forecast Results*. BAB000000-01717-4600-00007 REV 01. Las Vegas, Nevada: CRWMS M&O. ACC: MOL.19980710.0155.

101540 CRWMS M&O 1997. *Single Heater Test Status Report*. BAB000000-01717-5700-00002 REV 01. Las Vegas, Nevada: CRWMS M&O. ACC: MOL.19980416.0696.

111106 CRWMS M&O 1997. *Updated In Situ Thermal Testing Program Strat*egy. B00000000-01717-5705-00065 REV 01. Las Vegas, Nevada: CRWMS M&O. ACC: MOL.19990526.0296.

111115 CRWMS M&O 1998. *Drift Scale Test As-Built Report*. BAB000000-01717-5700-00003 REV 01. Las Vegas, Nevada: CRWMS M&O. ACC: MOL.19990107.0223.

108306 CRWMS M&O 1998. *Drift Scale Test Progress Report No. 1*. BAB000000-01717-5700-00004 REV 01. Las Vegas, Nevada: CRWMS M&O. ACC: MOL.19990209.0240.

159512 CRWMS M&O 1998. *Thermal Test Progress Report #1*. Las Vegas, Nevada: CRWMS M&O. ACC: MOL.19991104.0269.

129261 CRWMS M&O 1999. *Single Heater Test Final Report*. BAB000000-01717-5700-00005 REV 00 ICN 1. Las Vegas, Nevada: CRWMS M&O. ACC: MOL.20000103.0634.

159513 CRWMS M&O 1999. *Thermal Test Progress Report #3*. Las Vegas, Nevada: CRWMS M&O. ACC: MOL.19991104.0271.

154585 CRWMS M&O 1999. *Thermal Test Progress Report #2*. BABEAF000-01717-5700-00001 REV 00. Las Vegas, Nevada: CRWMS M&O. ACC: MOL.19991104.0270.

159126 Daily, W. and Owen, E. 1991. "Cross-Borehole Resistivity Tomography." *Geophysics, 56*, (8), 1228-1235. Tulsa, Oklahoma: Society of Exploration Geophysicists. TIC: 253164.

134360 Danko, G. and Mousset-Jones, P. 1993. "Modeling of the Ventilation for Emplacement Drift Re-Entry and Rock Drying." *High Level Radioactive Waste Management, Proceedings of the Fourth Annual International Conference, Las Vegas, Nevada, April 26-30, 1993*. *1*, 590-599. La Grange Park, Illinois: American Nuclear Society. TIC: 208542.

100282 DOE (U.S. Department of Energy) 1988. *Site Characterization Plan Yucca Mountain Site, Nevada Research and Development Area, Nevada*. DOE/RW-0199. Nine volumes. Washington, D.C.: U.S. Department of Energy, Office of Civilian Radioactive Waste Management. ACC: HQO.19881201.0002.

130104 DOE (U.S. Department of Energy) 1995. *In-Situ Thermal Testing Program Strategy*. DOE/YMSCO-003. Las Vegas, NV: YMSCO. TIC: 215726.

159475 DOE (U.S. Department of Energy) 2002. *Quality Assurance Requirements and Description*. DOE/RW-0333P, Rev. 12. Washington, D.C.: U.S. Department of Energy, Office of Civilian Radioactive Waste Management. ACC: MOL.20020819.0387.

100673 Flint, L.E. 1996. *Matrix Properties of Hydrogeologic Units at Yucca Mountain, Nevada*. Milestone 3GUP603M. Denver, Colorado: U.S. Geological Survey. ACC: MOL.19970324.0046.

100033 Flint, L.E. 1998. *Characterization of Hydrogeologic Units Using Matrix Properties, Yucca Mountain, Nevada*. Water-Resources Investigations Report 97-4243. Denver, Colorado: U.S. Geological Survey. ACC: MOL.19980429.0512.

159098 Freifeld, B. and Tsang, Y.W. 1998. "Active Hydrological Testing." Chapter 2 of *First Quarter TDIF Submission for the Drift Scale Test (Hydrological, Radar, Microseismic), Version 1.0*. Milestone SP2770M4. Berkeley, California: Lawrence Berkeley National Laboratory. ACC: MOL.19980812.0239.

158429 GS970608314224.006. Provisional Results: Geotechnical Data for Alcove 5 (DWFA), Main Drift of the ESF: Detailed Line Survey Data for the Heated Drift and Cross Drift. Submittal date: 06/24/1997.

100814 Harrar, J.E.; Carley, J.F.; Isherwood, W.F.; and Raber, E. 1990. *Report of the Committee to Review the Use of J-13 Well Water in Nevada Nuclear Waste Storage Investigations*. UCID-21867. Livermore, California: Lawrence Livermore National Laboratory. ACC: NNA.19910131.0274.

159108 Horita, J. and Wesolowski, D.J. 1994. "Liquid-Vapor Fractionation of Oxygen and Hydrogen Isotopes of Water from the Freezing to the Critical Temperature." *Geochemica et Cosmochimica Acta, 58*, (16), 3425-3437. New York, New York: Elsevier. TIC: 240153.

101868 Hvorslev, M.J. 1951. *Time Lag and Soil Permeability in Ground-Water Observations*. AEWES Bulletin 36. Vicksburg, Mississippi: U.S. Army Corps of Engineers, Waterways Experiment Station. TIC: 238956.

158278 LA0002FH6001WP.001. Single Heater Test - Raw Data. Submittal date: 02/25/2000.

158230 LA0106FH831151.002. Large Block Test Data. Submittal date: 06/06/2001.

158229 LA0106FH831151.003. Large Block Temperature Data. Submittal date: 06/06/2001.

158317 LA0111FH831151.002. Drift Scale Test (DST), Raw Data Sets. Submittal date: 11/06/2001.

159515 LA0208FH831151.001. DST DCS Raw Data (All) Includes SNO5 Raw. Submittal date: 08/08/2002.

159308 LA0208FH831151.002. ESF Drift Scale Test, ESF DCS Data TCO Hourly. Submittal date: 08/08/2002.

158319 LA9908FH6001WP.001. Drift Scale Test-Raw Data. Submittal date: 08/31/1999.

159047 LaBrecque, D.J.; Ramirez, A.L.; Daily, W.D.; Binley, A.M.; and Schima, S.A. 1996. "ERT Monitoring of Environmental Remediation Processes." *Measurement and Science Technology, 7*, ([3]), 375-383. [Bristol, England]: IOP Publishing. TIC: 236228.

101393 Lin, W. and Daily, W. 1984. *Transport Properties of Topopah Spring Tuff*. UCRL-53602. Livermore, California: Lawrence Livermore National Laboratory. ACC: NNA.19891026.0025.

159069 Lin, W.; Blair, S.C.; Wilder, D.; Carlson, S.; Wagoner, J.; DeLoach, L.; Danko, G.; Ramirez, A.L.; and Lee, K. 2001. *Large Block Test Final Report*. UCRL-ID-132246, Rev. 2. Livermore, California: Lawrence Livermore National Laboratory. TIC: 252918.

159099 Lin, W.; Roberts, R.; Carlberg, E.; Ruddle, D.; and Pletcher, R. 2002. *Moisture Retention Curves of Topopah Spring Tuff at Elevated Temperatures*. UCRL-ID-146579. Livermore, California: Lawrence Livermore National Laboratory. TIC: 253211.

157900 Lowry, W.E. 2001. *Engineered Barrier Systems Thermal-Hydraulic-Chemical Column Test Report*. TDR-EBS-MD-000018 REV 00. Las Vegas, Nevada: Bechtel SAIC Company. ACC: MOL.20020102.0206.

159132 Lum, C.C. 1997. *Complete Scanline Mapping of Drift Scale Test A*rea. Milestone SP5140M4. Albuquerque, New Mexico: Sandia National Laboratories. ACC: MOL.19971120.0002.

159101 Majer, E.L. and McEvilly, T.V. 1985. "Acoustic Emission and Wave Propagation Monitoring at the Spent Fuel Test: Climax, Nevada*." International Journal of Rock Mechanics and Mining Sciences and Geomechanics Abstracts, 22*, (4), 215-226. [New York, New York: Elsevier]. TIC: 222776.

159518 Mitchell, A. 1996. "Borehole Videos from the Exploratory Studies Facility Thermal Testing Facility-Thermomechanical Alcove." Memorandum from A. Mitchell (LANL) to Distribution, May 21, 1996, LA-EES-13-LV-05-96-021, with attachment ACC: MOL.19960711.0110.

159514 Pannell, G. 2001. "Heat Loss White Paper for KTI KTE0201." E-mail from G. Pannell to C. Gardner, April 4, 2001, with attachment. ACC: MOL.20010822.0143.

101698 Peterson, J.E. 1986. *The Application of Algebraic Reconstruction Techniques to Geophysical Problems*. LBL-21498. Berkeley, California: Lawrence Berkeley National Laboratory. TIC: 239765.

159102 Peterson, J.E., Jr. and Williams, K.H. 1998. "Acoustic Emission/Seismic Wave Monitoring Baseline Data." Chapter 5 of *ESF Drift Scale Test As-Built Data and Baseline Measurements (Hydrological, Radar, and Microseismic), Revision 1.0*. Milestone SPY193M4. Berkeley, California: Lawrence Berkeley National Laboratory. ACC: MOL.19981016.0046.

159128 Peterson, J.E., Jr. and Williams, K.H. 1998. "Pre-Heating Ground Penetrating Radar Baseline Data." Chapter 4 of *ESF Drift Scale Test As-Built Data and Baseline Measurements (Hydrological, Radar, and Microseismic), Revision 1.0*. Milestone SPY193M4. Berkeley, California: Lawrence Berkeley National Laboratory. ACC: MOL.19981016.0046.

159120 Peterson, J.E., Jr. and Williams, K.H. 1998. "Radar Imaging at the Drift Scale Heater Test." Chapter 4 of *First Quarter TDIF Submission for the Drift Scale Test (Hydrological, Radar, Microseismic), Version 1.0*. Milestone SP2770M4. Berkeley, California: Lawrence Berkeley National Laboratory. ACC: MOL.19980812.0239.

159100 Roberts, J.J. and Lin, W. 1995. *Hydrological Property Measurements of Topopah Spring Tuff*. UCRL-ID-119033. Livermore, California: Lawrence Livermore National Laboratory. ACC: MOV.19980504.0004.

159048 Roberts, J.J. and Lin, W. 1995. *Report on Laboratory Tests of Drying and Re-Wetting of Intact Rocks*. UCRL-ID-121513. Livermore, California: Lawrence Livermore National Laboratory. ACC: MOL.19960404.0013.

101710 Roberts, J.J. and Lin, W. 1997. "Electrical Properties of Partially Saturated Topopah Spring Tuff: Water Distribution as a Function of Saturation." *Water Resources Research, 33*, (4), 577-587. Washington, D.C.: American Geophysical Union. TIC: 239736.

117471 SNL (Sandia National Laboratories) 1997. *Unconfined Compression Tests on Specimens from the Drift Scale Test Area of the Exploratory Studies Facility at Yucca Mountain, Nevada*. Albuquerque, New Mexico: Sandia National Laboratories. ACC: MOL.19971120.0014.

118788 SNL (Sandia National Laboratories) 1998. *Laboratory Measurements of Thermal Conductivity as a Function of Saturation State for Welded and Nonwelded Tuff Specimens*. Albuquerque, New Mexico: Sandia National Laboratories. ACC: MOL.19980901.0177.

100646 Tsang, Y.W. and Cook, P. 1997. *Ambient Characterization of the ESF Drift Scale Test Area by Field Air Permeability Measurements*. Milestone SP9512M4. Berkeley, California: Lawrence Berkeley National Laboratory. ACC: MOL.19971201.0829.

105774 Tsang, Y.W. and Freifeld, B. 1998. "Hydrological Baseline Measurements." Chapter 2 of *ESF Drift Scale Test As-Built Data and Baseline Measurements (Hydrological, Radar, and Microseismic)*. Milestone SPY193M4, Rev. 1. Berkeley, California: Lawrence Berkeley National Laboratory. ACC: MOL.19981016.0046.

159097 Tsang, Y.W. and Freifeld, B. 1998. "Hydrological Characterization Data." Chapter 3 *of ESF Drift Scale Test As-Built Data and Baseline Measurements (Hydrological, Radar, and Microseismic)*. Milestone SPY193M4, Rev. 1. Berkeley, California: Lawrence Berkeley National Laboratory. ACC: MOL.19981016.0046.

101736 Waxman, M.H. and Thomas, E.C. 1974. "Electrical Conductivities in Shaly Sands: I. The Relation Between Hydrocarbon Saturation and Resistivity Index; II. The Temperature Coefficient of Electrical Conductivity." *Journal of Petroleum*

Technology, 26, 213-225. Dallas, Texas: Society of Petroleum Engineers. TIC: 239699.

159121 Williams, K.H. and Peterson, J.E., Jr. 1998. "Radar Imaging and Acoustic Emission Monitoring: Second Quarter Progress." Chapter 4 of *Second Quarter TDIF Submission for the Drift Scale Test (Hydrological, Radar, Microseismic), Version 0.0*. Milestone SP2790M4. Berkeley, California: Lawrence Berkeley National Laboratory. ACC: MOL.19980812.0240.

159104 Williams, K.H.; Majer, E.; and Peterson, J.E., Jr. 1998. "Acoustic Emission Monitoring/Seismic Wave Monitoring: First Quarter Data." Chapter 5 of *First Quarter TDIF Submission for the Drift Scale Test (Hydrological, Radar, Microseismic), Version 1.0*. Milestone SP2770M4. Berkeley, California: Lawrence Berkeley National Laboratory. ACC: MOL.19980812.0239.

159516 Williams, N.H. 2001. "Contract #: DE-AC08-01NV12101 - Drift Scale Test (DST) White Paper: Scaling Along the Roof of the Heated Drift." Letter from N.H. Williams (BSC) to S.P. Mellington (DOE/YMSCO), May 15, 2001, PROJ.05/01.033, with enclosure. ACC: MOL.20010622.0252.

100194 Yang, I.C.; Rattray, G.W.; and Yu, P. 1996. *Interpretation of Chemical and Isotopic Data from Boreholes in the Unsaturated Zone at Yucca Mountain, Nevada*. Water-Resources Investigations Report 96-4058. Denver, Colorado: U.S. Geological Survey. ACC: MOL.19980528.0216.

158176 YMP (Yucca Mountain Site Characterization Project) 2002. *Effects of Introduced Materials in the Drift Scale Test.* North Las Vegas, Nevada: Yucca Mountain Site Characterization Office. ACC: MOL.20020304.0044.

8.2 CODES, STANDARDS, REGULATIONS, AND PROCEDURES

033-YMP-QP-3.8, Rev. 1. *Control of the Electronic Management of Information*. Livermore, California: Lawrence Livermore National Laboratory. ACC: MOL.20020108.0169.

AP-2.14Q, Rev. 2, ICN 1. *Review of Technical Products and Data*. Washington, D.C.: U.S. Department of Energy, Office of Civilian Radioactive Waste Management. ACC: MOL.20020701.0183.

AP-2.22Q, Rev. 0. *Classification Criteria And Maintenance Of The Monitored Geologic Repository Q-List.* Washington, D.C.: U.S. Department of Energy, Office of Civilian Radioactive Waste Management. ACC: MOL.20020314.0046

AP-2.27Q, Rev. 0. *Planning for Science Activities.* Washington, D.C.: U.S. Department of Energy, Office of Civilian Radioactive Waste Management. ACC: MOL.20020701.0184

AP-3.15Q, Rev. 3, ICN 3. *Managing Technical Product Inputs*. Washington, D.C.: U.S. Department of Energy, Office of Civilian Radioactive Waste Management. ACC: MOL.20020830.0001.

AP-6.1Q, Rev. 6, ICN 5. *Controlled Distribution.* Washington, DC: U.S. Department of Energy, Office of Civilian Radioactive Waste Management. ACC: MOL.20020813.0055.

AP-7.5Q, Rev. 1. *Submittal, Review, and Acceptance of Deliverables.* Washington, D.C.: U.S. Department of Energy, Office of Civilian Radioactive Waste Management. ACC: MOL.20020701.0181.

AP-17.1Q, Rev. 2, ICN 3. *Record Source Responsibilities for Inclusionary Records*. Washington, D.C.: U.S. Department of Energy, Office of Civilian Radioactive Waste Management. ACC: MOL.20020813.0054.

AP-32.4, Rev. 0, ICN 1, BSCN 1. *Records Retention and Disposition.* Washington, D.C.: U.S. Department of Energy, Office of Civilian Radioactive Waste Management. ACC: MOL.20010212.0274.

AP-SI.1Q, Rev. 3, ICN 4. *Software Management.* Washington, D.C.: U.S. Department of Energy, Office of Civilian Radioactive Waste Management. ACC: MOL.20020520.0283.

AP-SIII.1Q, Rev. 1, ICN 1. *Scientific Notebooks*. Washington, D.C.: U.S. Department of Energy, Office of Civilian Radioactive Waste Management. ACC: MOL.20010905.0138.

AP-SIII.3Q, Rev. 1, ICN 2. *Submittal And Incorporation Of Data To The Technical Data Management System*. Washington, D.C.: U.S. Department of Energy, Office of Civilian Radioactive Waste Management. ACC: MOL.20020701.0177

AP-SIII.7Q, Rev. 0, ICN 1. *Scientific Investigation Laboratory and Field Testing*. Washington, D.C.: U.S. Department of Energy, Office of Civilian Radioactive Waste Management. ACC: MOL.20020701.0180.

AP-SIII.9Q, Rev. 0, ICN 1. *Scientific Analyses.* Washington, D.C.: U.S. Department of Energy, Office of Civilian Radioactive Waste Management. ACC: MOL.20020404.0083.

AP-SV.1Q, Rev. 0, ICN 2. *Control of the Electronic Management of Information.* Washington, D.C.: U.S. Department of Energy, Office of Civilian Radioactive Waste Management. ACC: MOL.20000831.0065.

ASTM D 4971-89. 1989. Standard Test Method for Determining the In Situ Modulus of Deformation of Rock Using the Diametrically Loaded 76-mm (3-in.) Borehole Jack. Philadelphia, Pennsylvania: American Society for Testing and Materials. TIC: 245311.

LANL-YMP-QP-S5.01, Rev. 1. *Electronic Information Management*. Los Alamos, [New Mexico]: Los Alamos National Laboratory. ACC: MOL.20020613.0394.

NWM-USGS-GCP-03, Rev. 4, Mod. 0. *Uranium-Thorium Disequilibrium Studies*. Denver, Colorado: U.S. Geological Survey. ACC: MOL.19990723.0011.

NWM-USGS-GCP-12 Rev. 4, Mod. 1. *Rb-Sr Isotope Geochemistry*. Denver, Colorado: U.S. Geological Survey. ACC: MOL.19990825.0067.

NWM-USGS-GP-32, Rev. 0. *Underground Geologic Mapping*. Denver, Colorado: U.S. Geological Survey. ACC: MOL.19941102.0023.

TIP-AC-02, Rev. 0. *Solutions Analysis Cations by Inductively Coupled Plasma Atomic Emission Spectroscopy (ICP/AES)*. Livermore, California: Lawrence Livermore National Laboratory. ACC: MOL.20010618.0439.

TIP-AC-03, Rev. 0. *Determination of Inorganic Anions by Ion Chromatography (EPA Method 300.00)*. Livermore, California: Lawrence Livermore National Laboratory. ACC: MOL.20010315.0345.

TIP-NF-33, Rev. 0. *Collection and Field Analysis of Water Samples from Boreholes In the Exploratory Studies Facility*. Livermore, California: Lawrence Livermore National Laboratory. ACC: MOL.20010110.0463.

YMP-LBNL-QIP-6.1, Rev. 8, Mod. 0. *Document Review*. Berkeley, California: Lawrence Berkeley National Laboratory. Submitted to the RPC.

YMP-LBNL-QIP-SV.0, Rev. 2, Mod. 1. *Management of YMP-LBNL Electronic Data*. Berkeley, California: Lawrence Berkeley National Laboratory. ACC: MOL.20020717.0319.

YMP-LBNL-TIP/AFT-2.0, Rev. 1, Mod. 0. *Determination of Moisture Content, Bulk Density, Porosity and Particle Density of Rock Samples.* Berkeley, California: Lawrence Berkeley National Laboratory. ACC: MOL.20020717.0323.

YMP-LBNL-TIP/TT-4.0, Rev. 1, Mod. 0. *Acoustic Emission Monitoring/Seismic Wave Monitoring.* Berkeley, California: Lawrence Berkeley National Laboratory. ACC: MOL.20020717.0323.

YMP-LBNL-TIP/TT-7.0, Rev. 0, Mod. 0. *Extraction and Analysis of the Stable Isotope Components of CO2 in Gas Samples*. Berkeley, California: Lawrence Berkeley National Laboratory. ACC: MOL.19990205.0145.

YMP-LBNL-TIP/TT-9.0, Rev. 0, Mod. 0. *Hydrogen Isotope Analyses of Waters*. Berkeley, California: Lawrence Berkeley National Laboratory. ACC: MOL.19990318.0083.

YMP-LBNL-TIP/TT-10.0, Rev. 0, Mod. 0. *Analysis of the Oxygen Isotopic Composition of Water Samples using the ISOPREP 18*. Berkeley, California: Lawrence Berkeley National Laboratory. ACC: MOL.19990224.0638.

8.3 SOURCE DATA, LISTED BY DATA TRACKING NUMBER

159136 GS011108312322.008. Uranium Concentrations and 234U/238U Activity Ratios Analyzed between February 1, 1999, and August 1, 2001 for Drift-Scale Heater Test Water Collected between June 1998 and April 2001, and Pore Water Collected between March 1996 and April 1999. Submittal date: 12/19/2001.

159137 GS011108312322.009. Strontium Isotope Ratios and Strontium Concentrations in Water Samples from the Drift Scale Test Analyzed from March 16, 1999 to June 27, 2001. Submittal date: 02/07/2002.

158430 GS970608314224.007. Provisional Results: Geotechnical Data for the Exploratory Studies Facility, Main Drift, Alcove 5 (DWFA): Heated Drift and Cross Drift Full Periphery Geotechnical Map (Drawing OA-46-300) and Rock Mass Quality Ratings Report. Submittal date: 06/24/1997.

153485 LA0009SL831151.001. Fracture Mineralogy of the ESF Single Heater Test Block, Alcove 5. Submittal date: 09/28/2000.

158426 LA0201SL831225.001. Chemical, Textural, and Mineralogical Characteristics of Sidewall Samples from the Drift Scale Test. Submittal date: 01/10/2002.

146449 LA9912SL831151.002. Percent Coverage by Fracture-Coating Minerals in Core ESF-HD-TEMP-2. Submittal date: 01/05/2000.

158431 LARO831422AQ97.002. Exploratory Studies Facility Test Coordination Office Notebook #2 for Borehole Wireline Measurements. Submittal date: 08/27/1999.

158335 LB000121123142.001. Passive Monitoring Data Collected from 12 Hydrology Holes of the ESF Drift Scale Test for the Period June 1, 1999 through October 31, 1999. Submittal date: 01/21/2000.

158337 LB000121123142.002. Active Hydrology Testing Data (Air Injection) Collected from 12 Hydrology Holes of the ESF Drift Scale Test for the Period June 1, 1999 through October 31, 1999. Submittal date: 01/21/2000.

146451 LB000121123142.003. Isotope Data for CO2 Gas Samples Collected From the Hydrology Holes of the ESF Drift Scale Test for the Period August 9, 1999 through November 30, 1999. Submittal date: 01/21/2000.

158338 LB000121123142.004. Ground Penetrating Radar Data Collected from Boreholes of the ESF Drift Scale Test for the Period June 1, 1999 to October 31, 1999. Submittal date: 01/21/2000.

158339 LB000121123142.005. Acoustic Emission Data Collected from Boreholes of the ESF Drift Scale Test for the Period December 21, 1998 through October 27, 1999. Submittal date: 01/21/2000.

158340 LB000718123142.001. Passive Monitoring Data Collected from 12 Hydrology Holes of the ESF Drift Scale Test for the Period November 1, 1999 through May 31, 2000. Submittal date: 07/18/2000.

158341 LB000718123142.002. Active Hydrology Testing Data (Air Injection) Collected from 12 Hydrology Holes of the ESF Drift Scale Test for the Period November 1, 1999 through May 31, 2000. Submittal date: 07/18/2000.

158342 LB000718123142.003. Isotope Data for CO2 Gas Samples Collected from the Hydrology Holes of the ESF Drift Scale Test for the Period April 18, 2000 through April 19, 2000. Submittal date: 07/18/2000.

153354 LB000718123142.004. Ground Penetrating Radar Data Collected from Boreholes of the ESF Drift Scale Test on April 13, 2000. Submittal date: 07/18/2000.

158343 LB000718123142.005. Acoustic Emission Data Collected from Boreholes of the ESF Drift Scale Test for the Period October 27, 1999 through March 21, 2000. Submittal date: 07/18/2000.

158344 LB0101ACEMDST1.001. Acoustic Emission Data Collected from Boreholes of the ESF Drift Scale Test for 04/13/00-07/02/00. Submittal date: 01/19/2001.

158345 LB0101AIRKDST1.001. Active Air K Testing Data Collected from 12 Hydrology Holes of the ESF Drift Scale Test for 7/24/00-7/28/00 and 10/18/00-10/27/00. Submittal date: 01/19/2001.

158346 LB0101GPRDST01.001. GPR Data Collected from Boreholes of the ESF Drift Scale Test on September 27-28, 2000. Submittal date: 01/19/2001.

158347 LB0101H2ODST01.001. Passive Monitoring Data-Pressure, Temperature, and Humidity - in the ESF DST Hydrology Holes (6/01/00-11/30/00). Submittal date: 01/12/2001.

159306 LB0102CO2DST98.001. Concentration Data for CO2 from Gas Samples Collected from Hydrology Holes in Drift-scale Test. Submittal date: 02/28/2001.

158437 LB0108ACEMDST5.001. Drift Scale Test Acoustic Emission Data. Submittal date: 10/29/2001.

158438 LB0108AIRKDST5.001. Active Air-K Testing. Submittal date: 08/27/2001.

156888 LB0108CO2DST05.001. Concentration and Isotope Data for CO2 and H2O from Gas Samples Collected from Hydrology Holes in Drift-Scale Test - May and August 1999, April 2000, January and April 2001. Submittal date: 08/27/2001.

158440 LB0108GPRDST05.001. Drift Scale Test Ground Penetrating Radar Data for February 2001. Submittal date: 08/27/2001.

158441 LB0108H2ODST05.001. DST Monitoring Data - Temperature, Pressure, Humidity. Submittal date: 08/27/2001.

158348 LB0203AIRKDSTE.001. Active Air-K Testing, Sept. 2001 - Jan. 2002. Submittal date: 03/13/2002.

158349 LB0203CO2DSTEH.001. Concentration/Isotope Data for CO2/H2O from Gas Samples Collected from Hydrology Holes in DST up to End of Heating. Submittal date: 03/13/2002.

158350 LB0203GPRDSTEH.001. Drift Scale Test Ground Penetrating Radar Data for June 2001 - Jan. 2002, Prior to End of Heating. Submittal date: 03/13/2002.

158351 LB0203H2ODSTEH.001. DST Monitoring Data - Temperature, Pressure, Humidity; Jun. 2001 - Jan. 2002. Submittal date: 03/13/2002.

159543 LB0204SHAIRK3Q.001. Single Heater Test Air-K (March-May 97). Submittal date: 04/16/2002.

159303 LB0206C14DSTEH.001. Carbon 14 Isotope Data from CO2 Gas Samples Collected from DST. Submittal date: 06/17/2002.

105587 LB960500834244.001. Hydrological Characterization of the Single Heater Test Area in ESF. Submittal date: 08/23/1996.

158287 LB970100123142.001. Air Injections in Boreholes #16 and #18 in the Single Heater Test Area. Submittal date: 01/17/1997.

158288 LB970100123142.002. Infrared Images in the Single Heater Test Area. Submittal date: 01/17/1997.

158289 LB970400123142.001. Images for Second Quarter Results of Infrared Mapping in the Single Heater Test Area. Submittal date: 04/18/1997.

158293 LB970500123142.001. Air Injection Data in Boreholes #16 and #18 in the Single Heater Test Area. Submittal date: 05/23/1997.

131500 LB970500123142.003. Laboratory Test Results of Hydrological Properties from Dry Drilled and Wet Drilled Cores in the Drift Scale Test Area and in the Single Heater Test Area of the Thermal Test Facility. Submittal date: 05/30/1997.

105589 LB970600123142.001. Ambient Characterization of the ESF Drift Scale Test Area by Field Air Permeability Measurements. Submittal date: 06/13/1997.

158295 LB970700123142.002. Third Quarter IR Pictures of the Single Heater Test Area. Submittal date: 07/17/1997.

118965 LB971000123142.001. Air Injections in Boreholes #16 and #18 in the Single Heater Test Area. Submittal date: 10/17/1997.

158296 LB971000123142.002. Fourth Quarter FY 97 IR Pictures of the Single Heater Test Area. Submittal date: 10/17/1997.

158297 LB980120123142.001. First Quarter FY98 IR Pictures of the Single Heater Test Area. Submittal date: 01/20/1998.

105590 LB980120123142.004. Air Injections in Boreholes 57 through 61, 74 through 78, 185 and 186 in the Drift Scale Test Area. Submittal date: 01/20/1998.

114134 LB980120123142.005. Hydrological Characterization by Air Injections Tests in Boreholes in Heated Drift in DST. Submittal date: 01/20/1998.

158352 LB980120123142.007. Data Represents the Measurement of Discrete Acoustic Energy of the Rock Measured Prior to Turning on the Heaters in the SHT. Submittal date: 01/20/1998.

158280 LB980120123142.008. Data from "Letter Report on First Quarter Results of Measurements in Hydrology Holes in the Single Heater Test Area, FY1998.". Submittal date: 05/28/1999.

113696 LB980420123142.001. Passive Monitoring Data for Hydrology Holes (Boreholes 57-61, 74-78, 185-186) Taken from November, 1997 to February, 1998. Submittal date: 04/20/1998.

113706 LB980420123142.002. Active Hydrology Testing Data in Boreholes 57-61, 74-78, and 185-186; Air Injection Tests and Gas Tracer Tests. Submittal date: 04/20/1998.

113717 LB980420123142.004. Acoustic Emission Data (Recorded Events and Calibration Files). Submittal date: 04/20/1998.

111471 LB980420123142.005. Isotope Data for CO2 from Gas Samples Collected from Drift Scale Test February 1998 in First Quarter TDIF Submission for the Drift Scale Test. Submittal date: 11/12/1998.

113733 LB980715123142.001. Passive Monitoring Data from Hydrology Holes (Boreholes 57-61, 74-78, 185-186) from March 1998 to May 1998 in 2nd Quarter TDIF Submission of the Drift Scale Test Heating Phase. Submittal date: 07/15/1998.

113742 LB980715123142.002. Active Hydrology Testing Data in Boreholes 57-61, 74-78, and 185-186; Air Injection Tests and Gas Tracer Tests in 2ND Quarter TDIF Submission of the Drift Scale Test Heating Phase. Submittal date: 07/15/1998.

111472 LB980715123142.003. Isotope Data for CO2 from Gas Samples Collected from Drift Scale Test June 4, 1998 in 2nd Quarter TDIF Submission of the Drift Scale Test Heating Phase. Submittal date: 07/15/1998.

118999 LB980901123142.001. Active Hydrology Testing Data in Boreholes 16 and 18. Submittal date: 08/26/1998.

119009 LB980901123142.002. Passive Monitoring Data (Temperature, Relative Humidity, and Gauge Pressure) for the Final TDIF Submittal for the Single Heater Test. Submittal date: 08/26/1998.

119016 LB980901123142.003. Ground Penetrating Radar Data for Final TDIF Submittal for the Single Heater Test. Submittal date: 08/26/1998.

119029 LB980901123142.006. Laboratory Test Results of Hydrological Properties from Post-Test Dry-Drilled Cores in the Single Heater Test Area for the Final TDIF Submittal for the Single Heater Test. Submittal date: 08/31/1998.

105593 LB980912332245.002. Gas Tracer Data from Niche 3107 of the ESF. Submittal date: 09/30/1998.

158353 LB981016123142.001. Passive Monitoring Data (Humidity, Pressure, Temperature) from Boreholes 57-61, 74-78, 185-186 Taken from June 1998 to August 1998 for the Third Quarter TDIF Submission for the Drift Scale Test. Submittal date: 10/16/1998.

129245 LB981016123142.002. Active Hydrology Testing Data (Air Injection) from Boreholes 57-61, 74-78, 185-186 Taken from August 1998 to September 1998 for the Third Quarter TDIF Submission for the Drift Scale Test. Submittal date: 10/16/1998.

113278 LB981016123142.004. Isotope Data for CO2 from Gas and Water Samples Taken from June 1998 to September 1998 for the Third Quarter TDIF Submission for the Drift Scale Test. Submittal date: 10/16/1998.

129247 LB990630123142.001. Fourth, Fifth, and Sixth Quarters TDIF Submission for the Drift Scale Test, September 1998 to May 1999. Submittal date: 06/30/1999.

158355 LB990630123142.002. Fourth, Fifth, and Sixth Quarters TDIF Submission for the Drift Scale Test, September 1998 to May 1999. Submittal date: 06/30/1999.

111476 LB990630123142.003. Fourth, Fifth, and Sixth Quarters TDIF Submission for the Drift Scale Test, September 1998 to May 1999. Submittal date: 06/30/1999.

158360 LB990630123142.004. Fourth, Fifth, and Sixth Quarters TDIF Submission for the Drift Scale Test, September 1998 to May 1999. Submittal date: 07/20/1999.

129274 LB990630123142.005. Fourth, Fifth, and Sixth Quarters TDIF Submission for the Drift Scale Test, September 1998 to May 1999. Submittal date: 07/20/1999.

158325 LL000804023142.009. Liquid Saturation Tomographs for the ESF Drift Scale Test (DST) Determined from ERT Measurements. Submittal date: 08/04/2000.

153288 LL001100931031.008. Aqueous Chemistry of Water Sampled from Boreholes of the Drift Scale Test (DST). Submittal date: 11/10/2000.

153616 LL001200231031.009. Aqueous Chemistry of Water Sampled from Boreholes of the Drift Scale Test (DST). Submittal date: 12/04/2000.

159134 LL020302223142.015. Aqueous Geochemistry of DST Samples Collected from HYD Boreholes. Submittal date: 03/07/2002.

159307 LL020405123142.019. Aqueous Geochemistry of Condensed Fluids Collected During Studies of Introduced Materials. Submittal date: 05/22/2002.

159105 LL020502523142.020. Electrical Properties of Topopah Spring Tuff as a Function of Saturation and Temperature. Submittal date: 07/05/2002.

159551 LL020710223142.024. Moisture Content of Rock from Neutron Logging Activities in the Drift Scale Test (DST): August 1997 through May 2002. Submittal date: 08/20/2002.

158237 LL950812704242.017. Report on Laboratory Tests of Drying and Re-Wetting of Intact Rocks. Submittal date: 08/07/1995.

158271 LL960400404244.012. Fracture Mapping of the East Side of the Large Block Test. Submittal date: 04/01/1996.

158274 LL960400504244.013. Fracture Mapping of the South Side of the Large Block Test. Submittal date: 04/01/1996.

158275 LL960400604244.014. Fracture Mapping of the West Side of the Large Block Test. Submittal date: 04/01/1996.

158276 LL960400704244.015. Fracture Mapping of the North Side of the Large Block Test. Submittal date: 04/01/1996.

158244 LL960905204244.022. Permeability Measurements on an Intact Core Sample from the Large Block Test. Submittal date: 09/24/1996.

158281 LL970101004244.026. First Quarter Results of ERT Measurements in the Single Heater Test. Submittal date: 01/08/1997.

158309 LL970101104244.027. First Quarter Results of Chemical Measurements in the Single Heater Test. Submittal date: 01/08/1997.

111481 LL970409604244.030. Second Quarter Results of Chemical Measurements in the Single Heater Test. Submittal date: 04/17/1997.

148609 LL970505404244.031. Second and Third Quarter Results of ERT Measurements for Single Heater Test. Submittal date: 05/23/1997.

111482 LL970703904244.034. Third Quarter Results of Chemical Measurements in the Single Heater Test. Submittal date: 07/15/1997.

127312 LL970709004244.035. Single Heater Test Samples (SHT) Showing Porosity, Relative Humidity and Water Saturation and Drift Scale Test Samples (DST) Showing Porosity, Matrix Potential and Water Saturation. Submittal date: 07/31/1997.

158313 LL970805504244.043. XYZ of Instruments in Single Heater Test (SHT) in RTD Holes 15, 17, 22, and 23; Packer Holes 16 and 18; Chemistry Holes 20 and 21. Submittal date: 08/14/1997.

158286 LL971002904244.044. Fourth Quarter FY97 Results of ERT Measurements in the Single Heater Test. Submittal date: 10/13/1997.

148611 LL971006604244.046. Fourth Quarter FY97 Results of Chemical Measurements in the Single Heater Test (SHT). Submittal date: 10/21/1997.

113894 LL971204304244.047. Neutron Logging Activities at the Large Block Test (LBT). Submittal date: 12/08/1997.

148610 LL980105204244.049. First Quarter FY98 Results of ERT Measurements in the Single Heater Test. Submittal date: 01/13/1998.

118963 LL980106904244.051. First Quarter FY98 Results of the Neutron Logging Report. Submittal date: 01/16/1998.

158332 LL980108804244.052. Electrical Resistivity Tomography (ERT) Monitoring of the Drift Scale Test. Submittal date: 01/22/1998.

158299 LL980109904243.015. Fourth Quarter FY 1997 and First Quarter FY 1998 Data on the O-MPBX at the Single Heater Test (SHT). Submittal date: 01/26/1998.

113782 LL980406404244.057. First and Second Quarter FY98 Results of ERT Measurements in the Drift Scale Test. Submittal date: 04/14/1998.

159107 LL980411004244.060. DST Baseline REKA Probe Measurements. Submittal date: 04/24/1998.

159111 LL980411104244.061. DST Baseline REKA Probe Measurements for Thermal Conductivity and Diffusivity. Submittal date: 04/24/1998.

113791 LL980808604244.065. Second Quarter FY98 Results of ERT Measurements in the Drift Scale Test. Submittal date: 08/21/1998.

159109 LL980902104244.070. DST Baseline REKA Probe Measurements for Thermal Conductivity and Diffusivity. Submittal date: 09/03/1998.

145385 LL980913304244.072. Data Submission Report for Electrical Resistance Tomography Results Obtained During the Large Block Test FY98. Submittal date: 09/24/1998.

135872 LL980918904244.074. Temperature, Relative Humidity and Gas Pressure Results During the Large Block Test FY 98. Submittal date: 09/29/1998.

145099 LL980919304244.075. Neutron Logging Activities at the Large Block Test (LBT). Submittal date: 09/30/1998.

148630 LL980919404244.076. Measurement of the Sensor Displacement While Heating the Large Block at the Large Block Test FY98. Submittal date: 09/30/1998.

158261 LL981001604244.079. The Imaging of the Resistivity Distribution Between Two Boreholes using an Automatic Data Collection and Switching System. Submittal date: 10/05/1998.

118959 LL981109904242.072. Electrical Properties of Tuff from the ESF as a Function of Water Saturation and Temperature. Submittal date: 11/19/1998.

158270 LL981202305912.004. Investigation of Bacterial Transport in the Large Block Test, a Thermally Perturbed Block of Topopah Spring Tuff. Submittal date: 12/03/1998.

158263 LL981208404244.092. X-Ray Radiography of Fracture Flow and Matrix Imbibition in Topopah Spring Tuff Under a Thermal Gradient. Submittal date: 12/08/1998.

113872 LL990702704244.099. Data for the Drift Scale Test. Submittal date: 07/13/1999.

153836 MO0001SEPDSTPC.000. Drift Scale Test (DST) Temperature, Power, Current, and Voltage Data for June 1, 1999 through October 31, 1999. Submittal date: 01/12/2000.

147304 MO0002ABBLSLDS.000. As-Built Borehole Locations and Sensor Locations for the Drift Scale Test Given in Local (DST) Coordinates. Submittal date: 02/01/2000.

150930 MO0005PORWATER.000. Perm-Sample Pore Water Data. Submittal date: 05/04/2000.

153707 MO0007SEPDSTPC.001. Drift Scale Test (DST) Temperature, Power, Current, and Voltage Data for November 1, 1999 through May 31, 2000. Submittal date: 07/13/2000.

153708 MO0012SEPDSTPC.002. Drift Scale Test (DST) Temperature, Power, Current, and Voltage Data for June 1, 2000 through November 30, 2000. Submittal date: 12/19/2000.

153711 O0101SEPFDDST.000. Field Measured Data of Water Samples from the Drift Scale Test. Submittal date: 01/03/2001.

158321 MO0107SEPDSTPC.003. Drift Scale Test (DST) Temperature, Power, Current, and Voltage Data for December 1, 2000 through May 31, 2001. Submittal date: 07/06/2001.

158320 MO0202SEPDSTTV.001. Drift Scale Test (DST) Temperature, Power, Current, and Voltage Data for June 1, 2001 through January 14, 2002. Submittal date: 02/28/2002.

159300 MO0207AL5WATER.001. Water Sampling in Alcove 5 (Results from 2/4/1997 through 4/20/1999). Submittal date: 07/11/2002.

113644 MO9807DSTSET01.000. Drift Scale Test (DST) Temperature, Power, Current, Voltage Data for November 7, 1997 through May 31, 1998. Submittal date: 07/09/1998.

113662 MO9810DSTSET02.000. Drift Scale Test (DST) Temperature, Power, Current, Voltage Data for June 1 through August 31, 1998. Submittal date: 10/09/1998.

113673 MO9906DSTSET03.000. Drift Scale Test (DST) Temperature, Power, Current, and Voltage Data for September 1, 1998 through May 31, 1999. Submittal date: 06/08/1999.

153841 SN0001F3912298.014. Measurements of Displacement Data for the Drift Scale Test (with Results from 6/1/1999 through 10/31/1999). Submittal date: 01/18/2000.

158372 SN0001F3912298.015. Measurements of Strain Data for the Drift Scale Test (with Results from 6/1/1999 through 10/31/1999). Submittal date: 01/18/2000.

153842 SN0001F3912298.016. Measurements of Displacement Data for the Drift Scale Test Corrected for Thermal Expansion (with Results from 6/1/1999 through 10/31/1999). Submittal date: 01/18/2000.

158373 SN0001F3912298.017. Measurements of Strain Data for the Drift Scale Test Corrected for Thermal Expansion (with Results from 6/1/1999 through 10/31/1999). Submittal date: 01/18/2000.

158374 SN0007F3912298.018. Measurements of Displacement Data for the Drift Scale Test (with Results from 11/1/1999 through 5/31/2000). Submittal date: 07/17/2000.

158387 SN0007F3912298.019. Measurements of Strain Data for the Drift Scale Test (with Results from 11/1/1999 through 5/31/2000). Submittal date: 07/17/2000.

158388 SN0007F3912298.020. Measurements of Displacement Data for the Drift Scale Test Corrected for Thermal Expansion (with Results from 11/1/1999 through 5/31/2000). Submittal date: 07/17/2000.

158391 SN0007F3912298.021. Measurements of Strain Data for the Drift Scale Test Corrected for Thermal Expansion (with Results from 11/1/1999 through 5/31/2000). Submittal date: 07/17/2000.

158392 SN0011F3912298.022. Plate-Loading Measured Displacement and Test Pressure Data (with Results from 10/16/2000 through 10/17/2000). Submittal date: 11/30/2000.

158399 SN0011F3912298.023. Plate-Loading Rock Mass Modulus Data (with Results from 10/16/2000 through 10/17/2000). Submittal date: 11/30/2000.

158400 SN0101F3912298.024. Measurements of Displacement Data for the Drift Scale Test (with Results from 6/1/2000 through 11/30/2000). Submittal date: 01/18/2001.

158401 SN0101F3912298.025. Measurements of Strain Data for the Drift Scale Test (with Results from 6/1/2000 through 11/30/2000). Submittal date: 01/18/2001.

158402 SN0101F3912298.026. Measurements of Displacement Data for the Drift Scale Test Corrected for Thermal Expansion (with Results from 6/1/2000 through 11/30/2000). Submittal date: 01/18/2001.

158407 SN0101F3912298.027. Measurements of Strain Data for the Drift Scale Test Corrected for Thermal Expansion (with Results from 6/1/2000 through 11/30/2000). Submittal date: 01/18/2001.

158408 SN0107F3912298.029. Measurements of Displacement Data for the Drift Scale Test (with Results from 12/1/2000 through 5/31/2001). Submittal date: 07/09/2001.

158409 SN0107F3912298.030. Measurements of Strain Data for the Drift Scale Test (with Results from 12/1/2000 through 5/31/2001). Submittal date: 07/09/2001.

158413 SN0107F3912298.031. Measurements of Displacement Data for the Drift Scale Test Corrected for Thermal Expansion (with Results from 12/1/2000 through 5/31/2001). Submittal date: 07/09/2001.

158414 SN0107F3912298.032. Measurements of Strain Data for the Drift Scale Test Corrected for Thermal Expansion (with Results from 12/1/2000 through 5/31/2001). Submittal date: 07/09/2001.

159133 SN0203F3903102.001. Drift Scale Test Water Sampling (with Results from 4/17/2001 through 1/14/2002). Submittal date: 03/29/2002.

158361 SN0203F3912298.033. Measurements of Displacement Data for the Drift Scale Test (with Results from 6/1/2001 through 1/14/2002). Submittal date: 03/26/2002.

158362 SN0203F3912298.034. Measurements of Strain Data for the Drift Scale Test (with Results from 6/1/2001 through 1/14/2002). Submittal date: 03/26/2002.

158363 SN0203F3912298.035. Measurements of Displacement Data for the Drift Scale Test Corrected for Thermal Expansion (with Results from 6/1/2001 through 1/14/2002). Submittal date: 03/26/2002.

158364 SN0203F3912298.036. Measurements of Strain Data for the Drift Scale Test Corrected for Thermal Expansion (with Results from 6/1/2001 through 1/14/2002). Submittal date: 03/26/2002.

158322 SN0203L2210196.007. Thermal Expansion and Thermal Conductivity of Test Specimens from the Drift Scale Test Area of the Exploratory Studies Facility at Yucca Mountain, Nevada. VA Supporting Data. Submittal date: 03/06/2002.

158314 SNF32020196001.010. Rock Mass Quality Data for the Thermal Testing Facility Alcove (Alcove #5) Stations 00+05 to 00+60 Meters. Submittal date: 09/24/1996.

158434 SNF32020196001.015. Rock Mass Quality Data for the Thermal Testing Facility Alcove (Alcove #5) Stations 00+60 to 01+35 Meters. Submittal date: 03/10/1997.

109620 SNF32070996001.005. Rock Mass Quality Data for the ESF South Ramp Stations 64+25 Meters to 66+95 Meters. Submittal date: 01/22/1997.

158315 SNF35110695001.001. Single Heater Test: As-Built Gage Layouts (Thermocouples, Thermistors, MPBX's). Submittal date: 09/25/1996.

113812 SNF35110695001.008. Evaluation and Comparative Analysis of Single Heater Test, Thermal and Thermomechanical Data: First Quarter FY98 Results (8/26/96 through 11/30/97). Submittal date: 01/06/1998.

113819 SNF35110695001.009. Thermal and Thermomechanical Data for the Single Heater Test Final Report. Submittal date: 08/24/1998.

158300 SNF35110695001.010. Goodman Jack Measurements in the Single Heater Test Block. Submittal date: 05/25/1999.

159130 SNF38040197001.001. Heated Drift Test: SNL As-Built Gauge Table (Thermomechanical Gauges Only). Submittal date: 01/06/1998.

159114 SNF39012298002.002. Measurements of Displacement Data for the Drift Scale Test (with Results from 11/1/1997 through 5/31/1998). Submittal date: 07/09/1998.

158417 SNF39012298002.003. Measurements of Strain Data for the Drift Scale Test (with Results from 11/9/1997 through 5/31/1998). Submittal date: 09/24/1998.

153837 SNF39012298002.004. Measurements of Displacement Data for the Drift Scale Test Corrected for Thermal Expansion (Results from 11/9/1997 through 5/31/1998). Submittal date: 09/24/1998.

158418 SNF39012298002.005. Measurements of Strain Data for the Drift Scale Test Corrected for Thermal Expansion (Results from 11/9/1997 through 5/31/1998). Submittal date: 09/24/1998.

158419 SNF39012298002.006. Measurements of Displacement Data for the Drift Scale Test (with Results from 6/1/1998 through 8/31/1998). Submittal date: 10/08/1998.

158365 SNF39012298002.007. Measurements of Strain Data for the Drift Scale Test (with Results from 6/1/1998 through 8/31/1998). Submittal date: 10/08/1998.

153839 SNF39012298002.008. Measurements of Displacement Data for the Drift Scale Test Corrected for Thermal Expansion (Results from 6/1/1998 through 8/31/1998). Submittal date: 10/08/1998.

158366 SNF39012298002.009. Measurements of Strain Data for the Drift Scale Test Corrected for Thermal Expansion (Results from 6/1/1998 through 8/31/1998). Submittal date: 10/08/1998.

158367 SNF39012298002.010. Measurements of Displacement Data for the Drift Scale Test (with Results from 9/1/1998 through 5/31/1999). Submittal date: 06/28/1999.

158368 SNF39012298002.011. Measurements of Strain Data for the Drift Scale Test (with Results from 9/1/1998 through 5/31/1999). Submittal date: 06/28/1999.

153840 SNF39012298002.012. Measurements of Displacement Data for the Drift Scale Test Corrected for Thermal Expansion (with Results from 9/1/1998 through 5/31/1999). Submittal date: 06/28/1999.

158369 SNF39012298002.013. Measurements of Strain Data for the Drift Scale Test Corrected for Thermal Expansion (with Results from 9/1/1998 through 5/31/1999). Submittal date: 06/28/1999.

158420 SNL02100196001.001. Unconfined Compression Tests on Specimens from the Drift Scale Test Area of the Exploratory Studies Facility at Yucca Mountain, Nevada. Submittal date: 05/14/1997.

109722 SNL22080196001.001. Thermal Properties of Test Specimens from the Single Heater Test Area in the Thermal Testing Facility at Yucca Mountain, Nevada. Submittal date: 08/15/1996.

158306 SNL22080196001.002. Unconfined Compression Tests on Specimens from the Single Heater Test Area in the Thermal Testing Facility at Yucca Mountain, Nevada. Submittal date: 08/22/1996.

119042 SNL22080196001.003. Posttest Laboratory Thermal and Mechanical Characterization for Single Heater Test (SHT) Block. Submittal date: 08/26/1998.

158213 SNL22100196001.006. Laboratory Measurements of Thermal Conductivity as a Function of Saturation State for Welded and Nonwelded Tuff Specimens. Submittal date: 06/08/1998.

158370 SNL23030598001.001. Unconfined Compression Tests on Cast-in-Place Concrete Specimens from the Drift Scale Test in the ESP (Exploratory Studies Facility) at Yucca Mountain, Nevada. Submittal date: 03/10/1998.

158422 SNL23030598001.003. Creep Testing of Cast-in-Place Concrete. Submittal date: 10/09/1998.

159115 UN0106SPA013GD.003. Drift Scale Thermal Test (DST) REKA Probe Acquired Data for Thermal Conductivity and Diffusivity for the Period 05/01/1998 to 04/30/2001 (Heated Measurements for Boreholes 151, 152, and 153). Submittal date: 06/13/2001.

159116 UN0106SPA013GD.004. Drift Scale Thermal Test (DST) REKA Probe Developed Data for Thermal Conductivity and Diffusivity for the Period 05/01/1998 to 04/30/2001 (Heated Measurements for Boreholes 151, 152, and 153). Submittal date: 06/28/2001.

159117 UN0109SPA013GD.005. Drift Scale Test (DST) Rapid Evaluation of K and Alpha (REKA) Probe Acquired Data for Thermal Conductivity and Diffusivity for the Period 05/01/2001 to 08/31/2001 (Heated Measurements for Boreholes 151, 152, and 153). Submittal date: 09/28/2001.

159118 UN0112SPA013GD.006. DST REKA Probe Acquired Data for Thermal Conductivity and Diffusivity for the Period 09/01/2001 to 12/31/2001 (Heated Measurements for Boreholes 151, 152, and 153). Submittal date: 12/31/2001.

159119 UN0201SPA013GD.007. DST REKA Probe Developed Data for Thermal Conductivity and Diffusivity for the Period 05/01/2001 to 12/31/2001 (Heated Measurements for Boreholes 151 and 152). Submittal date: 01/07/2002.

8.4 OUTPUT DATA, LISTED BY DATA TRACKING NUMBER

LB0208ACEMDSTH.001. Acoustic Emission for the Heating Phase of the DST. Submittal date: 9/18/2002.

LB0208AIRKDSTH.001. Air Permeability Data for the Heating Phase of the DST. Submittal date: 9/18/2002.

LB0208AIRKSHTC.001. Air Permeability Data for the Heating and Cooling Phases of the SHT. Submittal date: 9/18/2002.

LB0208GPRDSTHP.001. GPR for the Heating Phase of the DST. Submittal date: 9/18/2002.

LB0208GPRSHTCP.001. GPR for the Heating and Cooling Phases of the SHT. Submittal date: 9/18/2002.

LB0208H2ODSTHP.001. Passive Hydrological Data for the Heating Phase of the DST. Submittal date: 9/18/2002.

LB0208ISODSTHP.001. Isotope Data and CO_2 Analysis for the Heating Phase of the DST. Submittal date: 9/18/2002.

LL020709923142.023. Aqueous Geochemistry of Borehole Waters Collected in the Heating Phase of the DST. Submittal date: 9/18/2002.

LL020710523142.025. Temperatures, Heater Powers, and Rock Displacements of the Large Block Test. Submittal date: 9/18/2002.

LL020801723142.028. Electrical Resistance Tomographs of the Drift Scale Test, November 1997 through December 2001. Submittal date: 9/18/2002.

LL020801823142.029. Electrical Resistance Tomographs of the Single Heater Test, August 1996 through December 1997. Submittal date: 9/18/2002.

MO0208RESTRDST.002. Restructured Drift Scale Test (DST) Heating Phase Power and Temperature Data. Submittal date: 9/18/2002.

MO0208RESTRSHT.002. Restructured Single Heater Test (SHT) Heating Phase Power and Temperature Data. Submittal date: 9/18/2002.

SN0207F3912298.037. Summary of Smoothed Measurements of Displacement Data for the Heating Phase of the Drift Scale Test (with Results From 12/3/1997 through 1/14/2002). Submittal date: 9/18/2002.

SN0208F3511695.011. Summary of Rock Displacement Data from the Single Heater Test (with Results from 8/26/1996 through 1/31/1998). Submittal date: 9/18/2002.

SN0208F3903102.002. Summary of Thermal Test Water Samples and Field Measurements through 1/14/2002. Submittal date: 9/18/2002.

SN0208F3903102.003. Field Measurements and Fluoride Content from HF (Hydrogen-Fluoride) Tests. Submittal date: 9/18/2002.

SN0208F3912298.038. Summary of Smoothed Measurements of Strain Data for the Heating Phase of the Drift Scale Test (with Results from 12/3/1997 through 1/14/2002). Submittal date: 9/18/2002.

SN0208F3912298.039. Rock Mass Thermal Expansion Coefficients Determined from the Drift Scale Test Heating Phase MPBX Measurements. Submittal date: 9/18/2002.